Unclassified **NEA/CSNI/R(2005)5/VOL1**

Organisation de Coopération et de Développement Economiques
Organisation for Economic Co-operation and Development **06-Sep-2005**

English text only

NUCLEAR ENERGY AGENCY
COMMITTEE ON THE SAFETY OF NUCLEAR INSTALLATIONS

NEA/CSNI/R(2005)5/VOL1
Unclassified

INTERNATIONAL STANDARD PROBLEM NO. 48
CONTAINMENT CAPACITY

Synthesis Report

The enclosed CD-Rom contains full report (including appendices) and the Workshop proceedings.

The complete document is only available in pdf format.

JT00188855

English text only

ORGANISATION FOR ECONOMIC CO-OPERATION AND DEVELOPMENT

Pursuant to Article 1 of the Convention signed in Paris on 14th December 1960, and which came into force on 30th September 1961, the Organisation for Economic Co-operation and Development (OECD) shall promote policies designed:

- to achieve the highest sustainable economic growth and employment and a rising standard of living in member countries, while maintaining financial stability, and thus to contribute to the development of the world economy;
- to contribute to sound economic expansion in member as well as non-member countries in the process of economic development; and
- to contribute to the expansion of world trade on a multilateral, non-discriminatory basis in accordance with international obligations.

The original member countries of the OECD are Austria, Belgium, Canada, Denmark, France, Germany, Greece, Iceland, Ireland, Italy, Luxembourg, the Netherlands, Norway, Portugal, Spain, Sweden, Switzerland, Turkey, the United Kingdom and the United States. The following countries became members subsequently through accession at the dates indicated hereafter: Japan (28th April 1964), Finland (28th January 1969), Australia (7th June 1971), New Zealand (29th May 1973), Mexico (18th May 1994), the Czech Republic (21st December 1995), Hungary (7th May 1996), Poland (22nd November 1996), Korea (12th December 1996) and the Slovak Republic (14 December 2000). The Commission of the European Communities takes part in the work of the OECD (Article 13 of the OECD Convention).

NUCLEAR ENERGY AGENCY

The OECD Nuclear Energy Agency (NEA) was established on 1st February 1958 under the name of the OEEC European Nuclear Energy Agency. It received its present designation on 20th April 1972, when Japan became its first non-European full member. NEA membership today consists of 28 OECD member countries: Australia, Austria, Belgium, Canada, the Czech Republic, Denmark, Finland, France, Germany, Greece, Hungary, Iceland, Ireland, Italy, Japan, Luxembourg, Mexico, the Netherlands, Norway, Portugal, Republic of Korea, the Slovak Republic, Spain, Sweden, Switzerland, Turkey, the United Kingdom and the United States. The Commission of the European Communities also takes part in the work of the Agency.

The mission of the NEA is:

- to assist its member countries in maintaining and further developing, through international co-operation, the scientific, technological and legal bases required for a safe, environmentally friendly and economical use of nuclear energy for peaceful purposes, as well as
- to provide authoritative assessments and to forge common understandings on key issues, as input to government decisions on nuclear energy policy and to broader OECD policy analyses in areas such as energy and sustainable development.

Specific areas of competence of the NEA include safety and regulation of nuclear activities, radioactive waste management, radiological protection, nuclear science, economic and technical analyses of the nuclear fuel cycle, nuclear law and liability, and public information. The NEA Data Bank provides nuclear data and computer program services for participating countries.

In these and related tasks, the NEA works in close collaboration with the International Atomic Energy Agency in Vienna, with which it has a Co-operation Agreement, as well as with other international organisations in the nuclear field.

COMMITTEE ON THE SAFETY OF NUCLEAR INSTALLATIONS

The NEA Committee on the Safety of Nuclear Installations (CSNI) is an international committee made up of senior scientists and engineers, with broad responsibilities for safety technology and research programmes, and representatives from regulatory authorities. It was set up in 1973 to develop and co-ordinate the activities of the NEA concerning the technical aspects of the design, construction and operation of nuclear installations insofar as they affect the safety of such installations.

The committee's purpose is to foster international co-operation in nuclear safety amongst the OECD member countries. The CSNI's main tasks are to exchange technical information and to promote collaboration between research, development, engineering and regulatory organisations; to review operating experience and the state of knowledge on selected topics of nuclear safety technology and safety assessment; to initiate and conduct programmes to overcome discrepancies, develop improvements and research consensus on technical issues; to promote the coordination of work that serve maintaining competence in the nuclear safety matters, including the establishment of joint undertakings.

The committee shall focus primarily on existing power reactors and other nuclear installations; it shall also consider the safety implications of scientific and technical developments of new reactor designs.

In implementing its programme, the CSNI establishes co-operative mechanisms with NEA's Committee on Nuclear Regulatory Activities (CNRA) responsible for the program of the Agency concerning the regulation, licensing and inspection of nuclear installations with regard to safety. It also co-operates with NEA's Committee on Radiation Protection and Public Health (CRPPH), NEA's Radioactive Waste Management Committee (RWMC) and NEA's Nuclear Science Committee (NSC) on matters of common interest.

FOREWORD

At the CSNI meeting in June 2002, the proposal for an International Standard Problem on containment integrity (ISP 48) based on the NRC/NUPEC/Sandia test was approved. Objectives were to extend the understanding of capacities of actual containment structures based on results of the recent PCCV Model test and other previous research. The ISP was sponsored by the USNRC, and results had been made available thanks to NUPEC and to the USNRC. Sandia National Laboratory was contracted to manage the technical aspects of the ISP.

This report presents the analysis results of the calculation of the Limit State Test (LST), i.e. static pressure loading, and of the calculations of response to both thermal and mechanical loadings, provided by the ISP48 participants.

Volumes 2 and 3 contain the individual participant reports for both phases 2 and 3.

The CSNI Working Group on the Integrity and Ageing and in particular its sub-group on the behavior of concrete structures has produced extensive material over the last few years. The report NEA/CSNI/R(2002)13 Finite element analysis of ageing reinforced and prestressed concrete structures in nuclear power plants - An international review of current capabilities and priorities for future developments- provides an excellent and complete review of finite element issues related to concrete structures under static and quasi-static conditions. The complete list of references is given below.

- NEA/CSNI/R(2004)11 International Standard Problem No.48 - Containment Capacity. Phase 2 Report - Results of Pressure Loading Analysis
- NEA/CSNI/R(2004)8 Proceedings of the CSNI/RILEM Workshop on Use and Performance of Concrete in NPP Fuel Cycle Facilities - Hosted by Instituto de Ciencias de la Construcción, Eduardo Torroja, Madrid, Spain, on 15-16 March 2004
- NEA/CSNI/R(2002)21 Electrochemical techniques to detect corrosion in concrete structures in nuclear installations - Technical Note
- NEA/CSNI/R(2002)14 Report of the task group reviewing activities in the area of ageing of concrete structures used to construct nuclear power plant fuel-cyle facilities
- NEA/CSNI/R(2002)13 Finite element analysis of ageing reinforced and prestressed concrete structures in nuclear power plants - An international review of current capabilities and priorities for future developments
- NEA/CSNI/R(2002)7 OECD-NEA Workshop on the Evaluation of Defects, Repair Criteria & Methods of Repair for Concrete Structures in Nuclear Power Plants – GRS, Berlin 10/11 April 2002 (Volume I - Volume II)
- NEA/CSNI/R(2000)15 Proceedings of the Workshop on Instrumentation and Monitoring of Concrete Structures, Tractebel, Brussels, 22-23 March 2000

- NEA/CSNI/R(1999)11 Tendon Prestress Loss in NPP Containments (EdF, Poitiers)

- NEA/CSNI/R(1999)1 Proceedings of Workshop on Finite Element Analysis of Degraded Concrete Structures (BNL New York/Oct5. 1998)

The complete list of CSNI reports, and the text of reports from 1993 onwards, is available on http://www.nea.fr/html/nsd/docs

ACKNOWLEDGMENTS

This effort would not have been possible without the cooperation and support of many individuals and groups. The Committee on the Safety of Nuclear Installations (CSNI), the U.S. Nuclear Regulatory Commission (NRC), the Japan Nuclear Energy Safety Organization (JNES) (formerly the Nuclear Power Engineering Corporation, NUPEC), and Sandia National Laboratories (SNL) are pleased to have had the participation of the following organizations in this International Standard Problem on Containment Capacity. While there were many other individuals who contributed to this effort, the principal correspondents are listed below:

BE/HSE/NNC	British Energy	Graham Doughty
	Nuclear Installations Inspectorate/Health & Safety Executive	David Shepherd
	NNC Ltd.	Nawal Prinja
		James Curley
EGP	Energoprojekt Praha, UJV Rez. Div.	Jan Stepan
		Jan Maly
FORTUM	Fortum Nuclear Services	Pentti Varpasuo
GRS	Gesellschaft für Anlagen und Reaktorsicherheit mbH	Hans Grebner
		Jurgen Sievers
IRSN/CEA	Institut de Radioprotection et de Sûreté Nucléaire	Georges Nahas
	Commissariat a l'Energie Atomique	Thierry Charras
JPRG	Japan PCCV Research Group	
	The Japan Atomic Power Co.	Takeshi Kawasato
	Obayahsi Corporation	Takanori Ogata
KAERI	Korea Atomic Energy Research Institute	Jeong-Moon Seo
		Sang-jin Lee
		Hong-Po Lee
KOPEC	Korea Power Engineering Company	Nam-Ho Lee
		Il Hwan Moon
NRC/SNL/DEA	US Nuclear Regulatory Commission	Syed A. Ali
		Bret A. Tegeler
		Abdul Sheikh
	Sandia National Laboratories	Michael F. Hessheimer
	David Evans and Associates	Robert A. Dameron
SCANSCOT	Scanscot Technology	Ola Jovall
		Mikael Pålsson

While not formally participating in Phase 2 of this ISP, the support and contributions of the following organizations and individuals is also recognized:

EDF	Électricité de France	Jean-Pierre Touret Jean-Luc Valfort Sharokh Ghavmian
JNES	Japan Nuclear Energy Safety Organization	Satoru Shibata

These organizations received no financial support from CSNI, NRC, or SNL, and their efforts are gratefully acknowledged.

The CSNI also wishes to acknowledge the guidance, support, and encouragement of the CSNI's Eric Mathet; and Dr. James F. Costello (retired), formerly of the NRC's Engineering and Research Applications Branch, Division of Engineering Technology, Office of Reactor Research. The CSNI also thanks Michael Hessheimer, Manager, Systems and Structures Dept. at Sandia National Laboratories, USA for his outstanding work and dedication to make this effort a success.

EXECUTIVE SUMMARY

In June 2002, the OECD-NEA Committee on the Safety of Nuclear Installations (CSNI), with the encouragement of the US NRC, initiated an International Standard Problem on containment integrity (ISP 48) based on the NRC/NUPEC/Sandia test. The objectives of the ISP are to extend the understanding of capacities of actual containment structures based on results of the recent PCCV Model test and other previous research.

From 1997 through 2001 Sandia National Laboratories (SNL) conducted a Cooperative Containment Integrity Program under the joint sponsorship of the Nuclear Power Engineering Corporation (NUPEC) of Japan, and the NRC Office of Nuclear Regulatory Research. The purpose of the program was to investigate the response of representative models of nuclear containment structures to pressure loading beyond the design basis accident and to compare analytical predictions to measured behavior. A uniform 1:4-scale model of a prestressed concrete containment vessel (PCCV) was constructed and tested at SNL. This model was representative of the containment structure of an actual pressurized-water reactor plant in Japan.

The ISP consists of four phases over a period of 2 years:

Phase 1: Data Collection and Identification

Phase 2: Calculation of the Limit State Test (LST), i.e. static pressure loading

Phase 3: Calculation of response to both Thermal and Mechanical Loadings

Phase 4: Reporting Workshop

Eleven organizations (or teams) from nine OECD member countries accepted the invitation to participate in the ISP and perform calculations to predict the structural response of the PCCV model to static and transient pressure and thermal loading. Each participating organization was provided with the model and loading data and was asked to perform independent analyses to simulate the response of the PCCV model. The results of each team's calculations were compiled and the results presented at a final workshop in April 2005.

The prestressed concrete containment vessel (PCCV) model is a uniform 1:4-scale model of the containment structure of Unit 3 of the Ohi Nuclear Power Station in Japan. The approach to designing the model was to scale the design of the Ohi-3 containment to the extent possible and include as many representative features of the prototype as practical: liner, penetrations, reinforcement steel and tendons.

Fifty-five response parameters, referred to as standard output locations (SOLs), were selected to facilitate initial comparison of the Phase 2 calculations with the test results. The selection of these locations was based on the containment experience of the project team at Sandia and the results of preliminary analyses to characterize model responses and identify possible failure modes. The calculated responses match the test results and each other reasonably well up to the onset of global or general membrane, yielding where the results begin to diverge. Also, most of the analyses capture the

loss of stiffness due to cracking of the concrete at approximately 1.5 times the design pressure. The calculated responses for hoop liner and tendon strains again match the test data up to the onset of global yielding, however, the divergence beyond this point is more pronounced for liner and tendon strains than it is for displacements. In addition to submitting response predictions at the SOLs, each participant was also asked to provide a best estimate of failure pressure and mechanisms of the PCCV model. It is interesting to note that the differences in failure predictions are much more significant than the differences in the calculated responses would seem to suggest.

Phase 3 of ISP48 extends the results of the model tests and calculations by investigating the addition of temperature to the pressure loading.

The ISP participants agreed to consider two thermal load cases for Phase 3:

- Case 1: Saturated Steam Conditions (mandatory for all Phase 3 participants)
  - Monotonically increasing static pressure and temperature (saturated steam).
- Case 2: Station Blackout Scenario
  - A representative severe-accident scenario for a four-loop PWR including vessel failure and hydrogen detonation

With regard to the two questions raised with the addition of thermal loading to the overpressurization, the following observations are made:

With addition of temperature, would the onset of leakage occur later in the pressure history and, possibly, closer to the burst pressure?

- Results predict failure at both lower and higher pressure when temperature is considered.
- The margin between leak and rupture does not appear to change significantly for the cases considered.
- Change in 'failure' pressures are small (<10%) in the cases considered.
- Consideration of 'realistic' severe accident scenario (Case 2) yields lower 'failure' pressure than saturated steam conditions.
- Effects of material degradation are significant for 'realistic' severe accident scenarios.

How would including the effect(s) of accident temperatures change the prediction of failure location and failure mode?

- While leak or rupture pressures are not significantly changed, displacements are significantly greater, especially when considering material property degradation.
  - Case 1: Vertical displacements increase
  - Case 2: Radial displacements increase
- Failure at penetrations appears more likely, and may control, under combined pressure and temperature loading.

The work reported herein represents, arguably, the state of the art in the numerical simulation of the response of a prestressed concrete containment vessel (PCCV) model to pressure loads up to failure. A significant expenditure of time and money on the part of the sponsors, contractors, and Round Robin

participants was required to meet the objectives. Results and conclusions for each phase of the ISP are included in this final report along with a discussion of issues identified as a result of this effort. In general the results for Phase 2 demonstrate good agreement between the calculated and measured values up to about twice the design pressure. The results of Phase 3 show the relevance of temperature loads which can be very different depending on the postulated transient. Global behavior compared more favorably than local behavior.

TABLE OF CONTENTS

LIST OF APPENDICES

NEA/CSNI/R(2005)5 - Volume 2

Appendix C: British Energy
Nuclear Installations Inspectorate/Health & Safety Executive
NNC Ltd.
Appendix D: Energoprojekt Praha, UJV Rez. Div.
Appendix E: Fortum Nuclear Services Ltd.
Appendix F: Gesellschaft für Anlagen und Reaktorsicherheit mbH
Appendix G: Institut de Radioprotection et de Sûreté Nucléaire
Commissariat a l'Energie Atomique

NEA/CSNI/R(2005)5 - Volume 3

Appendix H: Japan PCCV Research Group
Appendix I: Korea Atomic Energy Research Institute
Appendix J: Korea Power Engineering Company
Appendix K: US Nuclear Regulatory Commission
Sandia National Laboratories
David Evans and Associates
Appendix L: Scanscot Technology

FIGURES

TABLES

1. INTRODUCTION

1.1 Background

At the CSNI meeting in June 2002, the proposal for an International Standard Problem on containment integrity (ISP 48) based on the NRC/NUPEC/Sandia test was approved (Ref. IAGE_CONC/ISP48/(03)2). Objectives are to extend the understanding of capacities of actual containment structures based on results of the recent PCCV Model test and other previous research. Sandia National Laboratories (SNL) conducted a Cooperative Containment Integrity Program under the joint sponsorship of the Nuclear Power Engineering Corporation (NUPEC) of Japan, and the NRC Office of Nuclear Regulatory Research. The purpose of the program was to investigate the response of representative models of nuclear containment structures to pressure loading beyond the design basis accident and to compare analytical predictions to measured behavior. A uniform 1:4-scale model of a prestressed concrete containment vessel (PCCV) was constructed and tested at SNL from 1997 through 2001. This model was representative of the containment structure of an actual pressurized-water reactor plant in Japan.

1.2 Scope of ISP48

The first meeting of the ISP48 members was held on November 20 & 21, 2002 in Stockholm, Sweden to define the scope and the schedule for the ISP. It was agreed that the ISP would consist of four phases:

Phase 1: Data Collection and Identification

Phase 2: Calculation of the Limit State Test (LST), i.e. static pressure loading

Phase 3: Calculation of response to both Thermal and Mechanical Loadings

Phase 4: Reporting Workshop

Under Phase 1, Sandia National Laboratories (SNL) was tasked with providing the data on the model design/construction and testing to complete the calculations in Phases 2 and 3. A detailed test report was published by the US Nuclear Regulatory Commission [1]. A condensed version of this report was prepared to meet the requirements of Phase 1 of the ISP.

Eleven organizations (or teams) accepted the invitation to participate in the ISP and completed calculations for either Phase 2 or Phase 3 or both. The participating organizations are:

BE/HSE/NNC	British Energy Nuclear Installations Inspectorate/Health & Safety Executive NNC Ltd.	UK
EDF	Électricité de France	France
EGP	Energoprojekt Praha, UJV Rez. Div.	Czech Rep.
FORTUM	Fortum Nuclear Services Ltd.	Finland
GRS	Gesellschaft für Anlagen und Reaktorsicherheit mbH	Germany
IRSN/CEA	Institut de Radioprotection et de Sûreté Nucléaire Commissariat a l'Energie Atomique	France
JPRG	Japan PCCV Research Group	Japan
KAERI	Korea Atomic Energy Research Institute	Korea

KOPEC	Korea Power Engineering Company	Korea
NRC/SNL/DEA	US Nuclear Regulatory Commission Sandia National Laboratories David Evans and Associates	US
SCANSCOT	Scanscot Technology	Sweden

Some of these organizations participated in the Pretest Round Robin Analysis organized by SNL in 1995 to predict the response of the PCCV model prior to testing [2] while for other participants this was a new problem. Each participating organization was provided with the model and loading data and was asked to perform independent analyses to simulate the response of the PCCV model.

In order to provide an initial basis for comparison of the Phase 2 calculations with the test data, each participant was asked to submit response time histories at the same 55 Standard Output Locations (SOLs) used in the PCCV Pretest Round Robin Analysis. Each participant was also asked to specify the pressure at which they calculated key structural milestones, such as cracking, liner yield and failure. The results of the Phase 2 calculations were reviewed at a meeting of the participants held in conjunction with the 8th meeting of the CSNI Working Group on the Integrity and Ageing of Components and Structures on March 19, 2004 in Madrid, Spain.

The results of the Phase 3 combined thermal and mechanical analysis were reviewed at a meeting of the participants held in conjunction with a Workshop on Containment Capacity and the 9th meeting of the CSNI Working Group on the Integrity and Ageing of Components and Structures, held April 4-8, 2004 in Lyon, France. The compiled results of the ISP are the subject of this report. The results of a companion Workshop on Containment Capacity will also published by CSNI [3]

1.3 Report Organization

This report presents the Phase 2 and 3 analysis results completed by the ISP48 participants. These results include predictions of the response of the PCCV model in terms of strain, displacement, or force at specified locations throughout the model, the pressure capacity of the PCCV model, and the failure mode and mechanisms. Section 2 summarizes the design, construction and instrumentation of the PCCV model. Section 3 summarizes the procedures and results of the overpressure tests. Section 4 presents the Phase 2 calculations and the composite plots presented in Appendix A. Section 5 summarizes the Phase 3 calculations and the composite plots are presented in Appendix B. Section 6 provides some observations from the comparison of results. Appendices C through L are the individual participant reports for both Phases 2 and 3.

2. PRESTRESSED CONCRETE CONTAINMENT VESSEL MODEL

The PCCV model was a 1:4-scale model of the prestressed concrete containment vessel (PCCV) of an actual nuclear poser plant in Japan, Ohi-3 (Figure 2.1). Ohi-3 is an 1127 MWe Pressurized Water Reactor (PWR) unit, one of four units comprising the Ohi Nuclear Power Station located in Fukui Prefecture, owned and operated by Kansai Electric Power Company.

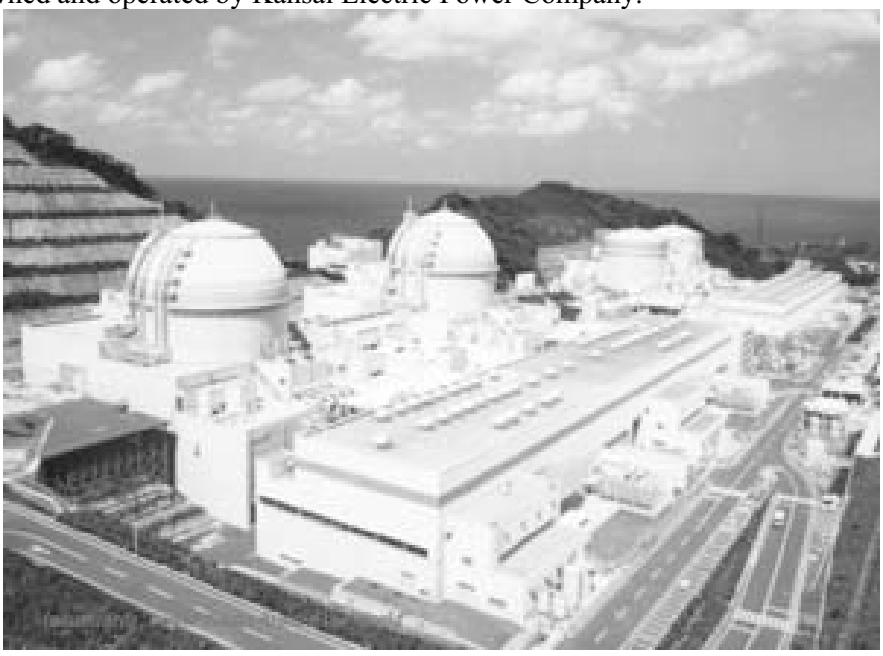

Figure 2.1 Ohi Nuclear Power Station, Ohi-cho, Fukui, Japan

2.1 Model Features and Scale

The Ohi-3 containment is a thin prestressed concrete cylindrical shell with a hemispherical dome and a continuous steel liner anchored to a reinforced concrete basemat which extends beyond the containment to support other plant structures. Consistent with the objectives of the sponsoring organizations, the features and scale of the PCCV model were chosen so that the response of the model would mimic the global behavior of the prototype and local details, particularly those around penetrations, would be represented. One of the primary considerations in determining the scale of the model was the desire to utilize construction materials that were identical, or nearly so, to the material used in the construction of the prototype. Preliminary design studies, conducted to determine the appropriate scale of the model, initially focused on a mixed scale model where the scale on the overall geometry would be 1:6, while the scale on the liner thickness would be 1:3. These preliminary studies indicated, however, that use of this mixed scale might upset the relationship between failure modes which might be expected in the prototype. In particular, the use of a steel liner which was twice as thick, relative to the prestressed concrete shell, as the prototype might retard the onset of liner tearing (leakage) failure modes and increase the likelihood of a structural failure mode occurring. As a result, it was decided that the scale of the model would be a uniform 1:4, with minor exceptions to accommodate fabrication and construction concerns. This was judged to be the minimum scale that would allow the steel liner to be constructed from prototypical materials and fabricated with details and procedures that were representative of the prototype. The overall geometry and dimensions of the PCCV model are shown in Figure 2.2.

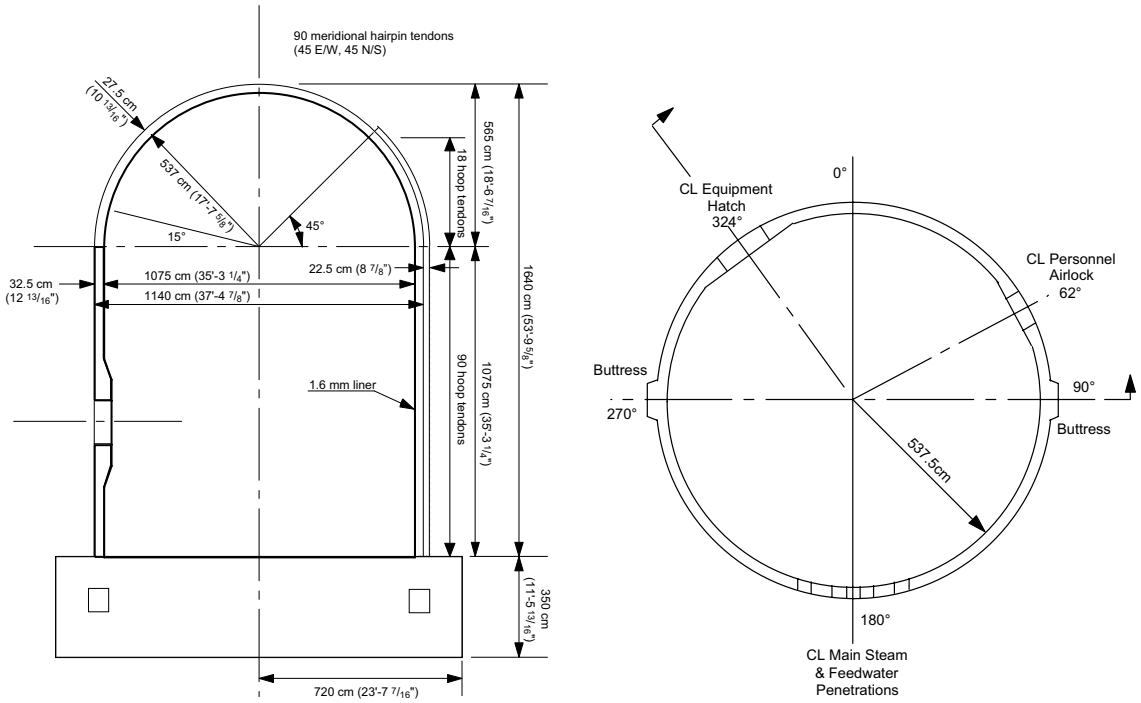

Figure 2.2 PCCV Model Elevation and Cross-Section

Although both NUPEC and SNL (under NRC sponsorship) had conducted component tests of both full-size and scaled penetrations, it was decided that PCCV model would include both functional representation of the major penetrations, namely the equipment hatch (E/H) and the personnel air lock (A/L), and non-functional representation of the main steam (M/S) and feed water (F/W) penetrations. The E/H and A/L penetrations were fully-functional, one-fourth scale models of the penetrations in the prototype, while only the penetration sleeves of the M/S and F/W penetrations, terminated with pressure seating blind flanges, were included in the model. The liner and concrete reinforcing details around these penetrations were also retained in the model.

During construction and instrumentation of the model, primary access to the interior was through the E/H, while the A/L was used to provide heating, cooling and ventilation for personnel working inside the model. The M/S and F/W penetrations provided portals for interior instrumentation cabling, power and, during testing, the pressurization medium. Prior to testing, after the E/H cover was installed and sealed, the A/L provided the means for final egress and sealing of the model with a specially designed pressure seating cover which could be closed from the outside of the model.

2.2 Project Schedule

The NUPEC/NRC Cooperative Containment Research Program commenced in June 1991. The tests were conducted at the Containment Technology Test Facility-West at Sandia National Laboratories, Albuquerque, New Mexico. Construction of the PCCV model commenced January 3, 1997 with initial site preparation. Milestones in the construction and testing of the PCCV model include the following:

12 February 1997	First Basemat Pour (F1)
19 June 1997	First Liner Panel Installed
15 April 1999	Final Dome Pour (D3)
12-14 October 1999	Pretest Round Robin Meeting
8 March-3 May 2000	Prestressing

25 June 2000	PCCV Construction Completed
12-14 September 2000	Structural Integrity and Integrated Leak Rate Test
27-28 September 2000	Limit State Test
22 August 2001	Posttest Round Robin Meeting
14 November 2002	Structural Failure Mode Test
3 May 2002	PCCV Demolition and Site Restoration Completed

2.3 Design

The Prestressed Concrete Containment Vessel model design was directed by NUPEC with overall responsibility for the design and construction contracted to Mitsubishi Heavy Industries, Ltd. (MHI), Tokyo. Responsibility for the design of the liner and penetrations was assigned to MHI's Kobe Shipyard and Machinery Works while the design of the concrete portions of the model were subcontracted to Obayashi Corp., Tokyo.

The basic philosophy guiding the design of the PCCV model was agreed upon very early in the program. Key elements of this design philosophy included:

- The PCCV model would be a uniform 1:4-scale model of the prototype prestressed concrete containment vessel of Ohi Unit 3.
- Elements of the model which would affect the ultimate strength would be equivalent to the prototype. The model liner would be one-fourth the thickness of the prototype liner. Reinforcing ratios would be maintained and the number and arrangement of the prestressing tendons would, to the extent possible, be identical to the prototype.
- The model should be capable of reproducing the failure modes postulated for the prototype, including

  a) Hoop Tensile failure of the cylinder wall

  b) Bending-Shear failure at the junction of the cylinder wall with the basemat

  c) Shear failure in the basemat above the tendon gallery

  d) Bearing failure at the tendon anchors

  e) Bending-Shear failure at the large penetrations

  f) Bending-Shear at the small penetrations

  g) Liner tearing due to strain concentrations at local discontinuities (stiffeners/anchors, thickened reinforcing plates at penetrations and embedments)

  h) Leakage at penetration seals due to ovalization or distortion of the sealing surfaces.

  Furthermore, to the extent possible, introduction of non-representative failure modes, as a result of scaling or other modeling artifacts, was to be avoided.

The general arrangement of the prototype and representative failure mode locations are shown in Figure 2.3.

While the PCCV model was not 'designed' in the conventional sense, its features were scaled directly from the Ohi-3 design with some simplification to facilitate construction without compromising the objectives of the test. The prototype, Ohi-3 was designed in accordance with the "Draft Technical

Code for Concrete Containment Vessels in Nuclear Power Plants" issued by MITI/ANRE in November, 1981. This draft code was formally adopted in 1993 as MITI Notification No. 452. The code is not identical to the ASME/ACI code which governs the design of concrete containments in the US, however, the basic design philosophies are similar, i.e. to ensure that all elements of the containment structure respond essentially elastically (with some minor exceptions for secondary stresses) to the specified design loading conditions.

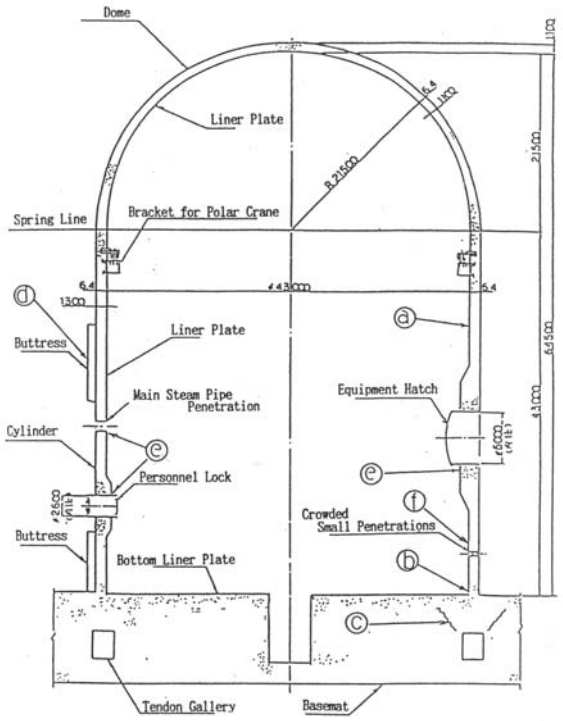

Figure 2.3 Elevation of PCCV Prototype and Potential Failure Locations

Construction of the prototype was also governed by Japanese Architectural Standard Specifications No. 5 and 5N for Reinforced Concrete Work at Nuclear Power Plants. Construction specifications for the PCCV model also followed these standards to the extent possible, however, modifications were made to adapt the specifications to US construction practices.

It is beyond the scope of this report to include all the details of the design and construction specifications. Those details are provided in the test report [1].

The completed PCCV model is shown in Figure 2.4.

Figure 2.4 Completed PCCV Model

2.4 Instrumentation

The basic instrumentation plan was outlined by NUPEC in early 1992 during the initial planning for the PCCV model test. Considering the basic design philosophy, described in Section 2.3, the basic instrumentation plan identified the following measurements to be taken during the PCCV pressure tests:

1. load (internal pressure),
2. displacement,
3. rebar strain,
4. concrete strain,
5. concrete crack mapping,
6. liner and liner anchor strain,
7. tendon force, and
8. temperature

These parameters were to be measured at a number of locations to be able to characterize both the global and local response of the model.

The basic instrumentation plan also specified a grid of azimuths and elevations which would form the basis for the instrumentation layout and provide a scheme for incorporating the nominal gage locations in the individual gage ID's. This basic grid of cardinal lines is shown in Figure 2.6.

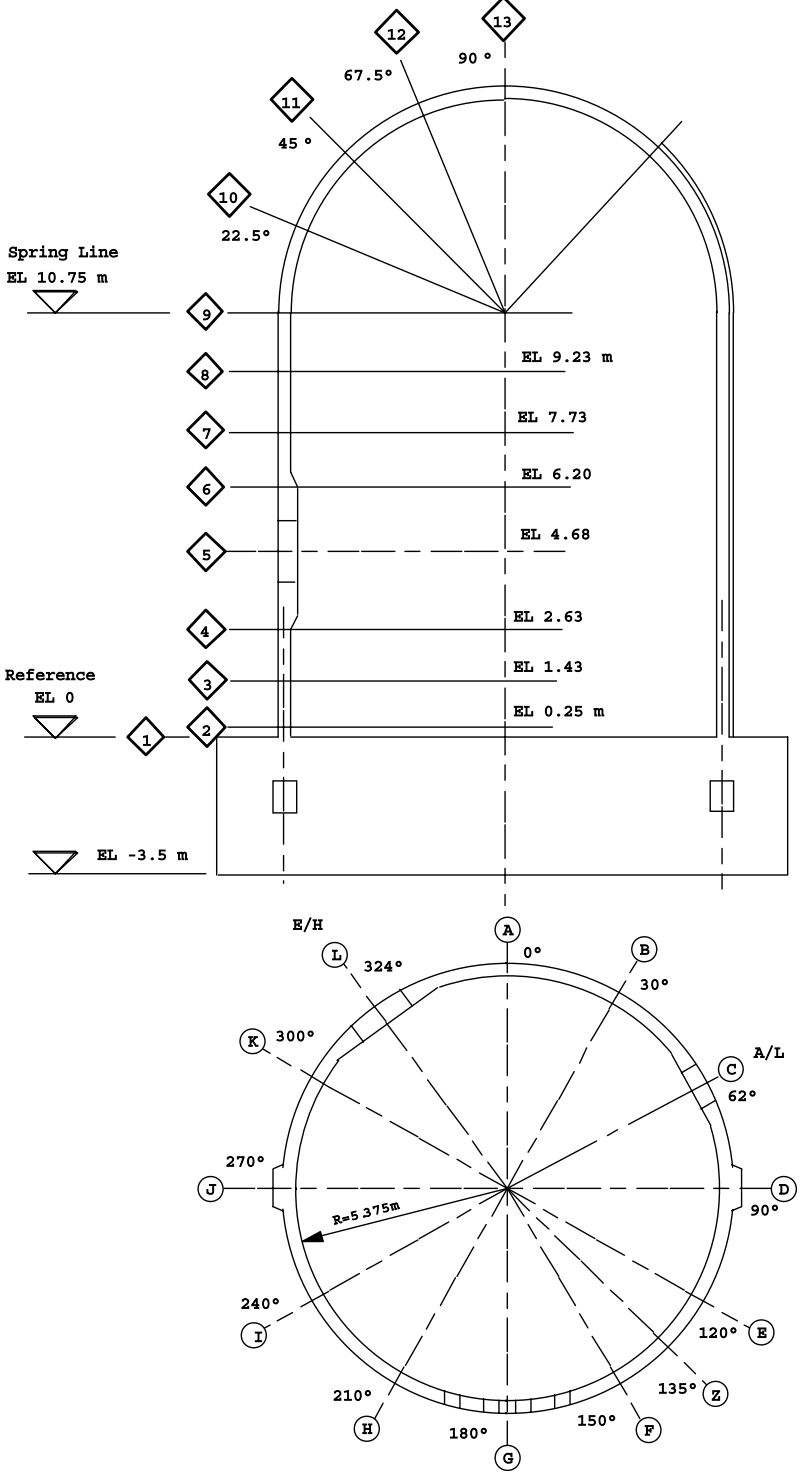

Figure 2.6 Cardinal Instrumentation Layout Lines

Thirteen cardinal elevations were established, from 1 at the top of the basemat (El. 0.00) to 13 at the dome apex. Twelve cardinal azimuths, spaced roughly 30º apart, were established with A at 0º (or

360º) to L at 324º. A thirteenth cardinal azimuth was established at 135º and designated Z. This azimuth was selected as representative of the global axisymmetric response of the containment, based on preliminary analysis results. While the PCCV model is not axisymmetric in terms of geometry and stiffness, Azimuth Z is reasonably distant from any major structural discontinuities and the net hoop prestressing force is close to the average.

Acoustic monitoring was not specified in the basic instrumentation plan but it was agreed to incorporate it into the final instrumentation plan to allow monitoring of the entire structure since it was likely that damage could occur at locations which were not monitored via other methods. The specific goals of the acoustic monitoring system were to:

- detect tendon wire breaks
- detect rebar breaks
- detect concrete cracking and crushing
- detect liner tearing and leakage

Acoustic monitoring of the PCCV model during both the prestressing and low and high pressure tests was performed Pure Technologies Inc. of Calgary, Canada under a turn-key contract. Pure Technologies developed the SoundPrint® acoustic monitoring system and has extensive experience in acoustically monitoring structures, especially prestressed concrete structures such as parking garages and bridges. This system was run independently of the main DAS. The system consisted of the acoustic sensors, essentially piezo-electric accelerometers bonded to the structure and connected to a separate data acquisition system. One of the unique features of this system is the capability to perform real-time data processing and analysis to identify event types and locations. Thirty-two sensors were glued the external surface of the model to monitor and 16 sensors were placed inside the model.

The nominal locations of the gages are shown in Figures 2.7 to 2.12. A detailed description of the instrumentation is provided in the test report [1]. The total number of each type of instrument installed on the PCCV Model is shown in Table 2.1.

Table 2.1 PCCV Instrument Summary

Instrument Type		**Number of Gages**
Strain	Liner	559
	Rebar	391
	Tendons (Tensmeg)	37
	Tendons (wire)	156
	Concrete	94
Displacements		101
Load Cells (1/3 of Tendons)		68
Temperature and Pressure		100
Acoustic		54
Total		**1560**

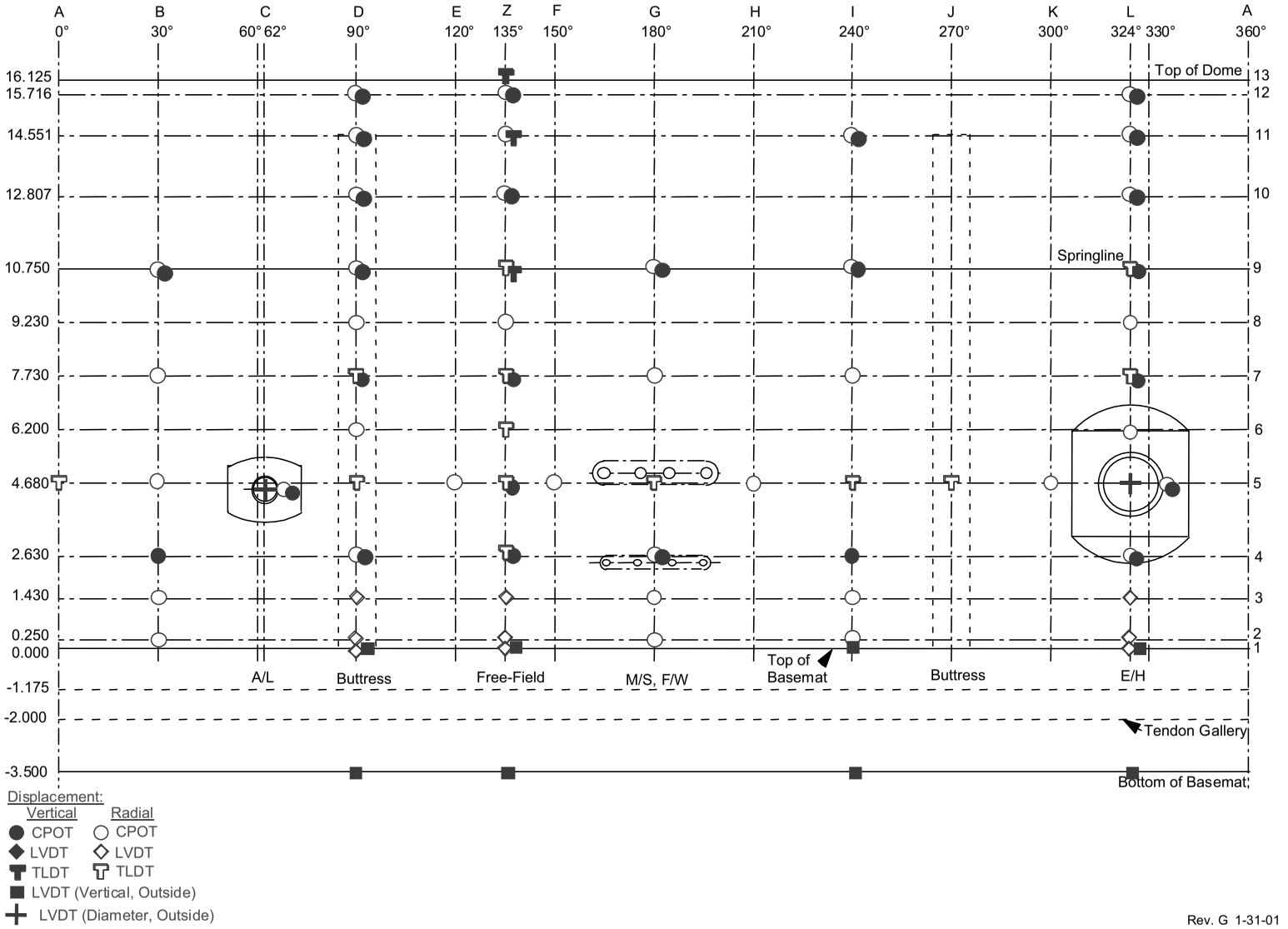

Figure 2.7 Displacement Instrumentation Locations

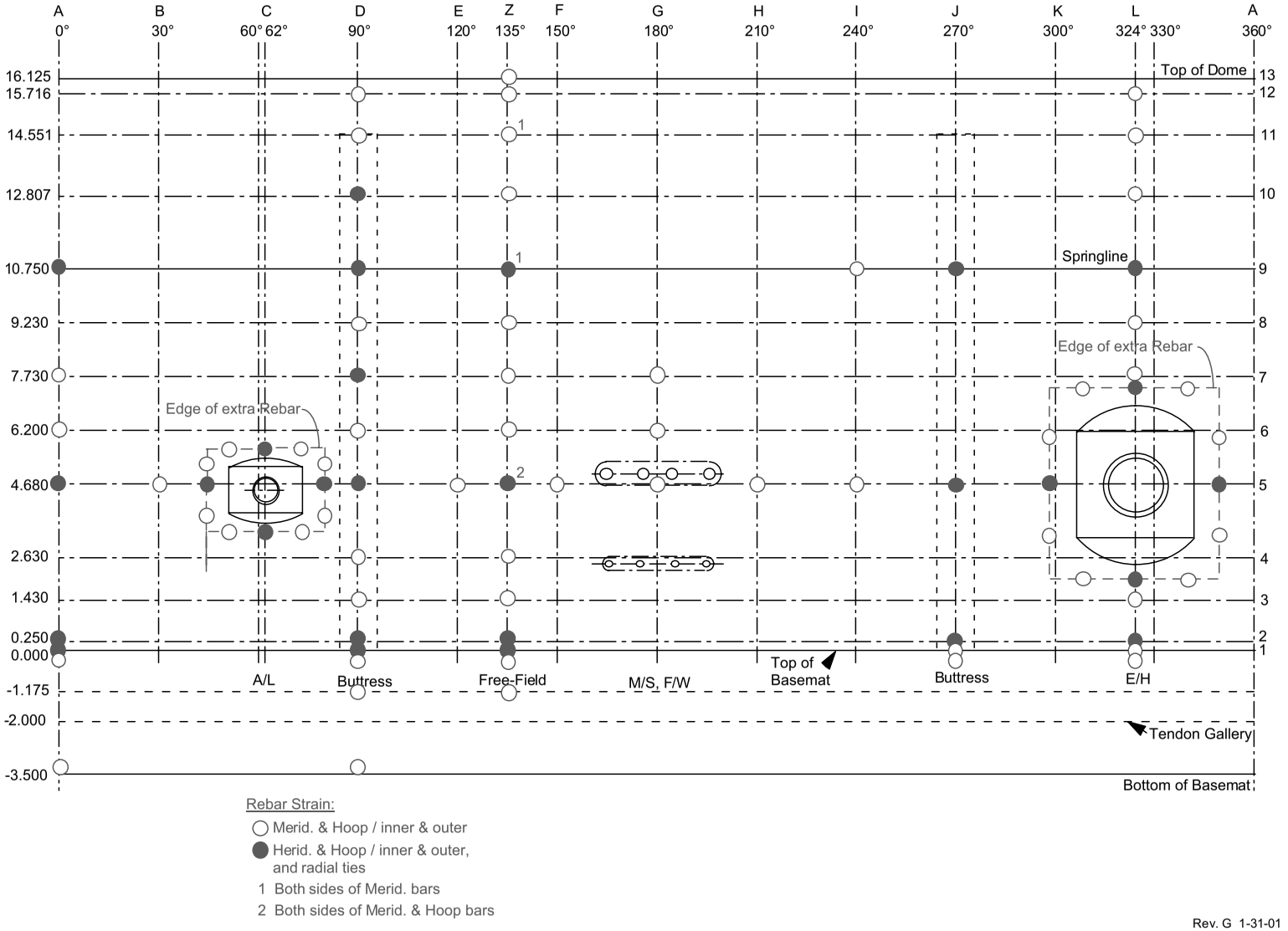

Figure 2.8 Rebar Instrumentation Locations

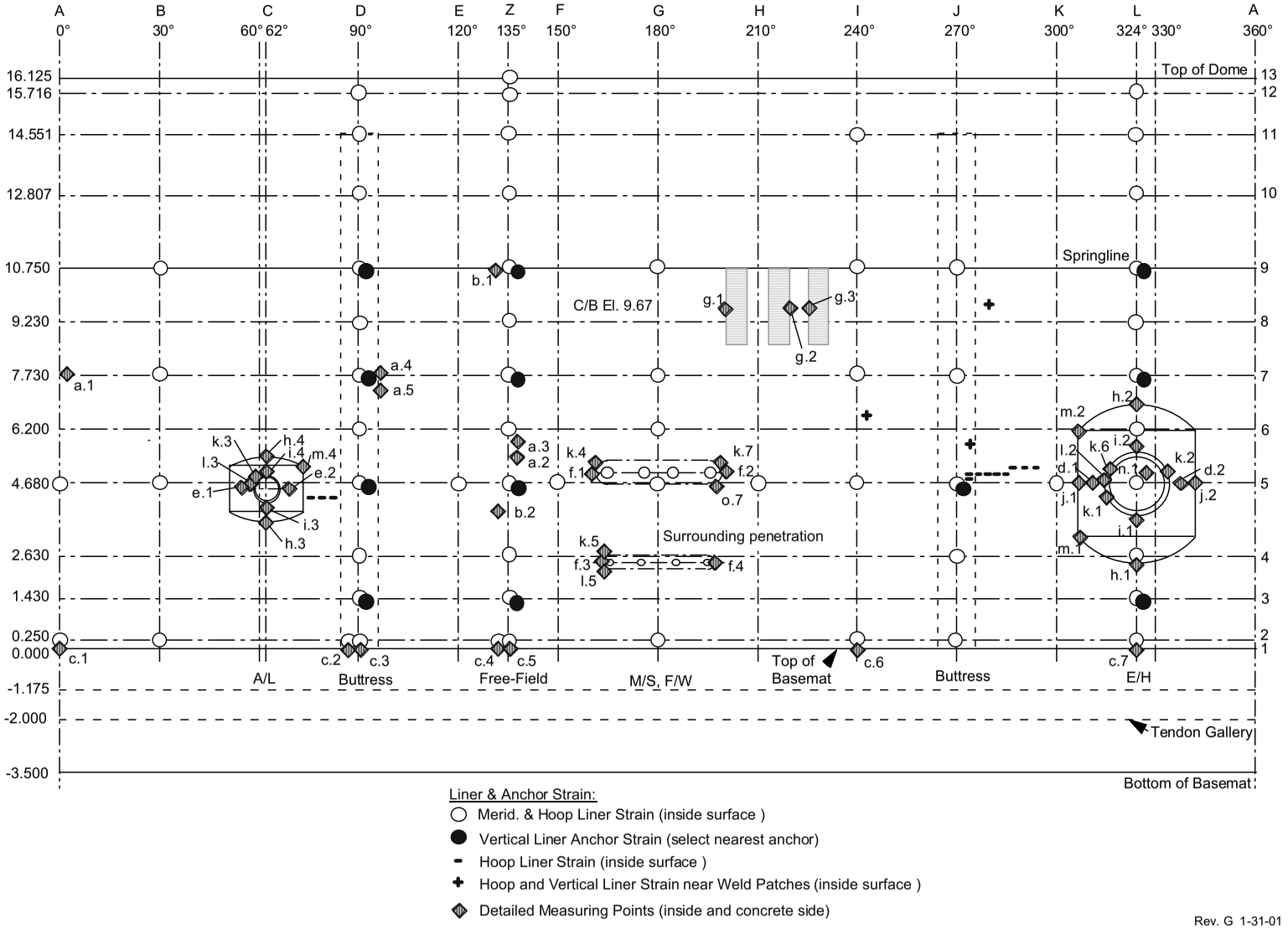

Figure 2.9 Liner and Liner Anchor Instrumentation Locations

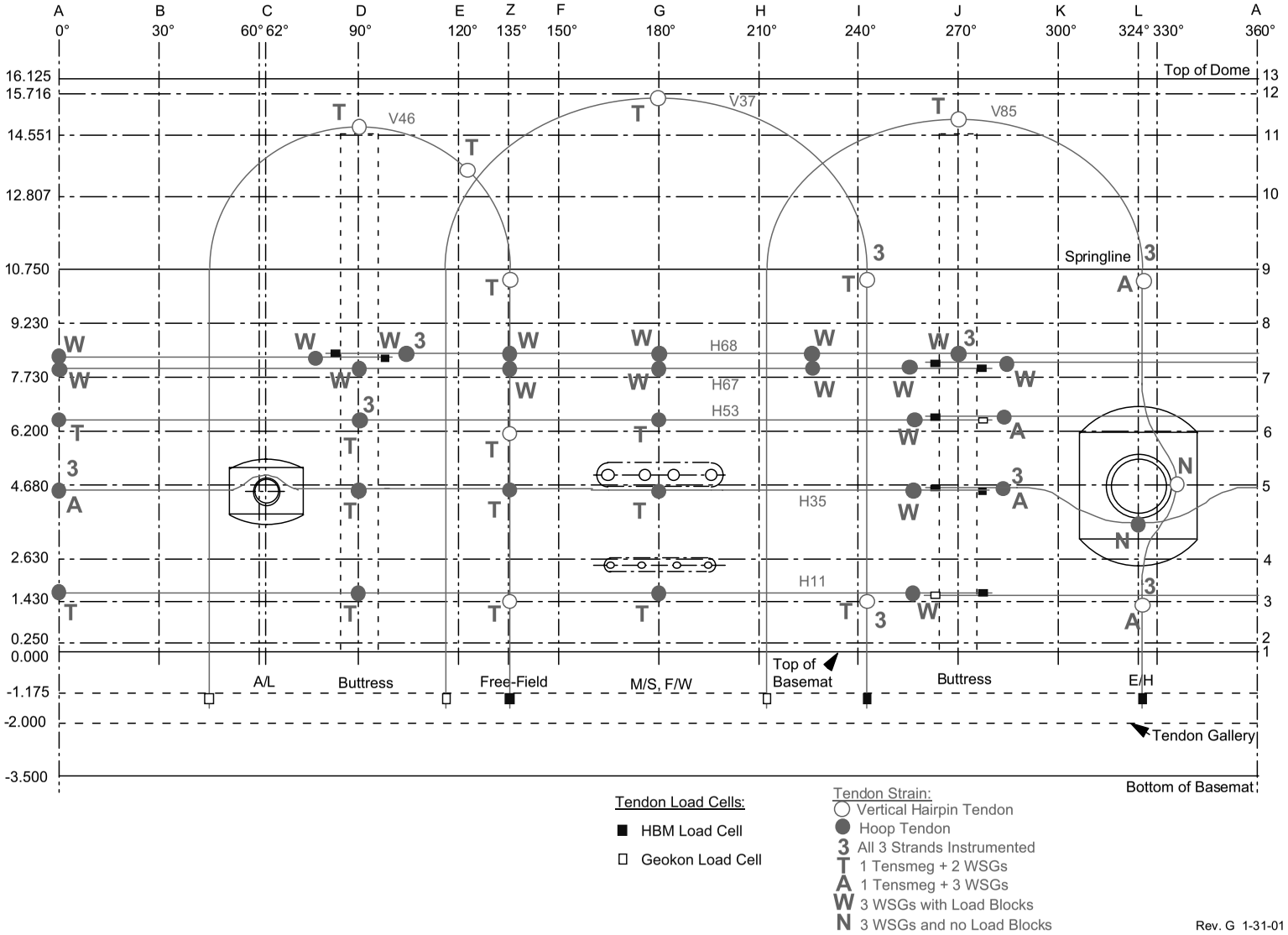

Figure 2.10 Tendon Instrumentation Locations

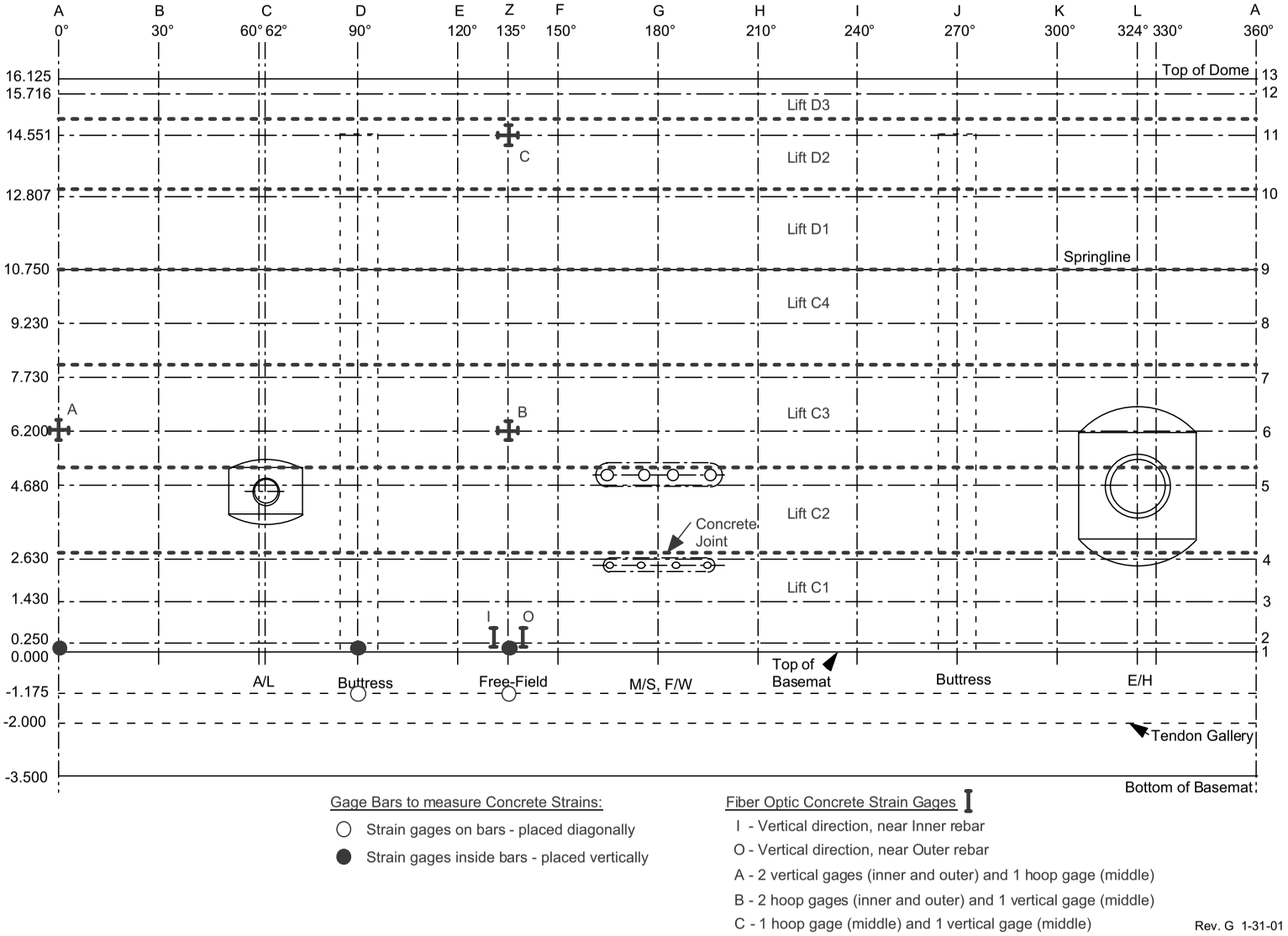

Figure 2.11 Concrete Instrumentation Locations

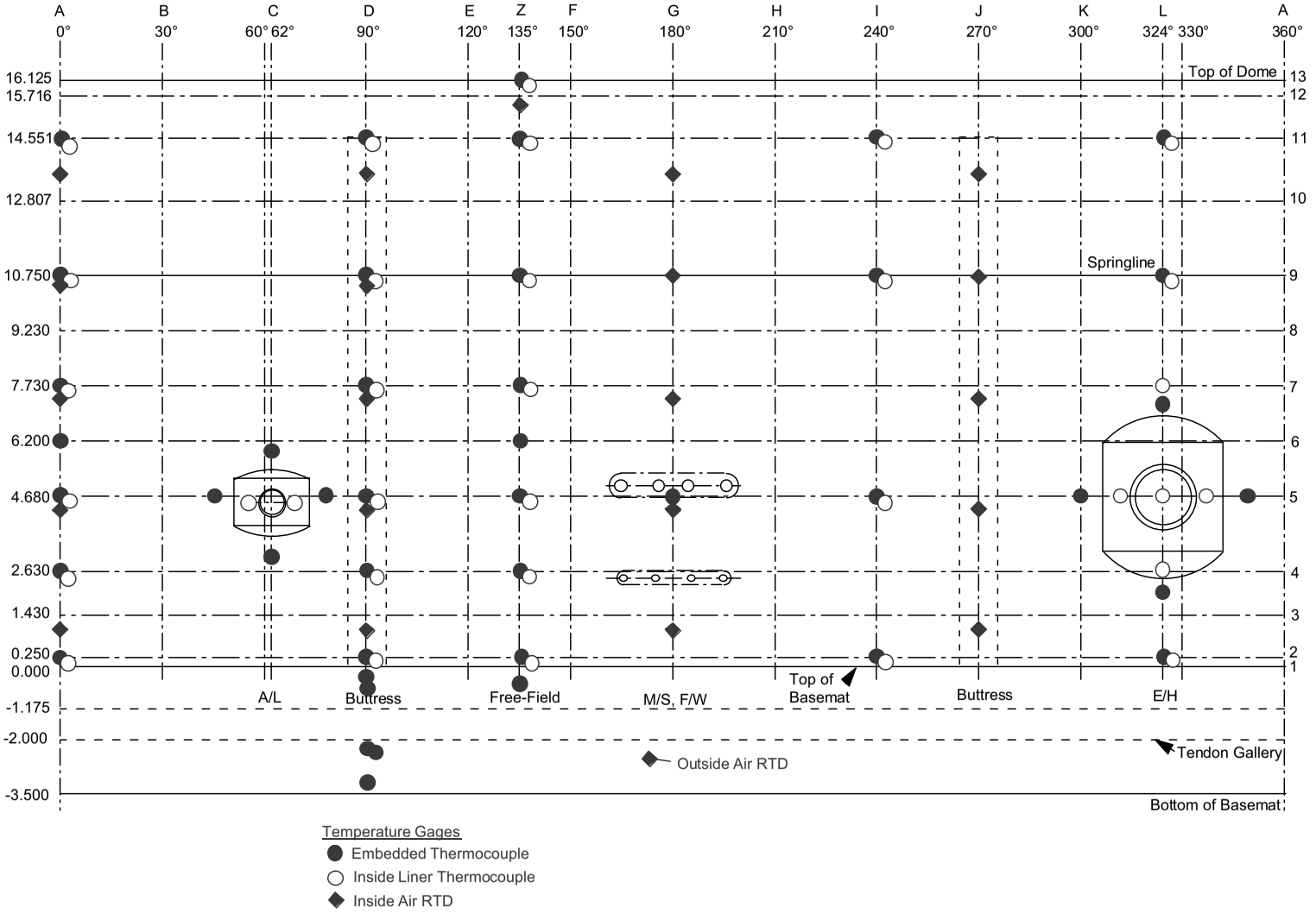

Figure 2.12 Temperature Instrumentation Locations

This page intentionally left blank

3. PCCV TESTING

For the test program, it was necessary to decide whether both thermal and pressure loads would be applied to the model, either separately or simultaneously, what the pressurization medium should be, and whether the transient characteristics of these loads should be considered. Programmatically, the decision to perform a **static, pneumatic** overpressurization test at **ambient temperature** was dictated by risk and cost considerations and previous experience.+

It should be noted that the **pneumatic** Limit State Test was the final test in the original program plan. This test was terminated following a functional failure, i.e. a leak, in the PCCV model, with only limited structural damage occurring. Subsequently, it was decided to re-pressurize the PCCV model, prior to demolition, in an attempt to observe larger inelastic response and, possibly, a global structural failure. This test was a combined **pneumatic-hydrostatic** test, where the PCCV model was sealed inside with an elastomeric membrane and filled nearly full with water, to reduce the volume of gas to be pressurized, and nitrogen gas was used to generate the overpressure.

The effect of elevated temperatures will be considered in Phase 3 of the ISP.

3.1 Test Planning

The basic objectives of the PCCV test were specified by NUPEC in the Master Project Plan. The stated objective of this plan was to… "investigate the ultimate behavior of PCCV under pressure beyond the design basis accident and to prove the pressure retaining capacity of PCCV". After extensive discussions between NUPEC, the NRC and SNL, a series of three tests were agreed upon. These tests are defined as follows and are illustrated in Figure 3.1.

- A leak check and System Functionality Test (SFT) @ 0.5 Pd (2.0 kgf/cm2 or 28.4 psig)
- A Structural Integrity Test (SIT) @1.125 Pd followed by an Integrated Leak Rate Test (ILRT) @ 0.9 Pd
- A Limit State Test (LST) to the static pressure capacity of the PCCV model (or the pressurization system, whichever comes first)

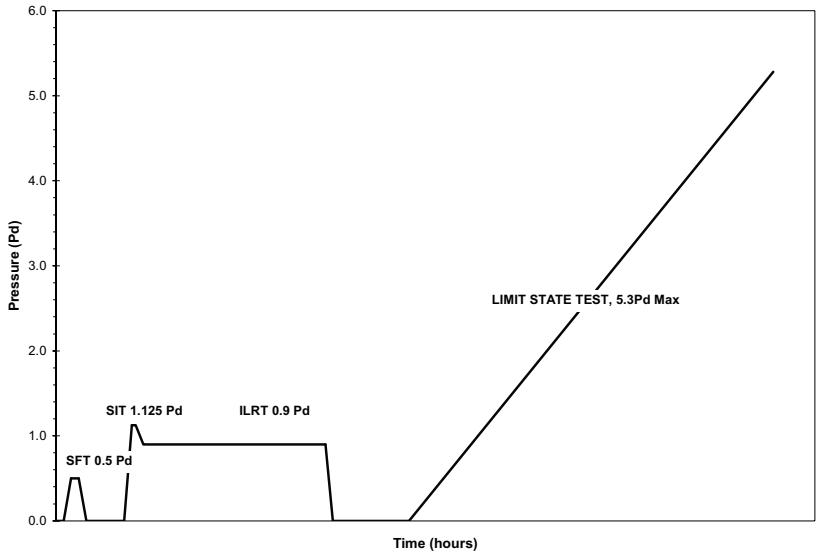

Figure 3.1 Pressurization Plan

A fourth test was added to the test program after the conclusion of the LST. After careful evaluation of the LST results, NUPEC, the NRC, SNL and their technical advisors concluded that all of the objectives of the test program were not fully met. SNL was tasked with designing and conducting a test which would allow the PCCV model to be pressurized beyond the level reached during the LST in an attempt to observe greater inelastic response of the model and, hopefully, generate a structural failure mode. This Structural Failure Mode Test (SFMT) is described in Section 3.2.2.

3.2 Test Operations

For purposes of ISP48, only the Limit State Test and, secondarily, the Structural Failure Mode Test are of interest. Details and results of the low pressure tests are provided in the test report [1].

3.2.1 Limit State Test

The Limit State Test (LST) was designed to fulfill the primary objectives of the PCCV test program, i.e. to investigate the response of representative models of nuclear containment structures to pressure loading beyond the design basis accident and to compare analytical predictions to measured behavior. The LST was conducted after the SIT and ILRT were completed and the data from these tests evaluated. The PCCV model was depressurized between the SIT/ILRT and the LST. The LST began at 10:00 AM, Tuesday, September, 26, 2000 and continued, without depressurization, until the test was terminated just before 5:00 PM on Wednesday, September 27.

The pressure and average temperature time histories during the LST, including depressurization, are plotted in Figure 3.2. The LST followed the planned pressurization sequence up to the point where the model began leaking.

Initially, the model pressurization sequence matched the pressurization steps followed for the SIT to allow for comparison of the model response to two identical cycles of loading. Pressurization continued in increments of approximately 0.2Pd until a pressure of 1.5 Pd (6.0 kgf/cm2 or 85.3 psig) was reached at approximately 4:30 PM. At this pressure, the first planned leak check was conducted by isolating the model and monitoring the temperature and pressure. After approximately 3 hours, a leak rate of 0.48% mass/day was calculated. Considering previous experience from the ILRT, which demonstrated that thermal expansion of the model during the day yielded apparent leak rates in this range, the results were interpreted to indicate that the PCCV model was leak-tight.

Pressurization of the model continued in increments of approximately 0.1Pd until a pressure of 2.0Pd (8.0 kgf/cm2 or 113.8 psig) was reached at approximately 11:00 PM. At this pressure the model was again isolated to perform a planned leak check. This leak check was also planned to be held for 8 hours to allow the test team to partially stand down for a rest period. A ‘skeleton crew’ consisting of the Test Conductor (TC), Data Acquisition System Operator (DO) and Nitrogen Supply Operator (NO) continued to monitor the response of the model and all other systems until approximately 7:00 AM on September 27. This pressure hold and leak check was also selected below the lower bound prediction for the onset of structural yielding (i.e. yielding of the rebar or tendons) to ensure that the model would remain relatively stable during this period. After approximately 8 hours, the calculated leak rate was 0.003%, i.e. essentially zero. This confirmed the interpretation of the leak check results at 1.5 Pd and also demonstrated the greater accuracy of the leak rate results when the model is thermally stable.

Pressurization of the model resumed at 7:00 AM in increments of 0.1Pd, with increasing dwell time between pressure steps, ~30 minutes, required to meet the gage stability criteria. As the pressure was increased to the next planned leak check at 2.5Pd, liner strain gages in the vicinity of the E/H (LSI-C-K5-12) began registering rapidly increasing strains in excess of 1%. At 2.4Pd, the acoustic system operator (AO) reported hearing a change in the acoustic output which might indicate that “something had happened”. At approximately 10:00 AM at a pressure of 2.5Pd (10.0 kgf/cm2 or 142.2 psig), the model was isolated for the third planned leak check. After approximately 1-1/2 hours, a fairly stable

leak rate of 1.628% mass per day was calculated. The leak rate calculations at 1.5, 2.0 and 2.5Pd are plotted in Figure 3.3. Coupled with the confirmation from the AO that the acoustic data continued to confirm that some new event had occurred, it became clear that the model was leaking, most likely from a tear in the liner in the vicinity of the E/H. Plots of the output of the four internal acoustic sensors surrounding the E/H at 2.3, 2.4 and 2.5 Pd are shown in Figure 3.4.

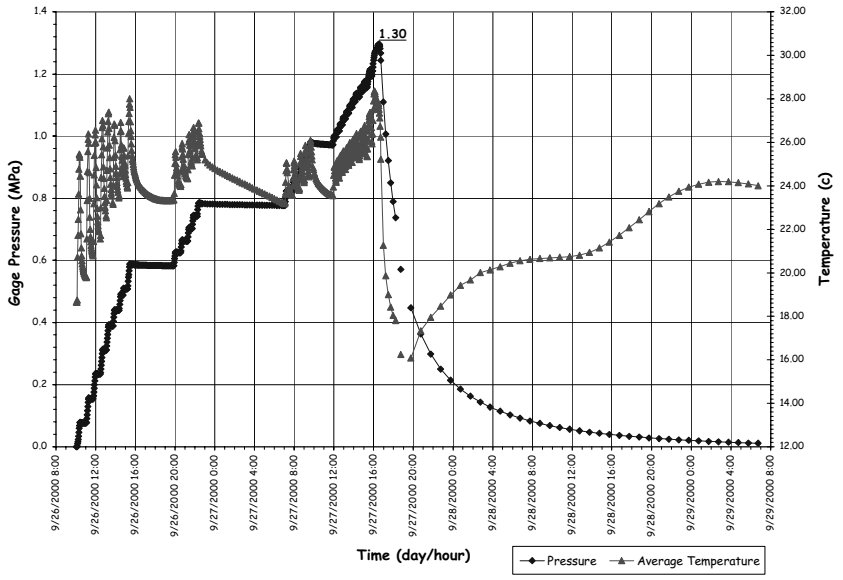

Figure 3.2 Limit State Test Pressure and Average Temperature

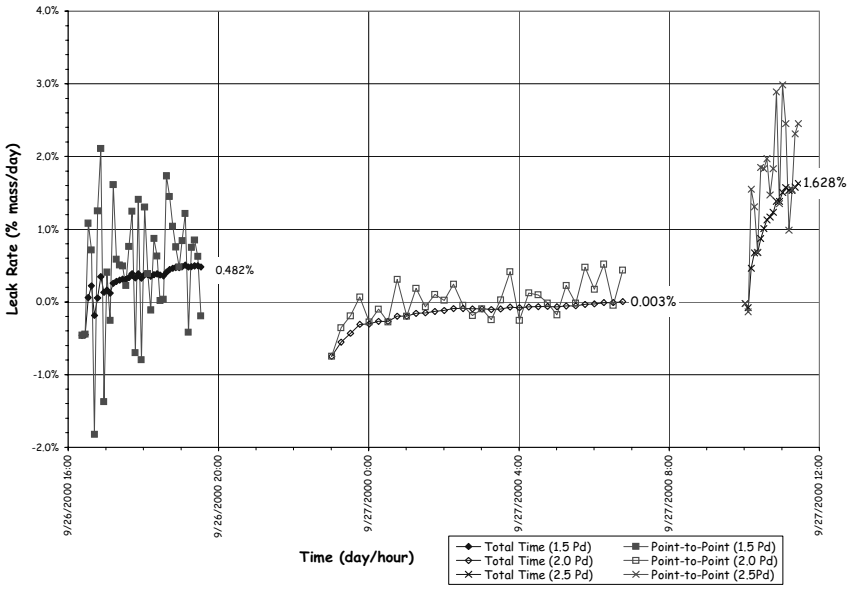

Figure 3.3 LST Calculated Leak Rates at 1.5, 2.0 and 2.5 Pd

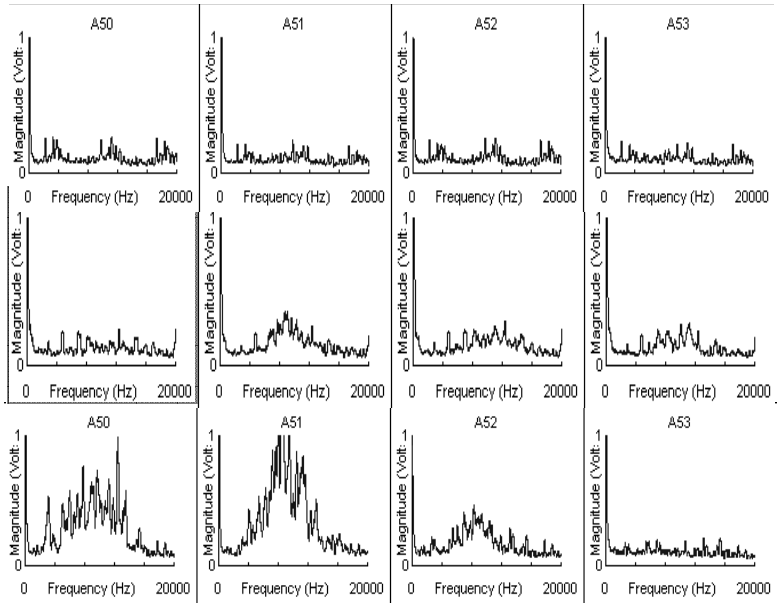

Figure 3.4 Internal Acoustic Sensor Signals @ the Equipment Hatch

After consulting with NUPEC and the NRC, the Test Conductor concluded that the model had functionally failed between 2.4 and 2.5 Pd and directed a change in the pressurization plan. Since the model was leaking, the next goal was to pressurize the model as high as possible to collect data on the inelastic response of the structure and to observe, if possible, a structural failure mode. Pressurization continued in increments of 0.05 Pd, as planned, however, the gage stability criterion was abandoned and the hold time at each pressure step was reduced to less than 10 minutes.

The PCCV model was pressurized to approximately 3.0Pd with increasing evidence of leakage and increasing liner strains. At 3.0Pd it became increasingly difficult to pressurize the model, and the nitrogen flow rate was increased to 99 std.m3/min (3500 scfm). At this flow rate, the pressure in the model was increase to 3.1Pd, however the pressure dropped steadily after reaching this pressure. The leak rate at this point was estimated to be 100% mass/day

The nitrogen flow rate was increased to the maximum capacity of the pressurization system, 142 std.m3/min (5000 scfm), and the pressure was increased to slightly over 3.3 Pd before the leak rate exceeded the capacity of the pressurization system. The pressure time history and flow rates during the final phase of the test are shown in Figures 3.5 and 3.6. Since it was no longer possible to increase the pressure in the model and the supply of nitrogen was nearly exhausted, the TC made the decision to begin terminating the test.

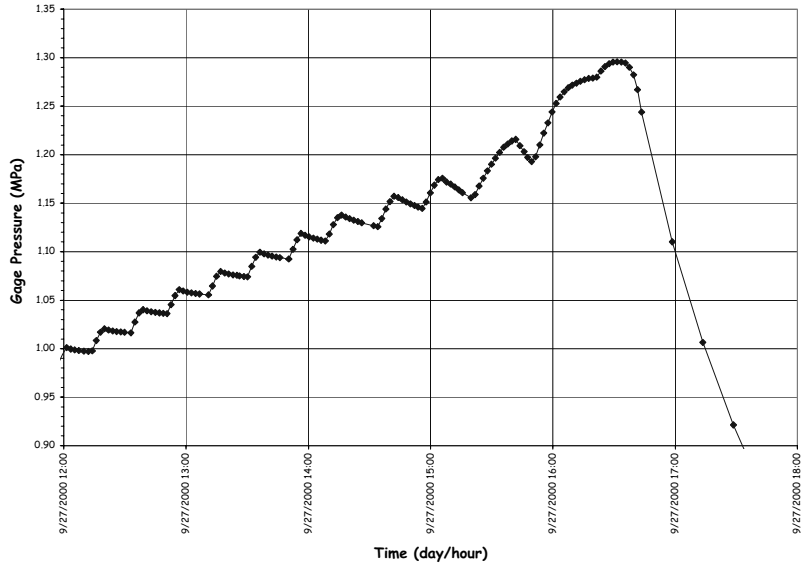

Figure 3.5 LST Pressure Time History, 2.5 to 3.3 Pd

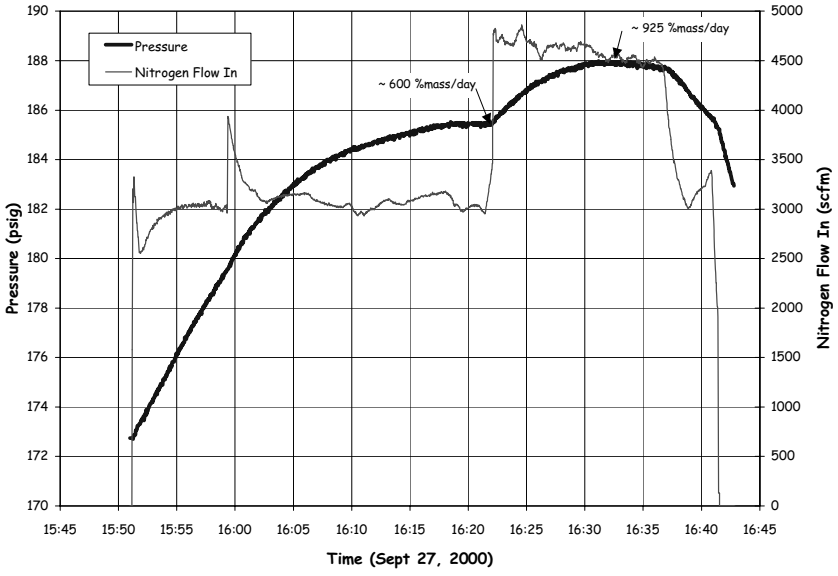

Figure 3.6 LST Pressure and Flow Rates @ Maximum Pressure

The isolation valve was closed and the model was allowed to depressurize on its own. The terminal leak rate was estimated to be on the order of 900% mass/day. (The maximum flow rate of nitrogen, 5000 scfm, is equivalent to a leak rate of 1000% mass/day.) Estimated leak rates during the final pressurization and depressurization phases are shown in Figures 3.7 and 3.8.

After the model pressure was reduced to 1.0 Pd, test personnel were able to enter the test site to inspect the model close-up. Nitrogen gas was observed (heard and felt) escaping through many small cracks in the concrete, around the penetration sleeves and at the tendon anchors. It was speculated that the liner acted as a leak chase, allowing nitrogen gas escaping through a tear or tears in the liner to travel between the liner and the concrete until it found an exit path through a crack in the concrete or a conduit in the tendon duct.

At maximum pressure, local liner strains of up to 6.5% were recorded and global hoop strains (computed from the radial displacement) at the mid-height of the cylinder averaged 0.4%. While large liner strains were observed and it was suspected that the liner might have torn in several locations, the remainder of the structure appeared to have suffered very little damage with the exception of more extensive concrete cracking at some locations. The largest crack was observed to the left of the E/H, shown in Figure 3.9.

After the model had completely depressurized, the model was purged with fresh air, the E/H was removed and detailed posttest inspection of the inside of the model began. A cursory inspection of the model identified 26 discrete tears at 18 separate locations.

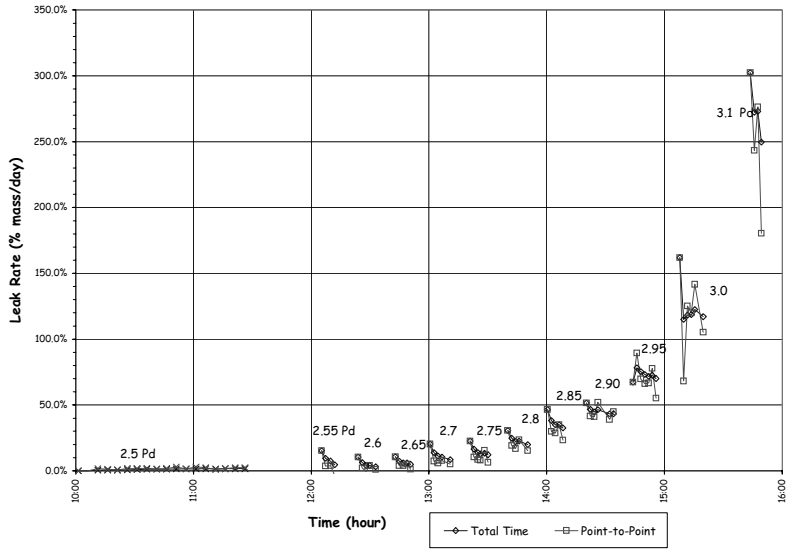

Figure 3.7 LST - Estimated Leak Rates (2.5-3.1 Pd)

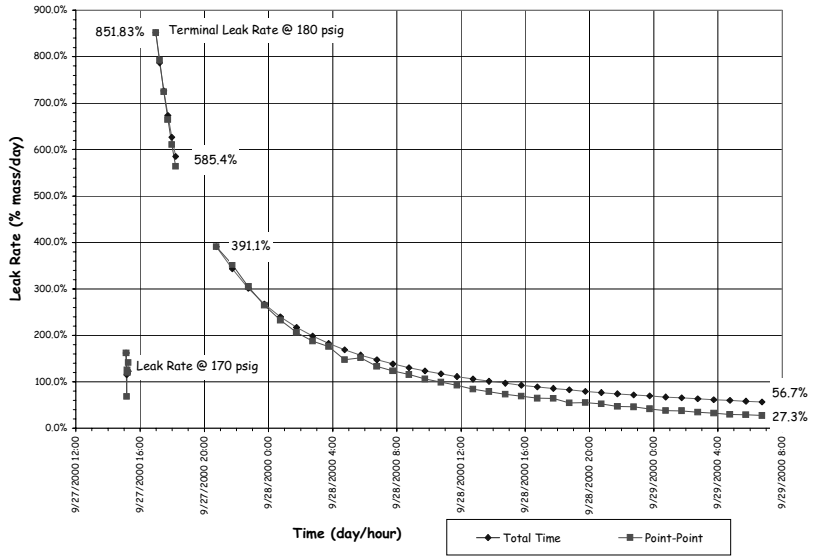

Figure 3.8 LST Estimated Terminal Leak Rates

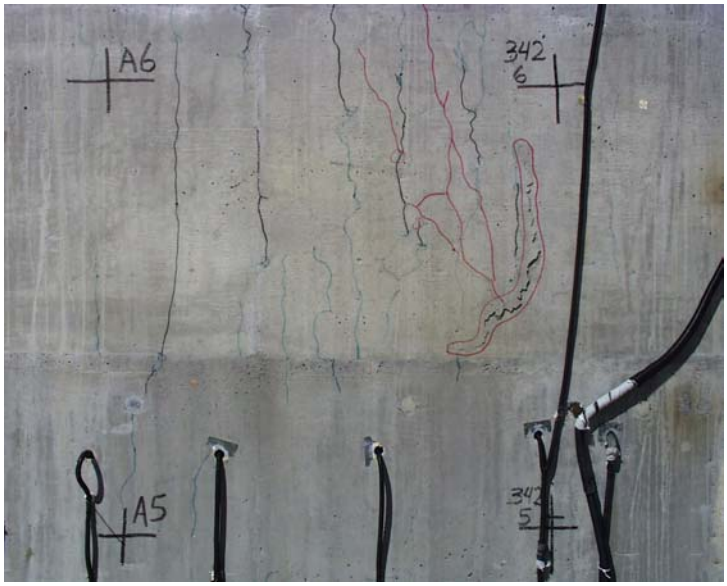

Figure 3.9 Post-LST Cracks @ Az. 350º, El 4680 to 6200 (Grid 45)

3.2.2 Structural Failure Mode Test

Almost immediately after the completion of the LST, there was a recognition that while the PCCV model had demonstrated its capacity to resist pressures well above the design pressure and confirmed, arguably, liner tearing and leaking as the functional failure mode. The test objectives were not, however, fully met with respect to observing large inelastic deformations, for comparison with analyses, and witnessing the structural failure mode of the PCCV model. SNL was tasked by NUPEC and the NRC with investigating the possibility of conducting a second limit state test.

Two issues needed to first be addressed to determine the technical feasibility of reloading the PCCV model. First was the question of whether the LST had caused sufficient damage to the structure such that any data obtained by reloading the structure would be compromised and of limited value for comparison with analytical results. The LST data was thoroughly reviewed and, with the exception of the liner and cracking of the concrete, there was no evidence of excessive structural damage. There was also no indication that the tendons had been strained beyond their yield limit and, except for a few isolated measurements, the same was true for the rebar. (Only 27 of the rebar gages registered strains in excess of 0.4%, with a maximum of 1.7%-which likely reflects the local perturbation caused by the presence of the gage.) Considering the radial displacement at the mid-height of the cylinder, compared to the pretest Round Robin predictions in Figure 3.10, clearly illustrates that the structure was on the verge of global yielding but had not undergone a significant amount of inelastic deformation. (In this context, only the yielding of the steel and rebar is being addressed. Obviously, the loss in stiffness that occurs with global concrete cracking at approximately 1.5Pd, cannot be recovered.) This was a positive finding for the prospect of reloading the model since most, if not all, of the capacity of the rebar and tendons was still available. Another important conclusion from the consideration of the LST data was that, if in fact, the model was on the verge of global structural yielding, the additional pressure required to cause larger inelastic deformations was not very large, perhaps only on the order of a few tenths to half the design pressure, i.e. an additional 1.0 to 2.0 kgf/cm2 (14 to 30 psig).

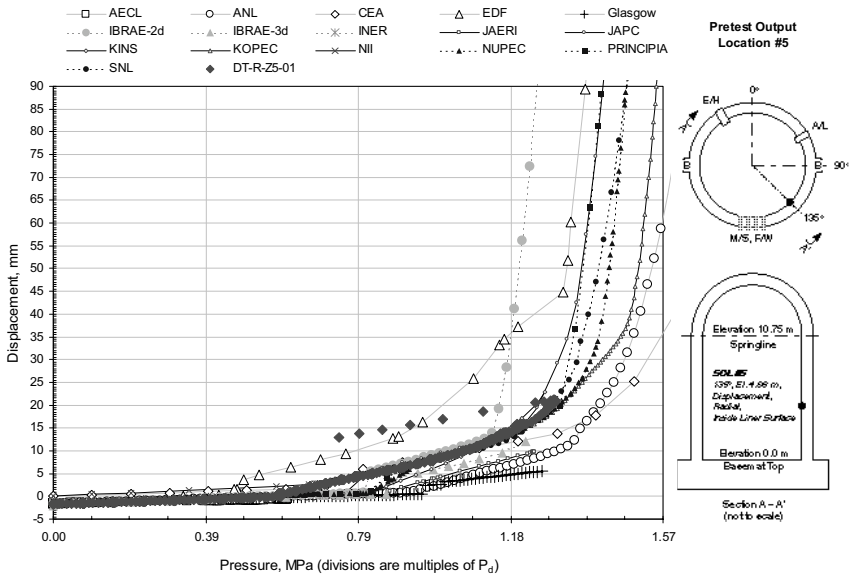

Figure 3.10 LST Radial Displacement @ Az. 135º, El. 4680

The second issue was the requirement to re-seal the model in order to re-pressurize it. Since large sections of the liner were removed as part of the post-LST inspection, the liner was no longer capable of providing an effective membrane to prevent premature leakage. Furthermore, even if the liner tears and cutouts were locally repaired or sealed, it was clear that other areas of the liner were susceptible to tearing at the same pressures (or perhaps even at lower pressures) which caused the liner to tear during the LST. It was necessary, therefore, to devise a cost-effective method of completely replacing the liner function in order to proceed with plans to re-pressurize the PCCV. The replacement 'liner' was also required to ensure that the model could be re-pressurized to a level beyond the maximum pressure achieved during the LST. (A corollary of this conclusion was that there was no further need to investigate the response of the liner and the instrumentation applied to the liner could be abandoned.)

Furthermore, the SFMT had to be completed within the current program budget and schedule for completing the project. The concept that was developed to re-pressurize the PCCV model is illustrated in Figure 3.11.

The concept consists of sealing the interior surface of the liner with an elastomeric membrane after removing all interior transducers on the liner. After closing the E/H and A/L, the model would be filled with water to 1.5m (5 ft.) from the dome apex, approximately 97% of the interior volume 1,591,000 ltr (350,000 gal). Filling the model with water would provide several advantages:

- The leak rate of water through any tears in the liner is much less than the corresponding leak rate of gas. Therefore, even if a leak path developed, the flow rate capacity of the pressurization system should be adequate to compensate for the leak.
- By maintaining a gas pocket in the model, the pressurization system used for the LST, using nitrogen gas as the pressurization medium, could be used for the SFMT without any major modifications. The only modification required was the installation of additional piping inside the model to allow the gas to be introduced at the dome apex and a pipe to fill (and drain, if necessary) the model. Reducing the volume of gas to be pressurized reduced the demand on the pressurization system in the event of a leak and also reduced the volume of gas required to conduct the test. In the case of the SFMT, a pressurized tube trailer could be used instead of the more expensive liquid nitrogen source required for the LST.

- Since the pressurization system could compensate for small leaks, it was not essential that the elastomeric liner be completely leak tight, only that the leaks were small enough to allow the model to be pressurized to the desired level.
- Leaks of water would be readily visible compared to gas leaks.
- In the event of a catastrophic rupture of the PCCV model, the energy stored in the model nearly filled with water was much less than the stored energy if pressurized to the same level with only gas. As a result, the safety exclusion zone around the model could be reduced if necessary.

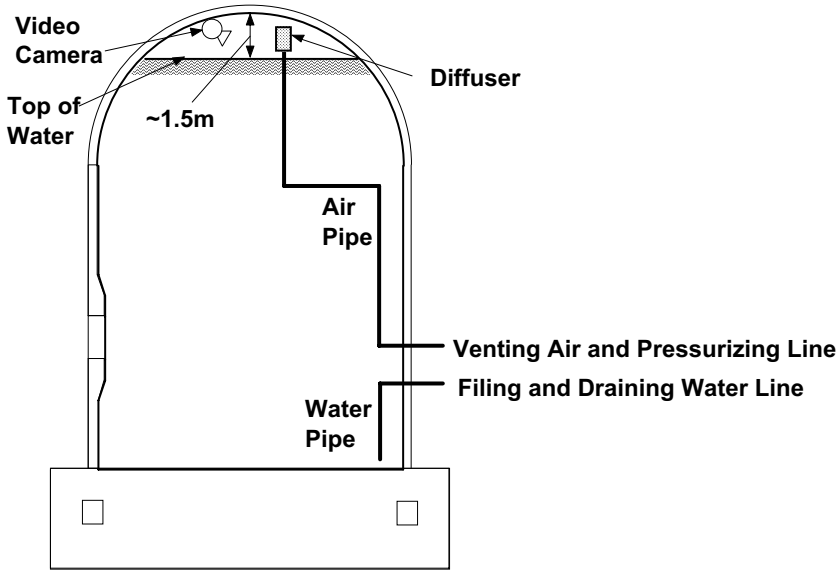

Figure 3.11 PCCV Structural Failure Mode Test Concept

At the same time, filling the model with water had some disadvantages:

- Any instruments or other electrically powered components (lights, cameras, etc.) inside the model had to be removed or completely sealed.
- The internal pressure would not be uniform due to the hydrostatic head, approximately 1.4 kgf/cm2 (20 psig).

These disadvantages, however, were not deemed to be significant, and efforts were then focused on selection of a suitable liner. A number of vendors were contacted and two proposals for sealing the liner were considered. One proposal was to prefabricate a 5 mm (200 mil) PVC sheet liner which would be installed inside the model by heat welding the seams and sealing around the penetrations using ring clamps. The second proposal was to apply a sprayed-on two-part polyurea coating, also a minimum of 5 mm (200 mil) thick. After considering both proposals, the sprayed-on lining was selected since it could be more readily adapted to the irregular liner surface and had significant cost and schedule advantages. The elastomeric liner was installed by Ershigs Corporation in August, 2001 after the interior model inspection was completed and all the surface instrumentation was removed.

After the elastomeric liner was installed the interior instrumentation for the SFMT was installed. A reduced set of instruments was selected to allow one data acquisition computer to scan all the gages in less than 60 seconds to support 'rapid' pressurization of the model. The instrumentation suite for the SFMT consisted of the following:

- All interior gages used for the LST were removed or abandoned. These were replaced by 20 water proof displacement transducers (LVDTs), 17 radial and 3 vertical, located as shown in Figure 3.12.
- Five interior pressure transducers, three below water at the base, cylinder mid-height and springline, two to measure the gas pressure.
- Two interior video cameras and lights to monitor the E/H and the water surface
- 18 Exterior Liner Strain Gages:
    - 14 @ Meridional @ Wall-Base junction
    - 4 @ Hoop stiffener details
- 82 Rebar Strain Gages (Standard Output Locations):
    - 35 rebar gages (all 22 SOL plus 13 meridional at Wall-Base)
    - 47 Gage bars (all surviving)
- All surviving Tendon strain gages and all Load Cells
- Soundprint® acoustic monitoring (external sensors only)
- Concrete Strain (6 SOFO gages)
- Four external digital video cameras at 0º, 90º, 270º and 360º, completely covering the PCCV cylinder wall.

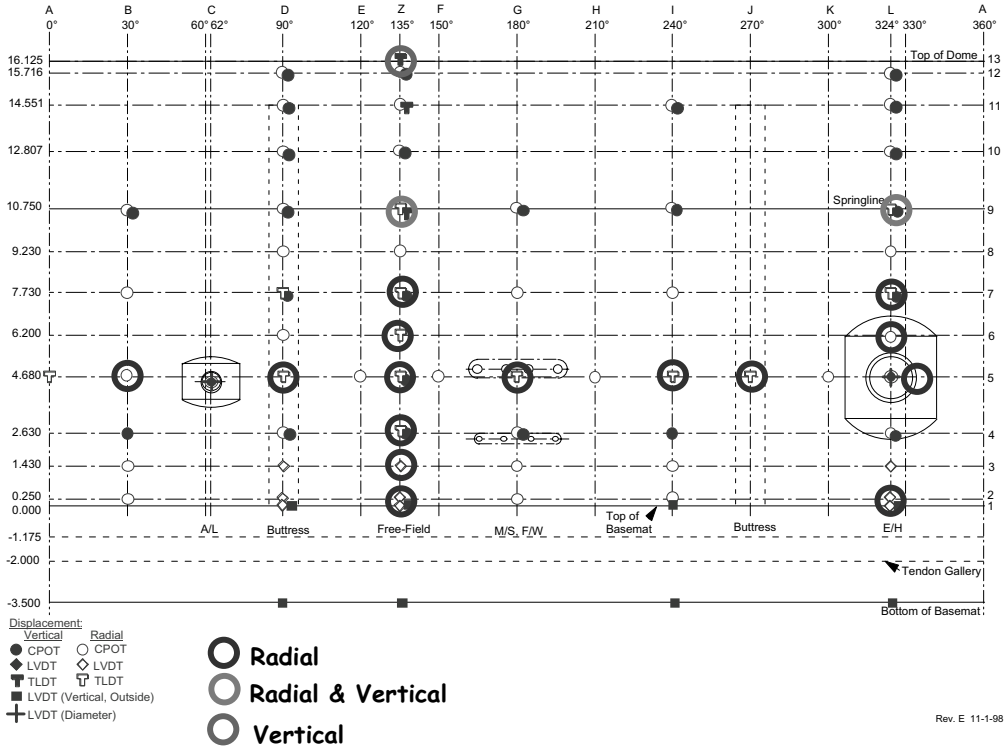

Figure 3.12 SFMT Displacement Transducer Layout

After completing the installation and completing all test-readiness checks, the equipment hatch cover was installed and after sealing the airlock, a low pressure pneumatic test was conducted to check for leaks on October 3, 2001. The leak test began at approximately 09:30 and a leak was detected (via the

acoustic system) at approximately 0.2 Pd (~12 psig). Pressure was increased to the target pressure of 0.5Pd (30 psig) at which time the vessel was isolated and monitored for a 24 hour leak test. The acoustic system (multiple sensors) continued to output signals consistent with a leak in the model and several potential leak locations were identified.

Once it was determined that the model was stable, the nitrogen supply was isolated and close inspection of the model was conducted. Through a combination of visual/auditory inspection, hand-held acoustic monitoring and application of soap-water solution, a number of locations where nitrogen gas was leaking from the model were discovered:

- The largest apparent leak was from a crack on the left-hand side of the 90-degree buttress at an elevation of approximately 6 meters (20 ft.) above the top of the basemat (Level 6 in our cardinal coordinate system). This leak was the first detected by the acoustic system and was immediately confirmed during the close-up inspection
- Secondary leaks, identified by the acoustic system, were confirmed at 150-degrees/3 and 6 meters (10 and 20 ft) and 210-degrees/4.5 meters (15 ft). These leaks appeared to be through previously existing cracks in the concrete. The leak at 150-degrees was along the horizontal construction joints between C1, C2 and C3 as well as along a vertical crack extending between C2 and C3. The leak at 210-dergrees also appeared to be through a previous crack.
- The acoustic system also suggested leaks at 300-degrees/1 to 2 meters (3 to 6-1/2 ft) and 360-degrees/0 meters, but close-up examination could not confirm leakage at either of these locations.
- During the close-up inspection, we also detected a leak at 30-degrees/5 meters (16 ft) which was not initially identified by the acoustic system.
- Close-up inspection of the penetrations also revealed leakage at the feedwater penetrations. There was no evidence of leakage at the E/H, A/L or M/S penetrations.

These results indicated that, in spite of the manufacturer's quality control procedures coupled with detailed visual inspection (individual locations which appeared suspect were also sealed with RTV prior to closing the model), the sprayed-on liner was not impermeable and once the gas escaped through the sprayed-on and steel liners, it migrated between the steel and concrete until it was able to find an exit path. It did not appear that the pressure was high enough to tear the sprayed-on liner when a leak was first detected.

The calculated leak rate was initially 70% mass/day at the maximum pressure of 2.1 kgf/cm2 (30 psi) decaying to 45% at 0.77 kgf/cm2 (11 psi) over 24 hours. The sound levels as detected by the SoundPrint system, which are roughly proportional to the rate of gas escaping, indicated a stable leak rate which was, to a large extent, independent of the pressure.

Based on these results, it was concluded that the leak was most likely due to a pre-existing hole(s) in the sprayed on liner which did not increase (or decrease) significantly during pressurization or during the leak test. (The equivalent orifice size reduced from about 6mm (0.25") at 2.1 kgf/cm2 (30 psi) to 5mm (0.20") at 0.8 kgf/cm2 (12 psi), based on the calculated leak rates.) As a result, it was decided that the SFMT could be conducted without repairing the sprayed-on liner and still have a reasonable chance that the leak would not grow significantly and overwhelm the capacity of the pressurization system. (Nevertheless, during an un-scheduled one-month postponement of the SFMT, the surface was re-tested with a ‘spark-tester’ and a few small holes were discovered and sealed with RTV. The model was then resealed and readied for filling with water.)

Filling of the PCCV with water and the SFMT began at approximately 09:00 November 6, after the initial data scan was taken, and continued until November 8, 2001. Slow leaks of water were initially observed late November 6, after the model was about one-fourth full, however, the amount of water

leaking was not significant. The pressure time histories at various elevations in the model from the start of filling up to the SFMT are shown in Figure 3.13. This figure illustrates the hydrostatic head and also reflects the slight loss of water due to leaks. The water level was 'topped off' on November 12, prior to the start of the SFMT.

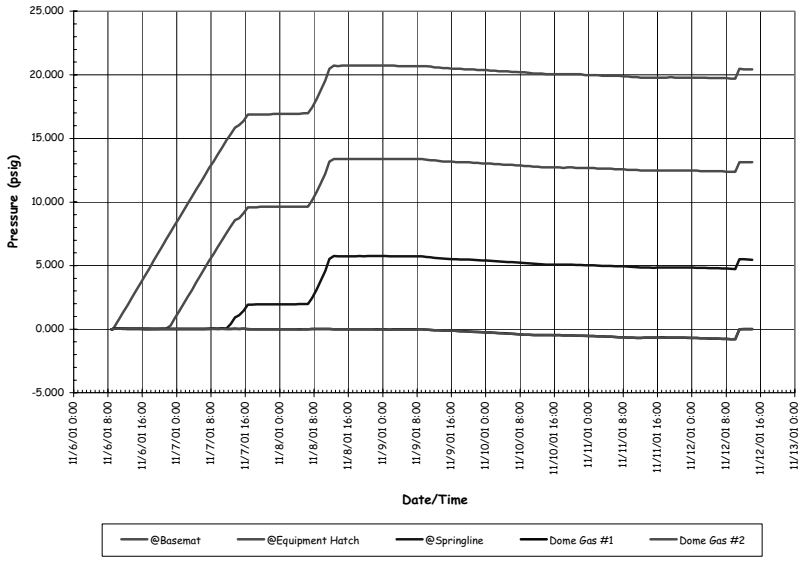

Figure 3.13 Pre-SFMT Hydrostatic Pressures

The test sequence planned for the SFMT was to 'rapidly' pressurize the model using nitrogen gas to compensate for the known leaks in the model. The minimum flow rate capacity of pressurization system, 14 std.m3/min (500 scfm), would increase pressure in the reduced void space at a rate of about 0.35 kgf/cm2 (5 psi) every minute. At this rate, the model could be pressurized to failure in less than an hour.

The SFMT began shortly after 10:00 AM on Wednesday, November 14, 2001. The pressure time histories are shown in Figure 3.14. The pressure time history of all 5 gages is shown along with the effective model pressure, which is calculated as a volume-weighted average. Any references to the SFMT pressures are to the effective pressure, unless noted otherwise.

The model was continuously pressurized at a rate of approximately 0.35 kgf/cm2 (5psi)/min. All active sensors were continuously scanned at intervals of approximately 30 seconds and the video cameras were continuously recording the response of the model. As the pressure was increased, evidence of leakage was visible as increasing wetting of the concrete surface. At 10:38 AM, the effective pressure in the model equaled the peak pressure achieved during the LST, 3.3 Pd (1.29 MPa or 188 psig). At approximately 10:39 AM, the acoustic system recorded a very high noise level event which was interpreted as the breaking of a tendon wire. At this point in the test, events occurred very quickly. Shortly after detecting the wire break, a small spray of water was observed at approximately 0º azimuth and additional tendon wire breaks were detected by the acoustic system with increasing frequency. The wire break events are plotted in Figure 3.15, along with the effective pressure and the radial displacement at Az. L (324º), Elevation 6 (6280), as a function of time.

The rate of pressurization was decreasing and the nitrogen flow rate was increased to maintain the pressurization rate. The gas pressure and flow rates are shown in Figure 3.16. The water surface inside the model, viewed through the internal video camera, was observed to be dropping slowly, but it was unclear if this was due to leakage or radial expansion of the vessel.

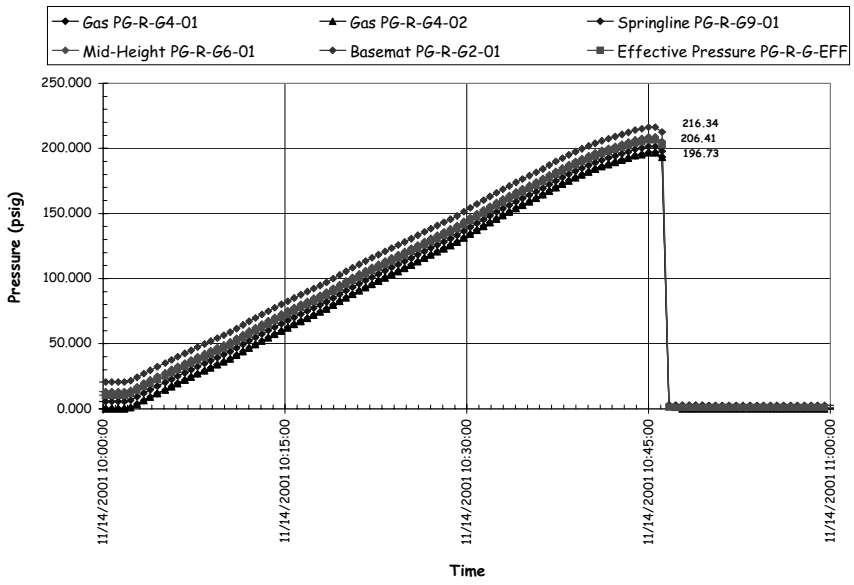

Figure 3.14 SFMT Pressure Time Histories

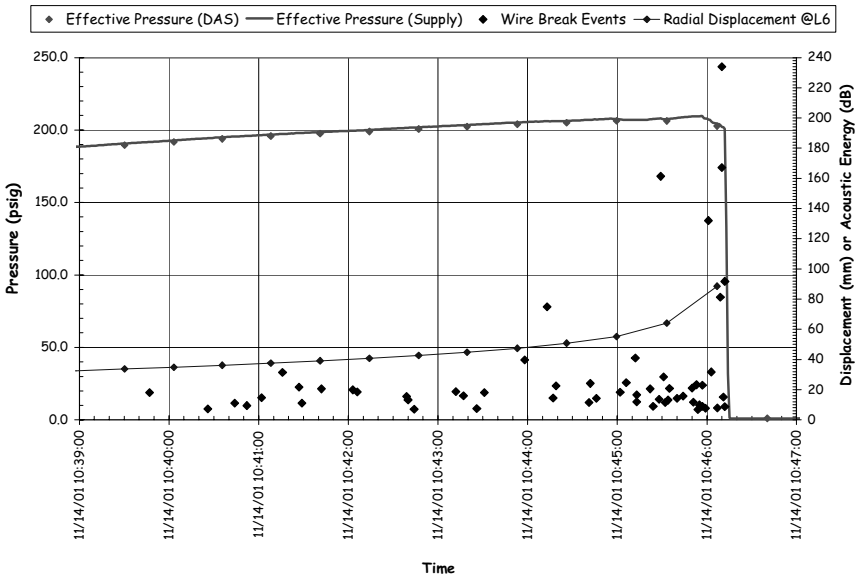

Figure 3.15 SFMT Wire Break Events vs. Pressure vs. Displacement

Pressurization of the model continued until a second spray of water was observed and then, suddenly, at 10:46:12.3, at an effective pressure of 3.63 Pd (1.42 MPa or 206.4 psig) the PCCV model ruptured violently at ~6º azimuth near the mid-height of the cylinder. The rupture propagated vertically in both directions and then radiated circumferentially about 2 meters above the top of the basemat, shearing off the cylinder wall. The dome and cylinder wall then came to rest on the instrumentation frame which appears to have prevented the model from toppling over. The entire collapse was over in slightly more than one second. The entire SFMT, including the sequence of rupture and collapse was recorded by the digital video cameras. A short movie (.mpg) file showing the rupture of the model is included on the data CD enclosed. The moment of rupture is shown from all four angles in Figure 3.17. The video recorded failure of the tendons including ejection of tendon anchors. The condition of the model after the SFMT is shown in Figure 3.18.

Because of program schedule constraints, demolition of the PCCV model commenced in December, 2001 and was completed in April 2002. During this period, attempts were made to further inspect the model and characterize the damage caused by the SFMT, however, these efforts were of limited value due to the difficulty of discriminating the damage caused during the SFMT from the demolition process. A few specimens from the model were retrieved, however, more for sentimental value than for providing any further technical insight into the behavior of the model.

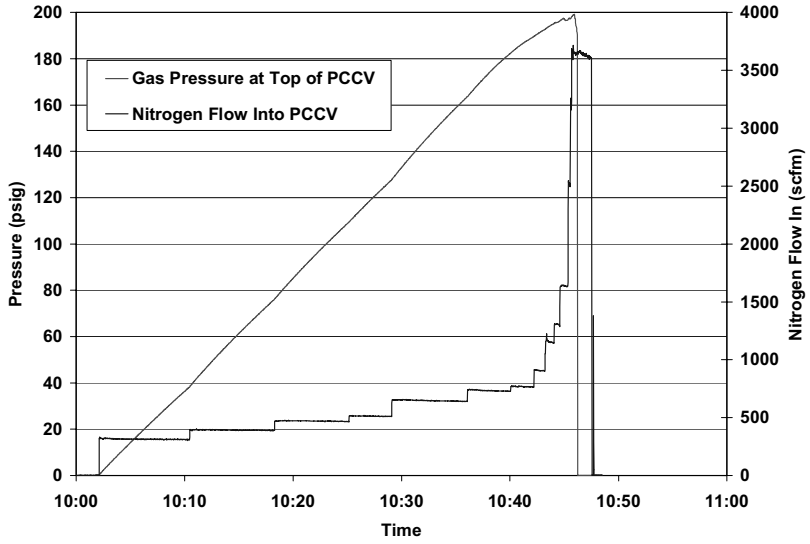

Figure 3.16 SFMT Pressurization System Data

(a) 0º Azimuth

(b) 90º Azimuth

(a) 180º Azimuth

(b) 270º Azimuth

Figure 3.17 SFMT: Rupture of the PCCV Model

Figure 3.18 PCCV Model after the Structural Failure Mode Test

3.3 Test Results

The response of the model was continuously recorded beginning March 3, 2000, prior to prestressing, through October 11, 2000, following the LST. Additional data was recorded, using a modified instrumentation suite, from November 6 to 14, 2001 for the SFMT. A detailed description of the data file structure and the data were provided in the test report [1].

The basic data was recorded for each instrument at discrete time steps. This basic data is referred to as the DYNAMIC data. It should be noted that the time reported in the data files is the DAS clock time at the start of a data scan. Since it took up to two minutes to complete a data scan (one minute for the SFMT), the actual time the data was recorded may be up to two minutes later than the recorded time. For pseudo-static loading, this is not a significant issue, but it may have some effect on the response recorded near the end of the LST and SFMT.

The Data of Record (DOR) is a subset of the dynamic data. The concept of the DOR was defined to facilitate comparison of the data with analysis results. Typically, the analysis results are described as a function of pressure. The DOR is intended to provide a single, stable response value at each pressure step. The DOR were recorded separately from the dynamic data when the gage stability criteria was met or at the direction of the test conductor.

The concept of DYNAMIC and DOR data is illustrated in Figure 3.19. In this figure the DYNAMIC data during and after the LST is plotted along with the DOR for the radial displacement at the cylinder mid-height at 135º. At lower pressures, the data are essentially identical, however at higher pressures

the drift due to model creep and/or leakage is apparent. Furthermore, the DOR data set does not capture the maximum pressure. In subsequent discussions of the DOR, the response at the maximum pressure from the DYNAMIC data has been appended to the DOR for completeness

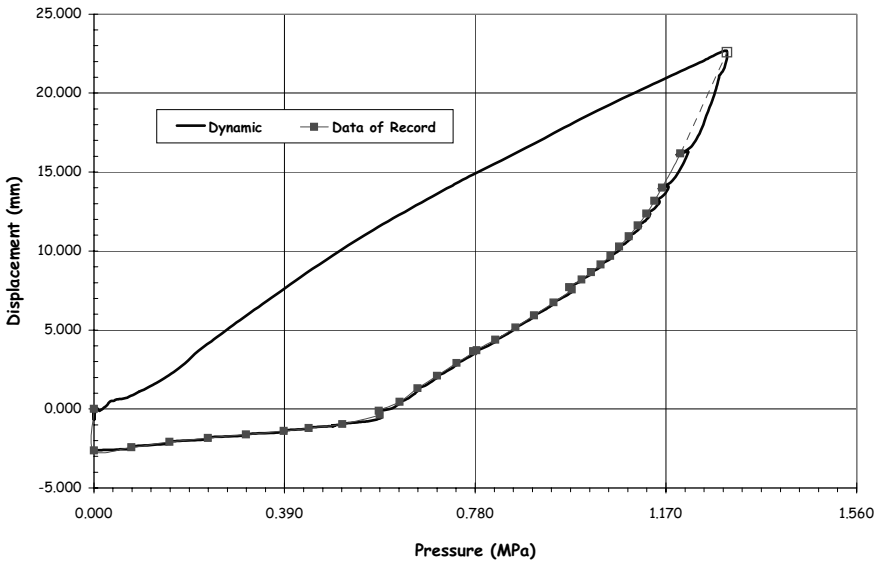

Figure 3.19 Radial Displacement @ AZ 135º, El. 6200

4. PHASE 2 CALCULATIONS

Each ISP participant was asked to provide a report summarizing their analysis approach and results. Each individual report is reproduced in Appendices C through L.

Fifty-five standard output locations, listed in Table 4.1, were selected to facilitate initial comparison of the Phase 2 calculations with the test results. The selection of these locations was based on the containment experience of the project team at Sandia and the results of preliminary analyses to characterize model responses and identify possible failure modes. The general locations are illustrated in Figure 4.1. This is the same set of variables used for the pretest Round Robin comparison. A gage, or set of gages, was installed at every standard output location for the LST. Due to the practical limitations, the model response was not measured at all these locations during the SFMT. The participants were asked to provide analysis results as a function of gage pressure at these locations. A summary of the results provided by each of the participants is given in Table 4.2. The calculated results were collected into composite plots for comparison with the LST and SFMT results at each SOL. These composite plots are provided in Appendix A.

To facilitate comparison of the calculated results with the pressure response of the model, most, if not all of the participants chose to 'initialize' their analysis results with the test data at the start of the LST. This was done to eliminate the variation in the calculation of the response due to dead load and prestressing as well as the effects of creep, shrinkage and changes in ambient conditions, which were not modeled. As a result, **most of the comparisons are for the change in the response variable due to pressure, not the total response**. Comparisons of analyses before initializing the response variables were much more inconsistent and a similar result would be expected for full-scale containments where the initial conditions might not be known.

In addition to submitting response predictions at the SOLs, each participant was also asked to provide a best estimate of failure pressure and mechanisms of the PCCV model. These are summarized in Table 4.3. Table 4.3 also summarizes predictions of the pressure for various milestones (onset of cracking, yielding, etc.) leading up to failure.

Table 4.1. Standard Output Locations for PCCV Round Robin Analysis

Loc. #	Type	Orientation	Az. (°)	El. (m)	Comments	General Location
1	Displacement	Vertical	135	0.00	Outside Cylinder	Top of Basemat
2	"	Radial	135	0.25	Inside Liner Surface	Base of Cylinder
3	"	Radial	135	1.43	"	"
4	"	Radial	135	2.63	"	"
5	"	Radial	135	4.68	"	E/H elev.
6	"	Radial	135	6.20	"	Approximate Midheight
7	"	Radial	135	10.75	"	Springline
8	"	Vertical	135	10.75	"	"
9	"	Horiz.(Rad)	135	14.55	"	Dome 45 deg
10	"	Vertical	135	14.55	"	"
11	"	Vertical	135	16.13	"	Dome apex
12	"	Radial	90	6.20	"	Midheight @ Buttress
13	"	Radial	90	10.75	"	Springline @ Buttress
14	"	Radial	324	4.675	"	Center of E/H
15	"	Radial	62	4.525	"	Center of A/L
16	Rebar Strain	Meridional	135	0.05	Inner Rebar Layer	Base of Cylinder
17	"	Meridional	135	0.05	Outer Rebar Layer	"
18	"	Meridional	135	0.25	Inner Rebar Layer	"
19	"	Meridional	135	0.25	Outer Rebar Layer	"
20	"	Meridional	135	1.43	Inner Rebar Layer	"
21	"	Meridional	135	1.43	Outer Rebar Layer	"
22	"	Hoop	135	6.20	Outer Rebar Layer	Midheight
23	"	Meridional	135	6.20	Outer Rebar Layer	"
24	"	Hoop	135	10.75	Outer Rebar Layer	Springline
25	"	Meridional	135	10.75	Inner Rebar Layer	"
26	"	Meridional	135	10.75	Outer Rebar Layer	"
27	"	Hoop	135	14.55	Outer Rebar Layer	Dome 45 deg
28	"	Meridional	135	14.55	Inner Rebar Layer	"
29	"	Meridional	135	14.55	Outer Rebar Layer	"
30	"	Meridional	90	0.05	Inner Rebar Layer	Base of Cylinder @ Buttress
31	"	Meridional	90	0.05	Outer Rebar Layer	"
32	"	Hoop	90	6.20	Outer Rebar Layer	Midheight @ Buttress
33	"	Meridional	90	6.20	Outer Rebar Layer	"
34	Liner Strain	Meridional	0	0.010	Inside Liner Surface	Base of Cylinder
35	"	Meridional	0	0.010	Outside Liner Surface	"
36	"	Meridional	135	0.25	Inside Liner Surface	"
37	"	Hoop	135	0.25	"	"
38	"	Meridional	135	6.20	"	Midheight
39	"	Hoop	135	6.20	"	"
40	"	Meridional	135	10.75	"	Springline
41	"	Hoop	135	10.75	"	"
42	"	Meridional	135	16.13	"	Dome apex
43	"	Meridional	90	6.20	"	Midheight @ Buttress
44	"	Hoop	90	6.20	"	"
45	"	Hoop	332	4.675	"	10 mm from thickened plate
46	"	Hoop	59	4.525	"	10 mm from thickened plate
47	Base Liner	Radial	135	0.00	100 mm Inside Cyl.	FF Basemat Liner Strain
48	Tendon Str.	Hairpin	180	15.60	Tendon - V37	Tendon Apex
49	"	Hairpin	135	10.75	Tendon - V46	Tendon Springline
50	"	Hoop	90	6.58	Tendon - H53	Mid Tendon
51	"	Hoop	180	6.58	Tendon - H53	1/4 - Tendon
52	"	Hoop	225	6.58	Tendon - H53	1/8 - Tendon
53	"	Hoop	0	4.57	Tendon - H35	Tendon btwn E/H and A/L
54	Tendon Force	Hairpin	241	-1.16	Tendon - V37	Tendon Gallery
55	"	Hoop	275	6.58	Tendon - H53	@ Buttress

Table 4.2 Results at Standard Output Location

					TEST DATA		BE/HSE/NNC				KAERI				
					LST	SFMT	ABAQUS 6.4	ANAMAT	EGP	GRS	IRSN-CEA	AXISYM	3D	KOPEC	NRC/SNL/DEA	SCANSCOT
Loc. #	Type	Orientation	Az. (deg)	El. (m)												
1	Displacement	Vertical	135	0												
2	Displacement	Radial	135	0.25												
3	Displacement	Radial	135	1.43												
4	Displacement	Radial	135	2.63												
5	Displacement	Radial	135	4.68												
6	Displacement	Radial	135	6.2												
7	Displacement	Radial	135	10.75												
8	Displacement	Vertical	135	10.75												
9	Displacement	Horiz. (Rad)	135	14.55												
10	Displacement	Vertical	135	14.55												
11	Displacement	Vertical	135	16.13												
12	Displacement	Radial	90	6.2												
13	Displacement	Radial	90	10.75												
14	Displacement	Radial	324	4.675												
15	Displacement	Radial	62	4.525												
16	Rebar Strain	Meridional	135	0.05												
17	Rebar Strain	Meridional	135	0.05												
18	Rebar Strain	Meridional	135	0.25												
19	Rebar Strain	Meridional	135	0.25												
20	Rebar Strain	Meridional	135	1.43												
21	Rebar Strain	Meridional	135	1.43												
22	Rebar Strain	Hoop	135	6.2												
23	Rebar Strain	Meridional	135	6.2												
24	Rebar Strain	Hoop	135	10.75												
25	Rebar Strain	Meridional	135	10.75												
26	Rebar Strain	Meridional	135	10.75												
27	Rebar Strain	Hoop	135	14.55												
28	Rebar Strain	Meridional	135	14.55												
29	Rebar Strain	Meridional	135	14.55												
30	Rebar Strain	Meridional	90	0.05												
31	Rebar Strain	Meridional	90	0.05												
32	Rebar Strain	Hoop	90	6.2												
33	Rebar Strain	Meridional	90	6.2												
34	Liner Strain	Meridional	0	0.01												
35	Liner Strain	Meridional	0	0.01												
36	Liner Strain	Meridional	135	0.25												
37	Liner Strain	Hoop	135	0.25												
38	Liner Strain	Meridional	135	6.2												
39	Liner Strain	Hoop	135	6.2												
40	Liner Strain	Meridional	135	10.75												
41	Liner Strain	Hoop	135	10.75												
42	Liner Strain	Meridional	135	16.13												
43	Liner Strain	Meridional	90	6.2												
44	Liner Strain	Hoop	90	6.2												
45	Liner Strain	Hoop	334	4.675												
46	Liner Strain	Hoop	58	4.525												
47	Base Liner	Radial	135	0												
48	Tendon Strain	Hairpin	180	15.6												
49	Tendon Strain	Hairpin	135	10.75												
50	Tendon Strain	Hoop	90	6.58												
51	Tendon Strain	Hoop	180	6.58												
52	Tendon Strain	Hoop	280	6.58												
53	Tendon Strain	Hoop	0	4.57												
54	Tendon Force	Hairpin	241	-1.16												
55	Tendon Force	Hoop	275	6.58												

This page intentionally left blank

Table 4.3 Summary of Results: Calculated Pressures (MPa) and Strains (%)

Participant	Concrete Cracking		Liner Yield	Hoop Tendon		Failure Modes		
	Hoop	Meridonal		Yield	2%	Pressure @ Failure	Free Field Hoop Strain	Mode
LST	**0.59-0.78**	**?**	**1.10**	**1.17**	**-**	**0.98**	**0.17%**	**Liner tear, 1% mass/day leak**
						1.29	**0.42%**	**Max. pressure @ 1000% mass/day leak**
BE / NNC	0.60	0.60	1.2 - 1.4			1.50	3.00%	Linear tear with extensive concrete cracking at buttress
EGP	0.60 0.44	0.96 0.44	0.98	1.25	1.53	aprox. 1.0	0.14%	cracking around EH
GRS	0.74-0.75	1.10	0.76	1.25	1.44	1.50	3.30%	Estimated tendon failure based on uniaxial measured failure strain of 3.3%
IRSN-CEA	0.68		0.84	0.94				
KAERI	0.59-0.62	0.59-0.62	0.95	1.38	1.47	1.50		Tendon failure strain 3.3%
KOPEC	0.60	0.58	0.84	1.43	1.47	1.52		Tendon Failure Strain 3.5%
NRC/SNL/DEA	0.62	1.14	0.85	1.15	-	1.26	0.35%	Liner Tear, leakage
SCANSCOT	0.55-0.7	0.8-1.0	0.8	1.12	1.35			More detailed model(s) needed to predict overpressure at liner rupture.

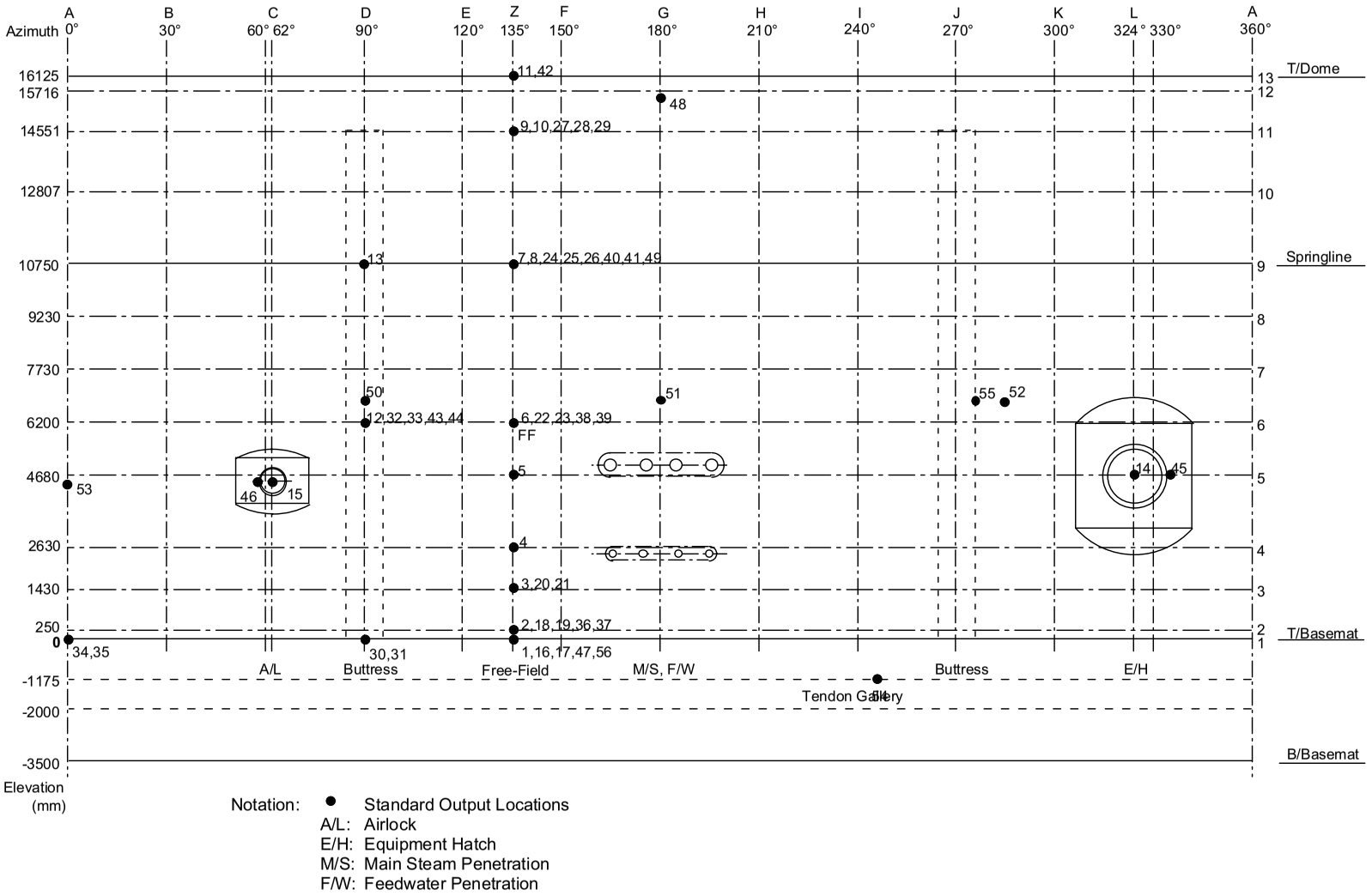

Figure 4.1 Standard Output Locations

5. PHASE 3 CALCULATIONS

5.1 Thermal Loading

Phase 3 of ISP48 extends the results of the model tests and calculations by investigating the addition of temperature to the pressure loading. The tests were conducted at ambient temperature based on risk and cost considerations and previous experience. Two questions were posed for Phase 3:

- With addition of temperature, would the onset of leakage occur later in the pressure history and, possibly, closer to the burst pressure?
- How would including the effect(s) of accident temperatures change the prediction of failure location and failure mode?

The ISP participants agreed to consider two thermal load cases for Phase 3:

- Case 1: Saturated Steam Conditions (mandatory for all Phase 3 participants)
    - Monotonically increasing static pressure and temperature (saturated steam).
- Case 2: Station Blackout Scenario (optional load case)
    - A representative severe-accident scenario for a four-loop PWR including vessel failure and hydrogen detonation

Saturated steam conditions were chosen for Case 1 since most analytical and experimental evaluations of containment capacity utilize this as an assumed bound on the combined effects of temperature and pressure. The saturated steam conditions for Case 1 are defined by standard steam tables, illustrated graphically in Figure 5.1.

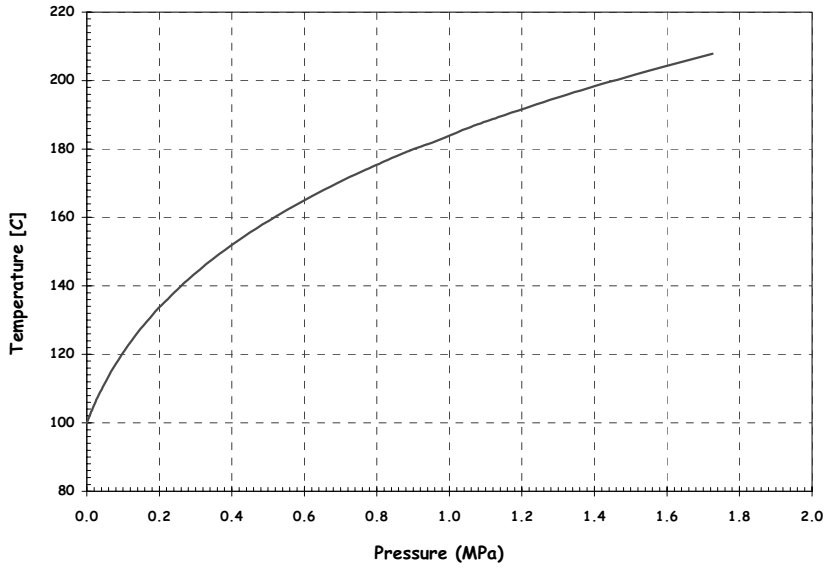

Figure 5.1 Case 1 Saturated Steam Conditions

For purposes of the response calculations, a pseudo-pressure/temperature time history was assumed to coincide with pressurization rate utilized during the SFMT, approximately 5 psi/min. These time histories are shown in Figure 5.2

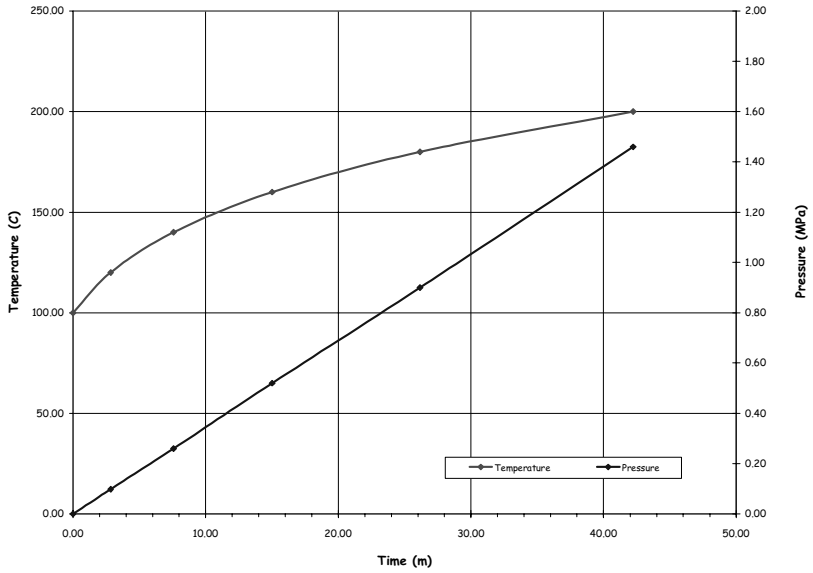

Figure 5.2 Case 1 Pseudo-Time Histories

During discussions on the Phase 3 loading, it was recognized that a more realistic severe accident scenario might provide different results and insights into the behavior of containments than merely considering saturated steam conditions. It was agreed to consider an optional load case based on a representative severe accident scenario.

A severe accident progression analysis for a Station Blackout initiating event was performed using the MELCOR[4] code. The MELCOR model was for a four-loop PWR with the containment configuration and volume similar to Ohi-3, the prototype for the PCCV model. This scenario begins at normal operating pressure and temperature then the reactor coolant pump trips, leading to a failure of the hot leg nozzle failure, followed by a hydrogen burn/detonation, and subsequent core melt and failure of the RPV. The interaction of the core with the basemat concrete leads to slowly increasing pressure and temperature. In a regular accident progression analysis, the failure of the containment would be included, however, since the purpose of this exercise was to determine the combination of temperature and pressure which would result in loss of containment, this feature of the model was turned off. The resulting pressure and temperature time histories are shown in Figure 5.3.

The peak pressure and temperature associated with the hydrogen burn/detonation was not calculated directly by MELCOR. These calculated peaks were increased to the values shown (0.8 MPa and ~600ºC) by consensus of the ISP participants to challenge the vessel early in the time history. An approximation of the calculated time history was used for the subsequent thermal and mechanical analyses.

It should be noted that rise times and durations of the pressure-temperature spikes are all long (on the order of minutes) relative to the fundamental periods of the structure. It was agreed that inertia effects were not significant and all analysis would be performed for static conditions. Furthermore, even though the late-time pressure-temperature rise is a result of the basemat concrete-core interaction, the

resulting direct damage to the structure would not be considered in the estimate of the capacity of the containment.

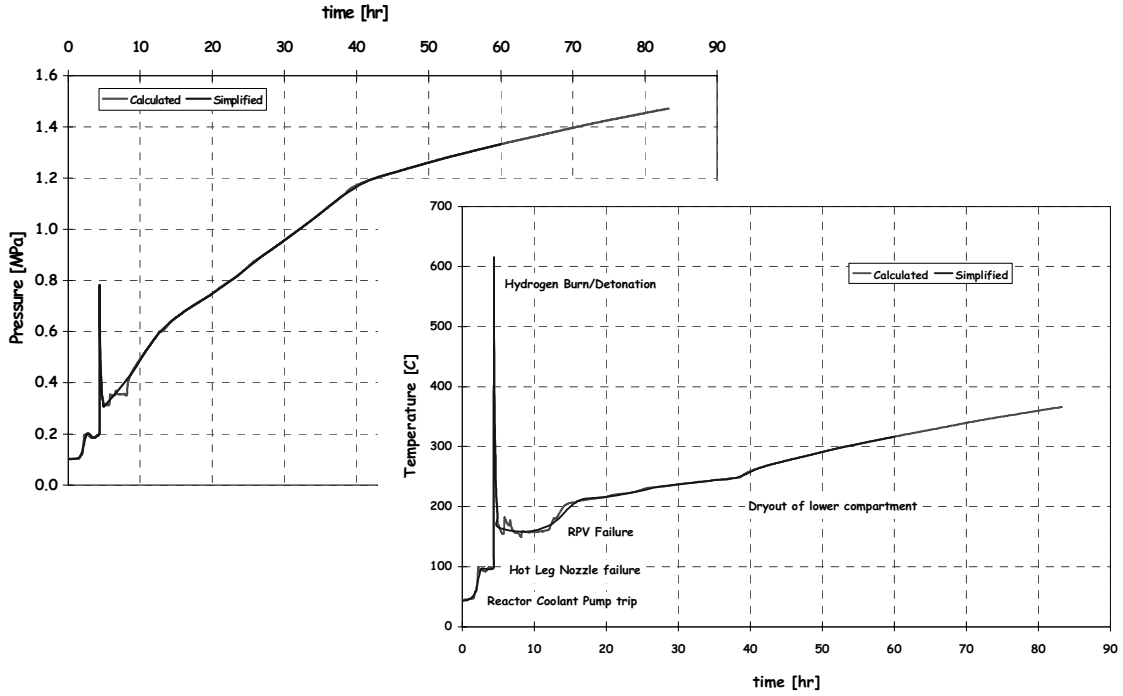

Figure 5.3 Case 2 Station Blackout Pressure and Temperature Time Histories

5.2 Thermal Analysis

The thermal and mechanical analyses were de-coupled with the heat transfer calculations being performed first using a full-scale axisymmetric model using a combination of applied temperature (liner), convection (cylinder wall and dome), and conduction (basemat/soil) boundary conditions. Thermal material properties and temperature dependent mechanical properties were based on handbook data. Thermal gradients were calculated at several locations and provided to the participants to perform combined temperature-pressure response calculations for the 1:4-scale model.

The thermal-mechanical solution strategy being adopted uses the ABAQUS finite element program, and a semi-coupled thermal mechanical analysis procedure using a combination of applied temperature (liner), convection (cylinder wall and dome), and conduction (basemat/soil) boundary conditions. The analysis advances through time (a pseudo-time history for Case 1 and about 60 hours for Case 2), at which point the combined pressure and temperature far exceed the capacity of the containment model. The results of these thermal analyses are provided as time and/or pressure dependent thermal gradients at representative cross-sections in the model. A set of temperature-dependent concrete and steel mechanical properties are also provided, though these properties only enter into the mechanical (stress) portion of the solution, not into the purely thermal solution. All of these properties are offered as a baseline suggestion and documentation of the source of the thermal gradients, but ISP48 participants are free to use properties from their own research if desired.

5.2.1 Assumptions for Heat Transfer Analysis

A full scale version of the PCCV axisymmetric model was used to conduct the thermal analysis since the thermal response does not scale geometrically. The resulting gradients are then scaled and applied to the 1:4-scale models for combined thermal-mechanical analysis.

In order to conduct the Heat Transfer analysis in ABAQUS, all elements relevant for thermal analysis were changed to diffusive heat transfer element types which only have temperature degrees of freedom. Thermal boundary conditions were imposed at the outer surface of the PCCV cylinder and dome wall consisting of free convection with air with a sink temperature ($T_{f,\leftarrow}$) of 25°C. For free convection with air, the heat transfer coefficient, h, varies with temperature according to the following relationship:

$h = 0.00382(\div T)^{1/3}$ lbf/in-s-°F (T in °F) for the full scale PCCV analysis, and

$h = 0.0153(\div T)^{1/3}$ lbf/in-s-°F for the 1:4 scale analysis. (These convert to 1.20 and 4.80 W-m^{-2}-°K.)

This is input to ABAQUS as a "non-uniform film coefficient" (FNU) through the User-defined subroutine related to the SFILM option.

The boundary condition on the basemat foundation consists of heat conduction with soil with a sink temperature ($T_{f,\square}$) of 25°C. The heat transfer coefficient was developed for the horizontal surface of the foundation in contact with the soil to be:

$h = 5.76x10^{45}$ lbf/in-s-°F for the full scale PCCV analysis, and $h = 2.30x10^{44}$ lbf/in-s-°F for the 1:4 scale PCCV. (These convert to 0.0181 and 0.0724 W-m^{-2}-°K.) This is input to ABAQUS as a constant film coefficient using the SFILM option and no User-defined subroutine.

The temperature input for the thermal analysis was applied through prescribed temperature boundary conditions on the nodes of the inner surface of the basemat, cylinder wall, and dome (i.e., on the liner), as shown in the figure below. For the Case 2 a steady state heat transfer analysis step preceded the dynamic heat transfer analysis with the time history temperature input. The steady state heat transfer step was used to bring the model up to an ambient/operating temperature of 25°C. Figure 5.4 shows the location of the prescribed boundary conditions for the axisymmetric model. Figure 5.5 shows the temperature contours for various steps in the heat transfer analysis. Also shown in Figure 5.6 are the sections through the containment wall and basemat where the temperature gradients are provided.

5.2.2 Material Properties and Variations due to Temperature

A literature review was conducted to choose and substantiate assumptions for concrete thermal properties, and for degradation of concrete and steel material properties. It should be noted that all of the fundamental mechanical properties (without thermal influence) that were used in the PCCV 1:4 scale test simulation analyses (ISP48 Phase 2, for example) were kept the same for the current exercise. Those related to heat transfer and those with some temperature dependency were then modified as described herein.

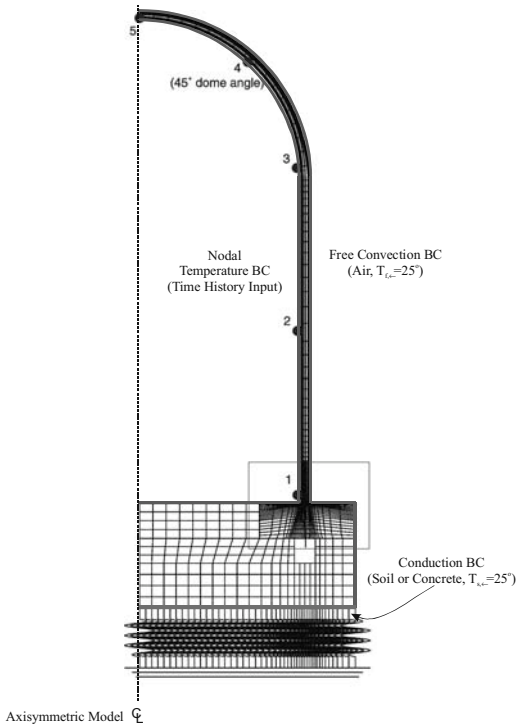

Figure 5.4 Axisymmetric Model with Thermal Boundary Conditions

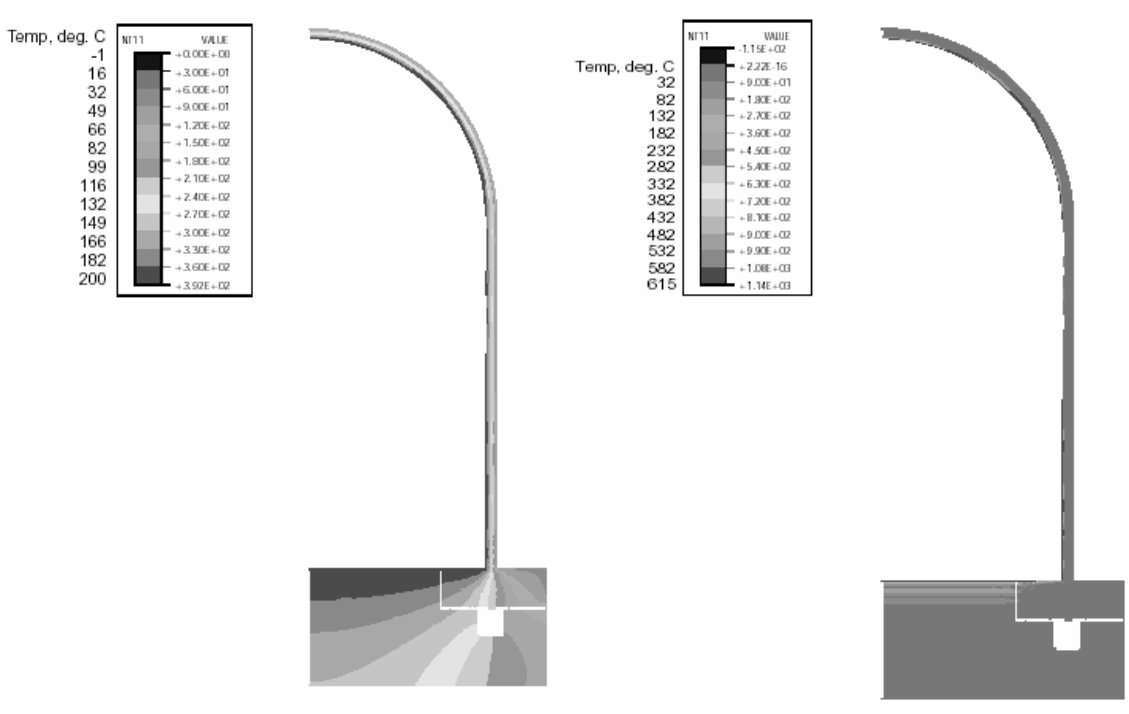

Case 1 Thermal Gradients @ T = 200°C **Case 2 Thermal Gradients @ T = 615°C**

Figure 5.5 Axisymmetric Model Thermal Gradients

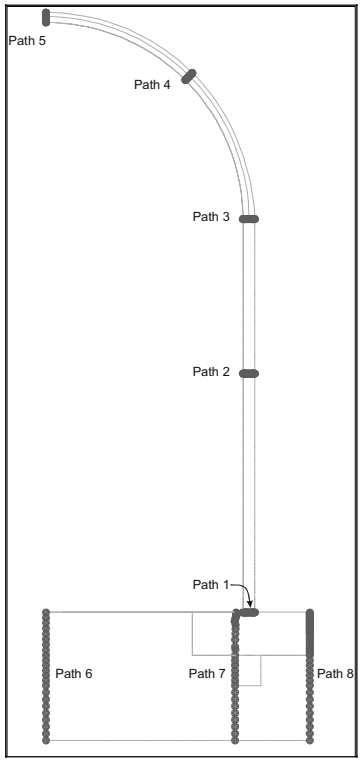

Figure 5.6 Thermal Gradient Locations

References 5 through 12 proved useful in support of this study. Though there are scores of publications on these subjects, we consider these to be a reasonably representative sample of the general literature. Reference 5 proved to be a particularly good summary of the various research. A summary of conclusions made in Reference 5 that we found relevant to our task for PCCVs and that we found to be generally consistent with other references is provided below.

- **Density**

  The average density of the concrete in the PCCV at the time of construction was reported as 2186 kgf/m3 for the nominal 300 kgf/cm3 (used in the basemat) and 2176 kgf/m3 for the nominal 450 kgf/cm3 (used in the tendon gallery, wall and dome) [1].

  Using a nominal 2% by volume of reinforcing steel and other embedments, a nominal value of 2290 kgf/m3 is used for the thermal analysis.

- **Specific Heat**

  Specific Heat of ordinary concrete at normal temperatures can vary from 0.50 to 1.13 $kJ\ kg^{41}K^{41}$. We used 0.879 $kJ\ \ kg^{41}K^{41}$ in the analysis.

  - generally it is assumed that changes in aggregate, mix, and age do not have a significant effect on this

- but moisture content does have a significant effect. Reducing moisture content from 25 to 12.5% by volume can reduce overall specific heat by 25%; we are assuming moisture content in the containment wall will be relatively low.

- at high temperatures, specific heat can go up considerably, approximately doubling from 150C to 500C; however, we will assume a constant value of specific heat since the very high temperature is of relatively short duration.

- **Thermal Conductivity**

  - assuming igneous amorphous aggregate Ą Thermal conductivity $= 1.0\,4\,1.6 Wm^{41} C^{41}$ (1.4 Wm^{-1} C^{-1} was used in the analysis.)

  - -not all that variable with temperature, but tends to decrease by ~10% to 30% between 20C and 200C

- **Thermal Spalling of Concrete**

  - may occur in either quiescent or violent fashion, and probability increases at higher heating rates

  - a primary cause is moisture content; greater the moisture the greater the spalling

  - high steel reinforcement ratios can also increase spalling

- **Strength**

  - significant reductions in strength determined when T>300C, and at 690C, strength reduced by 80%

  - a lot of scatter in experimental results, owing to different test conditions and to the composition of various concretes and aggregates. For conventional aggregates:

  - between 80 and 90C reductions range from 10 to 35%

  - between 90 and 200C, compressive strength ranges from continuing decrease to even slight increase.

  - from 200C on, there is continuous decrease.

  - rich mixes show greater reduction in strength

  - different water-cement ratios have little effect

  - also a significant time of exposure factor

  - there is some specimen shape and size effect. Small specimens lose more strength than large ones.

  - Poisson's ratio also drops from about 0.2 to 0.1 at 400C

  - tensile strength decreases showed similar trends as the compressive strength decreases

- modulus of elasticity reductions also showed similar trends as strength losses, but overall reductions are less. Tends to follow the square-root relationship commonly used.

5.2.3 Final Strength and Modulus Degradation Assumptions

A sampling of the degradation curves found in the literature review are shown in Figures 5.7 through 5.12. Figure 5.7 shows the trends for three basic kinds of tests found in the literature: "Unstressed" meaning that an unloaded specimen is heated and then loaded to failure while hot; "stressed" meaning the specimen is loaded to some initial stress and then heated; "unstressed residual" meaning that an unloaded specimen is heated and then cooled slowly, then loaded cool to failure. Figure 5.8 shows some additional results comparing aggregate types, all for the "unstressed" condition. Figure 5.9 shows a variety of data from Reference 8, and Figures 5.10 and 5.11 show data for Young's Modulus from References 8 and 9.

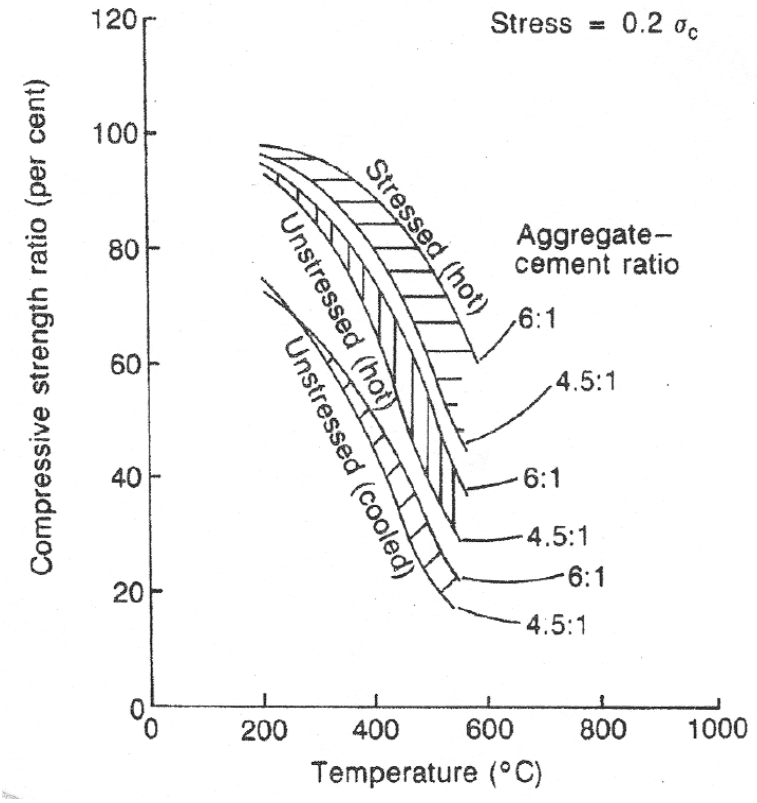

Figure 5.7 Compression Strength Ratio vs. Temp. (Ref. 5)

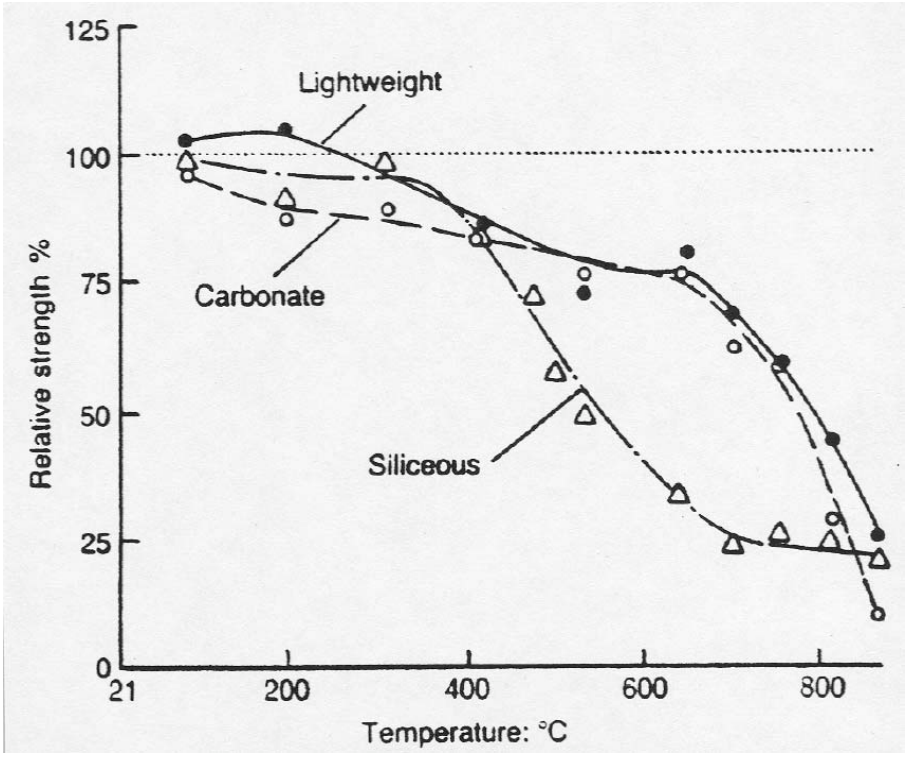

Figure 5.8 Compression Strength Ratio vs. Temp. (Ref. 6); Heated Without Load

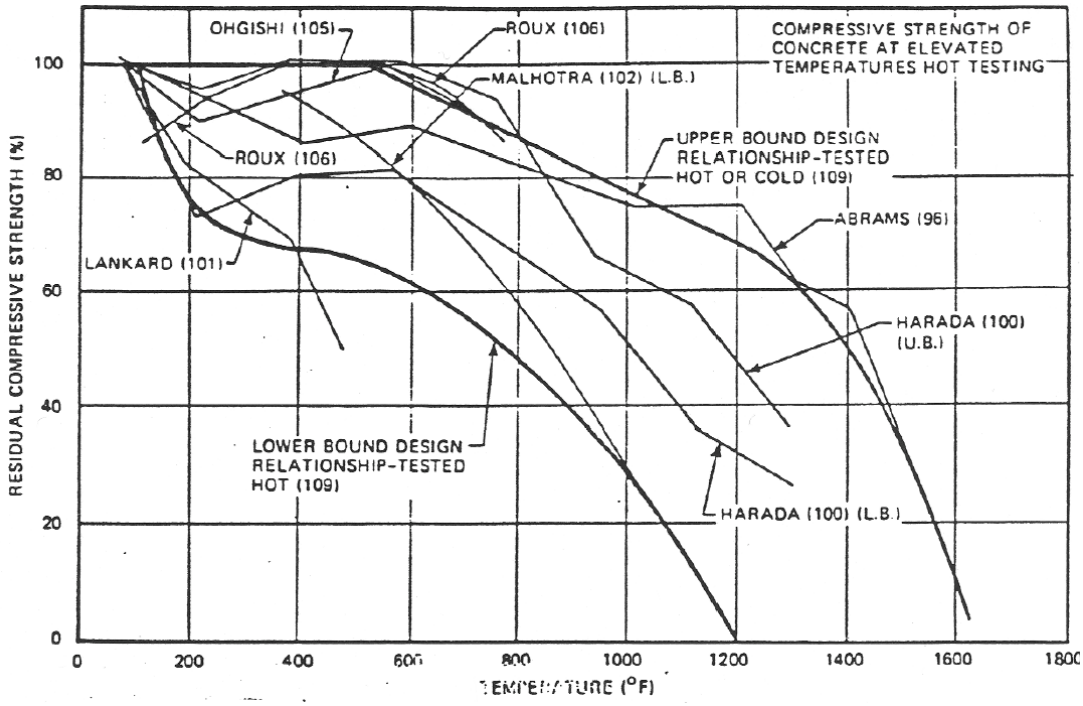

Figure 5.9 Compression Strength Ratio vs. Temp. (Ref. 8)

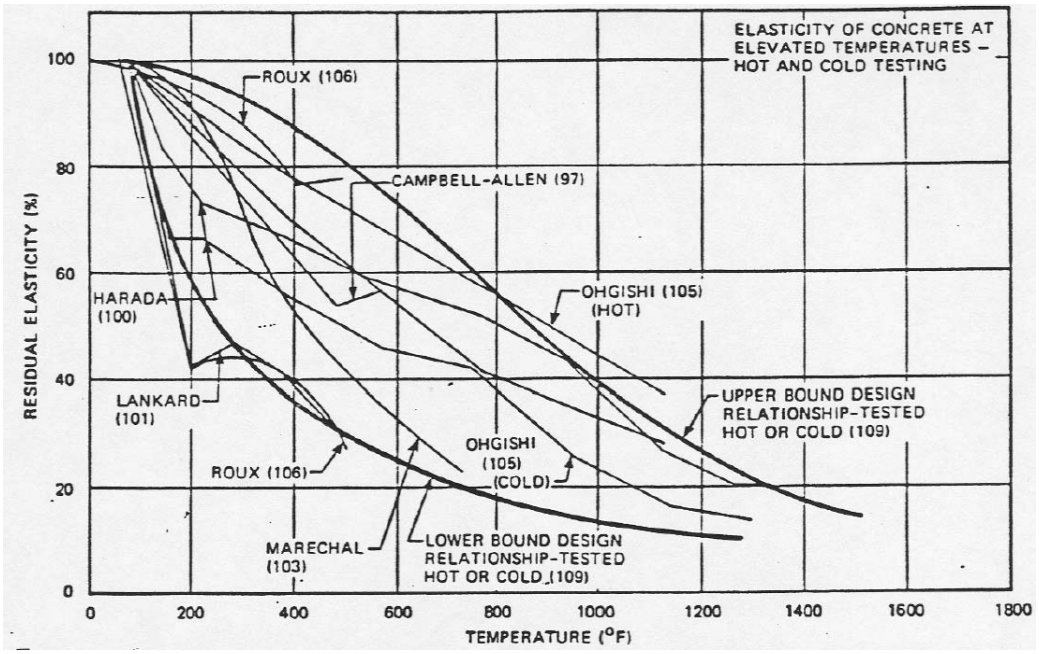

Figure 5.10 Young's Modulus Ratio vs. Temp. (Ref. 8)

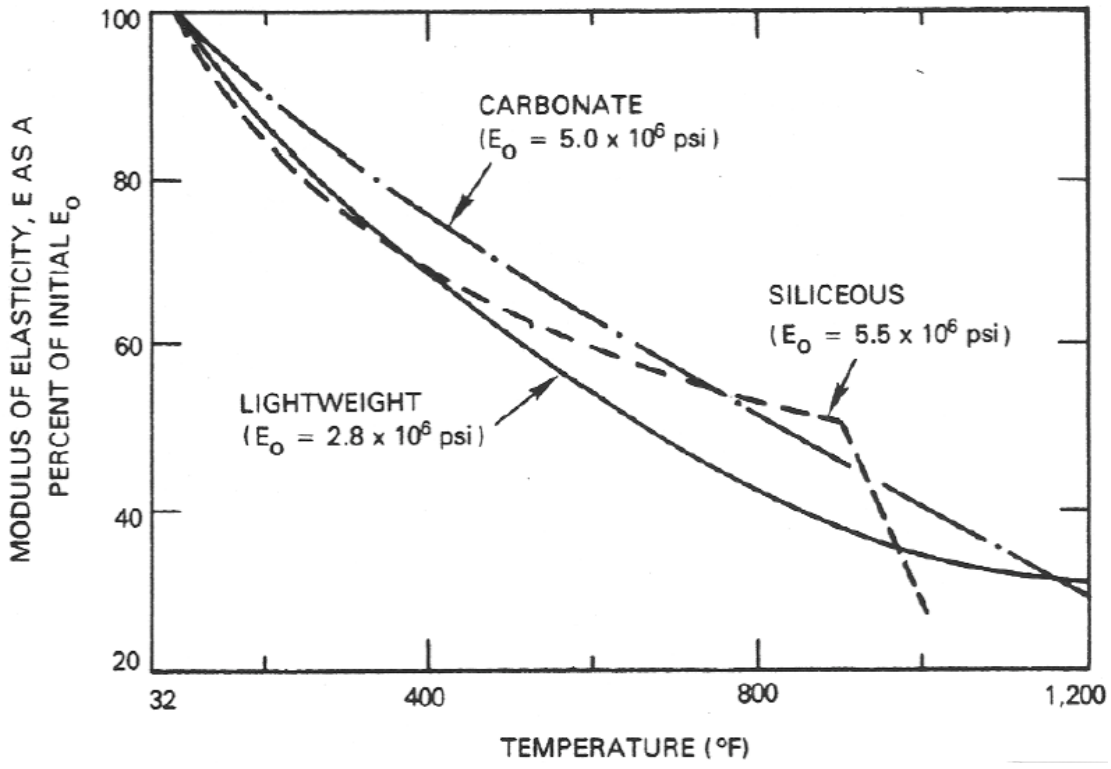

Figure 5.11 Young's Modulus Ratio vs. Temp. (Ref. 9)

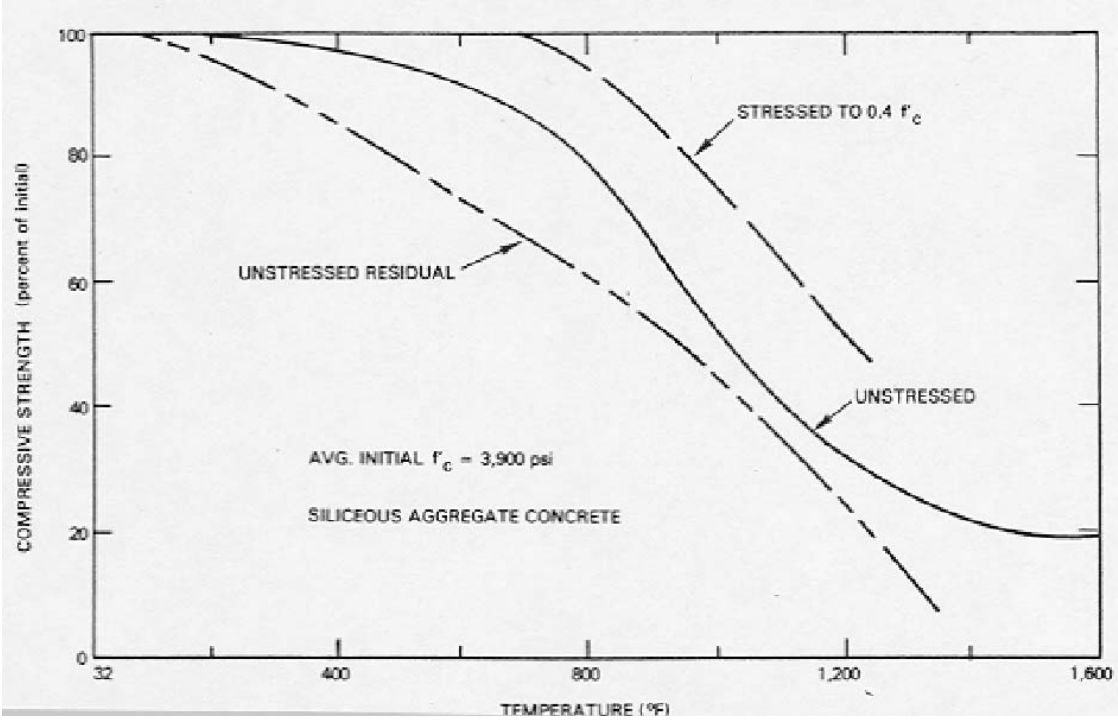

Figure 5.12 Compression Strength Ratio vs. Temp. (Ref. 9)

We have based a choice of a generic set of properties on an approximate "best estimate median" of the data rather than a bounding or conservative selection. We also feel it is reasonable to take the "unstressed hot" versions of data because in the PCCV loading scenarios, the temperatures and pressures are increasing simultaneously. The "stressed-hot" would imply a large pressure challenge existing and held constant during the temperature rise. The "actual" challenge in the PCCV is likely to be somewhere between an "unstressed-hot" case and a "stressed-hot" case.

Based on this and on the trends observed in other references, we have developed a smooth curve for strength degradation versus temperature as estimated below and plotted in Figure 5.13.

Concrete Strength Ratio, $S_{Rc} = \exp^4 (T/632)^{1.8}$ where T is in degrees C

The derivation of this curve was based on assumption of a basic shape as observed from the data, and then pegging the curve to the following points.

T (°C)	S_R
0	1.00
200	0.88
600	0.40
1000	1.10

Further, based on the literature, it appears reasonable to base the modulus on the standard ACI formula: $E = 57{,}000\sqrt{fc}\Re$(English Units) such that a Modulus Reduction Ratio can be defined as:

$$M_R = (S_R)^{\frac{1}{2}}$$

It should be noted, however, that the peak strain at which the concrete compressive strength limit is reached also shifts with increasing temperature. While at 25C, this strain is approximately 0.002, it can reach two to three times this value at high temperatures.

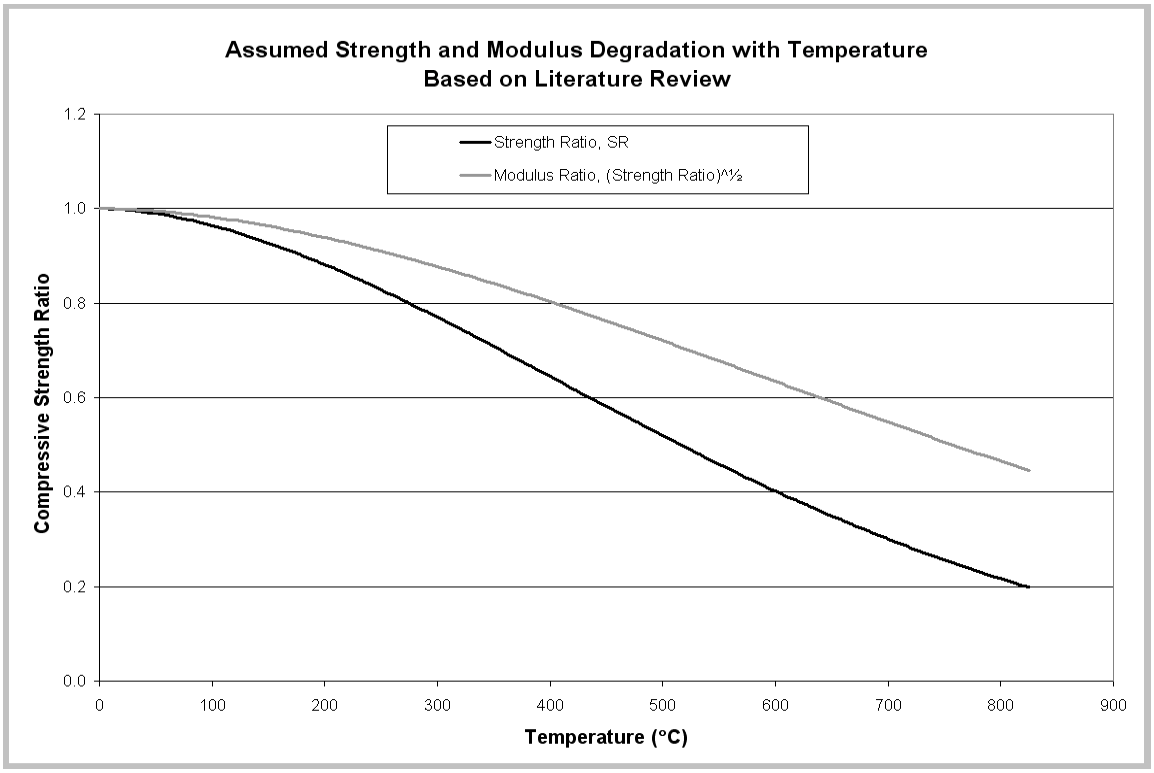

Figure 5.13 Concrete Compression Strength Ratio vs. Temperature

Temperature variation of steel is also included in the mechanical solution. This variation has been idealized based on curves provided in Reference 8 and trends is observed in other texts and papers:

Steel Yield Strength Ratio, $S_{Rs} = \exp^4((T\ 4\ 340)/300)^{1.9}$ where T is in degrees C.

$$S_{Rs} = 1.0, T\ \Omega 340C$$

For steel, the Young's Modulus tends to follow the yield strength one-to-one, rather than the square-root relationship found in concrete. The steel yield strength reduction is shown in Figure 5.14.

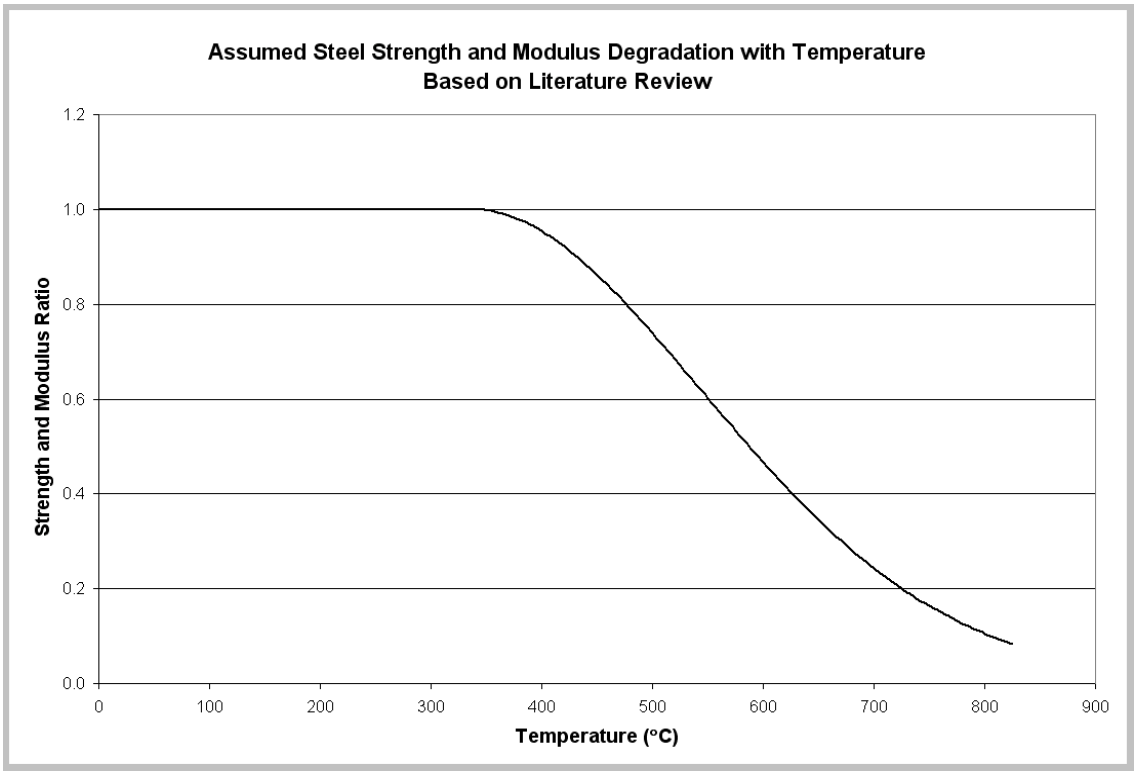

Figure 5.14 Steel Yield Strength and Modulus Ratio vs. Temperature

5.3 Combined Thermal and Mechanical Response Calculations

The results of the independent participant calculations were completed in January, 2005 Each of the participants completed analyses for Case 1 or both Case 1 and 2. Participants were also allowed to submit revised calculations for pressure only to account for any modeling changes between Phase 2 and 3. Each ISP participant was asked to provide a report summarizing their analysis approach and results. Each individual report is also reproduced along with the Phase 2 results in Appendices C through L.

A reduced set of twenty-two SOLs were selected to compare the Phase 3 calculations results. The selection of these locations was based on the Phase 2 experience. Participants were allowed to submit results at all of the 55 SOLs if they wished to do so. A summary of the results provided by each of the participants is given in Table 5.1 (the reduced set of SOLs is highlighted). The calculated results were collected into composite plots. These composite plots are provided in Appendix B. Although the test results did not include thermal loading, the comparison of the Case 1 results included the LST and SFMT data (when available, for reference. A few notes on the comparison plots:

- The participants agreed that the composite plots for liner strains should show mechanical strain, i.e. total strain minus thermal strain ($\boldsymbol{\zeta} \div \mathbf{T}$). It was felt that this value was more meaningful than comparing total strain for evaluating liner performance.

- Tendon strains and forces were initialized at zero pressure to match the residual values at the end of the LST . This was done to focus the comparison on the response to the applied pressure and thermal loads which might be masked by the differences in response to gravity and prestressing loads.

- The pressure time history for Case 2 was reported in absolute pressure. Most participants, however, treated the initial ambient pressure (~0.10 MPa) as overpressure. This slight error does not have any significant effect on the final results or conclusions for Case 2. The comparison plots for Case 2 have been adjusted so that all participant results are plotted in terms of absolute pressure.

Along with the meeting of the participants, a workshop was held in April, 2005 to review the results and develop a consensus on issues related to:

- Modeling and analysis methods
- Constitutive models for materials
- Limit state and structural failure criteria

The proceedings of this workshop, published by NEA [3], address these issues in detail.

In addition to submitting response predictions at the SOLs, each participant was also asked to provide a best estimate of various response milestones (onset of cracking, yielding, etc.) leading up to failure pressure of the PCCV model. These predictions are summarized for loading Cases 1 and 2 in the following tables. Tables 5.3 and 5.4 tabulate the calculated pressures at both the onset of concrete cracking (i.e. cracking calculated at a single integration point in the finite element) and through-thickness cracking when the individual cracks coalesce. Tables 5.5 and 5.6 summarize the pressures associated with various strain levels in the liner and normal reinforcing steel, while Tables 5.7 and 5.8 perform the same function for the hoop prestressing tendons. Tables 5.9 and 5.10 aggregate summarize the pressures associated with both functional failure, i.e. loss of containment associated with the onset of liner tearing, and structural failure, normally defined by the participants as rupture of the prestressing tendons.

Table 5.1 Results at Standard Output Location for Phase 3-Case 1

ISP 48 PHASE 3 CASE 1					BE/HSE/NNC	EDF	EGP	FORTUM	GRS	IRSN-CEA	JPRG	KOPEC	NRC/SNL/DEA	SCANSCOT
Loc. #	Type	Orientation	Az. (deg)	El. (m)	1	2	3	4	5	6	7	8	9	10
1	Displacement	Vertical	135	0	X			X		X	X	X	X	X
2	Displacement	Radial	135	0.25			X	X	X	X	X	X	X	X
3	Displacement	Radial	135	1.43			X	X	X	X	X	X	X	X
4	Displacement	Radial	135	2.63			X	X	X	X	X	X	X	X
5	Displacement	Radial	135	4.68			X	X	X	X	X	X	X	X
6	Displacement	Radial	135	6.2	X		X	X	X	X	X	X	X	X
7	Displacement	Radial	135	10.75	X		X	X	X	X	X	X	X	X
8	Displacement	Vertical	135	10.75	X		X	X	X	X	X	X	X	X
9	Displacement	Horiz. (Rad)	135	14.55			X	X	X	X	X	X	X	X
10	Displacement	Vertical	135	14.55			X	X	X	X	X	X	X	X
11	Displacement	Vertical	135	16.13	X		X	X	X	X	X	X	X	X
12	Displacement	Radial	90	6.2	X		X	X		X	X			X
13	Displacement	Radial	90	10.75	X		X	X		X	X			X
14	Displacement	Radial	324	4.675	X		X	X		X	X			X
15	Displacement	Radial	62	4.525			X	X		X	X			X
16	Rebar Strain	Meridional	135	0.05			X		X	X	X	X	X	X
17	Rebar Strain	Meridional	135	0.05			X		X	X	X	X	X	X
18	Rebar Strain	Meridional	135	0.25	X		X		X	X	X	X	X	X
19	Rebar Strain	Meridional	135	0.25	X		X		X	X	X	X	X	X
20	Rebar Strain	Meridional	135	1.43			X		X	X	X	X	X	X
21	Rebar Strain	Meridional	135	1.43			X		X	X	X	X	X	X
22	Rebar Strain	Hoop	135	6.2	X		X		X	X	X	X	X	X
23	Rebar Strain	Meridional	135	6.2	X		X		X	X	X	X	X	X
24	Rebar Strain	Hoop	135	10.75			X		X	X	X	X	X	X
25	Rebar Strain	Meridional	135	10.75			X		X	X	X	X	X	X
26	Rebar Strain	Meridional	135	10.75			X		X	X	X	X	X	X
27	Rebar Strain	Hoop	135	14.55			X		X	X	X	X	X	X
28	Rebar Strain	Meridional	135	14.55			X		X	X	X	X	X	X
29	Rebar Strain	Meridional	135	14.55			X		X	X	X	X	X	X
30	Rebar Strain	Meridional	90	0.05			X			X				X
31	Rebar Strain	Meridional	90	0.05			X			X				X
32	Rebar Strain	Hoop	90	6.2	X		X			X	X			X
33	Rebar Strain	Meridional	90	6.2	X		X			X	X			X
34	Liner Strain	Meridional	0	0.01	X				X	X			X	X
	Stress				X				X	X			X	X
35	Liner Strain	Meridional	0	0.01	X				X	X			X	X
	Stress				X				X	X			X	X
36	Liner Strain	Meridional	135	0.25	X		X		X	X	X	X	X	X
	Stress				X				X	X	X	X	X	X
37	Liner Strain	Hoop	135	0.25	X		X		X	X	X	X	X	X
	Stress				X				X	X	X	X	X	X
38	Liner Strain	Meridional	135	6.2	X		X		X	X	X	X	X	X
	Stress				X				X	X	X	X	X	X
39	Liner Strain	Hoop	135	6.2	X		X		X	X	X	X	X	X
	Stress				X				X	X	X	X	X	X
40	Liner Strain	Meridional	135	10.75	X		X		X	X	X	X	X	X
	Stress				X				X	X	X	X	X	X
41	Liner Strain	Hoop	135	10.75	X		X		X	X	X	X	X	X
	Stress				X				X	X	X	X	X	X
42	Liner Strain	Meridional	135	16.13	X		X		X	X	X	X	X	X
	Stress				X				X	X	X	X	X	X
43	Liner Strain	Meridional	90	6.2			X			X	X			X
44	Liner Strain	Hoop	90	6.2			X			X	X			X
45	Liner Strain	Hoop	334	4.675	X		X				X			X
46	Liner Strain	Hoop	58	4.525			X				X			X
47	Base Liner	Radial	135	0							X	X	X	
48	Tendon Strain	Hairpin	180	15.6	X		X	X	X	X	X		X	X
49	Tendon Strain	Hairpin	135	10.75						X	X			
50	Tendon Strain	Hoop	90	6.58	X		X	X	X	X	X		X	X
51	Tendon Strain	Hoop	180	6.58			X	X		X	X		X	X
52	Tendon Strain	Hoop	280	6.58	X		X	X		X	X		X	X
53	Tendon Strain	Hoop	0	4.57	X		X	X		X	X		X	X
54	Tendon Force	Hairpin	241	-1.16	X		X	X		X	X	X	X	X
55	Tendon Force	Hoop	275	6.58	X		X	X		X	X		X	X

Table 5.2 Results at Standard Output Location for Phase 3-Case2

ISP 48 PHASE 3 CASE 2					BE/HSE/NNC	EDF	EGP	FORTUM	GRS	IRSN-CEA	JPRG	KOPEC	NRC/SNL/DEA	SCANSCOT
Loc. #	Type	Orientation	Az. (deg)	El. (m)	1	2	3	4	5	6	7	8	9	10
1	Displacement	Vertical	135	0				X			X	X	X	X
2	Displacement	Radial	135	0.25			X	X			X	X	X	X
3	Displacement	Radial	135	1.43			X	X			X	X	X	X
4	Displacement	Radial	135	2.63			X	X			X	X	X	X
5	Displacement	Radial	135	4.68			X	X			X	X	X	X
6	Displacement	Radial	135	6.2			X	X	X		X	X	X	X
7	Displacement	Radial	135	10.75			X	X			X	X	X	X
8	Displacement	Vertical	135	10.75			X	X			X	X	X	X
9	Displacement	Horiz. (Rad)	135	14.55			X	X			X	X	X	X
10	Displacement	Vertical	135	14.55			X	X			X	X	X	X
11	Displacement	Vertical	135	16.13			X	X			X	X	X	X
12	Displacement	Radial	90	6.2			X	X			X			X
13	Displacement	Radial	90	10.75			X	X			X			X
14	Displacement	Radial	324	4.675			X	X			X			X
15	Displacement	Radial	62	4.525			X	X			X			X
16	Rebar Strain	Meridional	135	0.05			X				X	X	X	X
17	Rebar Strain	Meridional	135	0.05			X				X	X	X	X
18	Rebar Strain	Meridional	135	0.25			X				X	X	X	X
19	Rebar Strain	Meridional	135	0.25			X				X	X	X	X
20	Rebar Strain	Meridional	135	1.43			X				X	X	X	X
21	Rebar Strain	Meridional	135	1.43			X				X	X	X	X
22	Rebar Strain	Hoop	135	6.2			X		X		X	X	X	X
23	Rebar Strain	Meridional	135	6.2			X		X		X	X	X	X
24	Rebar Strain	Hoop	135	10.75			X				X	X	X	X
25	Rebar Strain	Meridional	135	10.75			X				X	X	X	X
26	Rebar Strain	Meridional	135	10.75			X				X	X	X	X
27	Rebar Strain	Hoop	135	14.55			X				X	X	X	X
28	Rebar Strain	Meridional	135	14.55			X				X	X	X	X
29	Rebar Strain	Meridional	135	14.55			X				X	X	X	X
30	Rebar Strain	Meridional	90	0.05			X							X
31	Rebar Strain	Meridional	90	0.05			X							X
32	Rebar Strain	Hoop	90	6.2			X				X			X
33	Rebar Strain	Meridional	90	6.2			X				X			X
34	Liner Strain	Meridional	0	0.01									X	X
	Stress												X	
35	Liner Strain	Meridional	0	0.01									X	X
	Stress												X	
36	Liner Strain	Meridional	135	0.25			X				X	X	X	X
	Stress										X	X	X	
37	Liner Strain	Hoop	135	0.25			X				X	X	X	X
	Stress										X	X	X	X
38	Liner Strain	Meridional	135	6.2			X		X		X	X	X	X
	Stress										X	X	X	
39	Liner Strain	Hoop	135	6.2			X		X		X	X	X	X
	Stress										X	X	X	X
40	Liner Strain	Meridional	135	10.75			X				X	X	X	X
	Stress										X	X	X	
41	Liner Strain	Hoop	135	10.75			X				X	X	X	X
	Stress										X	X	X	X
42	Liner Strain	Meridional	135	16.13			X				X	X	X	X
	Stress										X	X	X	X
43	Liner Strain	Meridional	90	6.2			X				X			X
44	Liner Strain	Hoop	90	6.2			X				X			X
45	Liner Strain	Hoop	334	4.675			X				X			X
46	Liner Strain	Hoop	58	4.525			X				X			X
47	Base Liner	Radial	135	0							X	X	X	
48	Tendon Strain	Hairpin	180	15.6			X	X			X		X	X
49	Tendon Strain	Hairpin	135	10.75							X			
50	Tendon Strain	Hoop	90	6.58			X	X	X		X		X	X
51	Tendon Strain	Hoop	180	6.58			X	X			X		X	X
52	Tendon Strain	Hoop	280	6.58			X	X			X		X	X
53	Tendon Strain	Hoop	0	4.57			X	X			X		X	X
54	Tendon Force	Hairpin	241	-1.16			X				X	X	X	X
55	Tendon Force	Hoop	275	6.58			X				X		X	X

Table 5.3 Phase 3-Pressure Only Results Summary: Concrete Cracking

(Pressures in MPa)

Participant	Cracking*			
	Hoop		Meridonal	
		Type, Location		Type, Location
Final **BE/HSE/NNC**	0.60 1.10	Initial cracking at inside surface of the wall Through wall	0.60 0.75	Initial cracking at inside surface of the wall Through wall
EDF				
Final **EGP**	0.60 0.44 0.00	through-wall cracking surface cracking around EH inirial cracking in buttres	0.96 0.44 0.00	through-wall cracking surface cracking around EH inirial cracking in dome
Final **FORTUM**	1.00	Through crack @ cyl midheight change in stiffness		
GRS	0.75	through-wall cracking starting from inside surface of the wall	1.10	initial cracking at inside surface of the wall
IRSN/CEA Case 1	0.48		0.52	
Final **JPRG** **Case1** **Case2**	- -		- -	
Final **KOPEC**	0.49MPa 0.57MPa	Initial cracking @ wall-base juncture Through crack @ cyl midheight	0.49MPa 0.84MPa	Initial cracking @ wall-base juncture Through crack @ cyl midheight
Final **NRC/SNL/DEA**	0.60 **Assumes "perfect welds" and no grinding flaws	Surface, midheight	0.60	Surface, inner-wall-base juncture
Final **SCANSCOT**	0,35MPa 0,55MPa	initial cracking side of E/H Through-wall cracking many locations	0.2MPa 0,8MPa	initial cracking over and under E/H Through-wall cracking many locations

Table 5.4 Phase 3-Pressure/Temperature Results Summary: Concrete Cracking

(Pressures in MPa)

Participant	Cracking*			
	Hoop		Meridonal	
		Type, Location		Type, Location
BE/HSE/NNC Case 1	0.60	Initial cracking at inside surface of the wall	0.60	Initial cracking at inside surface of the wall
	0.10	Initial cracking at outside surface of the wall	0.10	Initial cracking at outside surface of the wall
	1.10	Through wall	0.80	Through wall
EGP	0.00	initial cracking in buttress	0.00	initial cracking in dome
case 1	0MPa/100°C	surface cracking at outside surface	0MPa/100°C	surface cracking at outside surface
	0.76	through wall cracks		
FORTUM				
Case 1	1.05	Through crack @ cyl midheight, change in stiffness		
GRS	0.10	first cracks in cylindrical part at outer surface	0.10	first cracks in cylindrical part at outer surface
Case 1	0.8	through wall cracks	1.2	through wall cracks
Case 2	0.40	first cracks	0.65	first cracks
	0.85	through wall cracks	0.85	through wall cracks
IRSN/CEA Case 1	0.48		0.52	
JPRG Case1(P+T)	-		-	
JPRG Case2(P+T)	-		-	
Final				
KOPEC Case 1	0.1MPa	Initial Cracking@ wall-base juncture	0.1MPa	Initial Cracking@ wall-base juncture
	0.66MPa	through wall Cracks@ many location	0.86MPa	through wall Cracks@ many location
KOPEC Case 2	0.1MPa	Initial Cracking@ wall-base juncture	0.1MPa	Initial Cracking@ wall-base juncture
	0.26MPa	through wall Cracks@ wall-base juncture	0.42MPa	through wall Cracks@ many location
NRC/SNL/DEA	0.50 380°C 260min	Surface, midheight	0.40 240°C 260min	Surface, inner-wall-base juncture
	**Liner yields in compression at 0.5MPa, 220C, on initial pressure spike ***Pressure in Mpa, Temp in degrees C, time in minutes ****All data in this table is for Temp Case 2, because it is the controlling case.			
SCANSCOT Case 1	0MPa 0min 100°C	first cracking close to E/H outside of containment	0MPa 0min 100°C	first cracking many locations outside of containment
	0.58MPa 16.6min 160°C	Through-wall cracking many locations	0.87MPa 25.3min 178°C	Through-wall cracking many locations
SCANSCOT Case 2	0.2MPa 156min 95°C	first cracking close to E/H, A/L middle of containment wall	0.2MPa 260.18min 103°C	first cracking close to E/H middle of containment wall
	0.55MPa 260.47min 388°C	Through-wall cracking many locations	0.55MPa 260.47min 388°C	Through-wall cracking many locations

Table 5.5 Phase 3- Pressure Only Results Summary: Liner and Rebar Strains

(Pressures in MPa)

Participant	Liner Yield in tension	Liner Tearing (Leakage)		Rebar Yield	
	Hoop	Pressure	Criteria	Hoop	Meridonal
Final **BE/HSE/NNC**	0.75	1.10	Liner strain of 0.17% reached at SOL39 when leak rate in LST reached 1% mass/day		
EDF					
Final **EGP**	1.15	1.15	reaching of yield stress	1.15	1.45 1.25
Final **FORTUM**		1.30	critical global strain 0.01		
GRS	0.76			1.00	1.20
IRSN/CEA Case 1	0.82	1.00	Global strain = 0.3%	1.12	1.30
Final **JPRG**			Local strain=6.8%		
Case1	0.96MPa 28min	-		0.93MPa 27min	0.98 29min
Case2	0.94MPa 1752min	-		0.91MPa 1655min	0.97 1834min
Final **KOPEC**	0.98MPa	1.46MPa	max. strain=1.0%	1.16MPa	1.42MPa
Final **NRC/SNL/DEA**	1.02	1.33**	Local strain ~20%; from earlier local analysis, this occurred at global strain = 0.74%	1.10	1.30
Final **SCANSCOT**	0,8MPa	1,3MPa	max principal strain locally>2%	1MPa	1MPa

Table 5.6 Phase 3- Pressure/Temperature Results Summary: Liner and Rebar Strains

(Pressures in MPa)

Participant	Liner Yield in tension	Liner Tearing (Leakage)		Rebar Yield	
	Hoop	Pressure	Criteria	Hoop	Meridonal
BE/HSE/NNC Case 1	0.83	1.25	Liner strain of 0.17% reached at SOL39 when leak rate in LST reached 1% mass/day		
EGP case 1	0.75 Fixing into basemat	0.75	reaching of yield stress	1.06	0.83 Fixing into basemat
FORTUM Case 1		1.40	critical global strain 0.01		
GRS Case 1	1.10			0.70	0.20
Case 2	0.52			0.66	1.28
IRSN/CEA Case 1	0.82	1.00	Global strain = 0.3%	1.12	1.3
JPRG Case1(P+T)	1.04MPa 185C 30min	-	Local strain=6.8%	0.82MPa 176C 24min	0.89MPa 180C 26min
JPRG Case2(P+T)	0.31MPa 169C 298min	-		0.68MPa 512C 261min	0.91MPa 233C 1651min
Final **KOPEC Case 1**	0.81MPa	1.20MPa	max. strain=1.0%	0.88MPa	1.03MPa
KOPEC Case 2	0.19MPa	0.46MPa	max. strain=1.0%	0.788MPa	0.59MPa
NRC/SNL/DEA	1.10** 245°C 2200min	1.28 299°C 3160min	Local strain ~30%; (1.5 x incr. For temp.) extrapolation from earlier local analysis occurs at global strain = 1.11%	1.13 248°C 2280min	1.10 245°C 2200min
SCANSCOT Case 1	1.015MPa 29,55min 184°C	1.3MPa 37,6min 194°C	max principal strain localy>2%	0.872MPa 25.34min 178°C	1.015MPa 29.55min 184°C
SCANSCOT Case 2	**compression** 0.780MPa 260.6min 508°C **tension** 0.400MPa 276.4min 253°C	1.33MPa 3600min 316°C	max principal strain localy>2%	0.78MPa 260.6min 508°C	0.78MPa 260.6min 508°C

Table 5.7 Phase 3- Pressure Only Results Summary: Tendon Strains

(Pressures in MPa)

Participant	Hoop Tendon Strain			
	Yield	2%	Rupture	Criteria
Final **BE/HSE/NNC**	1.16		1.40	Hoop tendon strain of 0.34% at the maximum SFMT pressure in tendon H53
EDF				
Final **EGP**	1.25	1.53	1.25	reaching of yield stress
Final **FORTUM**			1.60	0.0119 strain
GRS	1.25	1.44	1.50	estimated tendon failure based on 3.3% failure strain
IRSN/CEA Case 1	0.88			
Final **JPRG**				Local strain=8%
Case1	1.21MPa 35min	1.44MPa 42min	-	
Case2	1.20MPa 2597min	-	-	
Final **KOPEC**	1.43MPa -	1.48MPa -	1.51MPa	max. strain=1.0%
Final **NRC/SNL/DEA**	1.18	1.35	1.42	2.00%
Final **SCANSCOT**	1,2MPa	1,32MPa	1,38MPa	Failure strain=3,8%

Table 5.8 Phase 3- Pressure/Temperature Results Summary: Tendon Strains

(Pressures in MPa)

Participant	Hoop Tendon Strain			
	Yield	2%	Rupture	Criteria
BE/HSE/NNC Case 1	0.96 Assumed yield strain of 0.2% obtained from tendon testing at SOL50		1.50	Hoop tendon strain of 0.34% at the maximum SFMT pressure in tendon H53
EGP case 1	>1.2 End of analysis at 1.2MPa			
FORTUM Case 1			1.69	0.0123 strain
GRS Case 1	1.30	1.40	1.50	estimated tendon failure based on 3.3% failure strain
Case 2	1.26			
IRSN/CEA Case 1	0.88			
JPRG Case1(P+T)	1.20MPa 191C 35min	1.44MPa 199C 42min	-	Local strain=8%
JPRG Case2(P+T)	1.18MPa 263C 2459min	-	-	
Final **KOPEC Case 1**	1.41MPa	1.46MPa	1.47MPa	Failure strain=3%
KOPEC Case 2	-	-	-	Failure strain=3%
NRC/SNL/DEA	1.15 254°C 2360min	1.30 302°C 3240min	1.33 310°C 3600min	2.00% (tendon temps not high enough to affect ductility)
SCANSCOT Case 1	1.227MPa 35.6min 192°C	1.38MPa 39.9min 197°C	1.449MPa 41.91min 199°C	Failure strain=3.8%
SCANSCOT Case 2	1.223MPa 2720min 277°C	P>1.33MPa	P>1.33MPa	Failure strain=3.8%

Table 5.9 Phase 3- Pressure Only Results Summary: Failure Predictions

(Pressures in MPa)

Participant	Pressure @ Failure	Free Field Hoop Strain @ Failure*	Max Radial Displacement @ Failure*	Failure Mode
Final **BE/HSE/NNC**	1.10 1.40	0.12% Mechanical strains at SOL39 @0.98Mpa	38.8mm Displacement at SOL 14 @1.295Mpa	Liner tearing causing high leakage rates Hoop tendon failure
EDF				
Final **EGP**	1.25	0.30%	16mm 27mm	global around EH
Final **FORTUM**	1.60		11.84 mm near E/H	loss of convergence in numerical solution algorithm
Final **GRS**	1.50	3.30%	200mm	Hoop tendon failure
IRSN/CEA Case 1				
Final **JPRG**				
Case1	-	(2.17%) EL.6.36m	(62.2mm) 135deg,EL.6.93m (107.0mm) near A/L	All steel materials don't reach critical strain. ( )Maximum value at the final step
Case2	-	(1.07%) EL.6.36m	(31.9mm) 135deg,EL.7.04m (51.1mm) near E/H	All steel materials don't reach critical strain. ( )Maximum value at the final step
Final **KOPEC**	1.51MPa	Failure strain=3%	113.9mm over	Tendon Failure Strain 3.0%
Final **NRC/SNL/DEA**	1.33**	0.74%	40 mm	Many liner tears near cylinder mid-height
Final **SCANSCOT**	1,38MPa	2.10%	91mm	Tendon failure HTD 38

Table 5.10 Phase 3- Pressure/Temperature Results Summary: Failure Predictions

(Pressures in MPa)

Participant	Pressure @ Failure	Free Field Hoop Strain @ Failure*	Max Radial Displacement @ Failure*	Failure Mode
BE/HSE/NNC Case 1	1.25	0.06% Mechanical strains at SOL39 @0.98Mpa	49.4mm Displacement at SOL 14 @1.295Mpa	Liner tearing causing high leakage rates
	1.50			Hoop tendon failure
EDF				
EGP case 1	>1.2 End of analysis at 1.2MPa			
FORTUM Case 1	1.69		16.94 near E/H	Hoop Tendon failure negative stiffness appearance in element stiffness matrix
Final **GRS Case 1**	1.50	2.9%	160 mm	Hoop tendon failure (failure strain 3.3%)
Case 2				no indication of failure at last load step with 1.3 MPa
IRSN/CEA Case 1				
JPRG Case1(P+T)	-	(2.24%) EL.5.69m	(70.0mm) 135deg,EL.6.93m (122.6mm) near A/L	All steel materials don't reach critical strain. ( )Maximum value at the final step
JPRG Case2(P+T)	-	(1.18%) EL.6.36m	(31.9mm) 135deg,EL.6.81m (73.5mm) near E/H	All steel materials don't reach critical strain. ( )Maximum value at the final step
Final **KOPEC Case 1**	1.47MPa	3% @ El. 6.2m	113.9mm over	Tendon Failure Strain 3%
KOPEC Case 2	-	-	-	Tendon Failure Strain 3%
NRC/SNL/DEA	1.28 299°C 3160min	1.11% at free-field Elev. 6.2 m	60 mm	1. Many liner tears near cylinder midheight. 2. Possible local failure at a piping penetration due to thermal deformation discontinuity
SCANSCOT Case 1	1.449MPa 41.91min 199°C	3%	134mm	Tendon failure HTD30
SCANSCOT Case 2	P>1.33MPa			No tendon rupture to low pressure

6. SUMMARY

The work reported herein represents, arguably, the state of the art in the numerical simulation of the response of a prestressed concrete containment vessel (PCCV) model to the pressure and thermal loads, normally associated with severe accidents, up to failure. A significant expenditure of time and money on the part of the sponsors, contractors, and ISP participants was required to meet the objectives. While it is difficult to summarize the results of this extraordinary effort in a few paragraphs, the following observations are offered for the reader's consideration:

(Note: These observations by the ISP coordinator, Sandia National Laboratories, and other participants do not necessarily represent the consensus of all the participants.)

6.1 Phase 2 Results

- The figures in Appendix A include the LST post test analysis results in comparison with LST and SFMT results. Most of the calculations show results beyond the maximum pressure achieved in the LST. These results were used to estimate the failure pressures for the liner, the tendons and the rebar, partly summarized in Table 4.3.
- The analysis models used by the ISP participants vary in complexity. Most are complex 3D finite element models which include geometric in-homogeneities, especially due to penetrations in the containment wall. Some axisymmetric models represent the containment behavior only far away from the penetrations. The manner of considering the penetrations is one source of discrepancy between the analysis results.
- Most of the comparison plots in Appendix A demonstrate that there is good agreement between the calculated and measured response of the model up to approximately twice the design pressure, P_d. This is the pressure where extensive hoop cracking has occurred, with the associated loss of stiffness, and yielding of the metallic components (tendons, rebar and liner) is starting to occur. Once generalized non-linear behavior begins to occur, agreement between the analytical results and the experimental data degrades. This may be due to the treatment of non-linear material behavior for the concrete, rebar, tendons and liner. Some cases which show poor agreement, even at pressures below $2P_d$, when the structure is still essentially elastic require further investigation to explain the differences. These may be examined in more detail during Phase 3.
- Displacements:
  - The global deformations and strains of the model containment, especially in regions far away from penetrations, are simulated quite well by axisymmetric models as well as full 3D models. 3D-models are necessary for simulation of local behavior in the vicinity of perturbations like the air lock, the equipment hatch, the main steam, the feedwater penetrations and the buttresses.
  - An axisymmetric model does not capture correctly the response of the dome.
  - The most accurate estimates of the global hoop strain are obtained from the average radial displacements at a given elevation (divided by the radius).
- Rebar strains:
  - The rebar strains compare less favorably (than the displacements) with analyses. This is primarily due to the difficulties in making point-to-point comparisons when local perturbations in the structure are not known or accurately modeled. Some differences also result from local perturbations resulting from the installation of the strain gages themselves.

- The meridional rebar strains at the wall-base junction appear to capture the bending response.
- The rebar strains at the mid-height of cylinder are consistent with displacement based strains.

- Liner strains:
  - For the locations compared in Appendix A, there is, in general good agreement between the calculated and experimental results, at least up to $2P_d$. Beyond this pressure the comparison is less favorable. (Note: Other data [1] not included in this report suggests that near geometric perturbations in the liner, where strain concentrations are present, the comparison between analysis and test results is less favorable, even at low pressures. This may be partially due to the assumptions and level of detail in the modeling of the liner and anchorage.
- Tendon strain/force:
  - In general the calculated change (increase) in tendon strain/force resulting from pressurization of the model are consistent and in agreement with test results.
  - In some cases there is significant variation in the initial tendon strains and forces due to the application of the prestressing. This is likely due to the assumptions and approach to applying the prestressing forces and modeling the interaction between the unbonded tendons and the concrete structure. These differences are hidden, to a large extent, in the comparison plots in Appendix A, since most of the calculated results were initialized to match the data at the onset of pressurization. Nevertheless, since the total response is critical to establishing failure limits, these initial variations are important and should not be ignored.
  - It appears that the effect of the pressure loading has much less influence on the vertical tendons than the hoop tendons and the hoop tendons are more highly stressed by pressure loading up to failure.
- Cracking:
  - Most of the analyses demonstrate that the formation of cracking in the concrete starts at about 1.5 P_d. One of the consequences is that the dependence of radial displacement (e.g. Fig. A-6) on pressure becomes nonlinear. This effect is in agreement with measured results.

6.2 Phase 3 Results

In general, the observations for the Phase 2, pressure only, results apply to the Phase 3 results. In addition, we can provide some observations regarding the two questions which were posed for Phase 3:

With addition of temperature, would the onset of leakage occur later in the pressure history and, possibly, closer to the burst pressure?

- Based on the results of Phase 3, no final conclusions can be drawn regarding whether the addition of temperature accelerates or retards failure of the vessel. Results predict failure, whether due to liner tearing or tendon rupture, at both lower and higher pressure when temperature is considered.

- The margin between leak and rupture does not appear to change significantly for the cases considered, i.e. the pressure differential between leak and rupture remains approximately constant even though the values may increase or decrease.

- The changes in 'failure' pressures, whether leak or rupture, are generally small (<10%) for the cases considered.

- Consideration of 'realistic' severe accident scenario (Case 2) might yield a lower 'failure' pressure than saturated steam conditions. While the results are not conclusive, they suggest that estimates of containment capacity based on saturated steam conditions only, may be unconservative, and more realistic scenarios might need to be considered.

- Effects of material degradation are significant for 'realistic' severe accident scenarios.

How would including the effect(s) of accident temperatures change the prediction of failure location and failure mode?

- While leak or rupture pressures are not significantly changed, both vertical and radial displacements are significantly greater when thermal loading is included, especially when considering material property degradation.

- A consequence of this result is that failure at penetrations, which are more susceptible to differential displacement, may be more likely, and may control under combined pressure and temperature loading.

Since there was no broad consensus on the conclusions to be drawn from these analyses, the conclusions of the individual participants are summarized in the following sections. More extensive discussion of these conclusions is included in the individual reports in the appendices.

6.2.1 British Energy/ Health & Safety Executive-Nuclear Installations Inspectorate/NNC Ltd.

- The elevated temperatures induce significant thermal expansion of the steel liner. The thermal straining of the liner results in rupture at approximately 1.25MPa. This is 14% higher than the rupture pressure of 1.1MPa obtained from the mechanical loading of the limit state test.

- The pre-loaded tendons are well insulated from the peak temperatures experienced in the accident transient. From the analysis results, the pressure required to induce tendon failure increases from 1.4MPa to approximately 1.50MPa. This is an increase of 7% compared to the limit state test. However, the modelling assumption of no sliding in the hoop tendons prevents load redistribution. Therefore, it can be concluded that in this case thermal loads do not change the pressure at tendon rupture.

- For the accident condition investigated, liner rupture is the initial failure mode. The design intent of liner rupture before catastrophic failure of the containment is maintained.

- If the margin between tendon failure and liner rupture is defined as the ratio of vessel pressurization required to cause the failures, the margin decreases from 1.27 for pressure only to 1.2 for pressure plus temperature loads.

- The temperature dependent effect of TTC in concrete is simulated using an effective modulus approach. For the accident condition investigated TTC is shown to have a small effect on PCCV strain distributions, but reduced vessel displacements are witnessed.

6.2.2 Energoprojekt Praha, UJV Rez. Div.

Commentary on model:

- the model used for the analysis describes global behavior of the structure altogether well especially for case 1 loading. Results of case 1 analysis for only pressure loading show better fit at the lower pressure with the test results in comparison with the Phase II analysis results. Reason is using of Abaqus/Standard analysis type in real time (a pseudo time sets in previous Abaqus/Explicit analysis was short and the results were affected by dynamic effects). Disadvantage is worse fit of results at higher pressure due to added small permanent stiffness of concrete elements.

- for the case 2 loading analysis there would be better to change the element mesh and use more elements across the wall thickness. The four linear elements used in current model are too coarse considering temperature gradient across the wall thickness.

- a global model is able to simulate behavior of the structure from strength point of view. But there is need to create detail models to analyze liner behavior and its tightness ability along with the liner anchors.

Commentary on results and results evaluation:

- comparison of the results of temperature-pressure loading analysis with the results of pressure loading analysis shows that temperature loading with the temperature gradient across the wall close to uniform is more favorable. On the other hand, long term high temperature loading causes temperature degradation into higher depth of wall. Rapid changes of temperature in containment are the most dangerous for liner, response of the rest of structure is suppressed by thermal capacity of structure material.

- the temperature degradation effects weren't too important in analyzed loading cases. Degradations of concrete have low effect due to tensile acting of concrete - pressure loading history corresponds to temperature loading history so there is high pressure at higher temperatures. Temperature degradation of steel has no effect in the case 1 loading due to low temperature. In case 2, there is considerable effect on liner during hydrogen detonation but due to relatively short time period of this loading there is no temperature degradation of rebar or tendons. Temperature degradation at final part of case 2 loading history could affect inner rebar row but the corresponding pressure loading is at the bearing capacity of the structure and likely there will be the structure failure before the temperature degradation could affect the rebar.

- beyond the direct influence of the temperature on degradation of material properties there are additional effects, e.g. thermal spalling of concrete at higher heating rates or redistribution and decrease of thermal stress in concrete. Simulation of these effects is more complicated (in global models) so it is difficult to include there direct into analysis. On the other hand, influence of thermal spalling of concrete is possible do decrease for example by applications of polypropylene fibers – higher temperature destroy the fibers and porosity of the concrete increases.

- the analysis results shows that the temperature couldn't change the failure mode of the structure significantly and, especially for long term thermal loading, the pressure will be the critical loading. On the other hand, thermal loading with fast changes of inner temperature is the critical loading for liner.

6.2.3 Fortum Nuclear Services Ltd.

(No written conclusions were provided.)

6.2.4 Gesellschaft für Anlagen und Reaktorsicherheit mbH

- The analyses results for Case 1 and Case 2 in terms of displacements show significant differences compared to the Phase 2 results (internal pressure only). Due to the temperature gradients in the wall, the displacement results of Phase 3 Case 1 are higher than the Phase 2 values, independent of the pressure about 5-10 mm for the radial displacements and increasing, up to 20 mm, for the vertical displacements.

- First extended regions of axial micro-cracks in the concrete are found for Case 1 at low pressure values, as e.g. for a pressure of 0.2 MPa, where a part of the wall thickness is cracked in the complete model starting from the outer surface. With increasing pressure micro-cracks penetrate the whole wall. At about 0.66 MPa the first formation of complete through wall arrangements of axial micro-cracks is calculated. At the transient load step with 1.14 MPa internal pressure almost all concrete parts of the model have micro-cracks which may cause leaks.

- Strains in the liner, the rebars and the concrete of the cylindrical part close to the inner and outer surface also show significant differences to the pressure only results, while the tendons near the middle of the wall show strains which are very similar to the pressure only values in the regions where comparison is possible. With the exception of the temperature and pressure peak of Case 2 the tendon results are very similar to Case 1 and the pressure only case. Obviously the tendons, which are located near the middle of the wall, are not significantly influenced by the thermal gradients. This means that the containment failure in terms of rupturing of the tendons is not changed by the additional temperatures. On the other hand the additional compressive stresses near the inner wall and tensile stresses near the outer wall caused by the thermal gradients strongly influence the behavior of the liner and the concrete cracking.

- For the pressure only case and the temperature Case 1, failure of the containment model due to rupture of circumferential tendons assumed at a failure strain of 3.3% is predicted at an internal pressure of about 1.45-1.50 MPa without consideration of geometric inhomogeneities due to penetrations in the wall. The calculated strains in some of the rebars show plastification, but the final values are below the critical ones with a sufficient margin.

- Due to the lower end pressure the results of the Case 2 calculations show that, although some plastification in the rebars occurs, the maximum strain values are sufficiently below critical values. For instance the maximum hoop tendon strain is below 1%. It is expected that critical strains in the tendons are reached if the transient, which is presently limited to 1.33 MPa at 60 h, is extrapolated with increasing pressure to further 25 h up to about 1.5 MPa.

6.2.5 Institut de Radioprotection et de Sûreté Nucléaire/Commissariat a l'Energie Atomique

(No written conclusions were provided.)

6.2.6 Japan PCCV Research Group

Liner tearing strain:

- The maximum strain of the liner for Case 1 with temperature is almost the same as that for pressure only. The temperature has little influence on the liner tearing pressure.

- The maximum strain of the liner for Case 2 with temperature is smaller than that for pressure alone. When temperature is included, liner tearing occurs at a higher pressure than for pressure alone.

Ultimate pressure:

- Since the strains of the hoop tendon become critical for Case 1, regardless of whether temperature is included, it is predicted that the structural failure for both occurs due to the rupture of the hoop tendon. Moreover, since the maximum strains of the hoop tendon are almost the same regardless of the temperature, the temperature has also little influence on the ultimate pressure. For Case 1, liner tearing precedes the occurrence of the structural failure due to the rupture of the rebar or tendon regardless of the thermal loading.

- For Case 2 with pressure only, the strains of the hoop tendon and the outer rebar reach critical at almost the same pressure. When temperature is included, the strain of the outer rebar becomes critical first. Structural failure occurs when the hoop tendon or the outer rebar rupture. Structural failure occurs at lower pressure when temperature is included.. When only pressure is considered liner tearing precedes structural failure, however when temperature is included structural failure occurs precedes liner tearing.

The scale effect in thermal stress analyses:

- In this study, the temperature distributions in the section obtained from the heat transfer analyses by a full-scale model are applied to the 1:4-scale model. Therefore, although the average temperature and the gradient of the 1:4-scale model are equal to those of the full-scale model, the thermal slope of the equivalent liner temperature of the 1:4-scale model is four times as that of the full-scale model because the wall thickness is one fourth.

- The thermal effect to the rupture of the PCCV is caused by addition of the thermal strain in case the change in the critical strain of the steel materials by heat is sufficiently small. The thermal strain in the 1:4-scale model may be as same as that in the full-scale model if their gradients are the same. Consequently the thermal strains to be added in the both models are the same in the balanced conditions only by the steel materials near the ultimate state. It follows from this, that the scale effect on the thermal load may be small.

6.2.7 Korea Power Engineering Company

- The liners are appeared to be yielded and/or ruptured at higher pressure when temperature and pressure are simultaneously applied in comparison with those of pressure only.

- A combined mechanical-thermal analysis simulating a saturated steam condition (Case 1) shows that the temperature history starting with 100 °C created a sudden increase in displacements at initial stage, but the slopes expressing the pressure-displacement relationship with increasing temperature and pressure appeared very similar to the trend for the pressure only case.

- The analysis results for Case 2 shows that the displacements due to the sudden increase of temperature and pressure for a very short time period did not fully recover when returned to the starting temperature and pressure. This can be interpreted as a sort of residual deformation from damage to the liner plate and/or concrete portion due to instantaneous high temperature and pressure loading. The ultimate capacity, however, can be expected to go down suddenly and the deformation will suddenly rise to a high degree inducing divergence.

- The buckling stress considering the horizontal spacing of liner anchor(150.15mm) is calculated to 122.2Mpa and thus most of stresses of Case 1 and Case 2 appeared beyond the calculated buckling stress.

- Tendon strains under both temperature and pressure are increased in comparison with those under pressure only. Temperature has definitely an effect on the ultimate pressure capacity of PCCV.

6.2.8 US Nuclear Regulatory Commission/Sandia National Laboratories/David Evans and Associates

The axisymmetric analyses for 1:4 and full scale finite element models of the PCCV subjected to pressure and temperature, with and without material property degradation, have led to the following conclusions:

- All of the cases, including pressure only, begin at 25C (77F), but because Case 1 is for Saturated Steam, the temperature starts out at 100C (212 F), so the thermal response for Case 1 shows generally an immediate jump in deformation associated with temperature relative to the pressure-only case.

- The deformations associated with temperature are very significant, especially for vertical displacement. For radial displacement at cylinder mid-height, displacement with temperature at 3Pd and 185C, are nearly double those for pressure alone. For vertical displacement at cylinder top (springline) displacement with temperature and 3Pd is nearly 8-times the pressure only displacement. At full scale, the thermally induced displacements can be very large and may lead to piping and equipment interference problems.

- For Case 1, in all cases, the differences due to thermally induced material property degradation, are very minor, and this tends to justify the use of an approximate material property degradation approach, at least for Case 1 Temperature.

- The Case 2 analyses were much more numerically sensitive and difficult to run, especially to get through the temperature/pressure spike at about time=4hours.

- For Case 2, the temperature again induces large displacements, and the vertical displacements are quite large. Also, the vertical displacements are not significantly influenced by the material property degradation.

- For Case 2, the radial displacements are significantly influenced by the material property degradation. At the cylinder wall mid-height, the thermal solution with and without material property degradation track closely together out to ~35 hours, or P= 2.8 Pd / T=240C, but then begin to separate. By time=50 hours, P=3.2Pd / T=295C, the cylinder mid-height radial displacements are nearly double for the temperature/property degradation case over the pressure case, and are about 50% higher than the pressure + temperature case without property degradation.

- It appears that thermal and property degradation analysis in a Case 2 scenario would reduce the pressure causing failure of the vessel. It appears that "global" failure of the vessel would be reduced from the 3.6Pd that occurred in the SFMT to approximately 3.4Pd. And local liner failure pressure would be affected since these are "driven" by global displacements and liner strains.

- The final prediction summaries are shown in the table as requested for the ISP. The liner tearing "leakage" pressure reduces from pressure-only prediction of 1.33 MPa to 1.28 MPa.

6.2.9 Scanscot Technology

Comments on analysis and modeling technique:

- To capture the true behavior of the containment loading response, including the effects of "disturbed regions" such as pre-stressing buttresses and major penetrations, a global 3D-model has to be utilized. The global 3D-model could then be complemented with local, more detailed sub-models at important regions, such as major penetrations.

- The explicit FEA solver technique provides a powerful tool to perform non-linear quasi-static analysis of containment structures. When dealing with material non-linearities and problems involving contact, the explicit solver provides a more straightforward approach compared to the implicit solver. This due to the fact that convergence of non-linear analysis sometimes can be rather cumbersome using implicit solvers. The results from our structural analyses also verify that explicit solvers provide accurate results compared to experimental test data.

Pressure load analysis:

- The structural response predicted by applying a three-dimensional model approach agrees very well with registered test data. Pressure levels related to cracking of concrete, yielding of the steel liner, and the collapse of the containment are captured in conformity with registered test data. To capture the pressure level at which rupture of the steel liner occurs, more detailed local models are needed, this is beyond the scope of this report. However, the analysis methods are capable of catching the zones where excessive yielding of the steel liner occurs, corresponding well with the first registered liner rupture position. The applied analysis methods also accurately predict the displacements of the containment, and strains in the steel liner, the rebars and the pre-stressing tendons.

Pressure + temperature load analysis:

- For cases when a temperature load is applied simultaneously with the pressure load the response will be quite different compared to pressure load only. The load effect is dependent on the temperature scenario, i.e. the maximum value of the temperature, and the rate of the temperature changes. For the case 1 temperature load scenario, onset of global yielding in the liner is delayed, while the ultimate capacity is unchanged. For the case 2 scenario however, yielding first in compression, and then in tension, occurs at rather low pressure levels due to a combination of the rapid changes in temperature and high temperature values inside the containment, this giving rise to restrained temperature expansion/contraction of the steel liner.

- The temperature load increases the deformation of the containment due to an increase in mean temperature, while the temperature gradient gives rise to early cracking of the outside part of the concrete wall.

- The maximum load-bearing capacity of the containment can be decreased by the increase in temperature. This due to the fact that the strength of the steel material is decreasing at elevated temperatures. However, for the cases studied in this report, the stipulated strength-temperature dependency does not result in such a decrease in strength.

Comments on results

- The structural response predicted by applying a 3D-model approach agrees very well with registered test data (radial displacements, tendon forces, stress and strain levels etc). Also, pressure levels related to important events such as cracking of concrete, yielding of the steel liner, and the collapse of the containment are captured in conformity with registered test data. To capture the pressure level at which rupture of the steel liner occurs, more detailed local sub-models are needed. However, the analysis determines the zones where excessive yielding of the steel liner occurs, corresponding reasonable well with the first registered liner rupture position.

- For cases when a temperature load is applied simultaneously with the pressure load the response will be quite different compared to pressure load only. The load effect is dependent on the temperature scenario, i.e. the maximum value of the temperature, and the rate of the temperature changes.

- For the case 1 temperature load scenario, onset of global yielding in the liner is delayed, while the ultimate capacity is unchanged. For the case 2 scenario however, yielding first in compression, and then in tension, occurs at rather low pressure levels due to a combination of the rapid changes in temperature and high temperature values inside the containment, this giving rise to restrained temperature expansion/contraction of the steel liner.

- The temperature load increases the deformation of the containment due to an increase in mean temperature, while the temperature gradient gives rise to early cracking of the outside part of the concrete wall.

- The maximum capacity of the containment can be decreased by an increase in temperature. This due to the fact that the strength of the steel material is degraded at elevated temperatures. However, for the cases studied in this report, the stipulated strength-temperature dependency does not result in such degradation.

7. REFERENCES

1. Hessheimer, M. F., Klamerus, E. W., Rightley, G. S., Lambert, L. D. and Dameron, R. A., "*Overpressurization Test of a 1:4-Scale Prestressed Concrete Containment Vessel Model*", NUREG/CR-6810, SAND2003-0840P, Sandia National Laboratories, Albuquerque NM. March, 2003.
2. Luk, V. K., "*Pretest Round Robin Analysis of a Prestressed Concrete Containment Vessel Model*", NUREG/CR-6678, SAND00-1535, Sandia National Laboratories, Albuquerque, NM, August, 2000.
3. Mathet, E., "Proceedings of the International Standard Problem 48 Workshop on Containment Capacity", Lyon, France, April, 2005. NEA/CSNI/R(2005)7
4. "MELCOR Computer Code Manuals", NUREG/CR-6119, SAND2000-2417, Sandia National Laboratories, Albuquerque, NM, December, 2000.
5. Bazant, Z.P., Kaplan, M.F., "Concrete at High Temperatures – Material Properties and Mathematical Models," Concrete Design and Construction Series, Longman Group Limited, 1996.
6. Khoury, G.A., "Compressive Strength of Concrete at High Temperatures: a Reassessment," Magazine of Concrete Research, 1992, 44, No. 161, Dec., pp. 291-309.
7. Bamforth, P.B., "The Long-Term Properties of Concrete Used in Prestressed Concrete Pressure Vessels," Taywood Engineering Ltd., Southall, Middlesex, "Inspection and Structural Validation of Nuclear Power Generation Plant," held in London, 11/25/93.
8. Freskakis, G.N., et al, "Strength Properties of Concrete at Elevated Temperatures, "Civil Engineering Nuclear Power, Vol.1, ASCE National Convention, Boston. April, 1979.
9. DeFish-Price, C., et-al (Rockwell International Report), "Effects of Long-Term Exposure to Elevated Temperatures on the Mechanical Properties of Hanford Concrete," a construction Technology Laboratories Report for the U.S. Department of Energy Under Contract DE-AC06-77RL01030, October, 1981.
10. M. S. Abrams, "Compressive Strength of Concrete at Temperatures to 1600F," Temperature and Concrete, ACI SP-25, American Concrete Institute, pp. 33-58 (1971).
11. N. G. Zoldners, "Thermal Properties of Concrete Under Sustained Elevated Temperatures: ACI SP-25, American Concrete Institute, p. 1-32 (1971).
12. Sanad, A. M., "Development of Generalised Stress-Strain Relationships for the Grillage Models of Cardington Concrete Slab," University of Edinburgh, School of Civil & Environmental Engineering, PIT Project Report, December, 1999.

Appendix A: Phase 2 Comparison Plots at Standard Output Locations : A-1 to A-57

Page intentionally left blank

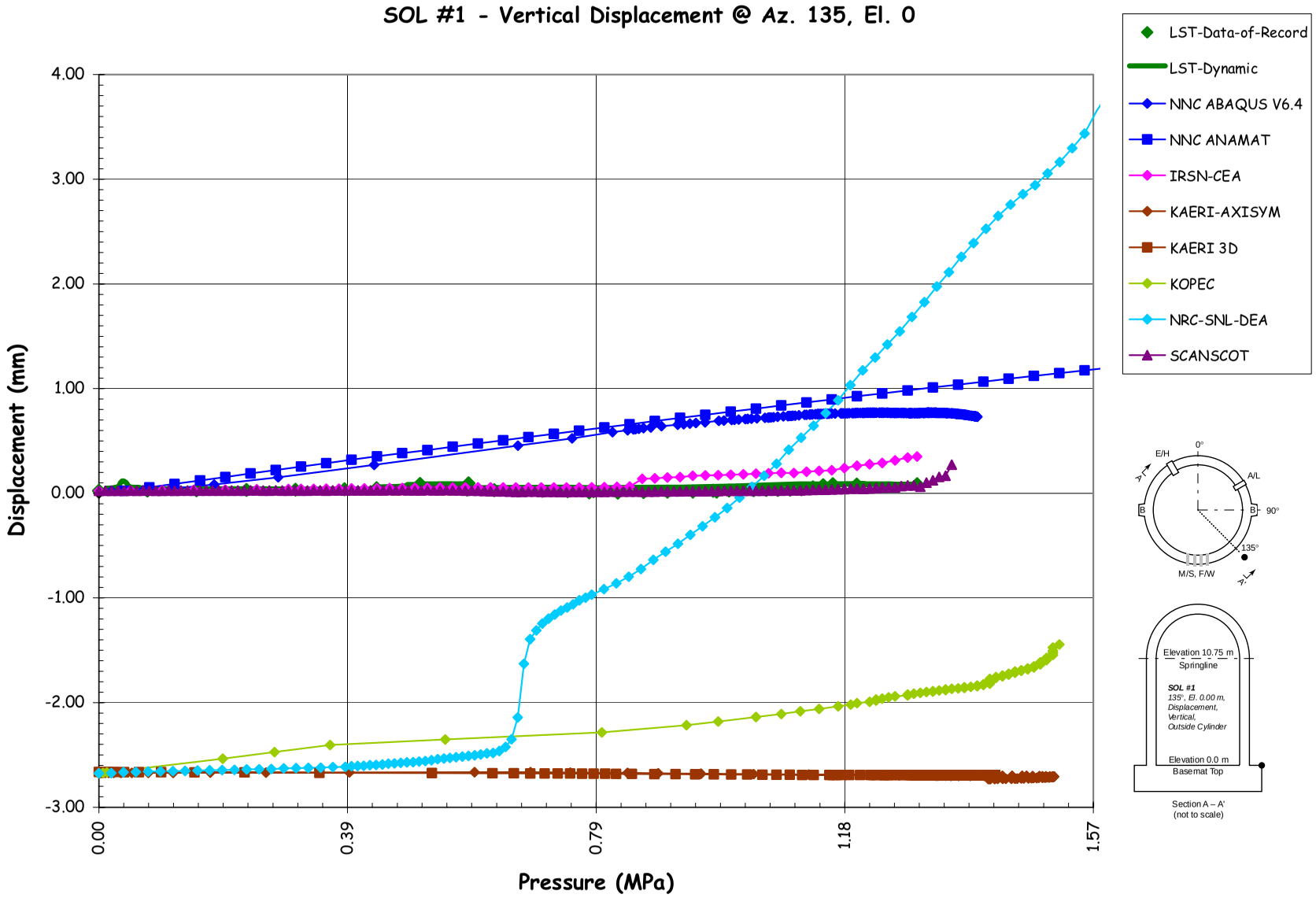
SOL #1 - Vertical Displacement @ Az. 135, El. 0
Displacement (mm)
4.00
3.00
2.00
1.00
0.00
-1.00
-2.00
-3.00
0.00
0.39
0.79
1.18
1.57
Pressure (MPa)
LST-Data-of-Record
LST-Dynamic
NNC ABAQUS V6.4
NNC ANAMAT
IRSN-CEA
KAERI-AXISYM
KAERI 3D
KOPEC
NRC-SNL-DEA
SCANSCOT
0°
E/H
A/L
B
B
90°
135°
M/S, F/W
Elevation 10.75 m
Springline
SOL #1
135°, El. 0.00 m,
Displacement,
Vertical,
Outside Cylinder
Elevation 0.0 m
Basemat Top
Section A – A'
(not to scale)

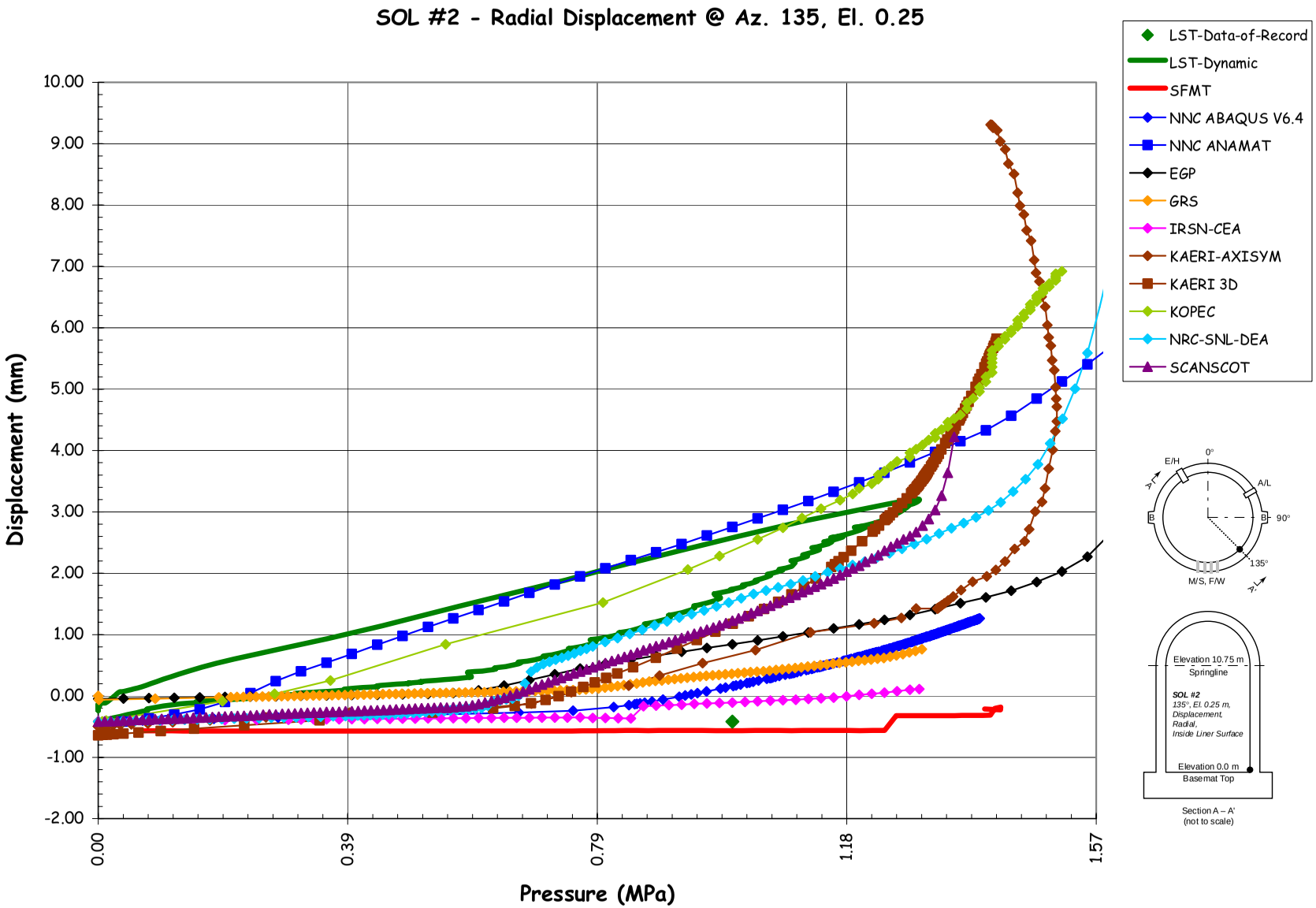
SOL #2 - Radial Displacement @ Az. 135, El. 0.25
Displacement (mm)
10.00
9.00
8.00
7.00
6.00
5.00
4.00
3.00
2.00
1.00
0.00
-1.00
-2.00
0.00
0.39
0.79
1.18
1.57
Pressure (MPa)
LST-Data-of-Record
LST-Dynamic
SFMT
NNC ABAQUS V6.4
NNC ANAMAT
EGP
GRS
IRSN-CEA
KAERI-AXISYM
KAERI 3D
KOPEC
NRC-SNL-DEA
SCANSCOT
0°
E/H
A/L
90°
135°
M/S, F/W
Elevation 10.75 m
Springline
SOL #2
135°, El. 0.25 m,
Displacement,
Radial,
Inside Liner Surface
Elevation 0.0 m
Basemat Top
Section A – A'
(not to scale)

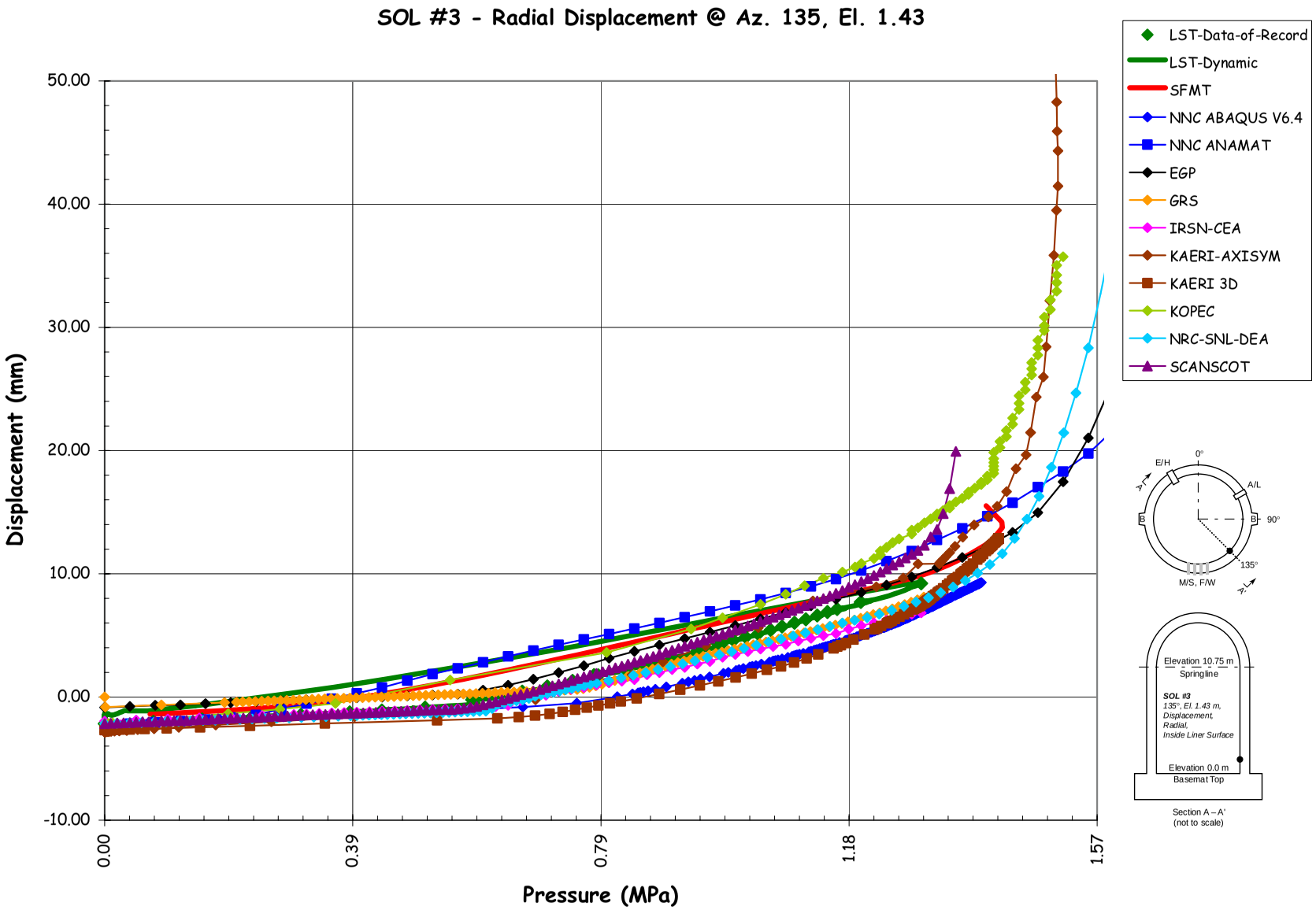
SOL #3 - Radial Displacement @ Az. 135, El. 1.43
Displacement (mm)
50.00
40.00
30.00
20.00
10.00
0.00
-10.00
0.00
0.39
0.79
1.18
1.57
Pressure (MPa)
LST-Data-of-Record
LST-Dynamic
SFMT
NNC ABAQUS V6.4
NNC ANAMAT
EGP
GRS
IRSN-CEA
KAERI-AXISYM
KAERI 3D
KOPEC
NRC-SNL-DEA
SCANSCOT
0°
E/H
A/L
B
B
90°
135°
M/S, F/W
A'
A'
Elevation 10.75 m
Springline
SOL #3
135°, El. 1.43 m,
Displacement,
Radial,
Inside Liner Surface
Elevation 0.0 m
Basemat Top
Section A – A'
(not to scale)

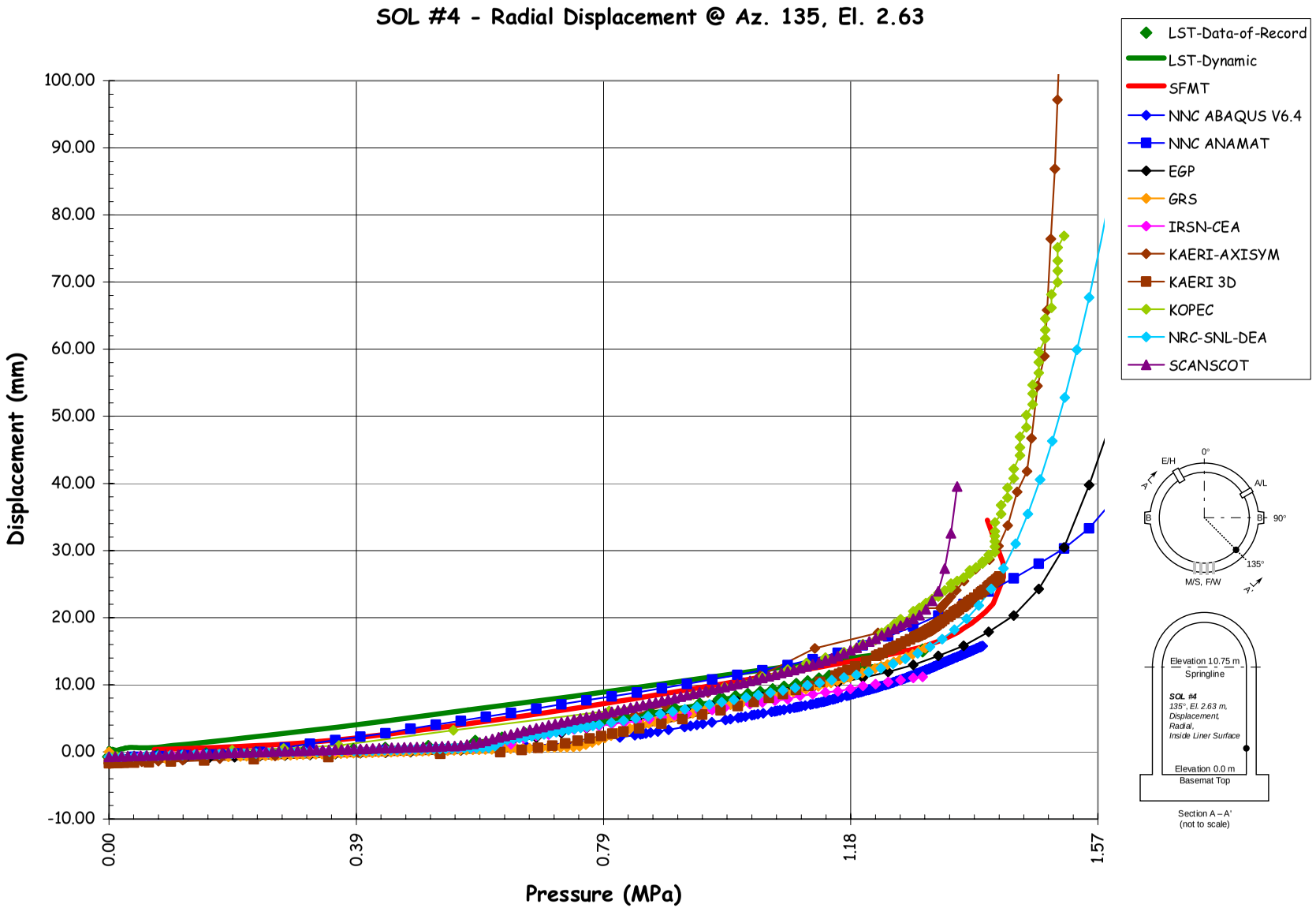
SOL #4 - Radial Displacement @ Az. 135, El. 2.63
Displacement (mm)
Pressure (MPa)
100.00
90.00
80.00
70.00
60.00
50.00
40.00
30.00
20.00
10.00
0.00
-10.00
0.00
0.39
0.79
1.18
1.57
LST-Data-of-Record
LST-Dynamic
SFMT
NNC ABAQUS V6.4
NNC ANAMAT
EGP
GRS
IRSN-CEA
KAERI-AXISYM
KAERI 3D
KOPEC
NRC-SNL-DEA
SCANSCOT
0°
E/H
A/L
90°
135°
M/S, F/W
Elevation 10.75 m
Springline
SOL #4
135°, El. 2.63 m,
Displacement,
Radial,
Inside Liner Surface
Elevation 0.0 m
Basemat Top
Section A – A'
(not to scale)

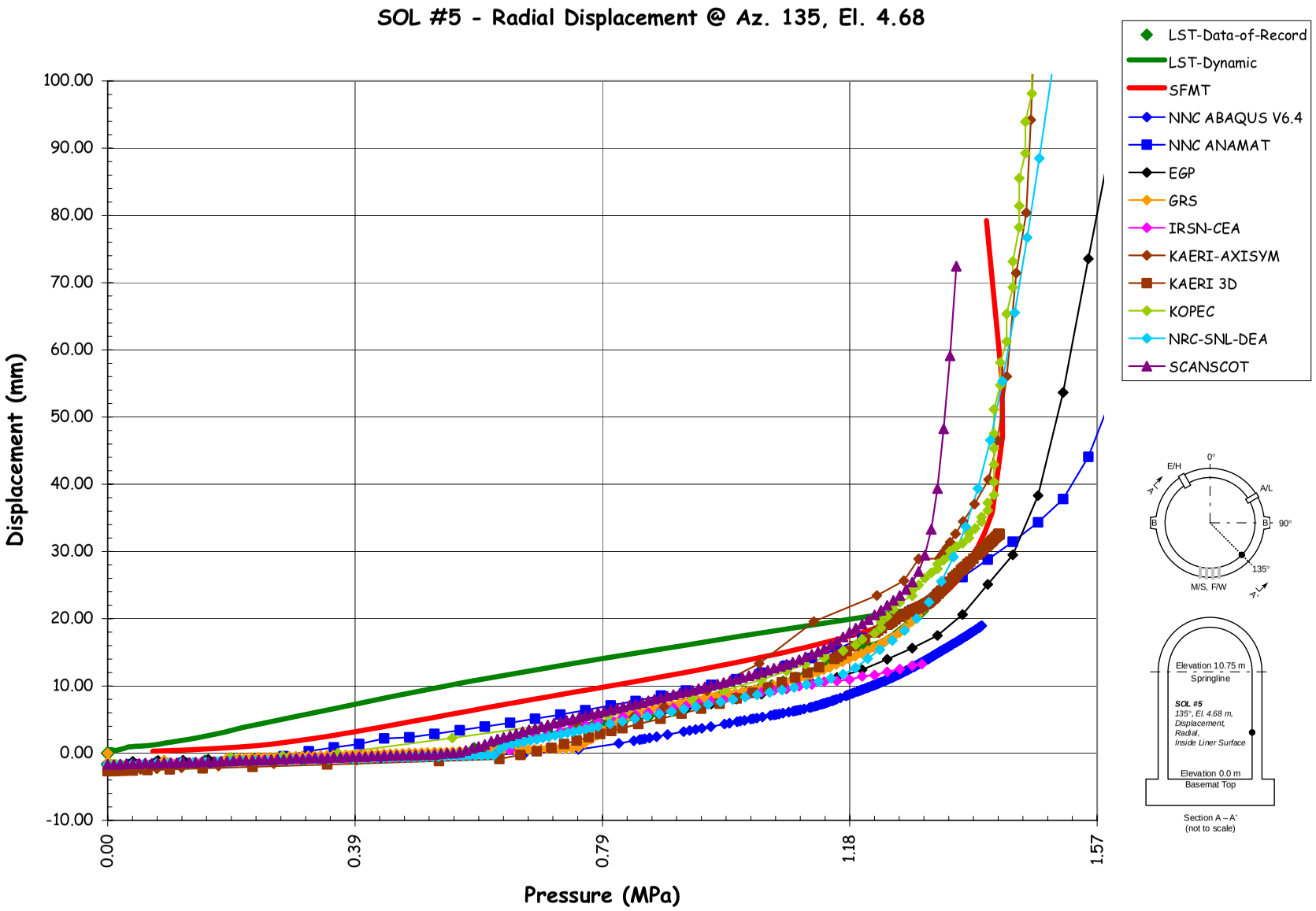
SOL #5 - Radial Displacement @ Az. 135, El. 4.68
Displacement (mm)
100.00
90.00
80.00
70.00
60.00
50.00
40.00
30.00
20.00
10.00
0.00
-10.00
0.00
0.39
0.79
1.18
1.57
Pressure (MPa)
LST-Data-of-Record
LST-Dynamic
SFMT
NNC ABAQUS V6.4
NNC ANAMAT
EGP
GRS
IRSN-CEA
KAERI-AXISYM
KAERI 3D
KOPEC
NRC-SNL-DEA
SCANSCOT
E/H
A/L
0°
90°
135°
M/S, F/W
Elevation 10.75 m
Springline
SOL #5
135°, El. 4.68 m,
Displacement,
Radial,
Inside Liner Surface
Elevation 0.0 m
Basemat Top
Section A – A'
(not to scale)

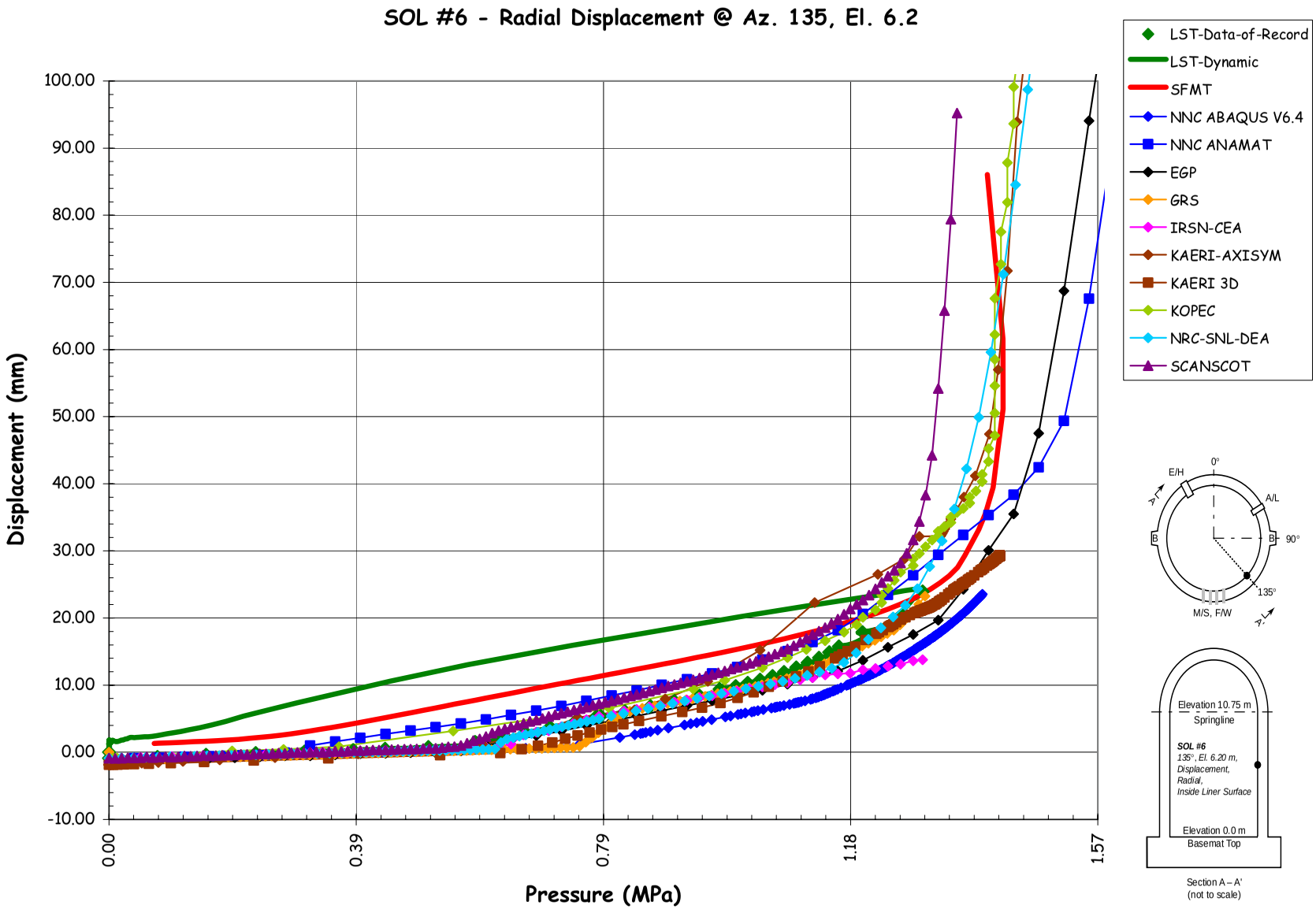
SOL #6 - Radial Displacement @ Az. 135, El. 6.2
Displacement (mm)
100.00
90.00
80.00
70.00
60.00
50.00
40.00
30.00
20.00
10.00
0.00
-10.00
0.00
0.39
0.79
1.18
1.57
Pressure (MPa)
LST-Data-of-Record
LST-Dynamic
SFMT
NNC ABAQUS V6.4
NNC ANAMAT
EGP
GRS
IRSN-CEA
KAERI-AXISYM
KAERI 3D
KOPEC
NRC-SNL-DEA
SCANSCOT
E/H
0°
A/L
B
B
90°
135°
M/S, F/W
Elevation 10.75 m
Springline
SOL #6
135°, El. 6.20 m,
Displacement,
Radial,
Inside Liner Surface
Elevation 0.0 m
Basemat Top
Section A – A'
(not to scale)

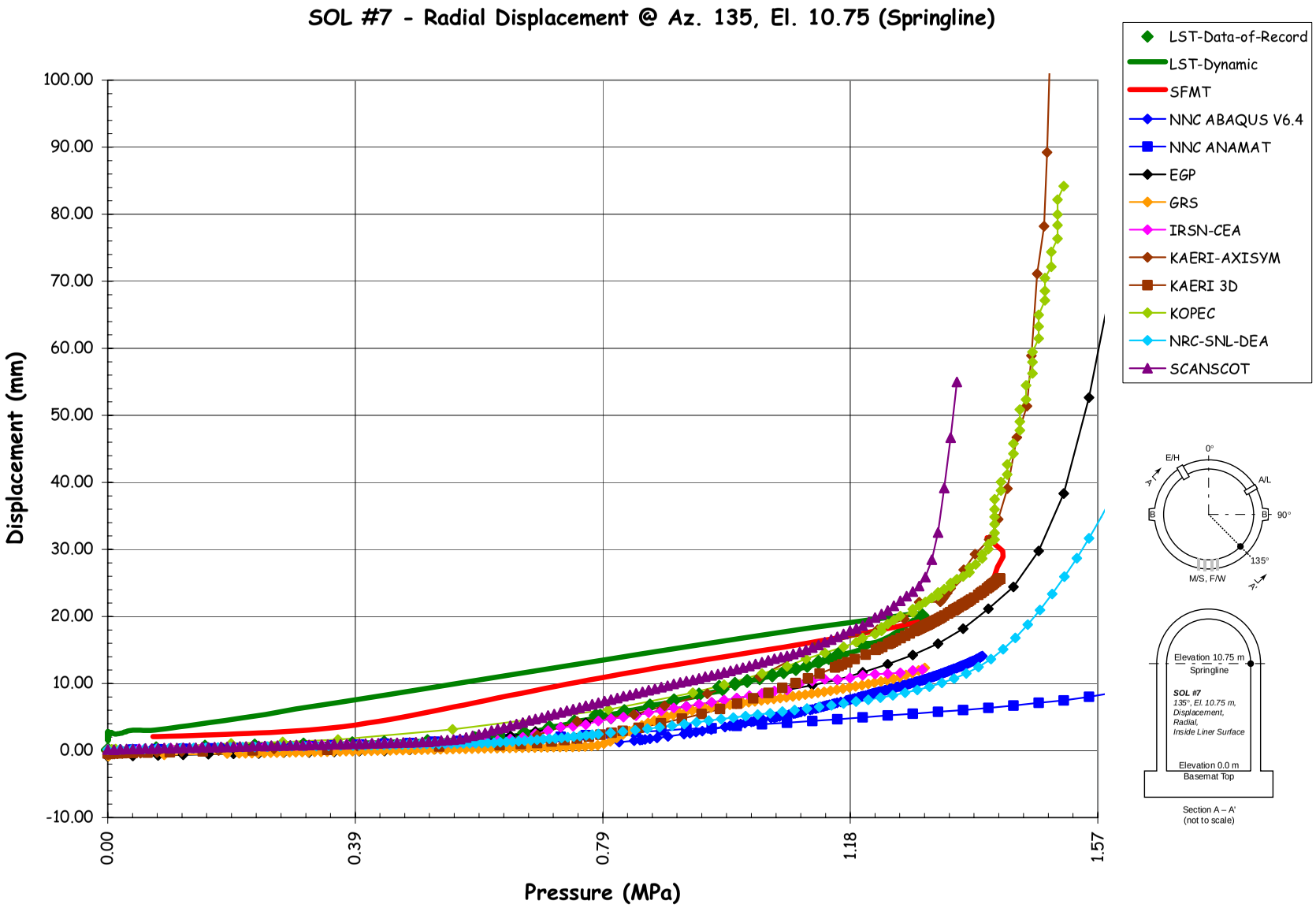
SOL #7 - Radial Displacement @ Az. 135, El. 10.75 (Springline)
Displacement (mm)
100.00
90.00
80.00
70.00
60.00
50.00
40.00
30.00
20.00
10.00
0.00
-10.00
0.00
0.39
0.79
1.18
1.57
Pressure (MPa)
LST-Data-of-Record
LST-Dynamic
SFMT
NNC ABAQUS V6.4
NNC ANAMAT
EGP
GRS
IRSN-CEA
KAERI-AXISYM
KAERI 3D
KOPEC
NRC-SNL-DEA
SCANSCOT
0°
E/H
A/L
90°
135°
M/S, F/W
Elevation 10.75 m
Springline
SOL #7
135°, El. 10.75 m,
Displacement,
Radial,
Inside Liner Surface
Elevation 0.0 m
Basemat Top
Section A – A'
(not to scale)

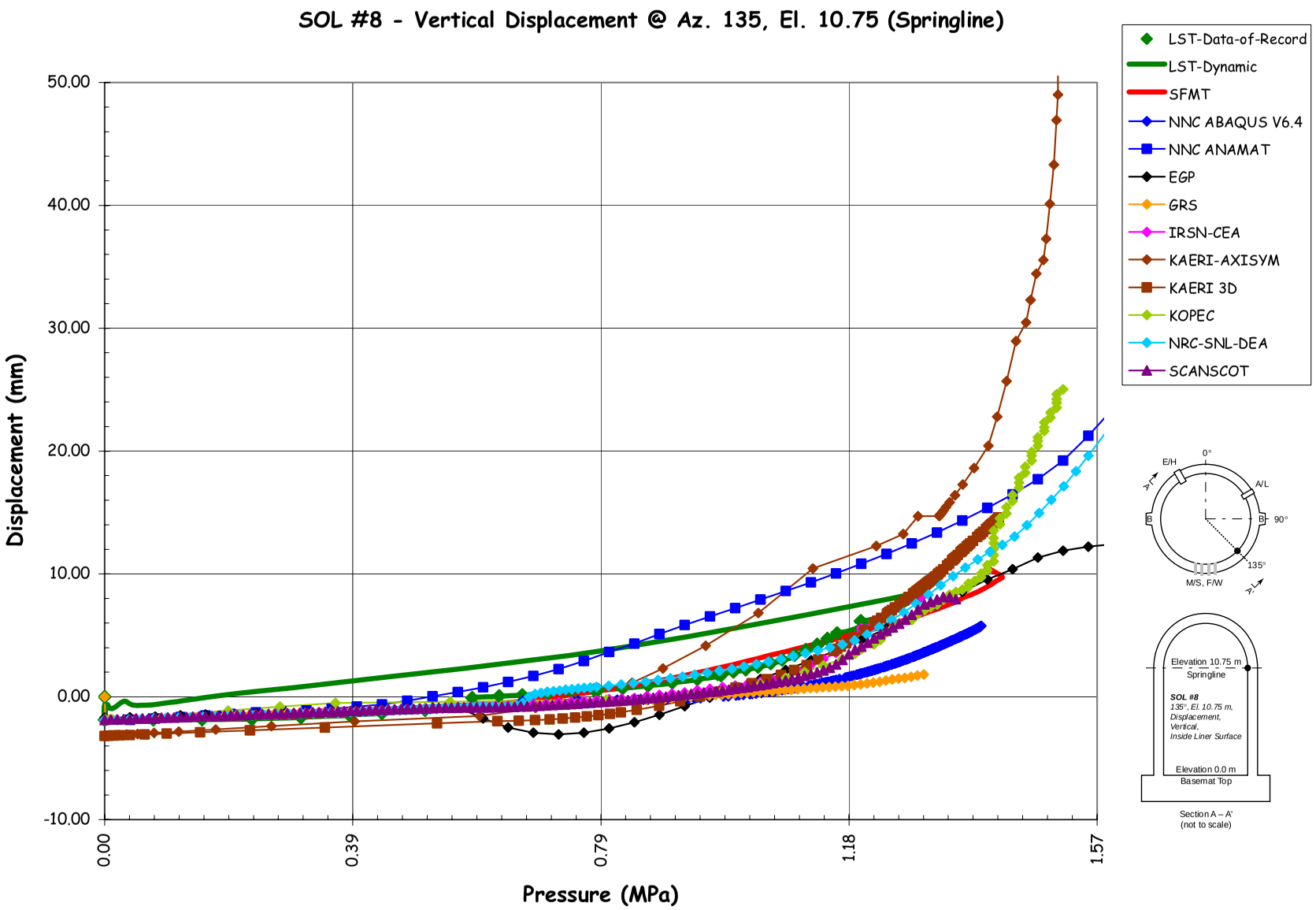
SOL #8 - Vertical Displacement @ Az. 135, El. 10.75 (Springline)
Displacement (mm)
50.00
40.00
30.00
20.00
10.00
0.00
-10.00
0.00
0.39
0.79
1.18
1.57
Pressure (MPa)
LST-Data-of-Record
LST-Dynamic
SFMT
NNC ABAQUS V6.4
NNC ANAMAT
EGP
GRS
IRSN-CEA
KAERI-AXISYM
KAERI 3D
KOPEC
NRC-SNL-DEA
SCANSCOT
0°
E/H
A/L
90°
135°
M/S, F/W
Elevation 10.75 m
Springline
SOL #8
135°, El. 10.75 m,
Displacement,
Vertical,
Inside Liner Surface
Elevation 0.0 m
Basemat Top
Section A – A'
(not to scale)

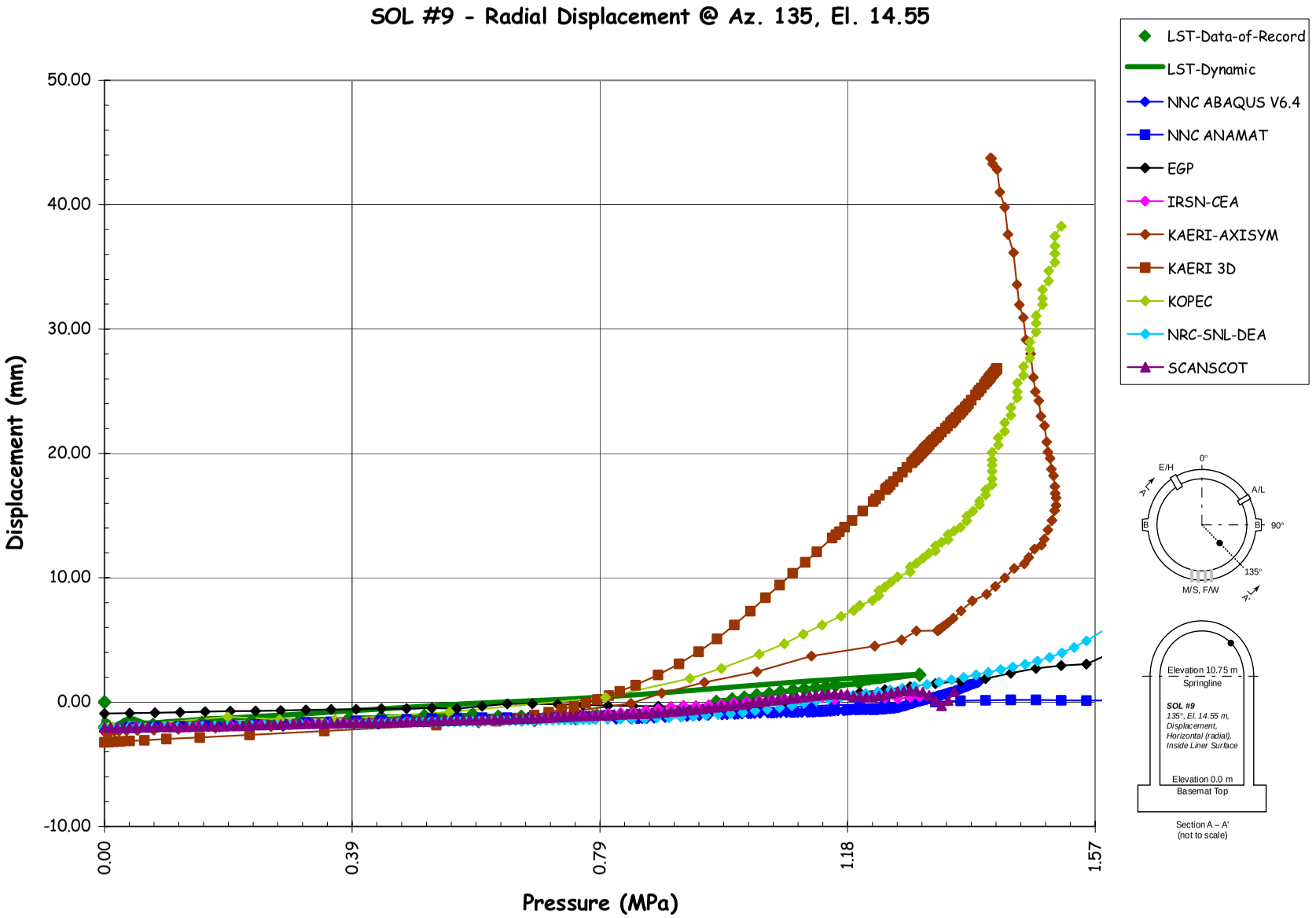
SOL #9 - Radial Displacement @ Az. 135, El. 14.55
Displacement (mm)
50.00
40.00
30.00
20.00
10.00
0.00
-10.00
0.00
0.39
0.79
1.18
1.57
Pressure (MPa)
LST-Data-of-Record
LST-Dynamic
NNC ABAQUS V6.4
NNC ANAMAT
EGP
IRSN-CEA
KAERI-AXISYM
KAERI 3D
KOPEC
NRC-SNL-DEA
SCANSCOT
E/H
0°
A/L
90°
135°
M/S, F/W
Elevation 10.75 m
Springline
SOL #9
135°, El. 14.55 m,
Displacement,
Horizontal (radial),
Inside Liner Surface
Elevation 0.0 m
Basemat Top
Section A – A'
(not to scale)

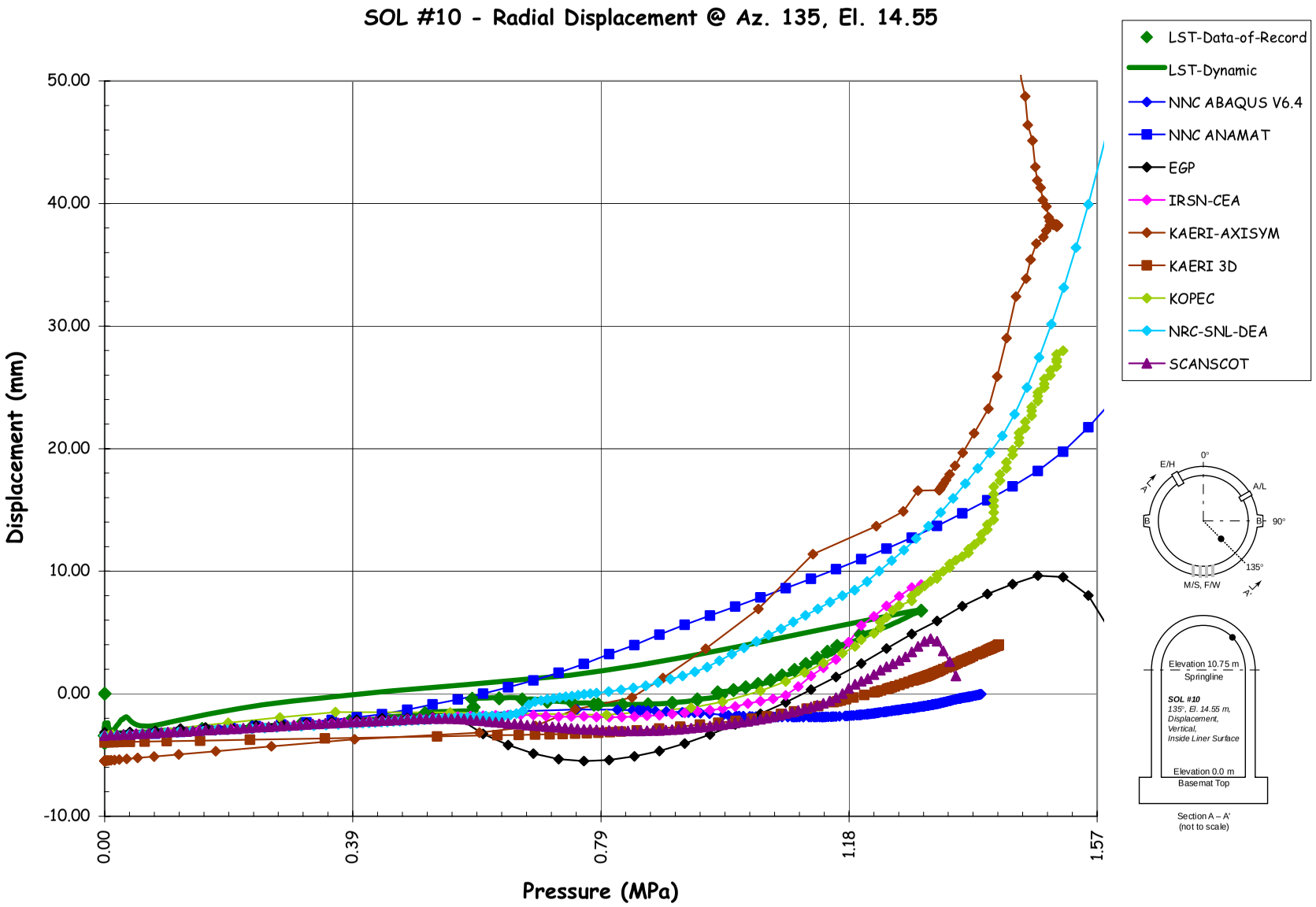
SOL #10 - Radial Displacement @ Az. 135, El. 14.55
Displacement (mm)
50.00
40.00
30.00
20.00
10.00
0.00
-10.00
0.00
0.39
0.79
1.18
1.57
Pressure (MPa)
LST-Data-of-Record
LST-Dynamic
NNC ABAQUS V6.4
NNC ANAMAT
EGP
IRSN-CEA
KAERI-AXISYM
KAERI 3D
KOPEC
NRC-SNL-DEA
SCANSCOT
E/H
0°
A/L
90°
135°
M/S, F/W
Elevation 10.75 m
Springline
SOL #10
135°, El. 14.55 m,
Displacement,
Vertical,
Inside Liner Surface
Elevation 0.0 m
Basemat Top
Section A – A'
(not to scale)

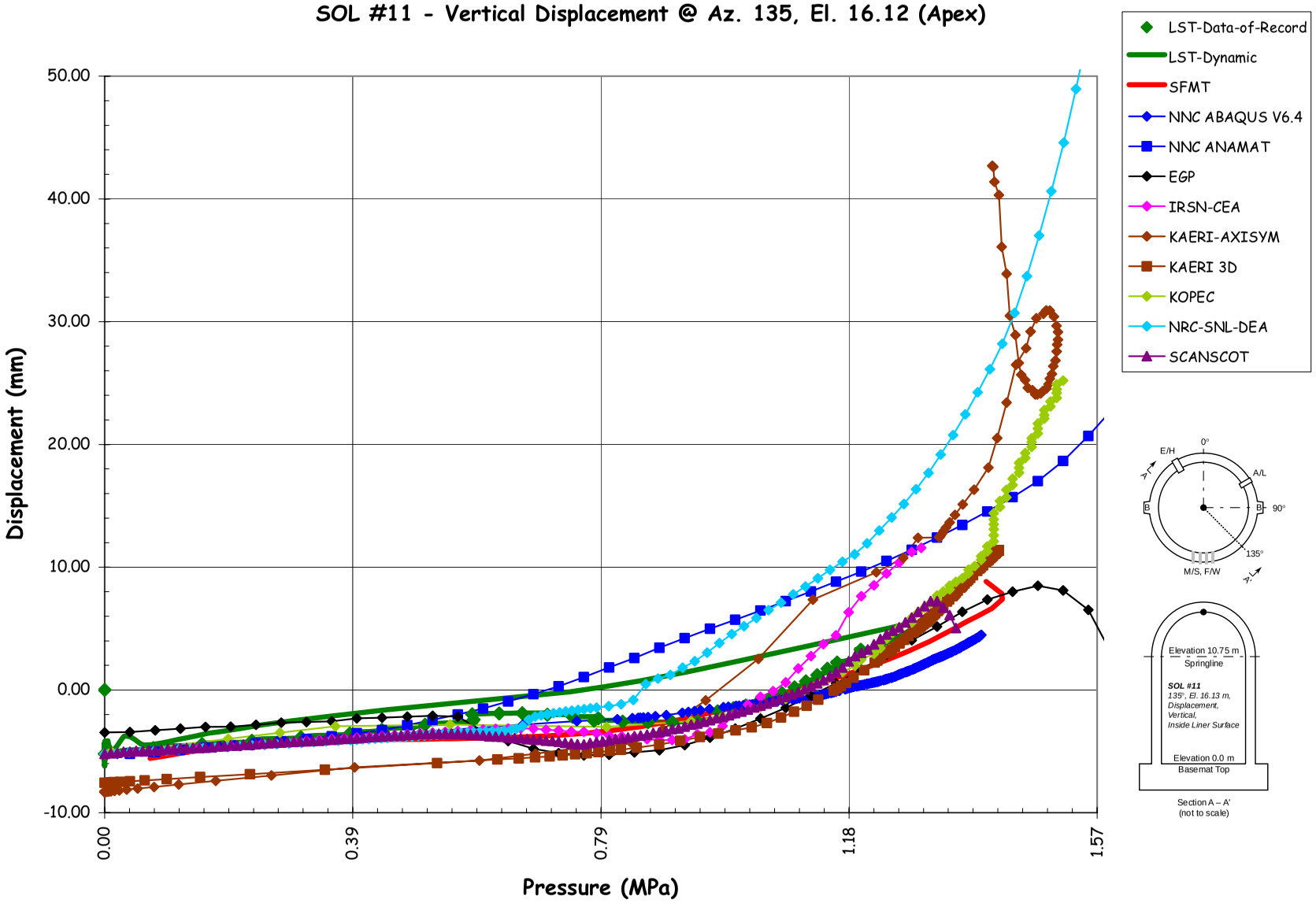
SOL #11 - Vertical Displacement @ Az. 135, El. 16.12 (Apex)
Displacement (mm)
50.00
40.00
30.00
20.00
10.00
0.00
-10.00
0.00
0.39
0.79
1.18
1.57
Pressure (MPa)
LST-Data-of-Record
LST-Dynamic
SFMT
NNC ABAQUS V6.4
NNC ANAMAT
EGP
IRSN-CEA
KAERI-AXISYM
KAERI 3D
KOPEC
NRC-SNL-DEA
SCANSCOT
E/H
0°
A/L
90°
135°
M/S, F/W
Elevation 10.75 m
Springline
SOL #11
135°, El. 16.13 m,
Displacement,
Vertical,
Inside Liner Surface
Elevation 0.0 m
Basemat Top
Section A – A'
(not to scale)

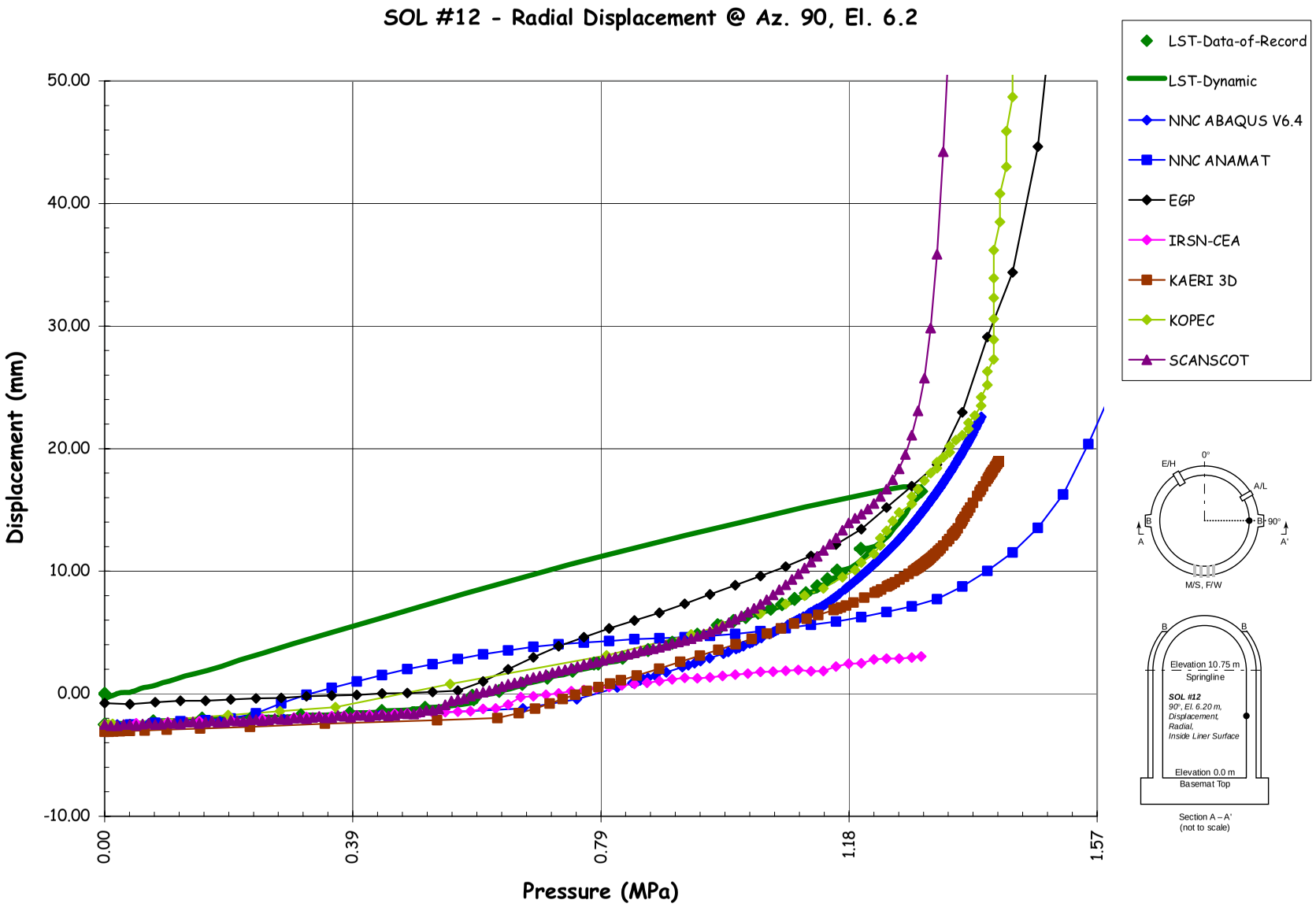
SOL #12 - Radial Displacement @ Az. 90, El. 6.2
Displacement (mm)
50.00
40.00
30.00
20.00
10.00
0.00
-10.00
0.00
0.39
0.79
1.18
1.57
Pressure (MPa)
LST-Data-of-Record
LST-Dynamic
NNC ABAQUS V6.4
NNC ANAMAT
EGP
IRSN-CEA
KAERI 3D
KOPEC
SCANSCOT
E/H
0°
A/L
90°
A
A'
M/S, F/W
B
B
Elevation 10.75 m
Springline
SOL #12
90°, El. 6.20 m,
Displacement,
Radial,
Inside Liner Surface
Elevation 0.0 m
Basemat Top
Section A – A'
(not to scale)

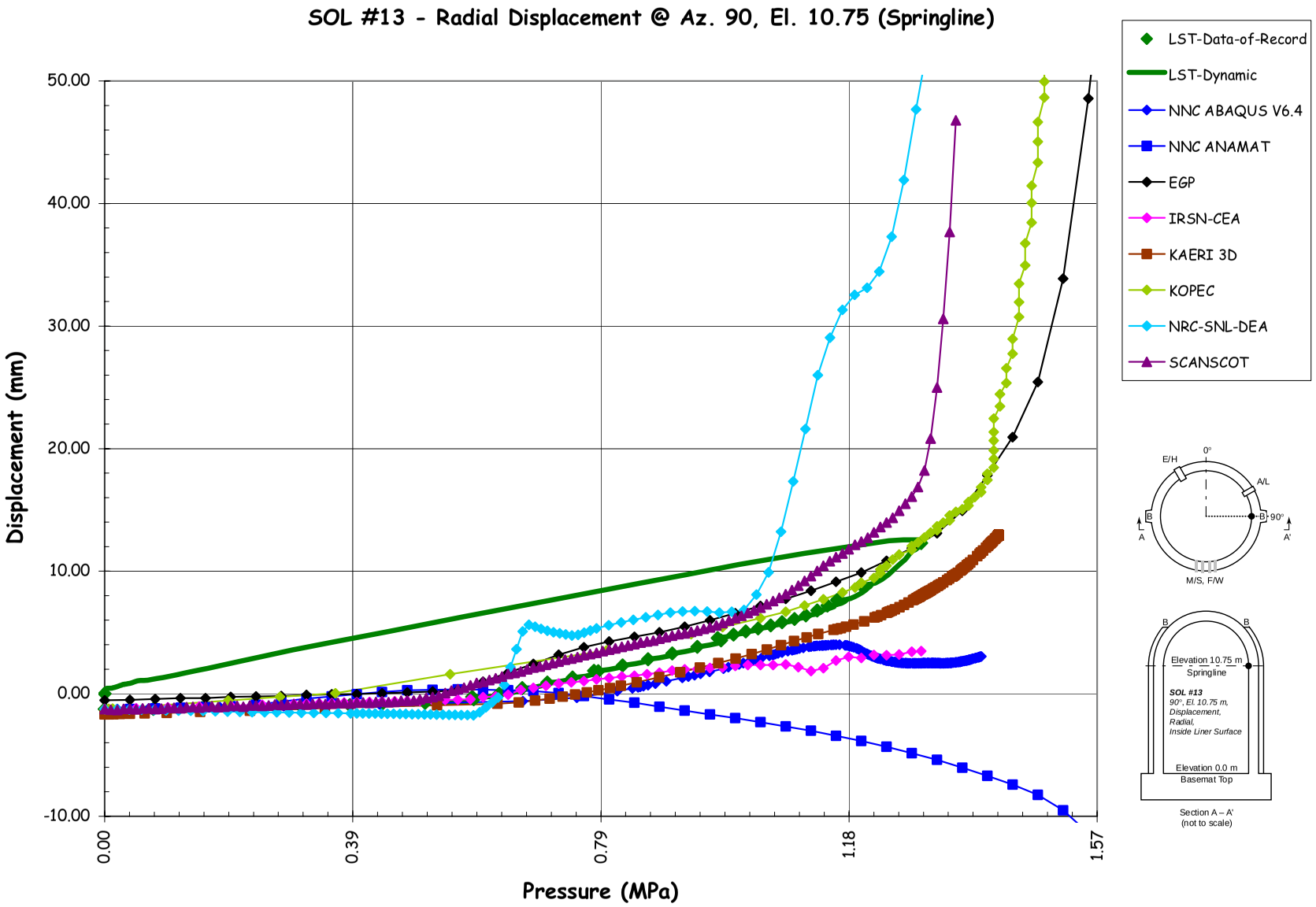
SOL #13 - Radial Displacement @ Az. 90, El. 10.75 (Springline)
Displacement (mm)
50.00
40.00
30.00
20.00
10.00
0.00
-10.00
0.00
0.39
0.79
1.18
1.57
Pressure (MPa)
LST-Data-of-Record
LST-Dynamic
NNC ABAQUS V6.4
NNC ANAMAT
EGP
IRSN-CEA
KAERI 3D
KOPEC
NRC-SNL-DEA
SCANSCOT
0°
E/H
A/L
B
B
90°
A
A'
M/S, F/W
B
B
Elevation 10.75 m
Springline
SOL #13
90°, El. 10.75 m,
Displacement,
Radial,
Inside Liner Surface
Elevation 0.0 m
Basemat Top
Section A – A'
(not to scale)

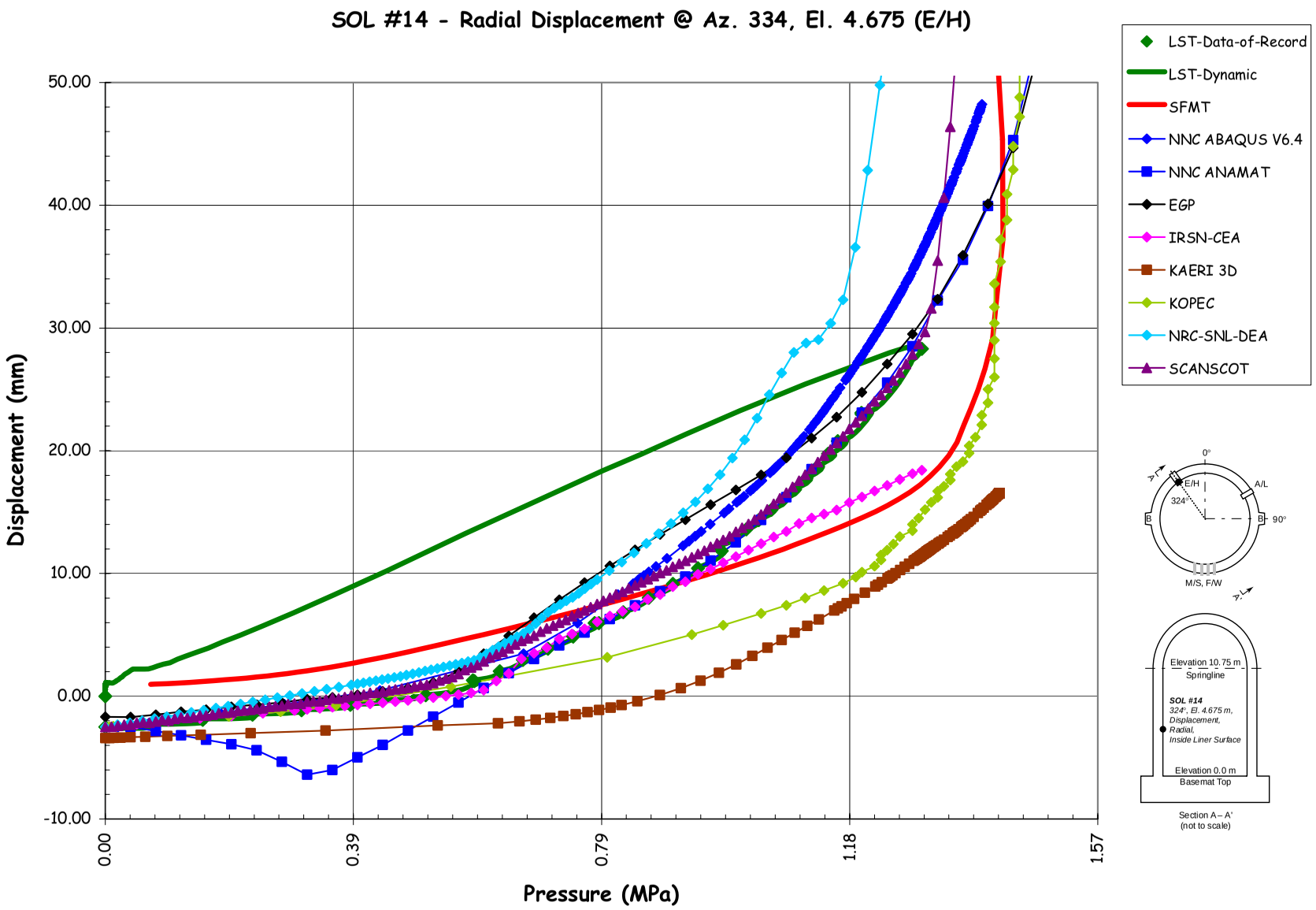
SOL #14 - Radial Displacement @ Az. 334, El. 4.675 (E/H)
Displacement (mm)
50.00
40.00
30.00
20.00
10.00
0.00
-10.00
0.00
0.39
0.79
1.18
1.57
Pressure (MPa)
LST-Data-of-Record
LST-Dynamic
SFMT
NNC ABAQUS V6.4
NNC ANAMAT
EGP
IRSN-CEA
KAERI 3D
KOPEC
NRC-SNL-DEA
SCANSCOT
0°
A/L
E/H
324°
90°
M/S, F/W
Elevation 10.75 m
Springline
SOL #14
324°, El. 4.675 m,
Displacement,
Radial,
Inside Liner Surface
Elevation 0.0 m
Basemat Top
Section A– A'
(not to scale)

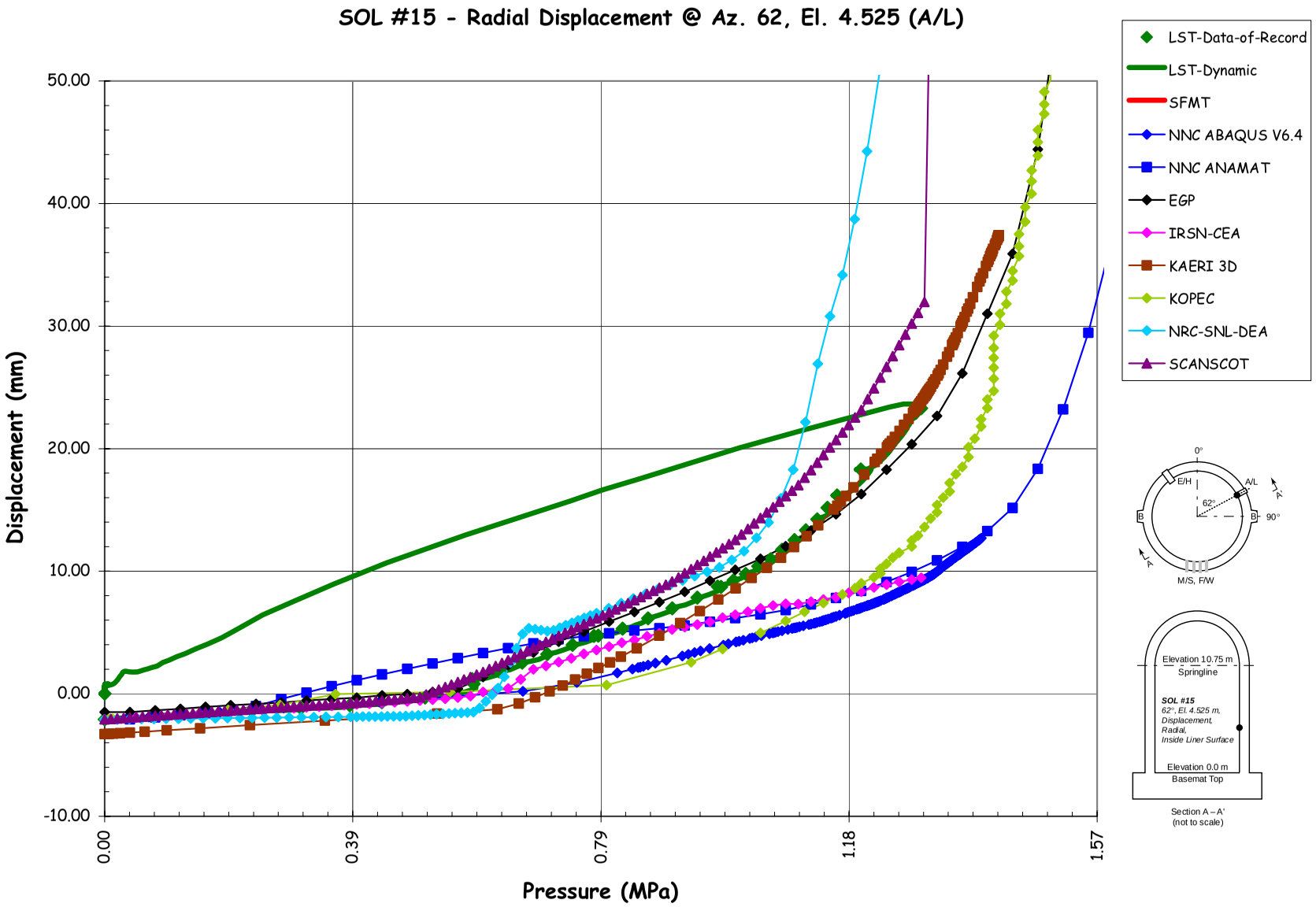
SOL #15 - Radial Displacement @ Az. 62, El. 4.525 (A/L)
Displacement (mm)
50.00
40.00
30.00
20.00
10.00
0.00
-10.00
0.00
0.39
0.79
1.18
1.57
Pressure (MPa)
LST-Data-of-Record
LST-Dynamic
SFMT
NNC ABAQUS V6.4
NNC ANAMAT
EGP
IRSN-CEA
KAERI 3D
KOPEC
NRC-SNL-DEA
SCANSCOT
0°
E/H
A/L
62°
90°
M/S, F/W
Elevation 10.75 m
Springline
SOL #15
62°, El. 4.525 m,
Displacement,
Radial,
Inside Liner Surface
Elevation 0.0 m
Basemat Top
Section A – A'
(not to scale)

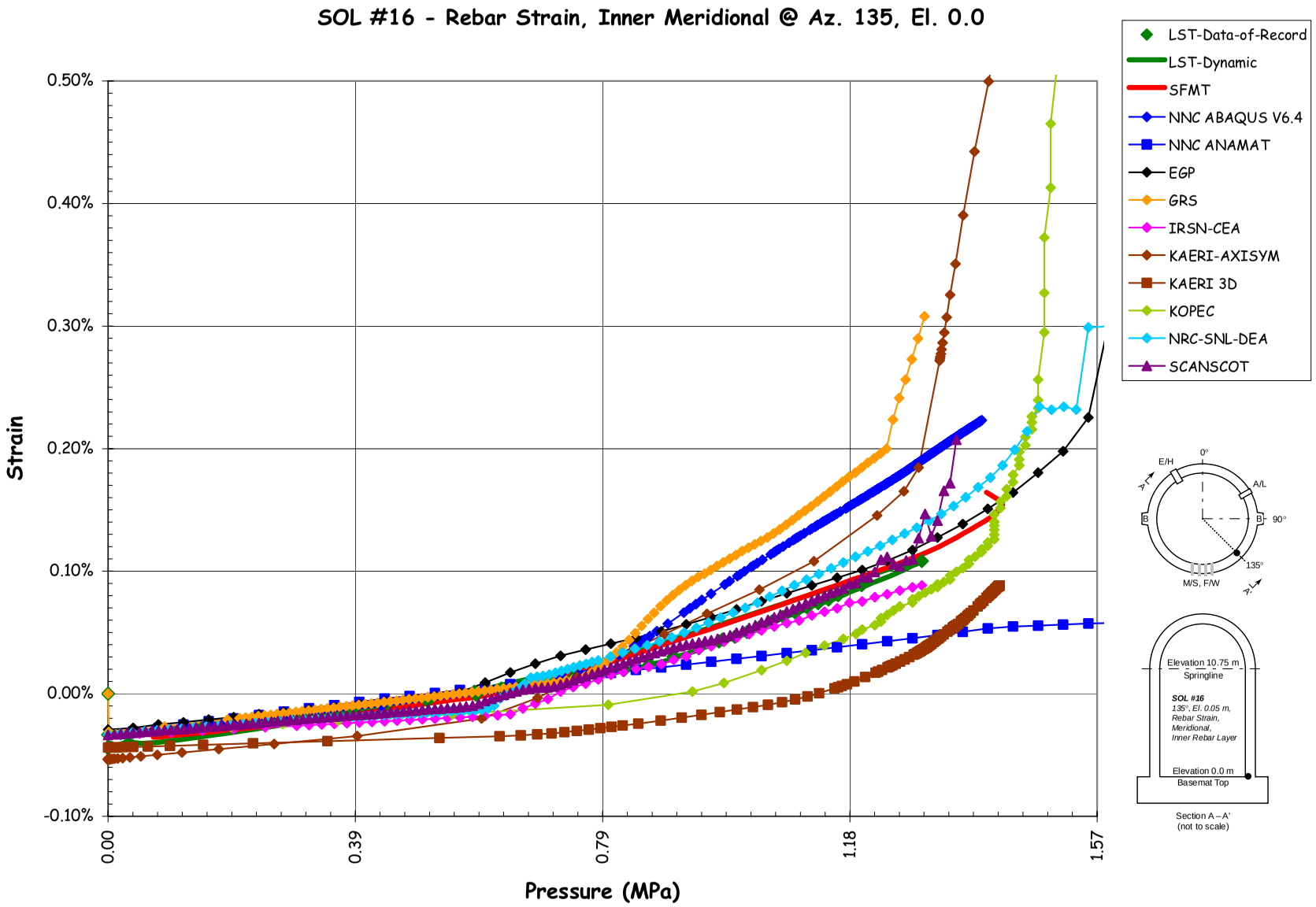
SOL #16 - Rebar Strain, Inner Meridional @ Az. 135, El. 0.0
Strain
0.50%
0.40%
0.30%
0.20%
0.10%
0.00%
-0.10%
0.00
0.39
0.79
1.18
1.57
Pressure (MPa)
LST-Data-of-Record
LST-Dynamic
SFMT
NNC ABAQUS V6.4
NNC ANAMAT
EGP
GRS
IRSN-CEA
KAERI-AXISYM
KAERI 3D
KOPEC
NRC-SNL-DEA
SCANSCOT
0°
E/H
A/L
90°
135°
M/S, F/W
Elevation 10.75 m
Springline
SOL #16
135°, El. 0.05 m,
Rebar Strain,
Meridional,
Inner Rebar Layer
Elevation 0.0 m
Basemat Top
Section A – A'
(not to scale)

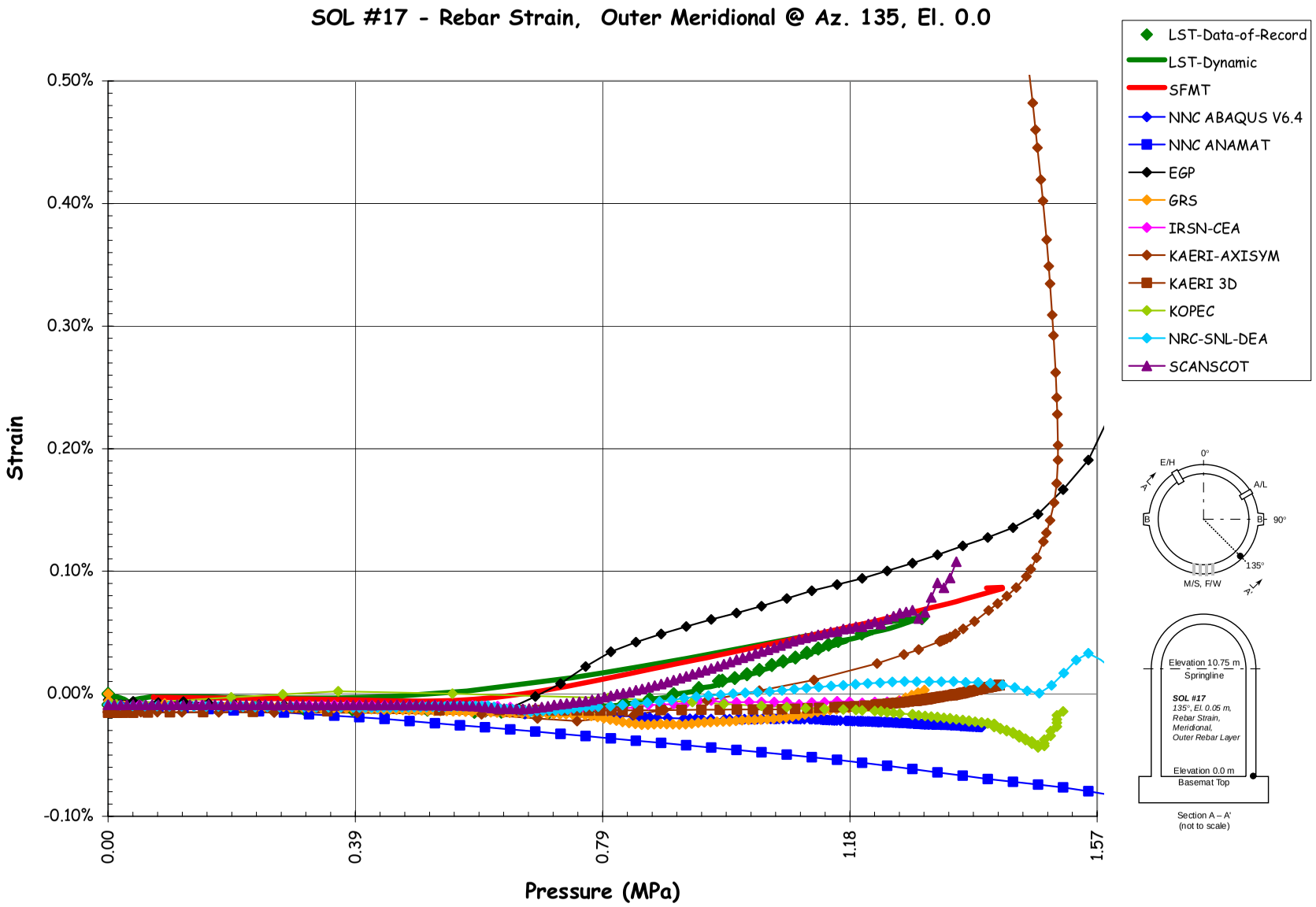
SOL #17 - Rebar Strain, Outer Meridional @ Az. 135, El. 0.0
Strain
0.50%
0.40%
0.30%
0.20%
0.10%
0.00%
-0.10%
0.00
0.39
0.79
1.18
1.57
Pressure (MPa)
LST-Data-of-Record
LST-Dynamic
SFMT
NNC ABAQUS V6.4
NNC ANAMAT
EGP
GRS
IRSN-CEA
KAERI-AXISYM
KAERI 3D
KOPEC
NRC-SNL-DEA
SCANSCOT
0°
E/H
A/L
90°
135°
M/S, F/W
Elevation 10.75 m
Springline
SOL #17
135°, El. 0.05 m,
Rebar Strain,
Meridional,
Outer Rebar Layer
Elevation 0.0 m
Basemat Top
Section A – A'
(not to scale)

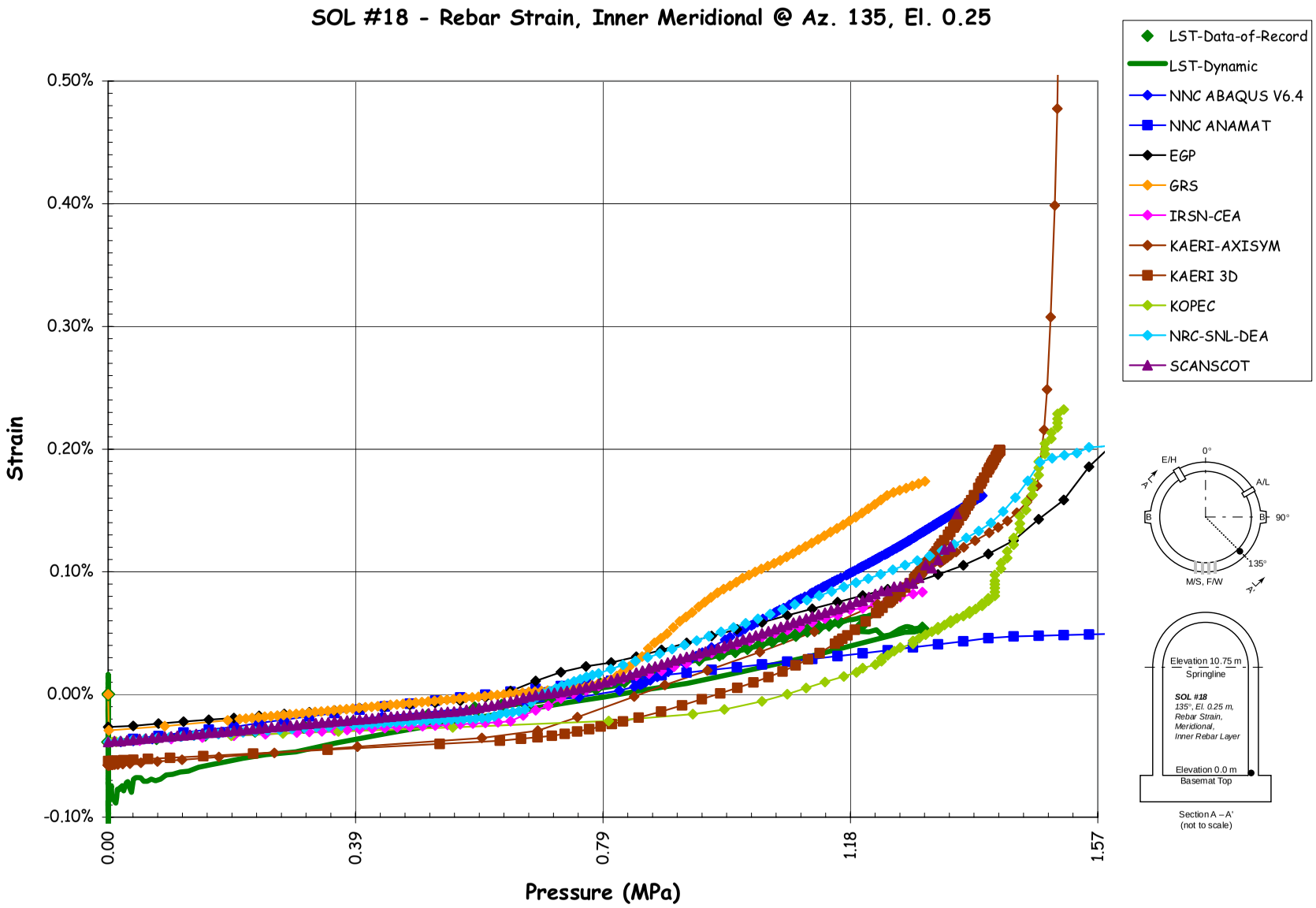
SOL #18 - Rebar Strain, Inner Meridional @ Az. 135, El. 0.25
LST-Data-of-Record
LST-Dynamic
NNC ABAQUS V6.4
NNC ANAMAT
EGP
GRS
IRSN-CEA
KAERI-AXISYM
KAERI 3D
KOPEC
NRC-SNL-DEA
SCANSCOT
0.50%
0.40%
0.30%
0.20%
0.10%
0.00%
-0.10%
Strain
0.00
0.39
0.79
1.18
1.57
Pressure (MPa)
0°
E/H
A/L
90°
135°
M/S, F/W
Elevation 10.75 m
Springline
SOL #18
135°, El. 0.25 m,
Rebar Strain,
Meridional,
Inner Rebar Layer
Elevation 0.0 m
Basemat Top
Section A – A'
(not to scale)

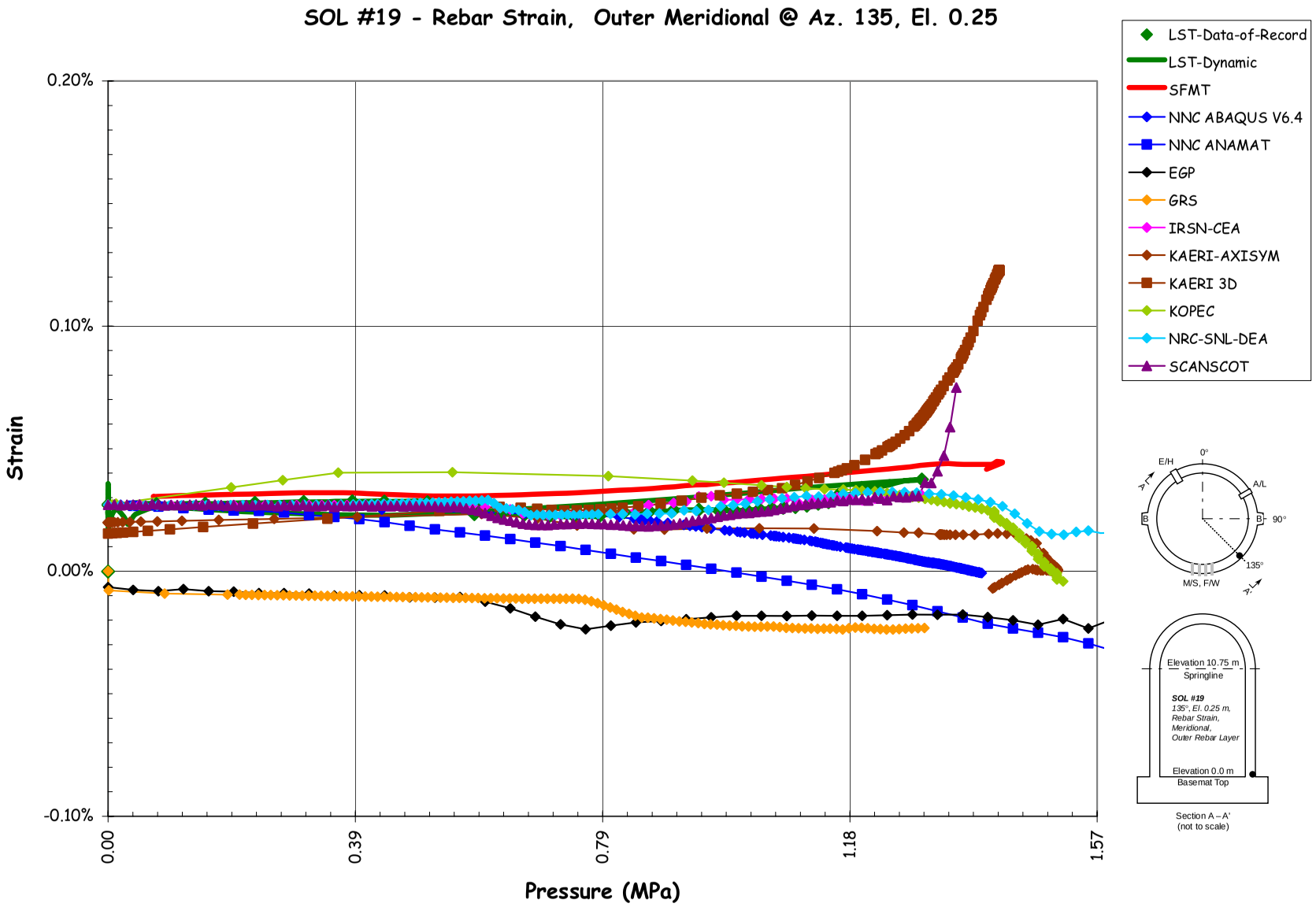
SOL #19 - Rebar Strain, Outer Meridional @ Az. 135, El. 0.25
LST-Data-of-Record
LST-Dynamic
SFMT
NNC ABAQUS V6.4
NNC ANAMAT
EGP
GRS
IRSN-CEA
KAERI-AXISYM
KAERI 3D
KOPEC
NRC-SNL-DEA
SCANSCOT
0.20%
0.10%
0.00%
-0.10%
Strain
0.00
0.39
0.79
1.18
1.57
Pressure (MPa)
0°
E/H
A/L
B
B
90°
135°
M/S, F/W
A
A'
Elevation 10.75 m
Springline
SOL #19
135°, El. 0.25 m,
Rebar Strain,
Meridional,
Outer Rebar Layer
Elevation 0.0 m
Basemat Top
Section A – A'
(not to scale)

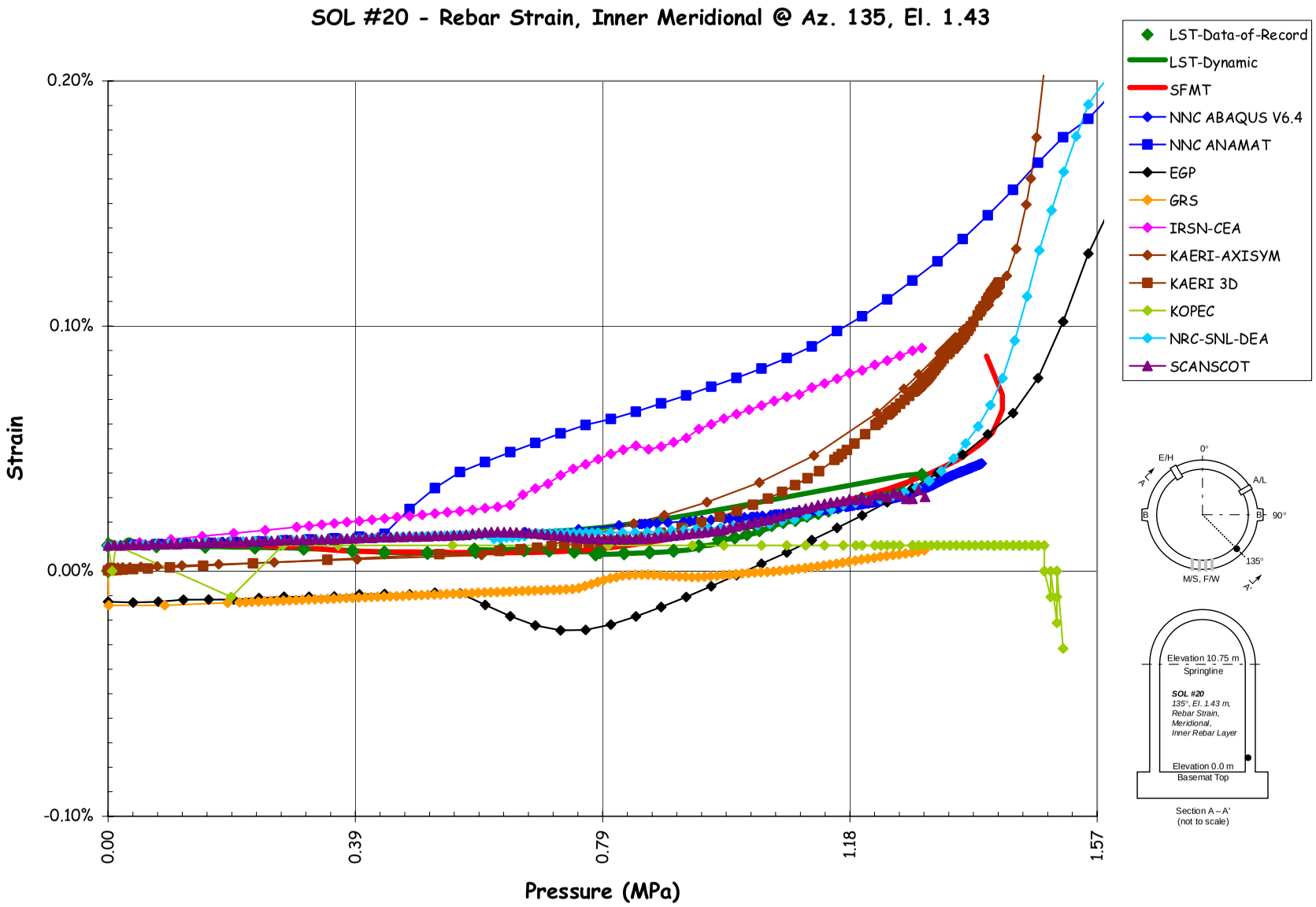
SOL #20 - Rebar Strain, Inner Meridional @ Az. 135, El. 1.43
LST-Data-of-Record
LST-Dynamic
SFMT
NNC ABAQUS V6.4
NNC ANAMAT
EGP
GRS
IRSN-CEA
KAERI-AXISYM
KAERI 3D
KOPEC
NRC-SNL-DEA
SCANSCOT
0.20%
0.10%
0.00%
-0.10%
Strain
0.00
0.39
0.79
1.18
1.57
Pressure (MPa)
E/H
A/L
0°
90°
135°
M/S, F/W
Elevation 10.75 m
Springline
SOL #20
135°, El. 1.43 m,
Rebar Strain,
Meridional,
Inner Rebar Layer
Elevation 0.0 m
Basemat Top
Section A – A'
(not to scale)

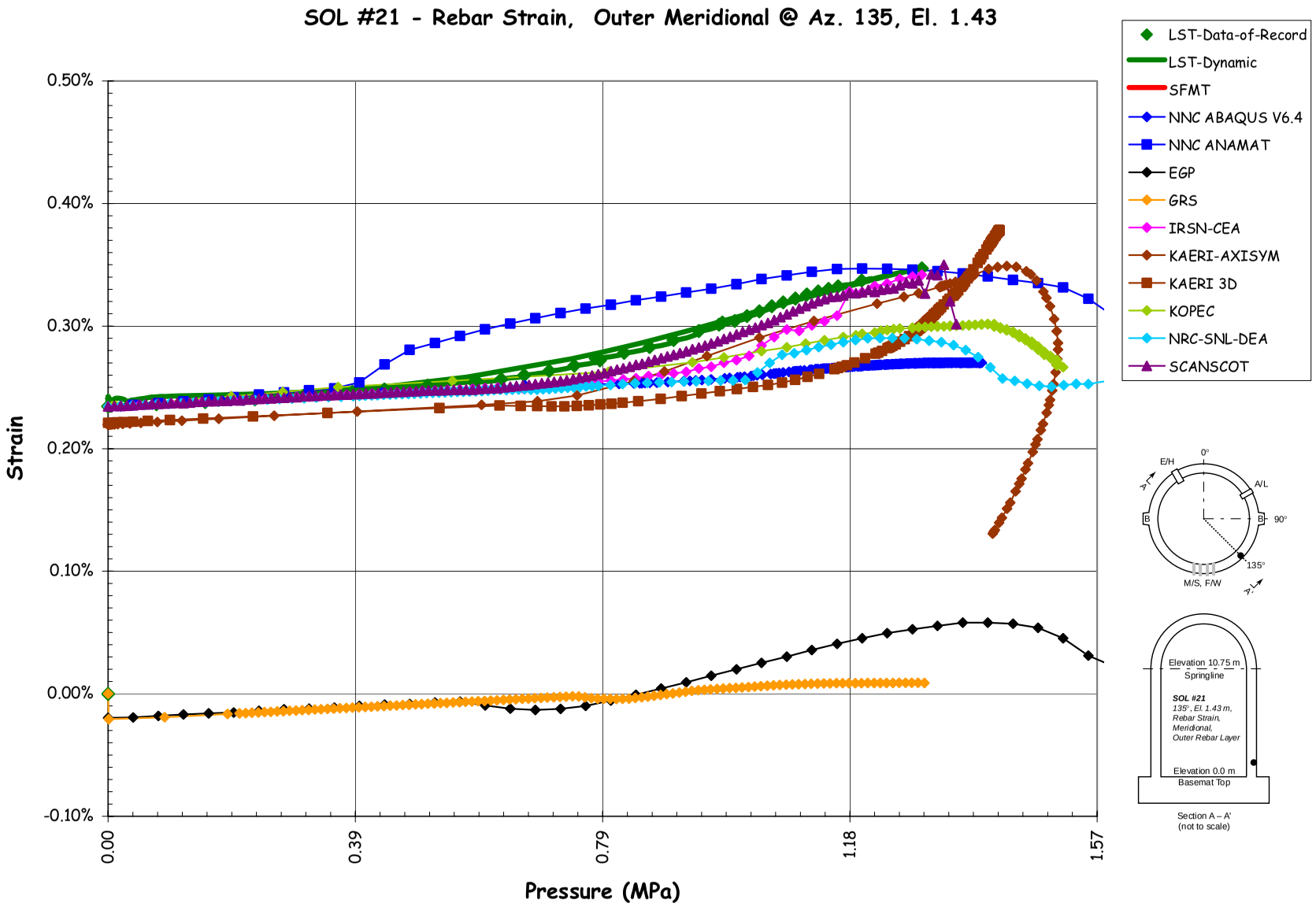
SOL #21 - Rebar Strain, Outer Meridional @ Az. 135, El. 1.43
Strain
0.50%
0.40%
0.30%
0.20%
0.10%
0.00%
-0.10%
0.00
0.39
0.79
1.18
1.57
Pressure (MPa)
LST-Data-of-Record
LST-Dynamic
SFMT
NNC ABAQUS V6.4
NNC ANAMAT
EGP
GRS
IRSN-CEA
KAERI-AXISYM
KAERI 3D
KOPEC
NRC-SNL-DEA
SCANSCOT
0°
E/H
A/L
B
B
90°
135°
M/S, F/W
Elevation 10.75 m
Springline
SOL #21
135°, El 1.43 m,
Rebar Strain,
Meridonal,
Outer Rebar Layer
Elevation 0.0 m
Basemat Top
Section A – A'
(not to scale)

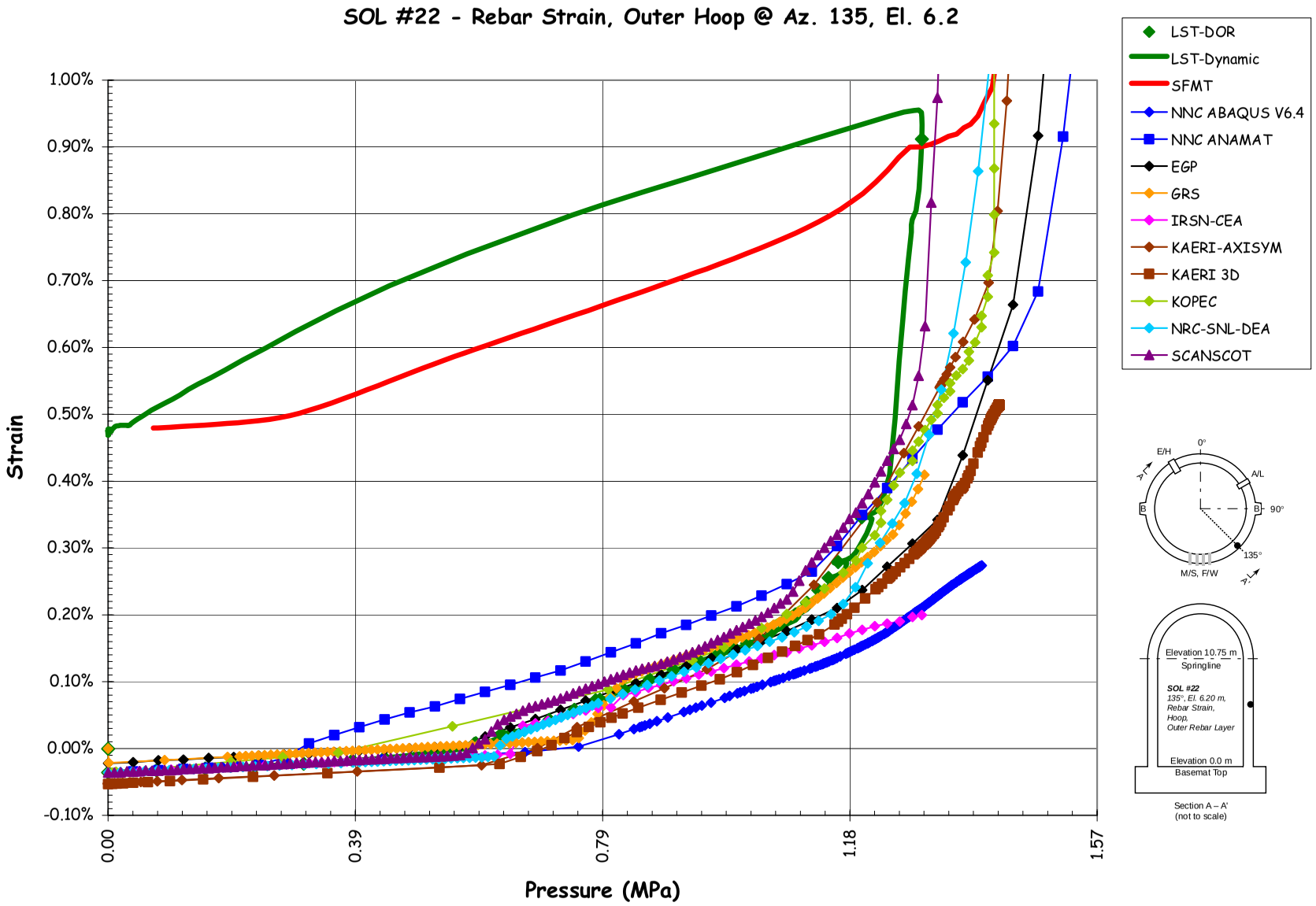
SOL #22 - Rebar Strain, Outer Hoop @ Az. 135, El. 6.2
Strain
1.00%
0.90%
0.80%
0.70%
0.60%
0.50%
0.40%
0.30%
0.20%
0.10%
0.00%
-0.10%
0.00
0.39
0.79
1.18
1.57
Pressure (MPa)
LST-DOR
LST-Dynamic
SFMT
NNC ABAQUS V6.4
NNC ANAMAT
EGP
GRS
IRSN-CEA
KAERI-AXISYM
KAERI 3D
KOPEC
NRC-SNL-DEA
SCANSCOT
0°
E/H
A/L
90°
135°
M/S, F/W
Elevation 10.75 m
Springline
SOL #22
135°, El. 6.20 m,
Rebar Strain,
Hoop,
Outer Rebar Layer
Elevation 0.0 m
Basemat Top
Section A – A'
(not to scale)

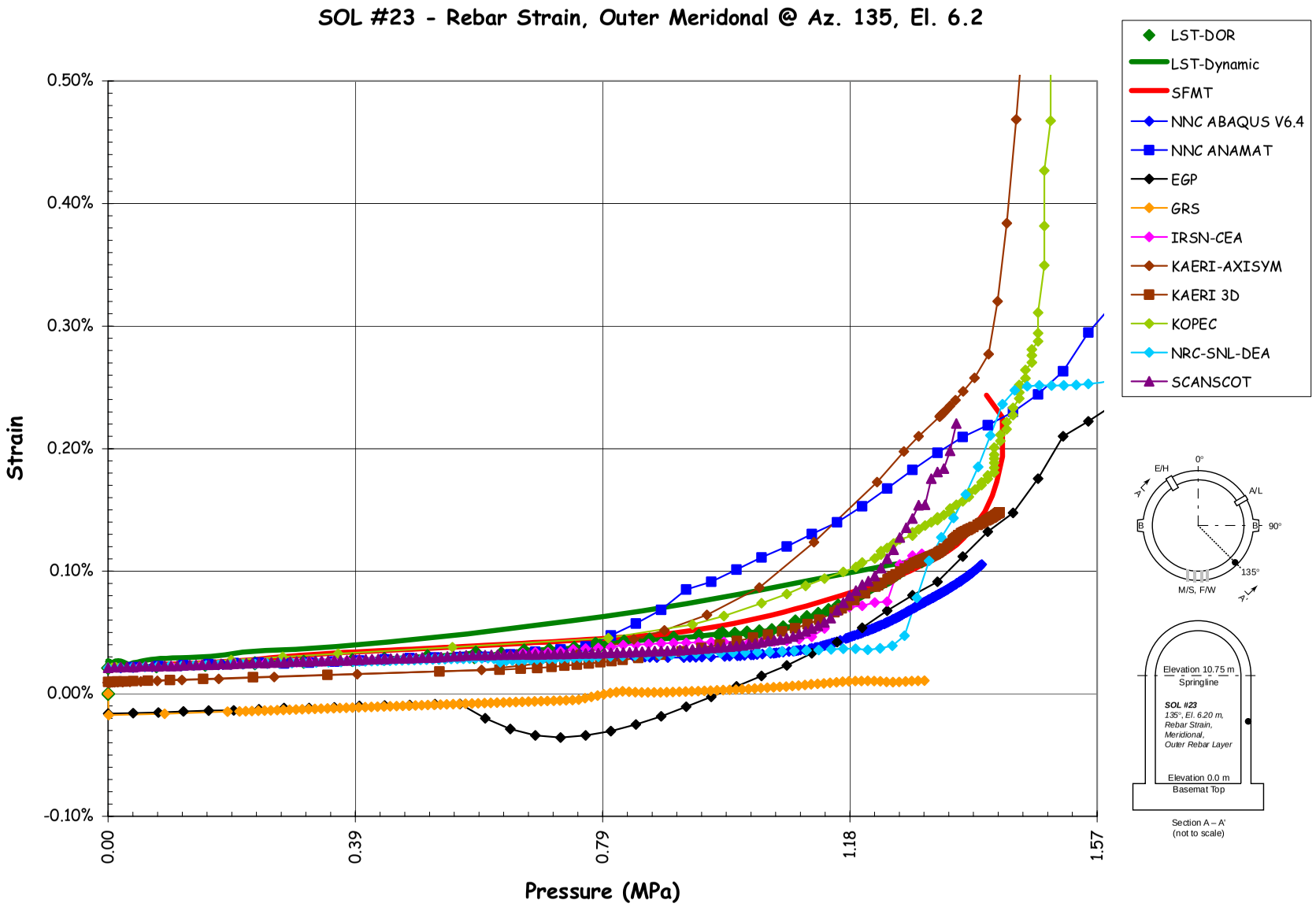
SOL #23 - Rebar Strain, Outer Meridonal @ Az. 135, El. 6.2
Strain
0.50%
0.40%
0.30%
0.20%
0.10%
0.00%
-0.10%
0.00
0.39
0.79
1.18
1.57
Pressure (MPa)
LST-DOR
LST-Dynamic
SFMT
NNC ABAQUS V6.4
NNC ANAMAT
EGP
GRS
IRSN-CEA
KAERI-AXISYM
KAERI 3D
KOPEC
NRC-SNL-DEA
SCANSCOT
0°
E/H
A/L
90°
135°
M/S, F/W
Elevation 10.75 m
Springline
SOL #23
135°, El. 6.20 m,
Rebar Strain,
Meridional,
Outer Rebar Layer
Elevation 0.0 m
Basemat Top
Section A – A'
(not to scale)

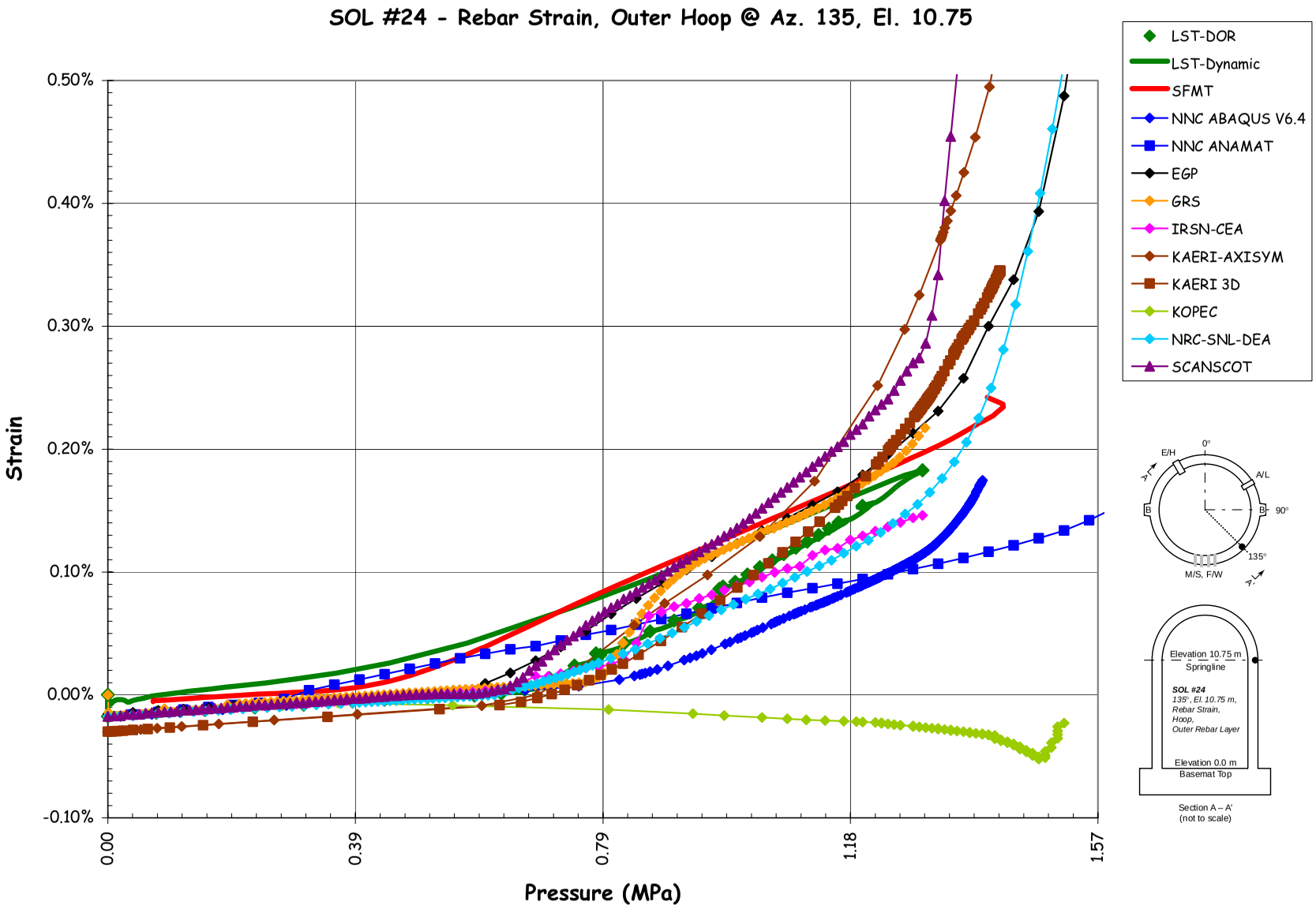
SOL #24 - Rebar Strain, Outer Hoop @ Az. 135, El. 10.75
Strain
0.50%
0.40%
0.30%
0.20%
0.10%
0.00%
-0.10%
0.00
0.39
0.79
1.18
1.57
Pressure (MPa)
LST-DOR
LST-Dynamic
SFMT
NNC ABAQUS V6.4
NNC ANAMAT
EGP
GRS
IRSN-CEA
KAERI-AXISYM
KAERI 3D
KOPEC
NRC-SNL-DEA
SCANSCOT
E/H
0°
A/L
90°
135°
M/S, F/W
Elevation 10.75 m
Springline
SOL #24
135°, El. 10.75 m,
Rebar Strain,
Hoop,
Outer Rebar Layer
Elevation 0.0 m
Basemat Top
Section A – A'
(not to scale)

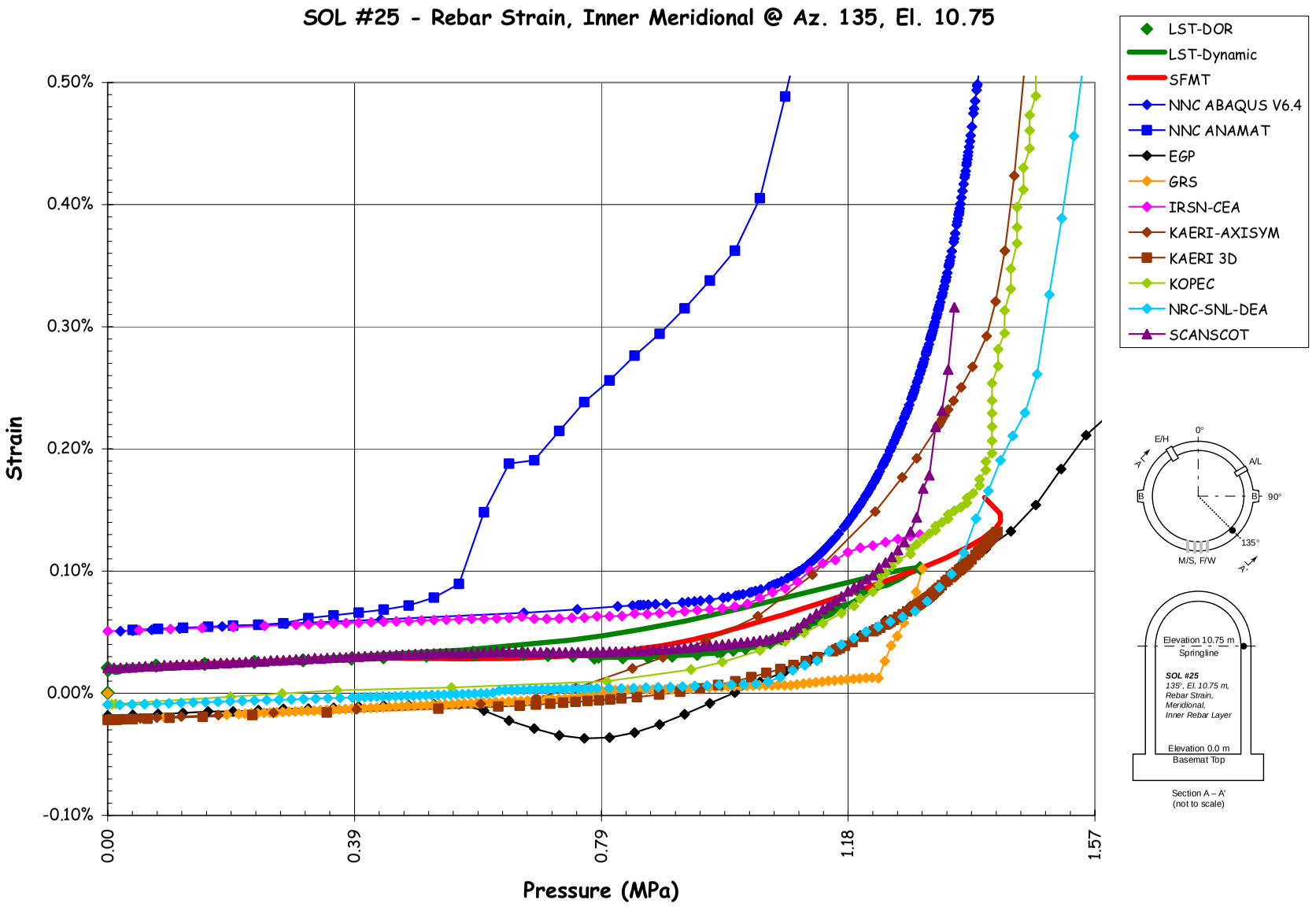
SOL #25 - Rebar Strain, Inner Meridional @ Az. 135, El. 10.75
Strain
0.50%
0.40%
0.30%
0.20%
0.10%
0.00%
-0.10%
0.00
0.39
0.79
1.18
1.57
Pressure (MPa)
LST-DOR
LST-Dynamic
SFMT
NNC ABAQUS V6.4
NNC ANAMAT
EGP
GRS
IRSN-CEA
KAERI-AXISYM
KAERI 3D
KOPEC
NRC-SNL-DEA
SCANSCOT
0°
E/H
A/L
90°
135°
M/S, F/W
Elevation 10.75 m
Springline
SOL #25
135°, El. 10.75 m,
Rebar Strain,
Meridional,
Inner Rebar Layer
Elevation 0.0 m
Basemat Top
Section A – A'
(not to scale)

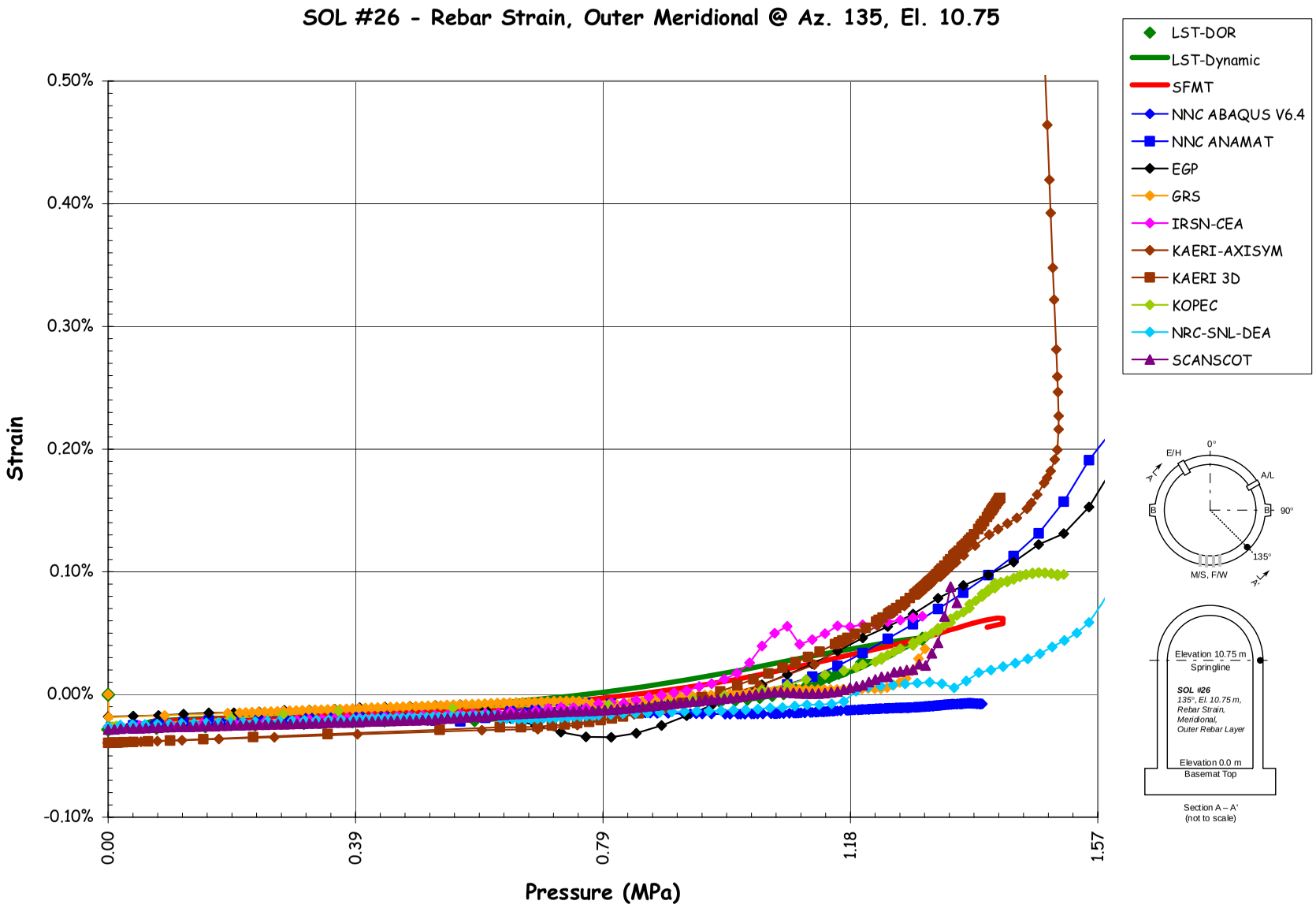
SOL #26 - Rebar Strain, Outer Meridional @ Az. 135, El. 10.75
Strain
0.50%
0.40%
0.30%
0.20%
0.10%
0.00%
-0.10%
0.00
0.39
0.79
1.18
1.57
Pressure (MPa)
LST-DOR
LST-Dynamic
SFMT
NNC ABAQUS V6.4
NNC ANAMAT
EGP
GRS
IRSN-CEA
KAERI-AXISYM
KAERI 3D
KOPEC
NRC-SNL-DEA
SCANSCOT
E/H
0°
A/L
90°
135°
M/S, F/W
Elevation 10.75 m
Springline
SOL #26
135°, El. 10.75 m,
Rebar Strain,
Meridional,
Outer Rebar Layer
Elevation 0.0 m
Basemat Top
Section A – A'
(not to scale)

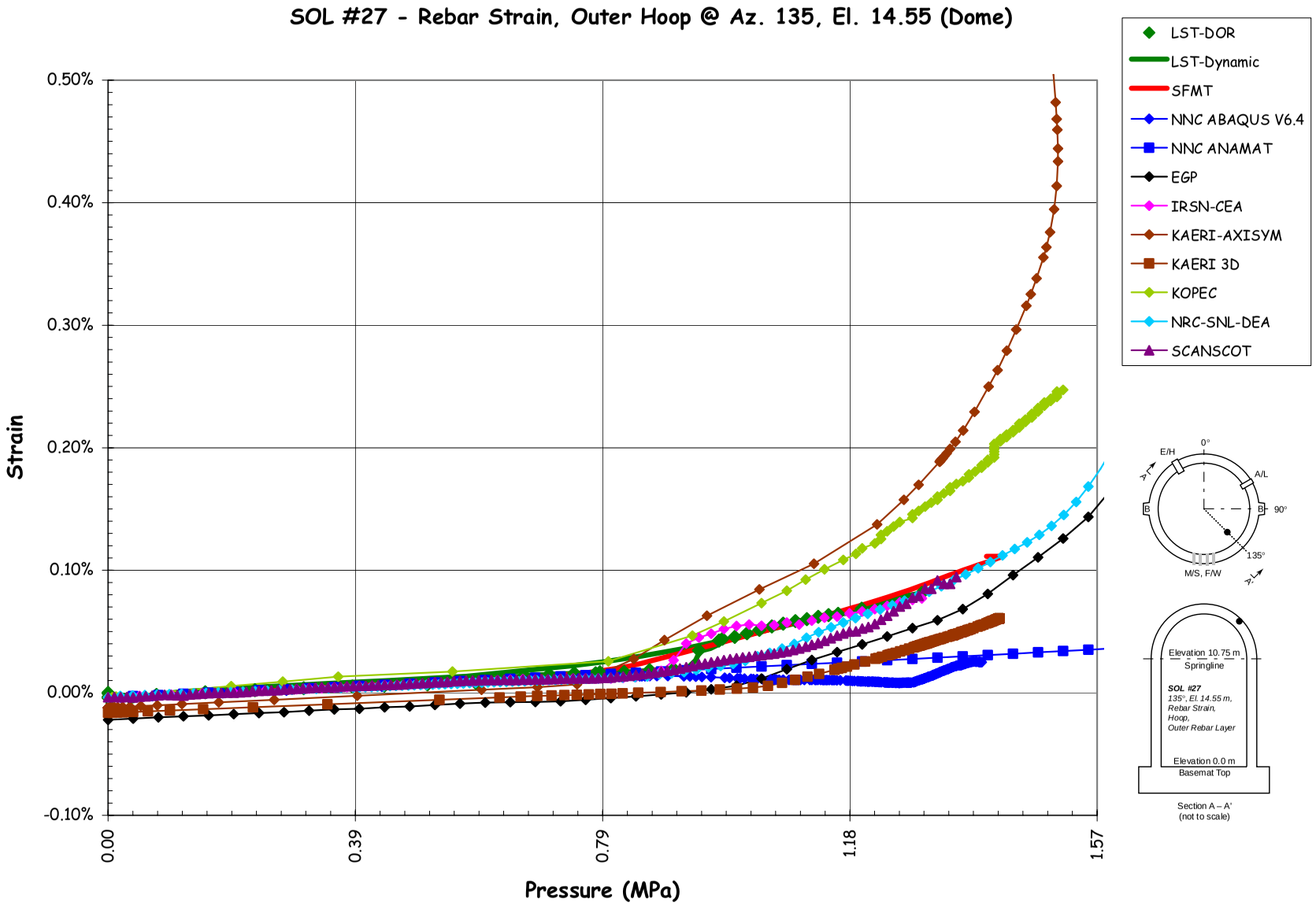
SOL #27 - Rebar Strain, Outer Hoop @ Az. 135, El. 14.55 (Dome)
Strain
0.50%
0.40%
0.30%
0.20%
0.10%
0.00%
-0.10%
0.00
0.39
0.79
1.18
1.57
Pressure (MPa)
LST-DOR
LST-Dynamic
SFMT
NNC ABAQUS V6.4
NNC ANAMAT
EGP
IRSN-CEA
KAERI-AXISYM
KAERI 3D
KOPEC
NRC-SNL-DEA
SCANSCOT
E/H
0°
A/L
90°
135°
M/S, F/W
Elevation 10.75 m
Springline
SOL #27
135°, El. 14.55 m,
Rebar Strain,
Hoop,
Outer Rebar Layer
Elevation 0.0 m
Basemat Top
Section A – A'
(not to scale)

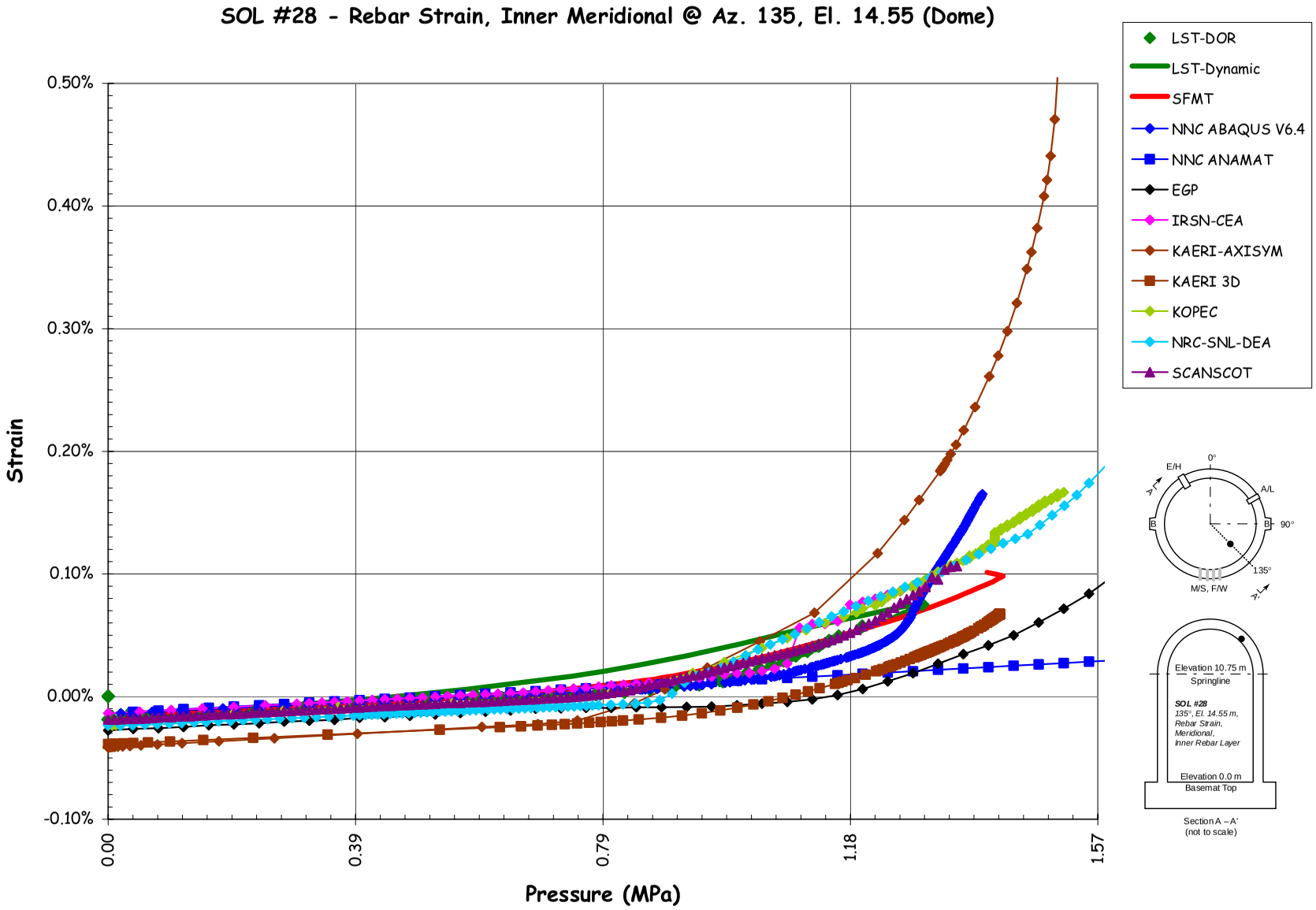
SOL #28 - Rebar Strain, Inner Meridional @ Az. 135, El. 14.55 (Dome)
LST-DOR
LST-Dynamic
SFMT
NNC ABAQUS V6.4
NNC ANAMAT
EGP
IRSN-CEA
KAERI-AXISYM
KAERI 3D
KOPEC
NRC-SNL-DEA
SCANSCOT
0.50%
0.40%
0.30%
0.20%
0.10%
0.00%
-0.10%
Strain
0.00
0.39
0.79
1.18
1.57
Pressure (MPa)
E/H
A/L
0°
90°
135°
M/S, F/W
Elevation 10.75 m
Springline
SOL #28
135°, El. 14.55 m,
Rebar Strain,
Meridional,
Inner Rebar Layer
Elevation 0.0 m
Basemat Top
Section A – A'
(not to scale)

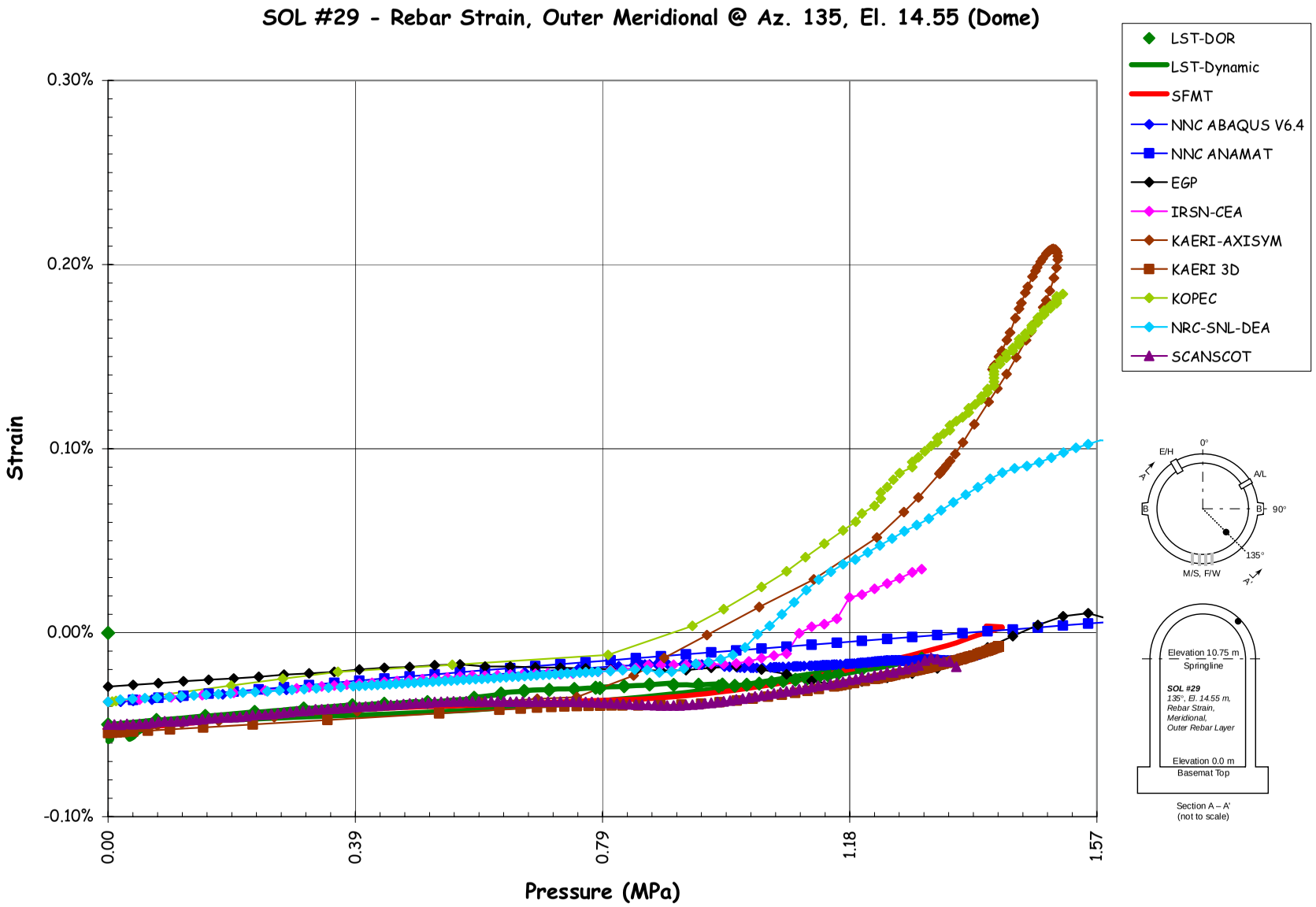
SOL #29 - Rebar Strain, Outer Meridional @ Az. 135, El. 14.55 (Dome)
Strain
0.30%
0.20%
0.10%
0.00%
-0.10%
0.00
0.39
0.79
1.18
1.57
Pressure (MPa)
LST-DOR
LST-Dynamic
SFMT
NNC ABAQUS V6.4
NNC ANAMAT
EGP
IRSN-CEA
KAERI-AXISYM
KAERI 3D
KOPEC
NRC-SNL-DEA
SCANSCOT
E/H
0°
A/L
90°
135°
M/S, F/W
Elevation 10.75 m
Springline
SOL #29
135°, El. 14.55 m,
Rebar Strain,
Meridional,
Outer Rebar Layer
Elevation 0.0 m
Basemat Top
Section A – A'
(not to scale)

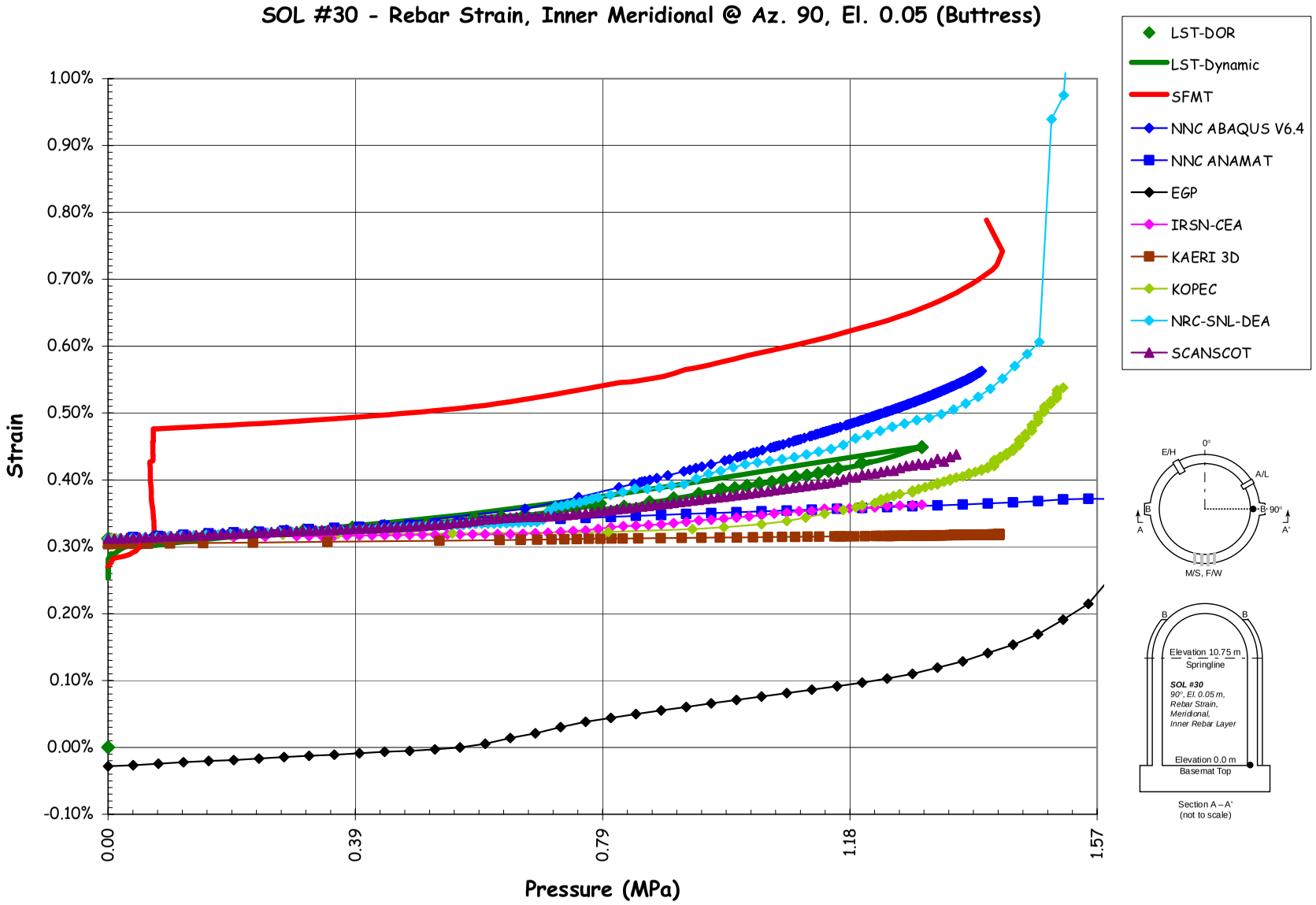
SOL #30 - Rebar Strain, Inner Meridional @ Az. 90, El. 0.05 (Buttress)
Strain
1.00%
0.90%
0.80%
0.70%
0.60%
0.50%
0.40%
0.30%
0.20%
0.10%
0.00%
-0.10%
0.00
0.39
0.79
1.18
1.57
Pressure (MPa)
LST-DOR
LST-Dynamic
SFMT
NNC ABAQUS V6.4
NNC ANAMAT
EGP
IRSN-CEA
KAERI 3D
KOPEC
NRC-SNL-DEA
SCANSCOT
E/H
0°
A/L
90°
M/S, F/W
Elevation 10.75 m
Springline
SOL #30
90°, El. 0.05 m,
Rebar Strain,
Meridional,
Inner Rebar Layer
Elevation 0.0 m
Basemat Top
Section A – A'
(not to scale)

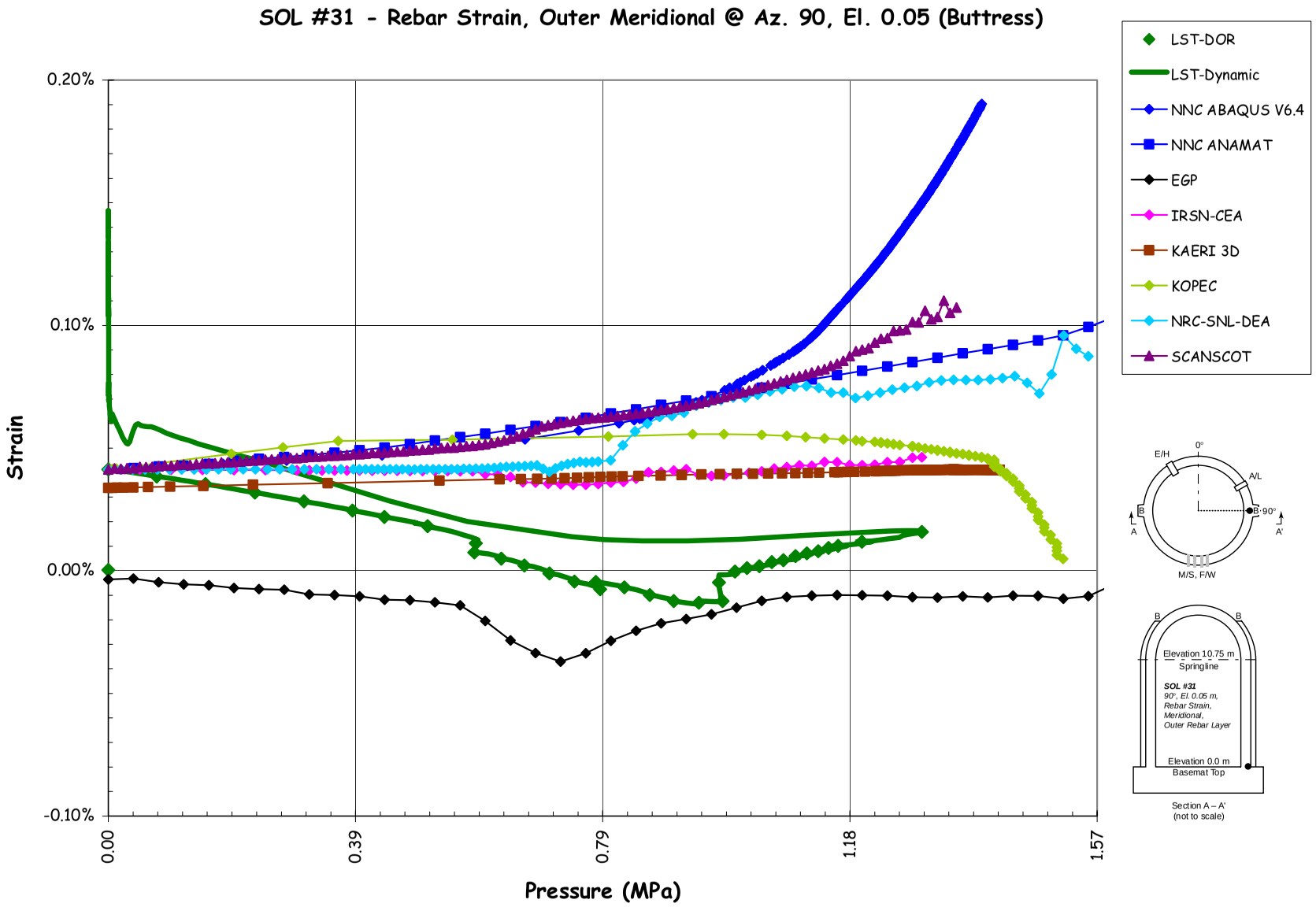
SOL #31 - Rebar Strain, Outer Meridional @ Az. 90, El. 0.05 (Buttress)
LST-DOR
LST-Dynamic
NNC ABAQUS V6.4
NNC ANAMAT
EGP
IRSN-CEA
KAERI 3D
KOPEC
NRC-SNL-DEA
SCANSCOT
0.20%
0.10%
0.00%
-0.10%
Strain
0.00
0.39
0.79
1.18
1.57
Pressure (MPa)
E/H
0°
A/L
90°
M/S, F/W
Elevation 10.75 m
Springline
SOL #31
90°, El. 0.05 m,
Rebar Strain,
Meridional,
Outer Rebar Layer
Elevation 0.0 m
Basemat Top
Section A – A'
(not to scale)

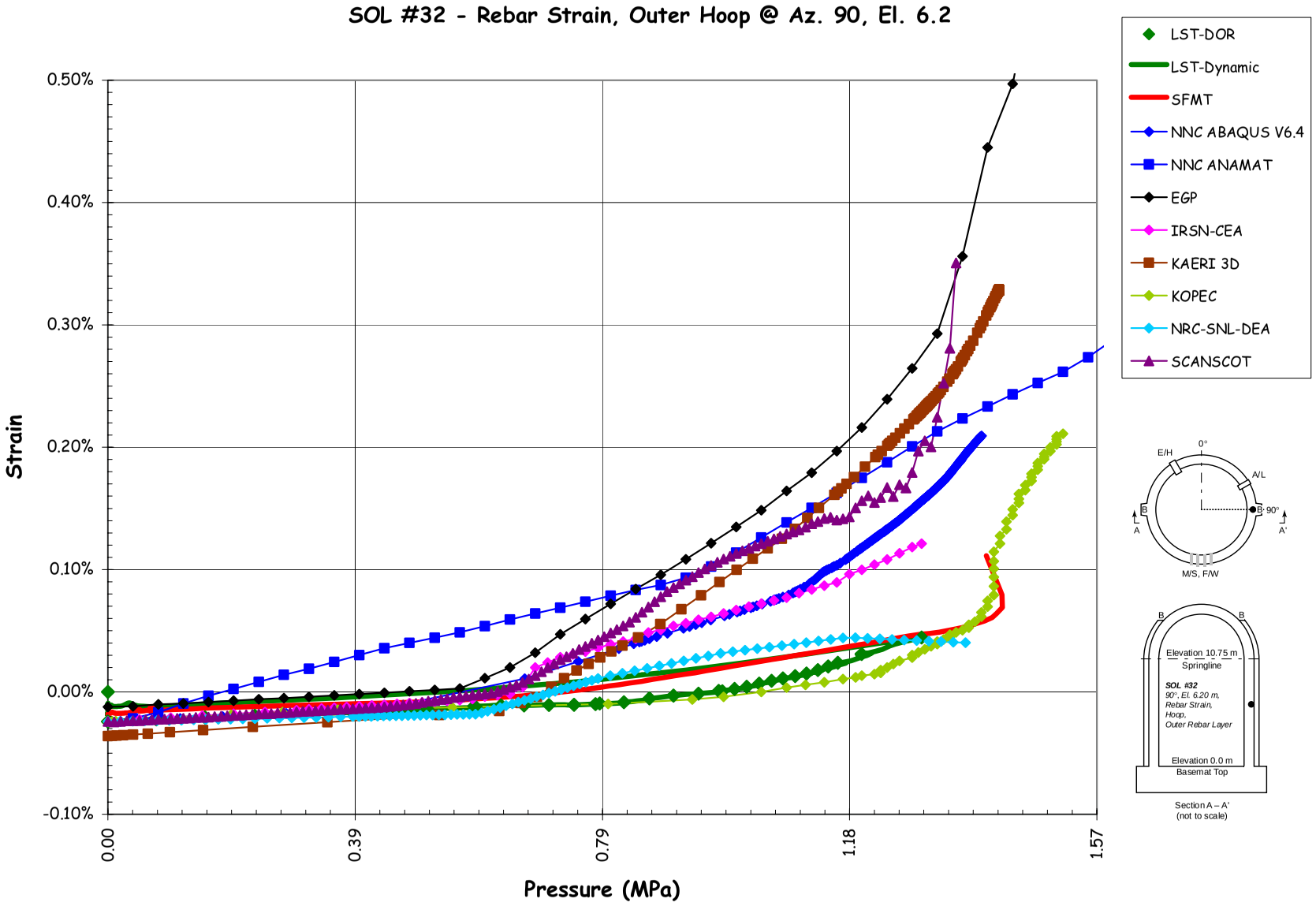
SOL #32 - Rebar Strain, Outer Hoop @ Az. 90, El. 6.2
Strain
0.50%
0.40%
0.30%
0.20%
0.10%
0.00%
-0.10%
0.00
0.39
0.79
1.18
1.57
Pressure (MPa)
LST-DOR
LST-Dynamic
SFMT
NNC ABAQUS V6.4
NNC ANAMAT
EGP
IRSN-CEA
KAERI 3D
KOPEC
NRC-SNL-DEA
SCANSCOT
E/H
0°
A/L
90°
M/S, F/W
Elevation 10.75 m
Springline
SOL #32
90°, El. 6.20 m,
Rebar Strain,
Hoop,
Outer Rebar Layer
Elevation 0.0 m
Basemat Top
Section A – A'
(not to scale)

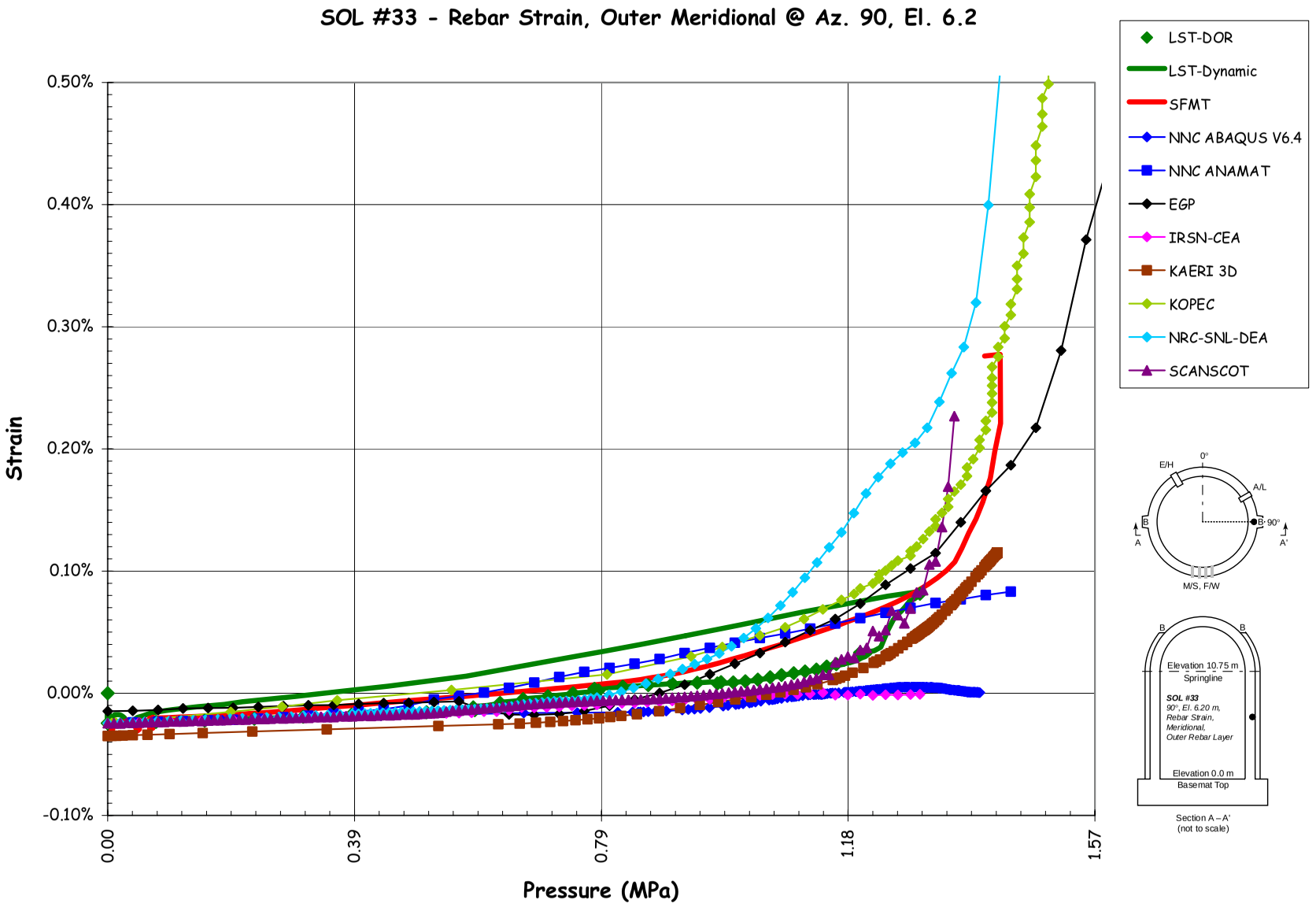
SOL #33 - Rebar Strain, Outer Meridional @ Az. 90, El. 6.2
Strain
0.50%
0.40%
0.30%
0.20%
0.10%
0.00%
-0.10%
0.00
0.39
0.79
1.18
1.57
Pressure (MPa)
LST-DOR
LST-Dynamic
SFMT
NNC ABAQUS V6.4
NNC ANAMAT
EGP
IRSN-CEA
KAERI 3D
KOPEC
NRC-SNL-DEA
SCANSCOT
E/H
0°
A/L
90°
M/S, F/W
Elevation 10.75 m
Springline
SOL #33
90°, El. 6.20 m,
Rebar Strain,
Meridional,
Outer Rebar Layer
Elevation 0.0 m
Basemat Top
Section A – A'
(not to scale)

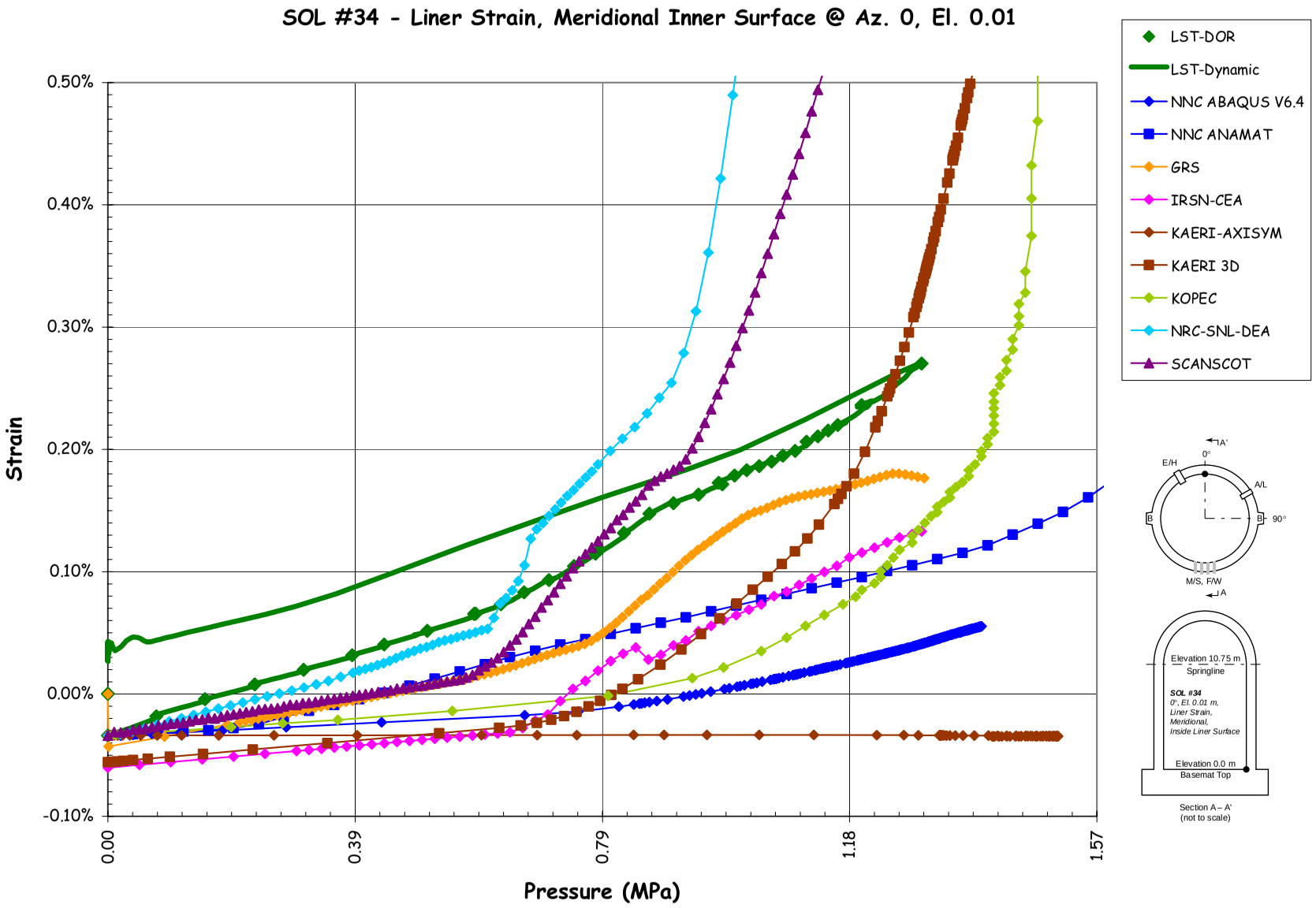
SOL #34 - Liner Strain, Meridional Inner Surface @ Az. 0, El. 0.01
Strain
0.50%
0.40%
0.30%
0.20%
0.10%
0.00%
-0.10%
0.00
0.39
0.79
1.18
1.57
Pressure (MPa)
LST-DOR
LST-Dynamic
NNC ABAQUS V6.4
NNC ANAMAT
GRS
IRSN-CEA
KAERI-AXISYM
KAERI 3D
KOPEC
NRC-SNL-DEA
SCANSCOT
A'
E/H
0°
A/L
B
B
90°
M/S, F/W
A
Elevation 10.75 m
Springline
SOL #34
0°, El. 0.01 m,
Liner Strain,
Meridional,
Inside Liner Surface
Elevation 0.0 m
Basemat Top
Section A – A'
(not to scale)

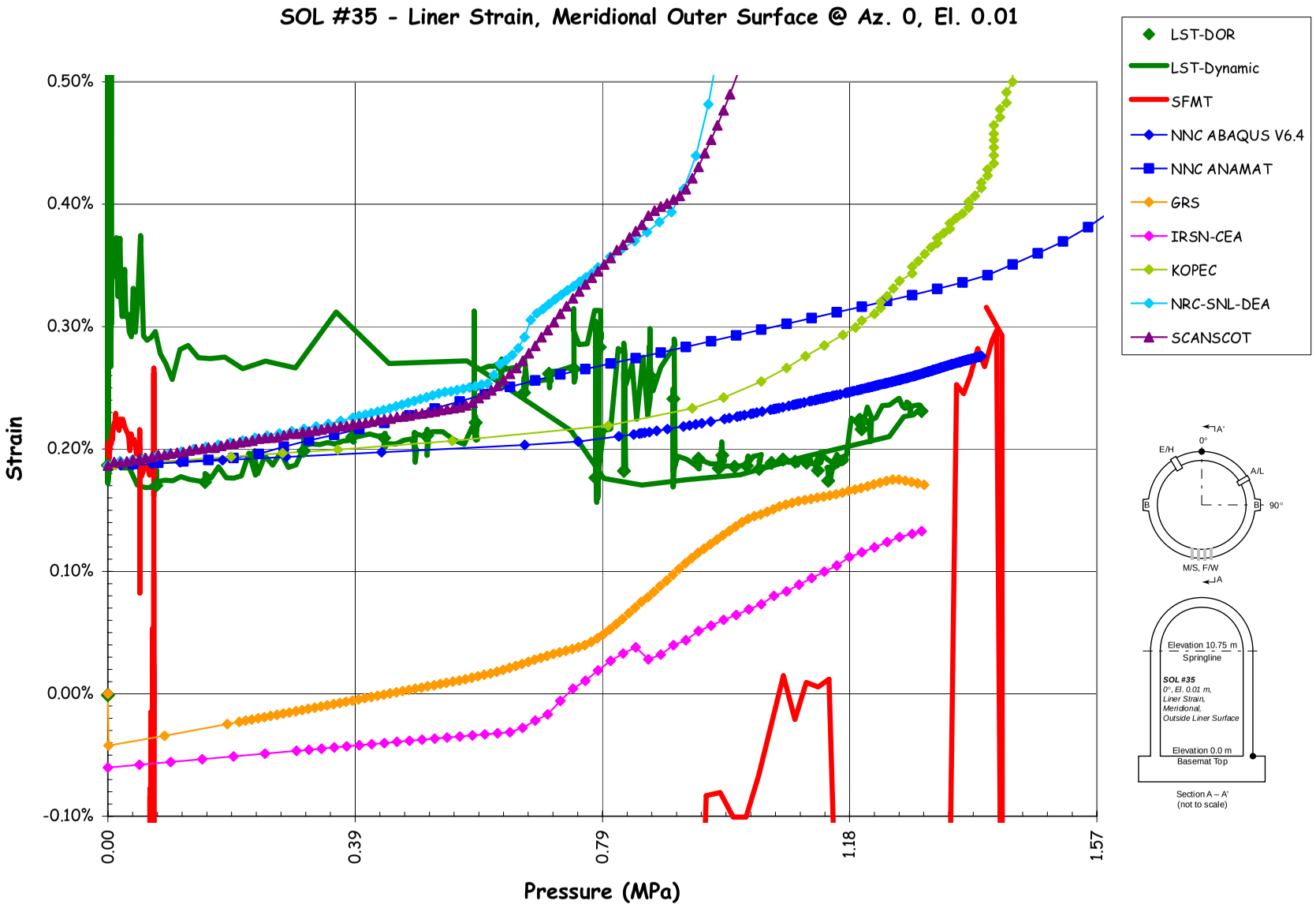
SOL #35 - Liner Strain, Meridional Outer Surface @ Az. 0, El. 0.01
Strain
0.50%
0.40%
0.30%
0.20%
0.10%
0.00%
-0.10%
0.00
0.39
0.79
1.18
1.57
Pressure (MPa)
LST-DOR
LST-Dynamic
SFMT
NNC ABAQUS V6.4
NNC ANAMAT
GRS
IRSN-CEA
KOPEC
NRC-SNL-DEA
SCANSCOT
A'
0°
E/H
A/L
B
B
90°
M/S, F/W
A
Elevation 10.75 m
Springline
SOL #35
0°, El. 0.01 m,
Liner Strain,
Meridional,
Outside Liner Surface
Elevation 0.0 m
Basemat Top
Section A – A'
(not to scale)

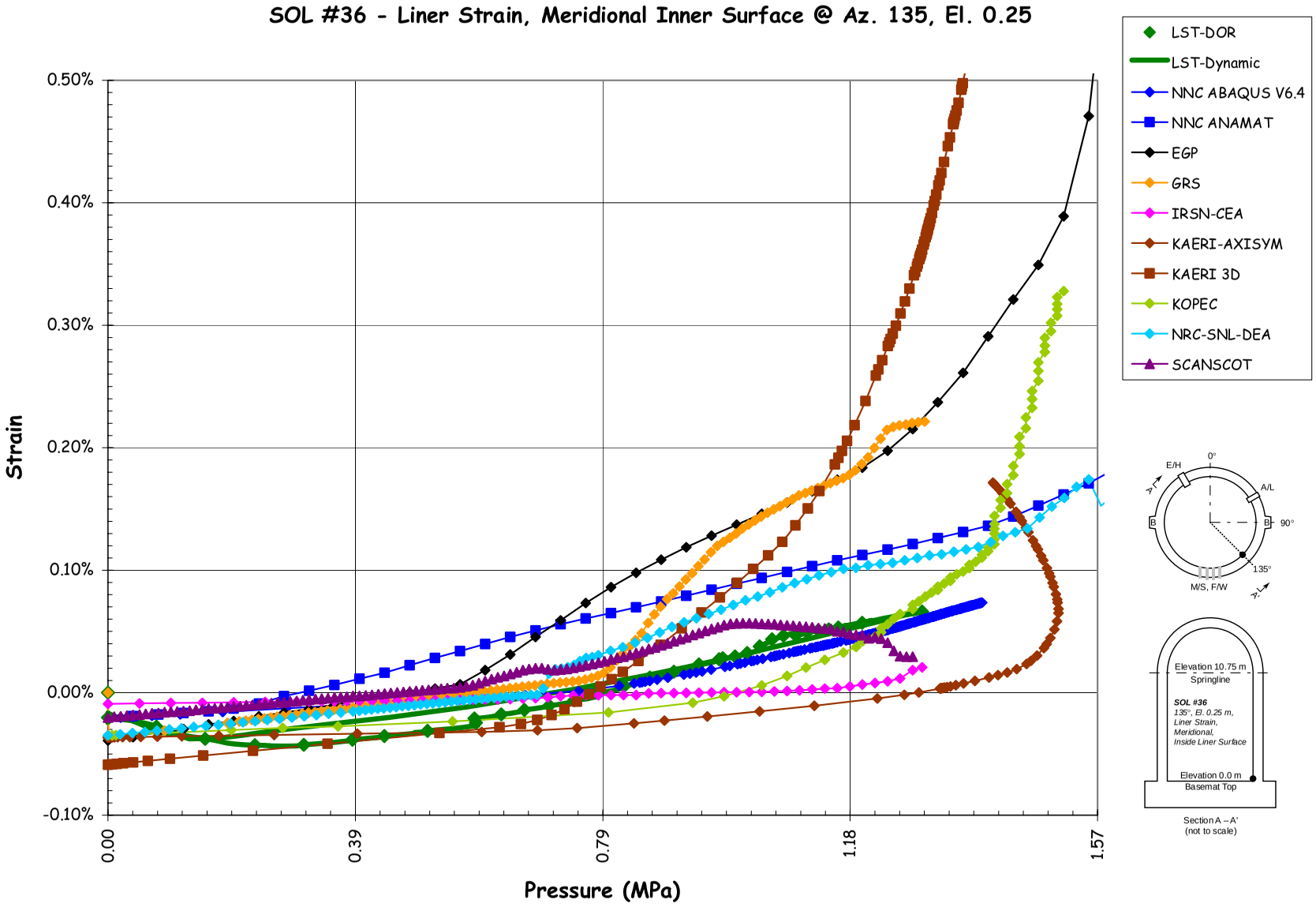
SOL #36 - Liner Strain, Meridional Inner Surface @ Az. 135, El. 0.25
Strain
0.50%
0.40%
0.30%
0.20%
0.10%
0.00%
-0.10%
0.00
0.39
0.79
1.18
1.57
Pressure (MPa)
LST-DOR
LST-Dynamic
NNC ABAQUS V6.4
NNC ANAMAT
EGP
GRS
IRSN-CEA
KAERI-AXISYM
KAERI 3D
KOPEC
NRC-SNL-DEA
SCANSCOT
E/H
0°
A/L
B
B
90°
135°
M/S, F/W
Elevation 10.75 m
Springline
SOL #36
135°, El. 0.25 m,
Liner Strain,
Meridional,
Inside Liner Surface
Elevation 0.0 m
Basemat Top
Section A – A'
(not to scale)

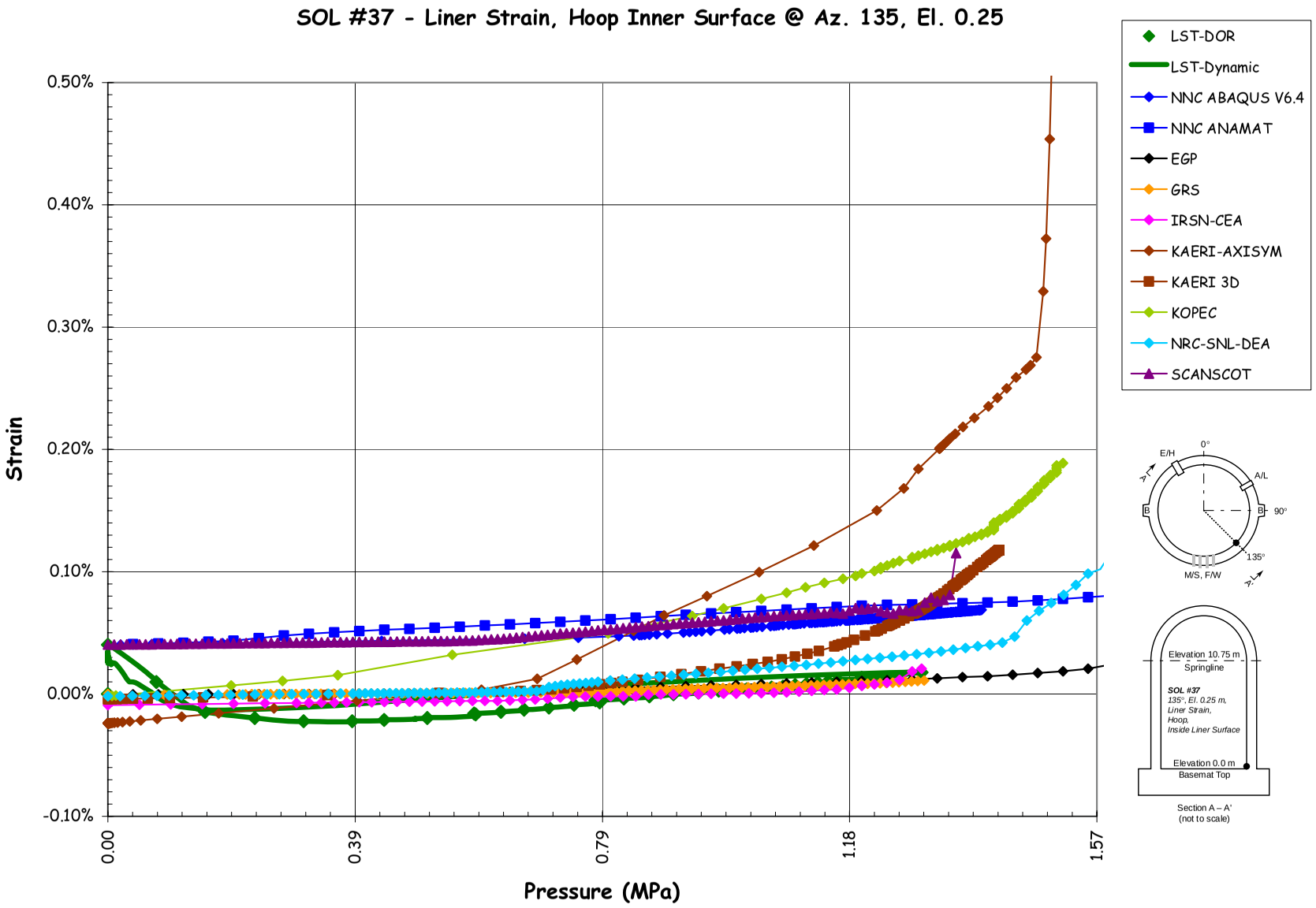
SOL #37 - Liner Strain, Hoop Inner Surface @ Az. 135, El. 0.25
Strain
0.50%
0.40%
0.30%
0.20%
0.10%
0.00%
-0.10%
0.00
0.39
0.79
1.18
1.57
Pressure (MPa)
LST-DOR
LST-Dynamic
NNC ABAQUS V6.4
NNC ANAMAT
EGP
GRS
IRSN-CEA
KAERI-AXISYM
KAERI 3D
KOPEC
NRC-SNL-DEA
SCANSCOT
E/H
0°
A/L
90°
135°
M/S, F/W
Elevation 10.75 m
Springline
SOL #37
135°, El. 0.25 m,
Liner Strain,
Hoop,
Inside Liner Surface
Elevation 0.0 m
Basemat Top
Section A – A'
(not to scale)

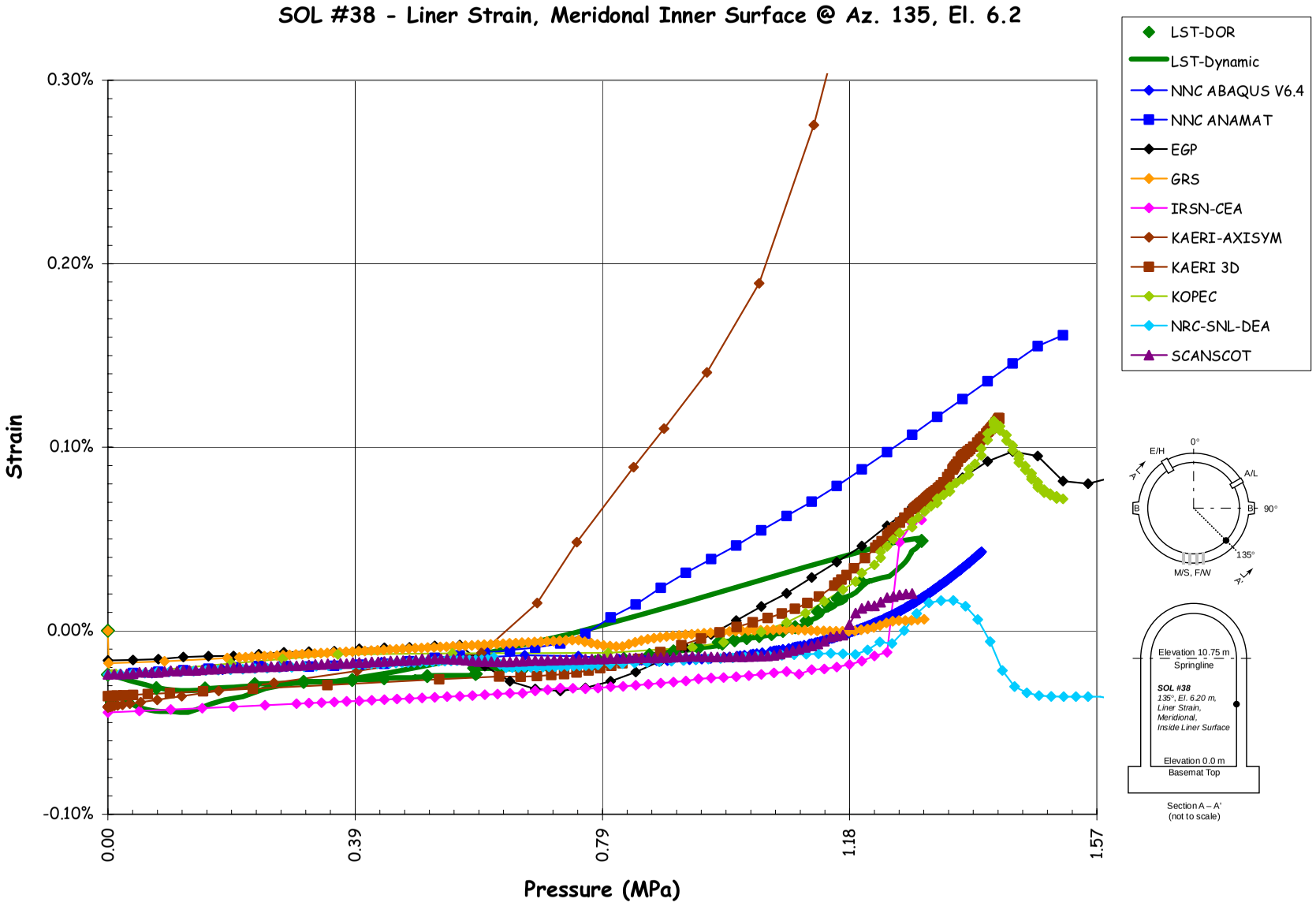
SOL #38 - Liner Strain, Meridonal Inner Surface @ Az. 135, El. 6.2
Strain
0.30%
0.20%
0.10%
0.00%
-0.10%
0.00
0.39
0.79
1.18
1.57
Pressure (MPa)
LST-DOR
LST-Dynamic
NNC ABAQUS V6.4
NNC ANAMAT
EGP
GRS
IRSN-CEA
KAERI-AXISYM
KAERI 3D
KOPEC
NRC-SNL-DEA
SCANSCOT
E/H
0°
A/L
90°
135°
M/S, F/W
Elevation 10.75 m
Springline
SOL #38
135°, El. 6.20 m,
Liner Strain,
Meridonal,
Inside Liner Surface
Elevation 0.0 m
Basemat Top
Section A – A'
(not to scale)

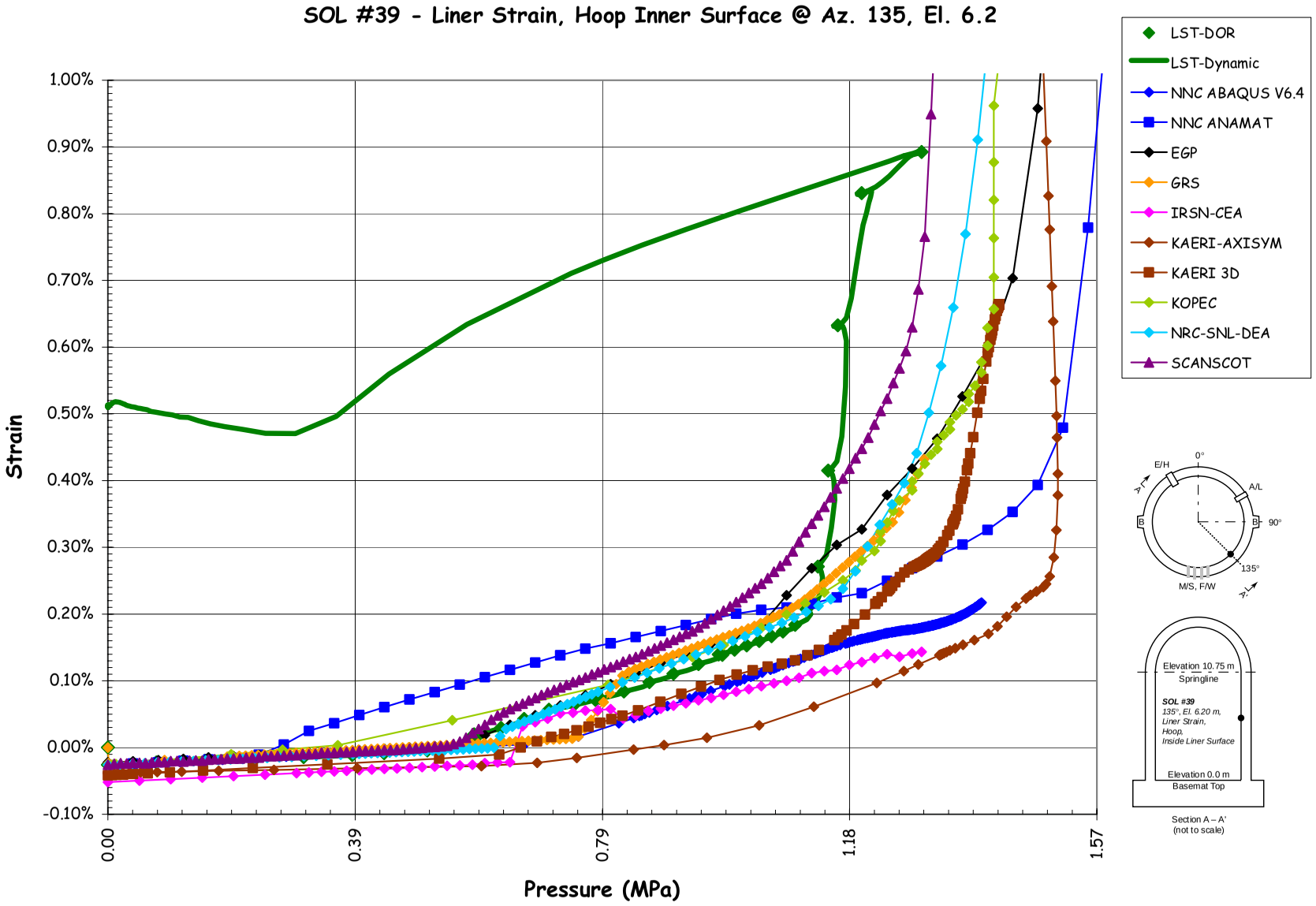
SOL #39 - Liner Strain, Hoop Inner Surface @ Az. 135, El. 6.2
Strain
1.00%
0.90%
0.80%
0.70%
0.60%
0.50%
0.40%
0.30%
0.20%
0.10%
0.00%
-0.10%
0.00
0.39
0.79
1.18
1.57
Pressure (MPa)
LST-DOR
LST-Dynamic
NNC ABAQUS V6.4
NNC ANAMAT
EGP
GRS
IRSN-CEA
KAERI-AXISYM
KAERI 3D
KOPEC
NRC-SNL-DEA
SCANSCOT
0°
E/H
A/L
90°
135°
M/S, F/W
Elevation 10.75 m
Springline
SOL #39
135°, El. 6.20 m,
Liner Strain,
Hoop,
Inside Liner Surface
Elevation 0.0 m
Basemat Top
Section A – A'
(not to scale)

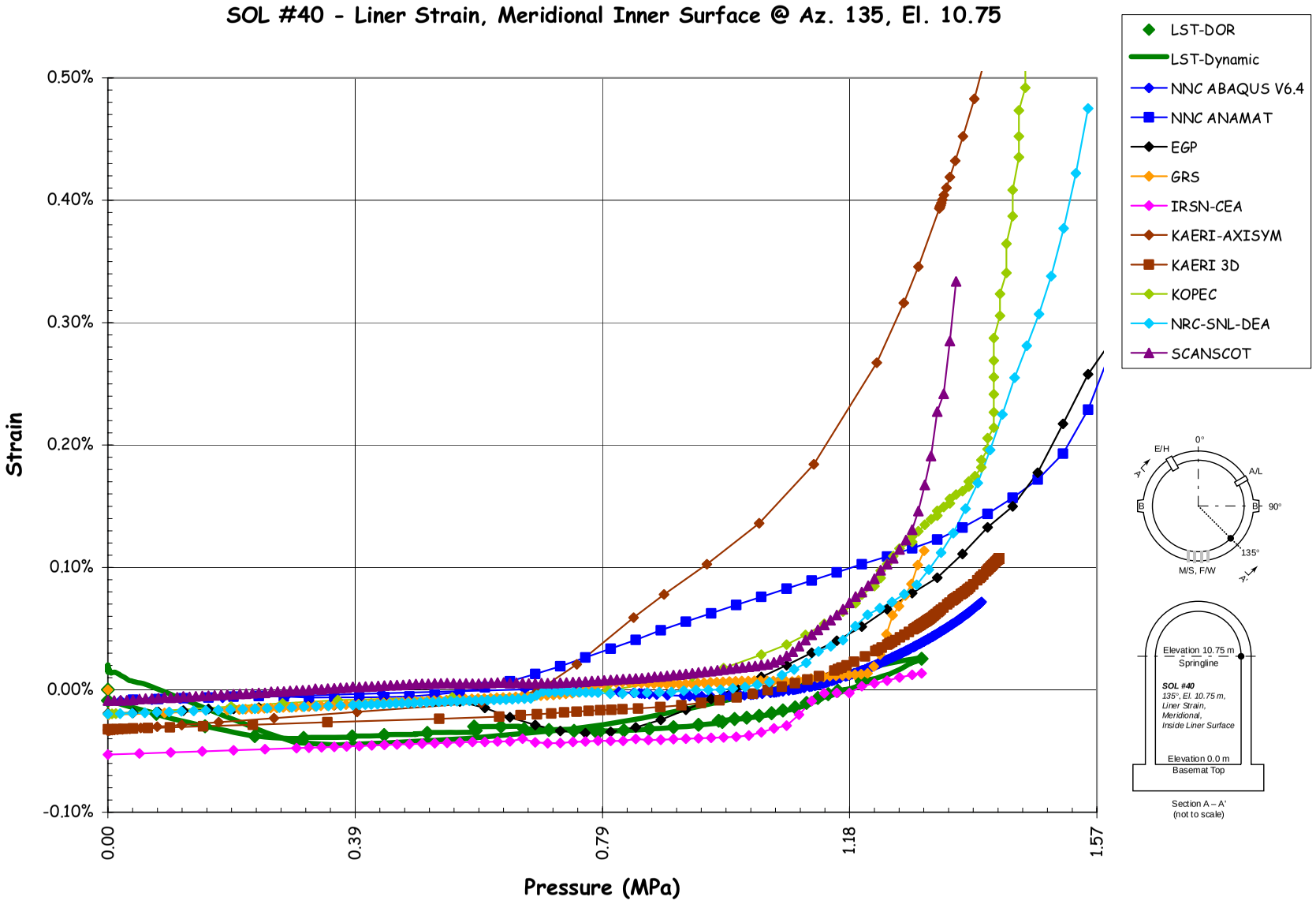
SOL #40 - Liner Strain, Meridional Inner Surface @ Az. 135, El. 10.75
Strain
0.50%
0.40%
0.30%
0.20%
0.10%
0.00%
-0.10%
0.00
0.39
0.79
1.18
1.57
Pressure (MPa)
LST-DOR
LST-Dynamic
NNC ABAQUS V6.4
NNC ANAMAT
EGP
GRS
IRSN-CEA
KAERI-AXISYM
KAERI 3D
KOPEC
NRC-SNL-DEA
SCANSCOT
0°
E/H
A/L
90°
135°
M/S, F/W
Elevation 10.75 m
Springline
SOL #40
135°, El. 10.75 m,
Liner Strain,
Meridional,
Inside Liner Surface
Elevation 0.0 m
Basemat Top
Section A – A'
(not to scale)

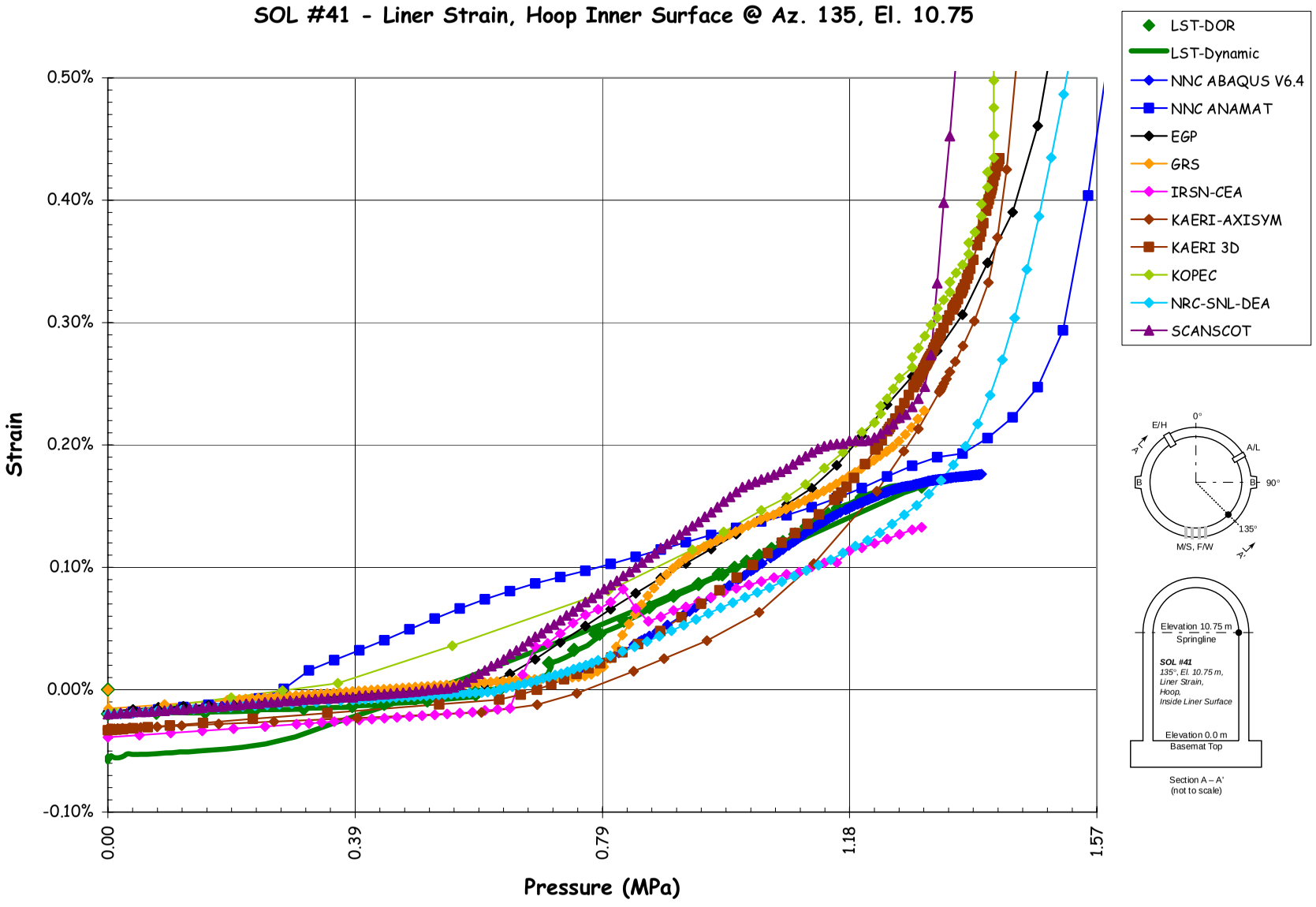
SOL #41 - Liner Strain, Hoop Inner Surface @ Az. 135, El. 10.75
Strain
0.50%
0.40%
0.30%
0.20%
0.10%
0.00%
-0.10%
0.00
0.39
0.79
1.18
1.57
Pressure (MPa)
LST-DOR
LST-Dynamic
NNC ABAQUS V6.4
NNC ANAMAT
EGP
GRS
IRSN-CEA
KAERI-AXISYM
KAERI 3D
KOPEC
NRC-SNL-DEA
SCANSCOT
E/H
0°
A/L
90°
135°
M/S, F/W
Elevation 10.75 m
Springline
SOL #41
135°, El. 10.75 m,
Liner Strain,
Hoop,
Inside Liner Surface
Elevation 0.0 m
Basemat Top
Section A – A'
(not to scale)

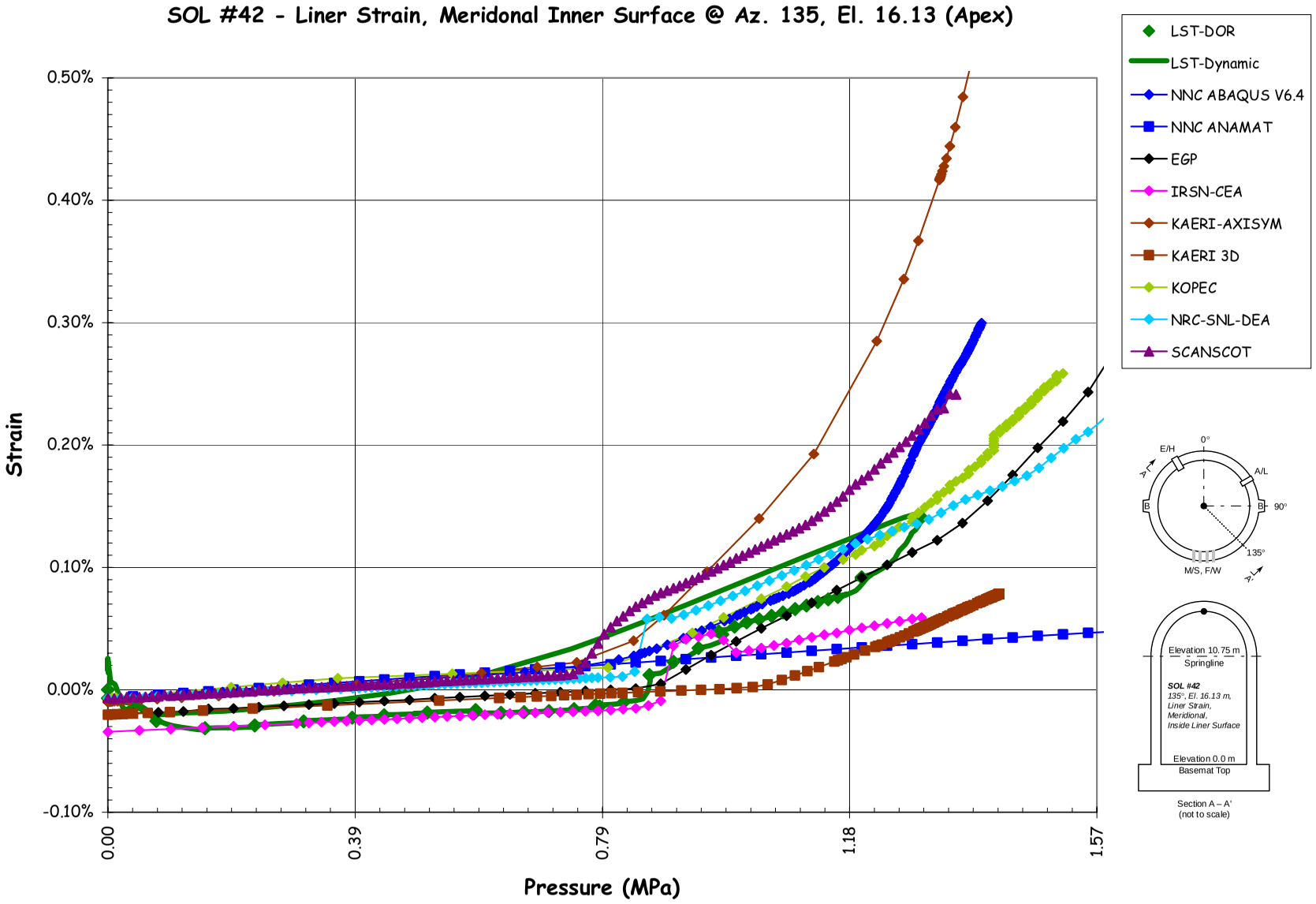
SOL #42 - Liner Strain, Meridonal Inner Surface @ Az. 135, El. 16.13 (Apex)
Strain
0.50%
0.40%
0.30%
0.20%
0.10%
0.00%
-0.10%
0.00
0.39
0.79
1.18
1.57
Pressure (MPa)
LST-DOR
LST-Dynamic
NNC ABAQUS V6.4
NNC ANAMAT
EGP
IRSN-CEA
KAERI-AXISYM
KAERI 3D
KOPEC
NRC-SNL-DEA
SCANSCOT
E/H
0°
A/L
90°
135°
M/S, F/W
Elevation 10.75 m
Springline
SOL #42
135°, El. 16.13 m,
Liner Strain,
Meridonal,
Inside Liner Surface
Elevation 0.0 m
Basemat Top
Section A – A'
(not to scale)

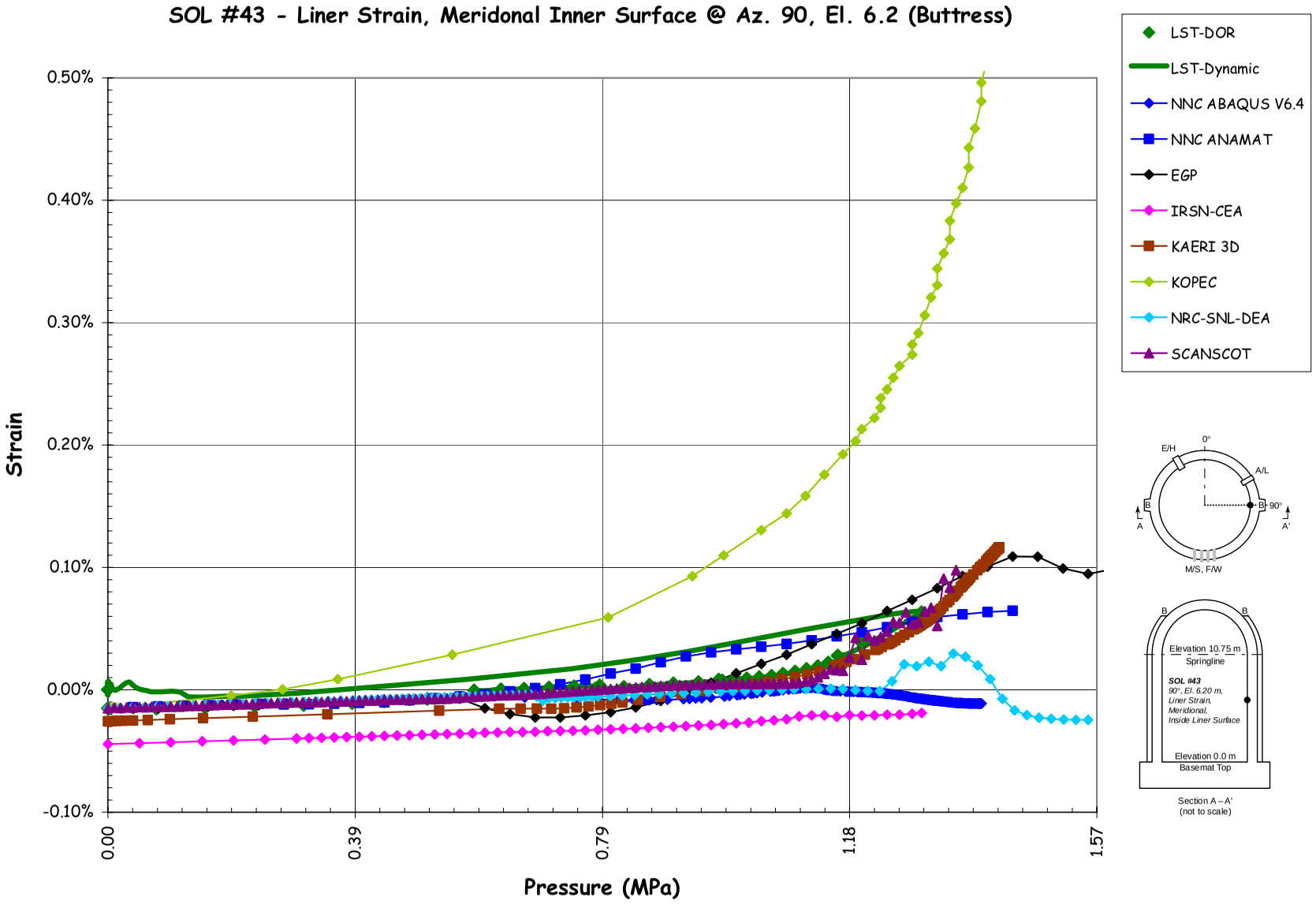
SOL #43 - Liner Strain, Meridonal Inner Surface @ Az. 90, El. 6.2 (Buttress)
Strain
0.50%
0.40%
0.30%
0.20%
0.10%
0.00%
-0.10%
0.00
0.39
0.79
1.18
1.57
Pressure (MPa)
LST-DOR
LST-Dynamic
NNC ABAQUS V6.4
NNC ANAMAT
EGP
IRSN-CEA
KAERI 3D
KOPEC
NRC-SNL-DEA
SCANSCOT
E/H
0°
A/L
90°
M/S, F/W
Elevation 10.75 m
Springline
SOL #43
90°, El. 6.20 m,
Liner Strain,
Meridional,
Inside Liner Surface
Elevation 0.0 m
Basemat Top
Section A – A'
(not to scale)

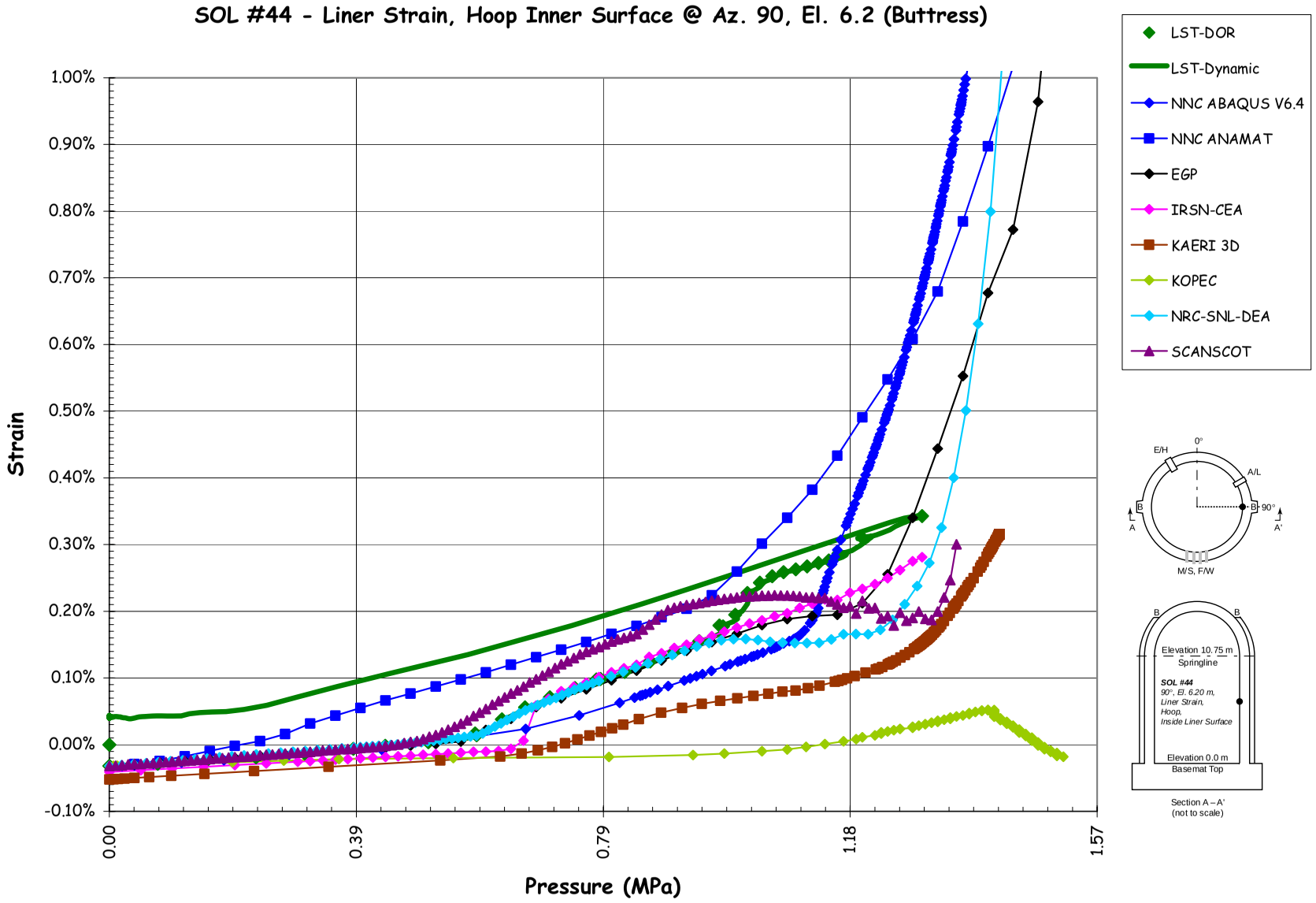
SOL #44 - Liner Strain, Hoop Inner Surface @ Az. 90, El. 6.2 (Buttress)
Strain
1.00%
0.90%
0.80%
0.70%
0.60%
0.50%
0.40%
0.30%
0.20%
0.10%
0.00%
-0.10%
0.00
0.39
0.79
1.18
1.57
Pressure (MPa)
LST-DOR
LST-Dynamic
NNC ABAQUS V6.4
NNC ANAMAT
EGP
IRSN-CEA
KAERI 3D
KOPEC
NRC-SNL-DEA
SCANSCOT
E/H
0°
A/L
90°
A
A'
M/S, F/W
B
B
Elevation 10.75 m
Springline
SOL #44
90°, El. 6.20 m,
Liner Strain,
Hoop,
Inside Liner Surface
Elevation 0.0 m
Basemat Top
Section A – A'
(not to scale)

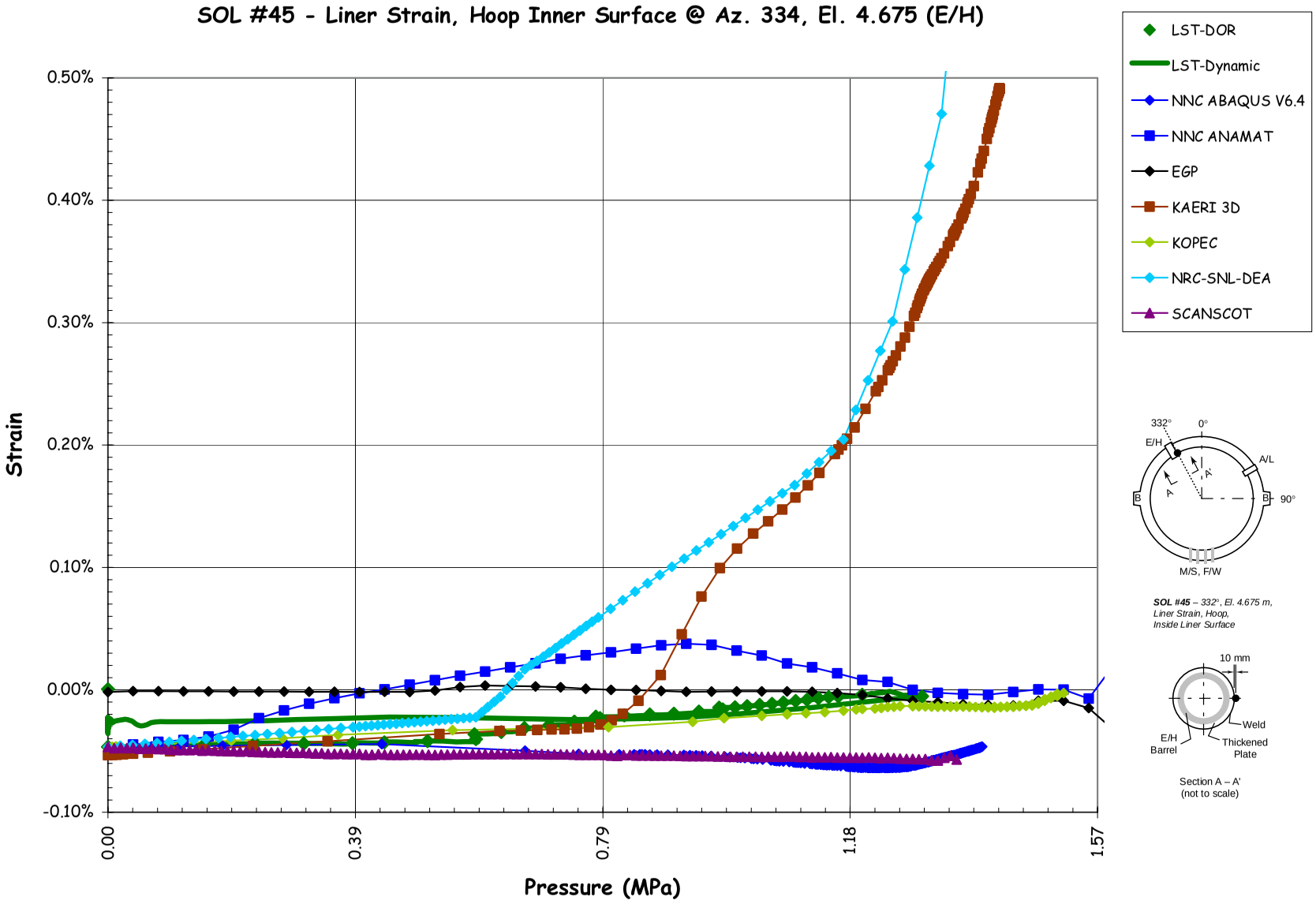
SOL #45 - Liner Strain, Hoop Inner Surface @ Az. 334, El. 4.675 (E/H)
LST-DOR
LST-Dynamic
NNC ABAQUS V6.4
NNC ANAMAT
EGP
KAERI 3D
KOPEC
NRC-SNL-DEA
SCANSCOT
0.50%
0.40%
0.30%
0.20%
0.10%
0.00%
-0.10%
Strain
0.00
0.39
0.79
1.18
1.57
Pressure (MPa)
332°
0°
E/H
A/L
90°
B
M/S, F/W
SOL #45 – 332°, El. 4.675 m,
Liner Strain, Hoop,
Inside Liner Surface
10 mm
Weld
E/H
Barrel
Thickened
Plate
Section A – A'
(not to scale)

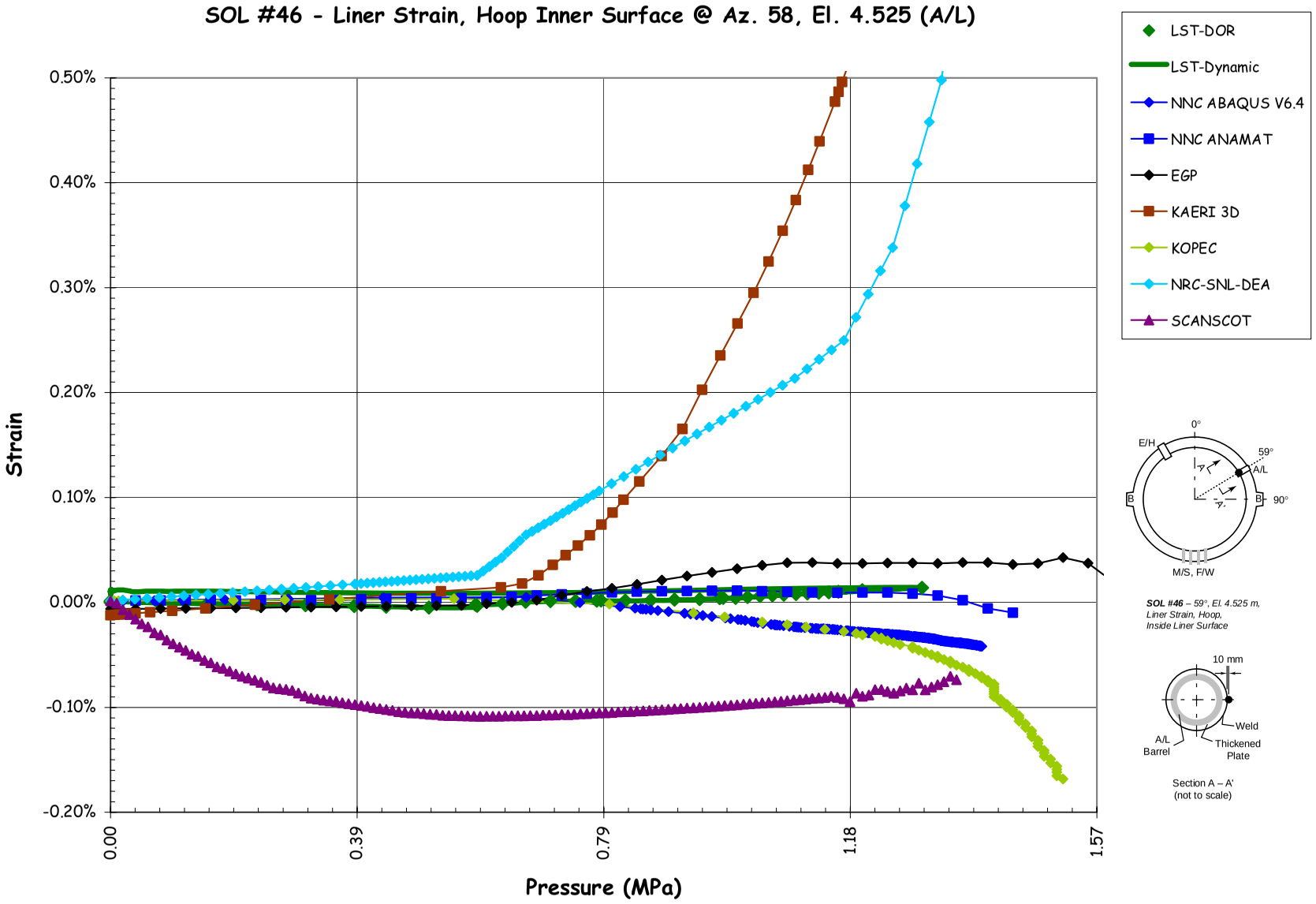
SOL #46 - Liner Strain, Hoop Inner Surface @ Az. 58, El. 4.525 (A/L)
Strain
0.50%
0.40%
0.30%
0.20%
0.10%
0.00%
-0.10%
-0.20%
0.00
0.39
0.79
1.18
1.57
Pressure (MPa)
LST-DOR
LST-Dynamic
NNC ABAQUS V6.4
NNC ANAMAT
EGP
KAERI 3D
KOPEC
NRC-SNL-DEA
SCANSCOT
0°
E/H
59°
A/L
B
B
90°
M/S, F/W
SOL #46 – 59°, El. 4.525 m, Liner Strain, Hoop, Inside Liner Surface
10 mm
Weld
A/L
Barrel
Thickened
Plate
Section A – A'
(not to scale)

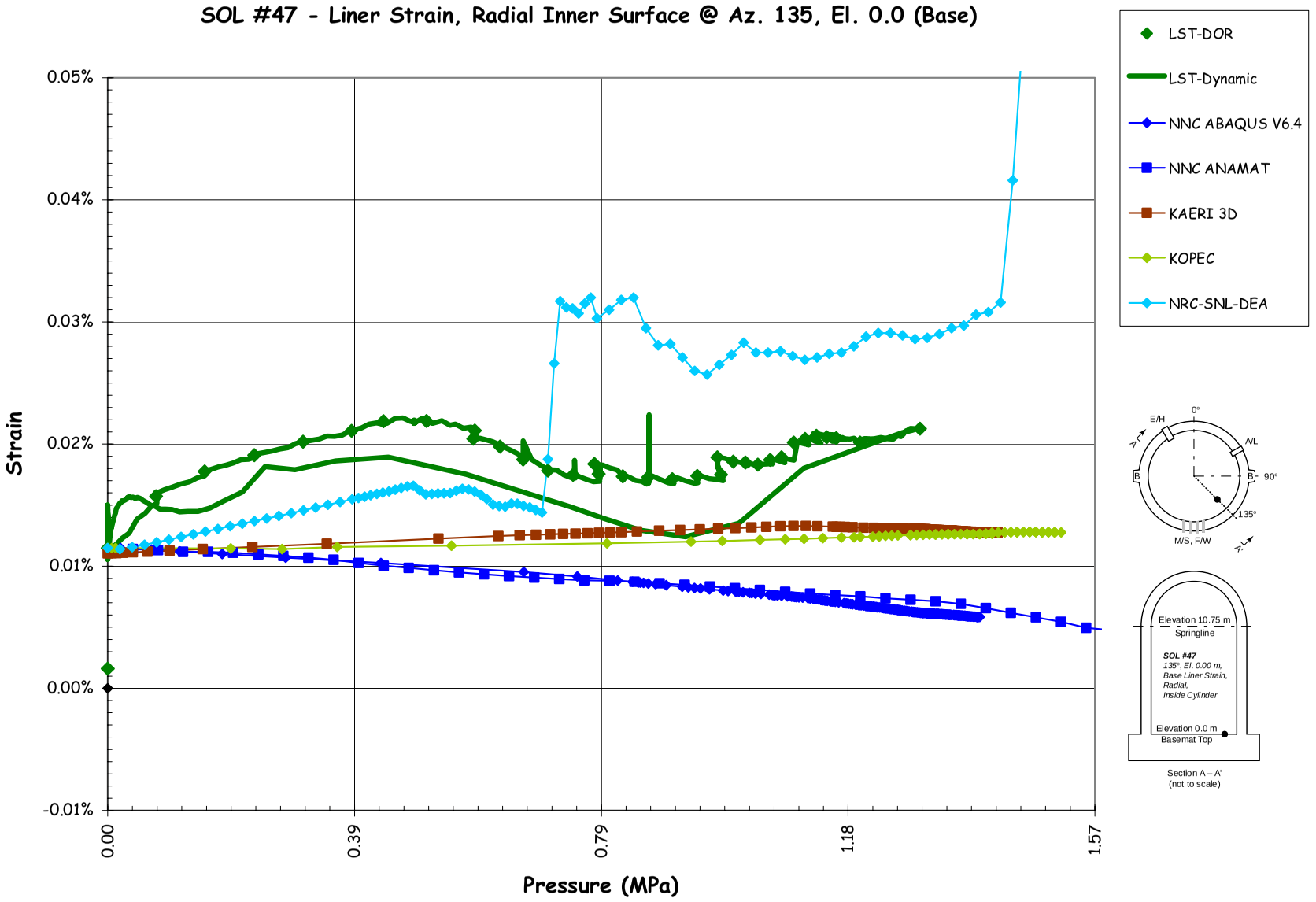
SOL #47 - Liner Strain, Radial Inner Surface @ Az. 135, El. 0.0 (Base)
LST-DOR
LST-Dynamic
NNC ABAQUS V6.4
NNC ANAMAT
KAERI 3D
KOPEC
NRC-SNL-DEA
0.05%
0.04%
0.03%
0.02%
0.01%
0.00%
-0.01%
Strain
0.00
0.39
0.79
1.18
1.57
Pressure (MPa)
E/H
A/L
B
B
90°
0°
135°
M/S, F/W
Elevation 10.75 m
Springline
SOL #47
135°, El. 0.00 m,
Base Liner Strain,
Radial,
Inside Cylinder
Elevation 0.0 m
Basemat Top
Section A – A'
(not to scale)

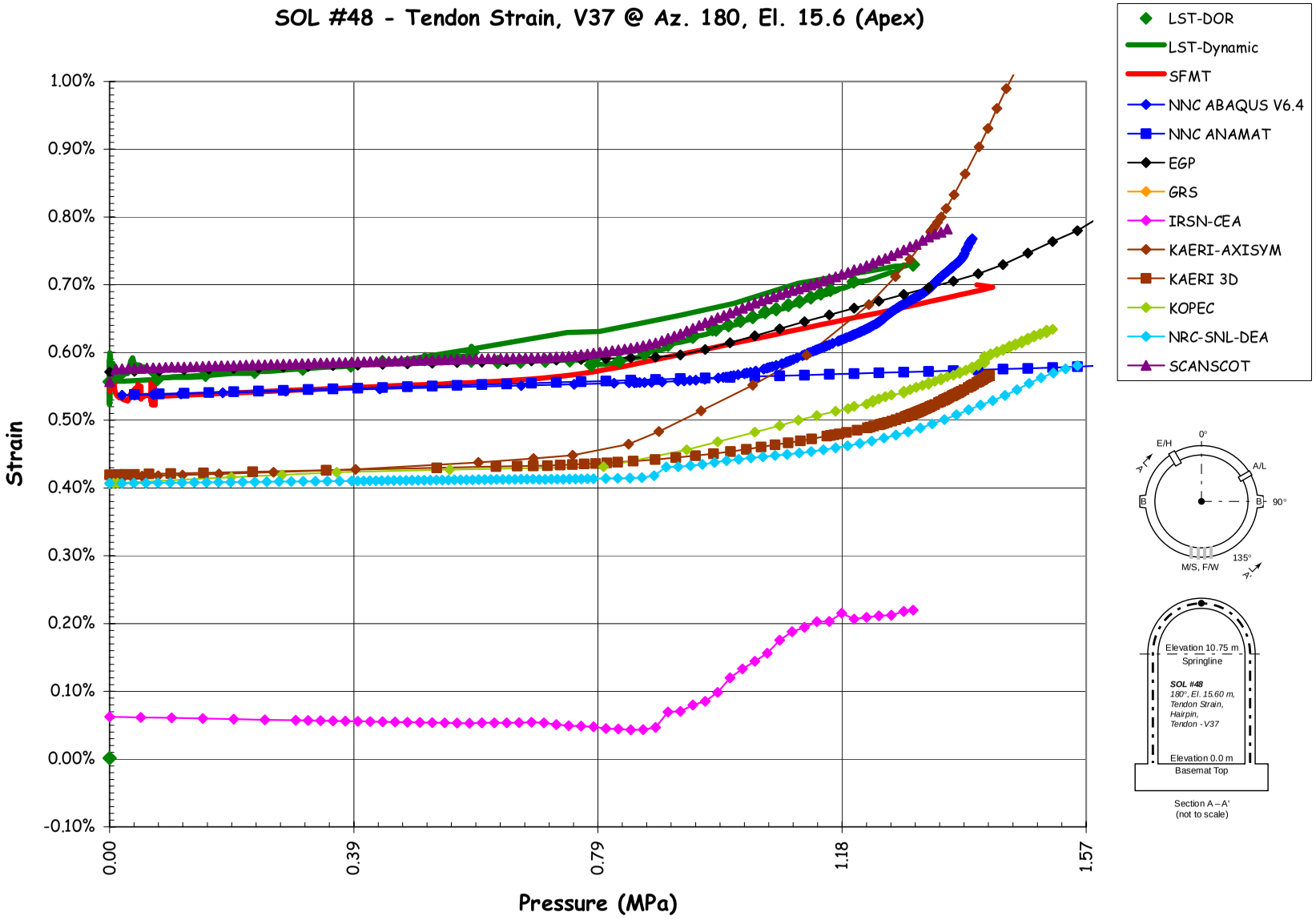
SOL #48 - Tendon Strain, V37 @ Az. 180, El. 15.6 (Apex)
Strain
1.00%
0.90%
0.80%
0.70%
0.60%
0.50%
0.40%
0.30%
0.20%
0.10%
0.00%
-0.10%
0.00
0.39
0.79
1.18
1.57
Pressure (MPa)
LST-DOR
LST-Dynamic
SFMT
NNC ABAQUS V6.4
NNC ANAMAT
EGP
GRS
IRSN-CEA
KAERI-AXISYM
KAERI 3D
KOPEC
NRC-SNL-DEA
SCANSCOT
0°
E/H
A/L
90°
M/S, F/W
135°
Elevation 10.75 m
Springline
SOL #48
180°, El. 15.60 m,
Tendon Strain,
Hairpin,
Tendon - V37
Elevation 0.0 m
Basemat Top
Section A – A'
(not to scale)

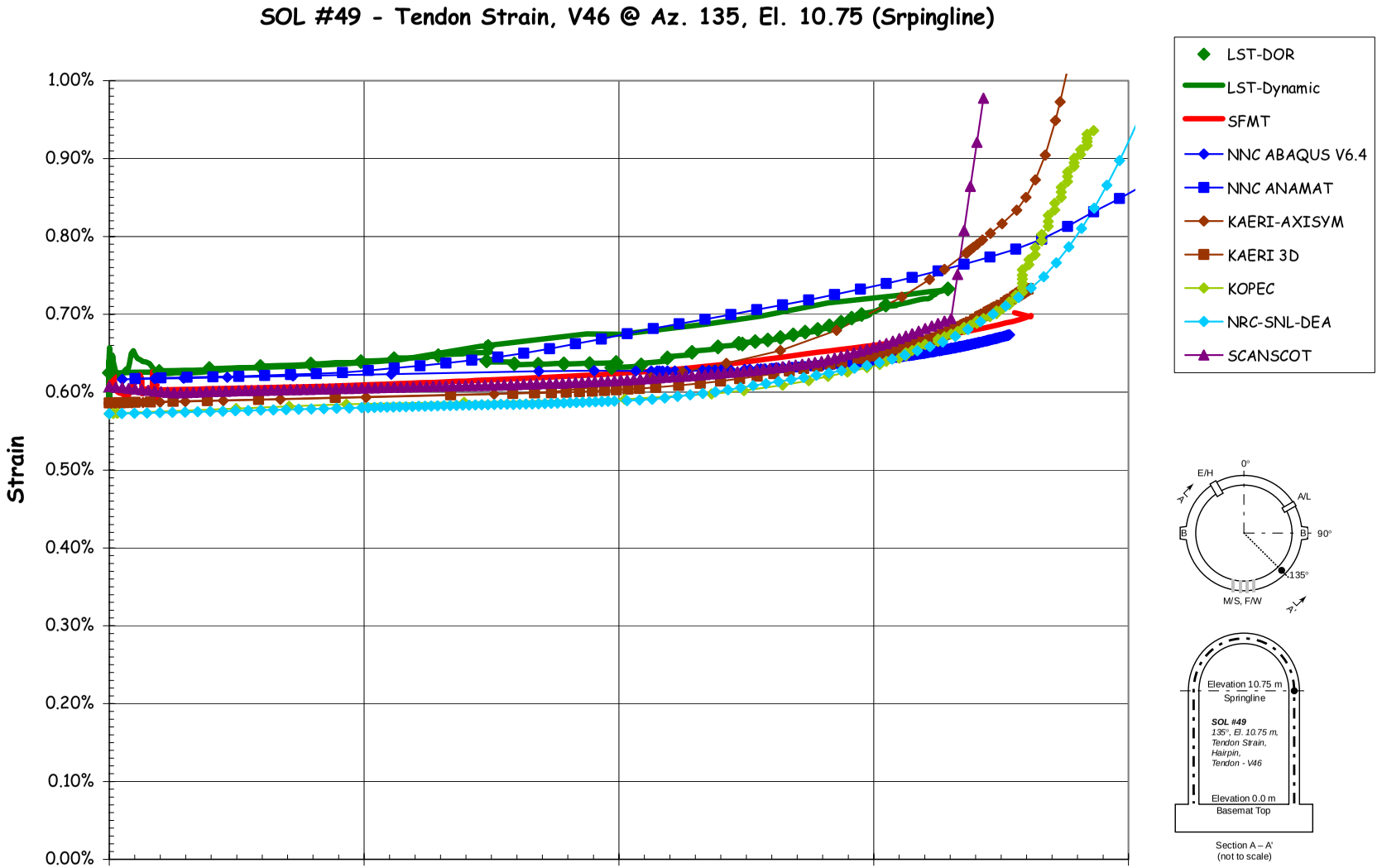
SOL #49 - Tendon Strain, V46 @ Az. 135, El. 10.75 (Srpingline)
Strain
1.00%
0.90%
0.80%
0.70%
0.60%
0.50%
0.40%
0.30%
0.20%
0.10%
0.00%
0.00
0.39
0.79
1.18
1.57
Pressure (MPa)
LST-DOR
LST-Dynamic
SFMT
NNC ABAQUS V6.4
NNC ANAMAT
KAERI-AXISYM
KAERI 3D
KOPEC
NRC-SNL-DEA
SCANSCOT
E/H
A/L
0°
90°
135°
M/S, F/W
Elevation 10.75 m
Springline
SOL #49
135°, El. 10.75 m,
Tendon Strain,
Hairpin,
Tendon - V46
Elevation 0.0 m
Basemat Top
Section A – A'
(not to scale)

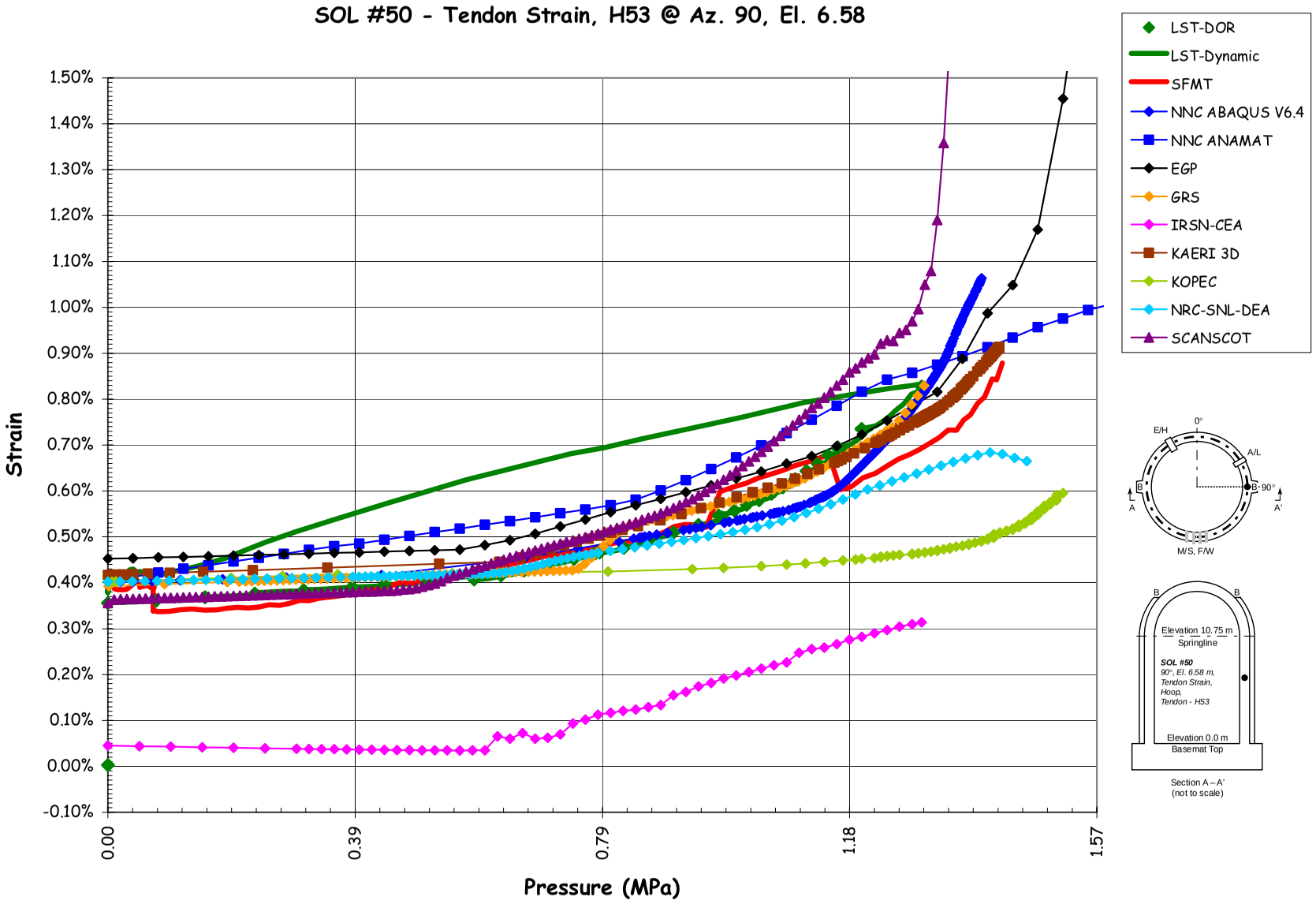
SOL #50 - Tendon Strain, H53 @ Az. 90, El. 6.58
Strain
1.50%
1.40%
1.30%
1.20%
1.10%
1.00%
0.90%
0.80%
0.70%
0.60%
0.50%
0.40%
0.30%
0.20%
0.10%
0.00%
-0.10%
0.00
0.39
0.79
1.18
1.57
Pressure (MPa)
LST-DOR
LST-Dynamic
SFMT
NNC ABAQUS V6.4
NNC ANAMAT
EGP
GRS
IRSN-CEA
KAERI 3D
KOPEC
NRC-SNL-DEA
SCANSCOT
E/H
0°
A/L
90°
A
A'
M/S, F/W
B
B
Elevation 10.75 m
Springline
SOL #50
90°, El. 6.58 m,
Tendon Strain,
Hoop,
Tendon - H53
Elevation 0.0 m
Basemat Top
Section A – A'
(not to scale)

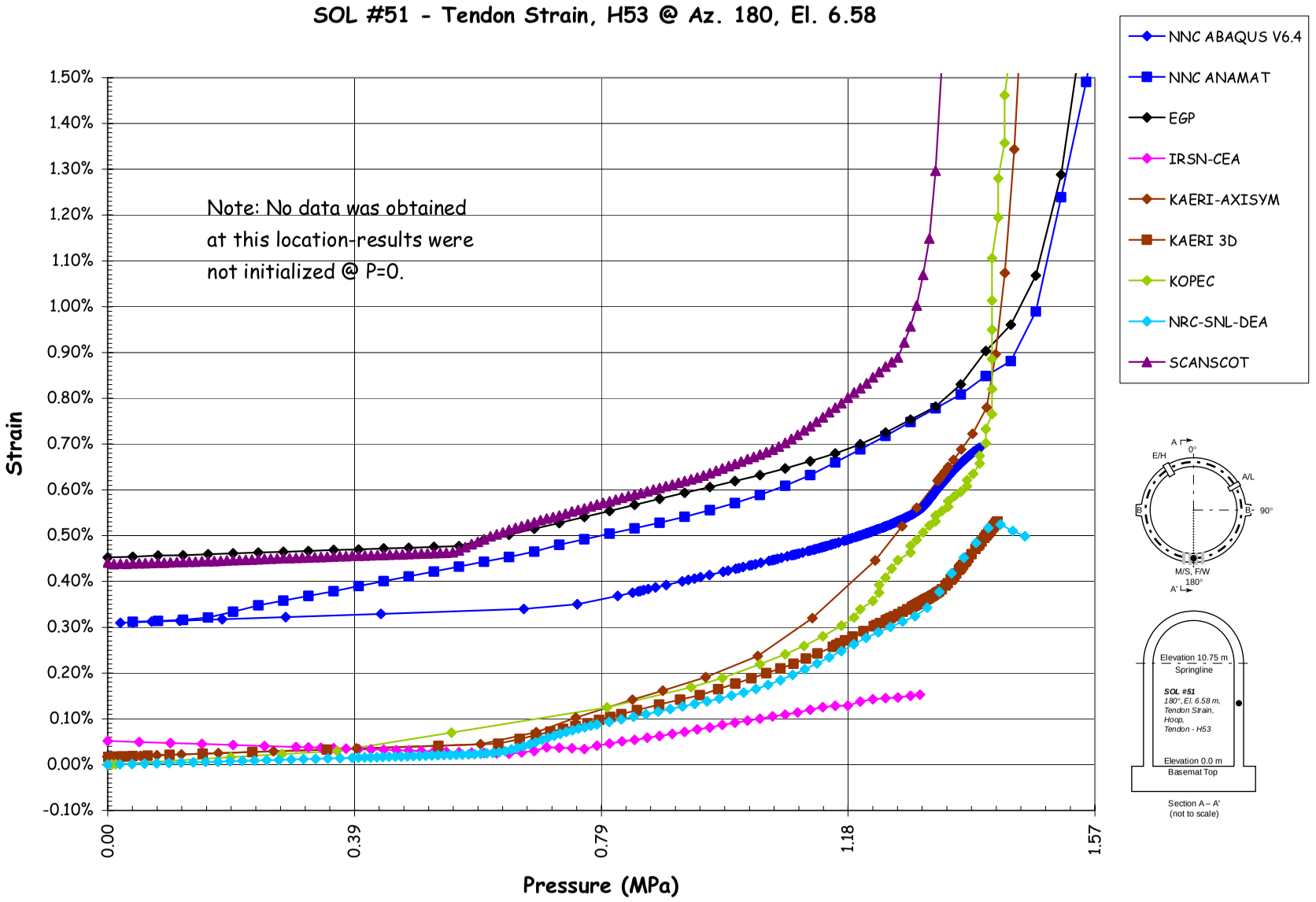
SOL #51 - Tendon Strain, H53 @ Az. 180, El. 6.58
Note: No data was obtained at this location-results were not initialized @ P=0.
Strain
1.50%
1.40%
1.30%
1.20%
1.10%
1.00%
0.90%
0.80%
0.70%
0.60%
0.50%
0.40%
0.30%
0.20%
0.10%
0.00%
-0.10%
0.00
0.39
0.79
1.18
1.57
Pressure (MPa)
NNC ABAQUS V6.4
NNC ANAMAT
EGP
IRSN-CEA
KAERI-AXISYM
KAERI 3D
KOPEC
NRC-SNL-DEA
SCANSCOT
A
0°
E/H
A/L
B
B
90°
M/S, F/W
180°
A'
Elevation 10.75 m
Springline
SOL #51
180°, El. 6.58 m,
Tendon Strain,
Hoop,
Tendon - H53
Elevation 0.0 m
Basemat Top
Section A – A'
(not to scale)

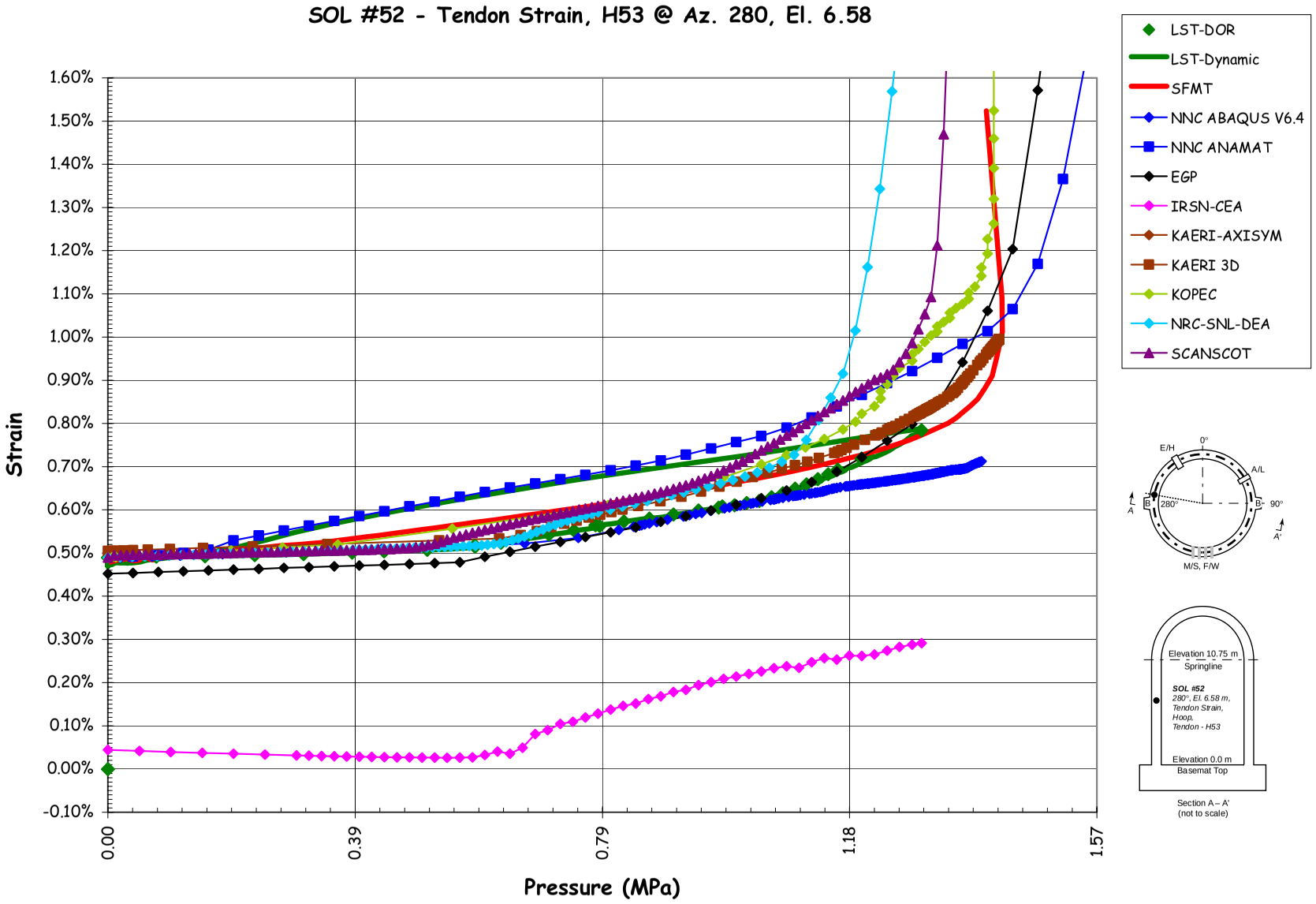
SOL #52 - Tendon Strain, H53 @ Az. 280, El. 6.58
Strain
1.60%
1.50%
1.40%
1.30%
1.20%
1.10%
1.00%
0.90%
0.80%
0.70%
0.60%
0.50%
0.40%
0.30%
0.20%
0.10%
0.00%
-0.10%
0.00
0.39
0.79
1.18
1.57
Pressure (MPa)
LST-DOR
LST-Dynamic
SFMT
NNC ABAQUS V6.4
NNC ANAMAT
EGP
IRSN-CEA
KAERI-AXISYM
KAERI 3D
KOPEC
NRC-SNL-DEA
SCANSCOT
E/H
0°
A/L
280°
90°
M/S, F/W
Elevation 10.75 m
Springline
SOL #52
280°, El. 6.58 m,
Tendon Strain,
Hoop,
Tendon - H53
Elevation 0.0 m
Basemat Top
Section A – A'
(not to scale)

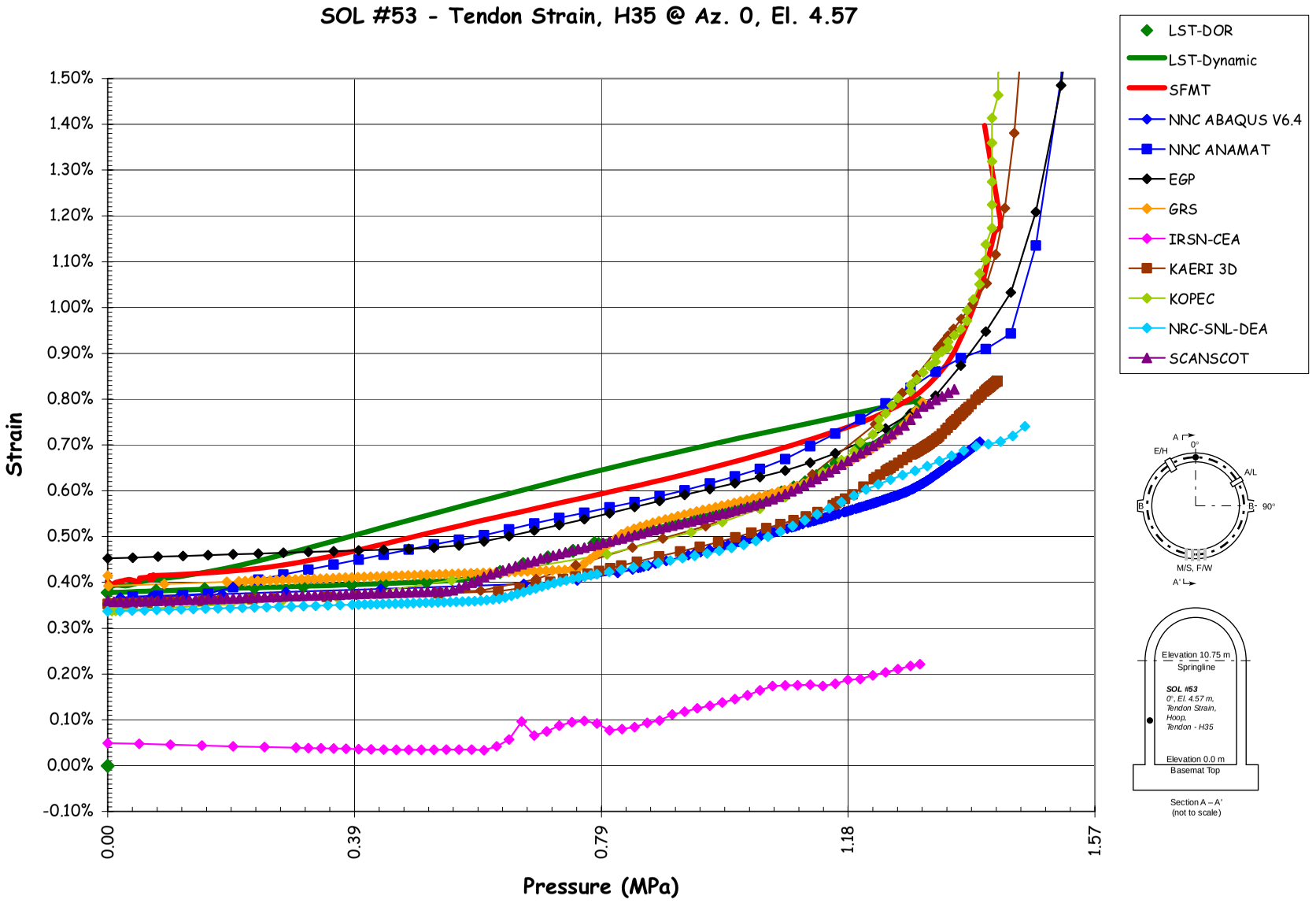
SOL #53 - Tendon Strain, H35 @ Az. 0, El. 4.57
Strain
1.50%
1.40%
1.30%
1.20%
1.10%
1.00%
0.90%
0.80%
0.70%
0.60%
0.50%
0.40%
0.30%
0.20%
0.10%
0.00%
-0.10%
0.00
0.39
0.79
1.18
1.57
Pressure (MPa)
LST-DOR
LST-Dynamic
SFMT
NNC ABAQUS V6.4
NNC ANAMAT
EGP
GRS
IRSN-CEA
KAERI 3D
KOPEC
NRC-SNL-DEA
SCANSCOT
A
0°
E/H
A/L
B
90°
M/S, F/W
A'
Elevation 10.75 m
Springline
SOL #53
0°, El. 4.57 m,
Tendon Strain,
Hoop,
Tendon - H35
Elevation 0.0 m
Basemat Top
Section A – A'
(not to scale)

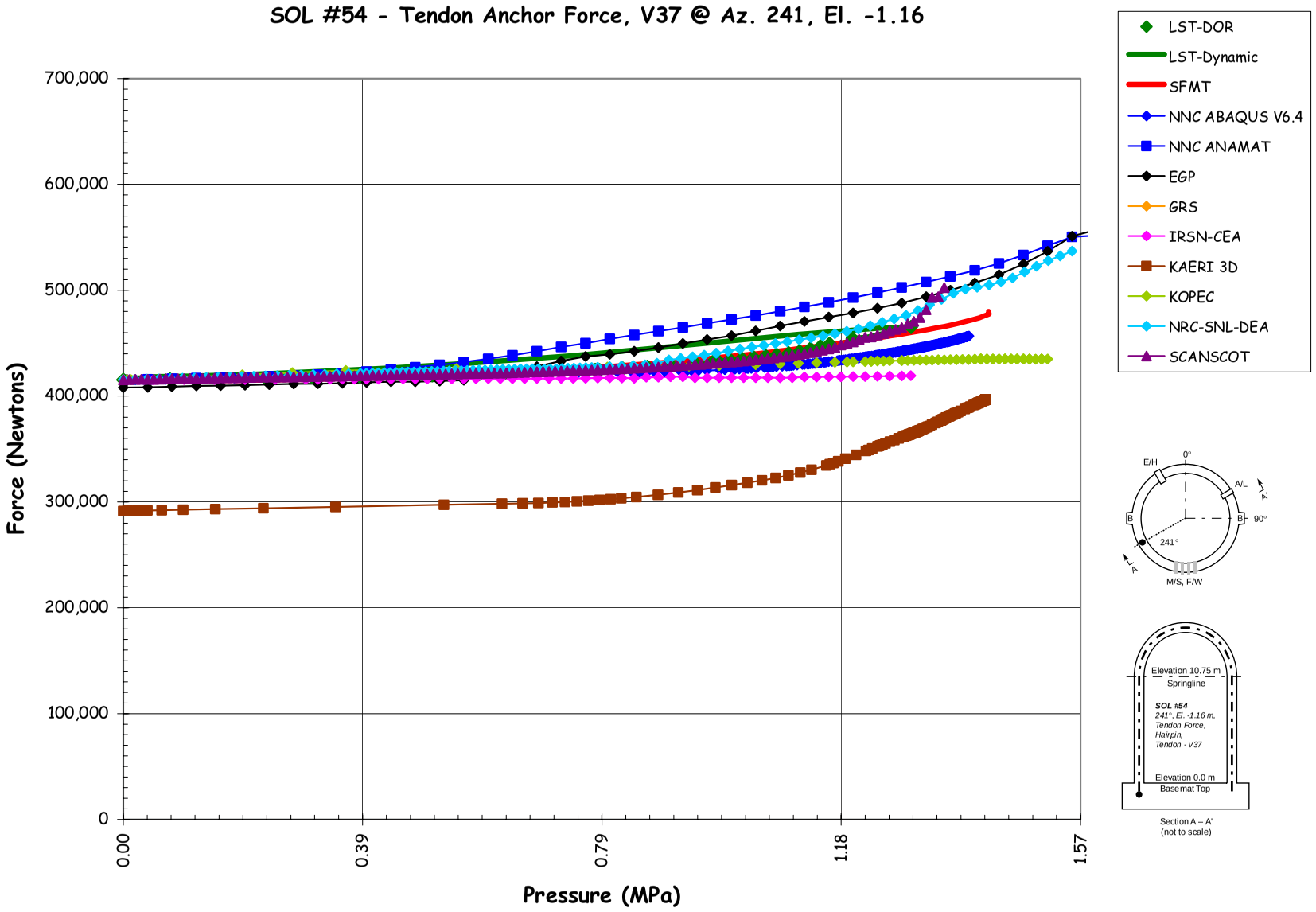
SOL #54 - Tendon Anchor Force, V37 @ Az. 241, El. -1.16
Force (Newtons)
700,000
600,000
500,000
400,000
300,000
200,000
100,000
0
0.00
0.39
0.79
1.18
1.57
Pressure (MPa)
LST-DOR
LST-Dynamic
SFMT
NNC ABAQUS V6.4
NNC ANAMAT
EGP
GRS
IRSN-CEA
KAERI 3D
KOPEC
NRC-SNL-DEA
SCANSCOT
0°
E/H
A/L
B
B
90°
241°
M/S, F/W
Elevation 10.75 m
Springline
SOL #54
241°, El. -1.16 m,
Tendon Force,
Hairpin,
Tendon - V37
Elevation 0.0 m
Basemat Top
Section A – A'
(not to scale)

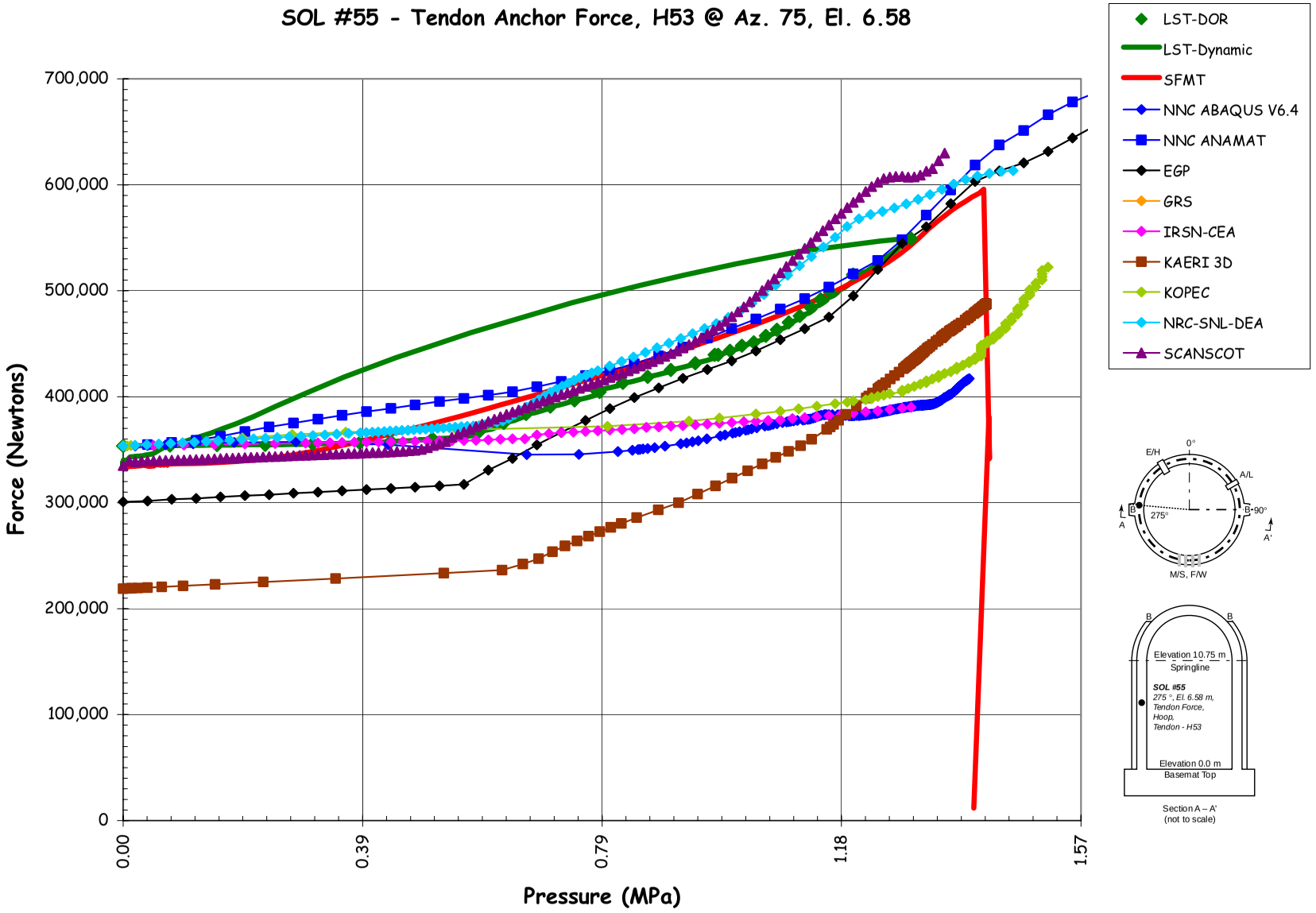
SOL #55 - Tendon Anchor Force, H53 @ Az. 75, El. 6.58
Force (Newtons)
700,000
600,000
500,000
400,000
300,000
200,000
100,000
0
0.00
0.39
0.79
1.18
1.57
Pressure (MPa)
LST-DOR
LST-Dynamic
SFMT
NNC ABAQUS V6.4
NNC ANAMAT
EGP
GRS
IRSN-CEA
KAERI 3D
KOPEC
NRC-SNL-DEA
SCANSCOT
0°
E/H
A/L
B
275°
B-90°
A
A'
M/S, F/W
B
B
Elevation 10.75 m
Springline
SOL #55
275 °, El. 6.58 m,
Tendon Force,
Hoop,
Tendon - H53
Elevation 0.0 m
Basemat Top
Section A – A'
(not to scale)

Appendix B: Phase 3 Case 1 Comparison Plots at Standard Output Locations: B-1 to B-66 Phase 3 Case 2: B-67 to B-135

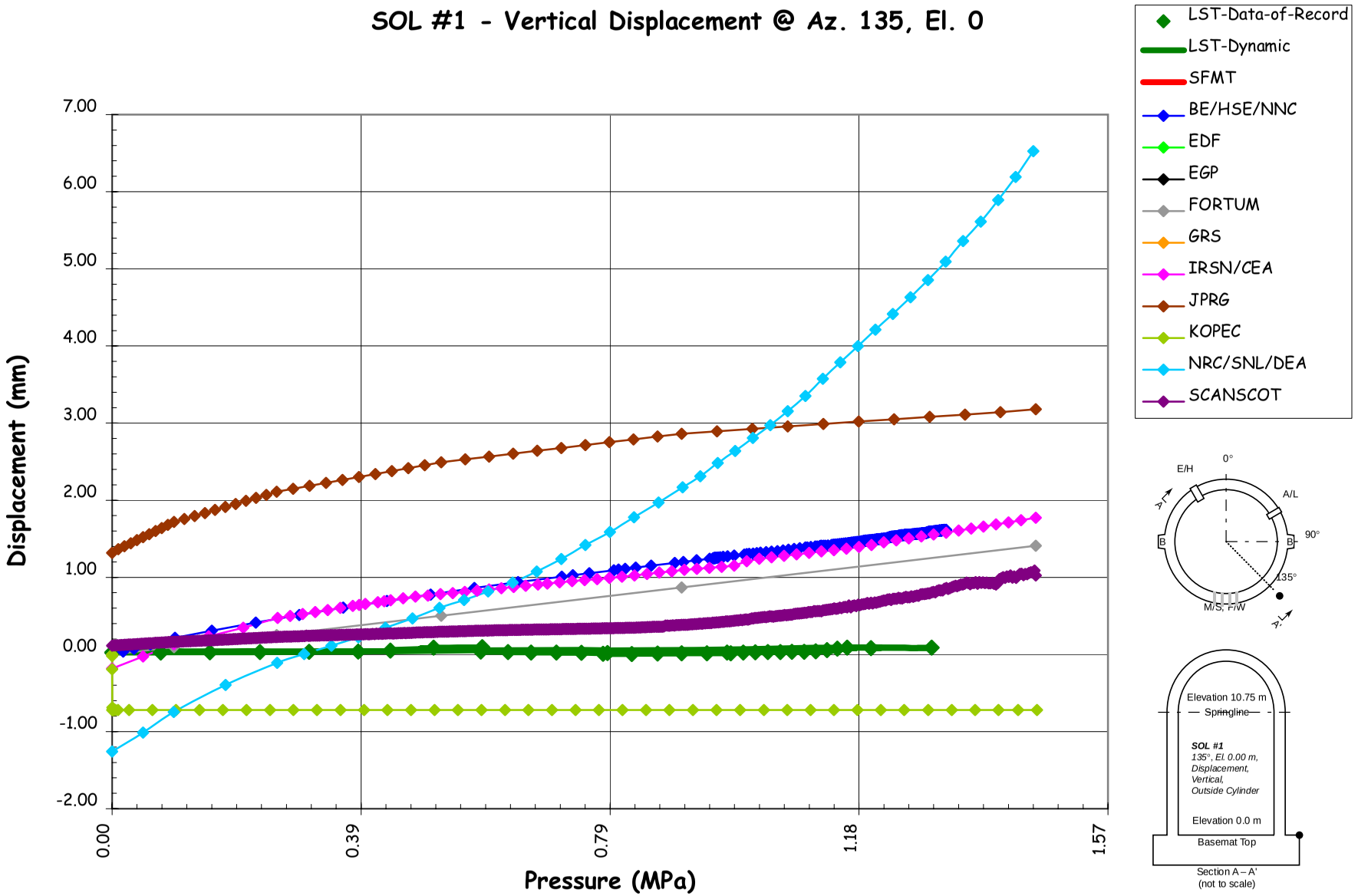
SOL #1 - Vertical Displacement @ Az. 135, El. 0
Displacement (mm)
7.00
6.00
5.00
4.00
3.00
2.00
1.00
0.00
-1.00
-2.00
0.00
0.39
0.79
1.18
1.57
Pressure (MPa)
LST-Data-of-Record
LST-Dynamic
SFMT
BE/HSE/NNC
EDF
EGP
FORTUM
GRS
IRSN/CEA
JPRG
KOPEC
NRC/SNL/DEA
SCANSCOT
0°
E/H
A/L
90°
135°
M/S, F/W
Elevation 10.75 m
Springline
SOL #1
135°, El. 0.00 m,
Displacement,
Vertical,
Outside Cylinder
Elevation 0.0 m
Basemat Top
Section A – A'
(not to scale)

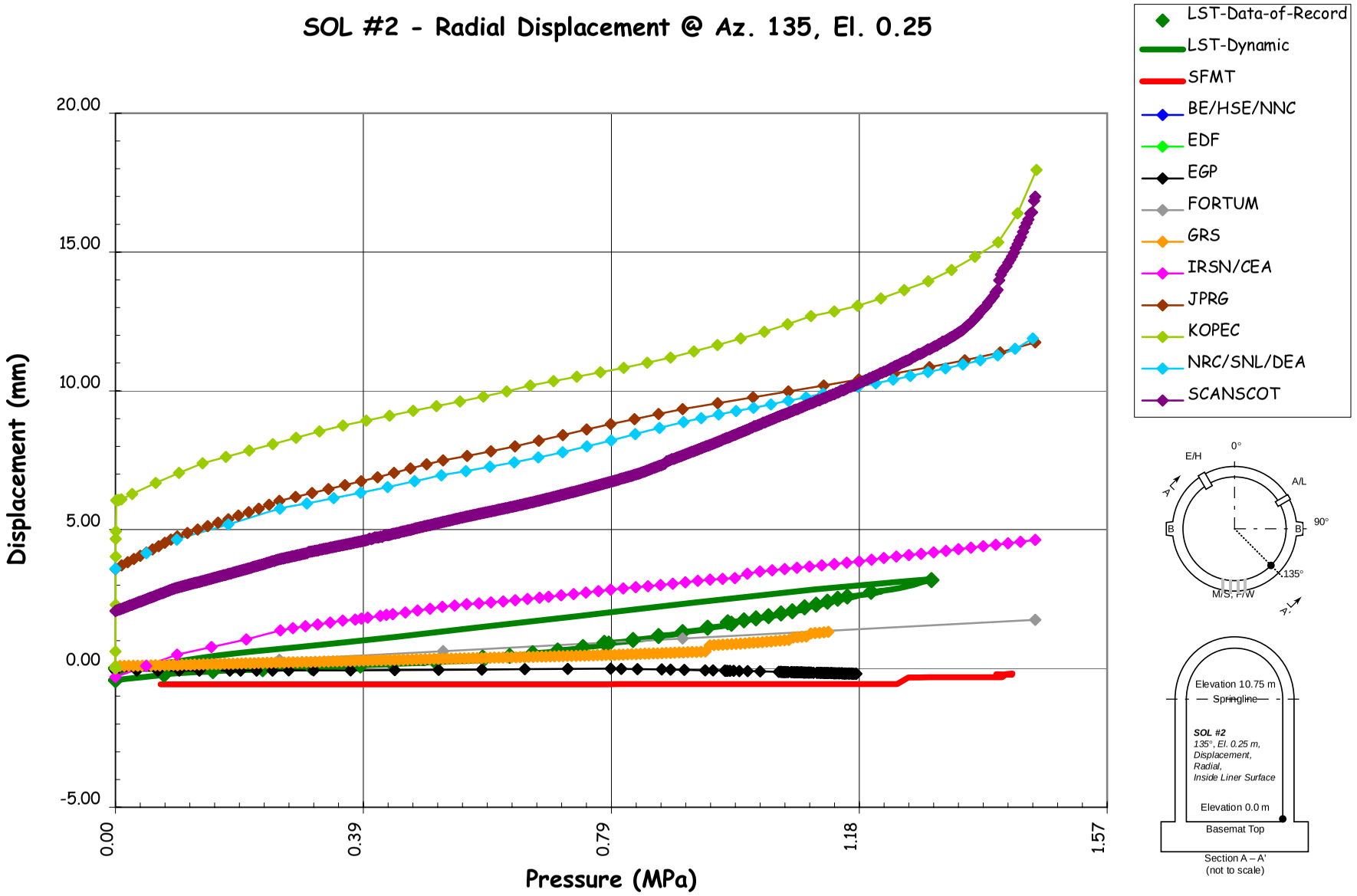
SOL #2 - Radial Displacement @ Az. 135, El. 0.25
Displacement (mm)
20.00
15.00
10.00
5.00
0.00
-5.00
0.00
0.39
0.79
1.18
1.57
Pressure (MPa)
LST-Data-of-Record
LST-Dynamic
SFMT
BE/HSE/NNC
EDF
EGP
FORTUM
GRS
IRSN/CEA
JPRG
KOPEC
NRC/SNL/DEA
SCANSCOT
E/H
A/L
0°
90°
135°
M/S, P/W
Elevation 10.75 m
Springline
SOL #2
135°, El. 0.25 m,
Displacement,
Radial,
Inside Liner Surface
Elevation 0.0 m
Basemat Top
Section A – A'
(not to scale)

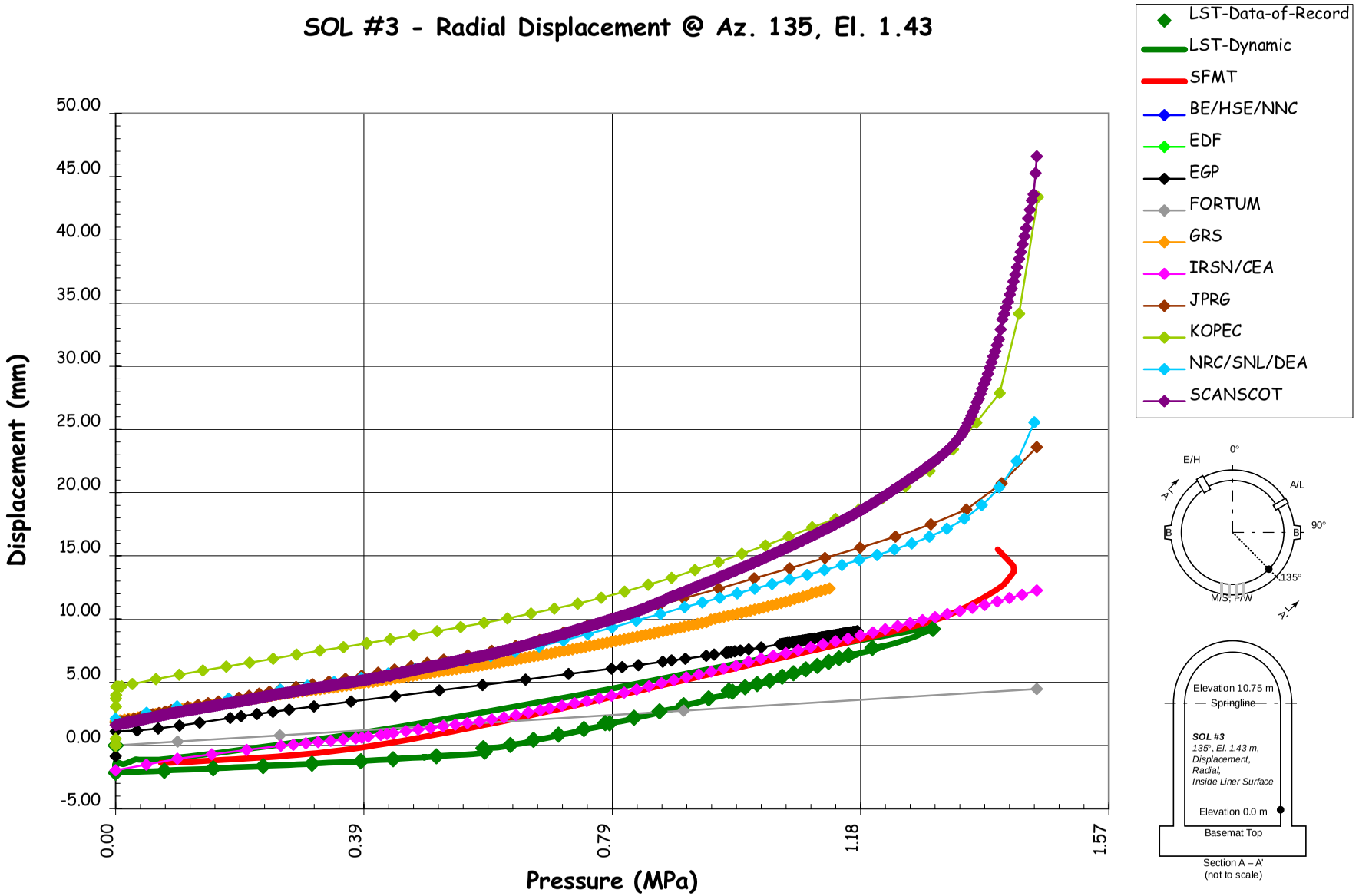
SOL #3 - Radial Displacement @ Az. 135, El. 1.43
Displacement (mm)
50.00
45.00
40.00
35.00
30.00
25.00
20.00
15.00
10.00
5.00
0.00
-5.00
0.00
0.39
0.79
1.18
1.57
Pressure (MPa)
LST-Data-of-Record
LST-Dynamic
SFMT
BE/HSE/NNC
EDF
EGP
FORTUM
GRS
IRSN/CEA
JPRG
KOPEC
NRC/SNL/DEA
SCANSCOT
0°
E/H
A/L
90°
135°
M/S, I-W
Elevation 10.75 m
Springline
SOL #3
135°, El. 1.43 m,
Displacement,
Radial,
Inside Liner Surface
Elevation 0.0 m
Basemat Top
Section A – A'
(not to scale)

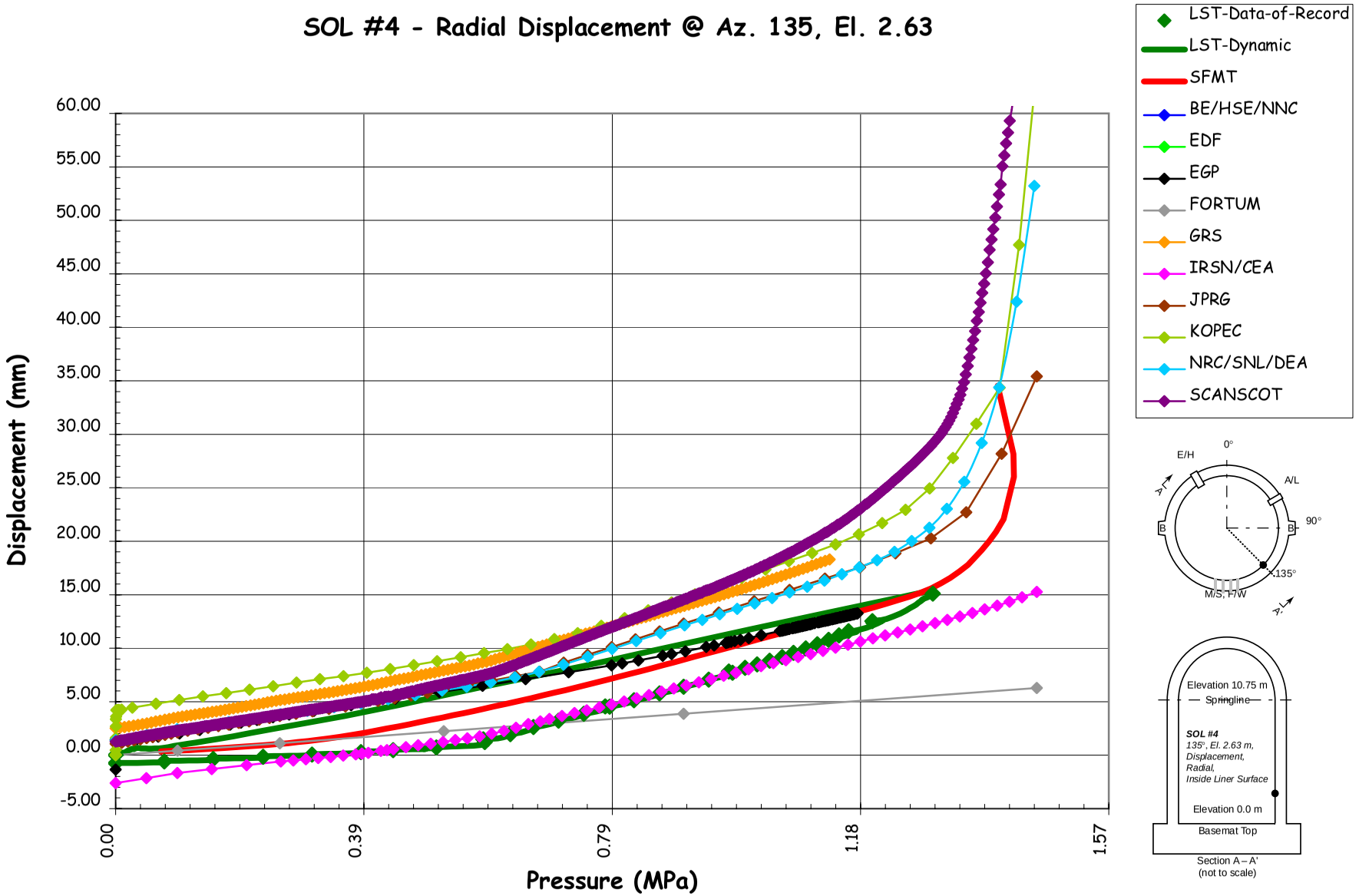
SOL #4 - Radial Displacement @ Az. 135, El. 2.63
Displacement (mm)
60.00
55.00
50.00
45.00
40.00
35.00
30.00
25.00
20.00
15.00
10.00
5.00
0.00
-5.00
0.00
0.39
0.79
1.18
1.57
Pressure (MPa)
LST-Data-of-Record
LST-Dynamic
SFMT
BE/HSE/NNC
EDF
EGP
FORTUM
GRS
IRSN/CEA
JPRG
KOPEC
NRC/SNL/DEA
SCANSCOT
0°
E/H
A/L
90°
135°
M/S, H/W
Elevation 10.75 m
Springline
SOL #4
135°, El. 2.63 m,
Displacement,
Radial,
Inside Liner Surface
Elevation 0.0 m
Basemat Top
Section A – A'
(not to scale)

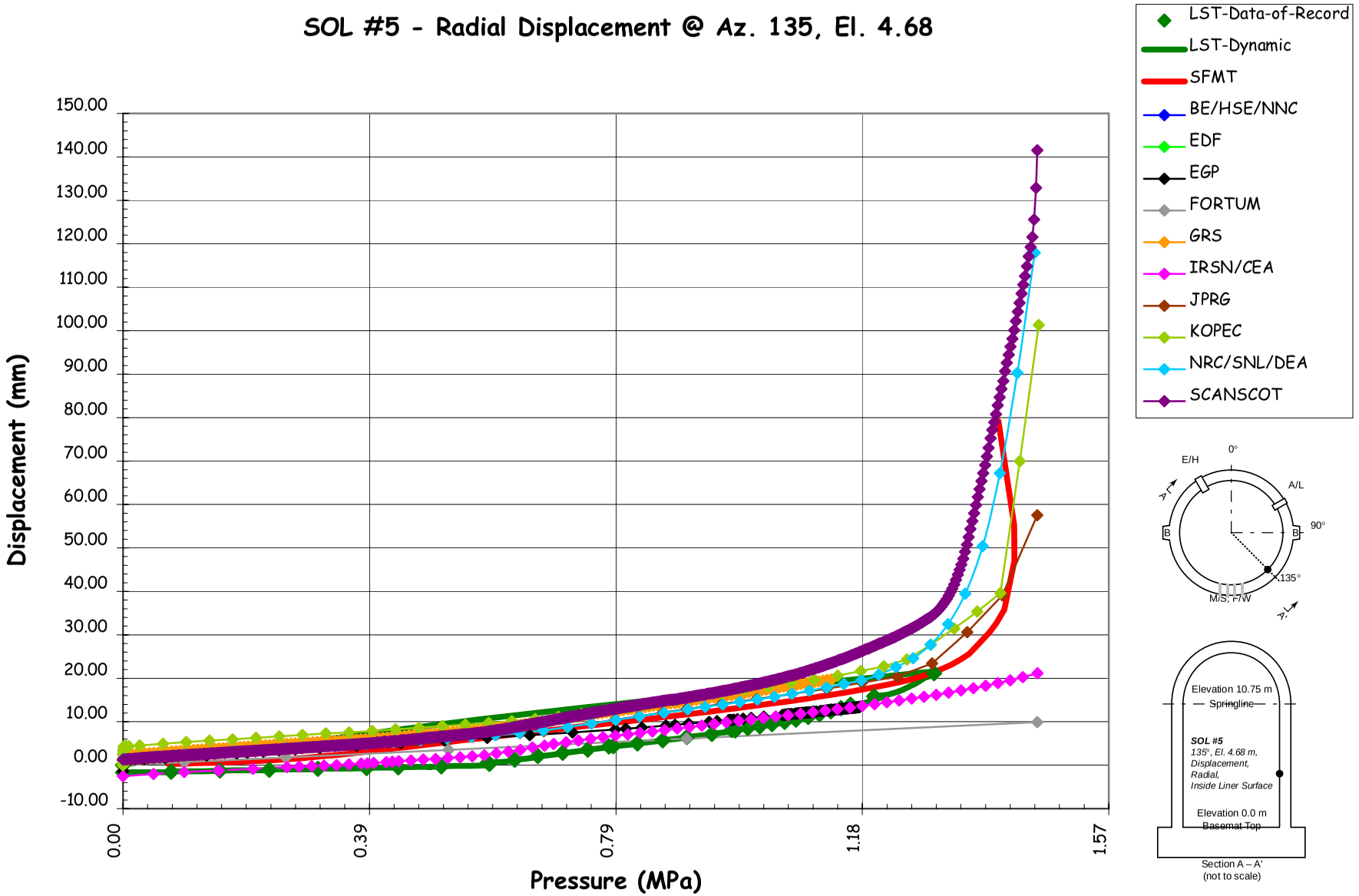
SOL #5 - Radial Displacement @ Az. 135, El. 4.68
Displacement (mm)
150.00
140.00
130.00
120.00
110.00
100.00
90.00
80.00
70.00
60.00
50.00
40.00
30.00
20.00
10.00
0.00
-10.00
0.00
0.39
0.79
1.18
1.57
Pressure (MPa)
LST-Data-of-Record
LST-Dynamic
SFMT
BE/HSE/NNC
EDF
EGP
FORTUM
GRS
IRSN/CEA
JPRG
KOPEC
NRC/SNL/DEA
SCANSCOT
E/H
0°
A/L
90°
135°
M/S, F/W
Elevation 10.75 m
Springline
SOL #5
135°, El. 4.68 m,
Displacement,
Radial,
Inside Liner Surface
Elevation 0.0 m
Basemat Top
Section A – A'
(not to scale)

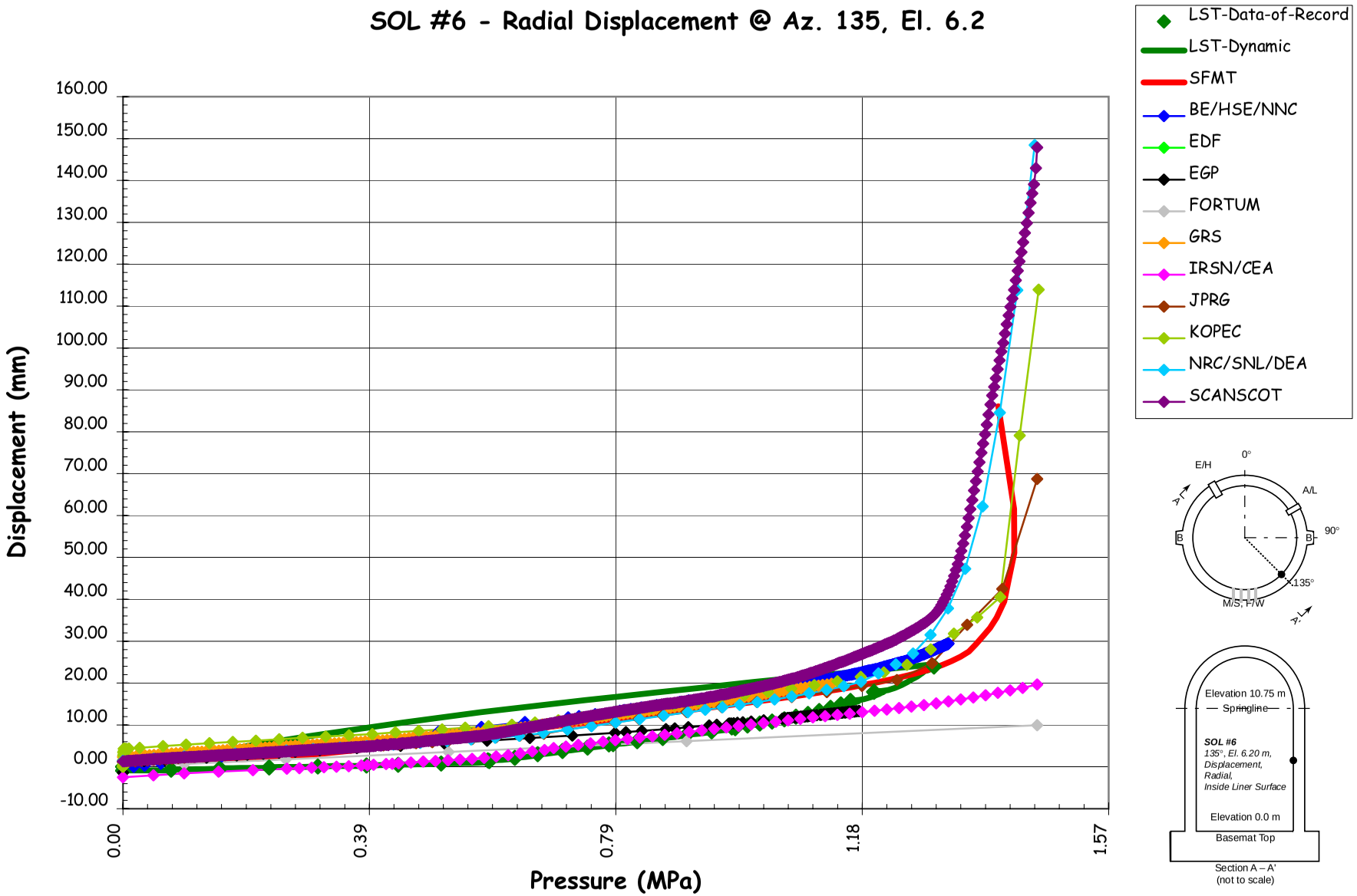
SOL #6 - Radial Displacement @ Az. 135, El. 6.2
Displacement (mm)
160.00
150.00
140.00
130.00
120.00
110.00
100.00
90.00
80.00
70.00
60.00
50.00
40.00
30.00
20.00
10.00
0.00
-10.00
0.00
0.39
0.79
1.18
1.57
Pressure (MPa)
LST-Data-of-Record
LST-Dynamic
SFMT
BE/HSE/NNC
EDF
EGP
FORTUM
GRS
IRSN/CEA
JPRG
KOPEC
NRC/SNL/DEA
SCANSCOT
0°
E/H
A/L
90°
135°
M/S, F/W
Elevation 10.75 m
Springline
SOL #6
135°, El. 6.20 m,
Displacement,
Radial,
Inside Liner Surface
Elevation 0.0 m
Basemat Top
Section A – A'
(not to scale)

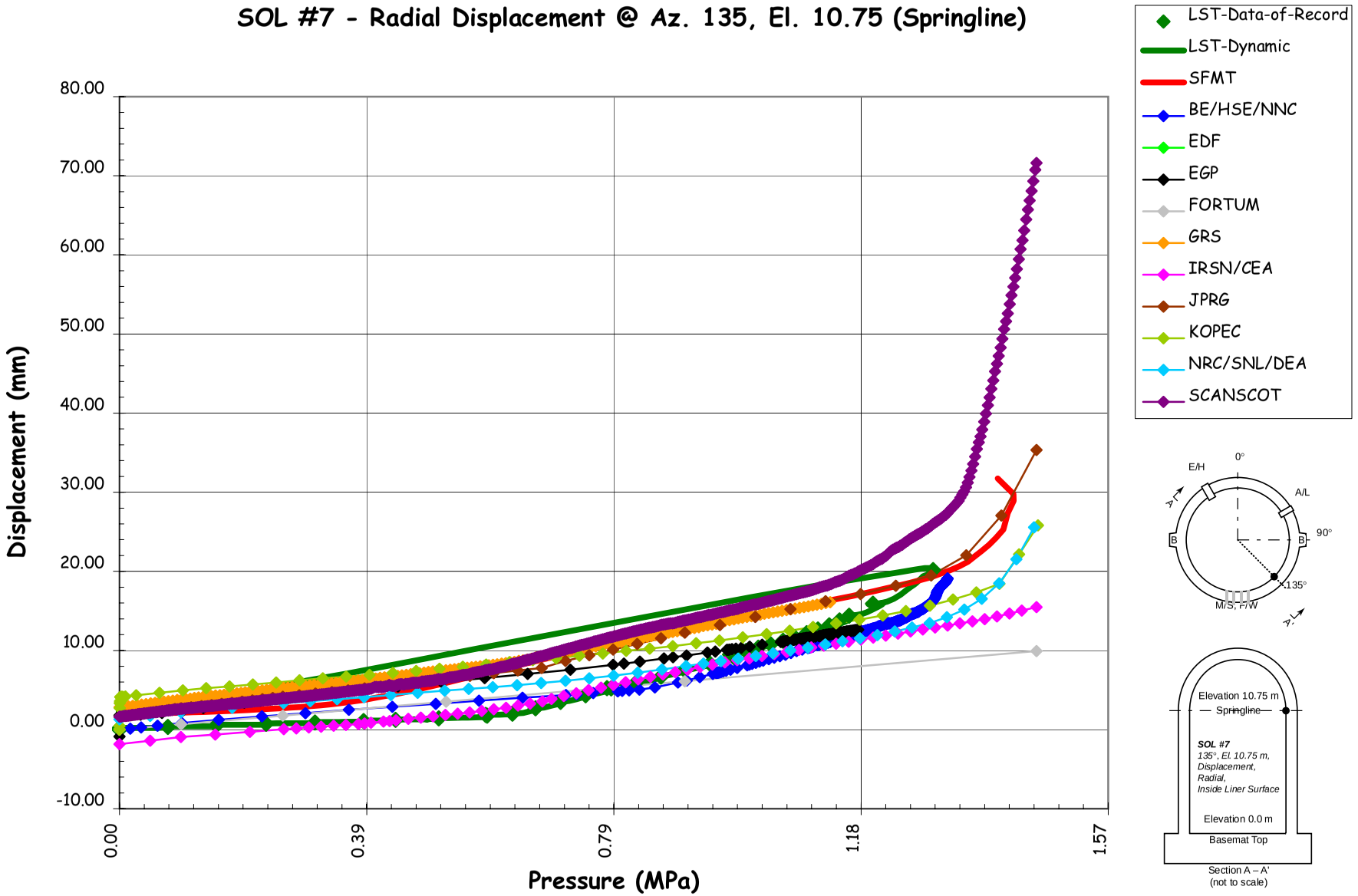
SOL #7 - Radial Displacement @ Az. 135, El. 10.75 (Springline)
Displacement (mm)
80.00
70.00
60.00
50.00
40.00
30.00
20.00
10.00
0.00
-10.00
0.00
0.39
0.79
1.18
1.57
Pressure (MPa)
LST-Data-of-Record
LST-Dynamic
SFMT
BE/HSE/NNC
EDF
EGP
FORTUM
GRS
IRSN/CEA
JPRG
KOPEC
NRC/SNL/DEA
SCANSCOT
0°
E/H
A/L
90°
135°
M/S, F/W
Elevation 10.75 m
Springline
SOL #7
135°, El. 10.75 m,
Displacement,
Radial,
Inside Liner Surface
Elevation 0.0 m
Basemat Top
Section A – A'
(not to scale)

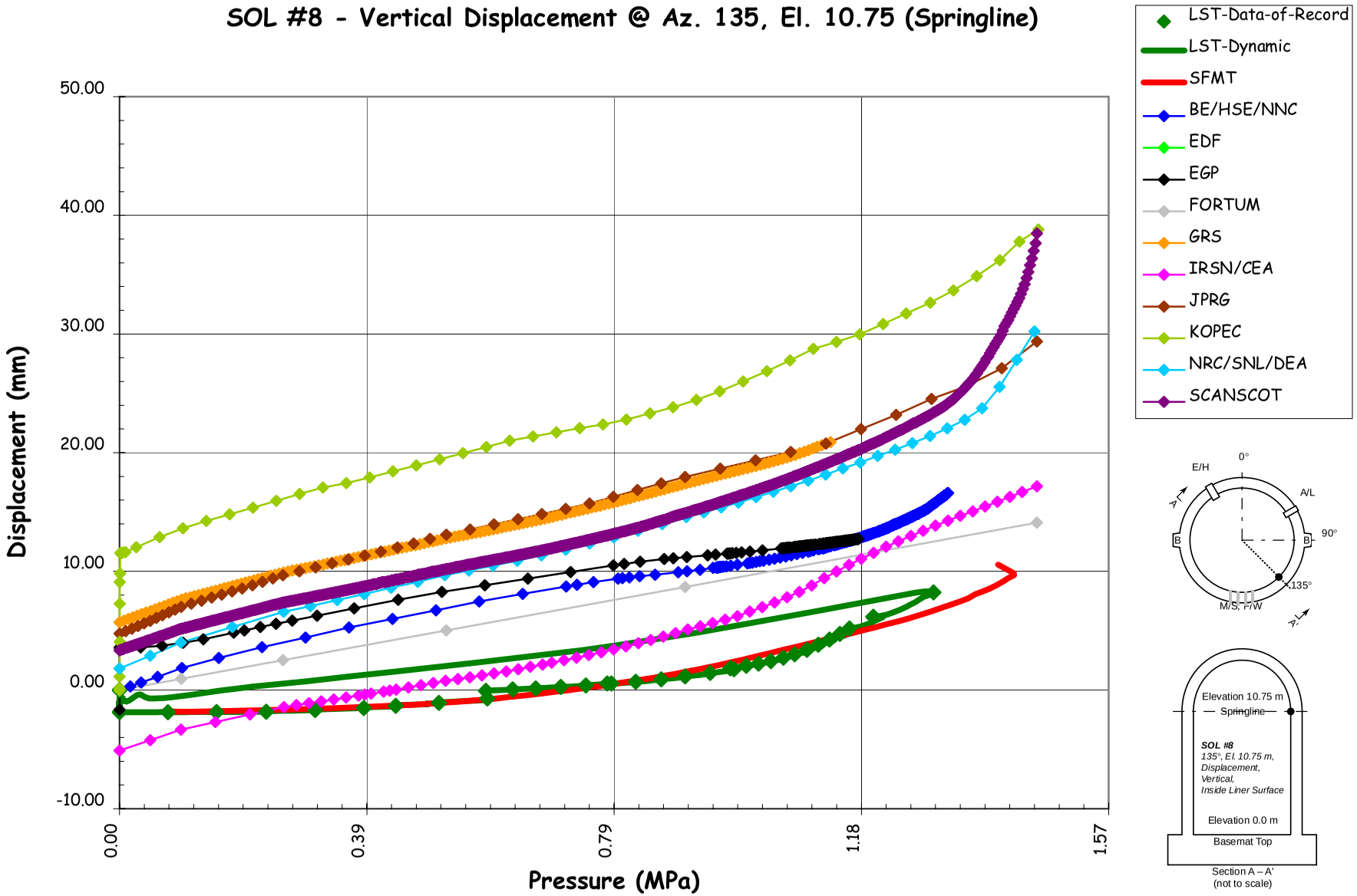
SOL #8 - Vertical Displacement @ Az. 135, El. 10.75 (Springline)
Displacement (mm)
50.00
40.00
30.00
20.00
10.00
0.00
-10.00
0.00
0.39
0.79
1.18
1.57
Pressure (MPa)
LST-Data-of-Record
LST-Dynamic
SFMT
BE/HSE/NNC
EDF
EGP
FORTUM
GRS
IRSN/CEA
JPRG
KOPEC
NRC/SNL/DEA
SCANSCOT
0°
E/H
A/L
90°
135°
M/S, F/W
Elevation 10.75 m
Springline
SOL #8
135°, El. 10.75 m,
Displacement,
Vertical,
Inside Liner Surface
Elevation 0.0 m
Basemat Top
Section A – A'
(not to scale)

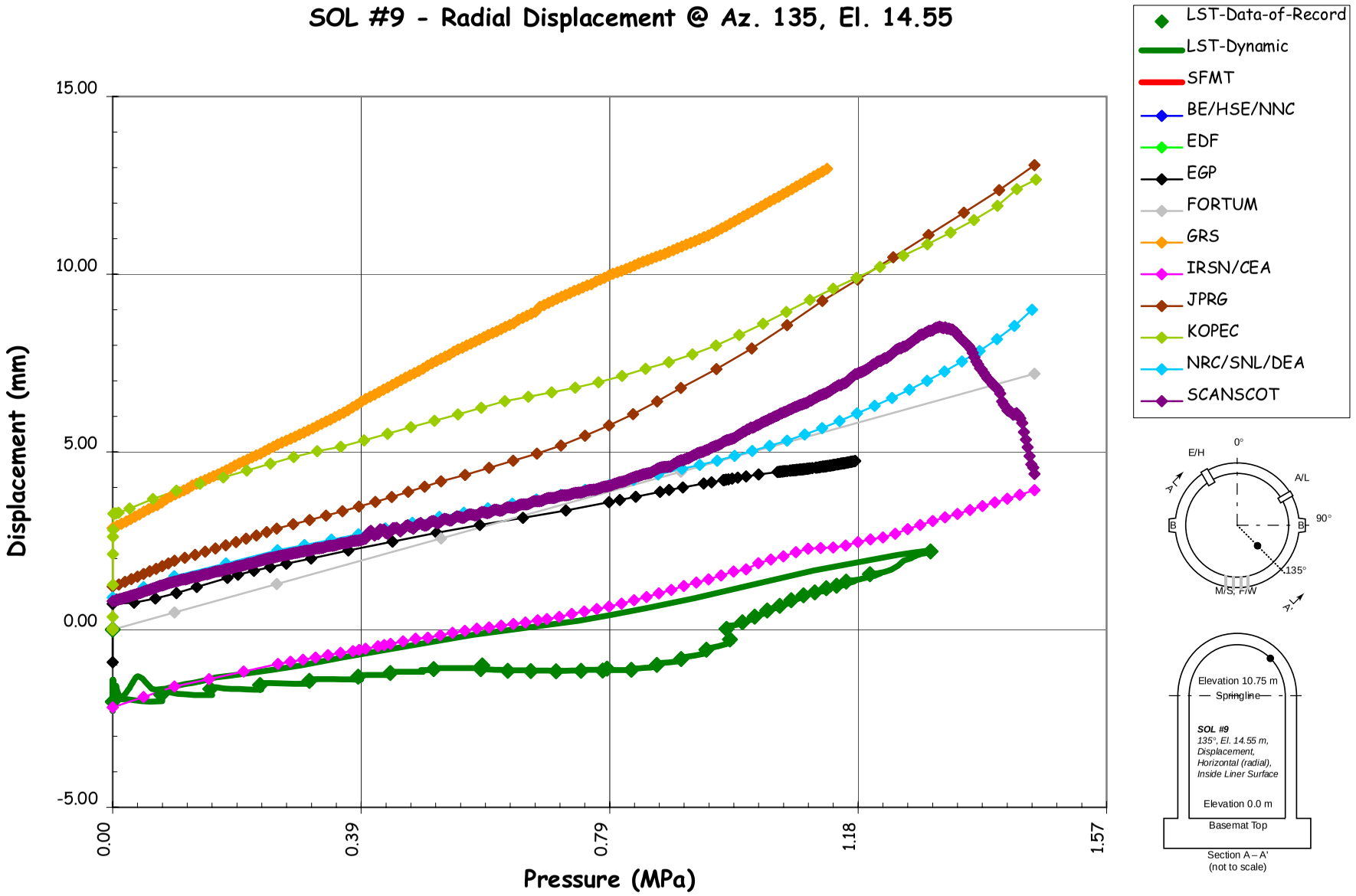
SOL #9 - Radial Displacement @ Az. 135, El. 14.55
Displacement (mm)
15.00
10.00
5.00
0.00
-5.00
0.00
0.39
0.79
1.18
1.57
Pressure (MPa)
LST-Data-of-Record
LST-Dynamic
SFMT
BE/HSE/NNC
EDF
EGP
FORTUM
GRS
IRSN/CEA
JPRG
KOPEC
NRC/SNL/DEA
SCANSCOT
0°
E/H
A/L
90°
135°
M/S, F/W
Elevation 10.75 m
Springline
SOL #9
135°, El. 14.55 m,
Displacement,
Horizontal (radial),
Inside Liner Surface
Elevation 0.0 m
Basemat Top
Section A – A'
(not to scale)

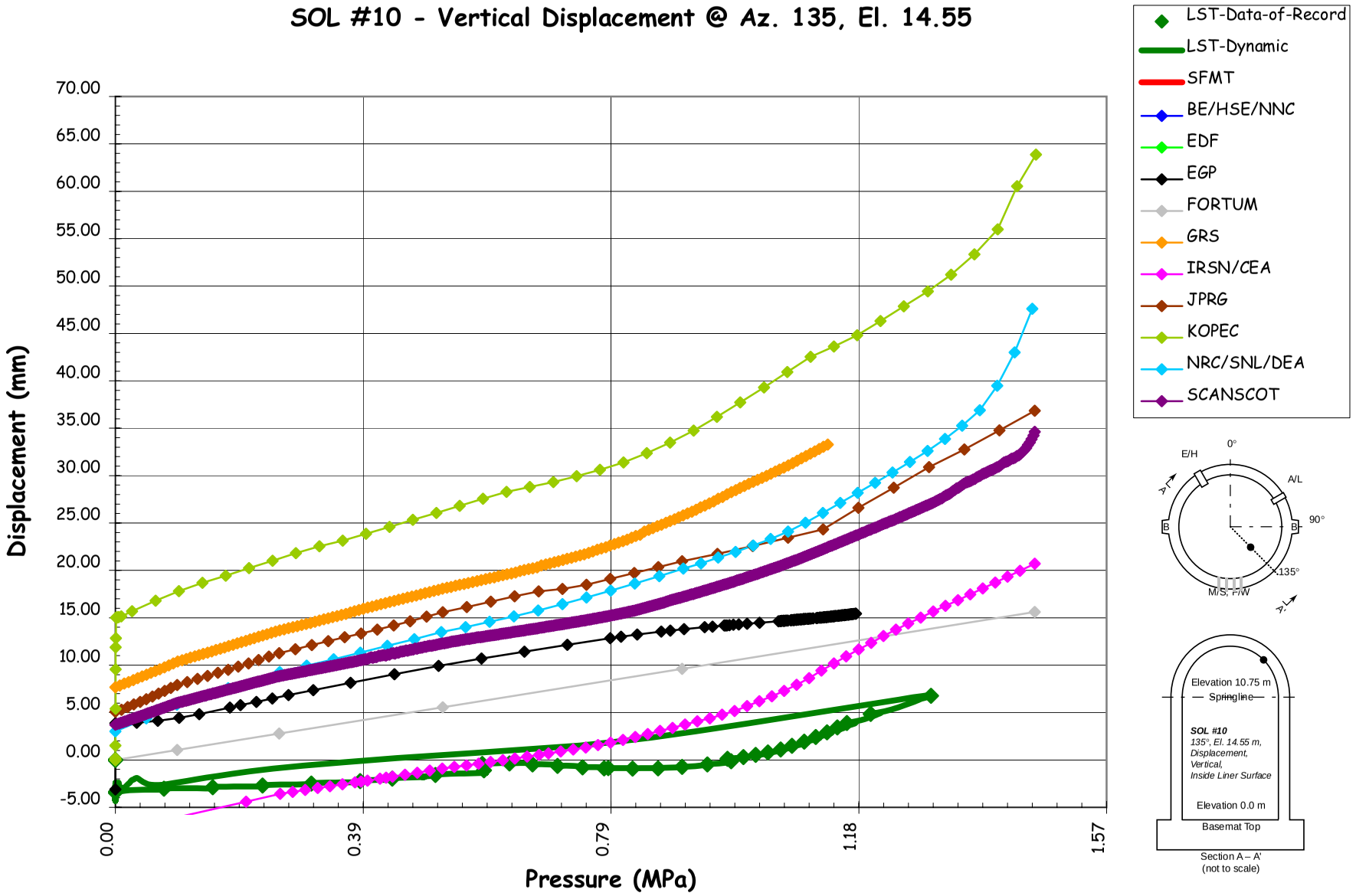
SOL #10 - Vertical Displacement @ Az. 135, El. 14.55
Displacement (mm)
70.00
65.00
60.00
55.00
50.00
45.00
40.00
35.00
30.00
25.00
20.00
15.00
10.00
5.00
0.00
-5.00
0.00
0.39
0.79
1.18
1.57
Pressure (MPa)
LST-Data-of-Record
LST-Dynamic
SFMT
BE/HSE/NNC
EDF
EGP
FORTUM
GRS
IRSN/CEA
JPRG
KOPEC
NRC/SNL/DEA
SCANSCOT
0°
E/H
A/L
90°
135°
M/S, F/W
Elevation 10.75 m
Springline
SOL #10
135°, El. 14.55 m,
Displacement,
Vertical,
Inside Liner Surface
Elevation 0.0 m
Basemat Top
Section A – A'
(not to scale)

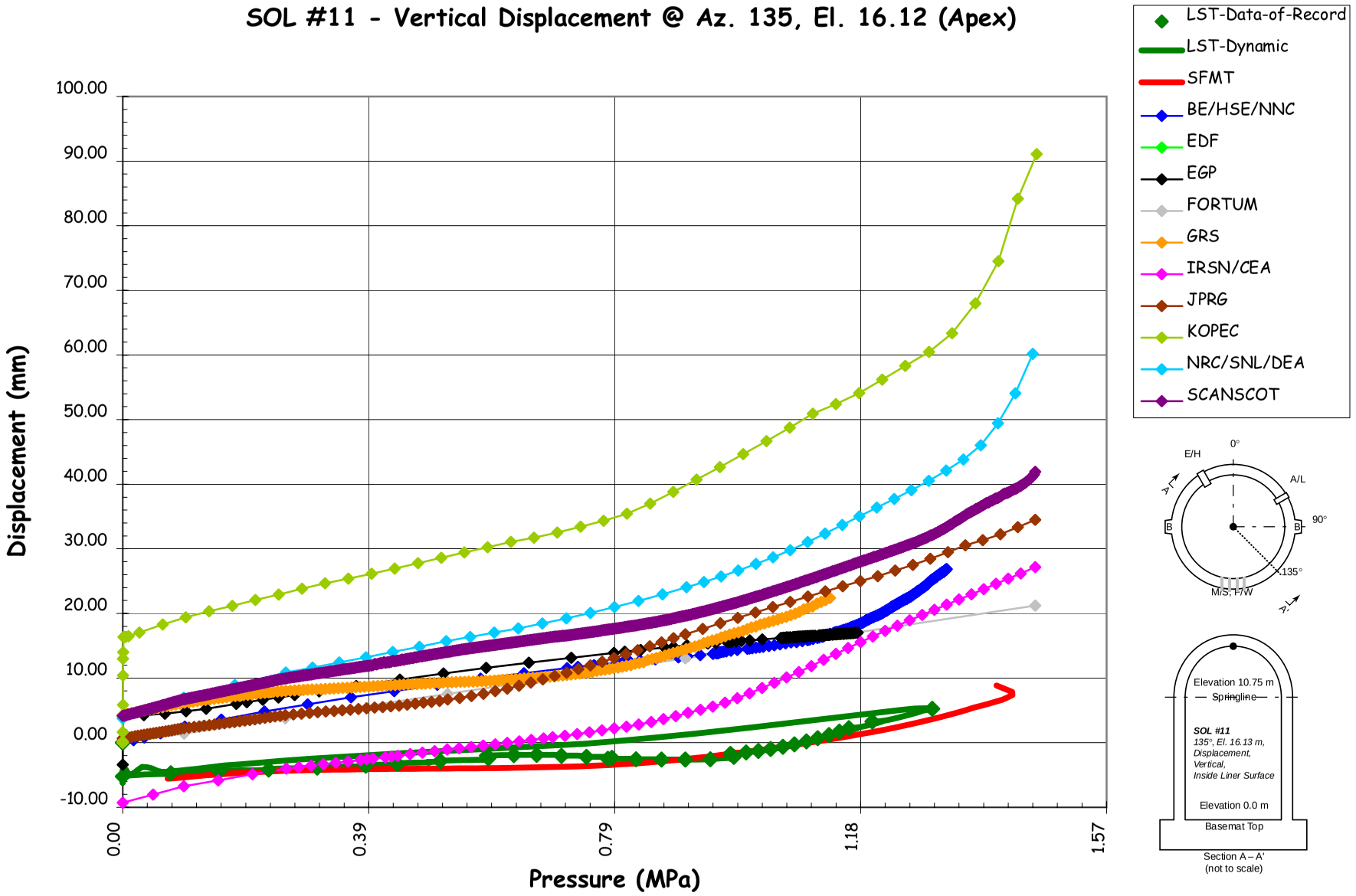
SOL #11 - Vertical Displacement @ Az. 135, El. 16.12 (Apex)
Displacement (mm)
100.00
90.00
80.00
70.00
60.00
50.00
40.00
30.00
20.00
10.00
0.00
-10.00
0.00
0.39
0.79
1.18
1.57
Pressure (MPa)
LST-Data-of-Record
LST-Dynamic
SFMT
BE/HSE/NNC
EDF
EGP
FORTUM
GRS
IRSN/CEA
JPRG
KOPEC
NRC/SNL/DEA
SCANSCOT
0°
E/H
A/L
90°
135°
M/S, I-7W
Elevation 10.75 m
Springline
SOL #11
135°, El. 16.13 m,
Displacement,
Vertical,
Inside Liner Surface
Elevation 0.0 m
Basemat Top
Section A – A'
(not to scale)

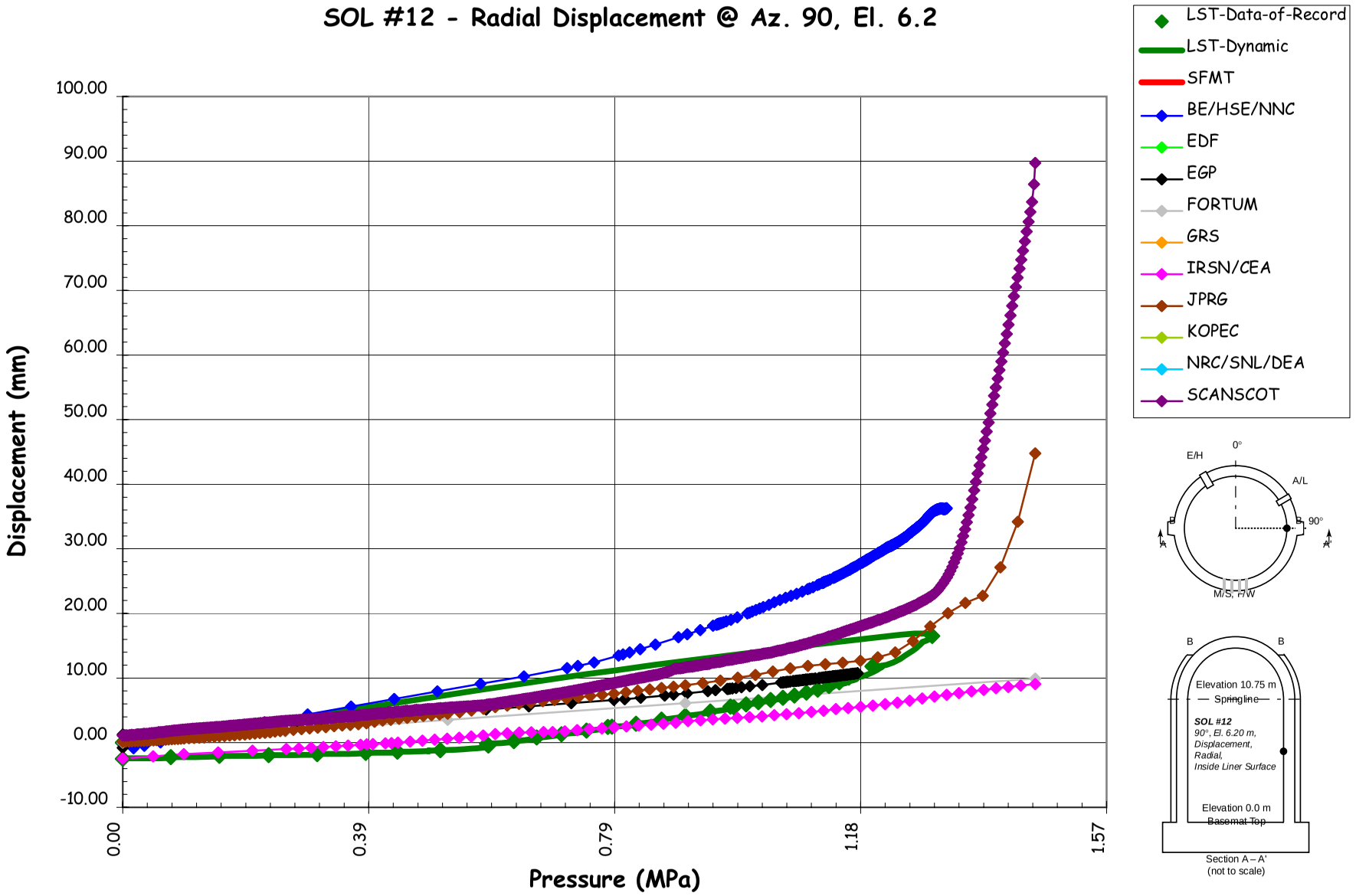
SOL #12 - Radial Displacement @ Az. 90, El. 6.2
Displacement (mm)
100.00
90.00
80.00
70.00
60.00
50.00
40.00
30.00
20.00
10.00
0.00
-10.00
0.00
0.39
0.79
1.18
1.57
Pressure (MPa)
LST-Data-of-Record
LST-Dynamic
SFMT
BE/HSE/NNC
EDF
EGP
FORTUM
GRS
IRSN/CEA
JPRG
KOPEC
NRC/SNL/DEA
SCANSCOT
0°
E/H
A/L
90°
M/S, HW
B
B
Elevation 10.75 m
Springline
SOL #12
90°, El. 6.20 m,
Displacement,
Radial,
Inside Liner Surface
Elevation 0.0 m
Basemat Top
Section A – A'
(not to scale)

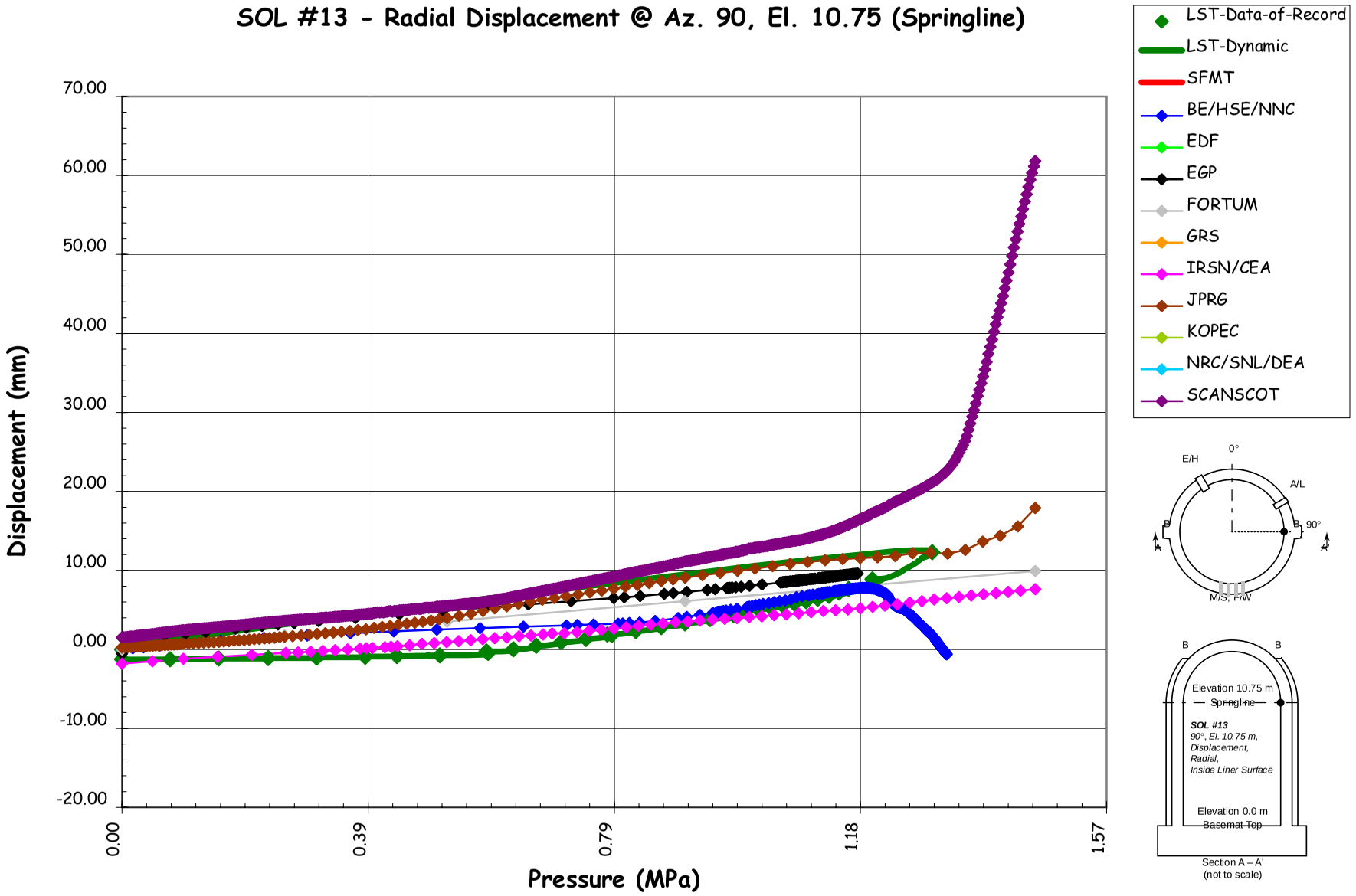
SOL #13 - Radial Displacement @ Az. 90, El. 10.75 (Springline)
Displacement (mm)
70.00
60.00
50.00
40.00
30.00
20.00
10.00
0.00
-10.00
-20.00
0.00
0.39
0.79
1.18
1.57
Pressure (MPa)
LST-Data-of-Record
LST-Dynamic
SFMT
BE/HSE/NNC
EDF
EGP
FORTUM
GRS
IRSN/CEA
JPRG
KOPEC
NRC/SNL/DEA
SCANSCOT
E/H
0°
A/L
90°
M/S, F/W
B
B
Elevation 10.75 m
Springline
SOL #13
90°, El. 10.75 m,
Displacement,
Radial,
Inside Liner Surface
Elevation 0.0 m
Basemat Top
Section A – A'
(not to scale)

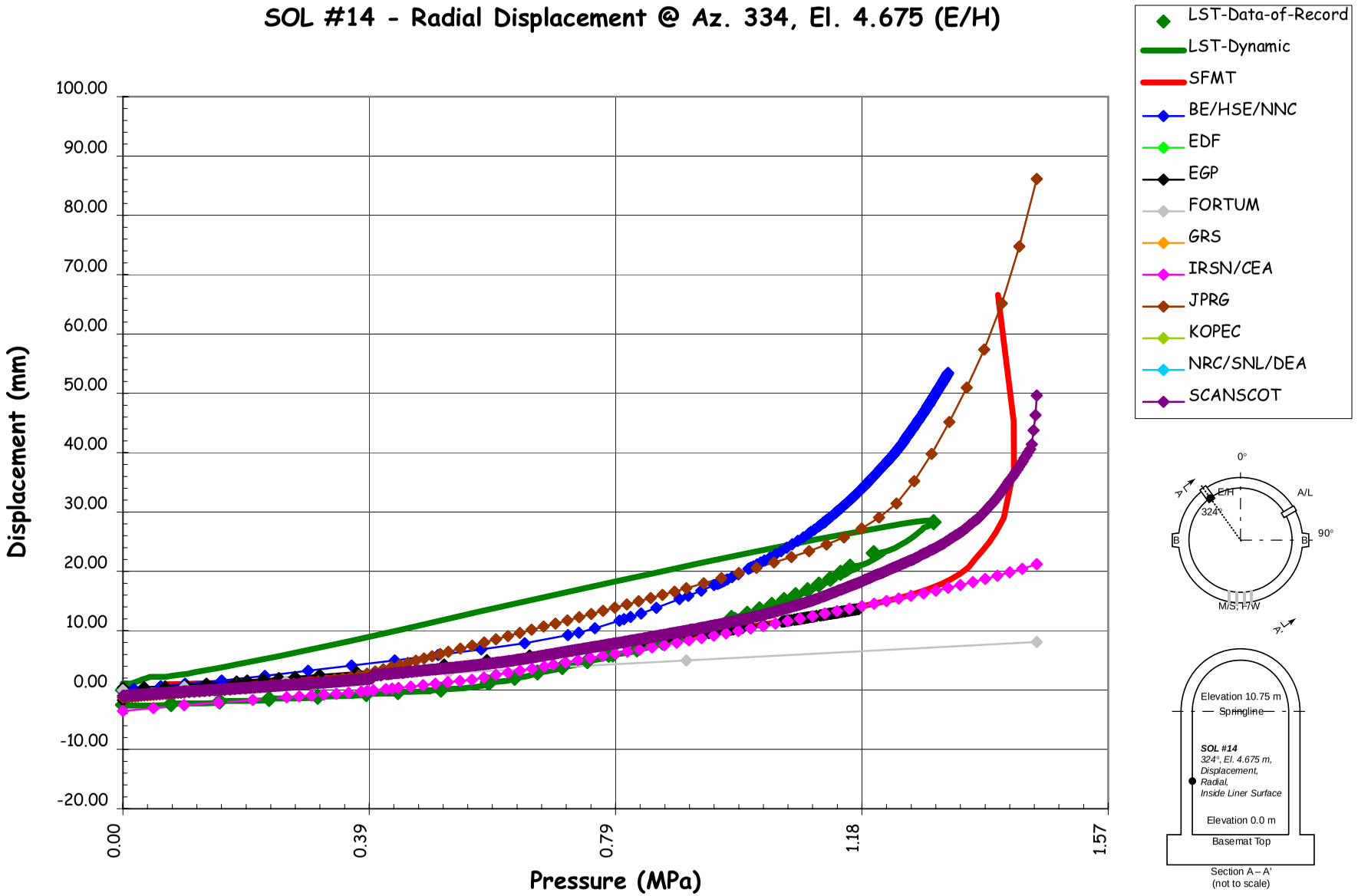
SOL #14 - Radial Displacement @ Az. 334, El. 4.675 (E/H)
Displacement (mm)
100.00
90.00
80.00
70.00
60.00
50.00
40.00
30.00
20.00
10.00
0.00
-10.00
-20.00
0.00
0.39
0.79
1.18
1.57
Pressure (MPa)
LST-Data-of-Record
LST-Dynamic
SFMT
BE/HSE/NNC
EDF
EGP
FORTUM
GRS
IRSN/CEA
JPRG
KOPEC
NRC/SNL/DEA
SCANSCOT
0°
E/H
A/L
324°
90°
B
B
M/S, I-/W
Elevation 10.75 m
Springline
SOL #14
324°, El. 4.675 m,
Displacement,
Radial,
Inside Liner Surface
Elevation 0.0 m
Basemat Top
Section A – A'
(not to scale)

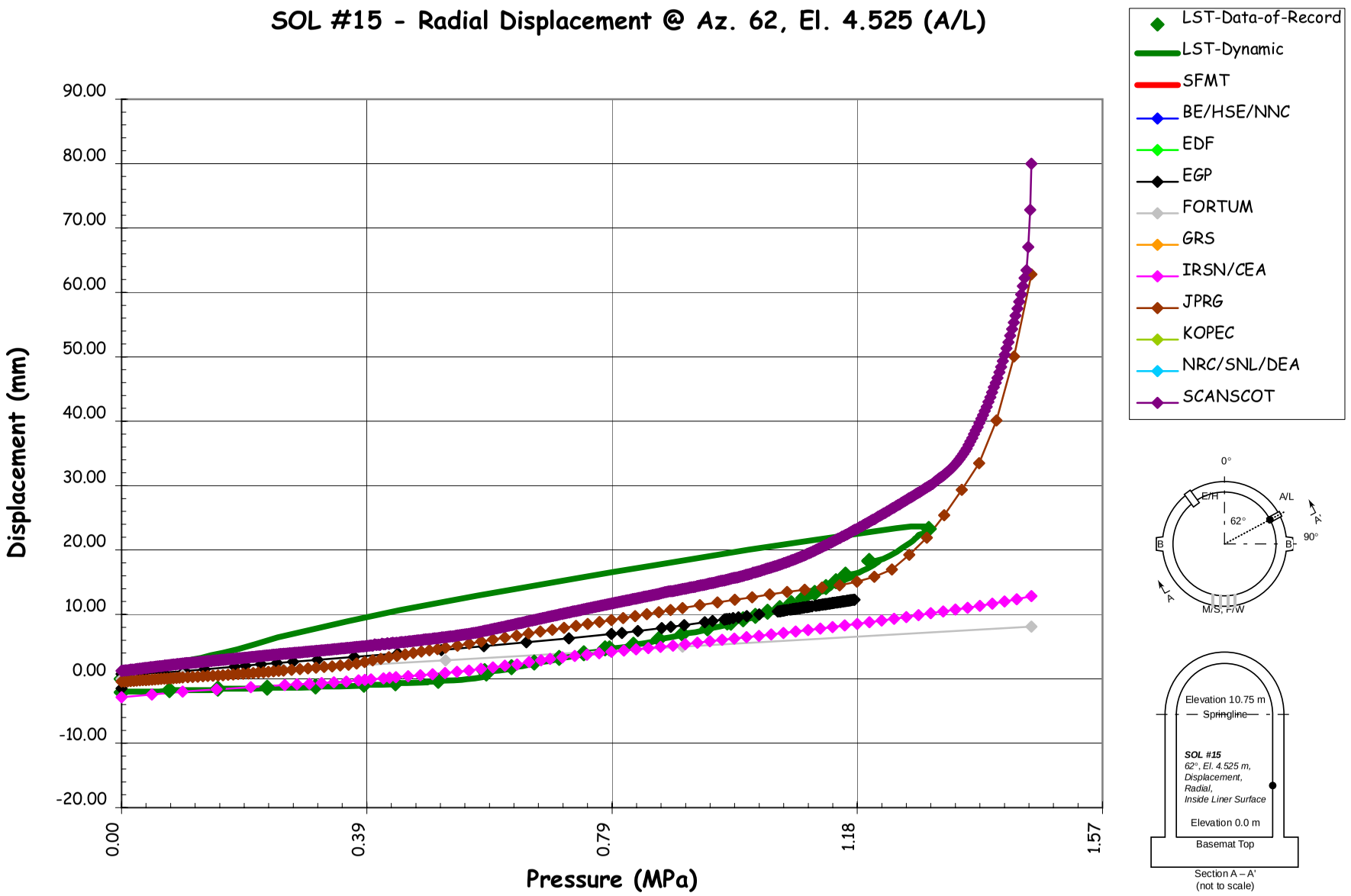
SOL #15 - Radial Displacement @ Az. 62, El. 4.525 (A/L)
Displacement (mm)
90.00
80.00
70.00
60.00
50.00
40.00
30.00
20.00
10.00
0.00
-10.00
-20.00
0.00
0.39
0.79
1.18
1.57
Pressure (MPa)
LST-Data-of-Record
LST-Dynamic
SFMT
BE/HSE/NNC
EDF
EGP
FORTUM
GRS
IRSN/CEA
JPRG
KOPEC
NRC/SNL/DEA
SCANSCOT
0°
E/H
A/L
62°
90°
M/S, F/W
Elevation 10.75 m
Springline
SOL #15
62°, El. 4.525 m,
Displacement,
Radial,
Inside Liner Surface
Elevation 0.0 m
Basemat Top
Section A – A'
(not to scale)

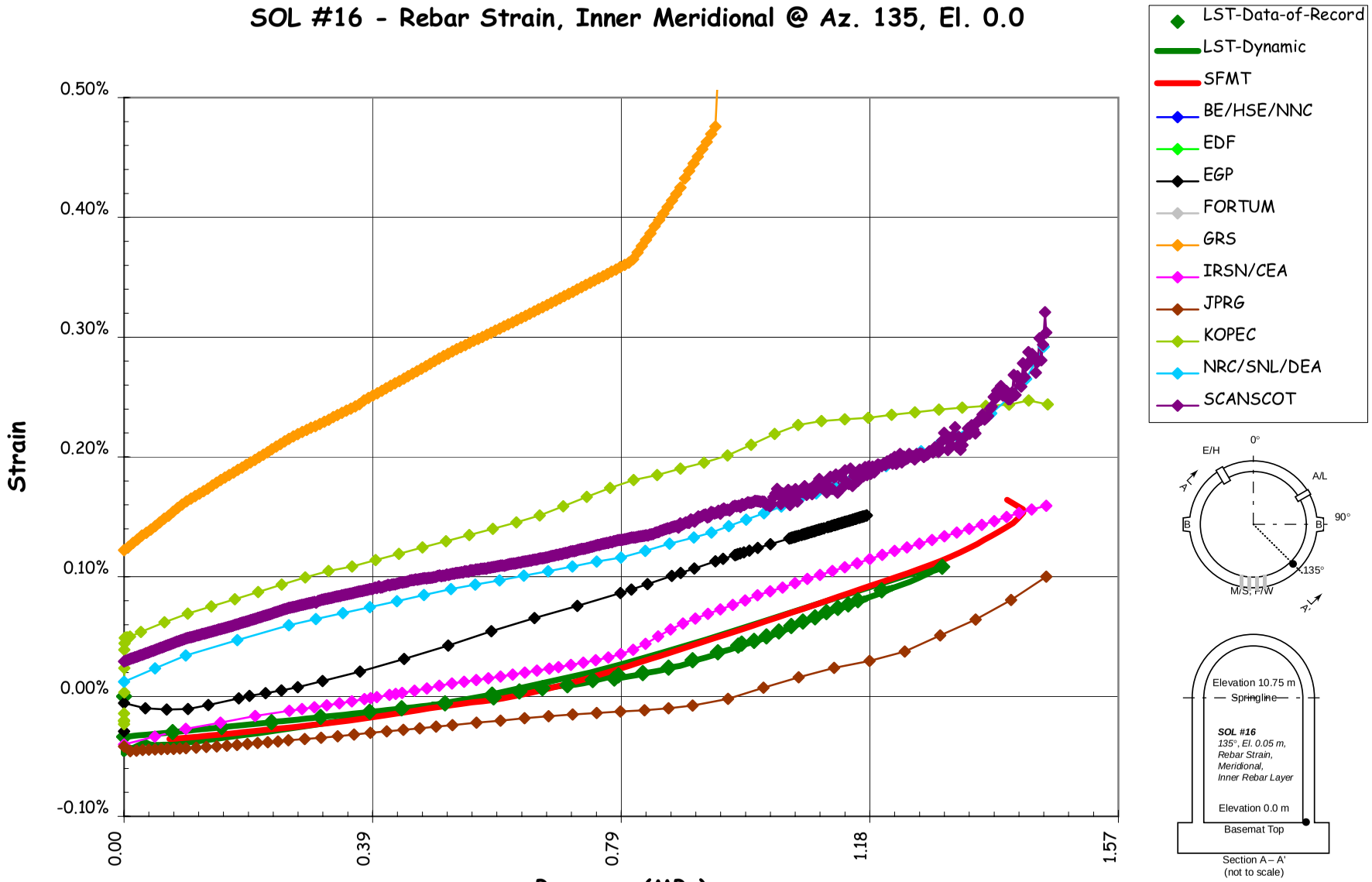
SOL #16 - Rebar Strain, Inner Meridional @ Az. 135, El. 0.0
Strain
0.50%
0.40%
0.30%
0.20%
0.10%
0.00%
-0.10%
0.00
0.39
0.79
1.18
1.57
Pressure (MPa)
LST-Data-of-Record
LST-Dynamic
SFMT
BE/HSE/NNC
EDF
EGP
FORTUM
GRS
IRSN/CEA
JPRG
KOPEC
NRC/SNL/DEA
SCANSCOT
0°
E/H
A/L
90°
135°
M/S, I-W
Elevation 10.75 m
Springline
SOL #16
135°, El. 0.05 m,
Rebar Strain,
Meridional,
Inner Rebar Layer
Elevation 0.0 m
Basemat Top
Section A – A'
(not to scale)

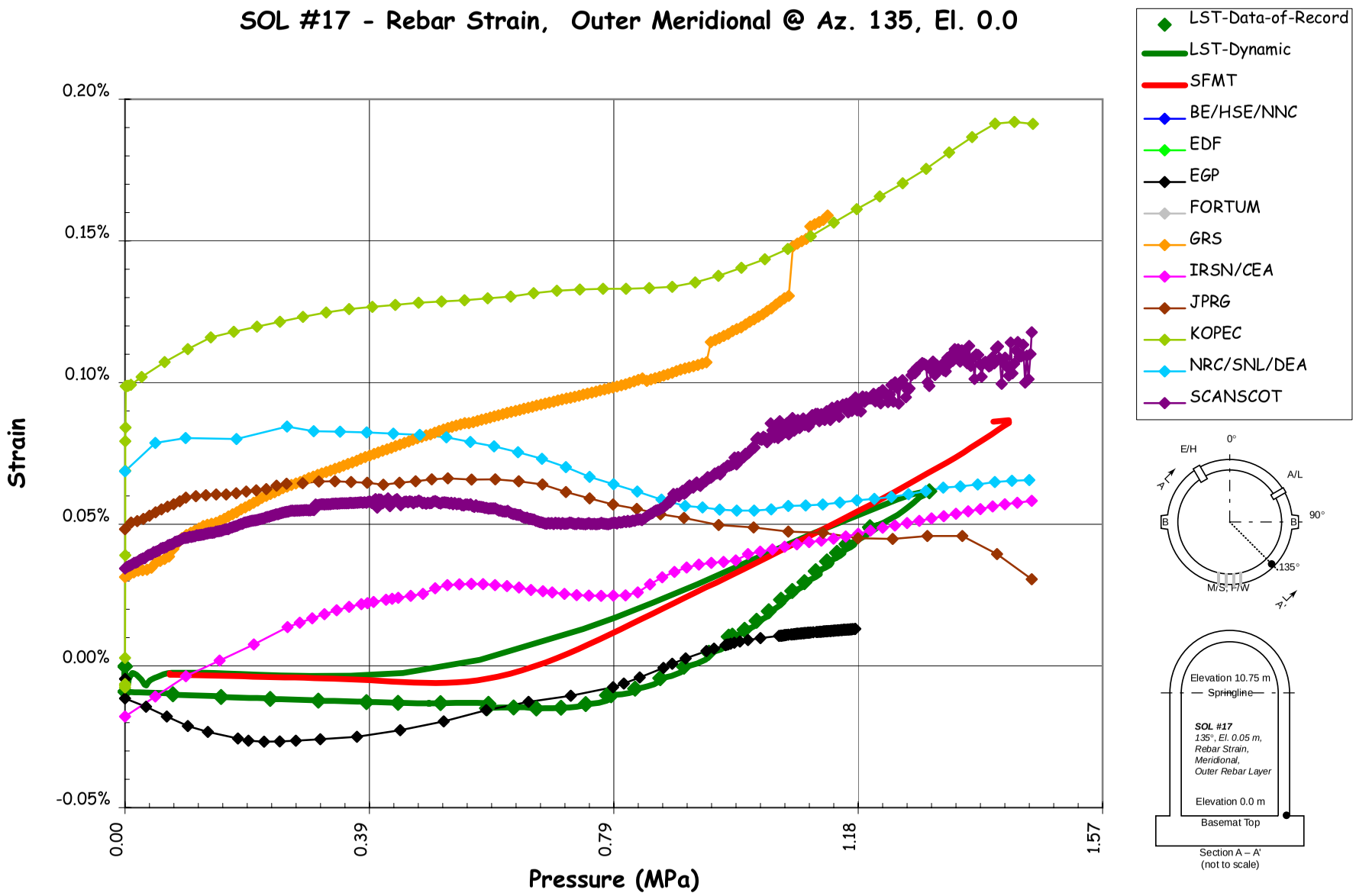
SOL #17 - Rebar Strain, Outer Meridional @ Az. 135, El. 0.0
Strain
0.20%
0.15%
0.10%
0.05%
0.00%
-0.05%
0.00
0.39
0.79
1.18
1.57
Pressure (MPa)
LST-Data-of-Record
LST-Dynamic
SFMT
BE/HSE/NNC
EDF
EGP
FORTUM
GRS
IRSN/CEA
JPRG
KOPEC
NRC/SNL/DEA
SCANSCOT
0°
E/H
A/L
90°
135°
M/S, T/W
Elevation 10.75 m
Springline
SOL #17
135°, El. 0.05 m,
Rebar Strain,
Meridional,
Outer Rebar Layer
Elevation 0.0 m
Basemat Top
Section A – A'
(not to scale)

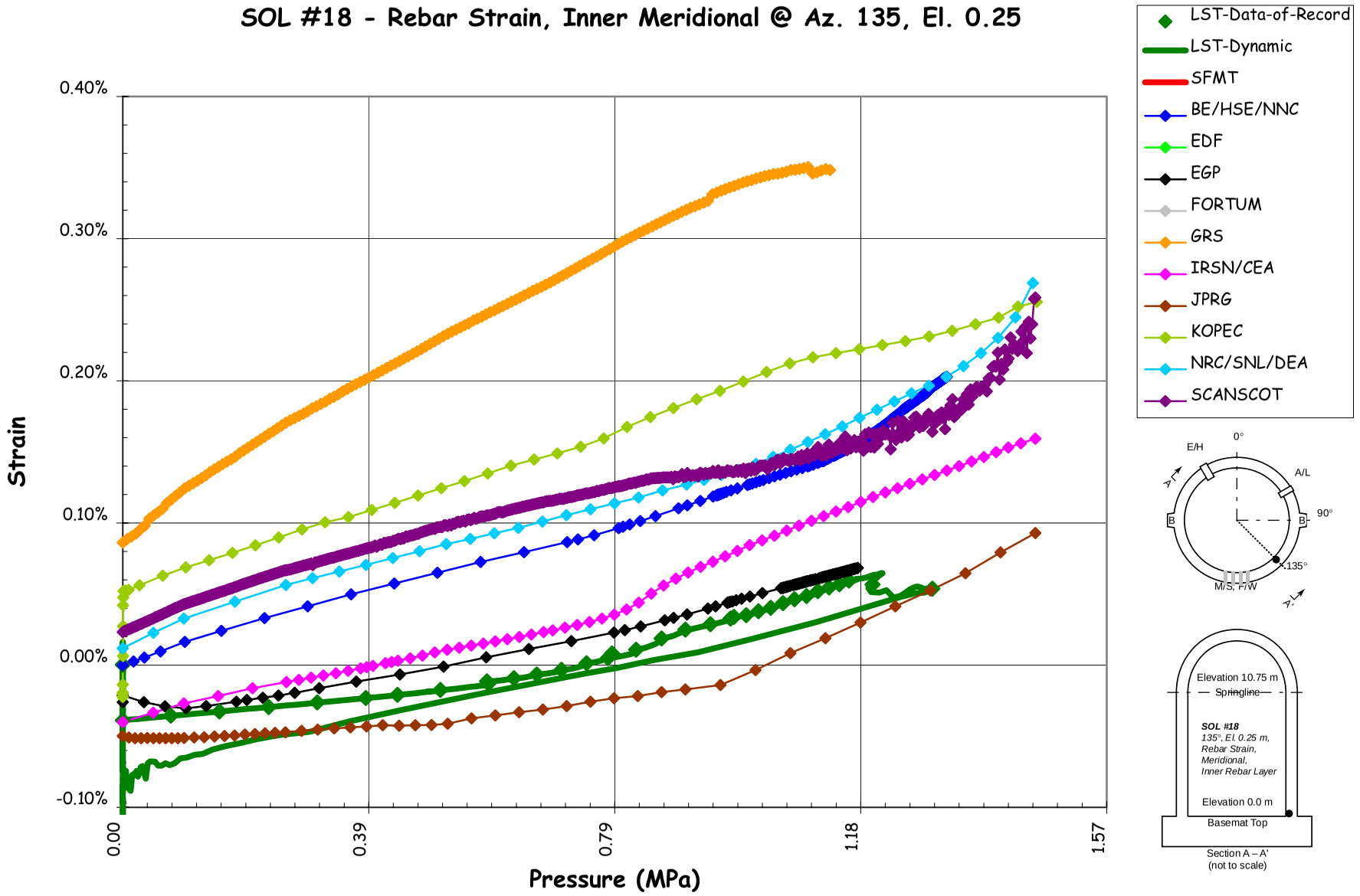
SOL #18 - Rebar Strain, Inner Meridional @ Az. 135, El. 0.25
Strain
0.40%
0.30%
0.20%
0.10%
0.00%
-0.10%
0.00
0.39
0.79
1.18
1.57
Pressure (MPa)
LST-Data-of-Record
LST-Dynamic
SFMT
BE/HSE/NNC
EDF
EGP
FORTUM
GRS
IRSN/CEA
JPRG
KOPEC
NRC/SNL/DEA
SCANSCOT
0°
E/H
A/L
90°
135°
M/S, F/W
Elevation 10.75 m
Springline
SOL #18
135°, El. 0.25 m,
Rebar Strain,
Meridional,
Inner Rebar Layer
Elevation 0.0 m
Basemat Top
Section A – A'
(not to scale)

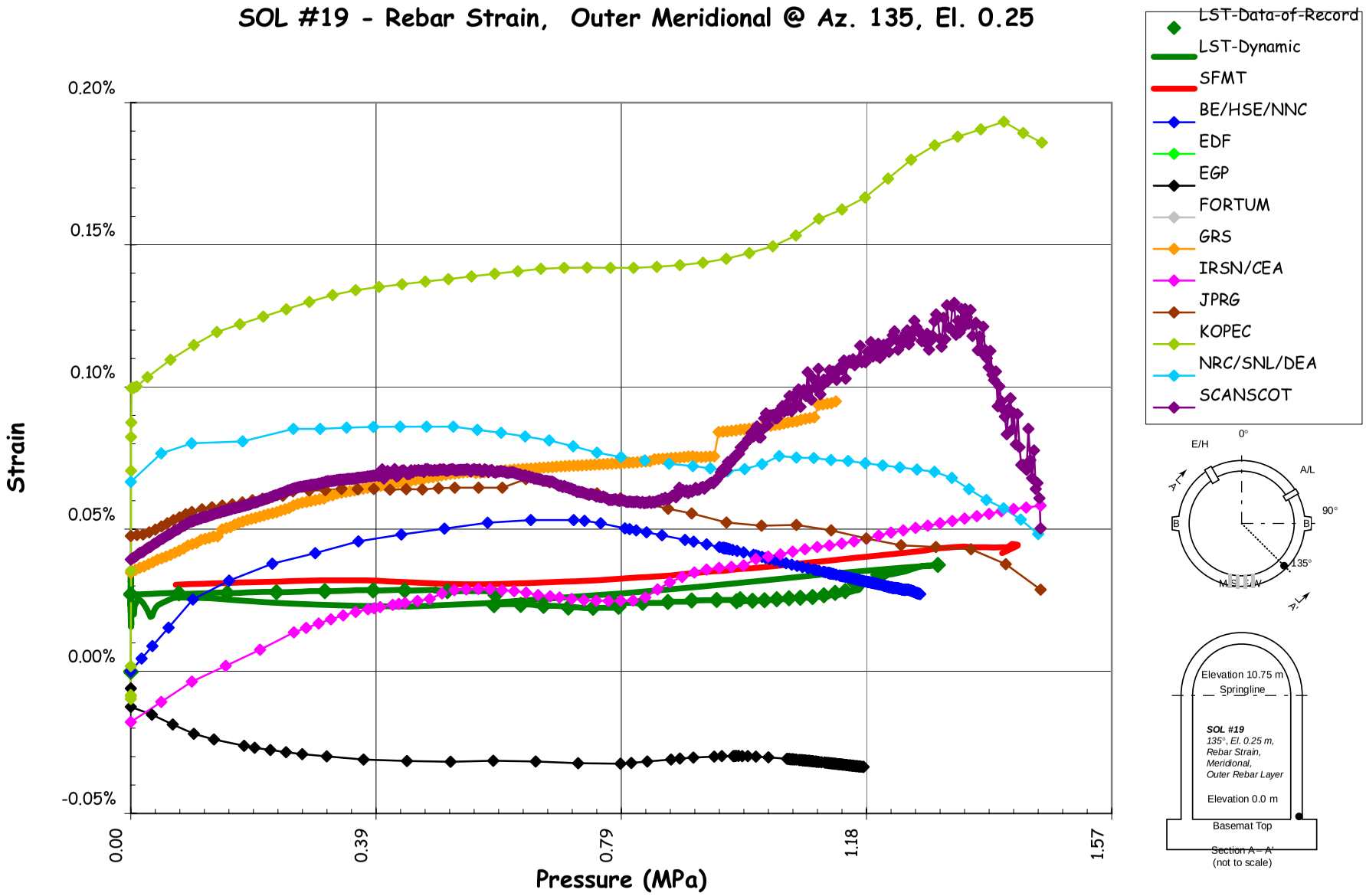
SOL #19 - Rebar Strain, Outer Meridional @ Az. 135, El. 0.25
Strain
0.20%
0.15%
0.10%
0.05%
0.00%
-0.05%
0.00
0.39
0.79
1.18
1.57
Pressure (MPa)
LST-Data-of-Record
LST-Dynamic
SFMT
BE/HSE/NNC
EDF
EGP
FORTUM
GRS
IRSN/CEA
JPRG
KOPEC
NRC/SNL/DEA
SCANSCOT
0°
E/H
A/L
90°
135°
Elevation 10.75 m
Springline
SOL #19
135°, El. 0.25 m,
Rebar Strain,
Meridional,
Outer Rebar Layer
Elevation 0.0 m
Basemat Top
Section A – A'
(not to scale)

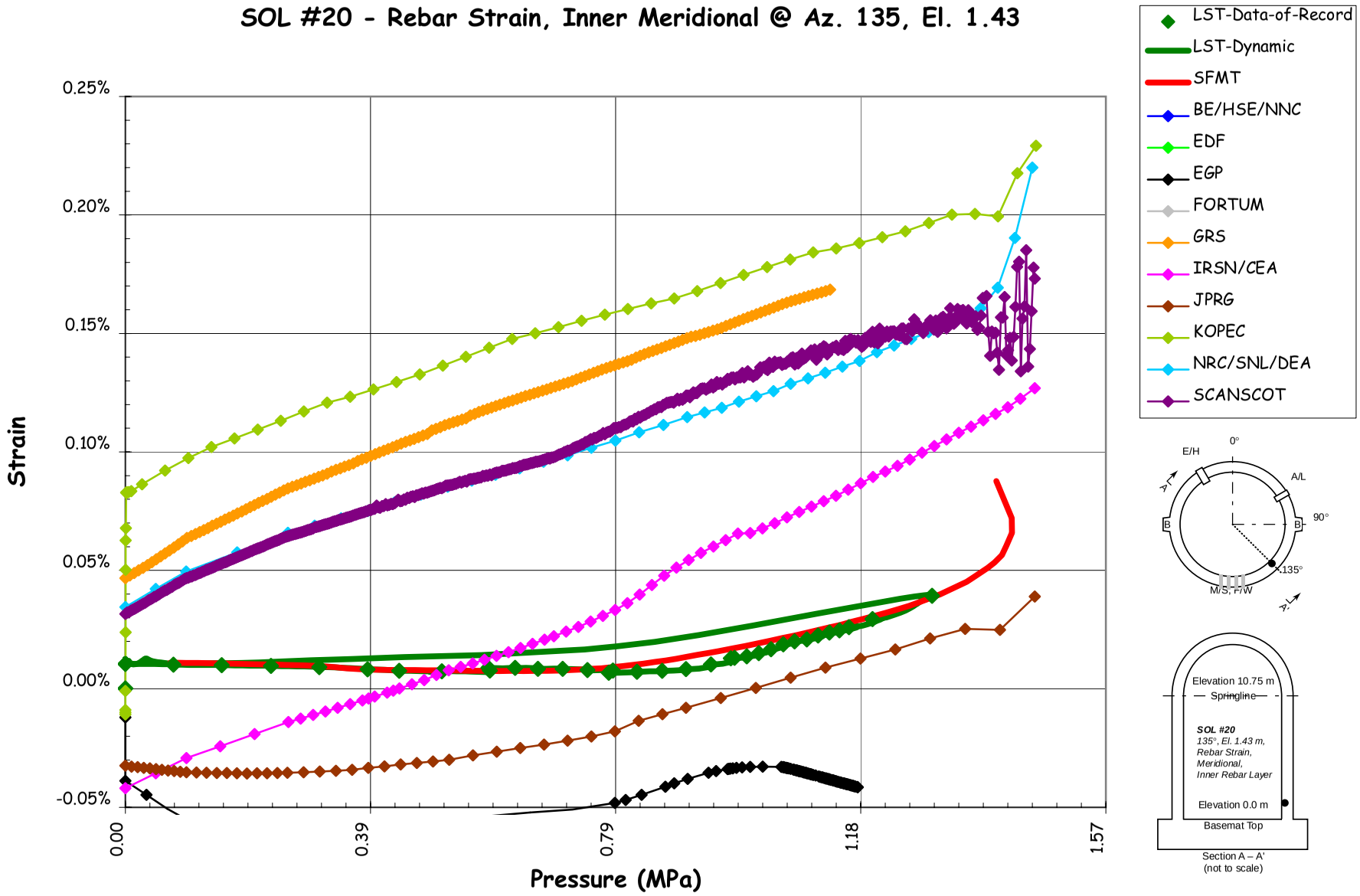
SOL #20 - Rebar Strain, Inner Meridional @ Az. 135, El. 1.43
Strain
0.25%
0.20%
0.15%
0.10%
0.05%
0.00%
-0.05%
0.00
0.39
0.79
1.18
1.57
Pressure (MPa)
LST-Data-of-Record
LST-Dynamic
SFMT
BE/HSE/NNC
EDF
EGP
FORTUM
GRS
IRSN/CEA
JPRG
KOPEC
NRC/SNL/DEA
SCANSCOT
0°
E/H
A/L
90°
B
135°
M/S; F/W
Elevation 10.75 m
Springline
SOL #20
135°, El. 1.43 m,
Rebar Strain,
Meridional,
Inner Rebar Layer
Elevation 0.0 m
Basemat Top
Section A – A'
(not to scale)

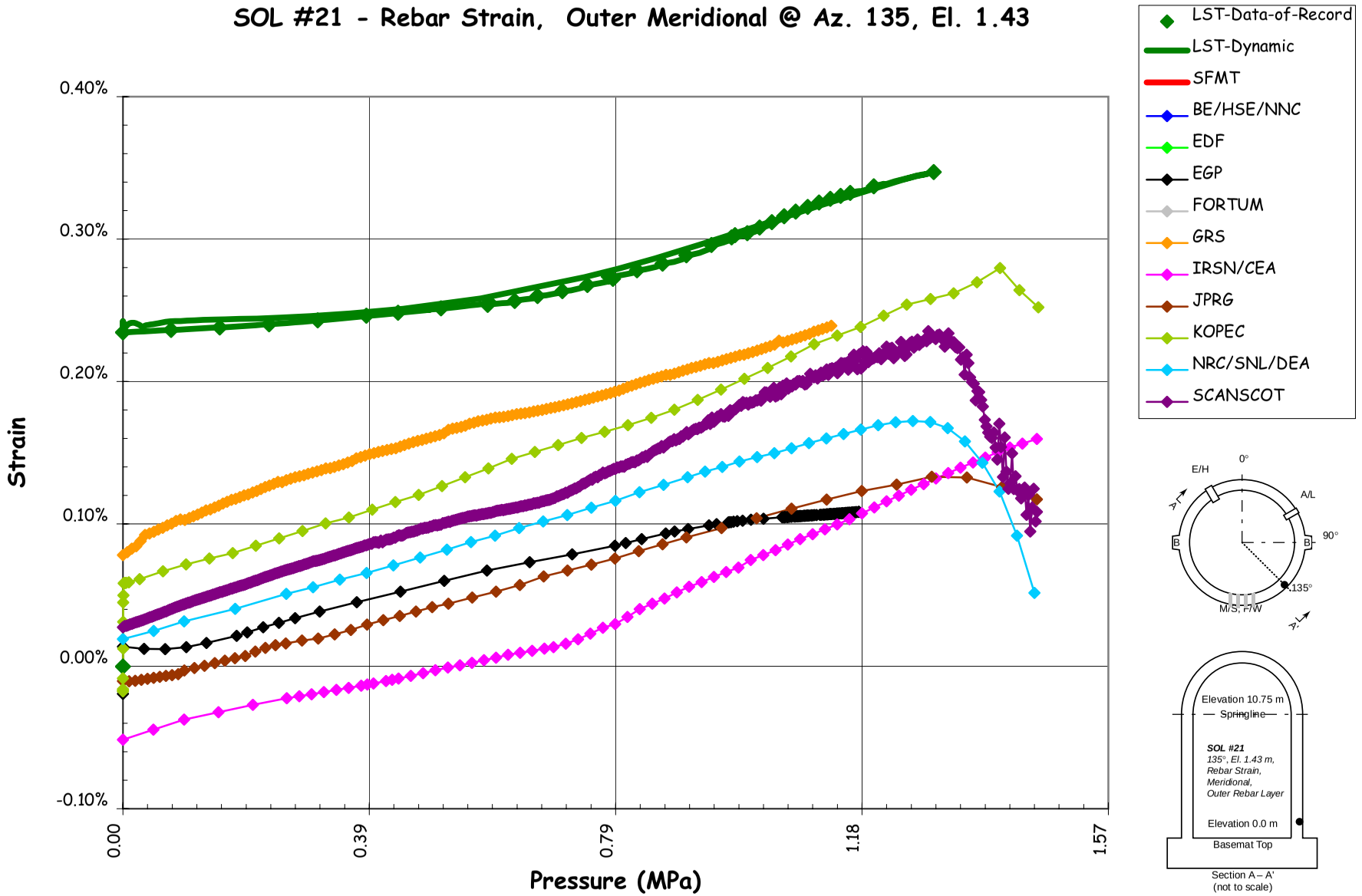
SOL #21 - Rebar Strain, Outer Meridional @ Az. 135, El. 1.43
Strain
0.40%
0.30%
0.20%
0.10%
0.00%
-0.10%
0.00
0.39
0.79
1.18
1.57
Pressure (MPa)
LST-Data-of-Record
LST-Dynamic
SFMT
BE/HSE/NNC
EDF
EGP
FORTUM
GRS
IRSN/CEA
JPRG
KOPEC
NRC/SNL/DEA
SCANSCOT
0°
E/H
A/L
90°
135°
M/S, F/W
Elevation 10.75 m
Springline
SOL #21
135°, El. 1.43 m,
Rebar Strain,
Meridional,
Outer Rebar Layer
Elevation 0.0 m
Basemat Top
Section A – A'
(not to scale)

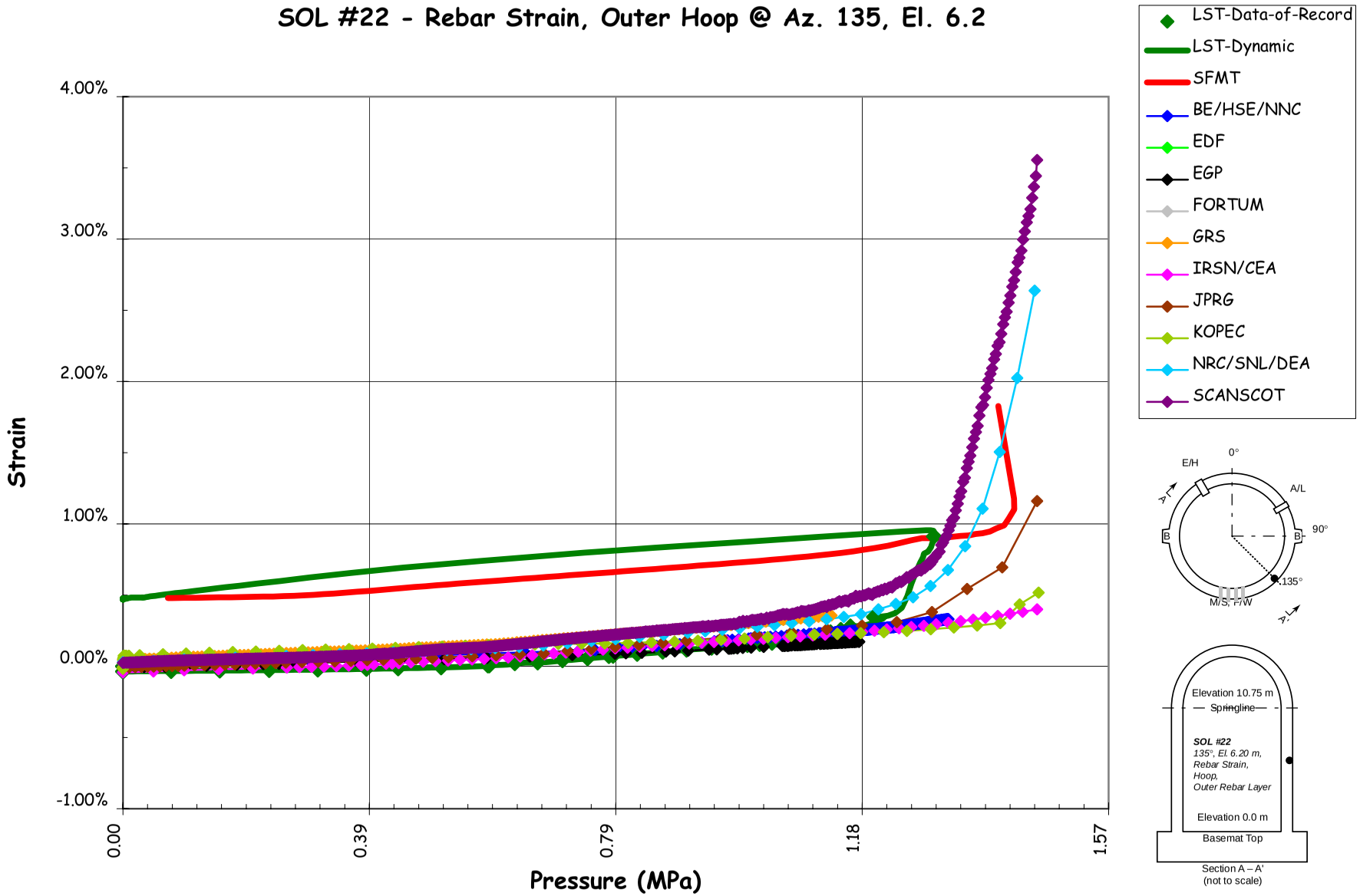
SOL #22 - Rebar Strain, Outer Hoop @ Az. 135, El. 6.2
Strain
4.00%
3.00%
2.00%
1.00%
0.00%
-1.00%
0.00
0.39
0.79
1.18
1.57
Pressure (MPa)
LST-Data-of-Record
LST-Dynamic
SFMT
BE/HSE/NNC
EDF
EGP
FORTUM
GRS
IRSN/CEA
JPRG
KOPEC
NRC/SNL/DEA
SCANSCOT
0°
E/H
A/L
90°
135°
M/S, F/W
Elevation 10.75 m
Springline
SOL #22
135°, El. 6.20 m,
Rebar Strain,
Hoop,
Outer Rebar Layer
Elevation 0.0 m
Basemat Top
Section A – A'
(not to scale)

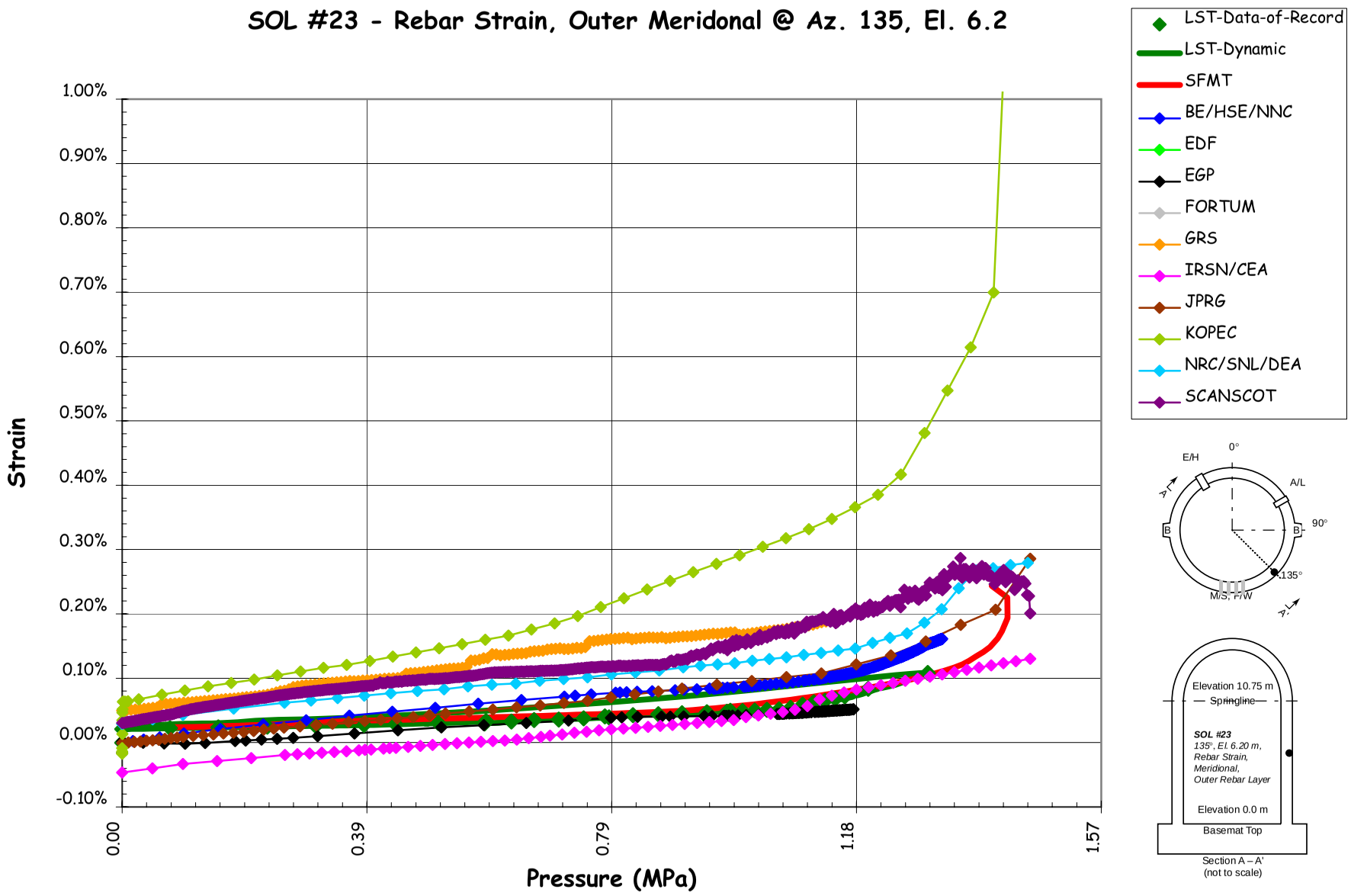
SOL #23 - Rebar Strain, Outer Meridonal @ Az. 135, El. 6.2
Strain
1.00%
0.90%
0.80%
0.70%
0.60%
0.50%
0.40%
0.30%
0.20%
0.10%
0.00%
-0.10%
0.00
0.39
0.79
1.18
1.57
Pressure (MPa)
LST-Data-of-Record
LST-Dynamic
SFMT
BE/HSE/NNC
EDF
EGP
FORTUM
GRS
IRSN/CEA
JPRG
KOPEC
NRC/SNL/DEA
SCANSCOT
0°
E/H
A/L
90°
135°
M/S, F/W
A
A'
B
B
Elevation 10.75 m
Springline
SOL #23
135°, El. 6.20 m,
Rebar Strain,
Meridional,
Outer Rebar Layer
Elevation 0.0 m
Basemat Top
Section A – A'
(not to scale)

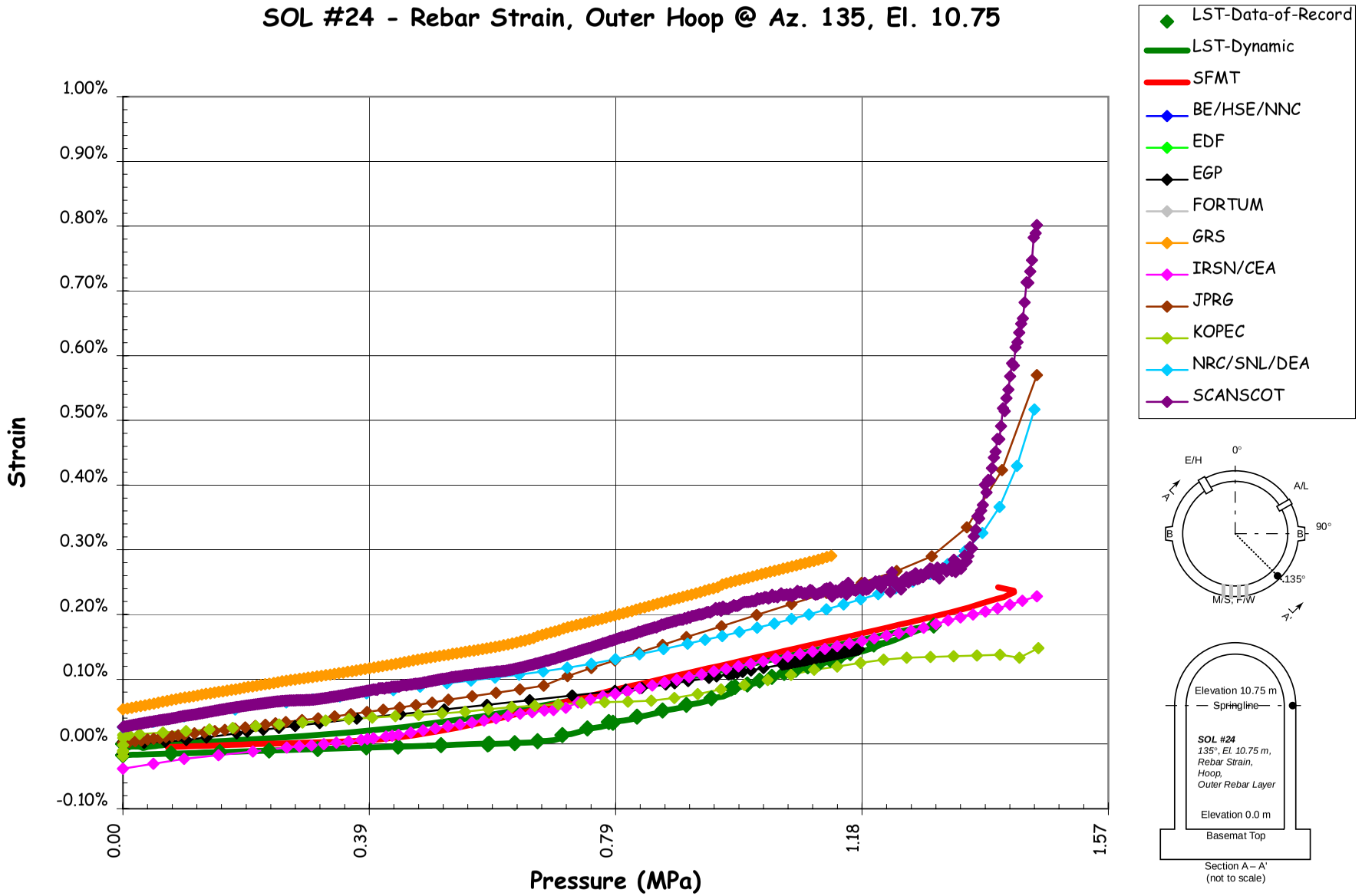
SOL #24 - Rebar Strain, Outer Hoop @ Az. 135, El. 10.75
Strain
1.00%
0.90%
0.80%
0.70%
0.60%
0.50%
0.40%
0.30%
0.20%
0.10%
0.00%
-0.10%
0.00
0.39
0.79
1.18
1.57
Pressure (MPa)
LST-Data-of-Record
LST-Dynamic
SFMT
BE/HSE/NNC
EDF
EGP
FORTUM
GRS
IRSN/CEA
JPRG
KOPEC
NRC/SNL/DEA
SCANSCOT
0°
E/H
A/L
90°
B
B
135°
M/S, F/W
A'
A'
Elevation 10.75 m
Springline
SOL #24
135°, El. 10.75 m,
Rebar Strain,
Hoop,
Outer Rebar Layer
Elevation 0.0 m
Basemat Top
Section A – A'
(not to scale)

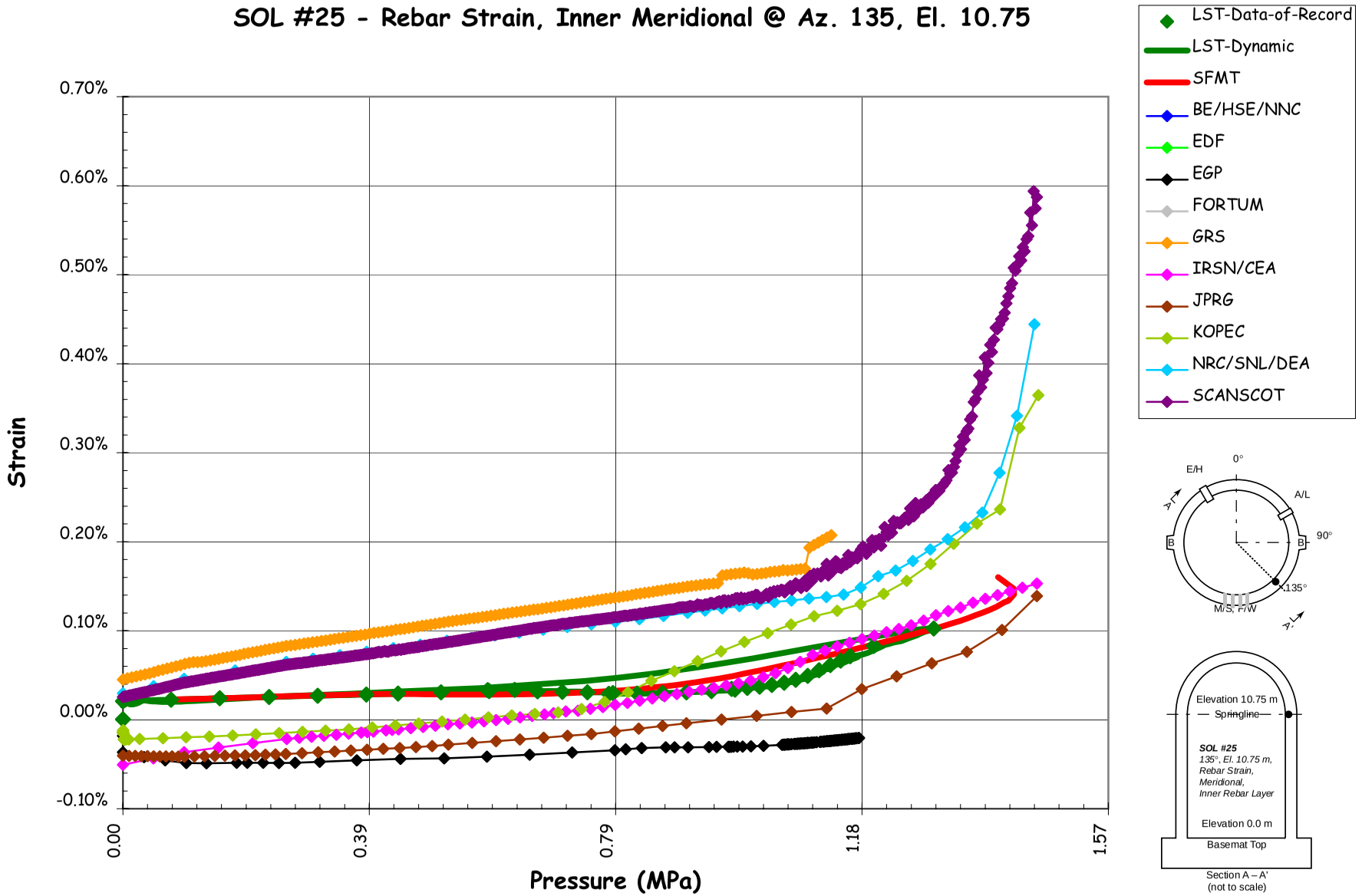
SOL #25 - Rebar Strain, Inner Meridional @ Az. 135, El. 10.75
Strain
0.70%
0.60%
0.50%
0.40%
0.30%
0.20%
0.10%
0.00%
-0.10%
0.00
0.39
0.79
1.18
1.57
Pressure (MPa)
LST-Data-of-Record
LST-Dynamic
SFMT
BE/HSE/NNC
EDF
EGP
FORTUM
GRS
IRSN/CEA
JPRG
KOPEC
NRC/SNL/DEA
SCANSCOT
0°
E/H
A/L
90°
135°
M/S, F/W
A'
A
Elevation 10.75 m
Springline
SOL #25
135°, El. 10.75 m,
Rebar Strain,
Meridional,
Inner Rebar Layer
Elevation 0.0 m
Basemat Top
Section A – A'
(not to scale)

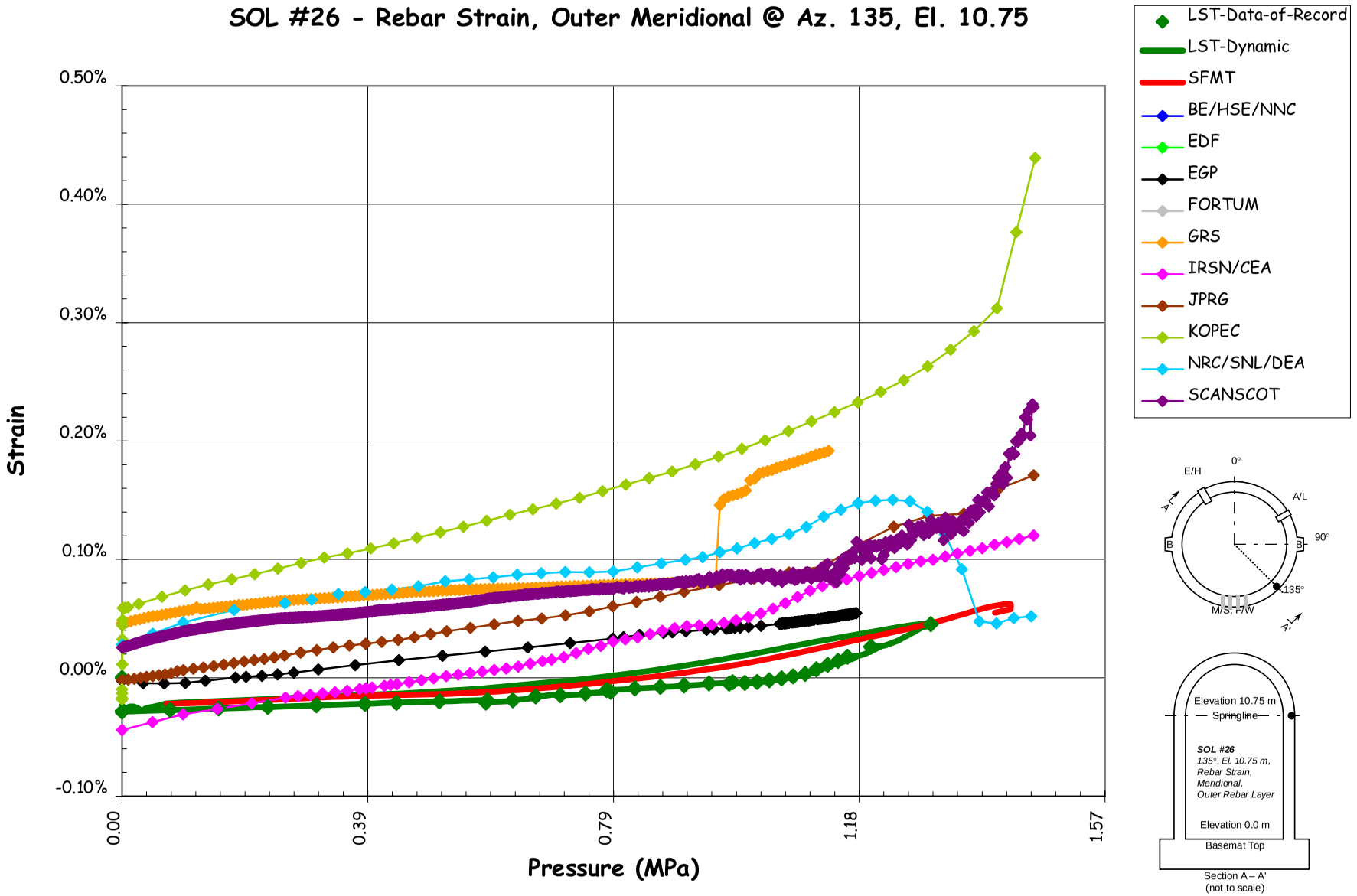
SOL #26 - Rebar Strain, Outer Meridional @ Az. 135, El. 10.75
Strain
0.50%
0.40%
0.30%
0.20%
0.10%
0.00%
-0.10%
0.00
0.39
0.79
1.18
1.57
Pressure (MPa)
LST-Data-of-Record
LST-Dynamic
SFMT
BE/HSE/NNC
EDF
EGP
FORTUM
GRS
IRSN/CEA
JPRG
KOPEC
NRC/SNL/DEA
SCANSCOT
0°
E/H
A/L
90°
135°
M/S, F/W
Elevation 10.75 m
Springline
SOL #26
135°, El. 10.75 m,
Rebar Strain,
Meridional,
Outer Rebar Layer
Elevation 0.0 m
Basemat Top
Section A – A'
(not to scale)

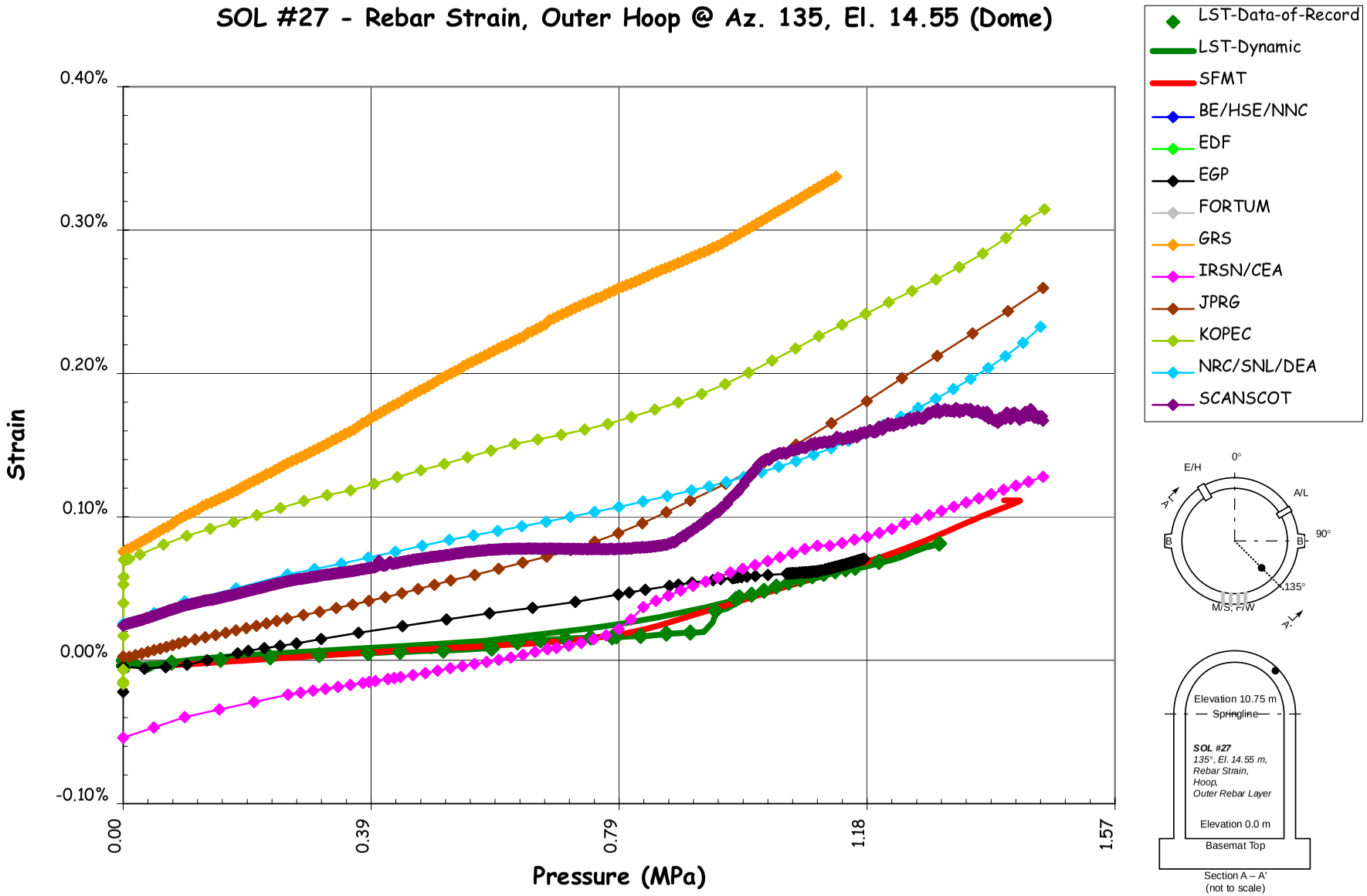
SOL #27 - Rebar Strain, Outer Hoop @ Az. 135, El. 14.55 (Dome)
Strain
0.40%
0.30%
0.20%
0.10%
0.00%
-0.10%
0.00
0.39
0.79
1.18
1.57
Pressure (MPa)
LST-Data-of-Record
LST-Dynamic
SFMT
BE/HSE/NNC
EDF
EGP
FORTUM
GRS
IRSN/CEA
JPRG
KOPEC
NRC/SNL/DEA
SCANSCOT
0°
E/H
A/L
90°
135°
M/S, F/W
Elevation 10.75 m
Springline
SOL #27
135°, El. 14.55 m,
Rebar Strain,
Hoop,
Outer Rebar Layer
Elevation 0.0 m
Basemat Top
Section A – A'
(not to scale)

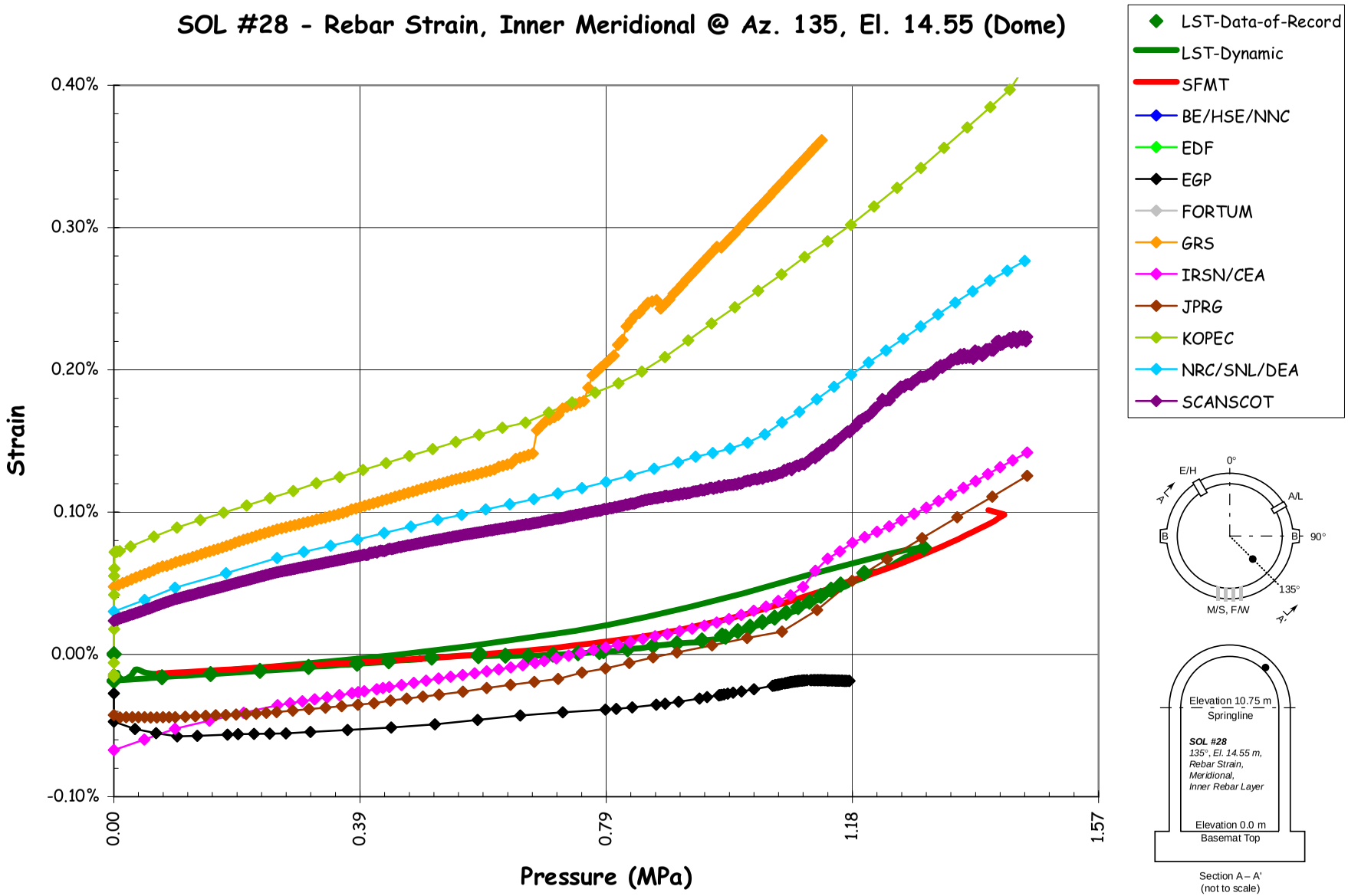
SOL #28 - Rebar Strain, Inner Meridional @ Az. 135, El. 14.55 (Dome)
Strain
0.40%
0.30%
0.20%
0.10%
0.00%
-0.10%
0.00
0.39
0.79
1.18
1.57
Pressure (MPa)
LST-Data-of-Record
LST-Dynamic
SFMT
BE/HSE/NNC
EDF
EGP
FORTUM
GRS
IRSN/CEA
JPRG
KOPEC
NRC/SNL/DEA
SCANSCOT
0°
E/H
A/L
90°
135°
M/S, F/W
Elevation 10.75 m
Springline
SOL #28
135°, El. 14.55 m,
Rebar Strain,
Meridional,
Inner Rebar Layer
Elevation 0.0 m
Basemat Top
Section A – A'
(not to scale)

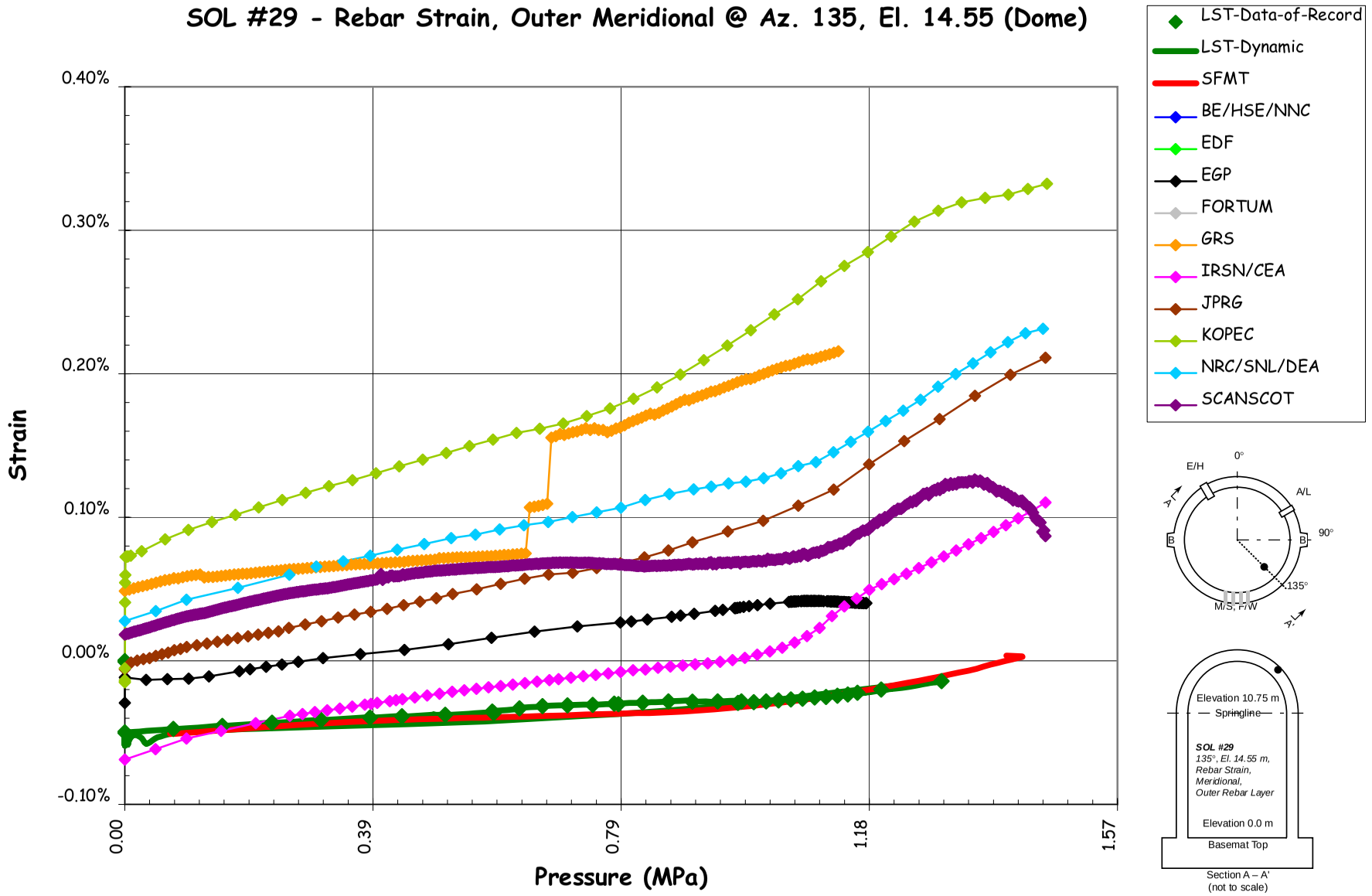
SOL #29 - Rebar Strain, Outer Meridional @ Az. 135, El. 14.55 (Dome)
Strain
0.40%
0.30%
0.20%
0.10%
0.00%
-0.10%
0.00
0.39
0.79
1.18
1.57
Pressure (MPa)
LST-Data-of-Record
LST-Dynamic
SFMT
BE/HSE/NNC
EDF
EGP
FORTUM
GRS
IRSN/CEA
JPRG
KOPEC
NRC/SNL/DEA
SCANSCOT
E/H
0°
A/L
90°
135°
M/S, F/W
Elevation 10.75 m
Springline
SOL #29
135°, El. 14.55 m,
Rebar Strain,
Meridional,
Outer Rebar Layer
Elevation 0.0 m
Basemat Top
Section A – A'
(not to scale)

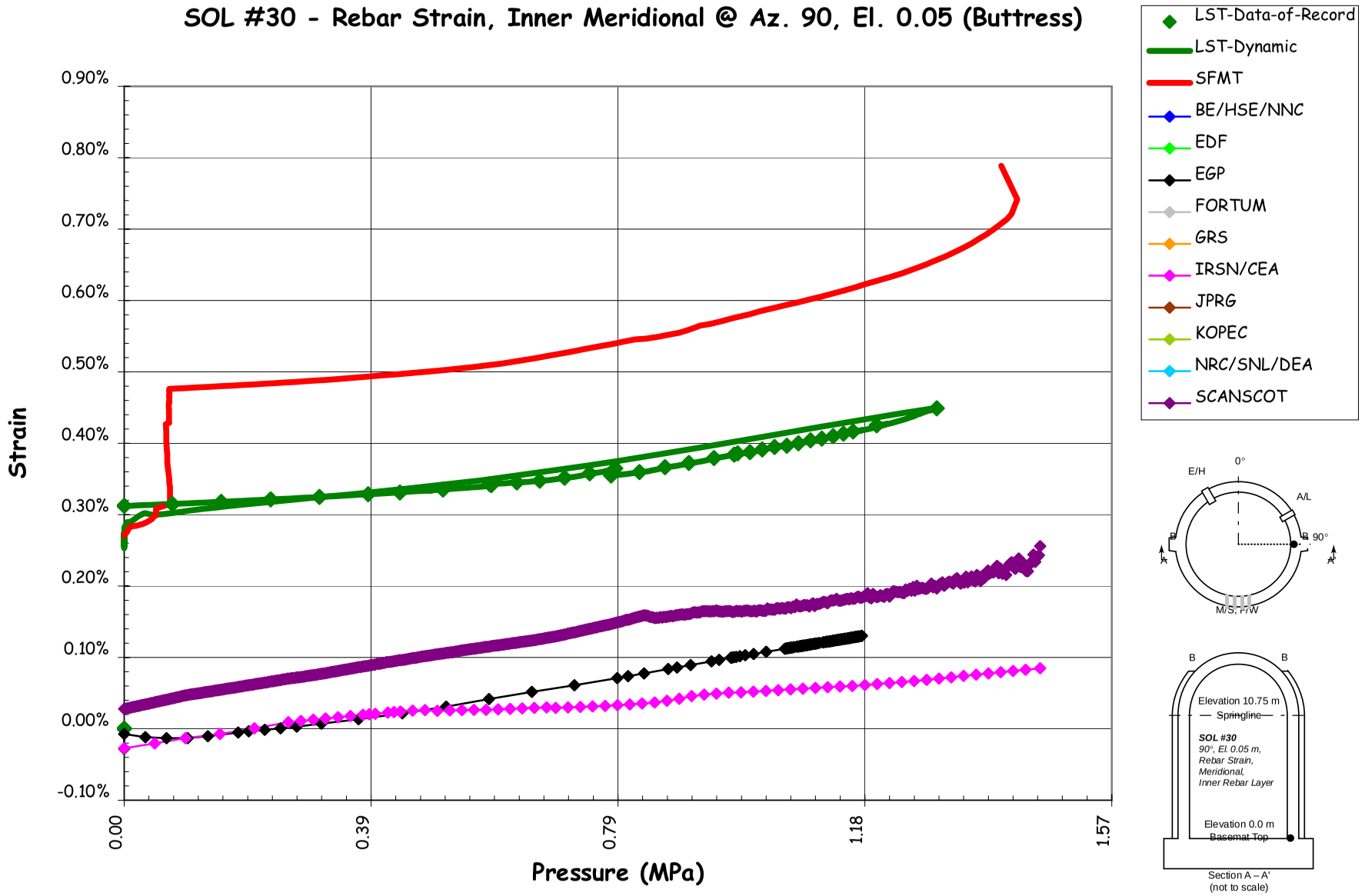
SOL #30 - Rebar Strain, Inner Meridional @ Az. 90, El. 0.05 (Buttress)
Strain
0.90%
0.80%
0.70%
0.60%
0.50%
0.40%
0.30%
0.20%
0.10%
0.00%
-0.10%
0.00
0.39
0.79
1.18
1.57
Pressure (MPa)
LST-Data-of-Record
LST-Dynamic
SFMT
BE/HSE/NNC
EDF
EGP
FORTUM
GRS
IRSN/CEA
JPRG
KOPEC
NRC/SNL/DEA
SCANSCOT
0°
E/H
A/L
B 90°
M/S, F/W
B
B
Elevation 10.75 m
Springline
SOL #30
90°, El. 0.05 m,
Rebar Strain,
Meridional,
Inner Rebar Layer
Elevation 0.0 m
Basemat Top
Section A – A'
(not to scale)

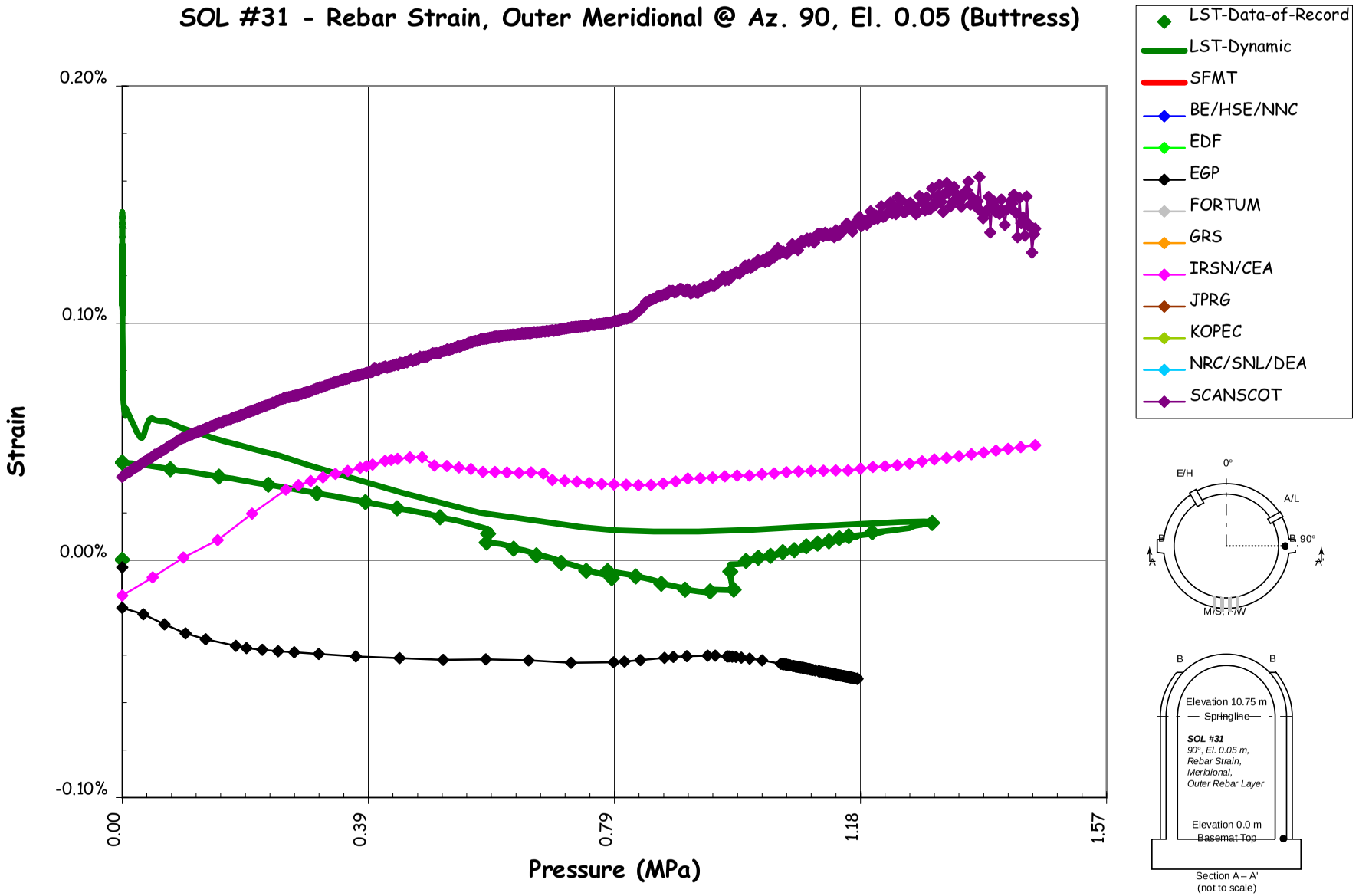
SOL #31 - Rebar Strain, Outer Meridional @ Az. 90, El. 0.05 (Buttress)
Strain
0.20%
0.10%
0.00%
-0.10%
0.00
0.39
0.79
1.18
1.57
Pressure (MPa)
LST-Data-of-Record
LST-Dynamic
SFMT
BE/HSE/NNC
EDF
EGP
FORTUM
GRS
IRSN/CEA
JPRG
KOPEC
NRC/SNL/DEA
SCANSCOT
0°
E/H
A/L
B
B
90°
A
A'
M/S, F/W
B
B
Elevation 10.75 m
Springline
SOL #31
90°, El. 0.05 m,
Rebar Strain,
Meridional,
Outer Rebar Layer
Elevation 0.0 m
Basemat Top
Section A – A'
(not to scale)

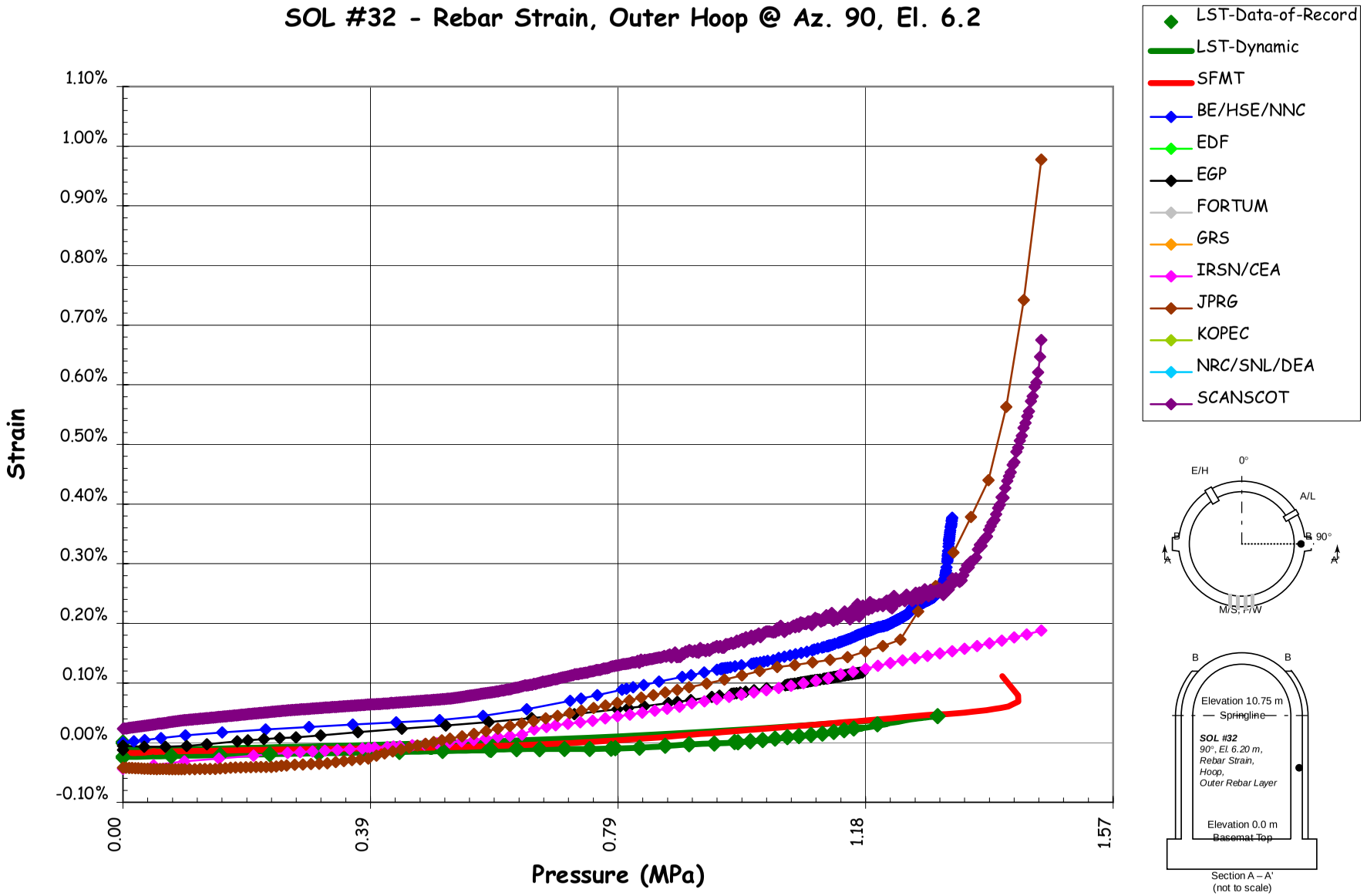
SOL #32 - Rebar Strain, Outer Hoop @ Az. 90, El. 6.2
Strain
1.10%
1.00%
0.90%
0.80%
0.70%
0.60%
0.50%
0.40%
0.30%
0.20%
0.10%
0.00%
-0.10%
0.00
0.39
0.79
1.18
1.57
Pressure (MPa)
LST-Data-of-Record
LST-Dynamic
SFMT
BE/HSE/NNC
EDF
EGP
FORTUM
GRS
IRSN/CEA
JPRG
KOPEC
NRC/SNL/DEA
SCANSCOT
0°
E/H
A/L
90°
M/S, F/W
B
B
Elevation 10.75 m
Springline
SOL #32
90°, El. 6.20 m,
Rebar Strain,
Hoop,
Outer Rebar Layer
Elevation 0.0 m
Basemat Top
Section A – A'
(not to scale)

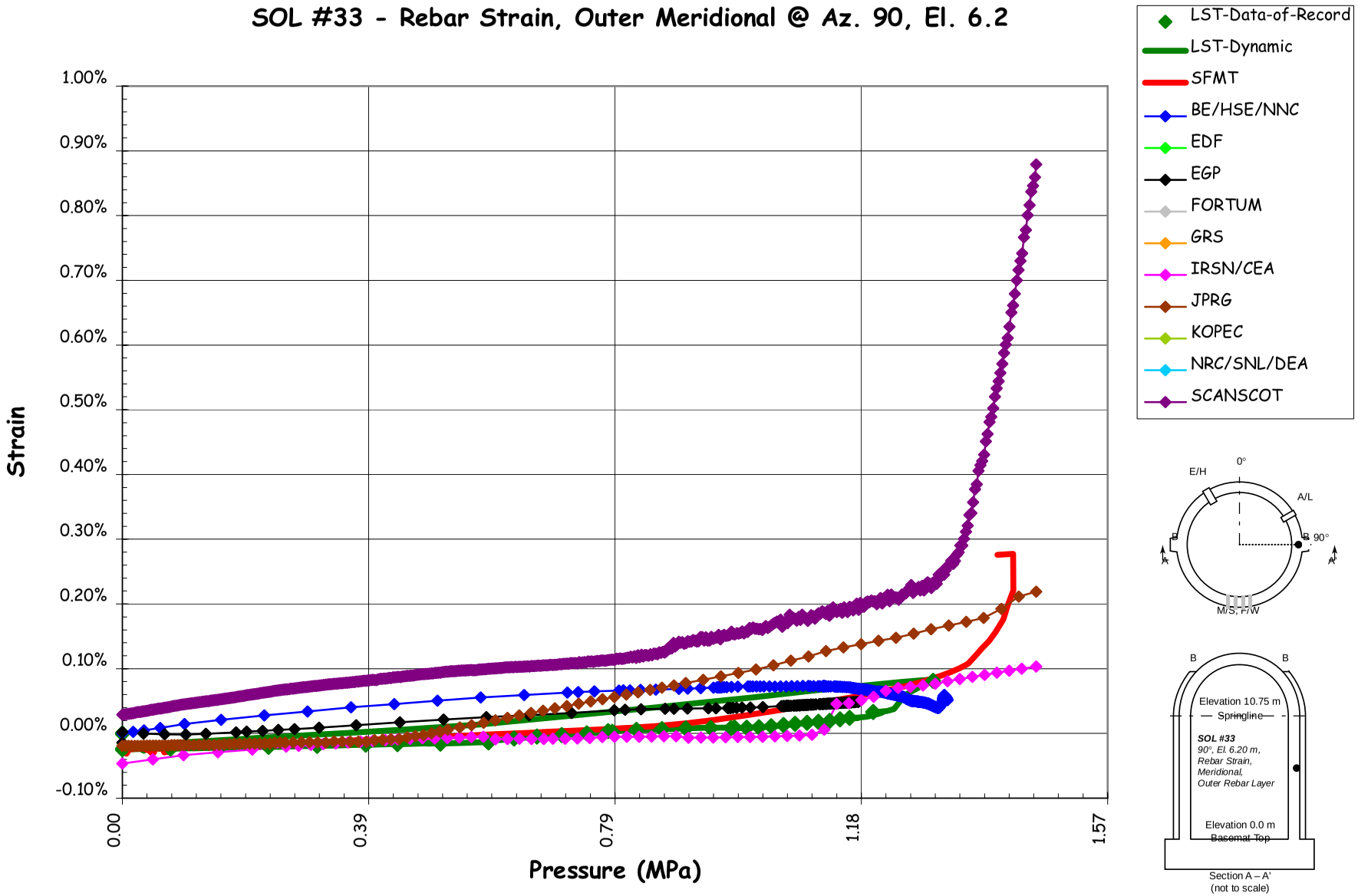
SOL #33 - Rebar Strain, Outer Meridional @ Az. 90, El. 6.2
Strain
1.00%
0.90%
0.80%
0.70%
0.60%
0.50%
0.40%
0.30%
0.20%
0.10%
0.00%
-0.10%
0.00
0.39
0.79
1.18
1.57
Pressure (MPa)
LST-Data-of-Record
LST-Dynamic
SFMT
BE/HSE/NNC
EDF
EGP
FORTUM
GRS
IRSN/CEA
JPRG
KOPEC
NRC/SNL/DEA
SCANSCOT
0°
E/H
A/L
90°
M/S, F/W
B
B
Elevation 10.75 m
Springline
SOL #33
90°, El. 6.20 m,
Rebar Strain,
Meridional,
Outer Rebar Layer
Elevation 0.0 m
Basemat Top
Section A – A'
(not to scale)

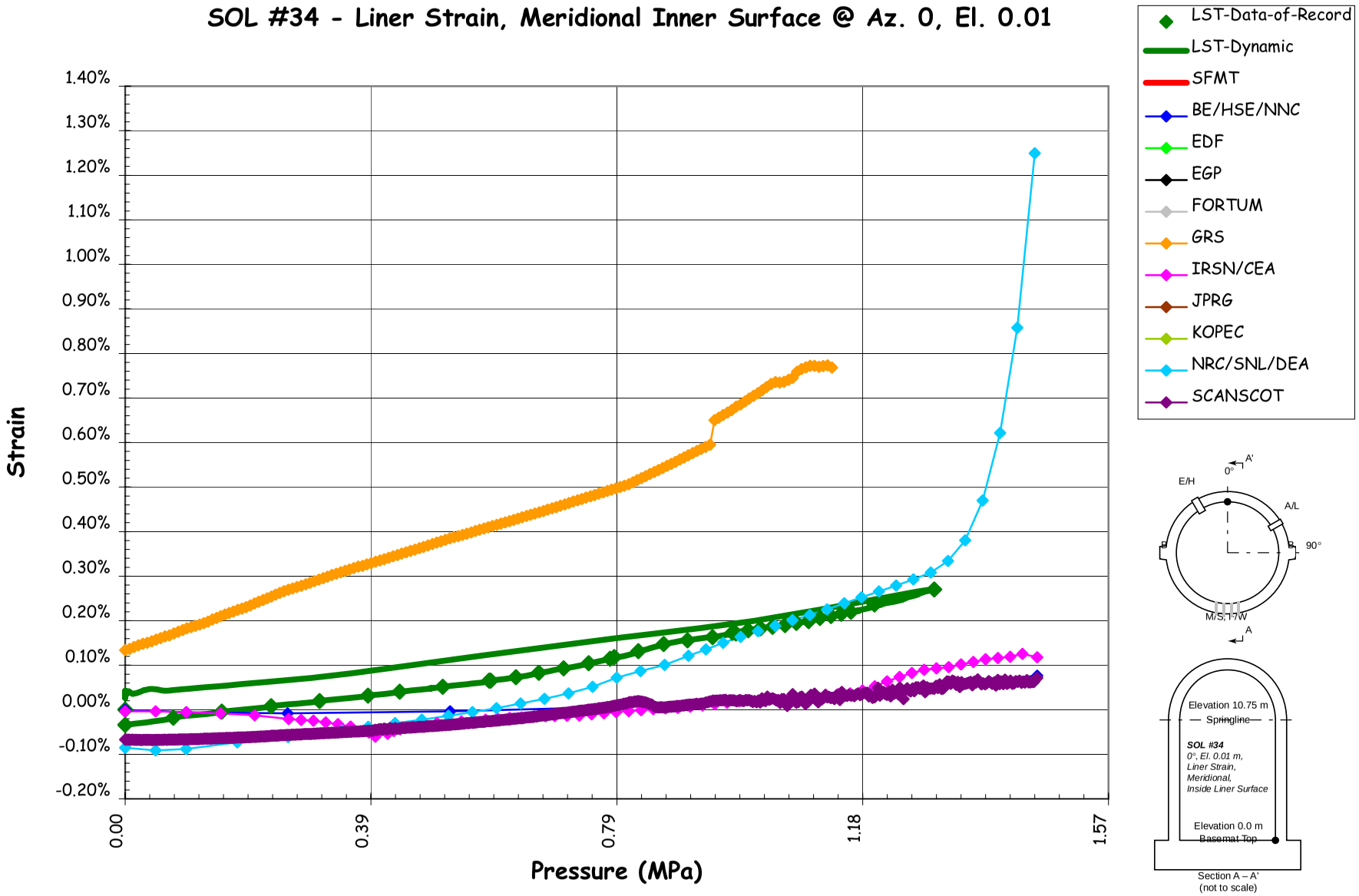
SOL #34 - Liner Strain, Meridional Inner Surface @ Az. 0, El. 0.01
Strain
1.40%
1.30%
1.20%
1.10%
1.00%
0.90%
0.80%
0.70%
0.60%
0.50%
0.40%
0.30%
0.20%
0.10%
0.00%
-0.10%
-0.20%
0.00
0.39
0.79
1.18
1.57
Pressure (MPa)
LST-Data-of-Record
LST-Dynamic
SFMT
BE/HSE/NNC
EDF
EGP
FORTUM
GRS
IRSN/CEA
JPRG
KOPEC
NRC/SNL/DEA
SCANSCOT
A'
0°
E/H
A/L
90°
M/S, I-W
A
Elevation 10.75 m
Springline
SOL #34
0°, El. 0.01 m,
Liner Strain,
Meridional,
Inside Liner Surface
Elevation 0.0 m
Basemat Top
Section A – A'
(not to scale)

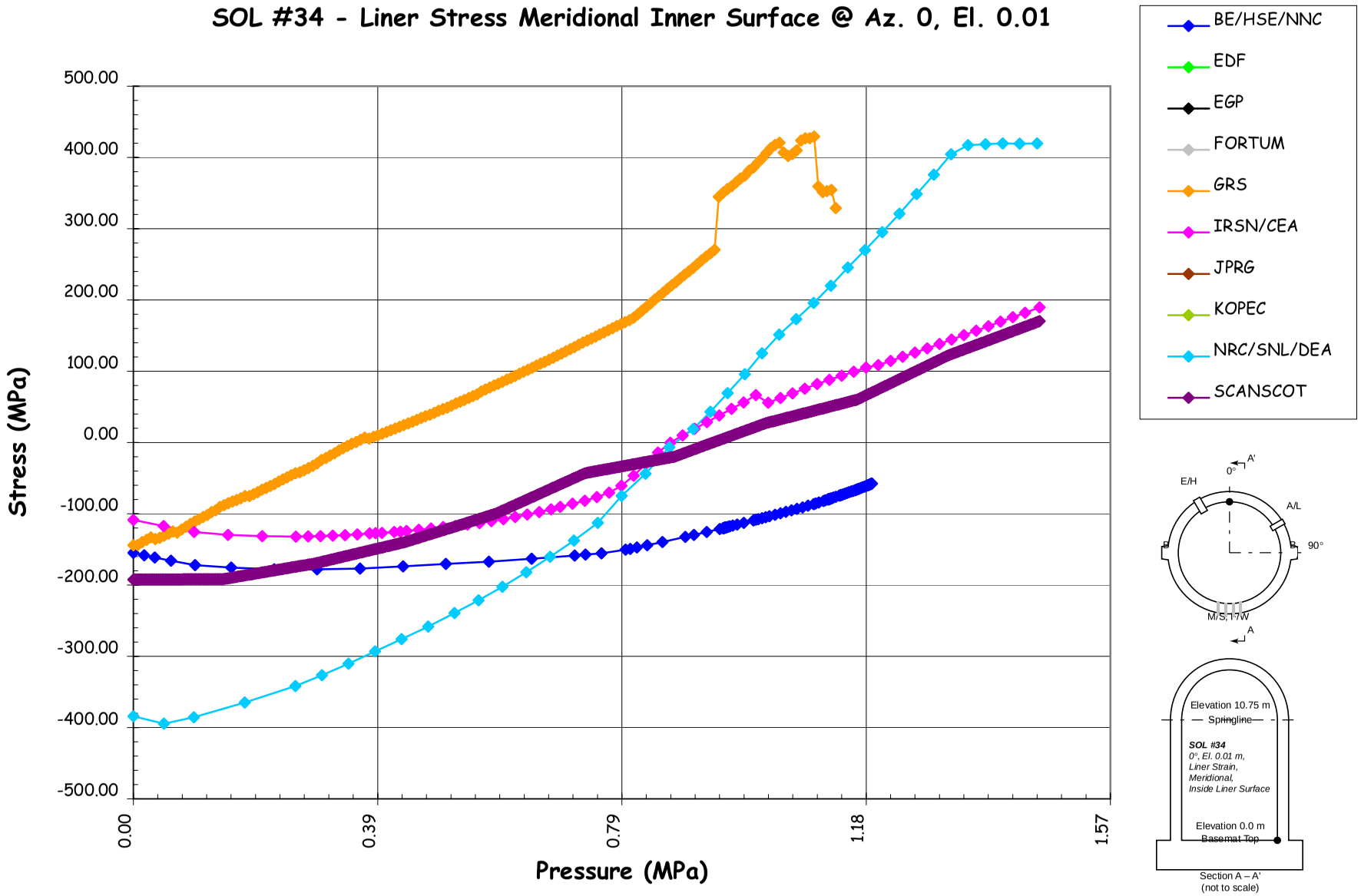
SOL #34 - Liner Stress Meridional Inner Surface @ Az. 0, El. 0.01
Stress (MPa)
500.00
400.00
300.00
200.00
100.00
0.00
-100.00
-200.00
-300.00
-400.00
-500.00
0.00
0.39
0.79
1.18
1.57
Pressure (MPa)
BE/HSE/NNC
EDF
EGP
FORTUM
GRS
IRSN/CEA
JPRG
KOPEC
NRC/SNL/DEA
SCANSCOT
A'
0°
E/H
A/L
90°
M/S, I-W
A
Elevation 10.75 m
Springline
SOL #34
0°, El. 0.01 m,
Liner Strain,
Meridional,
Inside Liner Surface
Elevation 0.0 m
Basemat Top
Section A – A'
(not to scale)

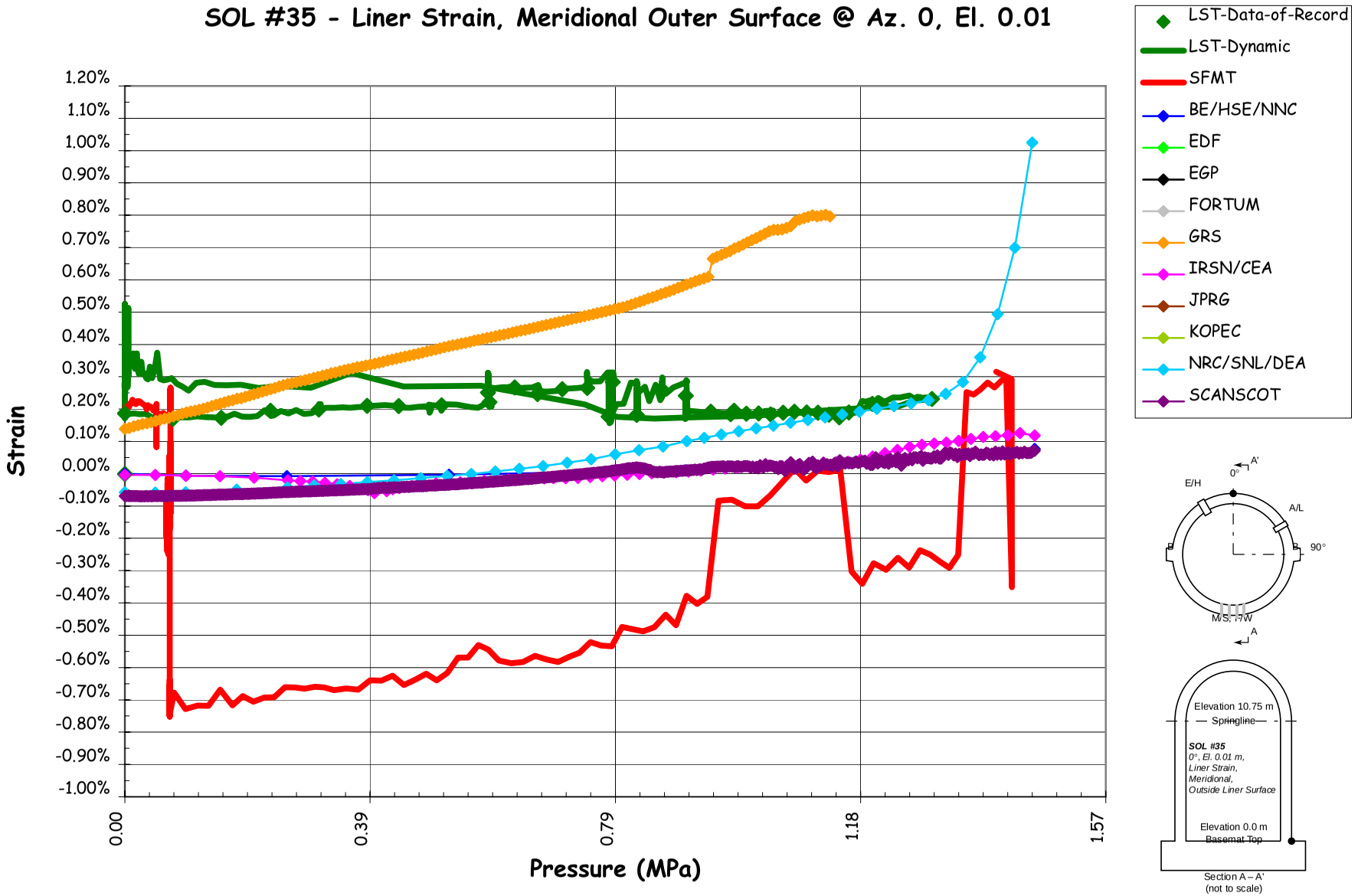
SOL #35 - Liner Strain, Meridional Outer Surface @ Az. 0, El. 0.01
Strain
1.20%
1.10%
1.00%
0.90%
0.80%
0.70%
0.60%
0.50%
0.40%
0.30%
0.20%
0.10%
0.00%
-0.10%
-0.20%
-0.30%
-0.40%
-0.50%
-0.60%
-0.70%
-0.80%
-0.90%
-1.00%
0.00
0.39
0.79
1.18
1.57
Pressure (MPa)
LST-Data-of-Record
LST-Dynamic
SFMT
BE/HSE/NNC
EDF
EGP
FORTUM
GRS
IRSN/CEA
JPRG
KOPEC
NRC/SNL/DEA
SCANSCOT
A'
0°
E/H
A/L
90°
MS, HW
A
Elevation 10.75 m
Springline
SOL #35
0°, El. 0.01 m,
Liner Strain,
Meridional,
Outside Liner Surface
Elevation 0.0 m
Basemat Top
Section A – A'
(not to scale)

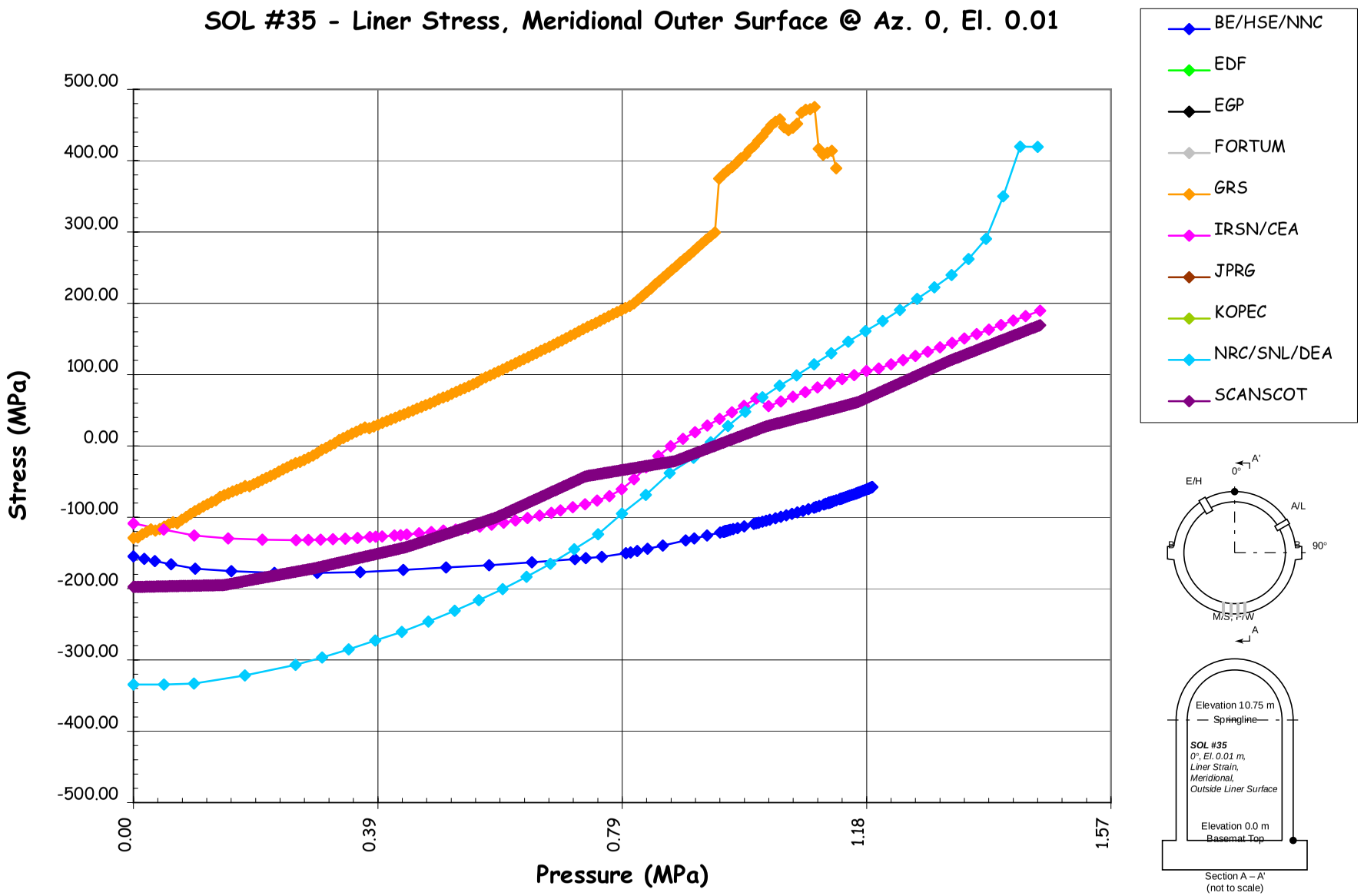
SOL #35 - Liner Stress, Meridional Outer Surface @ Az. 0, El. 0.01
Stress (MPa)
500.00
400.00
300.00
200.00
100.00
0.00
-100.00
-200.00
-300.00
-400.00
-500.00
0.00
0.39
0.79
1.18
1.57
Pressure (MPa)
BE/HSE/NNC
EDF
EGP
FORTUM
GRS
IRSN/CEA
JPRG
KOPEC
NRC/SNL/DEA
SCANSCOT
A'
0°
E/H
A/L
90°
M/S; I/W
A
Elevation 10.75 m
Springline
SOL #35
0°, El. 0.01 m,
Liner Strain,
Meridional,
Outside Liner Surface
Elevation 0.0 m
Basemat Top
Section A – A'
(not to scale)

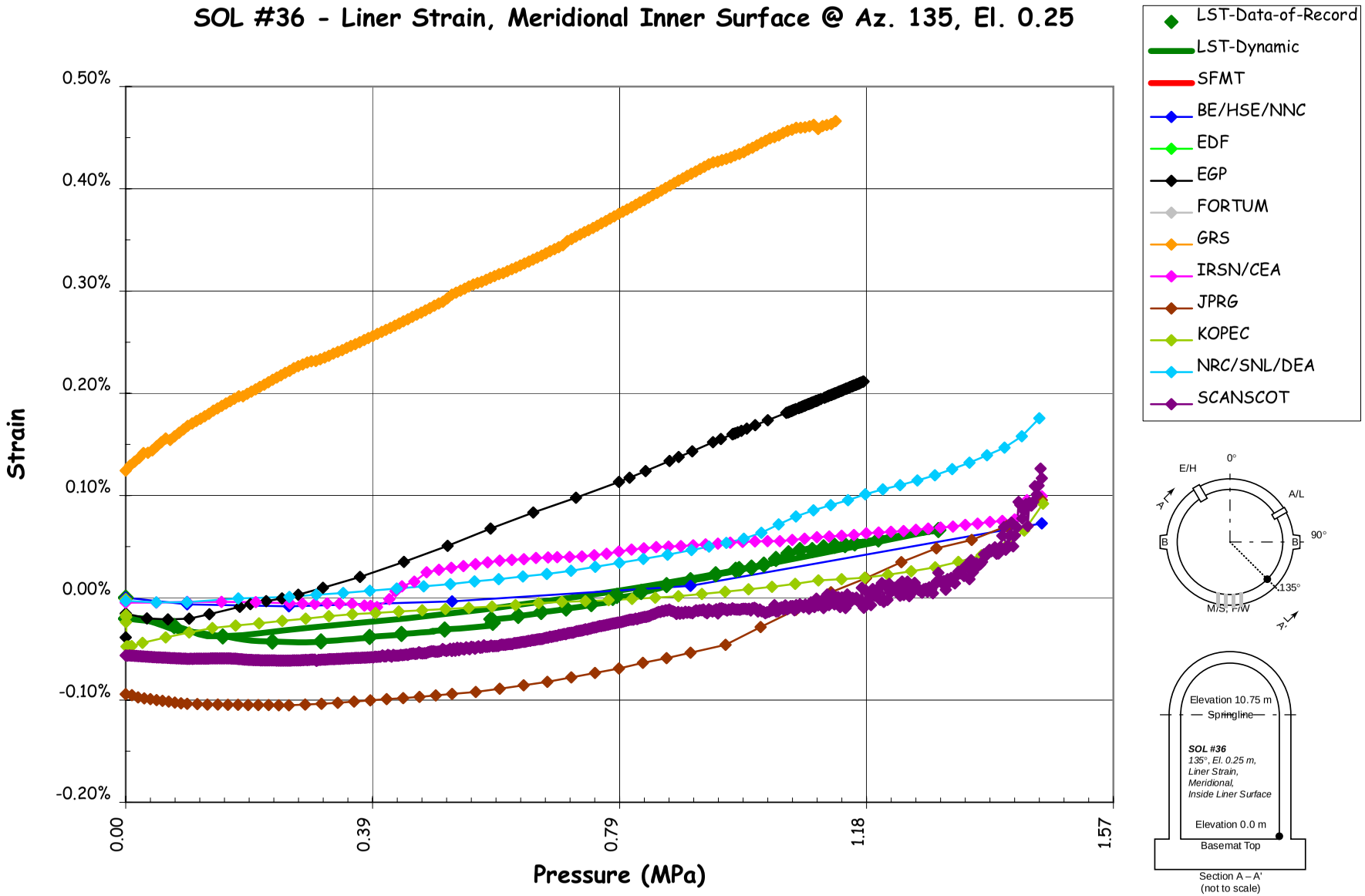
SOL #36 - Liner Strain, Meridional Inner Surface @ Az. 135, El. 0.25
Strain
0.50%
0.40%
0.30%
0.20%
0.10%
0.00%
-0.10%
-0.20%
0.00
0.39
0.79
1.18
1.57
Pressure (MPa)
LST-Data-of-Record
LST-Dynamic
SFMT
BE/HSE/NNC
EDF
EGP
FORTUM
GRS
IRSN/CEA
JPRG
KOPEC
NRC/SNL/DEA
SCANSCOT
0°
E/H
A/L
90°
135°
M/S, F/W
Elevation 10.75 m
Springline
SOL #36
135°, El. 0.25 m,
Liner Strain,
Meridional,
Inside Liner Surface
Elevation 0.0 m
Basemat Top
Section A – A'
(not to scale)

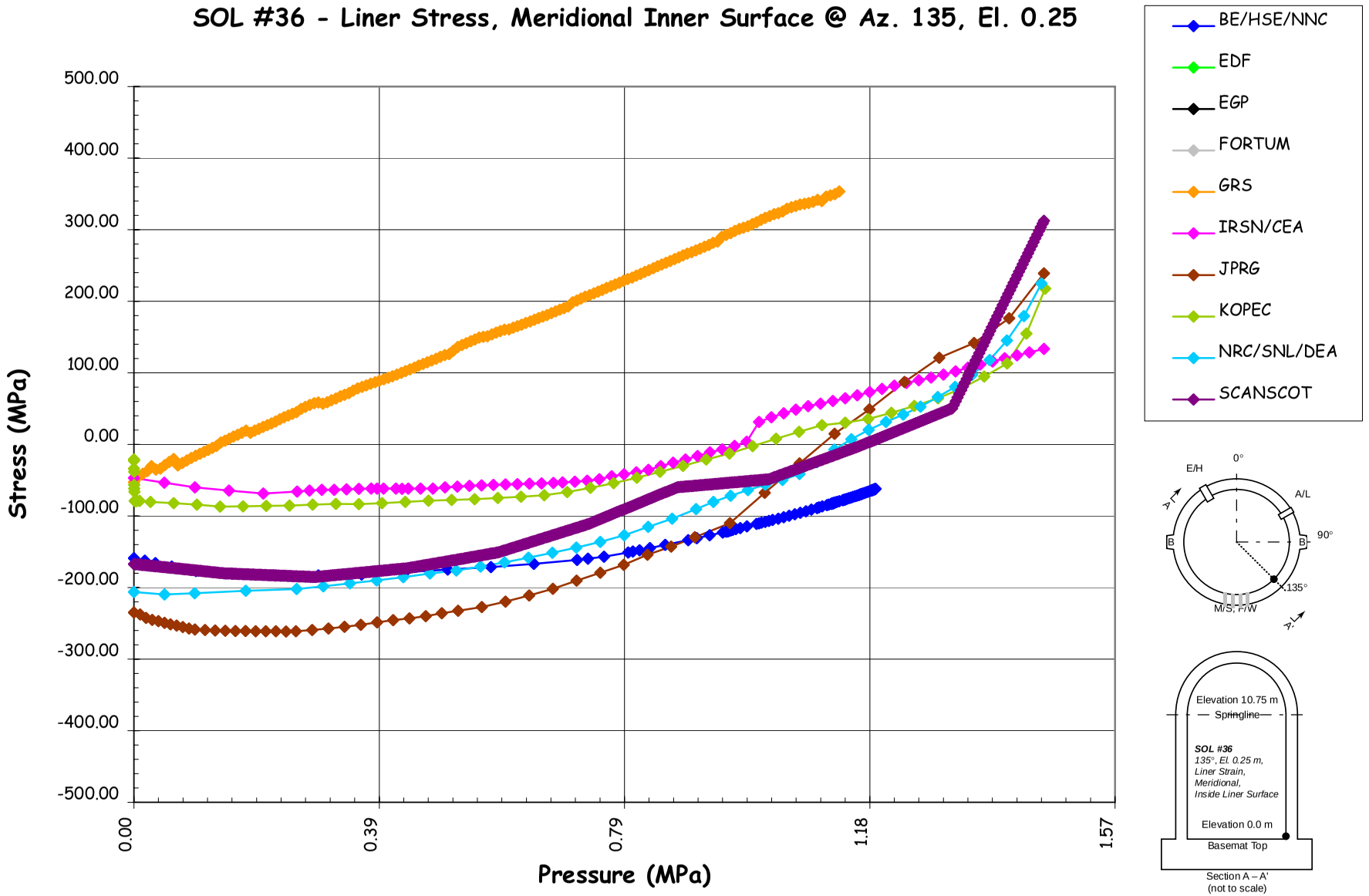
SOL #36 - Liner Stress, Meridional Inner Surface @ Az. 135, El. 0.25
Stress (MPa)
500.00
400.00
300.00
200.00
100.00
0.00
-100.00
-200.00
-300.00
-400.00
-500.00
0.00
0.39
0.79
1.18
1.57
Pressure (MPa)
BE/HSE/NNC
EDF
EGP
FORTUM
GRS
IRSN/CEA
JPRG
KOPEC
NRC/SNL/DEA
SCANSCOT
E/H
0°
A/L
90°
135°
M/S, F/W
Elevation 10.75 m
Springline
SOL #36
135°, El. 0.25 m,
Liner Strain,
Meridional,
Inside Liner Surface
Elevation 0.0 m
Basemat Top
Section A – A'
(not to scale)

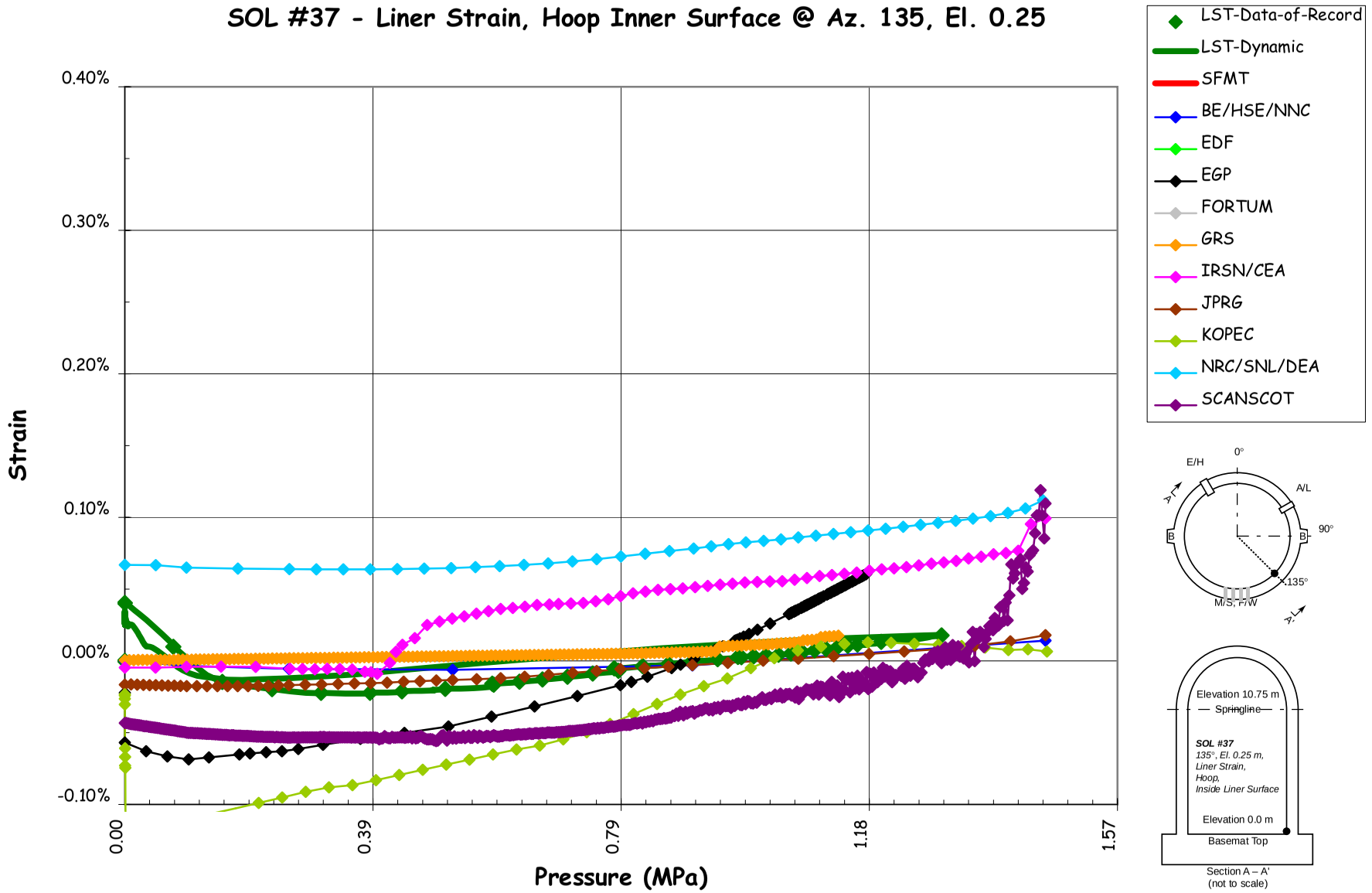
SOL #37 - Liner Strain, Hoop Inner Surface @ Az. 135, El. 0.25
Strain
0.40%
0.30%
0.20%
0.10%
0.00%
-0.10%
0.00
0.39
0.79
1.18
1.57
Pressure (MPa)
LST-Data-of-Record
LST-Dynamic
SFMT
BE/HSE/NNC
EDF
EGP
FORTUM
GRS
IRSN/CEA
JPRG
KOPEC
NRC/SNL/DEA
SCANSCOT
0°
E/H
A/L
90°
135°
M/S, F/W
P/T
P/L
Elevation 10.75 m
Springline
SOL #37
135°, El. 0.25 m,
Liner Strain,
Hoop,
Inside Liner Surface
Elevation 0.0 m
Basemat Top
Section A – A'
(not to scale)

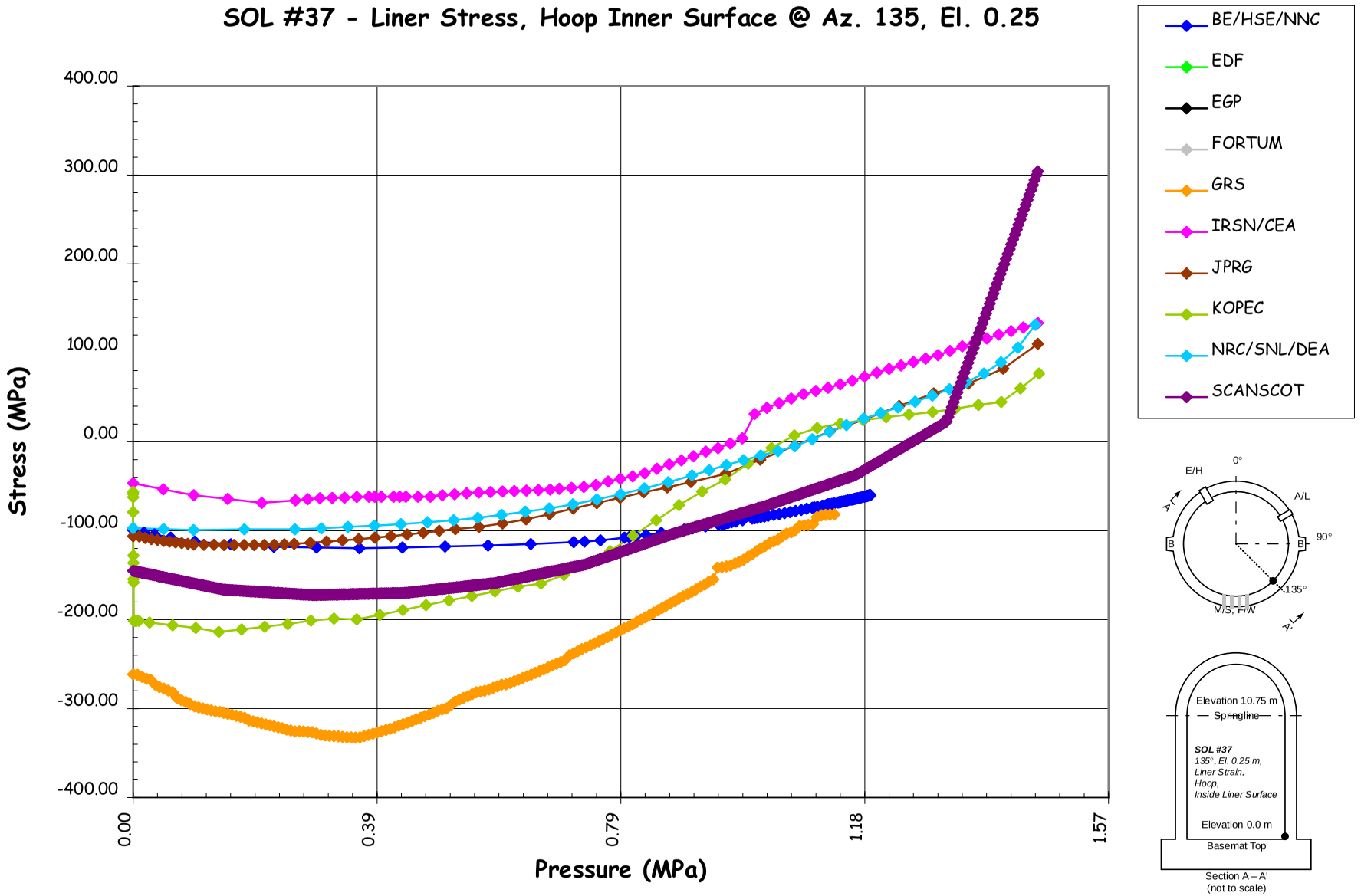
SOL #37 - Liner Stress, Hoop Inner Surface @ Az. 135, El. 0.25
Stress (MPa)
400.00
300.00
200.00
100.00
0.00
-100.00
-200.00
-300.00
-400.00
0.00
0.39
0.79
1.18
1.57
Pressure (MPa)
BE/HSE/NNC
EDF
EGP
FORTUM
GRS
IRSN/CEA
JPRG
KOPEC
NRC/SNL/DEA
SCANSCOT
0°
E/H
A/L
90°
135°
M/S, F/W
Elevation 10.75 m
Springline
SOL #37
135°, El. 0.25 m,
Liner Strain,
Hoop,
Inside Liner Surface
Elevation 0.0 m
Basemat Top
Section A – A'
(not to scale)

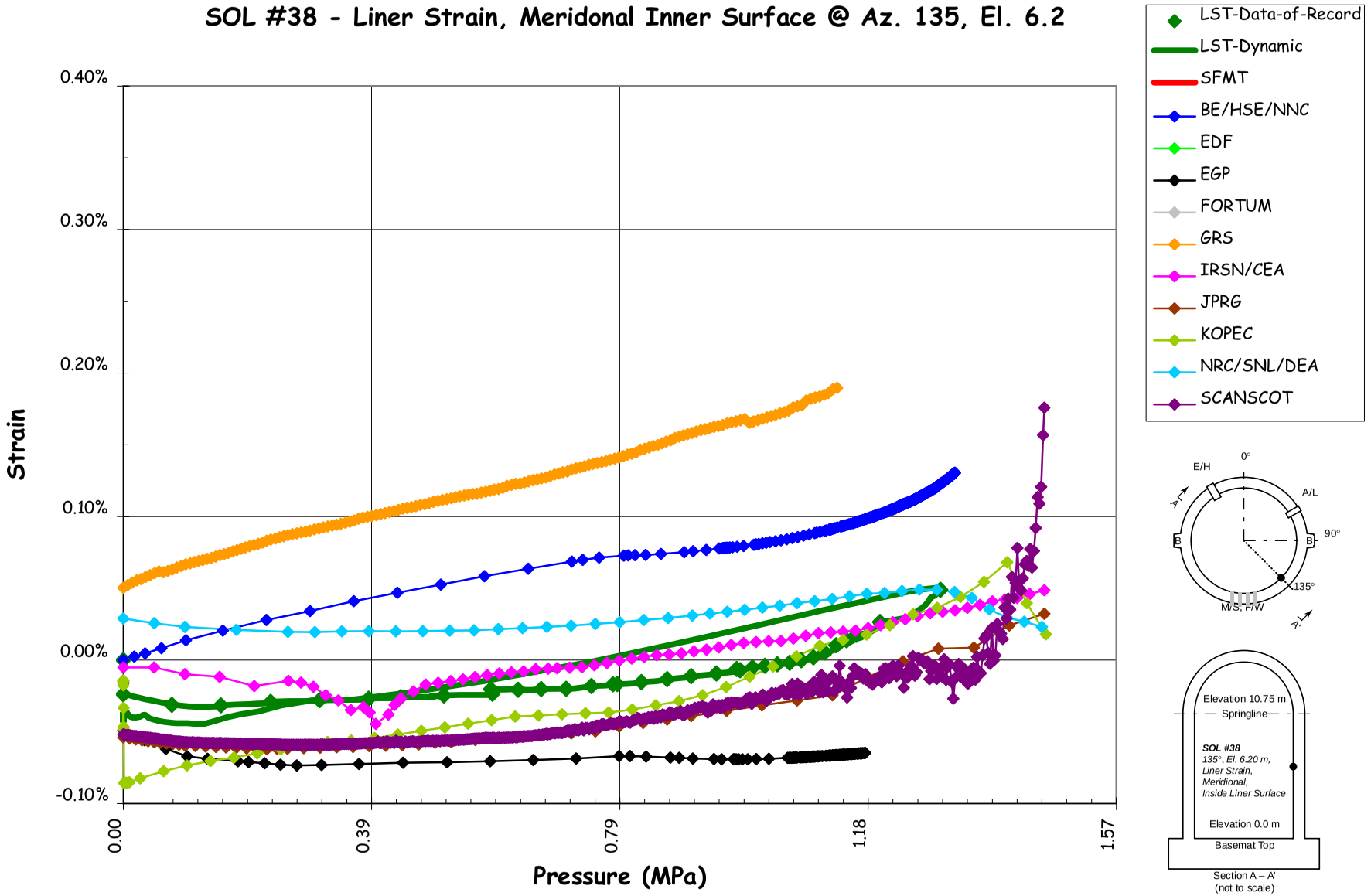
SOL #38 - Liner Strain, Meridonal Inner Surface @ Az. 135, El. 6.2
Strain
0.40%
0.30%
0.20%
0.10%
0.00%
-0.10%
0.00
0.39
0.79
1.18
1.57
Pressure (MPa)
LST-Data-of-Record
LST-Dynamic
SFMT
BE/HSE/NNC
EDF
EGP
FORTUM
GRS
IRSN/CEA
JPRG
KOPEC
NRC/SNL/DEA
SCANSCOT
0°
E/H
A/L
90°
B
135°
M/S, P/W
Elevation 10.75 m
Springline
SOL #38
135°, El. 6.20 m,
Liner Strain,
Meridional,
Inside Liner Surface
Elevation 0.0 m
Basemat Top
Section A – A'
(not to scale)

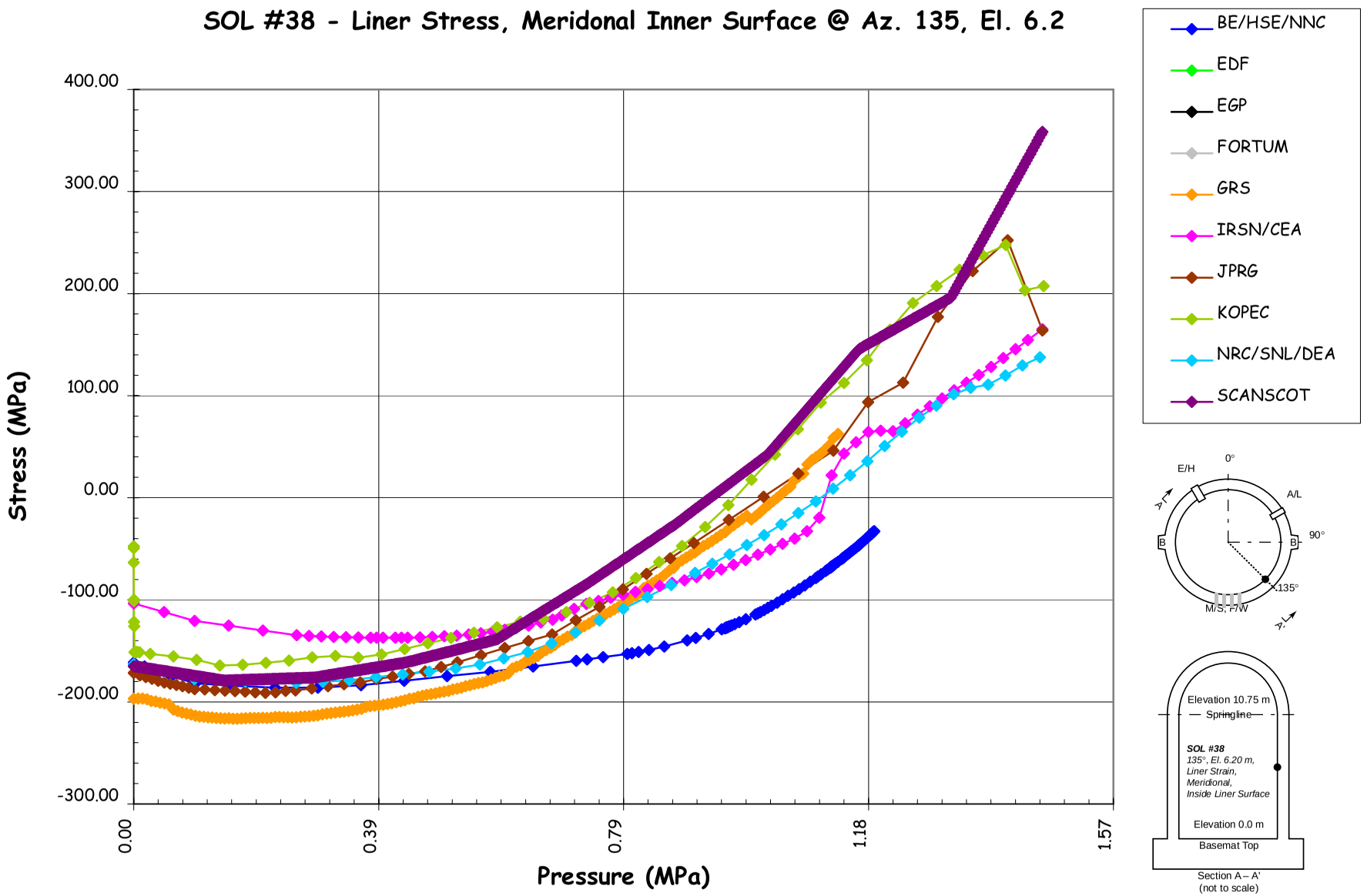
SOL #38 - Liner Stress, Meridonal Inner Surface @ Az. 135, El. 6.2
Stress (MPa)
400.00
300.00
200.00
100.00
0.00
-100.00
-200.00
-300.00
0.00
0.39
0.79
1.18
1.57
Pressure (MPa)
BE/HSE/NNC
EDF
EGP
FORTUM
GRS
IRSN/CEA
JPRG
KOPEC
NRC/SNL/DEA
SCANSCOT
E/H
0°
A/L
90°
B
B
135°
M/S, F/W
A
A
Elevation 10.75 m
Springline
SOL #38
135°, El. 6.20 m,
Liner Strain,
Meridional,
Inside Liner Surface
Elevation 0.0 m
Basemat Top
Section A – A'
(not to scale)

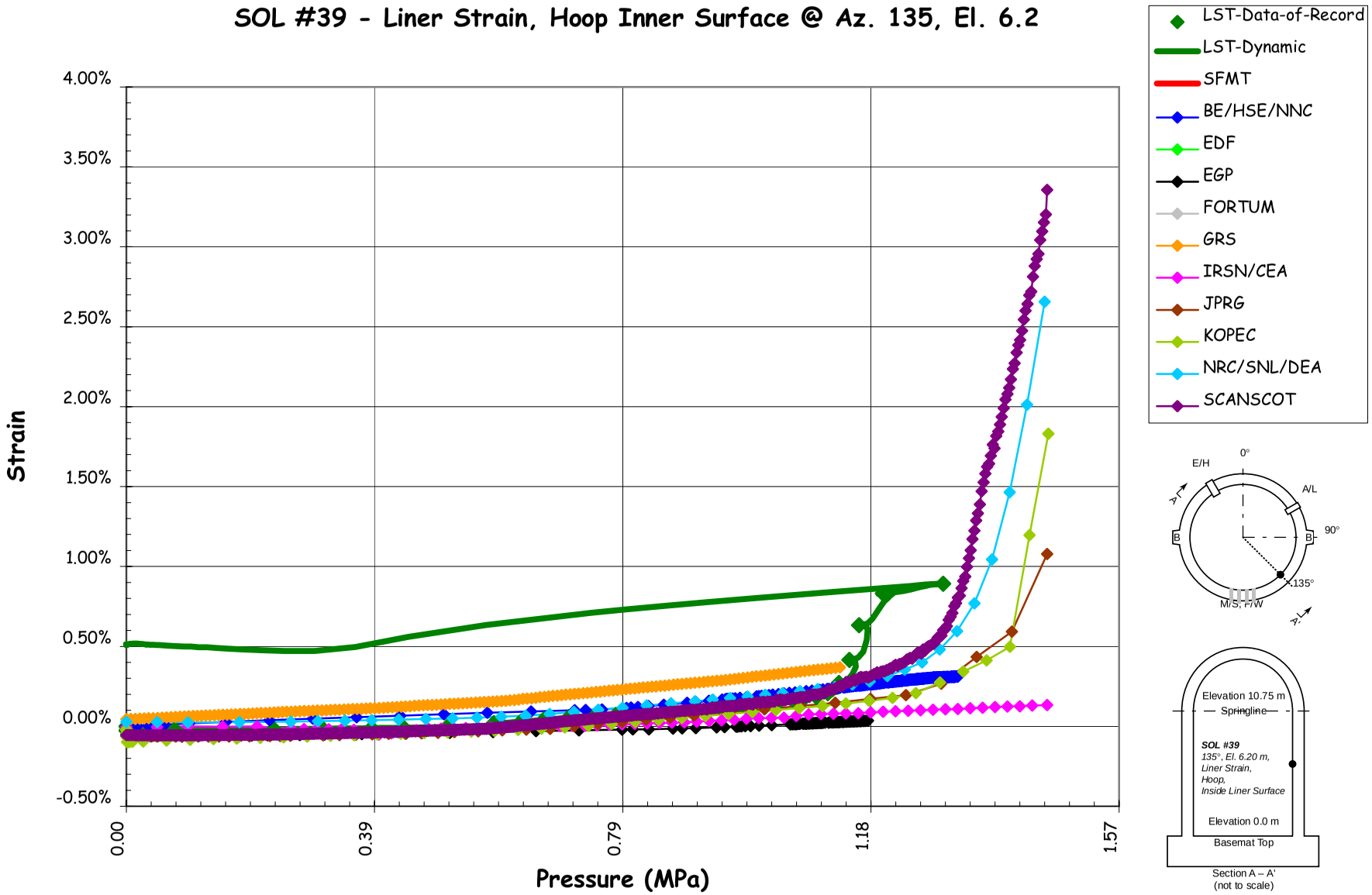
SOL #39 - Liner Strain, Hoop Inner Surface @ Az. 135, El. 6.2
Strain
4.00%
3.50%
3.00%
2.50%
2.00%
1.50%
1.00%
0.50%
0.00%
-0.50%
0.00
0.39
0.79
1.18
1.57
Pressure (MPa)
LST-Data-of-Record
LST-Dynamic
SFMT
BE/HSE/NNC
EDF
EGP
FORTUM
GRS
IRSN/CEA
JPRG
KOPEC
NRC/SNL/DEA
SCANSCOT
0°
E/H
A/L
90°
135°
M/S, F/W
Elevation 10.75 m
Springline
SOL #39
135°, El. 6.20 m,
Liner Strain,
Hoop,
Inside Liner Surface
Elevation 0.0 m
Basemat Top
Section A – A'
(not to scale)

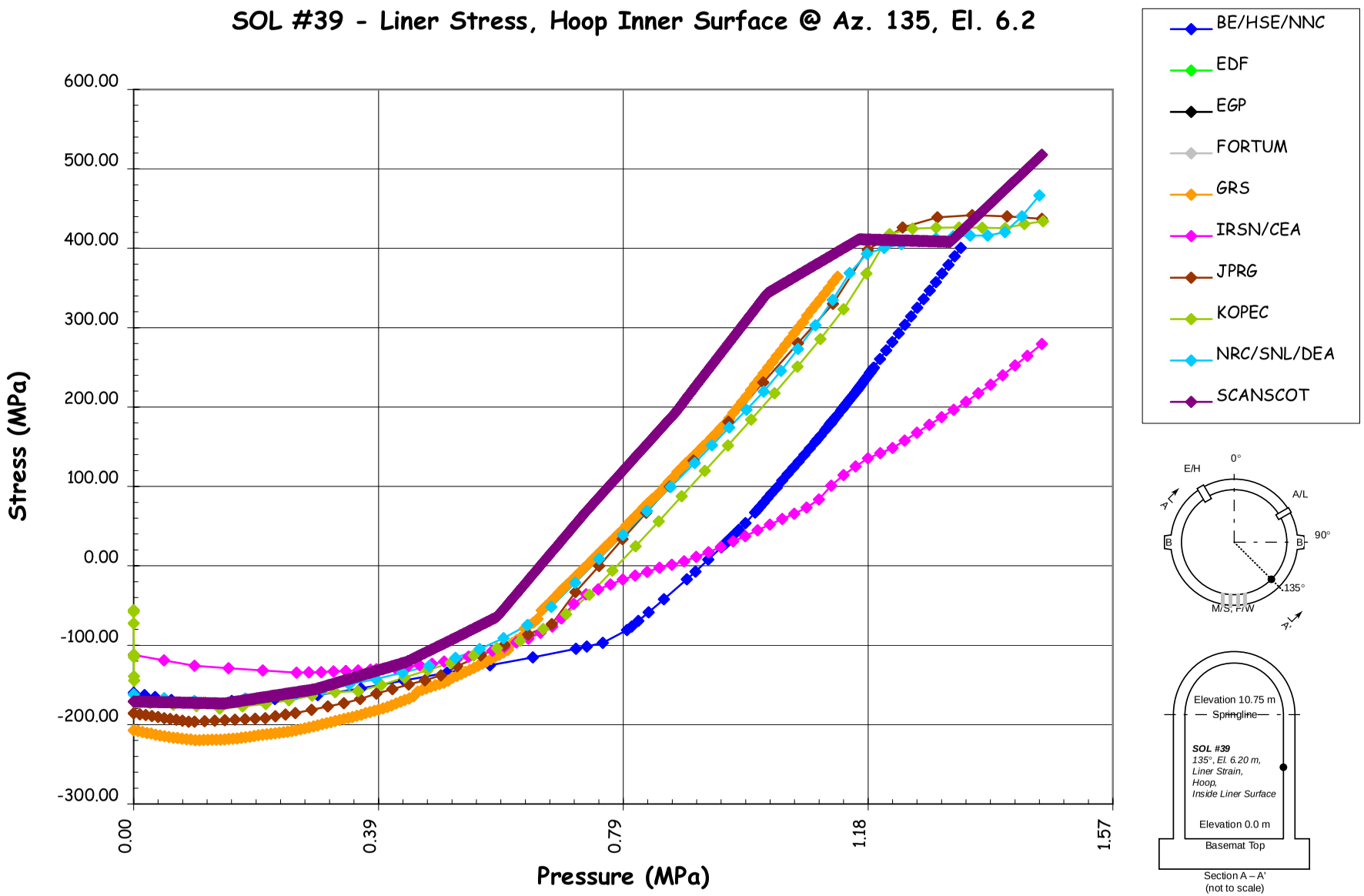
SOL #39 - Liner Stress, Hoop Inner Surface @ Az. 135, El. 6.2
Stress (MPa)
600.00
500.00
400.00
300.00
200.00
100.00
0.00
-100.00
-200.00
-300.00
0.00
0.39
0.79
1.18
1.57
Pressure (MPa)
BE/HSE/NNC
EDF
EGP
FORTUM
GRS
IRSN/CEA
JPRG
KOPEC
NRC/SNL/DEA
SCANSCOT
0°
E/H
A/L
90°
135°
M/S, F/W
Elevation 10.75 m
Springline
SOL #39
135°, El. 6.20 m,
Liner Strain,
Hoop,
Inside Liner Surface
Elevation 0.0 m
Basemat Top
Section A – A'
(not to scale)

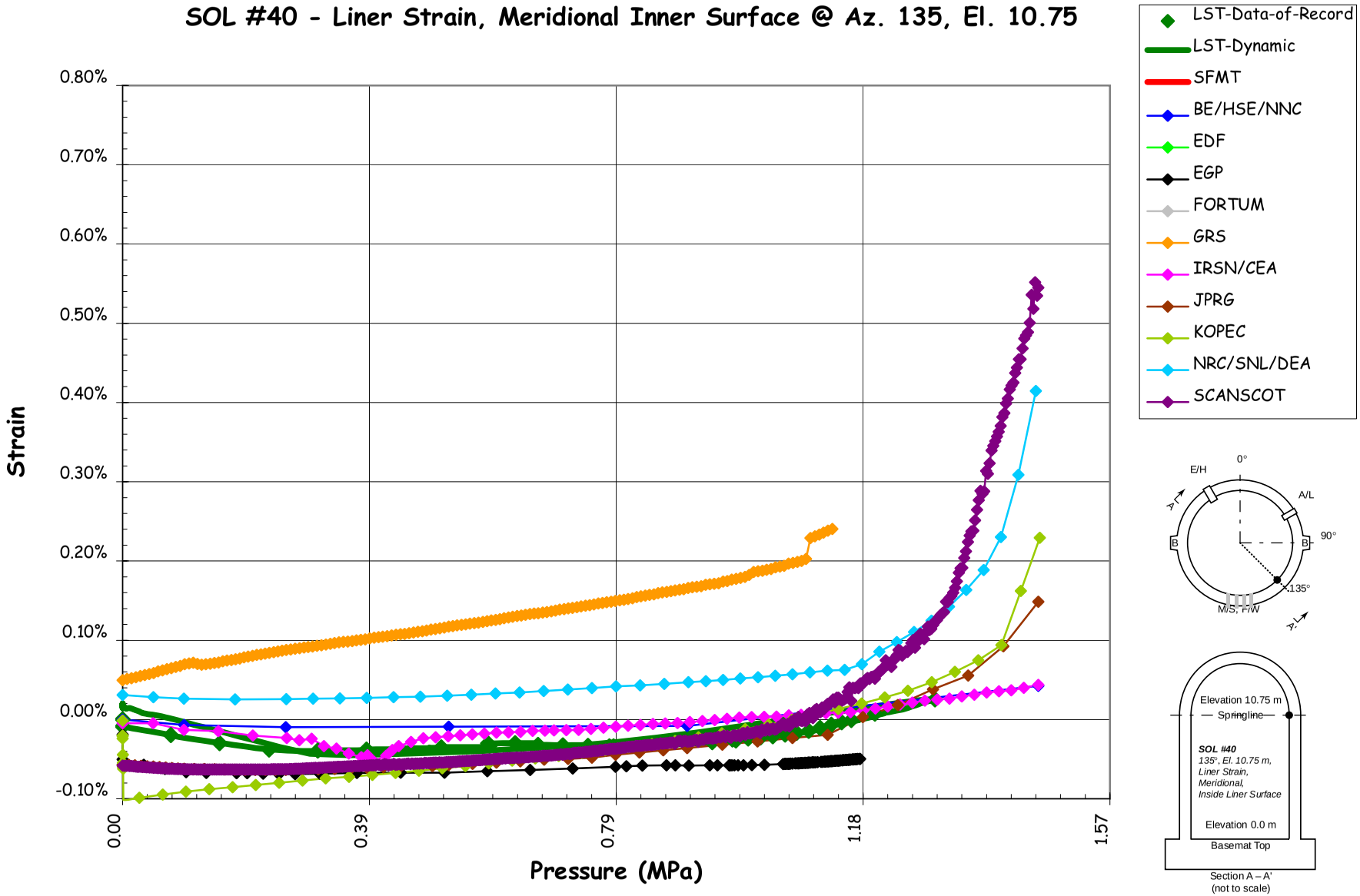
SOL #40 - Liner Strain, Meridional Inner Surface @ Az. 135, El. 10.75
Strain
0.80%
0.70%
0.60%
0.50%
0.40%
0.30%
0.20%
0.10%
0.00%
-0.10%
0.00
0.39
0.79
1.18
1.57
Pressure (MPa)
LST-Data-of-Record
LST-Dynamic
SFMT
BE/HSE/NNC
EDF
EGP
FORTUM
GRS
IRSN/CEA
JPRG
KOPEC
NRC/SNL/DEA
SCANSCOT
0°
E/H
A/L
90°
135°
M/S, F/W
Elevation 10.75 m
Springline
SOL #40
135°, El. 10.75 m,
Liner Strain,
Meridional,
Inside Liner Surface
Elevation 0.0 m
Basemat Top
Section A – A'
(not to scale)

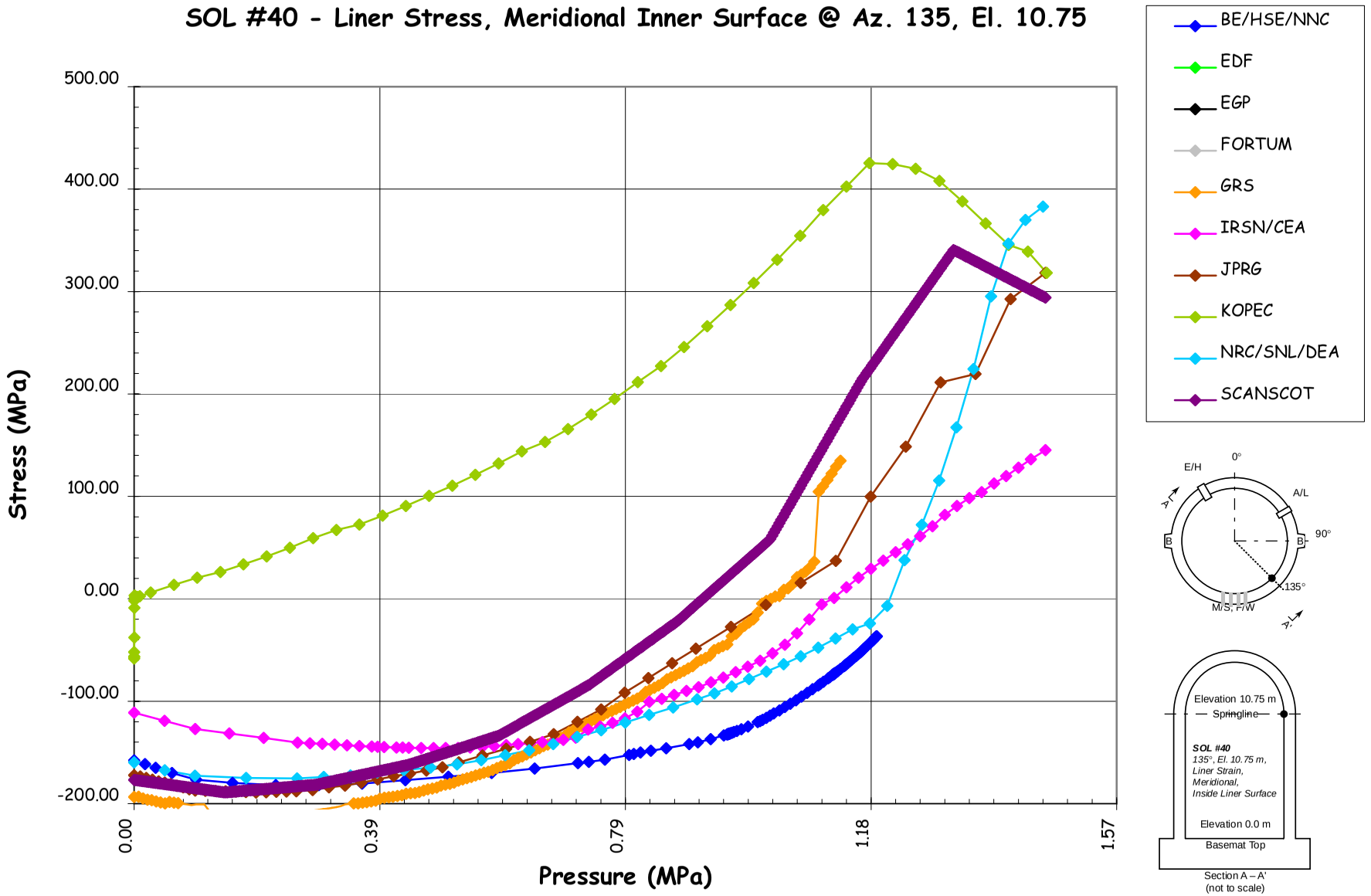
SOL #40 - Liner Stress, Meridional Inner Surface @ Az. 135, El. 10.75
Stress (MPa)
500.00
400.00
300.00
200.00
100.00
0.00
-100.00
-200.00
0.00
0.39
0.79
1.18
1.57
Pressure (MPa)
BE/HSE/NNC
EDF
EGP
FORTUM
GRS
IRSN/CEA
JPRG
KOPEC
NRC/SNL/DEA
SCANSCOT
E/H
0°
A/L
90°
135°
M/S, P/W
Elevation 10.75 m
Springline
SOL #40
135°, El. 10.75 m,
Liner Strain,
Meridional,
Inside Liner Surface
Elevation 0.0 m
Basemat Top
Section A – A'
(not to scale)

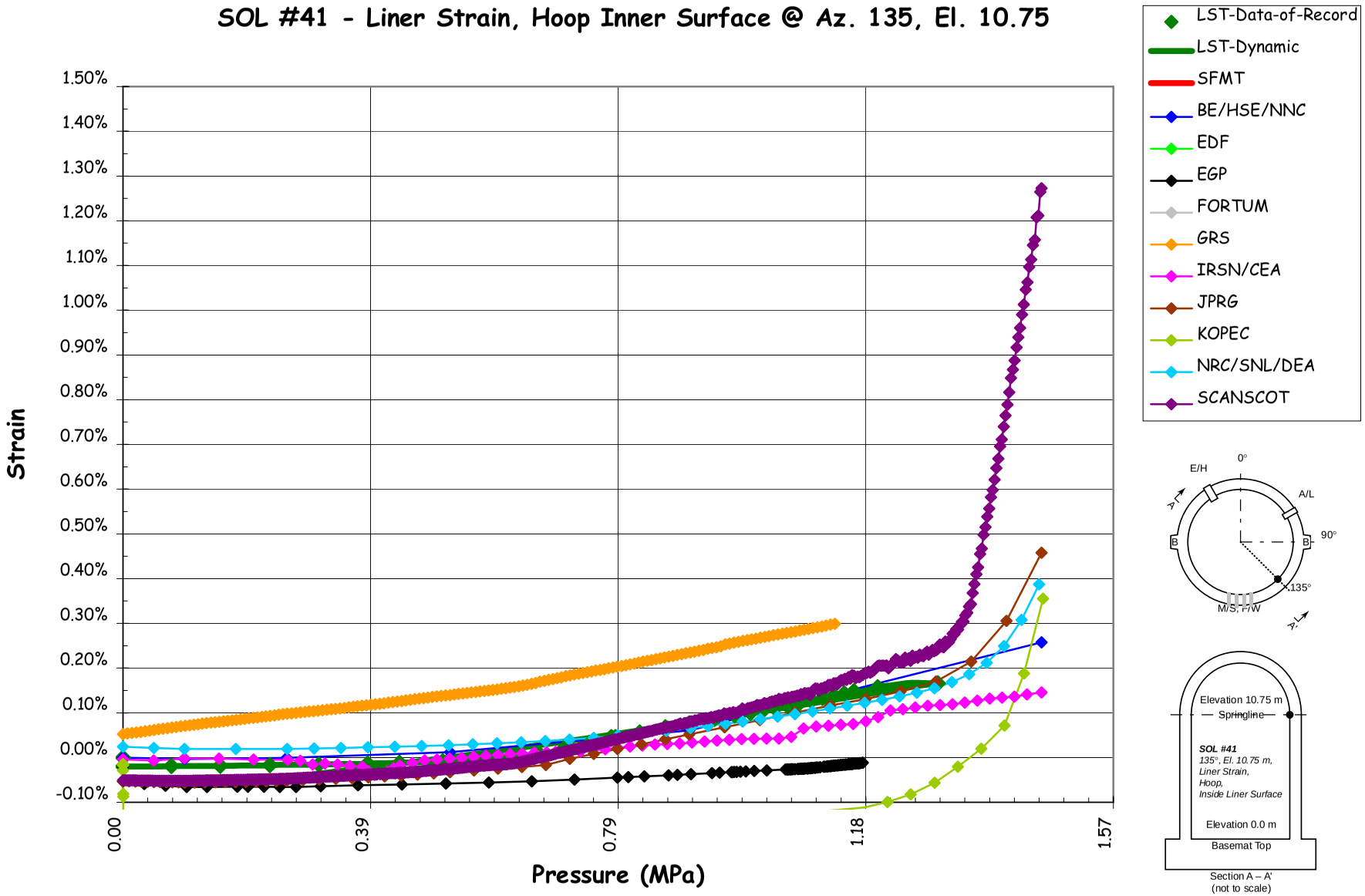
SOL #41 - Liner Strain, Hoop Inner Surface @ Az. 135, El. 10.75
Strain
1.50%
1.40%
1.30%
1.20%
1.10%
1.00%
0.90%
0.80%
0.70%
0.60%
0.50%
0.40%
0.30%
0.20%
0.10%
0.00%
-0.10%
0.00
0.39
0.79
1.18
1.57
Pressure (MPa)
LST-Data-of-Record
LST-Dynamic
SFMT
BE/HSE/NNC
EDF
EGP
FORTUM
GRS
IRSN/CEA
JPRG
KOPEC
NRC/SNL/DEA
SCANSCOT
0°
E/H
A/L
90°
135°
M/S, P/W
Elevation 10.75 m
Springline
SOL #41
135°, El. 10.75 m,
Liner Strain,
Hoop,
Inside Liner Surface
Elevation 0.0 m
Basemat Top
Section A – A'
(not to scale)

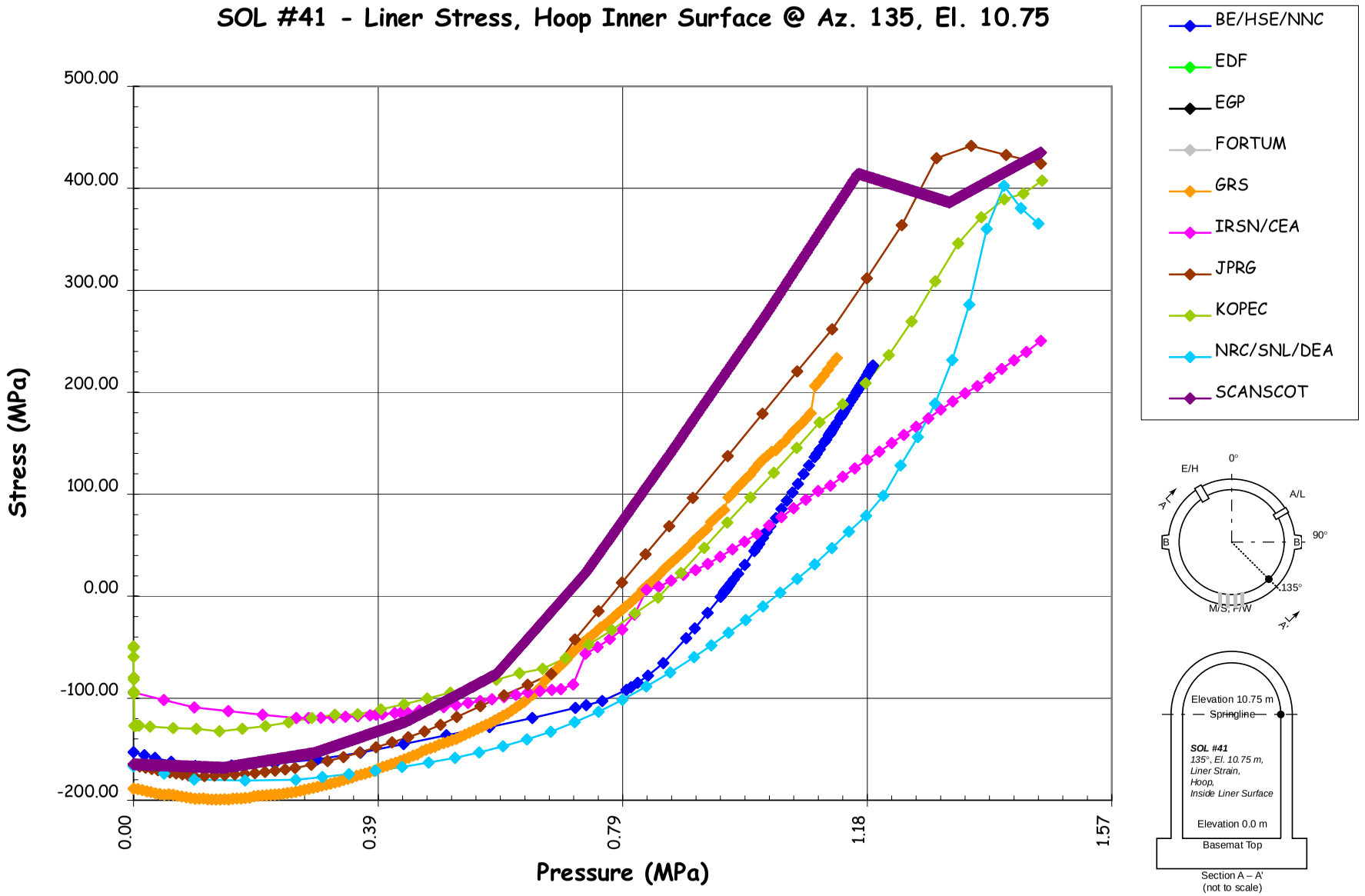
SOL #41 - Liner Stress, Hoop Inner Surface @ Az. 135, El. 10.75
Stress (MPa)
500.00
400.00
300.00
200.00
100.00
0.00
-100.00
-200.00
0.00
0.39
0.79
1.18
1.57
Pressure (MPa)
BE/HSE/NNC
EDF
EGP
FORTUM
GRS
IRSN/CEA
JPRG
KOPEC
NRC/SNL/DEA
SCANSCOT
E/H
0°
A/L
90°
135°
M/S, F/W
Elevation 10.75 m
Springline
SOL #41
135°, El. 10.75 m,
Liner Strain,
Hoop,
Inside Liner Surface
Elevation 0.0 m
Basemat Top
Section A – A'
(not to scale)

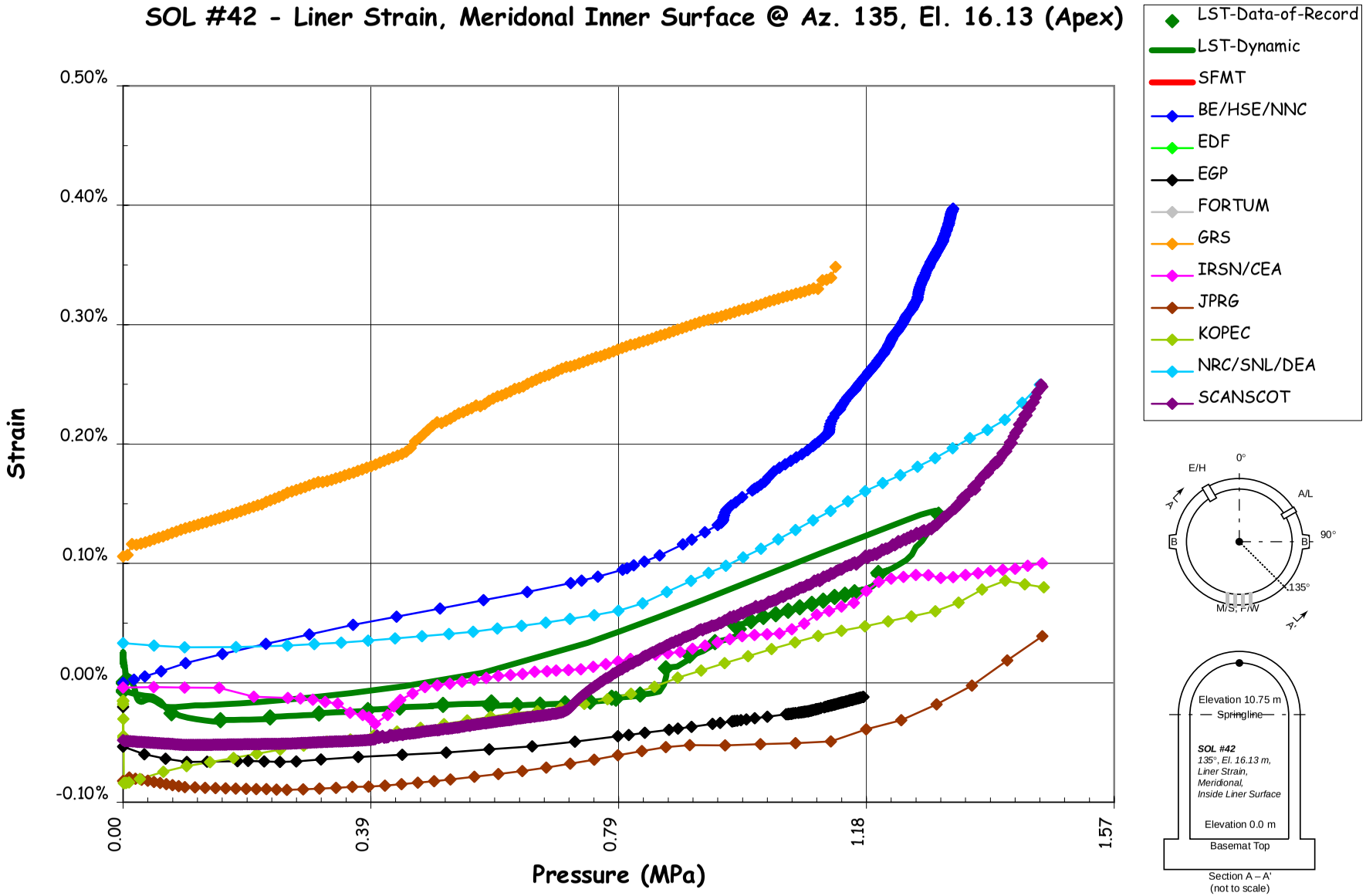
SOL #42 - Liner Strain, Meridonal Inner Surface @ Az. 135, El. 16.13 (Apex)
Strain
0.50%
0.40%
0.30%
0.20%
0.10%
0.00%
-0.10%
0.00
0.39
0.79
1.18
1.57
Pressure (MPa)
LST-Data-of-Record
LST-Dynamic
SFMT
BE/HSE/NNC
EDF
EGP
FORTUM
GRS
IRSN/CEA
JPRG
KOPEC
NRC/SNL/DEA
SCANSCOT
0°
E/H
A/L
90°
135°
M/S, F/W
Elevation 10.75 m
Springline
SOL #42
135°, El. 16.13 m,
Liner Strain,
Meridional,
Inside Liner Surface
Elevation 0.0 m
Basemat Top
Section A – A'
(not to scale)

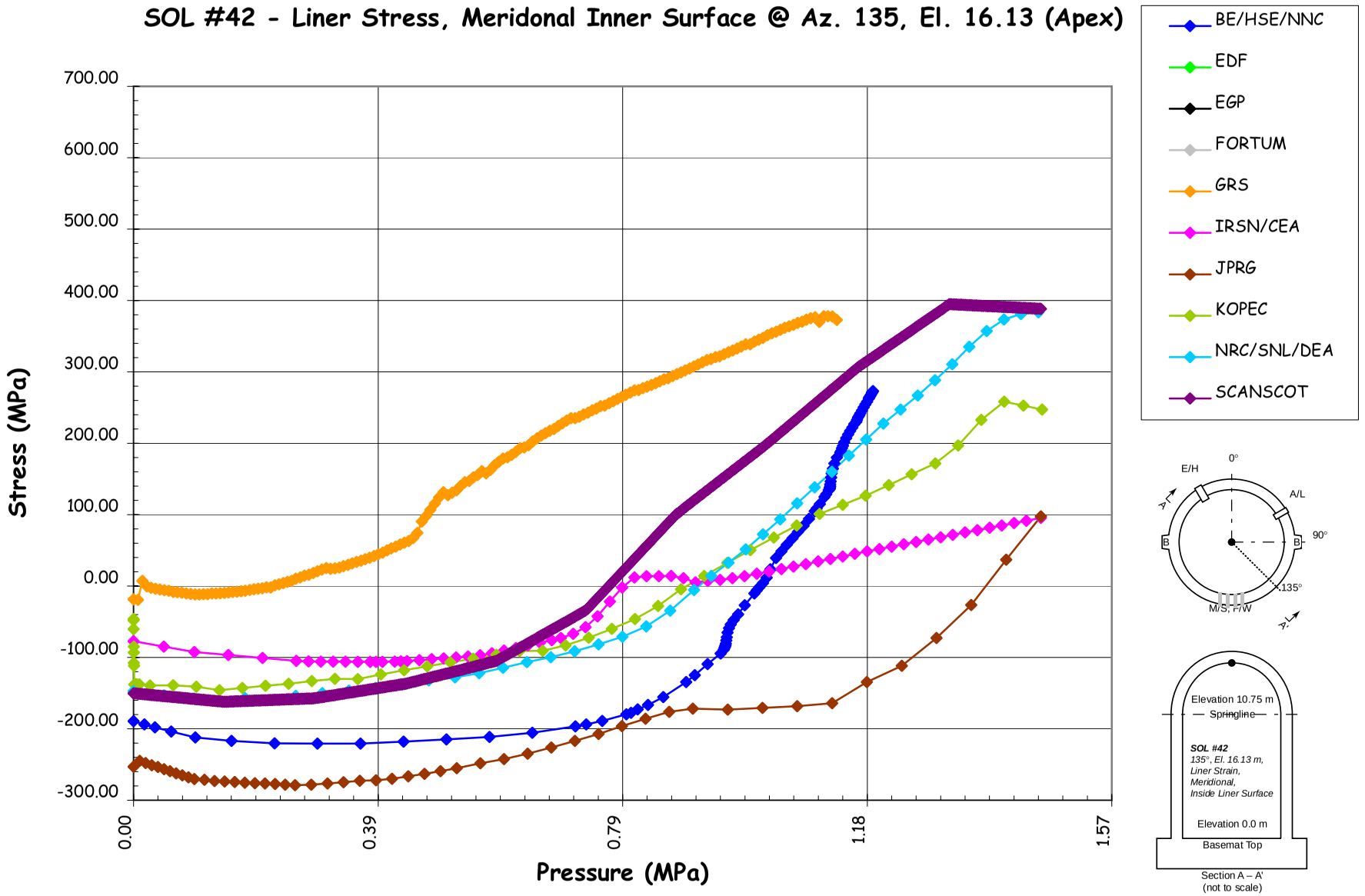
SOL #42 - Liner Stress, Meridonal Inner Surface @ Az. 135, El. 16.13 (Apex)
Stress (MPa)
700.00
600.00
500.00
400.00
300.00
200.00
100.00
0.00
-100.00
-200.00
-300.00
0.00
0.39
0.79
1.18
1.57
Pressure (MPa)
BE/HSE/NNC
EDF
EGP
FORTUM
GRS
IRSN/CEA
JPRG
KOPEC
NRC/SNL/DEA
SCANSCOT
0°
E/H
A/L
90°
135°
M/S, F/W
Elevation 10.75 m
Springline
SOL #42
135°, El. 16.13 m,
Liner Strain,
Meridional,
Inside Liner Surface
Elevation 0.0 m
Basemat Top
Section A – A'
(not to scale)

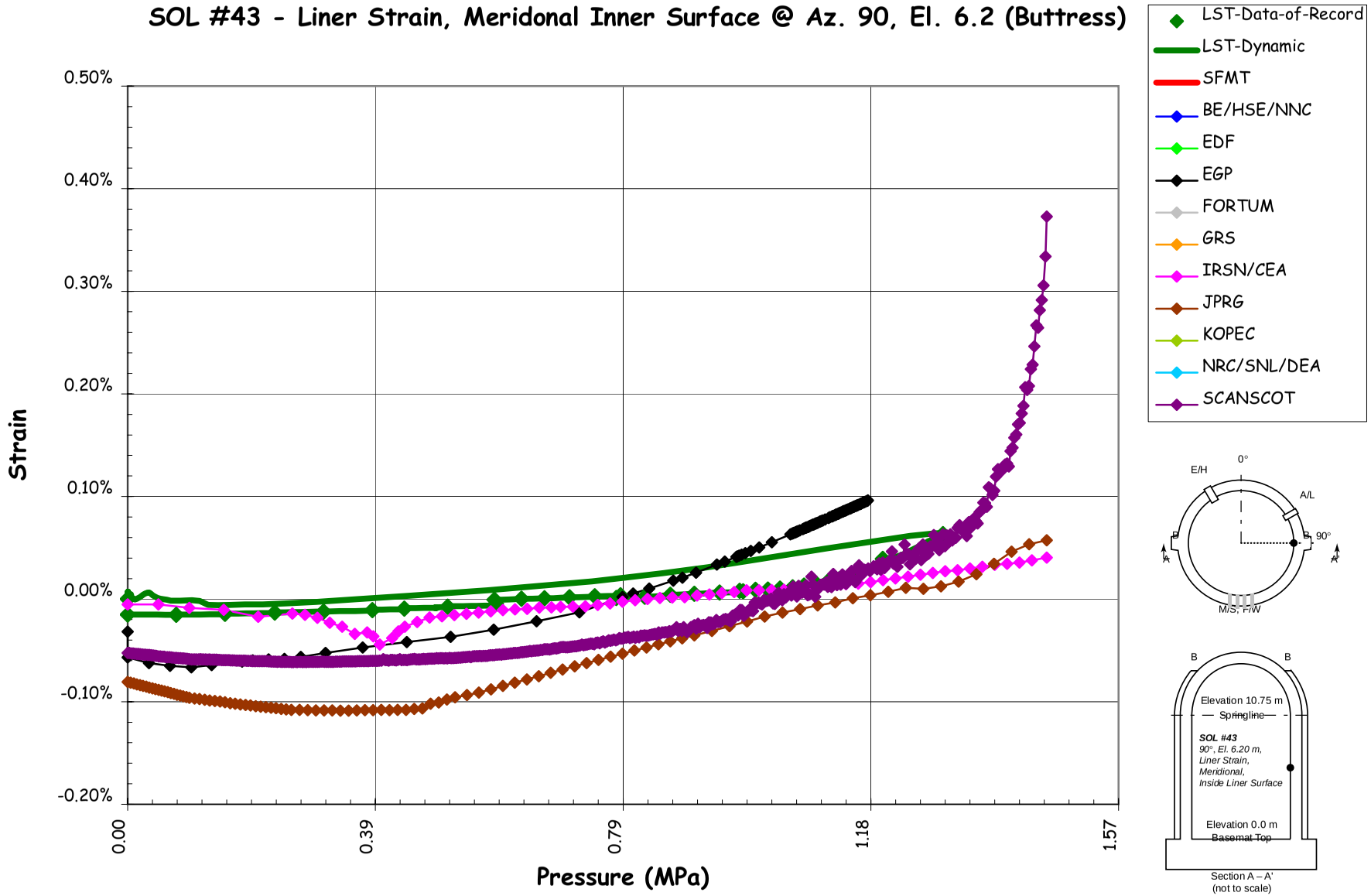
SOL #43 - Liner Strain, Meridonal Inner Surface @ Az. 90, El. 6.2 (Buttress)
Strain
0.50%
0.40%
0.30%
0.20%
0.10%
0.00%
-0.10%
-0.20%
0.00
0.39
0.79
1.18
1.57
Pressure (MPa)
LST-Data-of-Record
LST-Dynamic
SFMT
BE/HSE/NNC
EDF
EGP
FORTUM
GRS
IRSN/CEA
JPRG
KOPEC
NRC/SNL/DEA
SCANSCOT
0°
E/H
A/L
90°
M/S, F/W
B
B
Elevation 10.75 m
Springline
SOL #43
90°, El. 6.20 m,
Liner Strain,
Meridional,
Inside Liner Surface
Elevation 0.0 m
Basemat Top
Section A – A'
(not to scale)

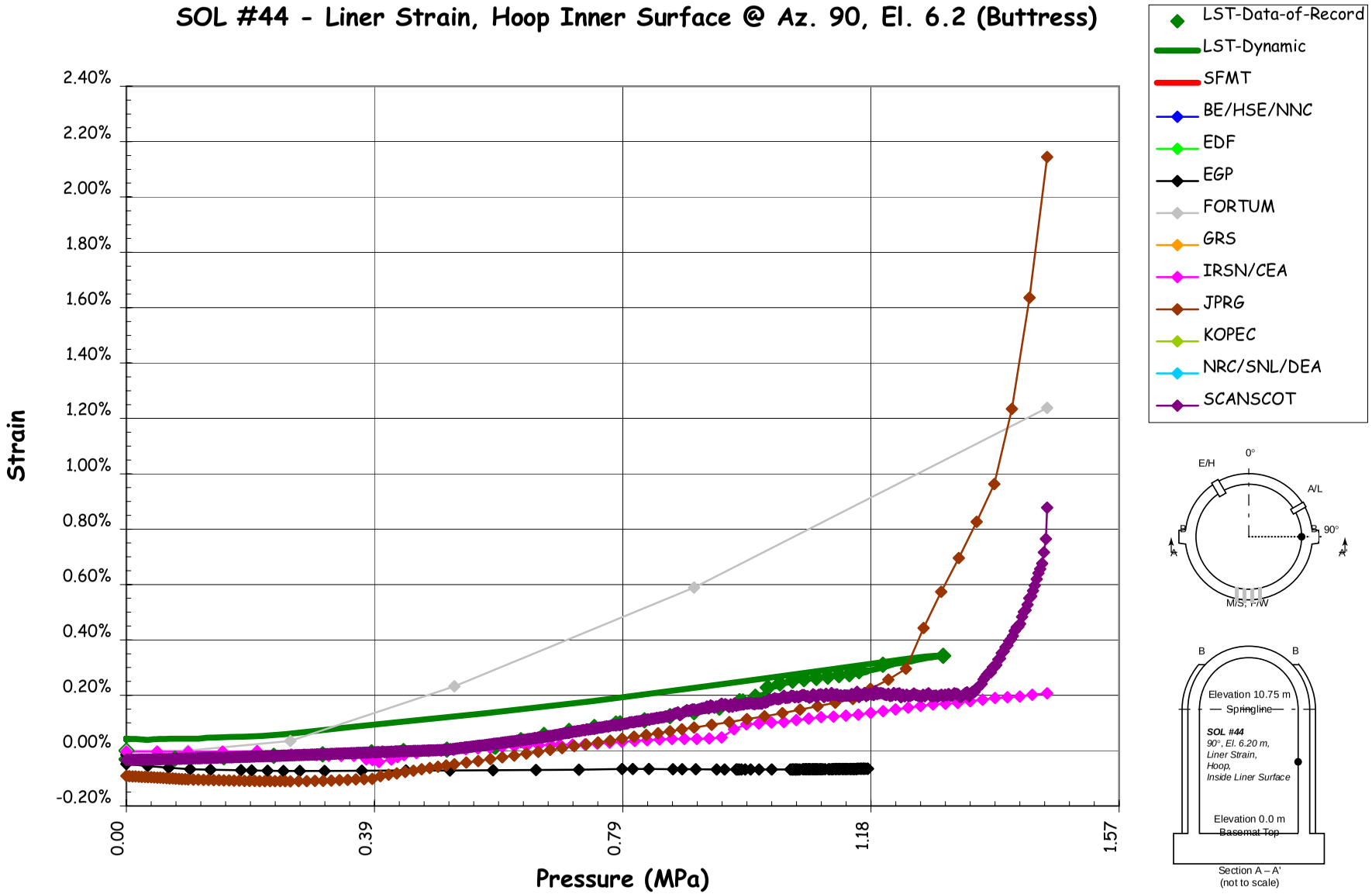
SOL #44 - Liner Strain, Hoop Inner Surface @ Az. 90, El. 6.2 (Buttress)
Strain
2.40%
2.20%
2.00%
1.80%
1.60%
1.40%
1.20%
1.00%
0.80%
0.60%
0.40%
0.20%
0.00%
-0.20%
0.00
0.39
0.79
1.18
1.57
Pressure (MPa)
LST-Data-of-Record
LST-Dynamic
SFMT
BE/HSE/NNC
EDF
EGP
FORTUM
GRS
IRSN/CEA
JPRG
KOPEC
NRC/SNL/DEA
SCANSCOT
0°
E/H
A/L
90°
M/S, F/W
B
B
Elevation 10.75 m
Springline
SOL #44
90°, El. 6.20 m,
Liner Strain,
Hoop,
Inside Liner Surface
Elevation 0.0 m
Basemat Top
Section A – A'
(not to scale)

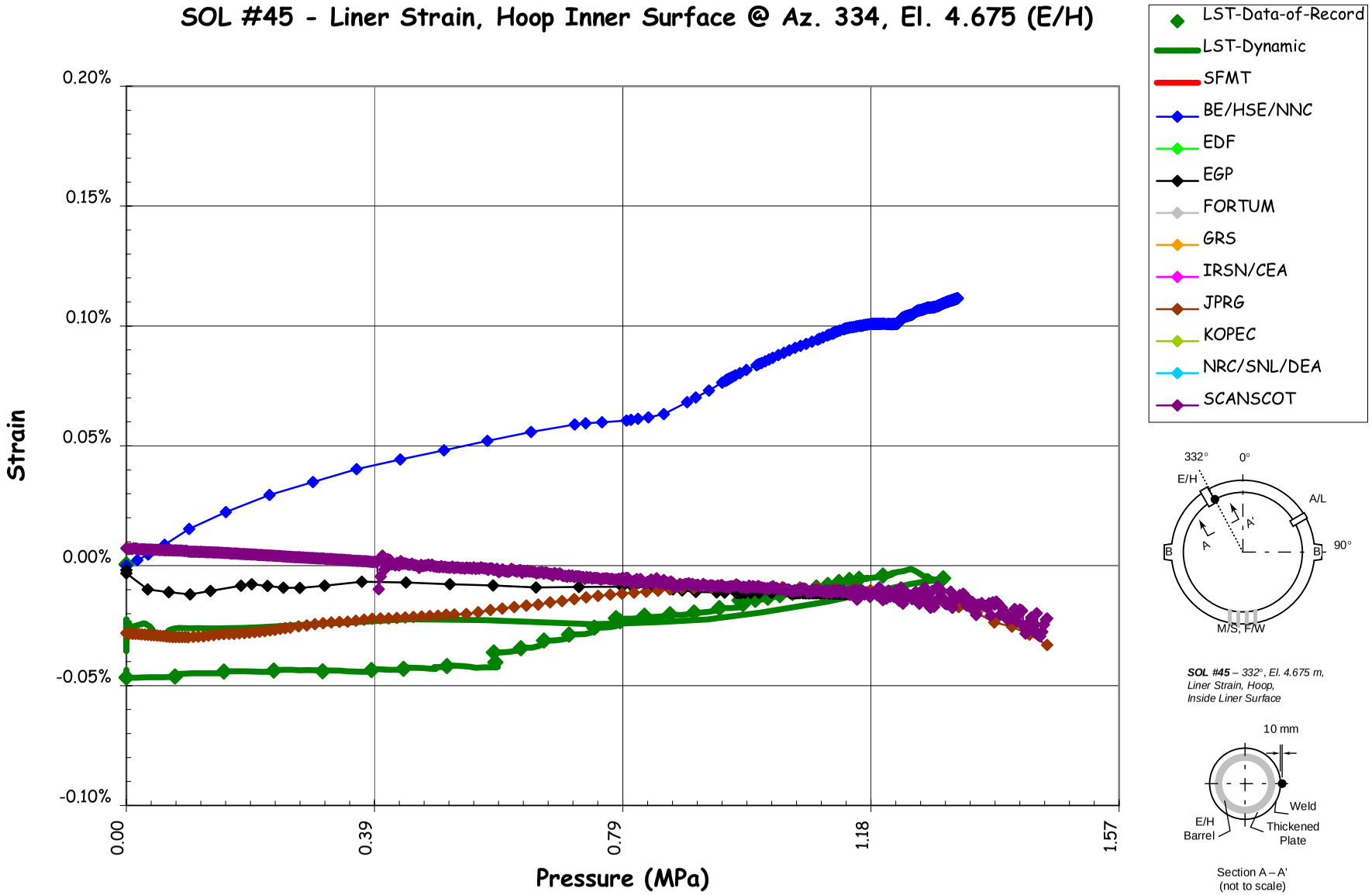
SOL #45 - Liner Strain, Hoop Inner Surface @ Az. 334, El. 4.675 (E/H)
Strain
0.20%
0.15%
0.10%
0.05%
0.00%
-0.05%
-0.10%
0.00
0.39
0.79
1.18
1.57
Pressure (MPa)
LST-Data-of-Record
LST-Dynamic
SFMT
BE/HSE/NNC
EDF
EGP
FORTUM
GRS
IRSN/CEA
JPRG
KOPEC
NRC/SNL/DEA
SCANSCOT
332°
0°
E/H
A/L
90°
M/S, F/W
SOL #45 – 332°, El. 4.675 m,
Liner Strain, Hoop,
Inside Liner Surface
10 mm
Weld
E/H
Barrel
Thickened
Plate
Section A – A'
(not to scale)

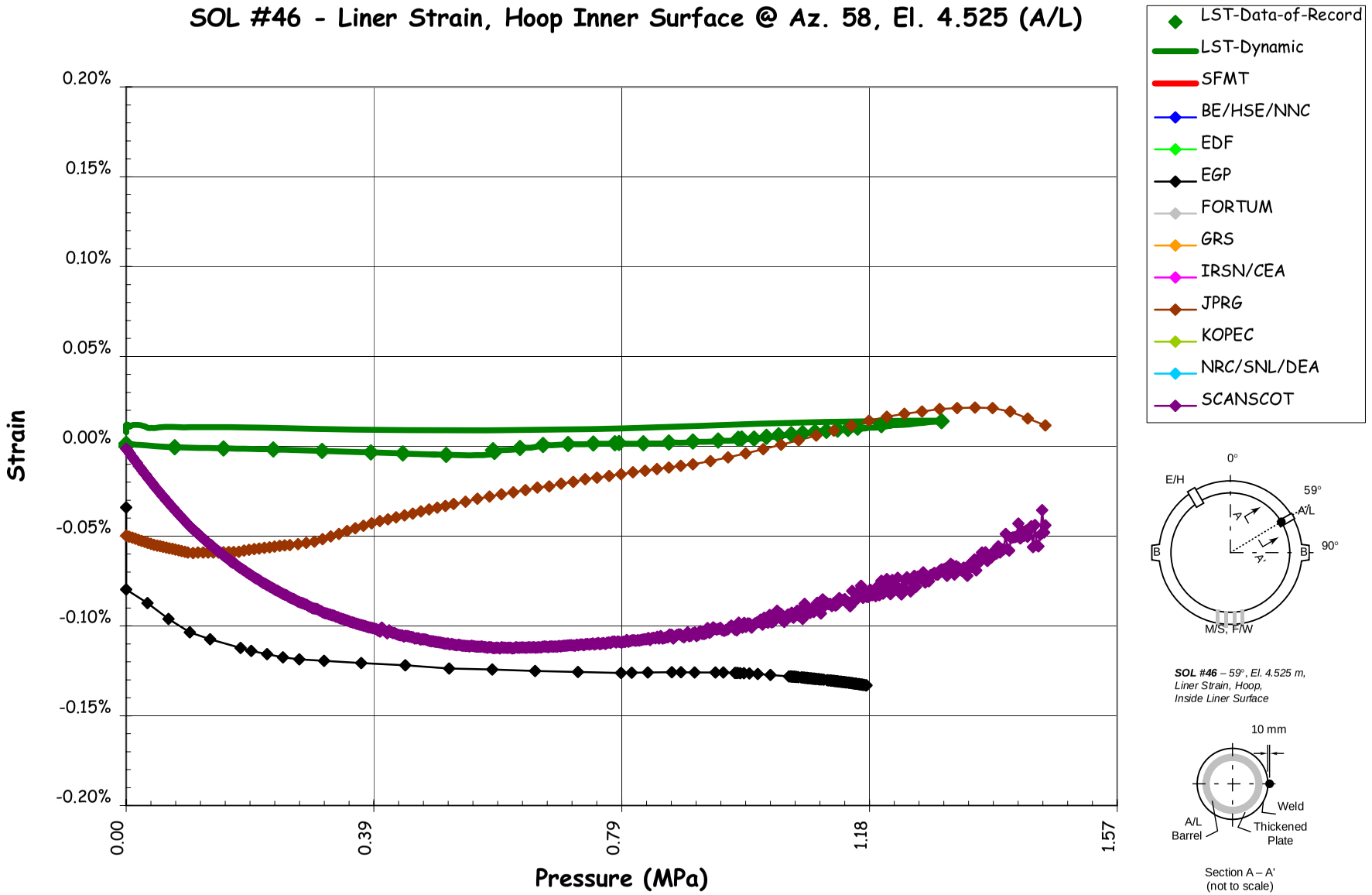
SOL #46 - Liner Strain, Hoop Inner Surface @ Az. 58, El. 4.525 (A/L)
Strain
0.20%
0.15%
0.10%
0.05%
0.00%
-0.05%
-0.10%
-0.15%
-0.20%
0.00
0.39
0.79
1.18
1.57
Pressure (MPa)
LST-Data-of-Record
LST-Dynamic
SFMT
BE/HSE/NNC
EDF
EGP
FORTUM
GRS
IRSN/CEA
JPRG
KOPEC
NRC/SNL/DEA
SCANSCOT
0°
E/H
59°
A/L
90°
B
B
M/S, F/W
SOL #46 – 59°, El. 4.525 m, Liner Strain, Hoop, Inside Liner Surface
10 mm
Weld
A/L Barrel
Thickened Plate
Section A – A' (not to scale)

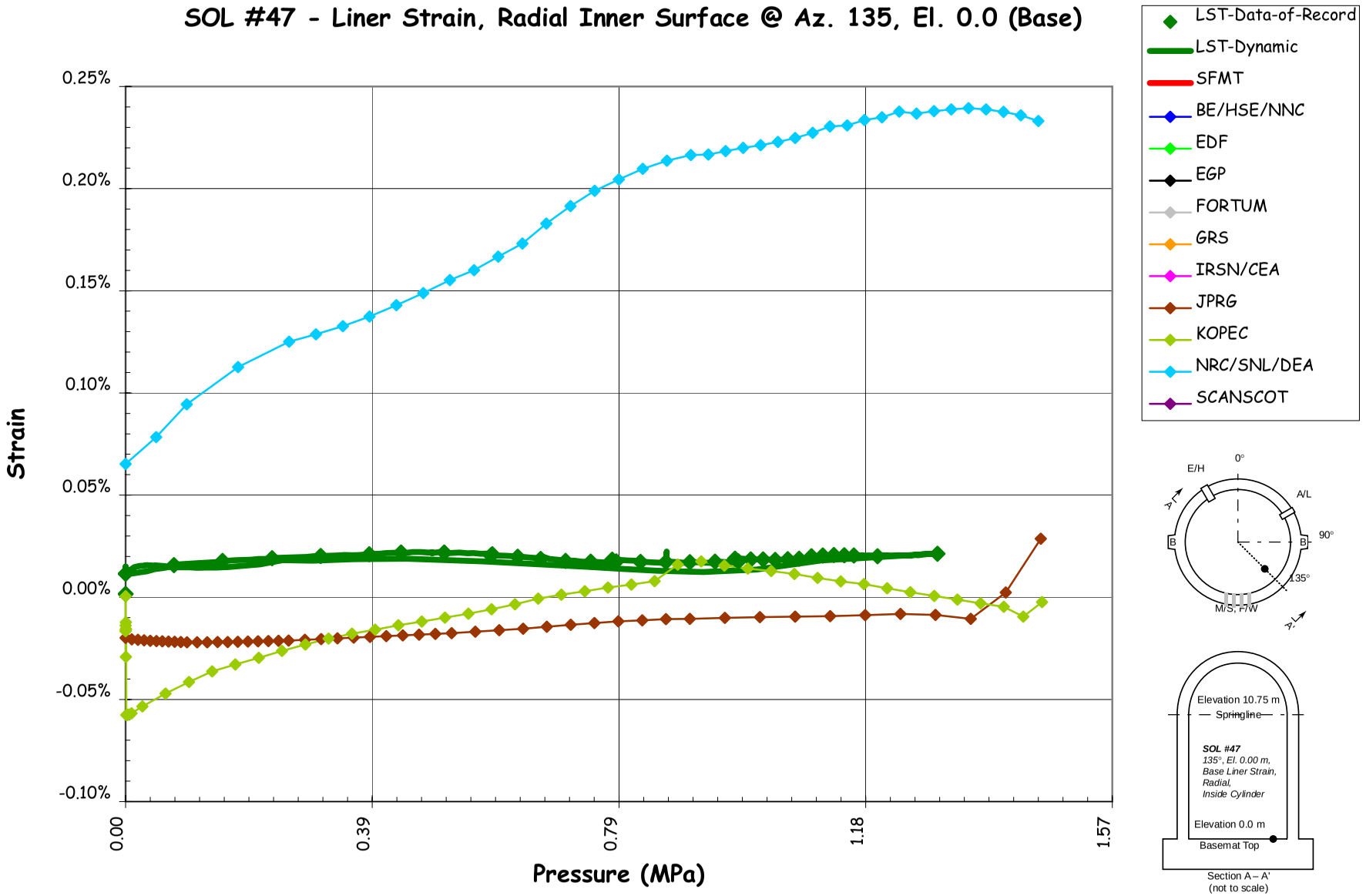
SOL #47 - Liner Strain, Radial Inner Surface @ Az. 135, El. 0.0 (Base)
Strain
0.25%
0.20%
0.15%
0.10%
0.05%
0.00%
-0.05%
-0.10%
0.00
0.39
0.79
1.18
1.57
Pressure (MPa)
LST-Data-of-Record
LST-Dynamic
SFMT
BE/HSE/NNC
EDF
EGP
FORTUM
GRS
IRSN/CEA
JPRG
KOPEC
NRC/SNL/DEA
SCANSCOT
0°
E/H
A/L
90°
135°
M/S, F/W
Elevation 10.75 m
Springline
SOL #47
135°, El. 0.00 m,
Base Liner Strain,
Radial,
Inside Cylinder
Elevation 0.0 m
Basemat Top
Section A – A'
(not to scale)

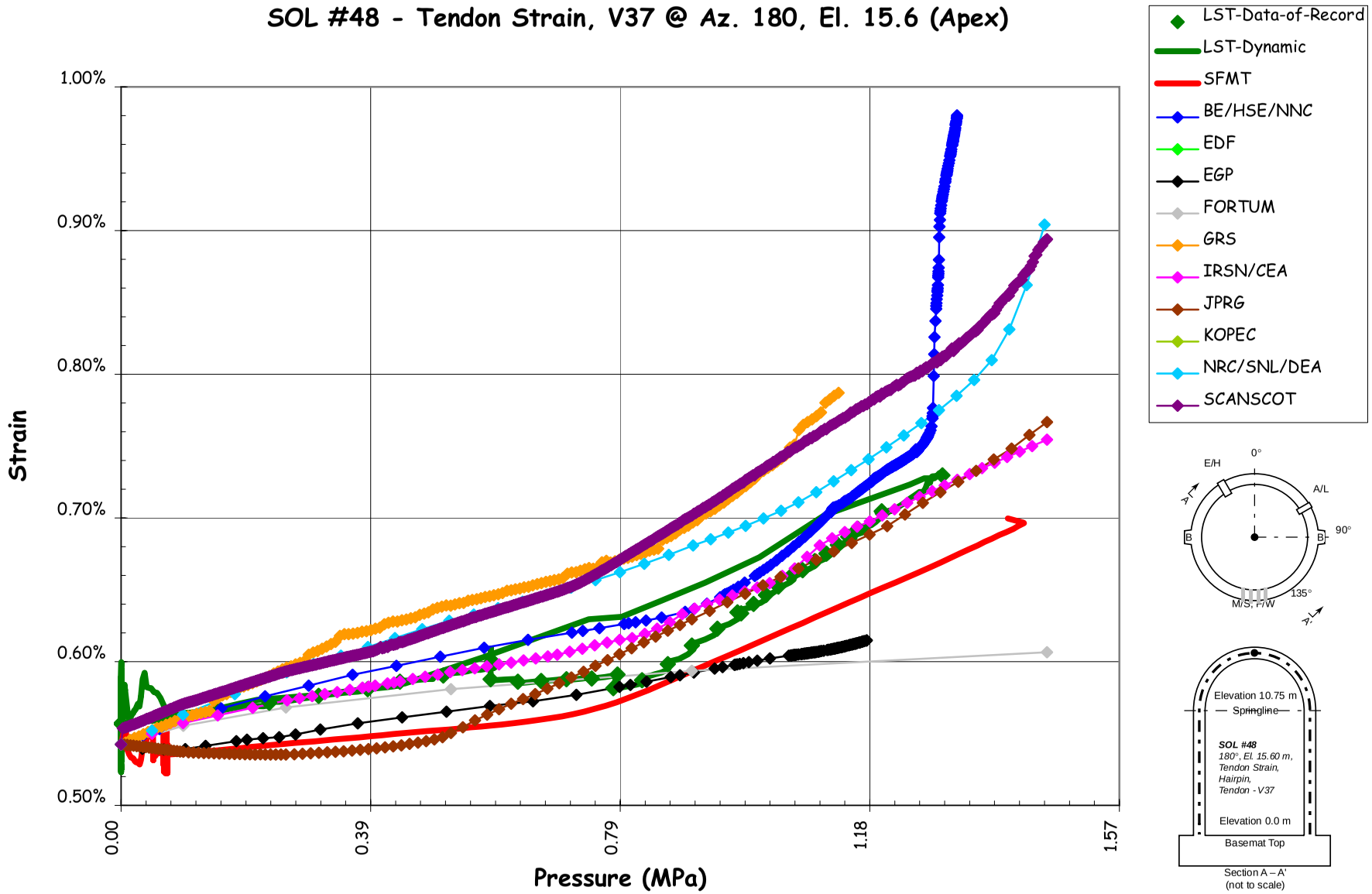
SOL #48 - Tendon Strain, V37 @ Az. 180, El. 15.6 (Apex)
Strain
1.00%
0.90%
0.80%
0.70%
0.60%
0.50%
0.00
0.39
0.79
1.18
1.57
Pressure (MPa)
LST-Data-of-Record
LST-Dynamic
SFMT
BE/HSE/NNC
EDF
EGP
FORTUM
GRS
IRSN/CEA
JPRG
KOPEC
NRC/SNL/DEA
SCANSCOT
0°
E/H
A/L
90°
135°
M/S, F/W
A'
B
B'
A'
Elevation 10.75 m
Springline
SOL #48
180°, El. 15.60 m,
Tendon Strain,
Hairpin,
Tendon - V37
Elevation 0.0 m
Basemat Top
Section A – A'
(not to scale)

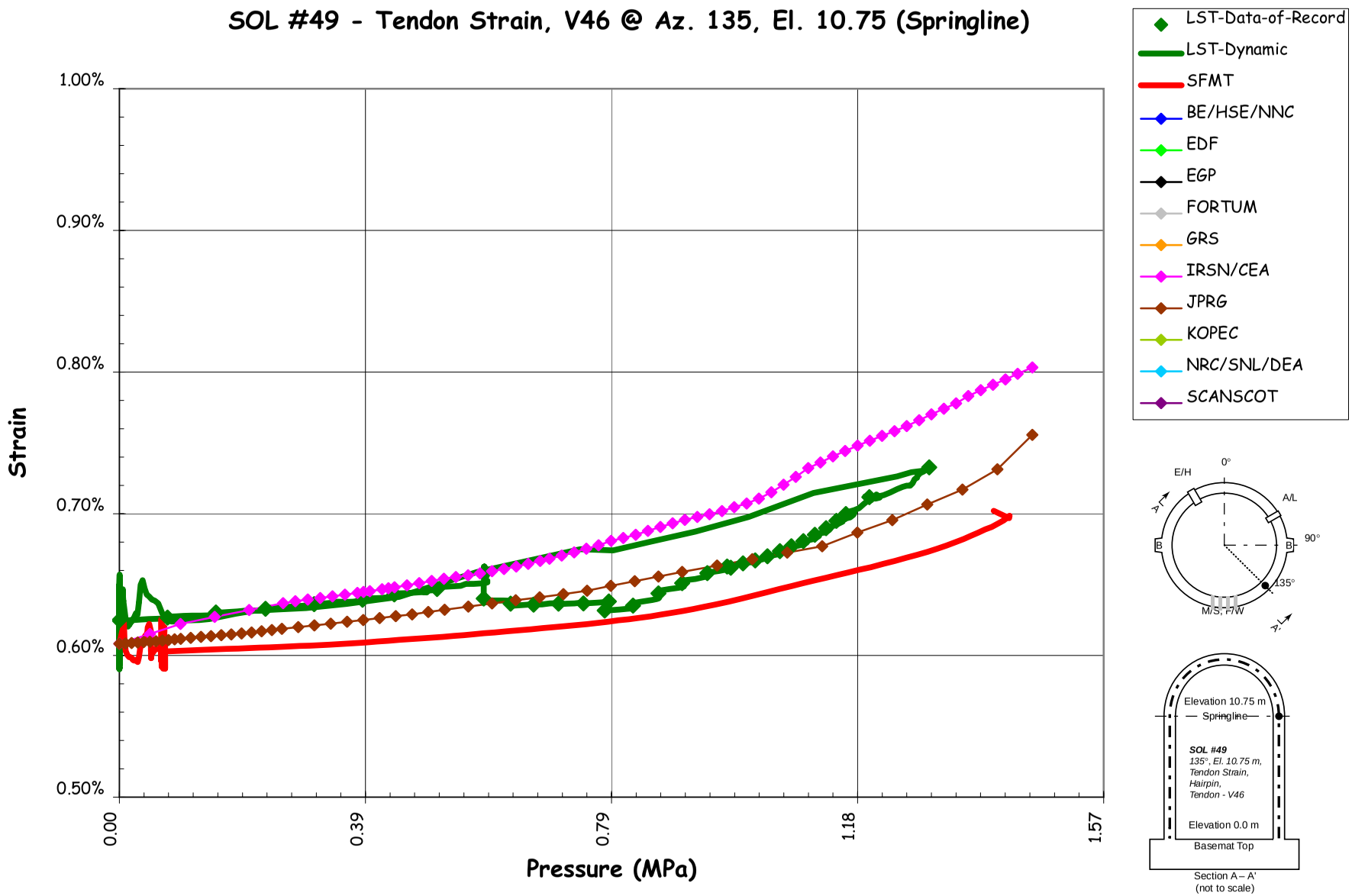
SOL #49 - Tendon Strain, V46 @ Az. 135, El. 10.75 (Springline)
Strain
1.00%
0.90%
0.80%
0.70%
0.60%
0.50%
0.00
0.39
0.79
1.18
1.57
Pressure (MPa)
LST-Data-of-Record
LST-Dynamic
SFMT
BE/HSE/NNC
EDF
EGP
FORTUM
GRS
IRSN/CEA
JPRG
KOPEC
NRC/SNL/DEA
SCANSCOT
0°
E/H
A/L
90°
135°
M/S, HW
A
A'
B
B
Elevation 10.75 m
Springline
SOL #49
135°, El. 10.75 m,
Tendon Strain,
Hairpin,
Tendon - V46
Elevation 0.0 m
Basemat Top
Section A – A'
(not to scale)

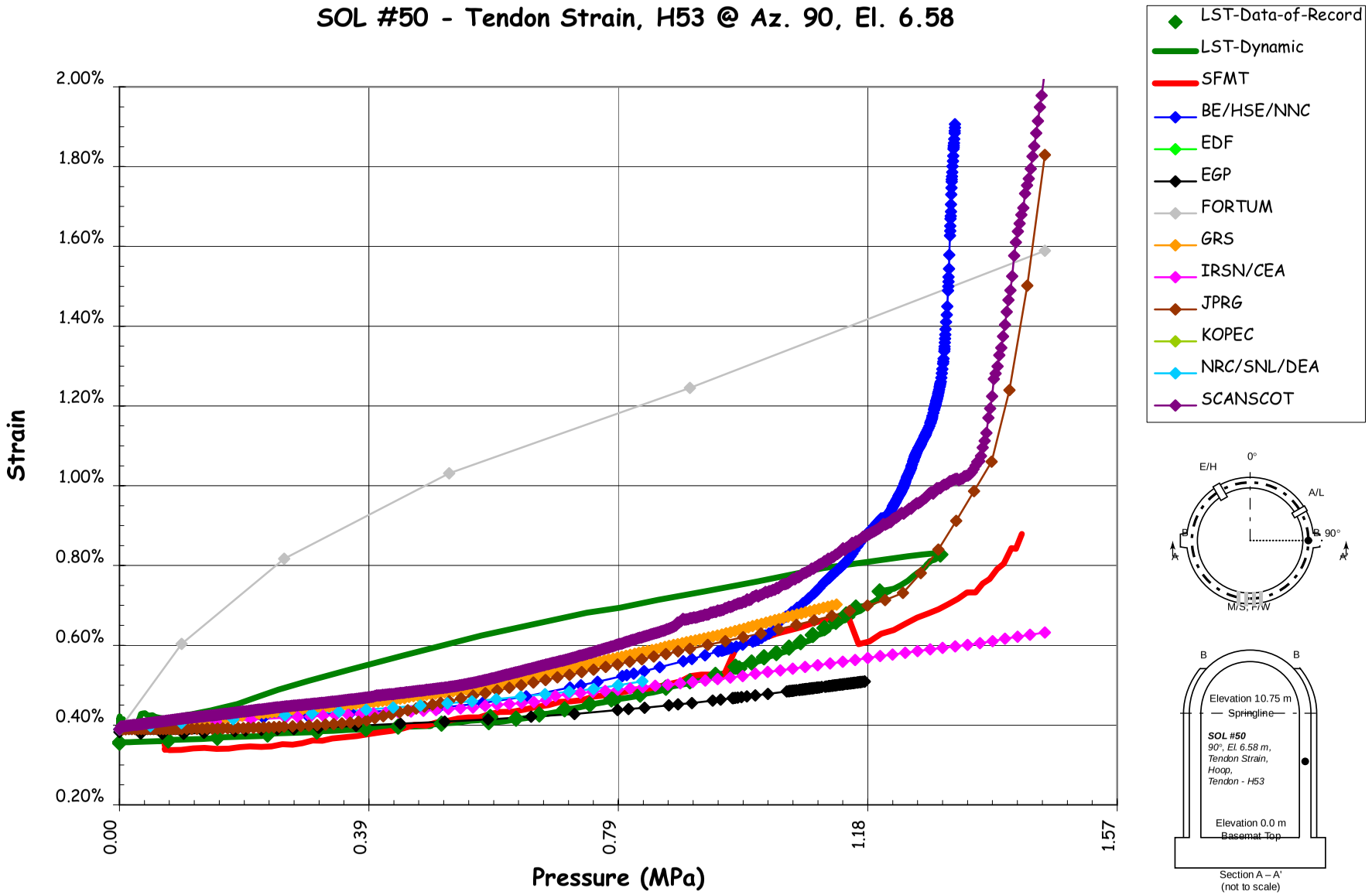
SOL #50 - Tendon Strain, H53 @ Az. 90, El. 6.58
Strain
2.00%
1.80%
1.60%
1.40%
1.20%
1.00%
0.80%
0.60%
0.40%
0.20%
0.00
0.39
0.79
1.18
1.57
Pressure (MPa)
LST-Data-of-Record
LST-Dynamic
SFMT
BE/HSE/NNC
EDF
EGP
FORTUM
GRS
IRSN/CEA
JPRG
KOPEC
NRC/SNL/DEA
SCANSCOT
0°
E/H
A/L
90°
M/S, F/W
B
B
Elevation 10.75 m
Springline
SOL #50
90°, El. 6.58 m,
Tendon Strain,
Hoop,
Tendon - H53
Elevation 0.0 m
Basemat Top
Section A – A'
(not to scale)

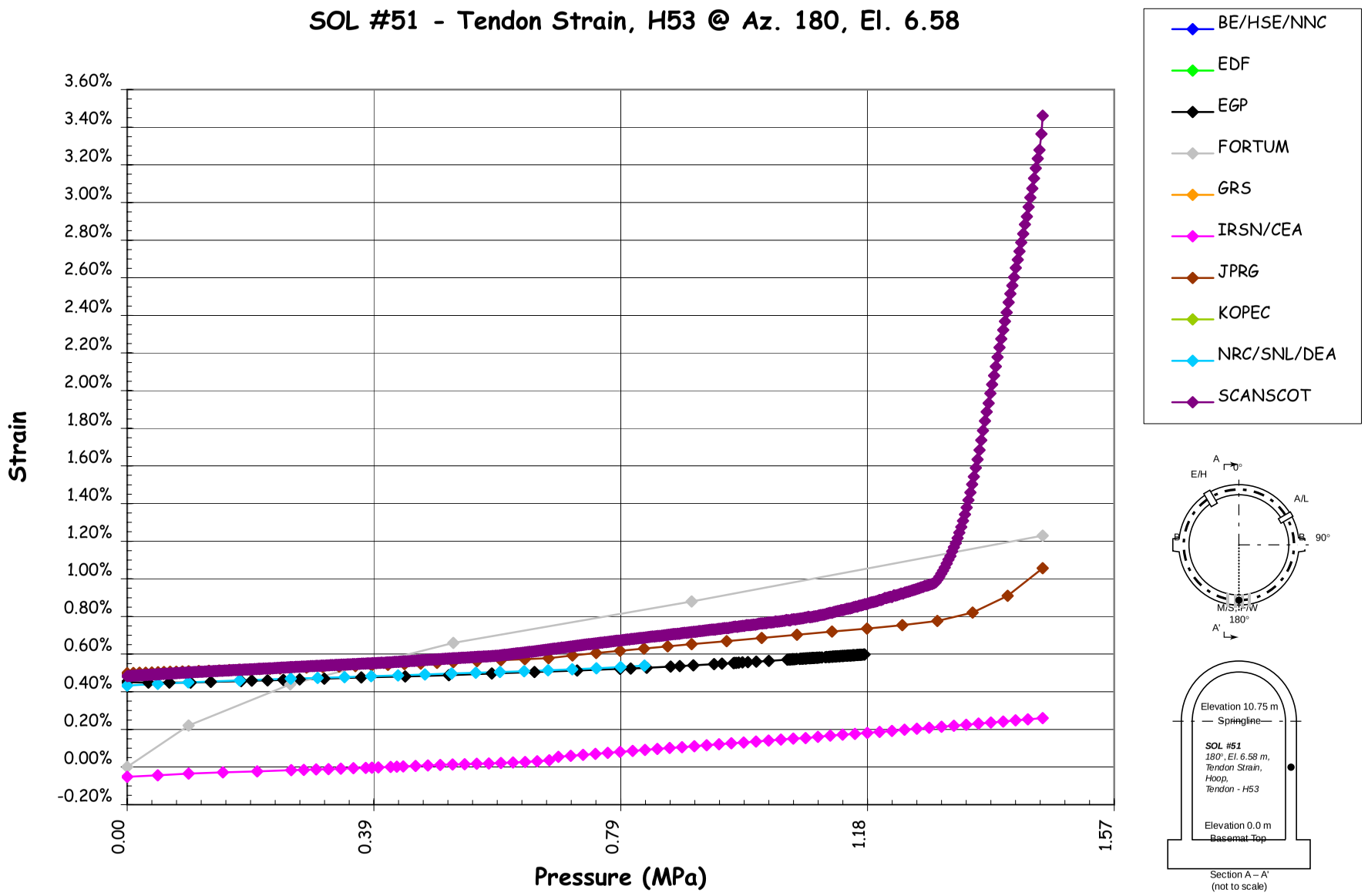
SOL #51 - Tendon Strain, H53 @ Az. 180, El. 6.58
Strain
3.60%
3.40%
3.20%
3.00%
2.80%
2.60%
2.40%
2.20%
2.00%
1.80%
1.60%
1.40%
1.20%
1.00%
0.80%
0.60%
0.40%
0.20%
0.00%
-0.20%
0.00
0.39
0.79
1.18
1.57
Pressure (MPa)
BE/HSE/NNC
EDF
EGP
FORTUM
GRS
IRSN/CEA
JPRG
KOPEC
NRC/SNL/DEA
SCANSCOT
A
0°
E/H
A/L
90°
M/S.H/W
180°
A'
Elevation 10.75 m
Springline
SOL #51
180°, El. 6.58 m,
Tendon Strain,
Hoop,
Tendon - H53
Elevation 0.0 m
Basemat Top
Section A – A'
(not to scale)

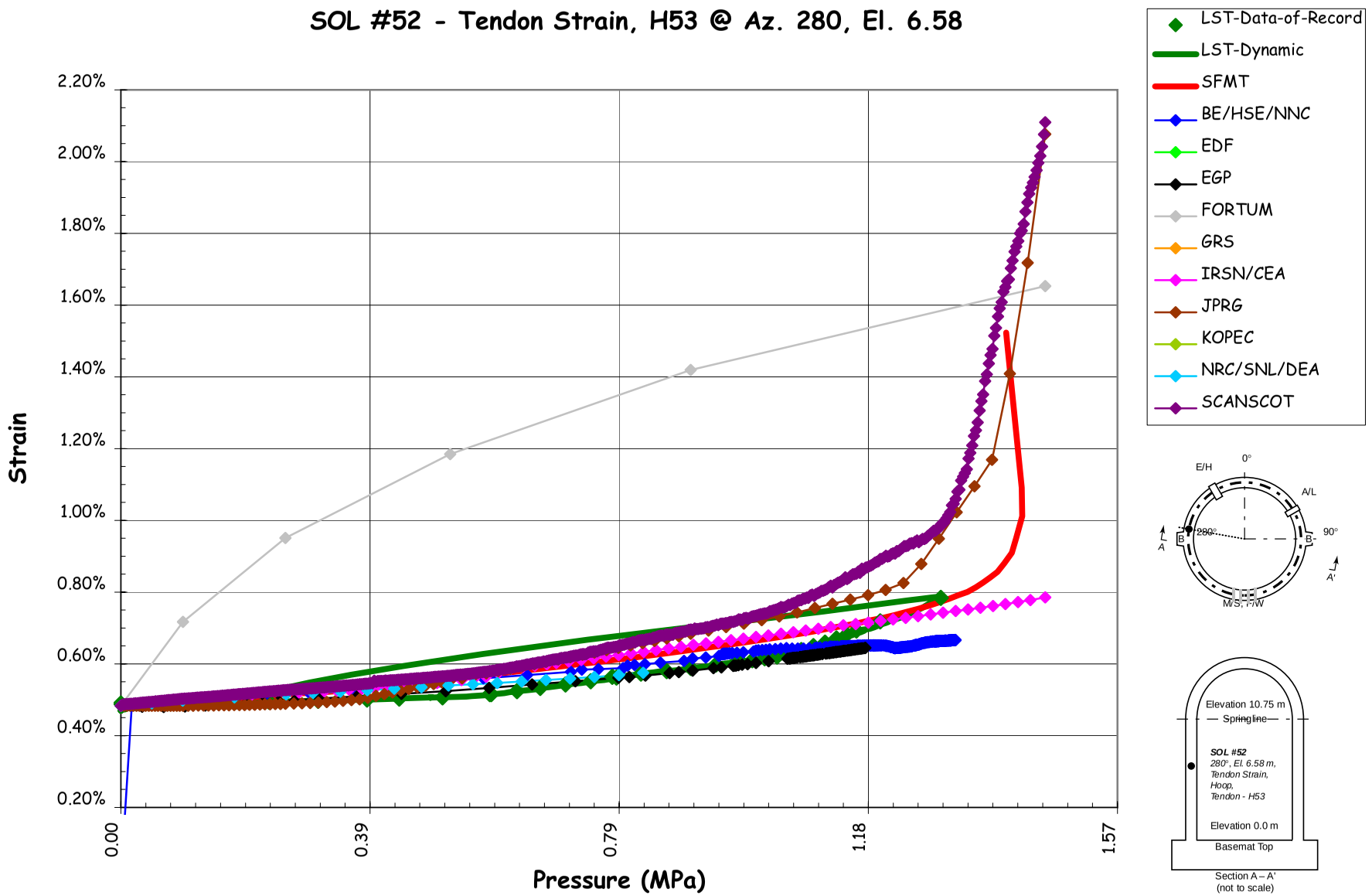
SOL #52 - Tendon Strain, H53 @ Az. 280, El. 6.58
Strain
2.20%
2.00%
1.80%
1.60%
1.40%
1.20%
1.00%
0.80%
0.60%
0.40%
0.20%
0.00
0.39
0.79
1.18
1.57
Pressure (MPa)
LST-Data-of-Record
LST-Dynamic
SFMT
BE/HSE/NNC
EDF
EGP
FORTUM
GRS
IRSN/CEA
JPRG
KOPEC
NRC/SNL/DEA
SCANSCOT
E/H
0°
A/L
280°
90°
A
A'
M/S, H/W
Elevation 10.75 m
Springline
SOL #52
280°, El. 6.58 m,
Tendon Strain,
Hoop,
Tendon - H53
Elevation 0.0 m
Basemat Top
Section A – A'
(not to scale)

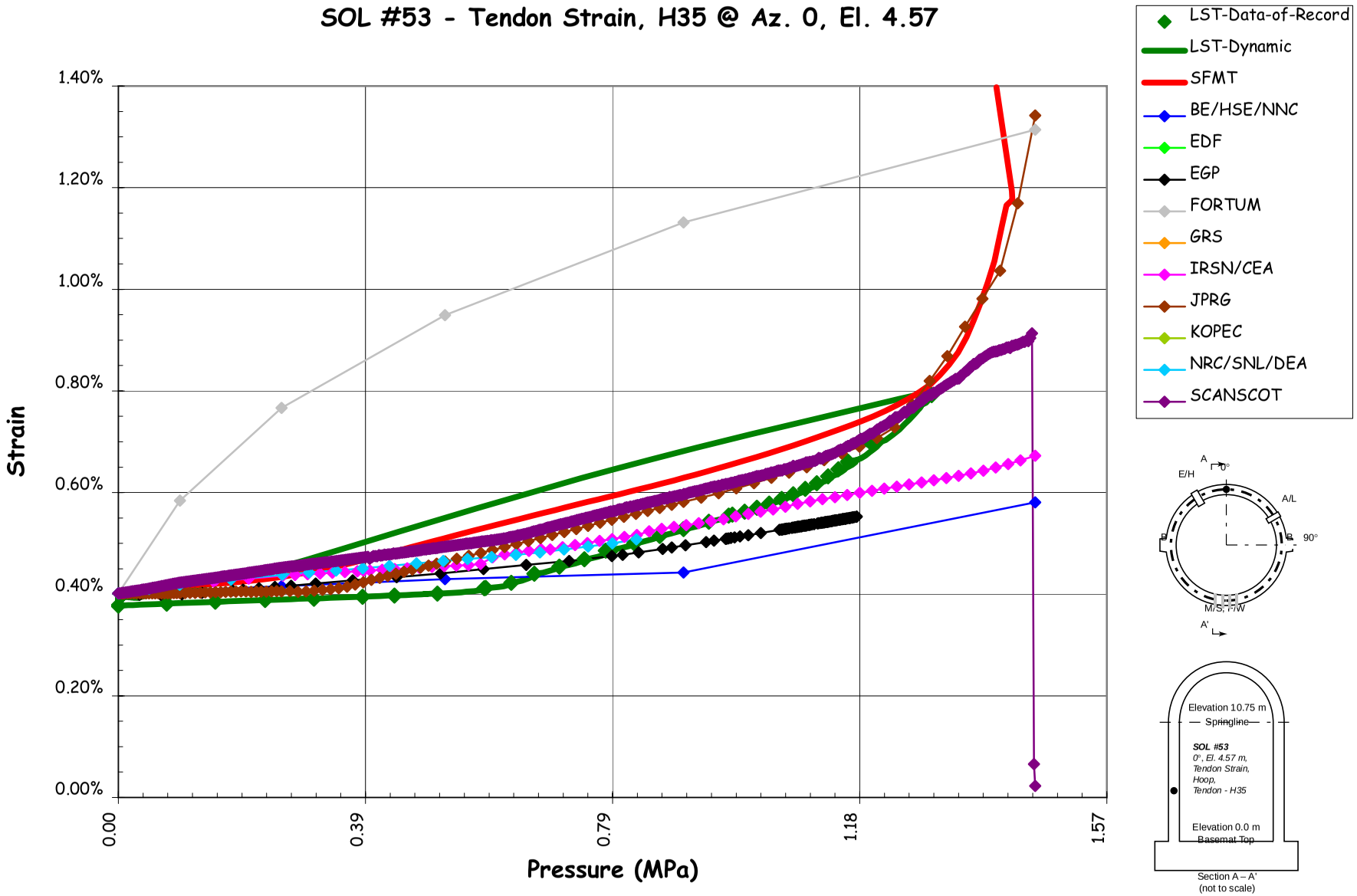
SOL #53 - Tendon Strain, H35 @ Az. 0, El. 4.57
Strain
1.40%
1.20%
1.00%
0.80%
0.60%
0.40%
0.20%
0.00%
0.00
0.39
0.79
1.18
1.57
Pressure (MPa)
LST-Data-of-Record
LST-Dynamic
SFMT
BE/HSE/NNC
EDF
EGP
FORTUM
GRS
IRSN/CEA
JPRG
KOPEC
NRC/SNL/DEA
SCANSCOT
A
E/H
0°
A/L
B
B
90°
M/S, H-W
A'
Elevation 10.75 m
Springline
SOL #53
0°, El. 4.57 m,
Tendon Strain,
Hoop,
Tendon - H35
Elevation 0.0 m
Basemat Top
Section A – A'
(not to scale)

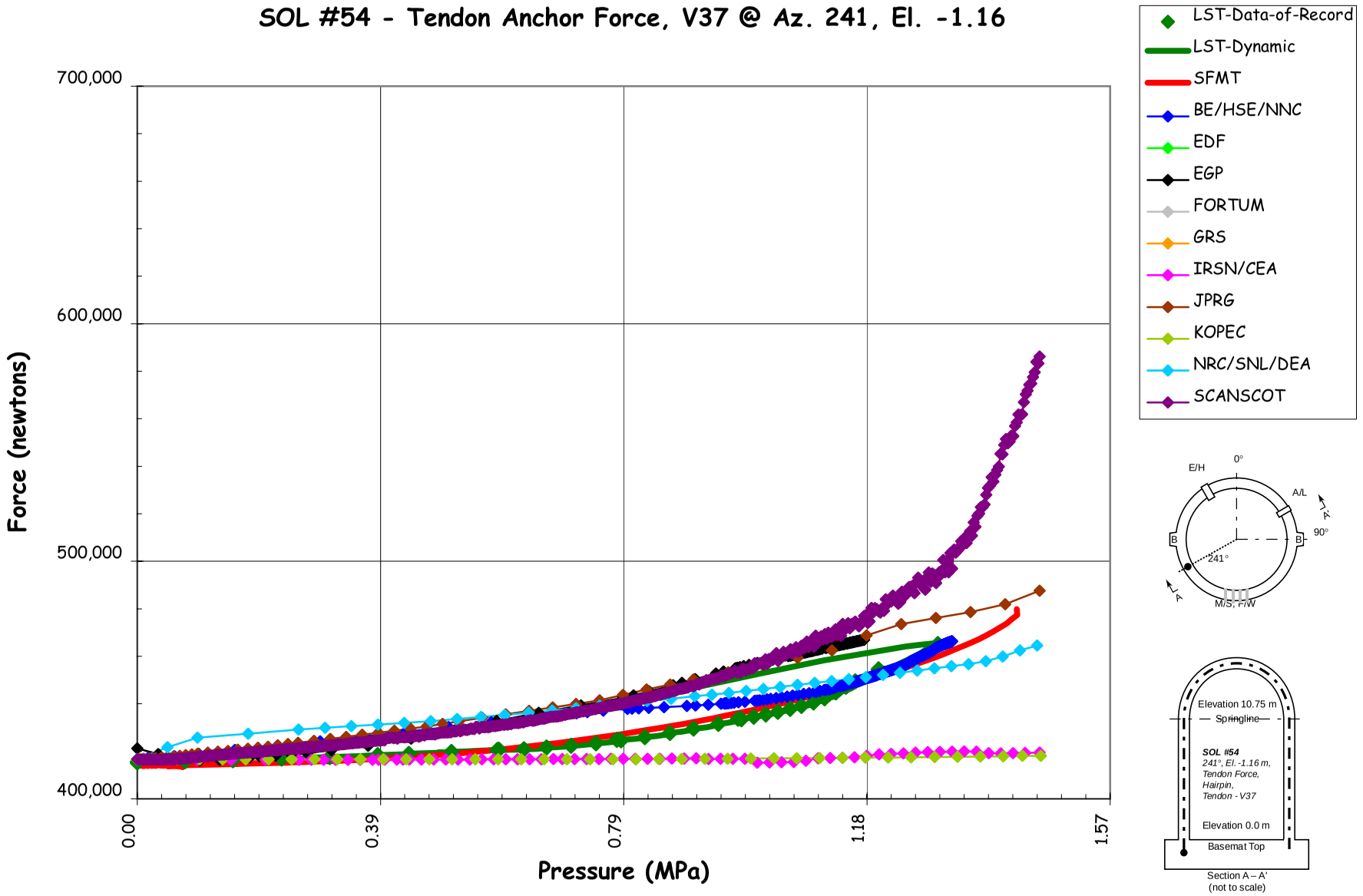
SOL #54 - Tendon Anchor Force, V37 @ Az. 241, El. -1.16
Force (newtons)
700,000
600,000
500,000
400,000
0.00
0.39
0.79
1.18
1.57
Pressure (MPa)
LST-Data-of-Record
LST-Dynamic
SFMT
BE/HSE/NNC
EDF
EGP
FORTUM
GRS
IRSN/CEA
JPRG
KOPEC
NRC/SNL/DEA
SCANSCOT
E/H
0°
A/L
90°
B
B
241°
A
A
M/S, F/W
Elevation 10.75 m
Springline
SOL #54
241°, El. -1.16 m,
Tendon Force,
Hairpin,
Tendon - V37
Elevation 0.0 m
Basemat Top
Section A – A'
(not to scale)

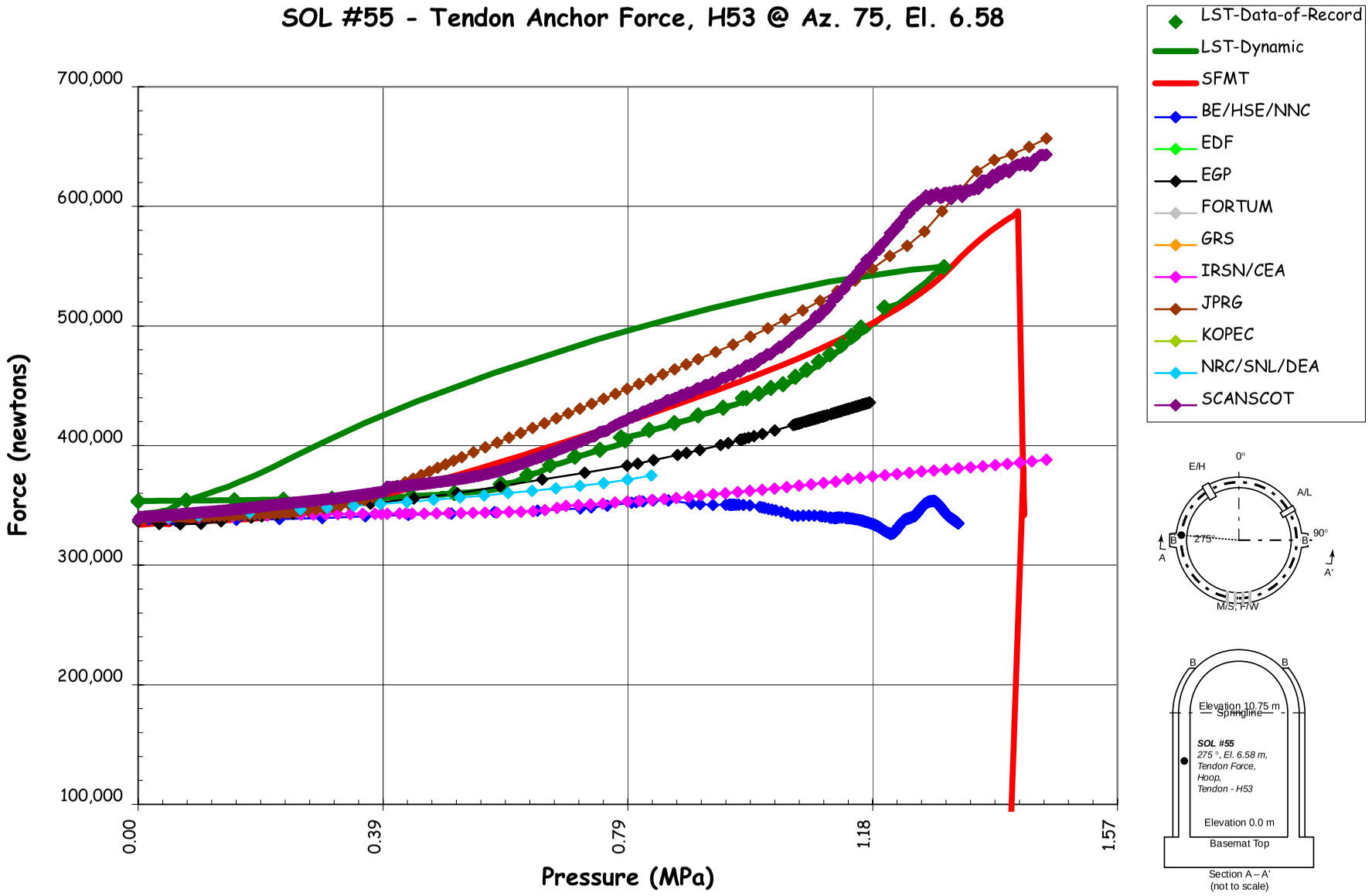
SOL #55 - Tendon Anchor Force, H53 @ Az. 75, El. 6.58
Force (newtons)
700,000
600,000
500,000
400,000
300,000
200,000
100,000
0.00
0.39
0.79
1.18
1.57
Pressure (MPa)
LST-Data-of-Record
LST-Dynamic
SFMT
BE/HSE/NNC
EDF
EGP
FORTUM
GRS
IRSN/CEA
JPRG
KOPEC
NRC/SNL/DEA
SCANSCOT
0°
E/H
A/L
90°
275°
B
A
A'
M/S, F/W
Elevation 10.75 m
Springline
SOL #55
275 °, El. 6.58 m,
Tendon Force,
Hoop,
Tendon - H53
Elevation 0.0 m
Basemat Top
Section A – A'
(not to scale)

Page intentionally left blank

Appendix B: Phase 3 - Case 2 - Comparison Plots at Standard Output Locations: B-67 to B-135

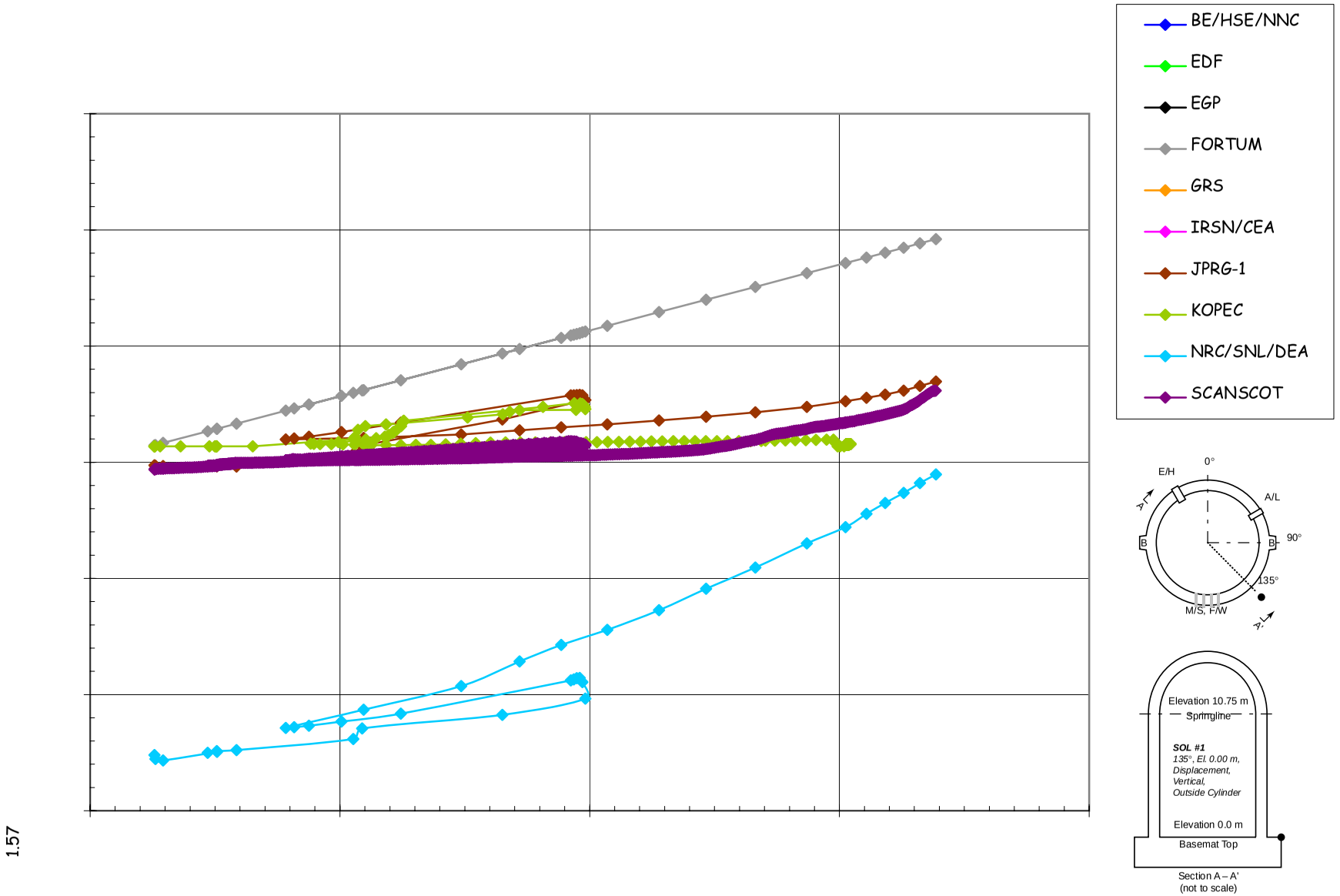
BE/HSE/NNC
EDF
EGP
FORTUM
GRS
IRSN/CEA
JPRG-1
KOPEC
NRC/SNL/DEA
SCANSCOT
0°
E/H
A/L
90°
135°
M/S, F/W
Elevation 10.75 m
Springline
SOL #1
135°, El. 0.00 m,
Displacement,
Vertical,
Outside Cylinder
Elevation 0.0 m
Basemat Top
Section A – A'
(not to scale)

1.57

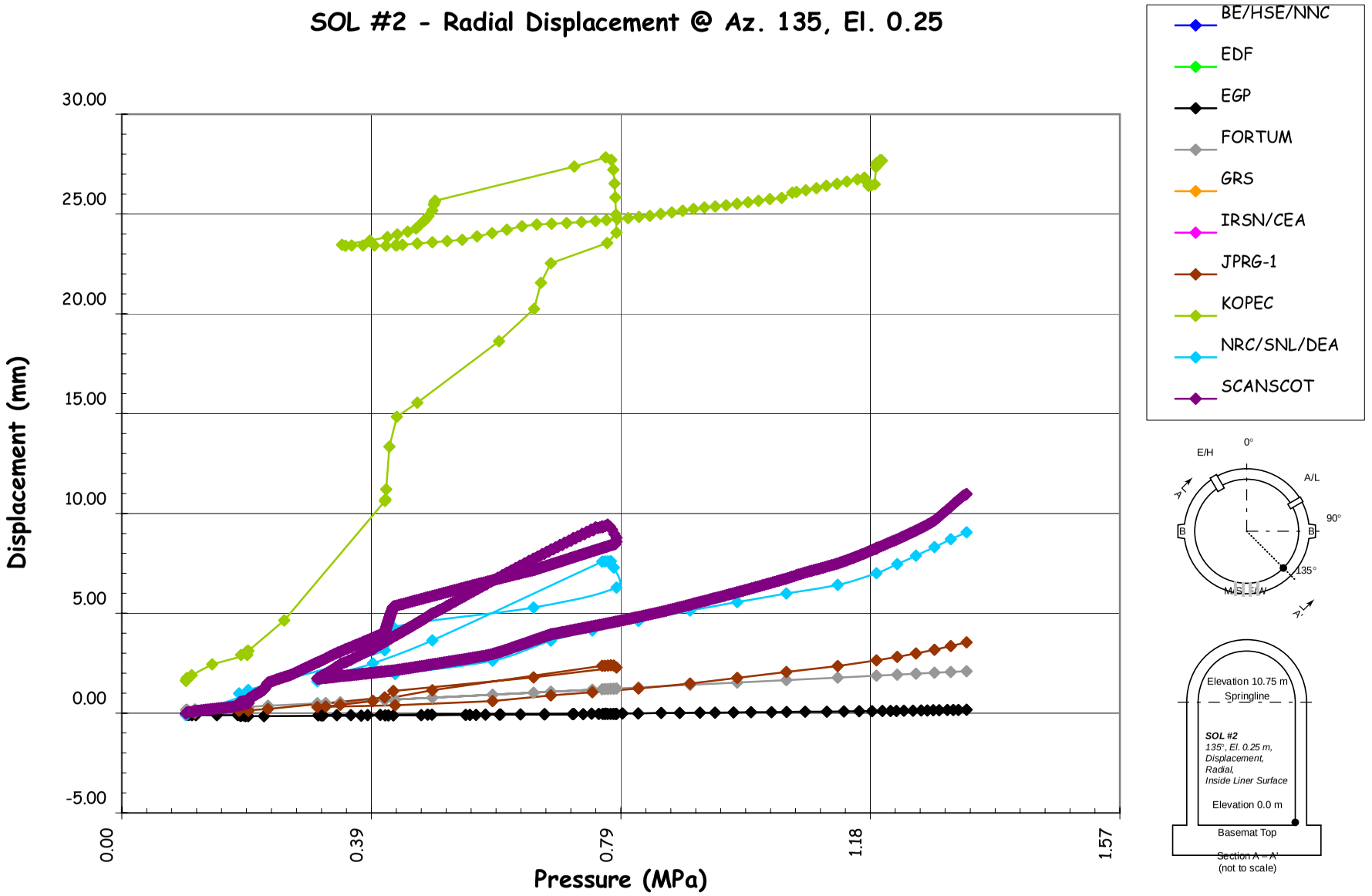

Phase_3_Case_2_P_and_T_Final.xls:SOL 2

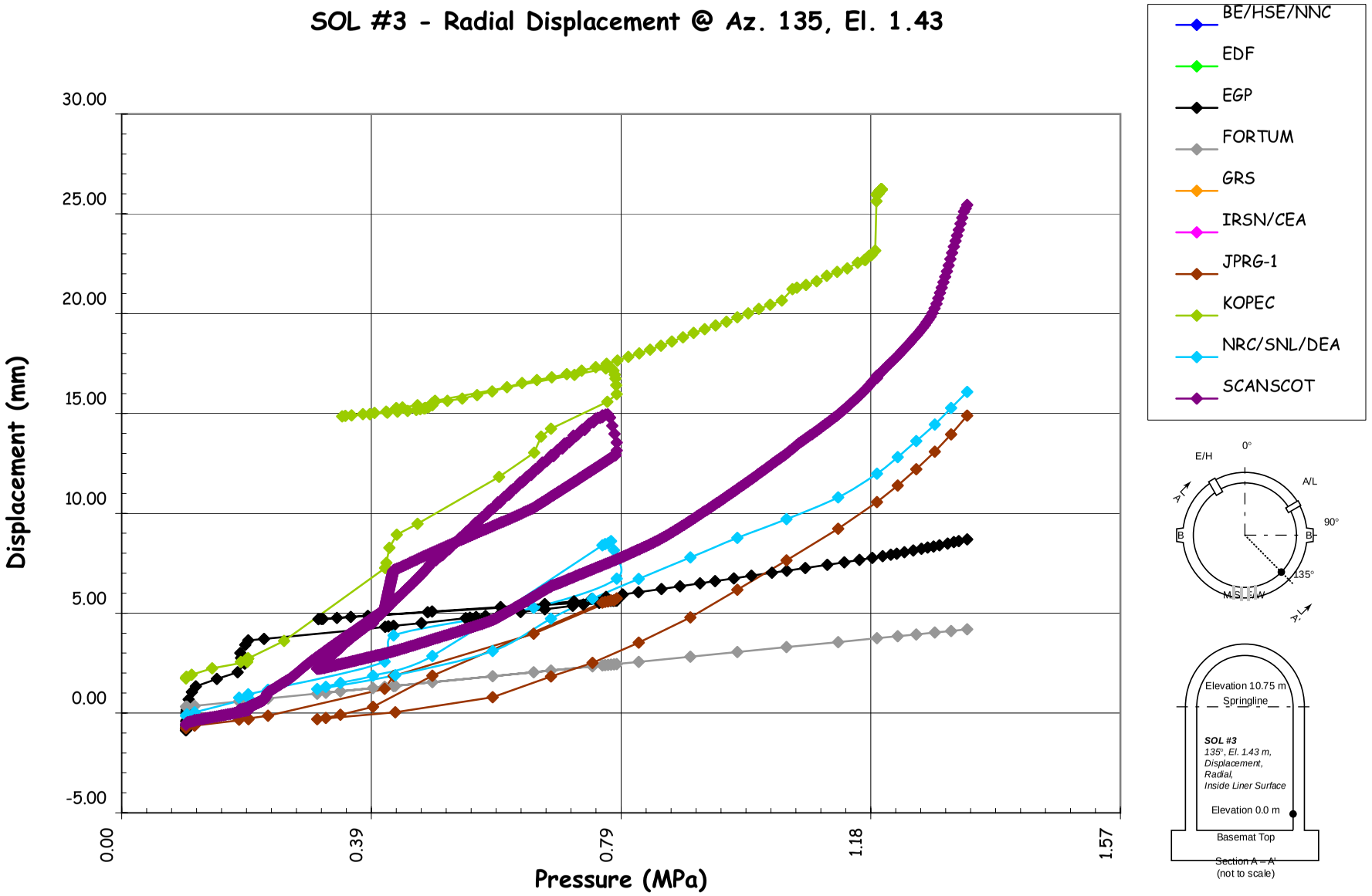
SOL #3 - Radial Displacement @ Az. 135, El. 1.43
Displacement (mm)
30.00
25.00
20.00
15.00
10.00
5.00
0.00
-5.00
0.00
0.39
0.79
1.18
1.57
Pressure (MPa)
BE/HSE/NNC
EDF
EGP
FORTUM
GRS
IRSN/CEA
JPRG-1
KOPEC
NRC/SNL/DEA
SCANSCOT
0°
E/H
A/L
90°
135°
Elevation 10.75 m
Springline
SOL #3
135°, El. 1.43 m,
Displacement,
Radial,
Inside Liner Surface
Elevation 0.0 m
Basemat Top
Section A – A'
(not to scale)

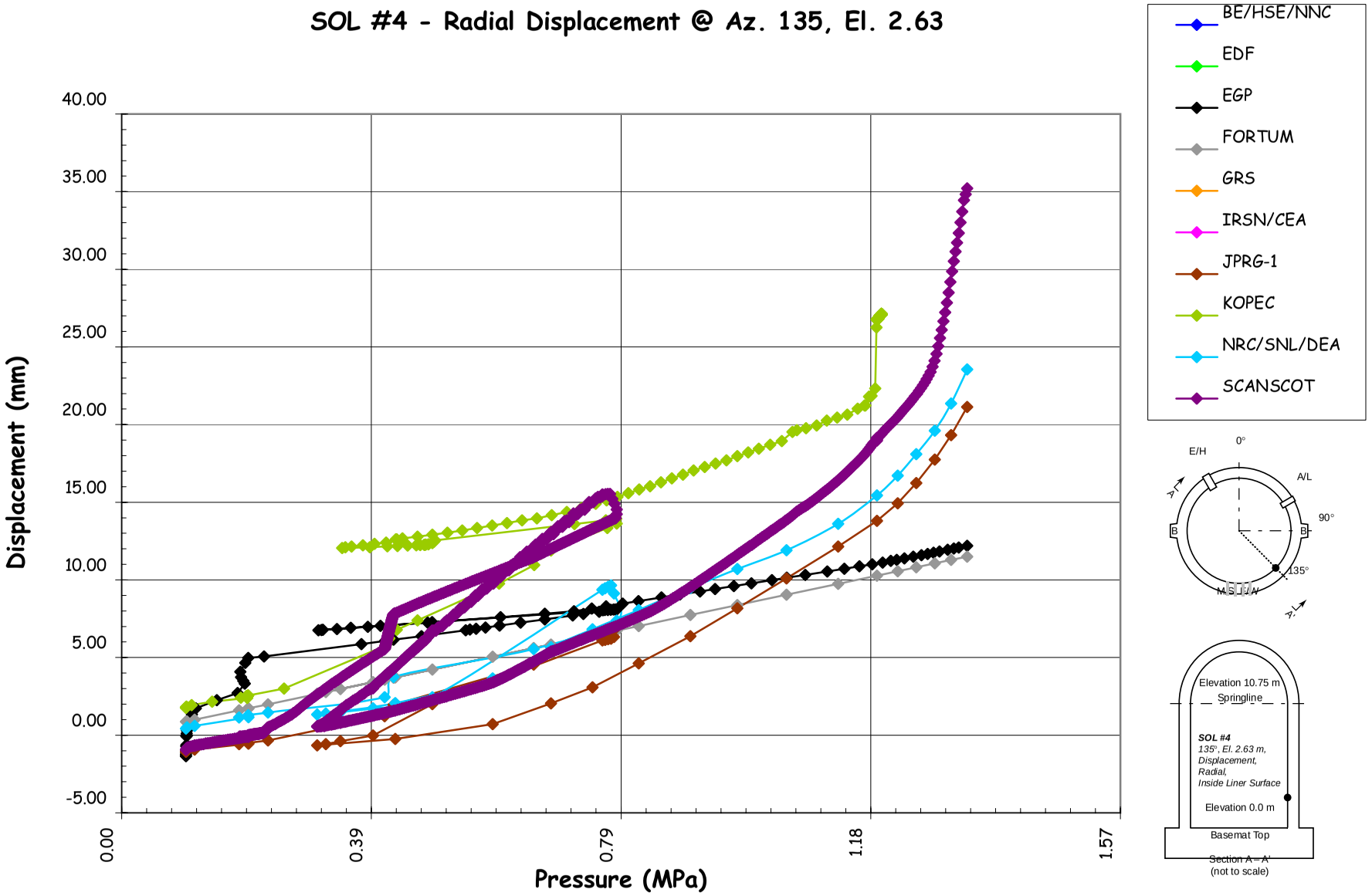
SOL #4 - Radial Displacement @ Az. 135, El. 2.63
Displacement (mm)
40.00
35.00
30.00
25.00
20.00
15.00
10.00
5.00
0.00
-5.00
0.00
0.39
0.79
1.18
1.57
Pressure (MPa)
BE/HSE/NNC
EDF
EGP
FORTUM
GRS
IRSN/CEA
JPRG-1
KOPEC
NRC/SNL/DEA
SCANSCOT
0°
E/H
A/L
90°
135°
Elevation 10.75 m
Springline
SOL #4
135°, El. 2.63 m,
Displacement,
Radial,
Inside Liner Surface
Elevation 0.0 m
Basemat Top
Section A – A'
(not to scale)

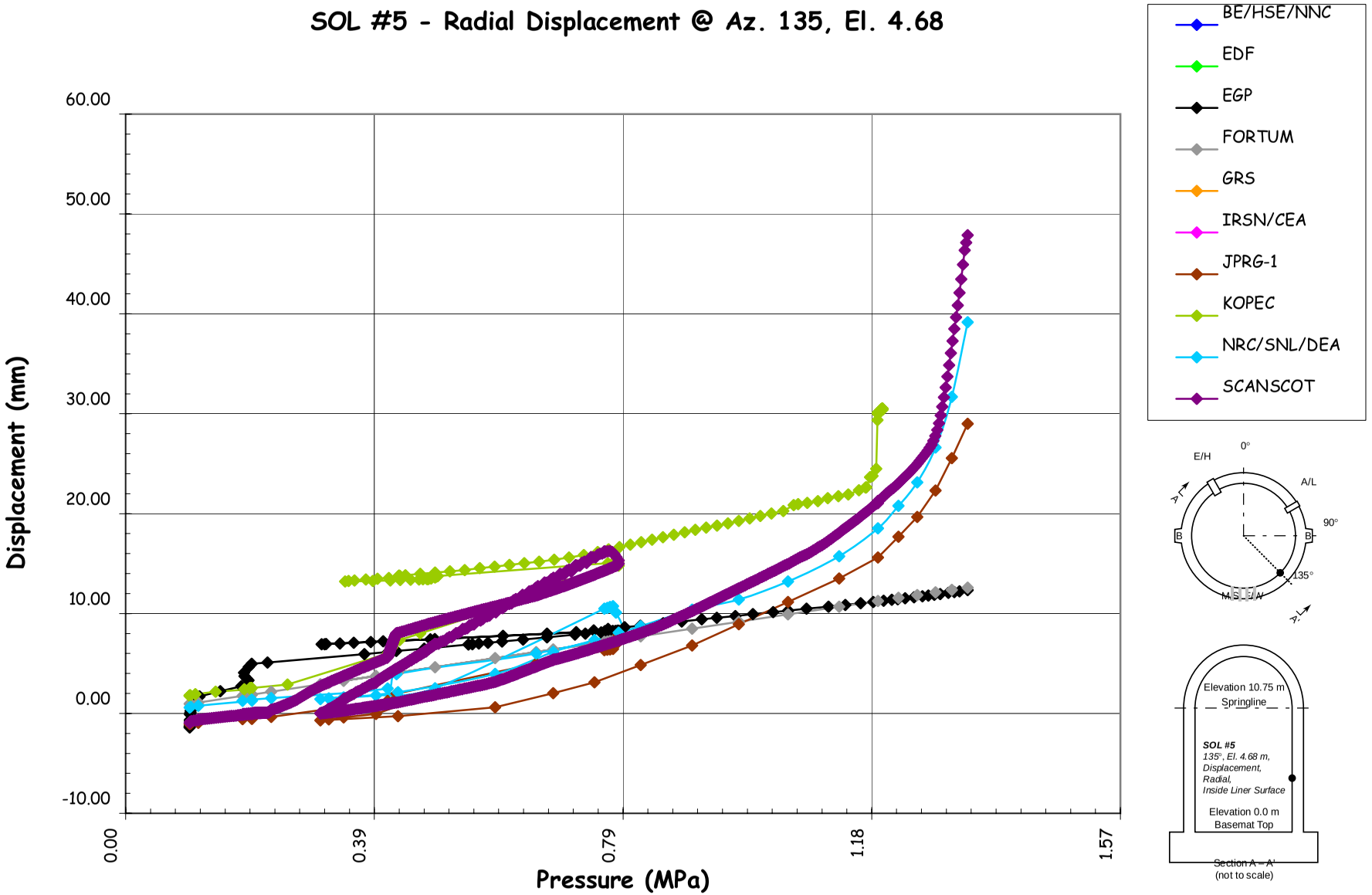
SOL #5 - Radial Displacement @ Az. 135, El. 4.68
Displacement (mm)
60.00
50.00
40.00
30.00
20.00
10.00
0.00
-10.00
0.00
0.39
0.79
1.18
1.57
Pressure (MPa)
BE/HSE/NNC
EDF
EGP
FORTUM
GRS
IRSN/CEA
JPRG-1
KOPEC
NRC/SNL/DEA
SCANSCOT
0°
E/H
A/L
90°
135°
Elevation 10.75 m
Springline
SOL #5
135°, El. 4.68 m,
Displacement,
Radial,
Inside Liner Surface
Elevation 0.0 m
Basemat Top
Section A – A'
(not to scale)

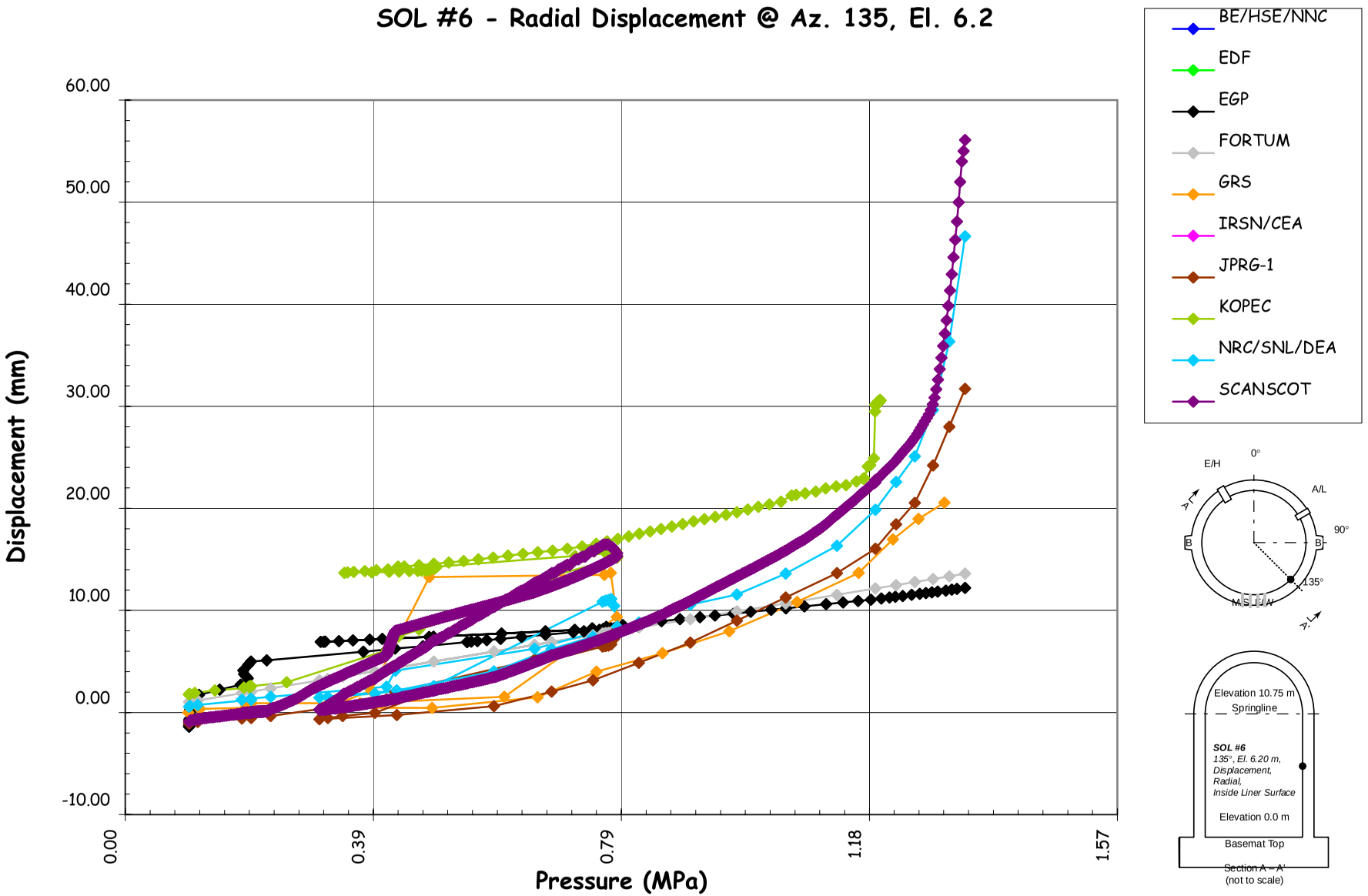

Phase_3_Case_2_P_and_T_Final.xls:SOL 6

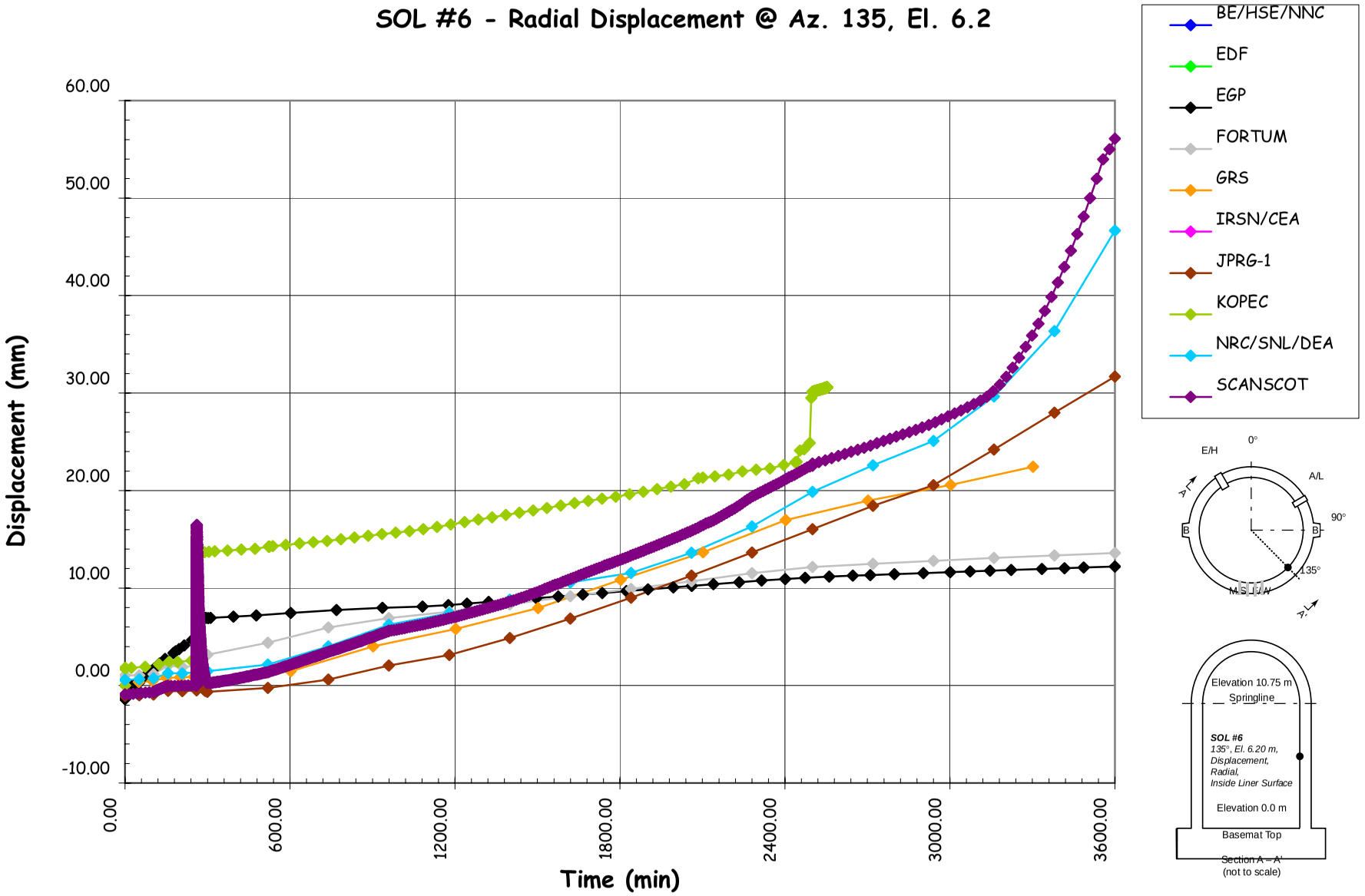
SOL #6 - Radial Displacement @ Az. 135, El. 6.2
Displacement (mm)
60.00
50.00
40.00
30.00
20.00
10.00
0.00
-10.00
0.00
600.00
1200.00
1800.00
2400.00
3000.00
3600.00
Time (min)
BE/HSE/NNC
EDF
EGP
FORTUM
GRS
IRSN/CEA
JPRG-1
KOPEC
NRC/SNL/DEA
SCANSCOT
0°
E/H
A/L
90°
B
B
135°
M.S.
A'
A'
Elevation 10.75 m
Springline
SOL #6
135°, El. 6.20 m,
Displacement,
Radial,
Inside Liner Surface
Elevation 0.0 m
Basemat Top
Section A – A'
(not to scale)

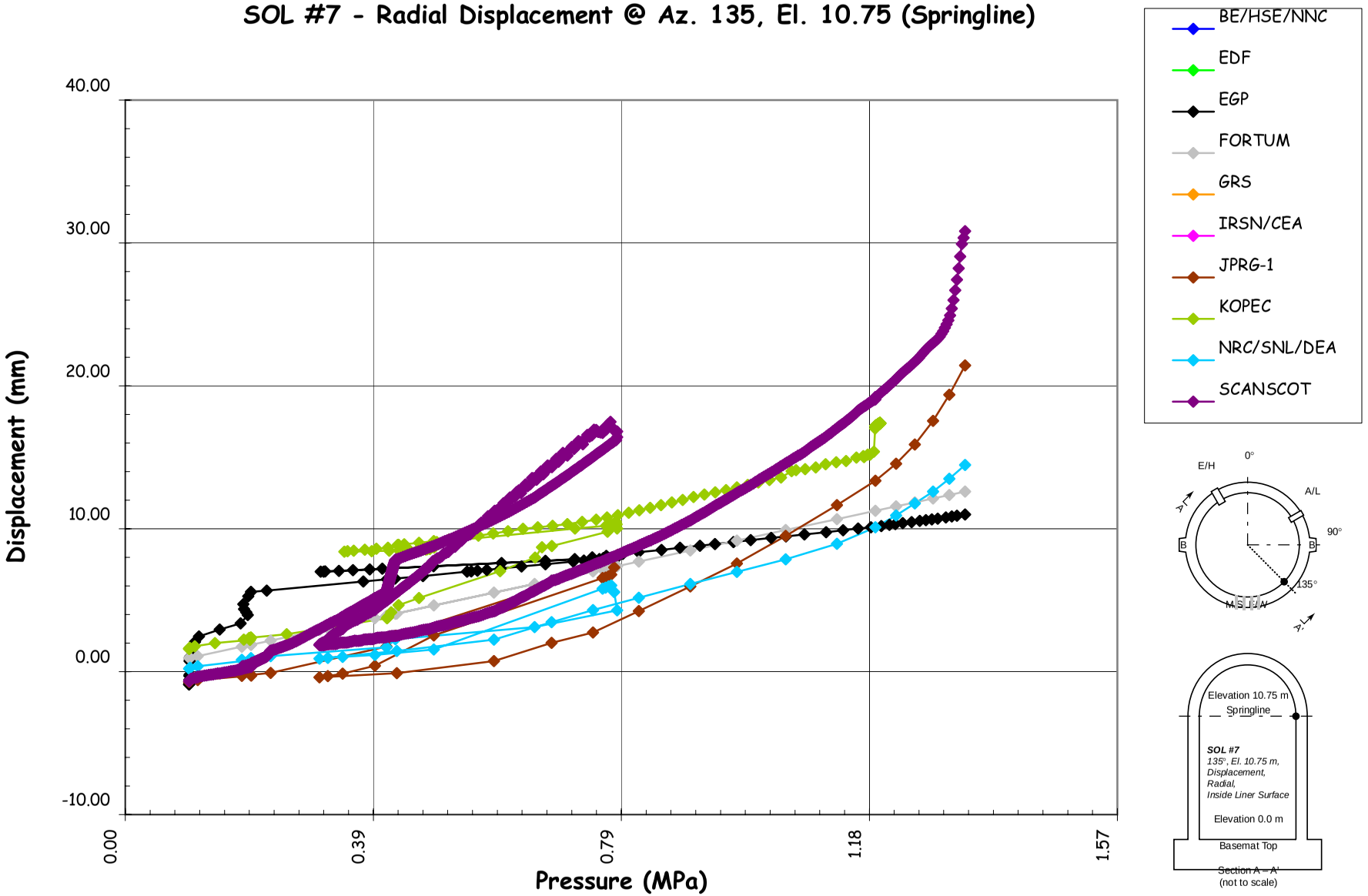
SOL #7 - Radial Displacement @ Az. 135, El. 10.75 (Springline)
Displacement (mm)
40.00
30.00
20.00
10.00
0.00
-10.00
0.00
0.39
0.79
1.18
1.57
Pressure (MPa)
BE/HSE/NNC
EDF
EGP
FORTUM
GRS
IRSN/CEA
JPRG-1
KOPEC
NRC/SNL/DEA
SCANSCOT
E/H
0°
A/L
90°
135°
M.S.U.A
Elevation 10.75 m
Springline
SOL #7
135°, El. 10.75 m,
Displacement,
Radial,
Inside Liner Surface
Elevation 0.0 m
Basemat Top
Section A – A'
(not to scale)

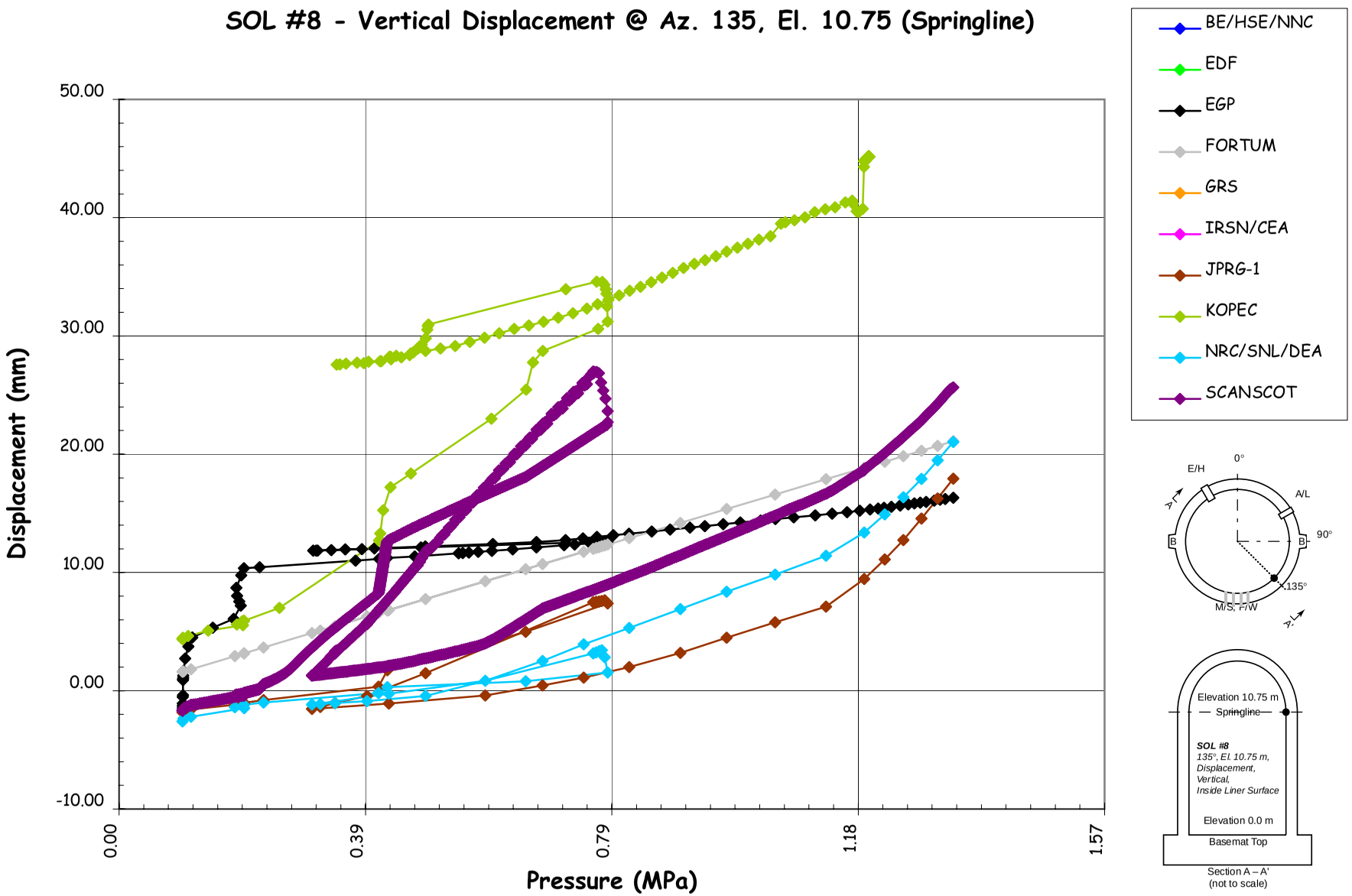
SOL #8 - Vertical Displacement @ Az. 135, El. 10.75 (Springline)
Displacement (mm)
50.00
40.00
30.00
20.00
10.00
0.00
-10.00
0.00
0.39
0.79
1.18
1.57
Pressure (MPa)
BE/HSE/NNC
EDF
EGP
FORTUM
GRS
IRSN/CEA
JPRG-1
KOPEC
NRC/SNL/DEA
SCANSCOT
0°
E/H
A/L
90°
135°
M/S, F/W
Elevation 10.75 m
Springline
SOL #8
135°, El. 10.75 m,
Displacement,
Vertical,
Inside Liner Surface
Elevation 0.0 m
Basemat Top
Section A – A'
(not to scale)

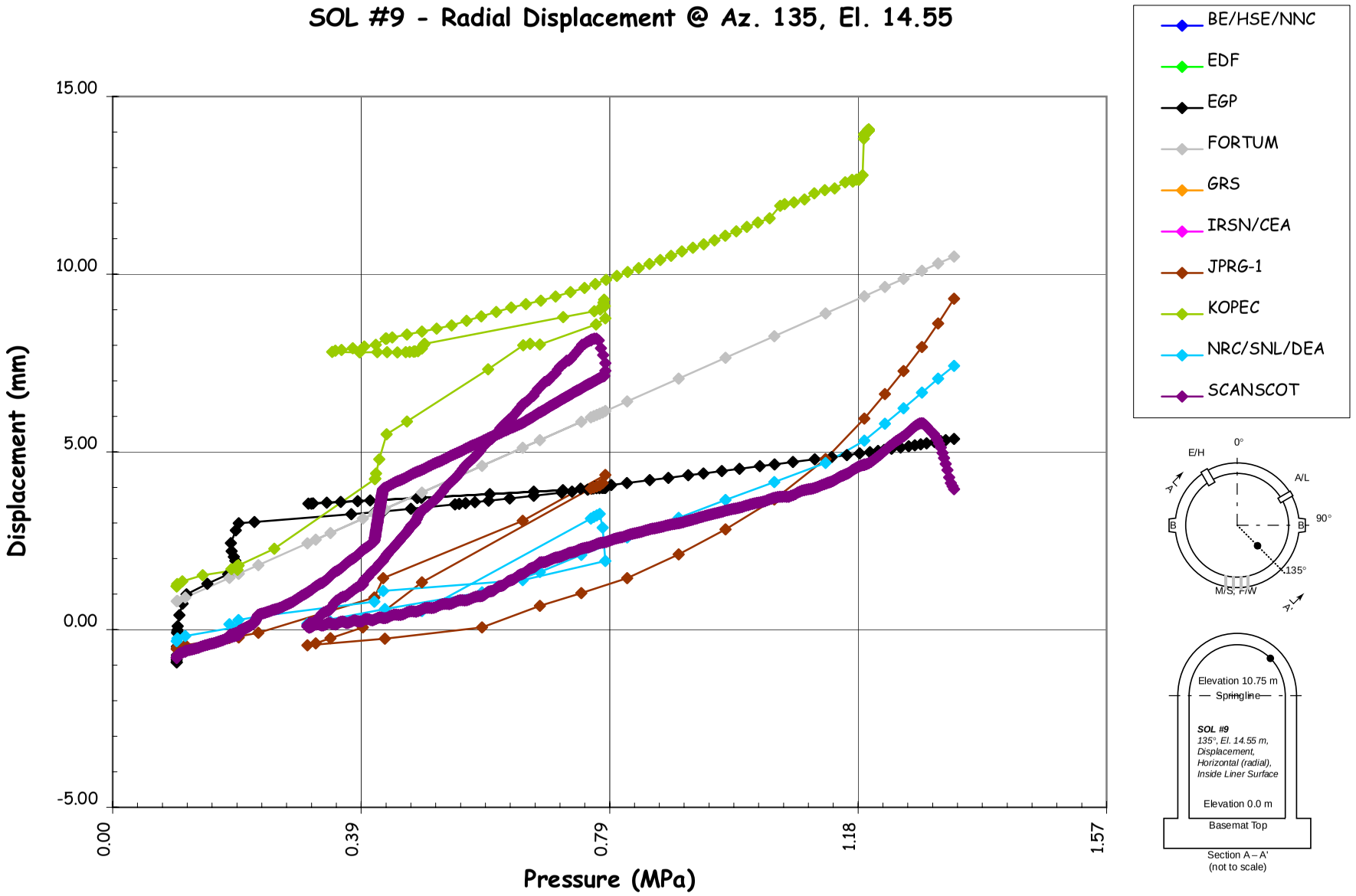
SOL #9 - Radial Displacement @ Az. 135, El. 14.55
Displacement (mm)
15.00
10.00
5.00
0.00
-5.00
0.00
0.39
0.79
1.18
1.57
Pressure (MPa)
BE/HSE/NNC
EDF
EGP
FORTUM
GRS
IRSN/CEA
JPRG-1
KOPEC
NRC/SNL/DEA
SCANSCOT
0°
E/H
A/L
90°
135°
M/S, F/W
Elevation 10.75 m
Springline
SOL #9
135°, El. 14.55 m,
Displacement,
Horizontal (radial),
Inside Liner Surface
Elevation 0.0 m
Basemat Top
Section A – A'
(not to scale)

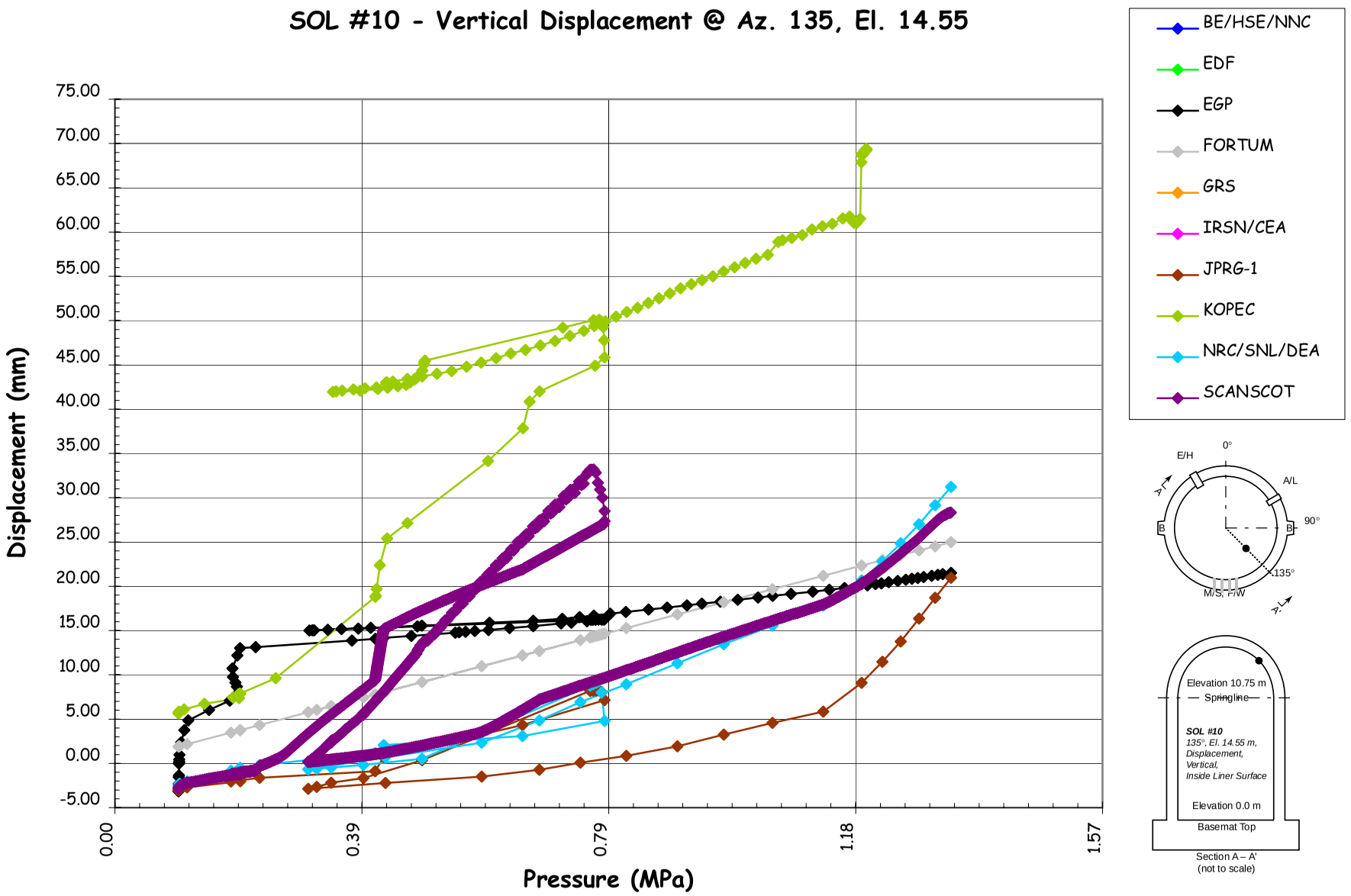
SOL #10 - Vertical Displacement @ Az. 135, El. 14.55
Displacement (mm)
75.00
70.00
65.00
60.00
55.00
50.00
45.00
40.00
35.00
30.00
25.00
20.00
15.00
10.00
5.00
0.00
-5.00
0.00
0.39
0.79
1.18
1.57
Pressure (MPa)
BE/HSE/NNC
EDF
EGP
FORTUM
GRS
IRSN/CEA
JPRG-1
KOPEC
NRC/SNL/DEA
SCANSCOT
0°
E/H
A/L
90°
135°
M/S, F/W
Elevation 10.75 m
Springline
SOL #10
135°, El. 14.55 m,
Displacement,
Vertical,
Inside Liner Surface
Elevation 0.0 m
Basemat Top
Section A – A'
(not to scale)

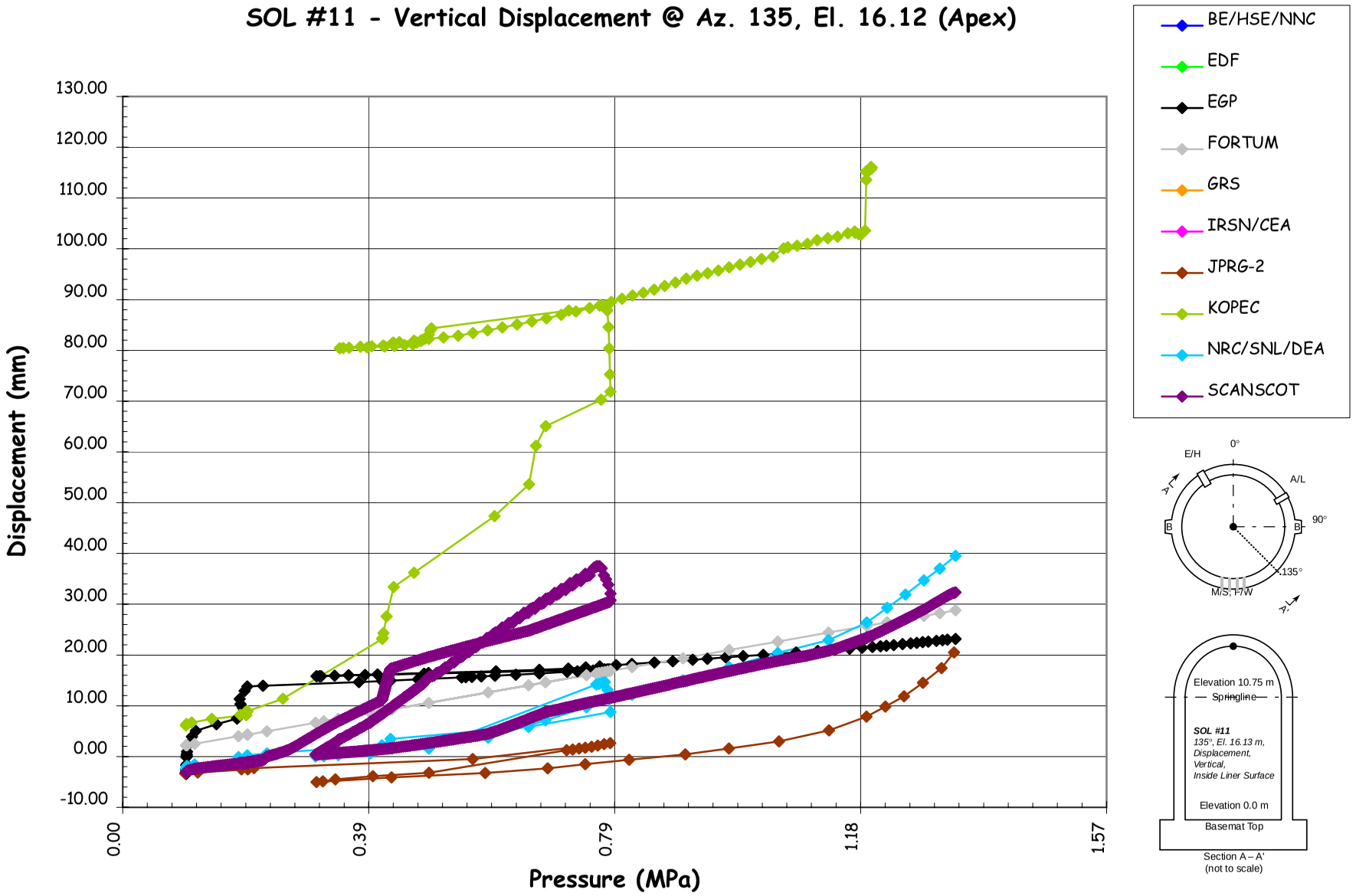
SOL #11 - Vertical Displacement @ Az. 135, El. 16.12 (Apex)
Displacement (mm)
130.00
120.00
110.00
100.00
90.00
80.00
70.00
60.00
50.00
40.00
30.00
20.00
10.00
0.00
-10.00
0.00
0.39
0.79
1.18
1.57
Pressure (MPa)
BE/HSE/NNC
EDF
EGP
FORTUM
GRS
IRSN/CEA
JPRG-2
KOPEC
NRC/SNL/DEA
SCANSCOT
0°
E/H
A/L
90°
135°
M/S, I-N
Elevation 10.75 m
Springline
SOL #11
135°, El. 16.13 m,
Displacement,
Vertical,
Inside Liner Surface
Elevation 0.0 m
Basemat Top
Section A – A'
(not to scale)

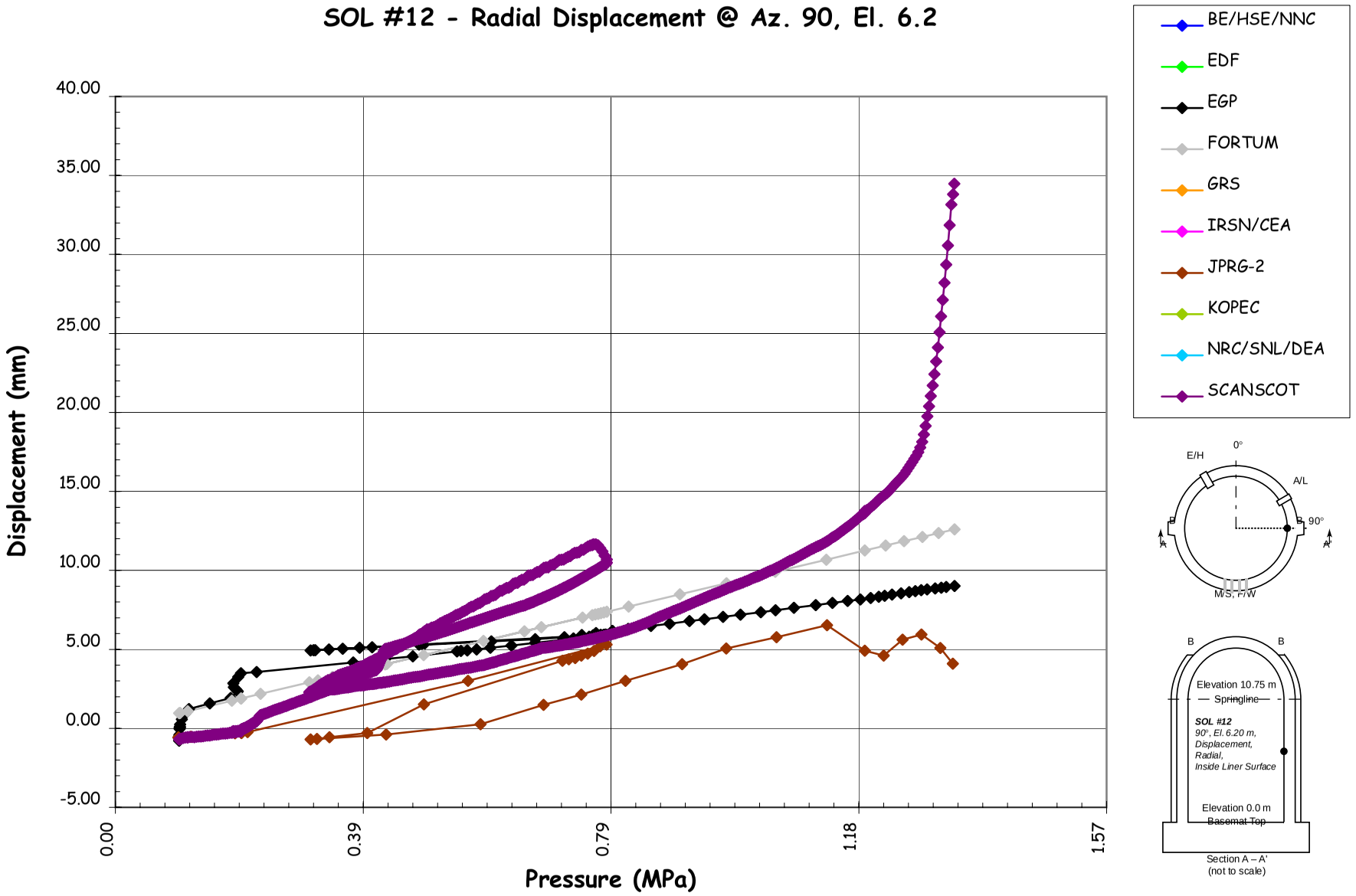
SOL #12 - Radial Displacement @ Az. 90, El. 6.2
Displacement (mm)
40.00
35.00
30.00
25.00
20.00
15.00
10.00
5.00
0.00
-5.00
0.00
0.39
0.79
1.18
1.57
Pressure (MPa)
BE/HSE/NNC
EDF
EGP
FORTUM
GRS
IRSN/CEA
JPRG-2
KOPEC
NRC/SNL/DEA
SCANSCOT
0°
E/H
A/L
90°
MS, FW
B
B
Elevation 10.75 m
Springline
SOL #12
90°, El. 6.20 m,
Displacement,
Radial,
Inside Liner Surface
Elevation 0.0 m
Basemat Top
Section A – A'
(not to scale)

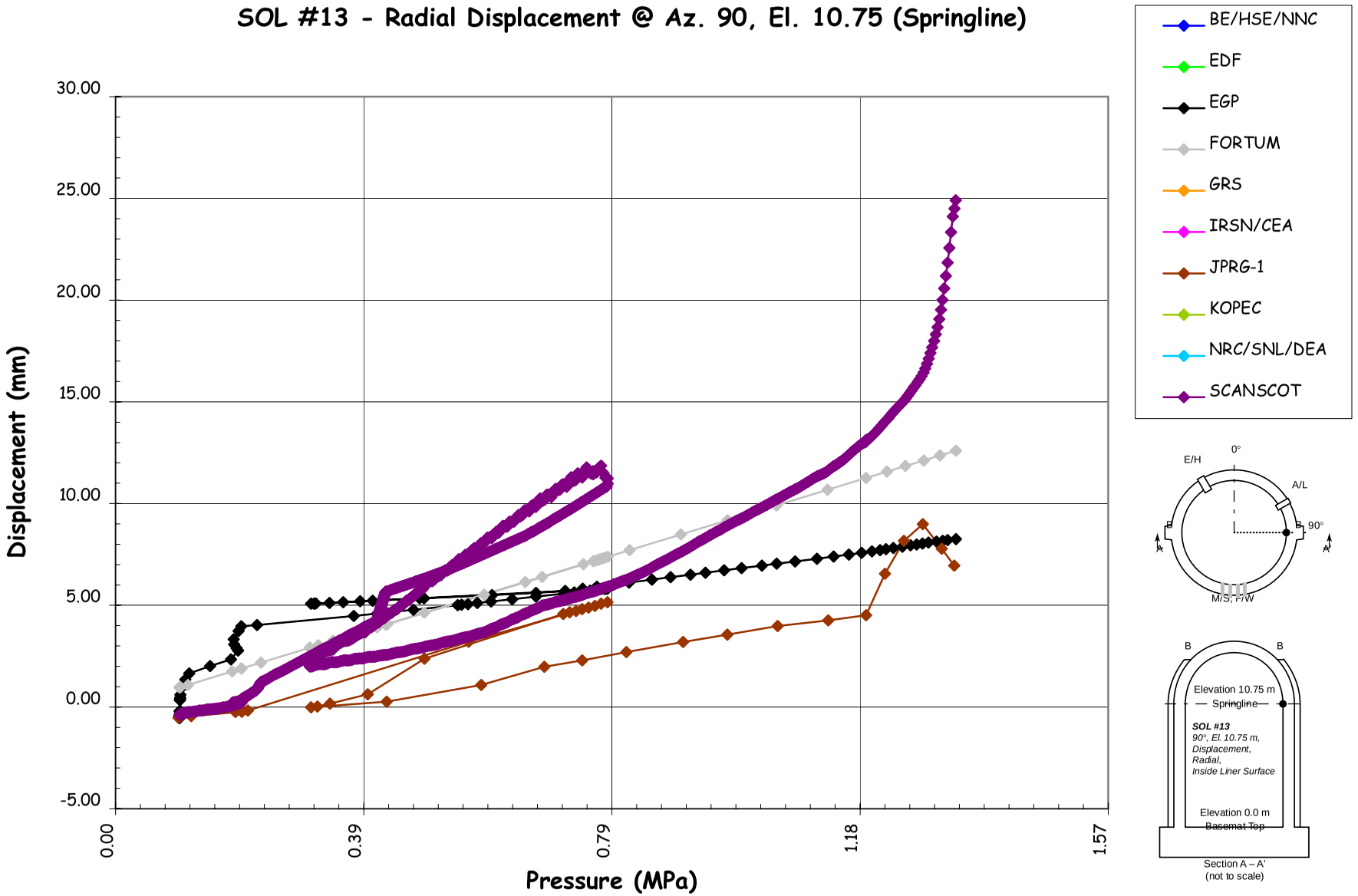
SOL #13 - Radial Displacement @ Az. 90, El. 10.75 (Springline)
Displacement (mm)
30.00
25.00
20.00
15.00
10.00
5.00
0.00
-5.00
0.00
0.39
0.79
1.18
1.57
Pressure (MPa)
BE/HSE/NNC
EDF
EGP
FORTUM
GRS
IRSN/CEA
JPRG-1
KOPEC
NRC/SNL/DEA
SCANSCOT
E/H
0°
A/L
90°
M/S, F/W
B
B
Elevation 10.75 m
Springline
SOL #13
90°, El. 10.75 m,
Displacement,
Radial,
Inside Liner Surface
Elevation 0.0 m
Basemat Top
Section A – A'
(not to scale)

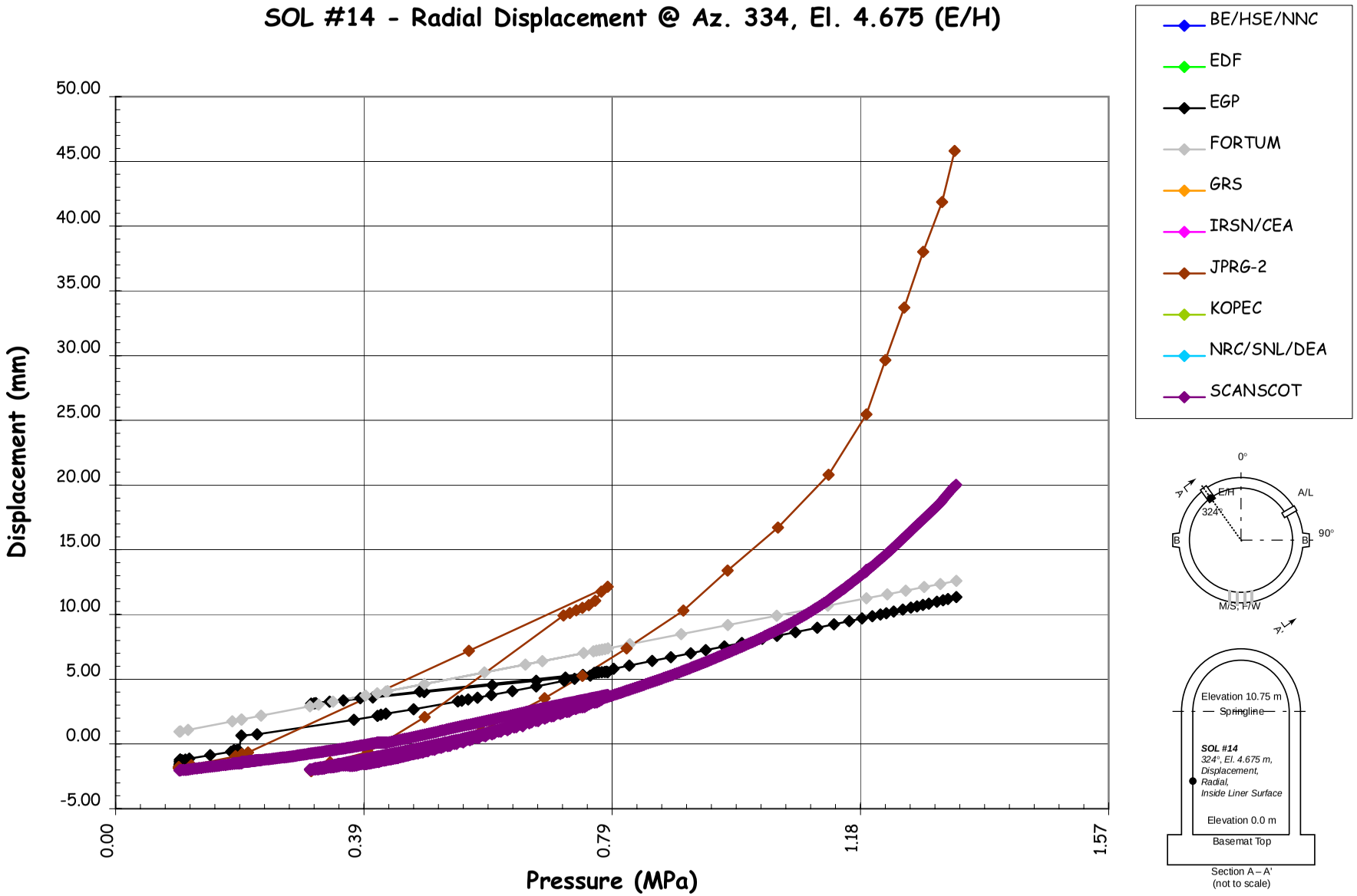
SOL #14 - Radial Displacement @ Az. 334, El. 4.675 (E/H)
Displacement (mm)
50.00
45.00
40.00
35.00
30.00
25.00
20.00
15.00
10.00
5.00
0.00
-5.00
0.00
0.39
0.79
1.18
1.57
Pressure (MPa)
BE/HSE/NNC
EDF
EGP
FORTUM
GRS
IRSN/CEA
JPRG-2
KOPEC
NRC/SNL/DEA
SCANSCOT
0°
E/H
A/L
324°
90°
B
B
M/S, I-W
Elevation 10.75 m
Springline
SOL #14
324°, El. 4.675 m,
Displacement,
Radial,
Inside Liner Surface
Elevation 0.0 m
Basemat Top
Section A – A'
(not to scale)

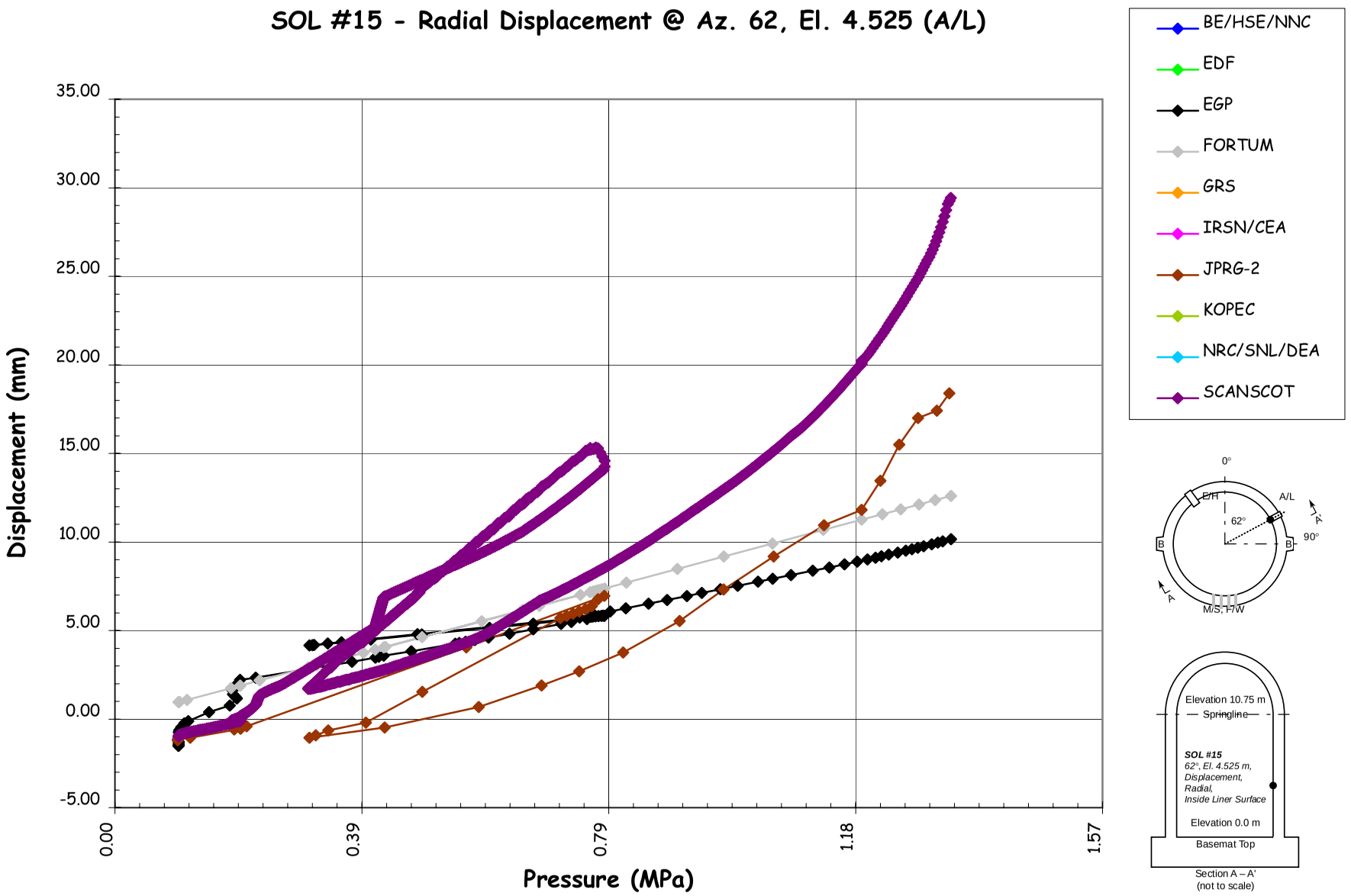
SOL #15 - Radial Displacement @ Az. 62, El. 4.525 (A/L)
Displacement (mm)
35.00
30.00
25.00
20.00
15.00
10.00
5.00
0.00
-5.00
0.00
0.39
0.79
1.18
1.57
Pressure (MPa)
BE/HSE/NNC
EDF
EGP
FORTUM
GRS
IRSN/CEA
JPRG-2
KOPEC
NRC/SNL/DEA
SCANSCOT
0°
E/H
A/L
62°
90°
B
B
M/S, HW
Elevation 10.75 m
Springline
SOL #15
62°, El. 4.525 m,
Displacement,
Radial,
Inside Liner Surface
Elevation 0.0 m
Basemat Top
Section A – A'
(not to scale)

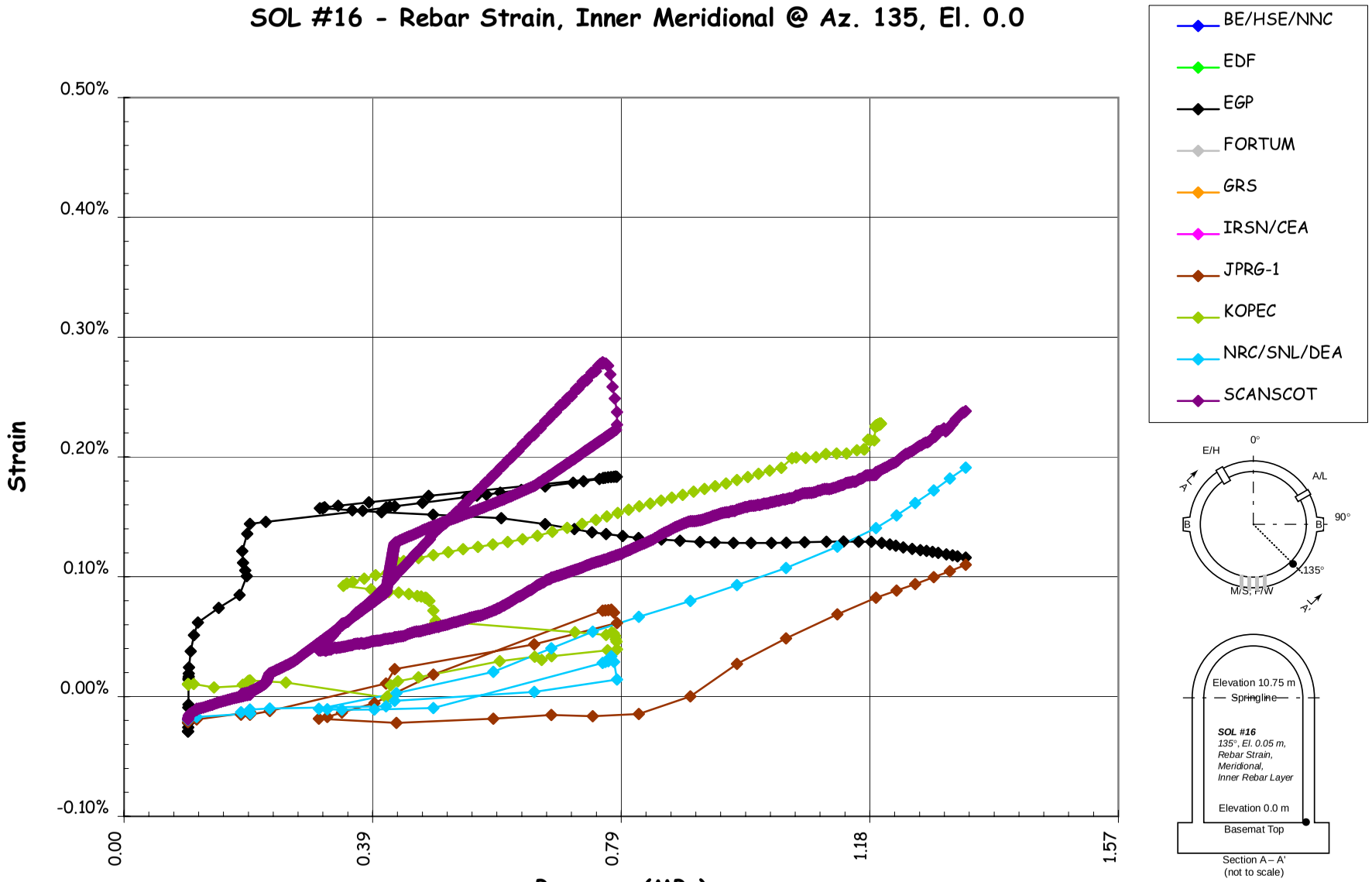
SOL #16 - Rebar Strain, Inner Meridional @ Az. 135, El. 0.0
Strain
0.50%
0.40%
0.30%
0.20%
0.10%
0.00%
-0.10%
0.00
0.39
0.79
1.18
1.57
Pressure (MPa)
BE/HSE/NNC
EDF
EGP
FORTUM
GRS
IRSN/CEA
JPRG-1
KOPEC
NRC/SNL/DEA
SCANSCOT
0°
E/H
A/L
90°
135°
M/S, I-W
Elevation 10.75 m
Springline
SOL #16
135°, El. 0.05 m,
Rebar Strain,
Meridional,
Inner Rebar Layer
Elevation 0.0 m
Basemat Top
Section A – A'
(not to scale)

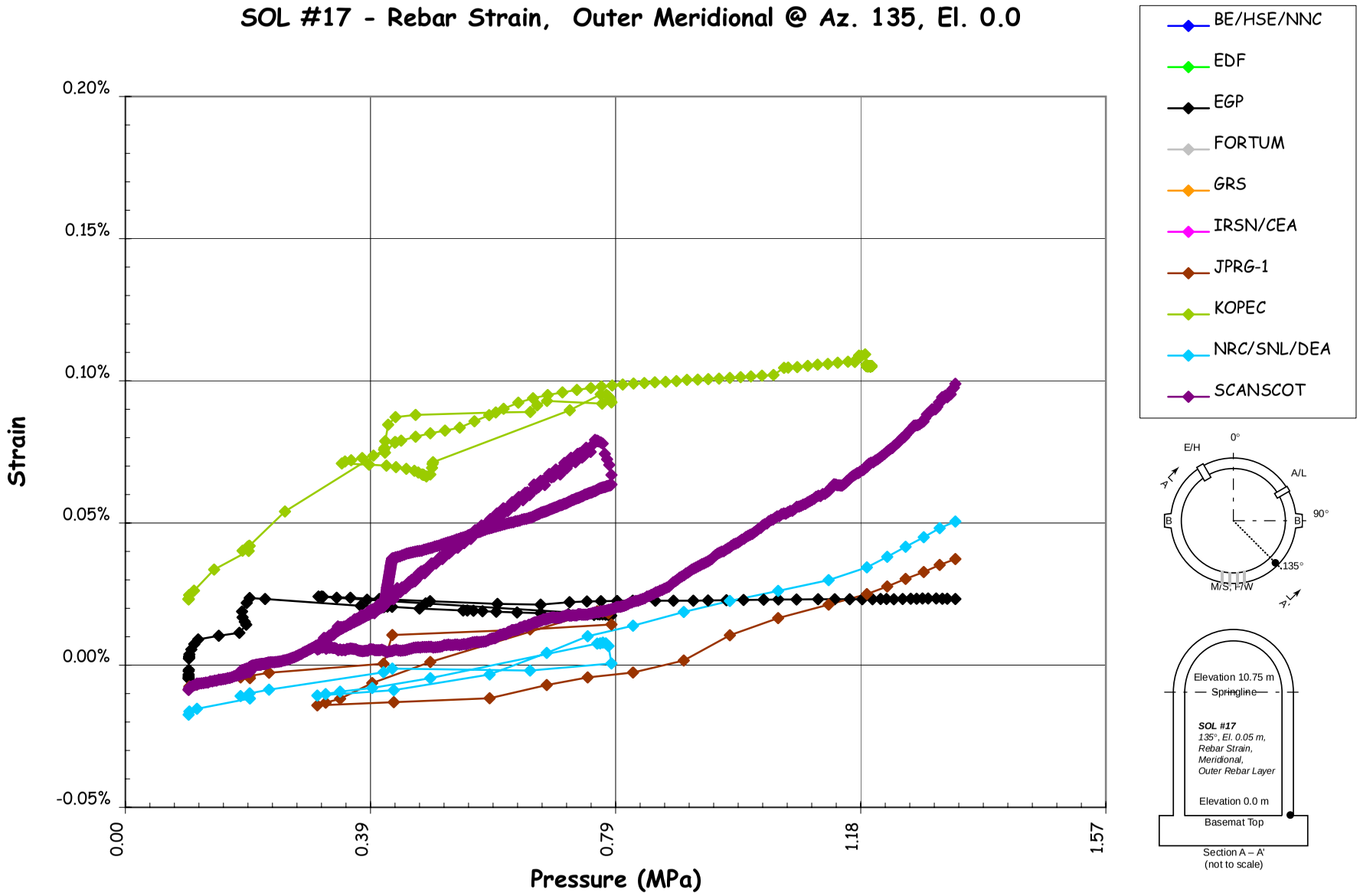
SOL #17 - Rebar Strain, Outer Meridional @ Az. 135, El. 0.0
Strain
0.20%
0.15%
0.10%
0.05%
0.00%
-0.05%
0.00
0.39
0.79
1.18
1.57
Pressure (MPa)
BE/HSE/NNC
EDF
EGP
FORTUM
GRS
IRSN/CEA
JPRG-1
KOPEC
NRC/SNL/DEA
SCANSCOT
0°
E/H
A/L
90°
135°
M/S, T/W
Elevation 10.75 m
Springline
SOL #17
135°, El. 0.05 m,
Rebar Strain,
Meridional,
Outer Rebar Layer
Elevation 0.0 m
Basemat Top
Section A – A'
(not to scale)

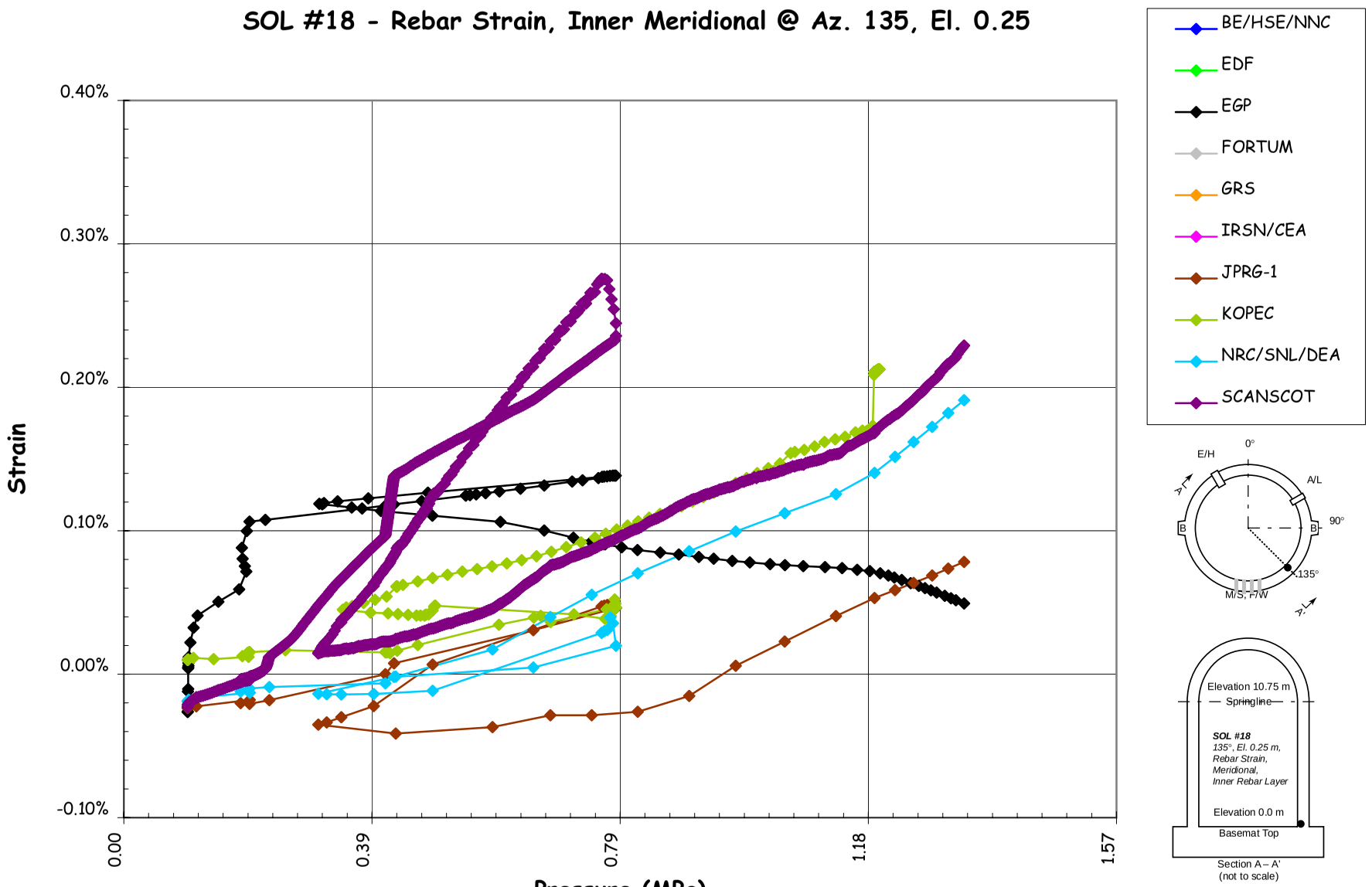
SOL #18 - Rebar Strain, Inner Meridional @ Az. 135, El. 0.25
Strain
0.40%
0.30%
0.20%
0.10%
0.00%
-0.10%
0.00
0.39
0.79
1.18
1.57
Pressure (MPa)
BE/HSE/NNC
EDF
EGP
FORTUM
GRS
IRSN/CEA
JPRG-1
KOPEC
NRC/SNL/DEA
SCANSCOT
0°
E/H
A/L
90°
135°
M/S, F/W
Elevation 10.75 m
Springline
SOL #18
135°, El. 0.25 m,
Rebar Strain,
Meridional,
Inner Rebar Layer
Elevation 0.0 m
Basemat Top
Section A – A'
(not to scale)

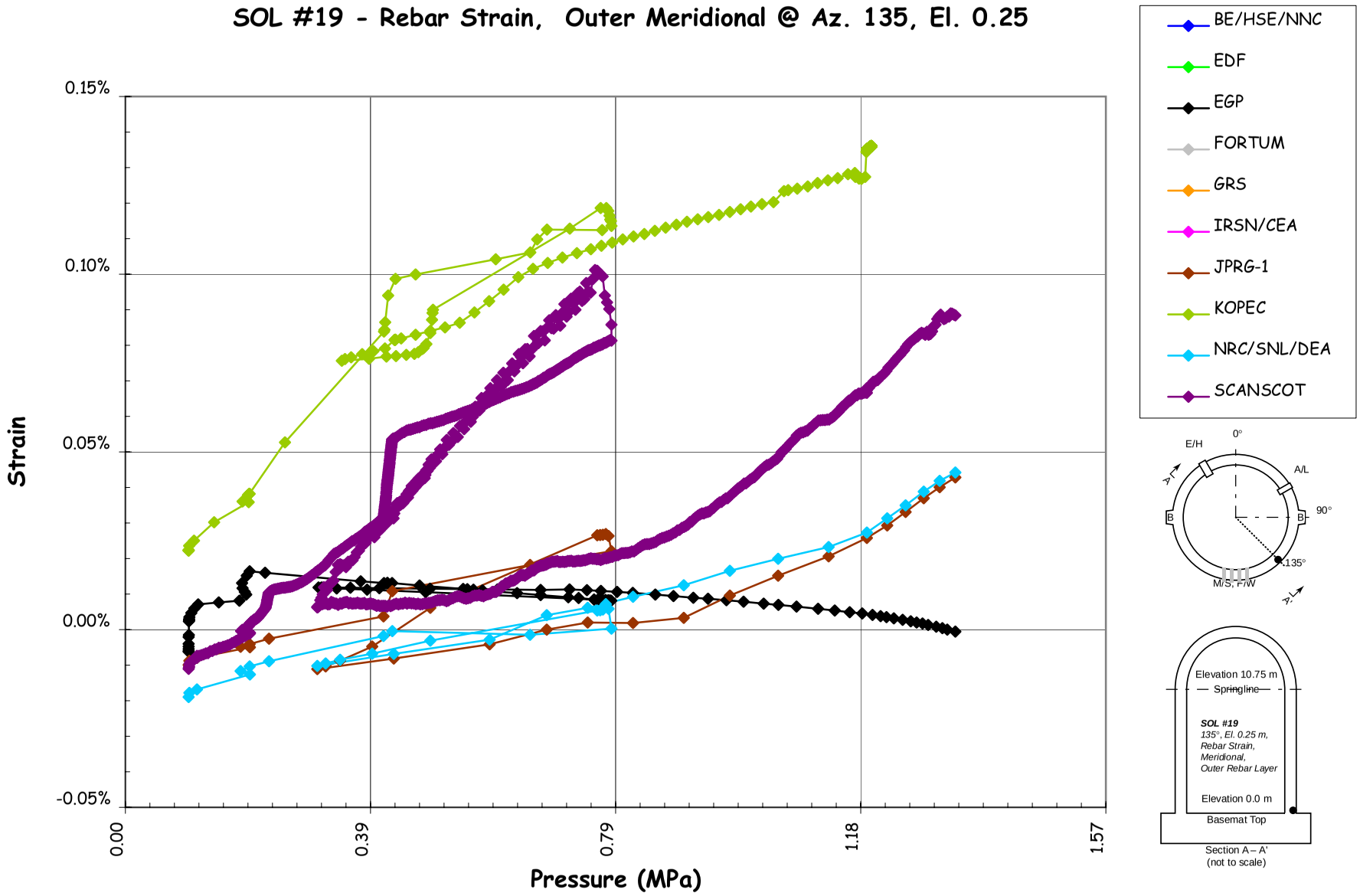
SOL #19 - Rebar Strain, Outer Meridional @ Az. 135, El. 0.25
Strain
0.15%
0.10%
0.05%
0.00%
-0.05%
0.00
0.39
0.79
1.18
1.57
Pressure (MPa)
BE/HSE/NNC
EDF
EGP
FORTUM
GRS
IRSN/CEA
JPRG-1
KOPEC
NRC/SNL/DEA
SCANSCOT
0°
E/H
A/L
90°
135°
M/S, F/W
Elevation 10.75 m
Springline
SOL #19
135°, El. 0.25 m,
Rebar Strain,
Meridional,
Outer Rebar Layer
Elevation 0.0 m
Basemat Top
Section A – A'
(not to scale)

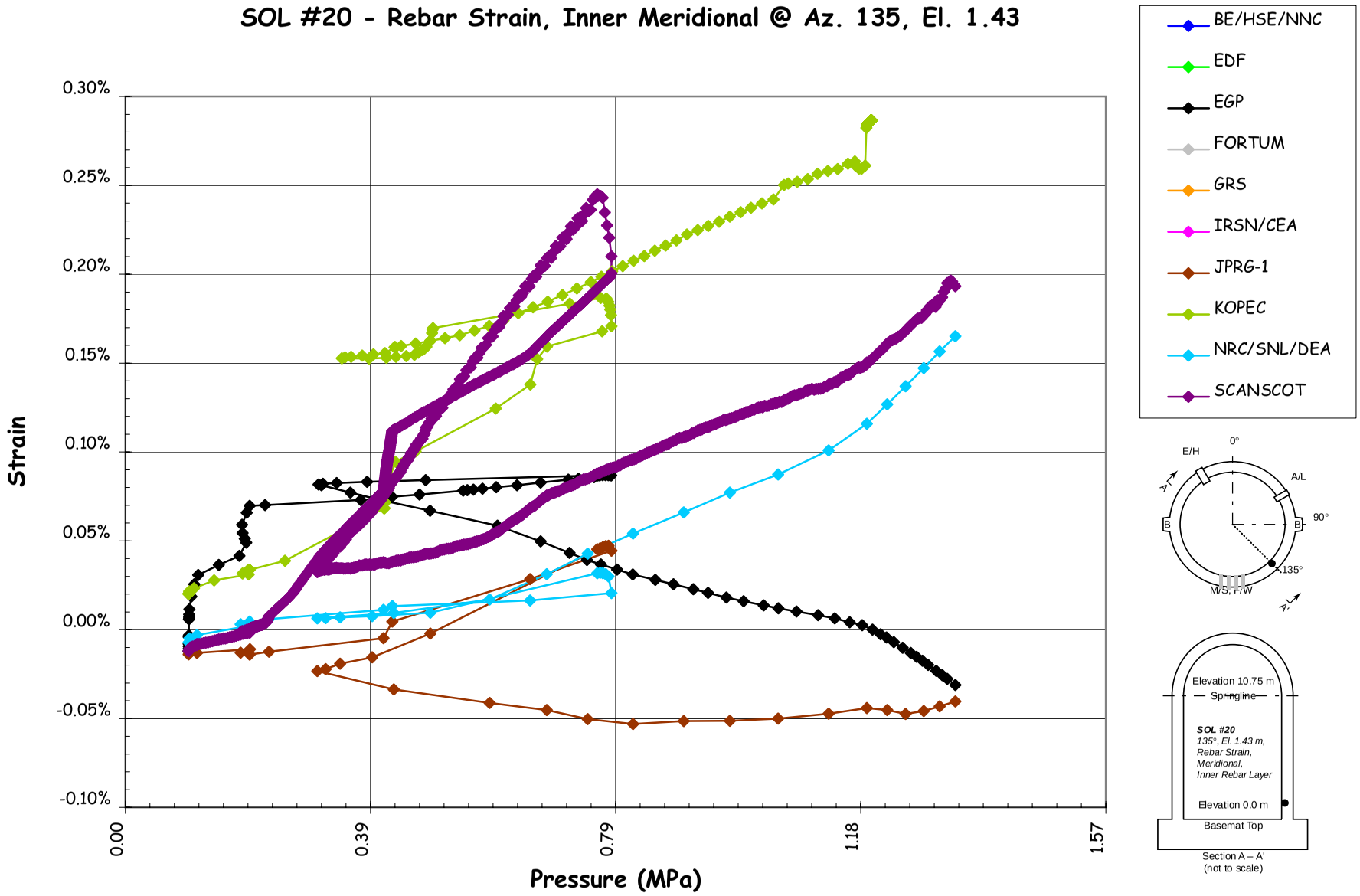
SOL #20 - Rebar Strain, Inner Meridional @ Az. 135, El. 1.43
Strain
0.30%
0.25%
0.20%
0.15%
0.10%
0.05%
0.00%
-0.05%
-0.10%
0.00
0.39
0.79
1.18
1.57
Pressure (MPa)
BE/HSE/NNC
EDF
EGP
FORTUM
GRS
IRSN/CEA
JPRG-1
KOPEC
NRC/SNL/DEA
SCANSCOT
0°
E/H
A/L
90°
B
135°
M/S; F/W
Elevation 10.75 m
Springline
SOL #20
135°, El. 1.43 m,
Rebar Strain,
Meridional,
Inner Rebar Layer
Elevation 0.0 m
Basemat Top
Section A – A'
(not to scale)

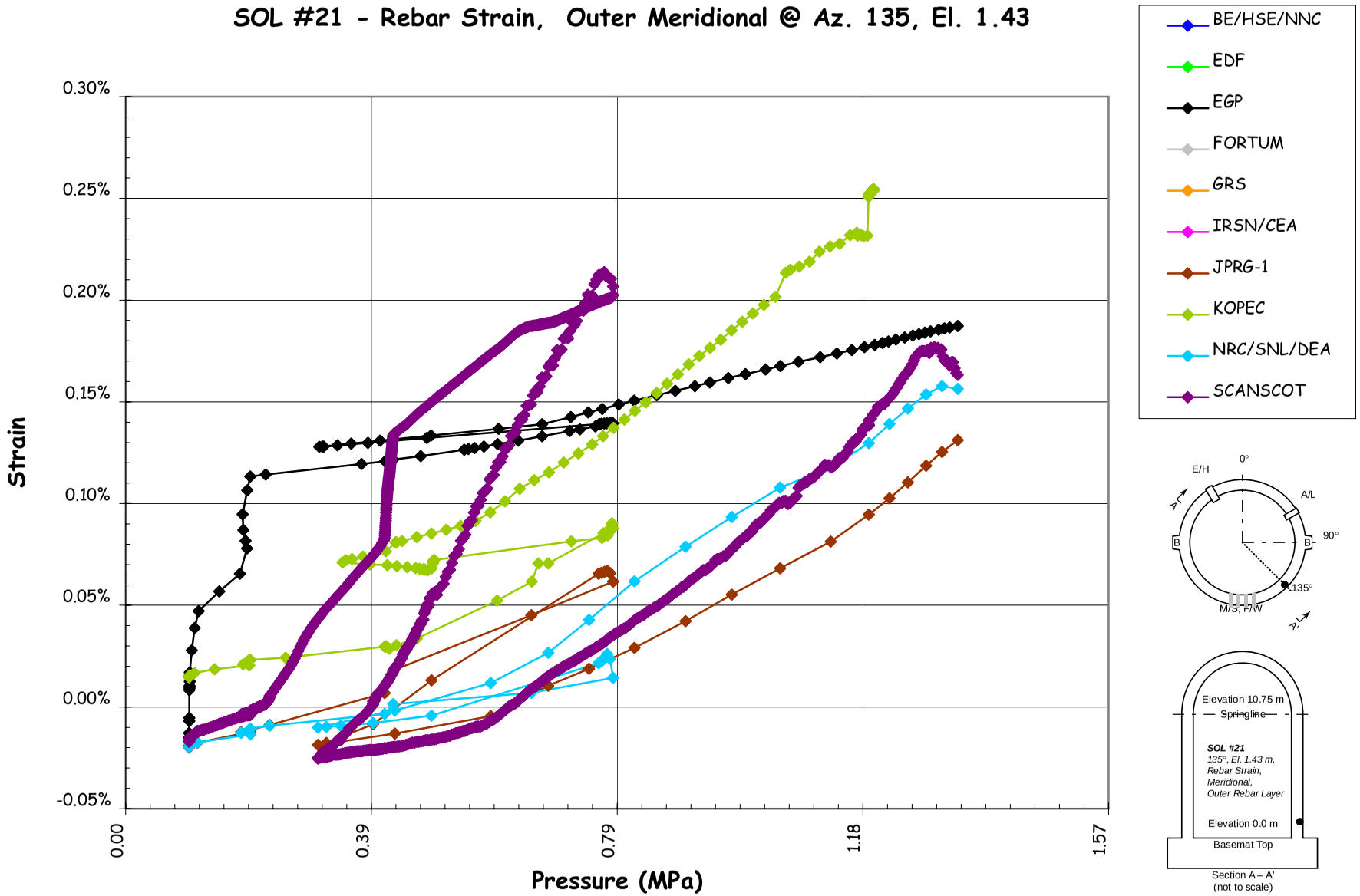
SOL #21 - Rebar Strain, Outer Meridional @ Az. 135, El. 1.43
Strain
0.30%
0.25%
0.20%
0.15%
0.10%
0.05%
0.00%
-0.05%
0.00
0.39
0.79
1.18
1.57
Pressure (MPa)
BE/HSE/NNC
EDF
EGP
FORTUM
GRS
IRSN/CEA
JPRG-1
KOPEC
NRC/SNL/DEA
SCANSCOT
0°
E/H
A/L
90°
135°
M/S, F/W
Elevation 10.75 m
Springline
SOL #21
135°, El. 1.43 m,
Rebar Strain,
Meridional,
Outer Rebar Layer
Elevation 0.0 m
Basemat Top
Section A – A'
(not to scale)

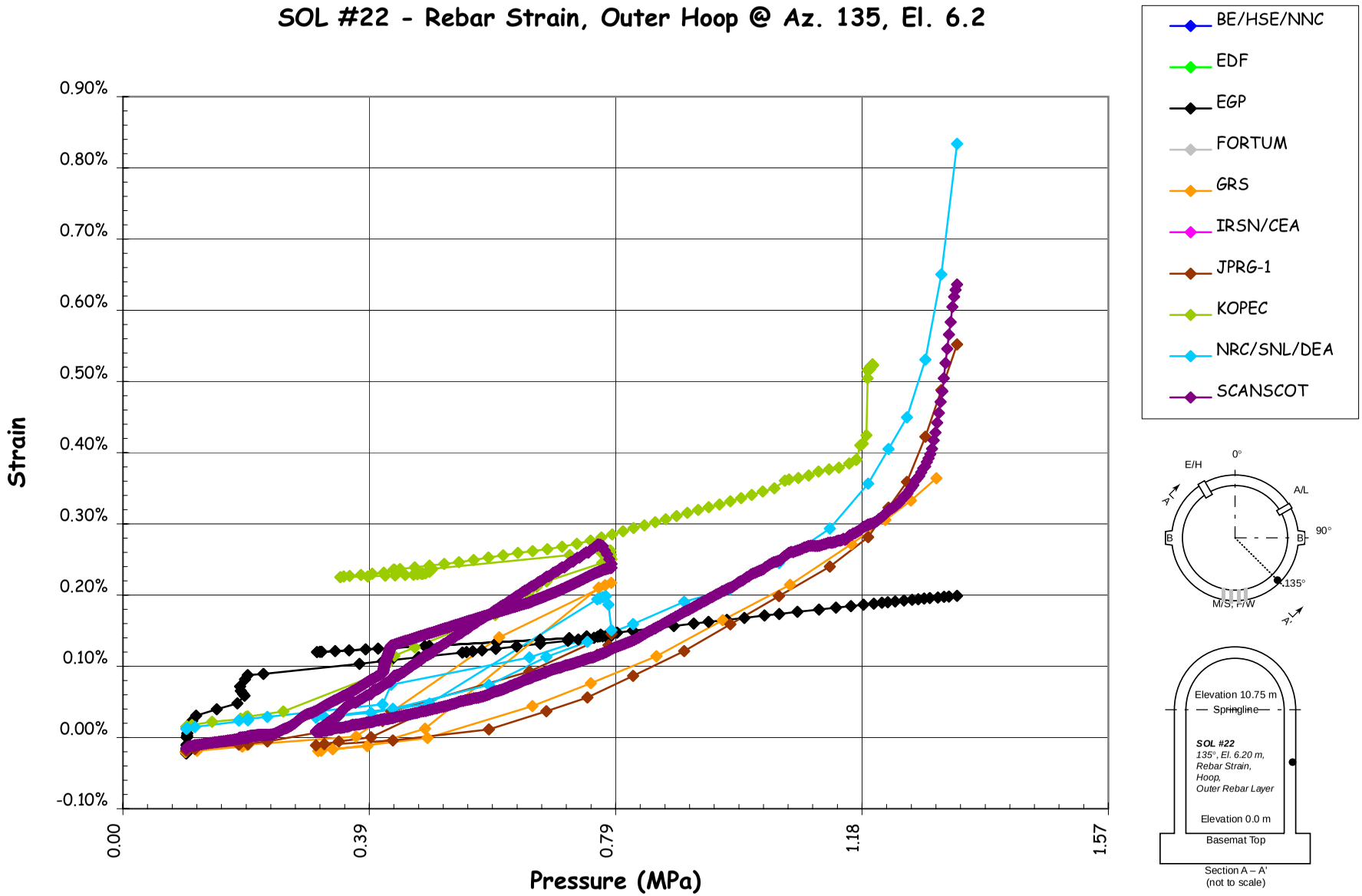
SOL #22 - Rebar Strain, Outer Hoop @ Az. 135, El. 6.2
Strain
0.90%
0.80%
0.70%
0.60%
0.50%
0.40%
0.30%
0.20%
0.10%
0.00%
-0.10%
0.00
0.39
0.79
1.18
1.57
Pressure (MPa)
BE/HSE/NNC
EDF
EGP
FORTUM
GRS
IRSN/CEA
JPRG-1
KOPEC
NRC/SNL/DEA
SCANSCOT
0°
E/H
A/L
90°
B
B
135°
M/S, F/W
A
A
Elevation 10.75 m
Springline
SOL #22
135°, El. 6.20 m,
Rebar Strain,
Hoop,
Outer Rebar Layer
Elevation 0.0 m
Basemat Top
Section A – A'
(not to scale)

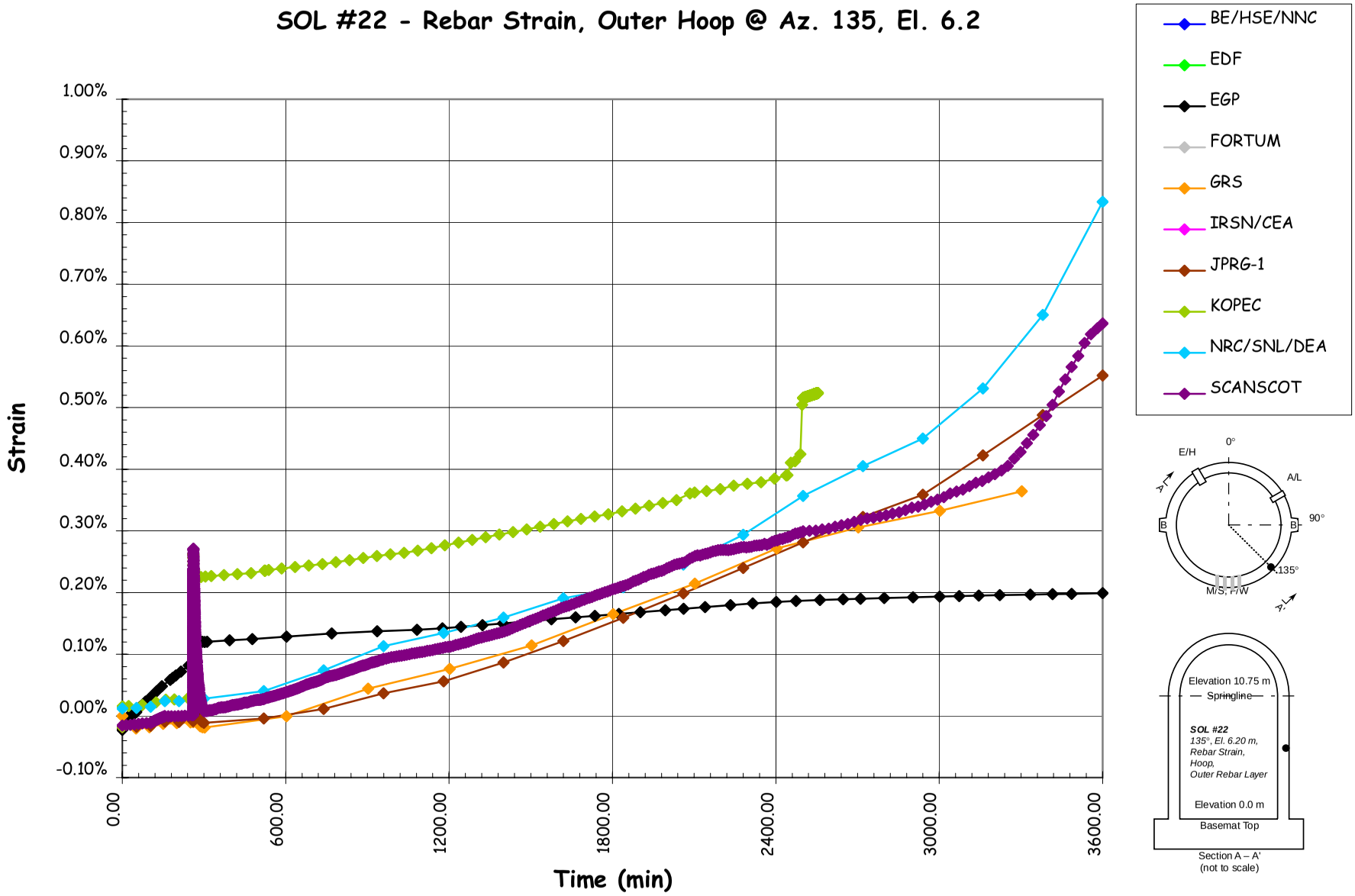
SOL #22 - Rebar Strain, Outer Hoop @ Az. 135, El. 6.2
Strain
1.00%
0.90%
0.80%
0.70%
0.60%
0.50%
0.40%
0.30%
0.20%
0.10%
0.00%
-0.10%
0.00
600.00
1200.00
1800.00
2400.00
3000.00
3600.00
Time (min)
BE/HSE/NNC
EDF
EGP
FORTUM
GRS
IRSN/CEA
JPRG-1
KOPEC
NRC/SNL/DEA
SCANSCOT
0°
E/H
A/L
90°
135°
M/S; F/W
Elevation 10.75 m
Springline
SOL #22
135°, El. 6.20 m,
Rebar Strain,
Hoop,
Outer Rebar Layer
Elevation 0.0 m
Basemat Top
Section A – A'
(not to scale)

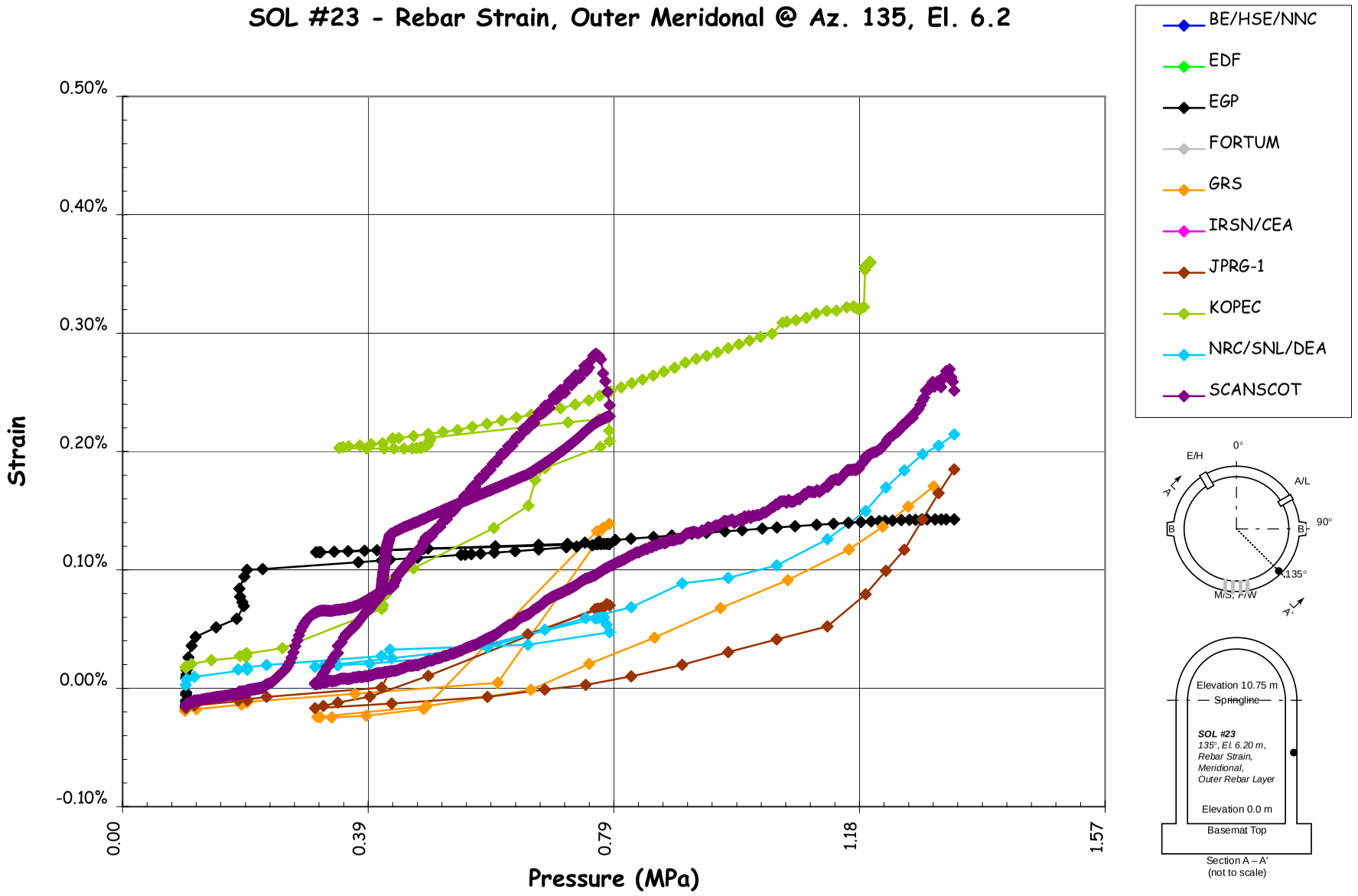
SOL #23 - Rebar Strain, Outer Meridonal @ Az. 135, El. 6.2
Strain
0.50%
0.40%
0.30%
0.20%
0.10%
0.00%
-0.10%
0.00
0.39
0.79
1.18
1.57
Pressure (MPa)
BE/HSE/NNC
EDF
EGP
FORTUM
GRS
IRSN/CEA
JPRG-1
KOPEC
NRC/SNL/DEA
SCANSCOT
0°
E/H
A/L
90°
135°
M/S, F/W
Elevation 10.75 m
Springline
SOL #23
135°, El. 6.20 m,
Rebar Strain,
Meridional,
Outer Rebar Layer
Elevation 0.0 m
Basemat Top
Section A – A'
(not to scale)

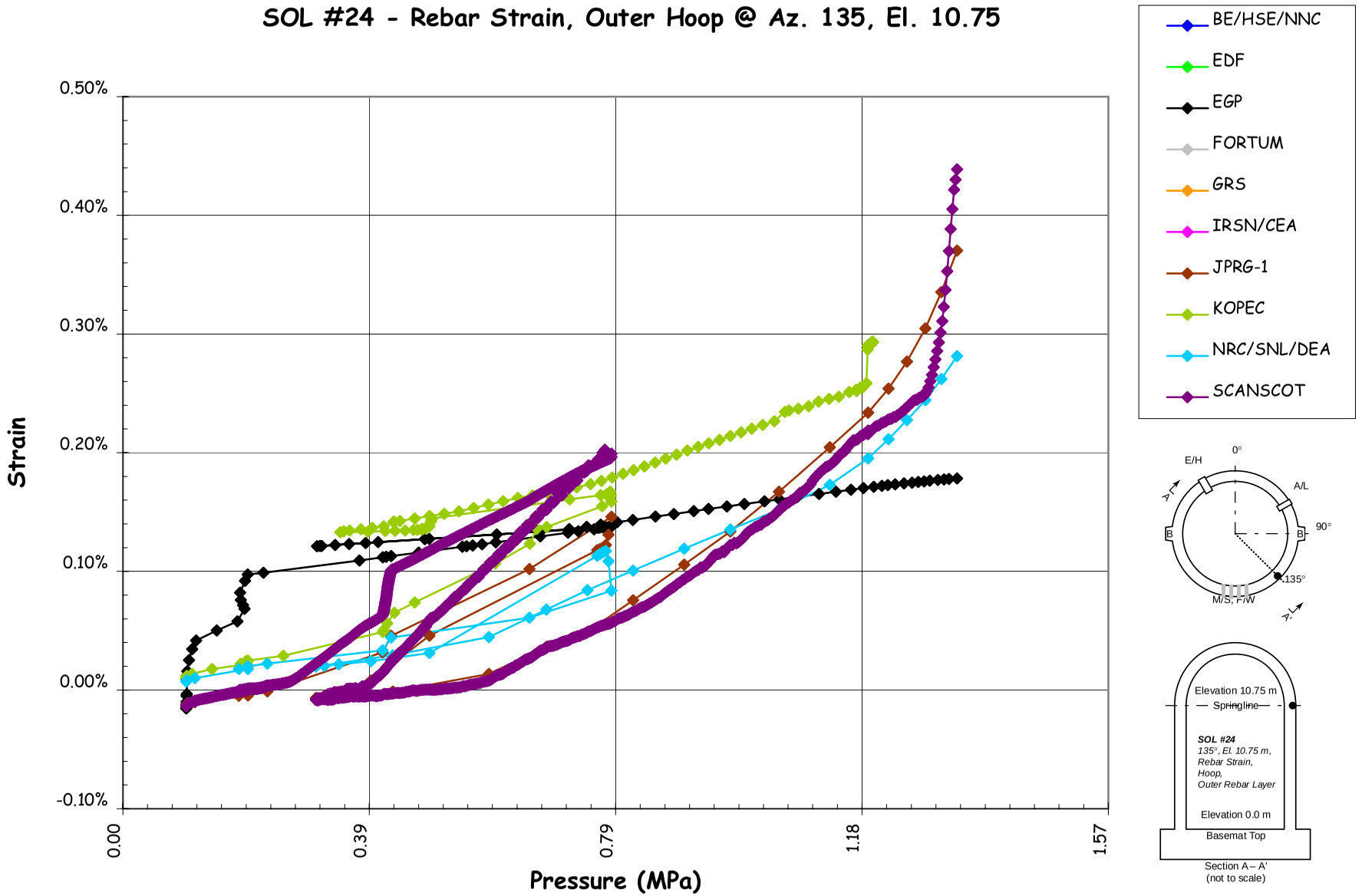
SOL #24 - Rebar Strain, Outer Hoop @ Az. 135, El. 10.75
Strain
0.50%
0.40%
0.30%
0.20%
0.10%
0.00%
-0.10%
0.00
0.39
0.79
1.18
1.57
Pressure (MPa)
BE/HSE/NNC
EDF
EGP
FORTUM
GRS
IRSN/CEA
JPRG-1
KOPEC
NRC/SNL/DEA
SCANSCOT
E/H
A/L
0°
90°
135°
M/S, F/W
Elevation 10.75 m
Springline
SOL #24
135°, El. 10.75 m,
Rebar Strain,
Hoop,
Outer Rebar Layer
Elevation 0.0 m
Basemat Top
Section A – A'
(not to scale)

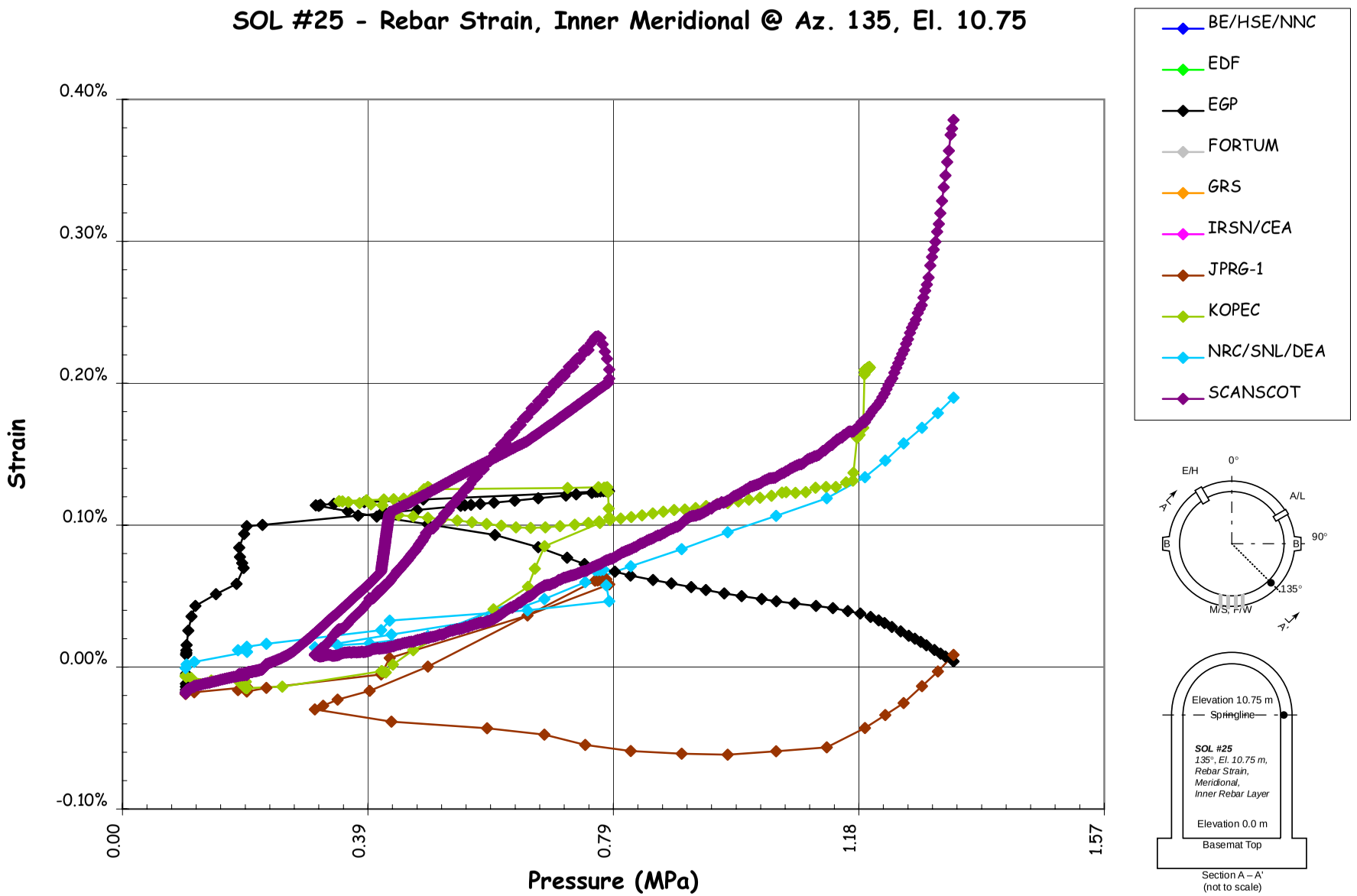
SOL #25 - Rebar Strain, Inner Meridional @ Az. 135, El. 10.75
Strain
0.40%
0.30%
0.20%
0.10%
0.00%
-0.10%
0.00
0.39
0.79
1.18
1.57
Pressure (MPa)
BE/HSE/NNC
EDF
EGP
FORTUM
GRS
IRSN/CEA
JPRG-1
KOPEC
NRC/SNL/DEA
SCANSCOT
0°
E/H
A/L
90°
135°
M/S, F/W
Elevation 10.75 m
Springline
SOL #25
135°, El. 10.75 m,
Rebar Strain,
Meridional,
Inner Rebar Layer
Elevation 0.0 m
Basemat Top
Section A – A'
(not to scale)

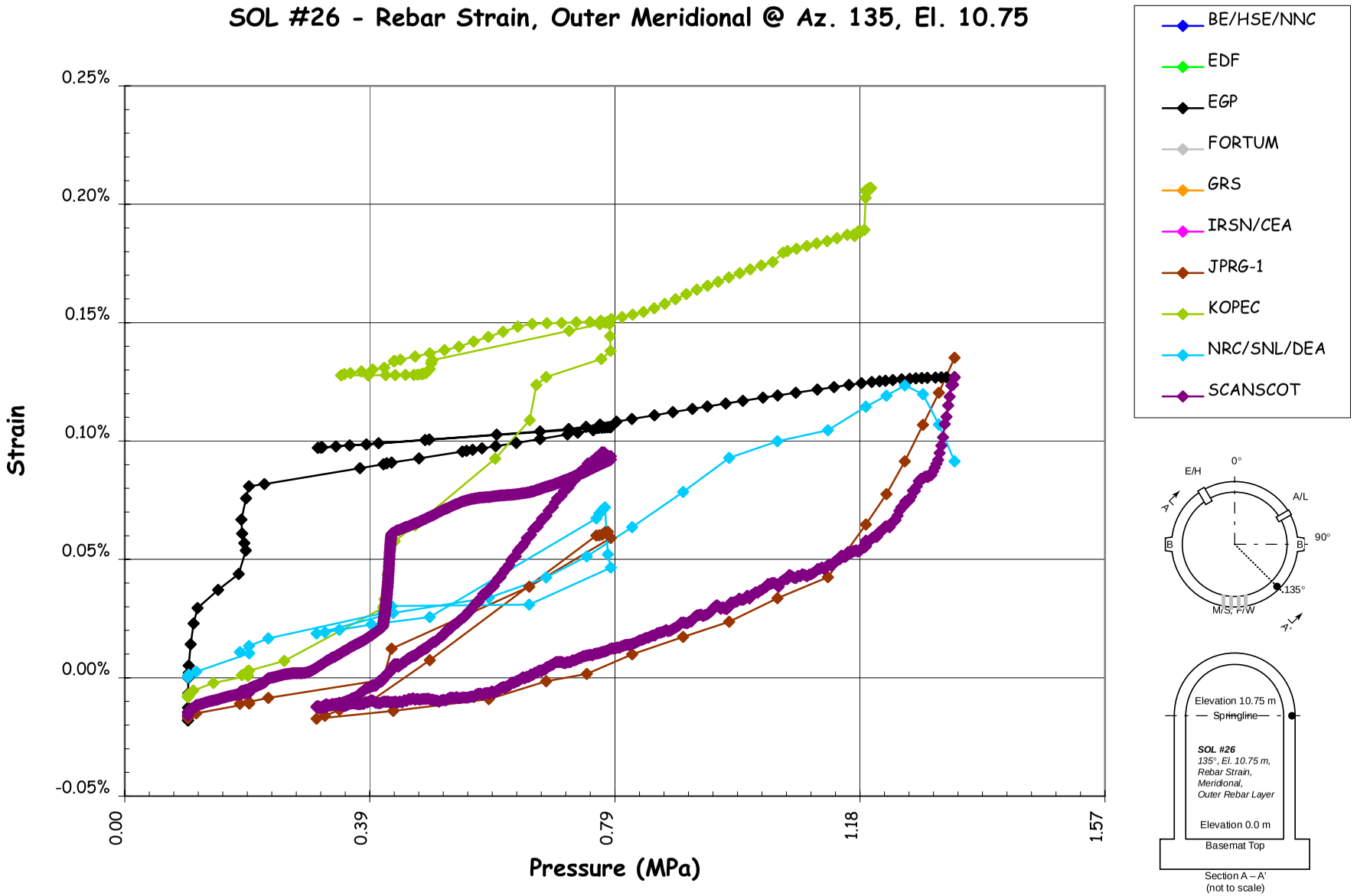
SOL #26 - Rebar Strain, Outer Meridional @ Az. 135, El. 10.75
Strain
0.25%
0.20%
0.15%
0.10%
0.05%
0.00%
-0.05%
0.00
0.39
0.79
1.18
1.57
Pressure (MPa)
BE/HSE/NNC
EDF
EGP
FORTUM
GRS
IRSN/CEA
JPRG-1
KOPEC
NRC/SNL/DEA
SCANSCOT
0°
E/H
A/L
90°
135°
M/S, P/W
Elevation 10.75 m
Springline
SOL #26
135°, El. 10.75 m,
Rebar Strain,
Meridional,
Outer Rebar Layer
Elevation 0.0 m
Basemat Top
Section A – A'
(not to scale)

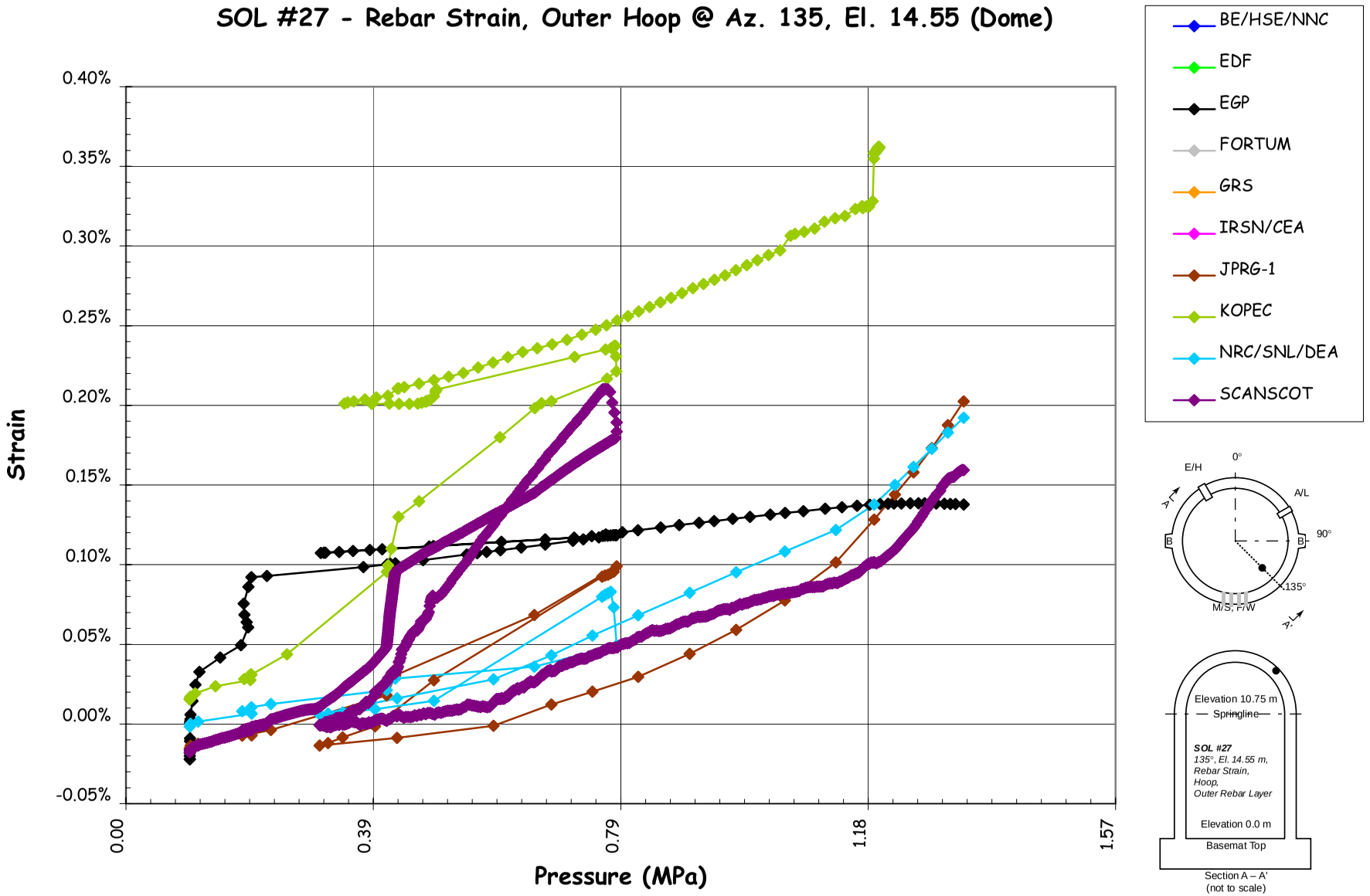
SOL #27 - Rebar Strain, Outer Hoop @ Az. 135, El. 14.55 (Dome)
Strain
0.40%
0.35%
0.30%
0.25%
0.20%
0.15%
0.10%
0.05%
0.00%
-0.05%
0.00
0.39
0.79
1.18
1.57
Pressure (MPa)
BE/HSE/NNC
EDF
EGP
FORTUM
GRS
IRSN/CEA
JPRG-1
KOPEC
NRC/SNL/DEA
SCANSCOT
E/H
0°
A/L
90°
135°
M/S, F/W
Elevation 10.75 m
Springline
SOL #27
135°, El. 14.55 m,
Rebar Strain,
Hoop,
Outer Rebar Layer
Elevation 0.0 m
Basemat Top
Section A – A'
(not to scale)

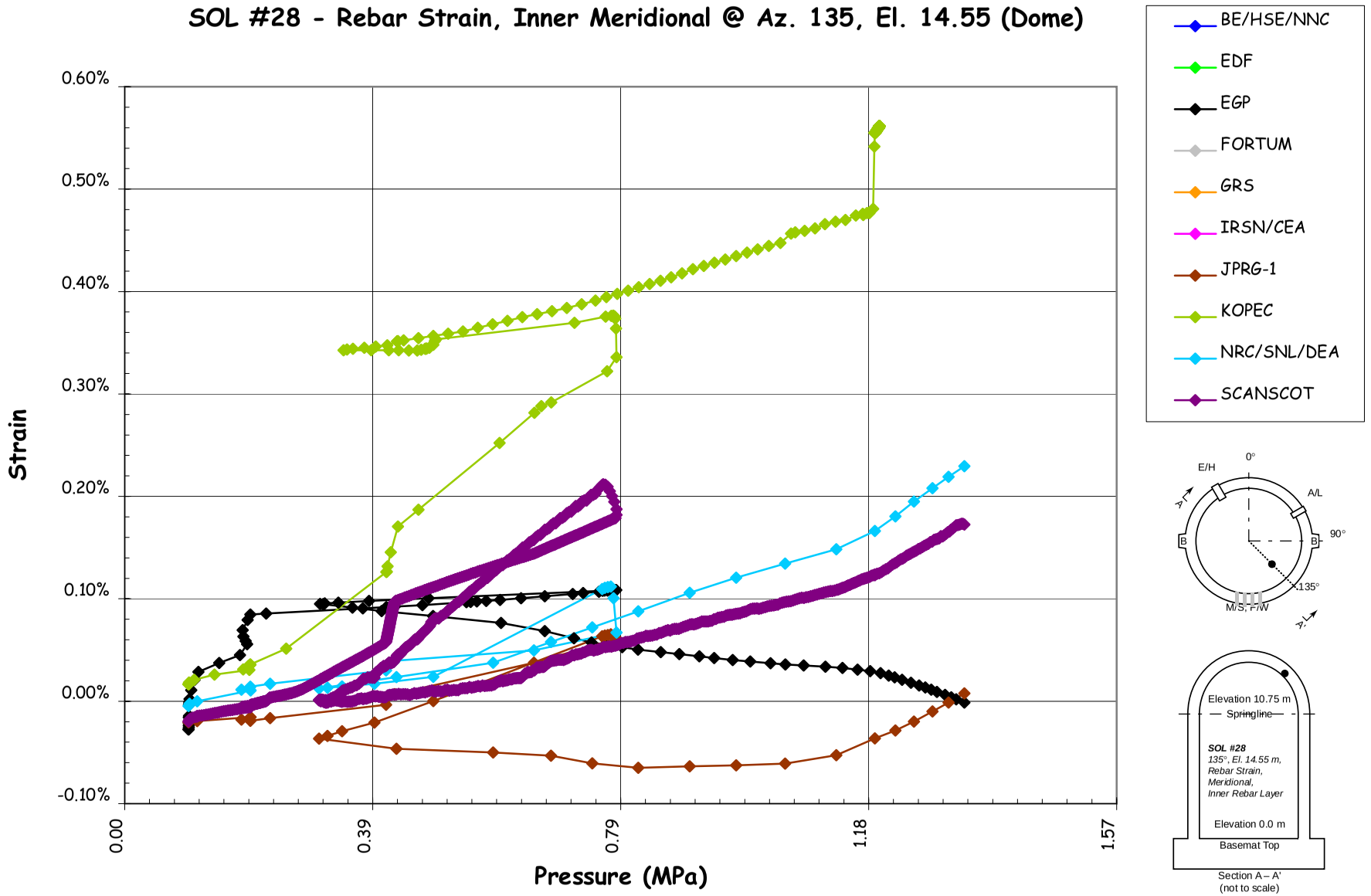
SOL #28 - Rebar Strain, Inner Meridional @ Az. 135, El. 14.55 (Dome)
Strain
0.60%
0.50%
0.40%
0.30%
0.20%
0.10%
0.00%
-0.10%
0.00
0.39
0.79
1.18
1.57
Pressure (MPa)
BE/HSE/NNC
EDF
EGP
FORTUM
GRS
IRSN/CEA
JPRG-1
KOPEC
NRC/SNL/DEA
SCANSCOT
0°
E/H
A/L
90°
135°
M/S, F/W
Elevation 10.75 m
Springline
SOL #28
135°, El. 14.55 m,
Rebar Strain,
Meridional,
Inner Rebar Layer
Elevation 0.0 m
Basemat Top
Section A – A'
(not to scale)

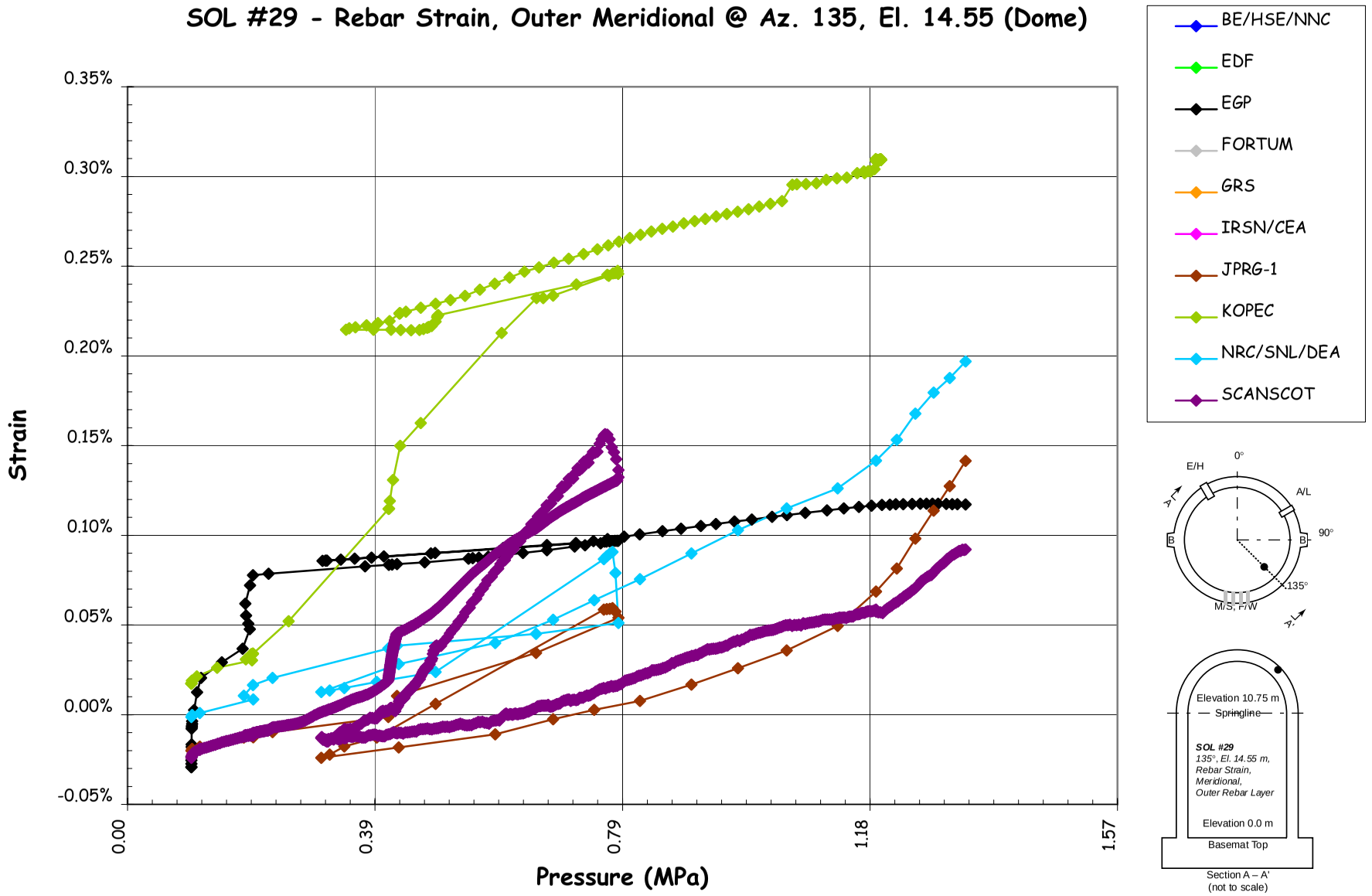
SOL #29 - Rebar Strain, Outer Meridional @ Az. 135, El. 14.55 (Dome)
Strain
0.35%
0.30%
0.25%
0.20%
0.15%
0.10%
0.05%
0.00%
-0.05%
0.00
0.39
0.79
1.18
1.57
Pressure (MPa)
BE/HSE/NNC
EDF
EGP
FORTUM
GRS
IRSN/CEA
JPRG-1
KOPEC
NRC/SNL/DEA
SCANSCOT
0°
E/H
A/L
90°
135°
M/S, F/W
Elevation 10.75 m
Springline
SOL #29
135°, El. 14.55 m,
Rebar Strain,
Meridional,
Outer Rebar Layer
Elevation 0.0 m
Basemat Top
Section A – A'
(not to scale)

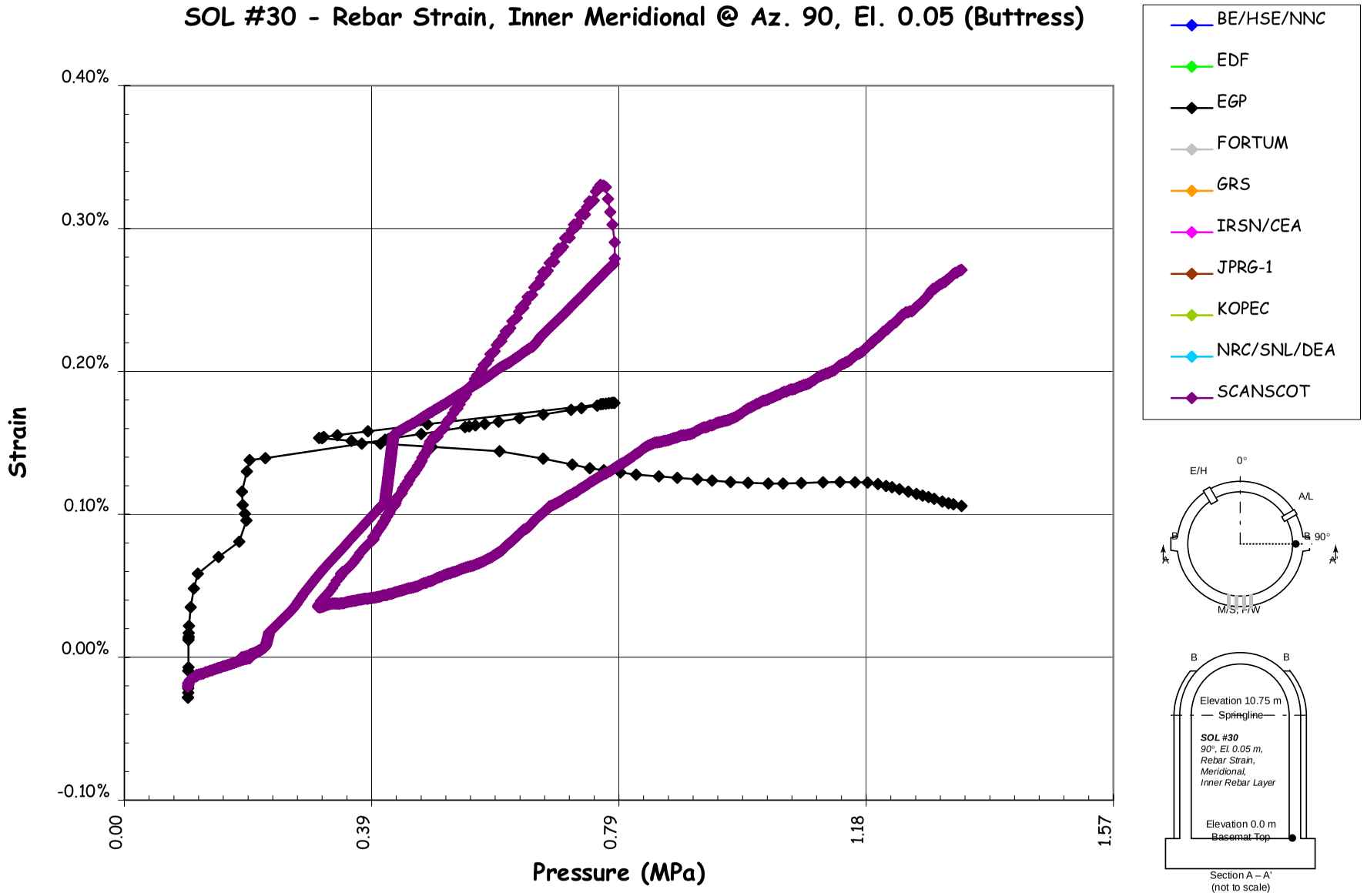
SOL #30 - Rebar Strain, Inner Meridional @ Az. 90, El. 0.05 (Buttress)
Strain
0.40%
0.30%
0.20%
0.10%
0.00%
-0.10%
0.00
0.39
0.79
1.18
1.57
Pressure (MPa)
BE/HSE/NNC
EDF
EGP
FORTUM
GRS
IRSN/CEA
JPRG-1
KOPEC
NRC/SNL/DEA
SCANSCOT
0°
E/H
A/L
B
B
90°
M/S, F/W
B
B
Elevation 10.75 m
Springline
SOL #30
90°, El. 0.05 m,
Rebar Strain,
Meridional,
Inner Rebar Layer
Elevation 0.0 m
Basemat Top
Section A – A'
(not to scale)

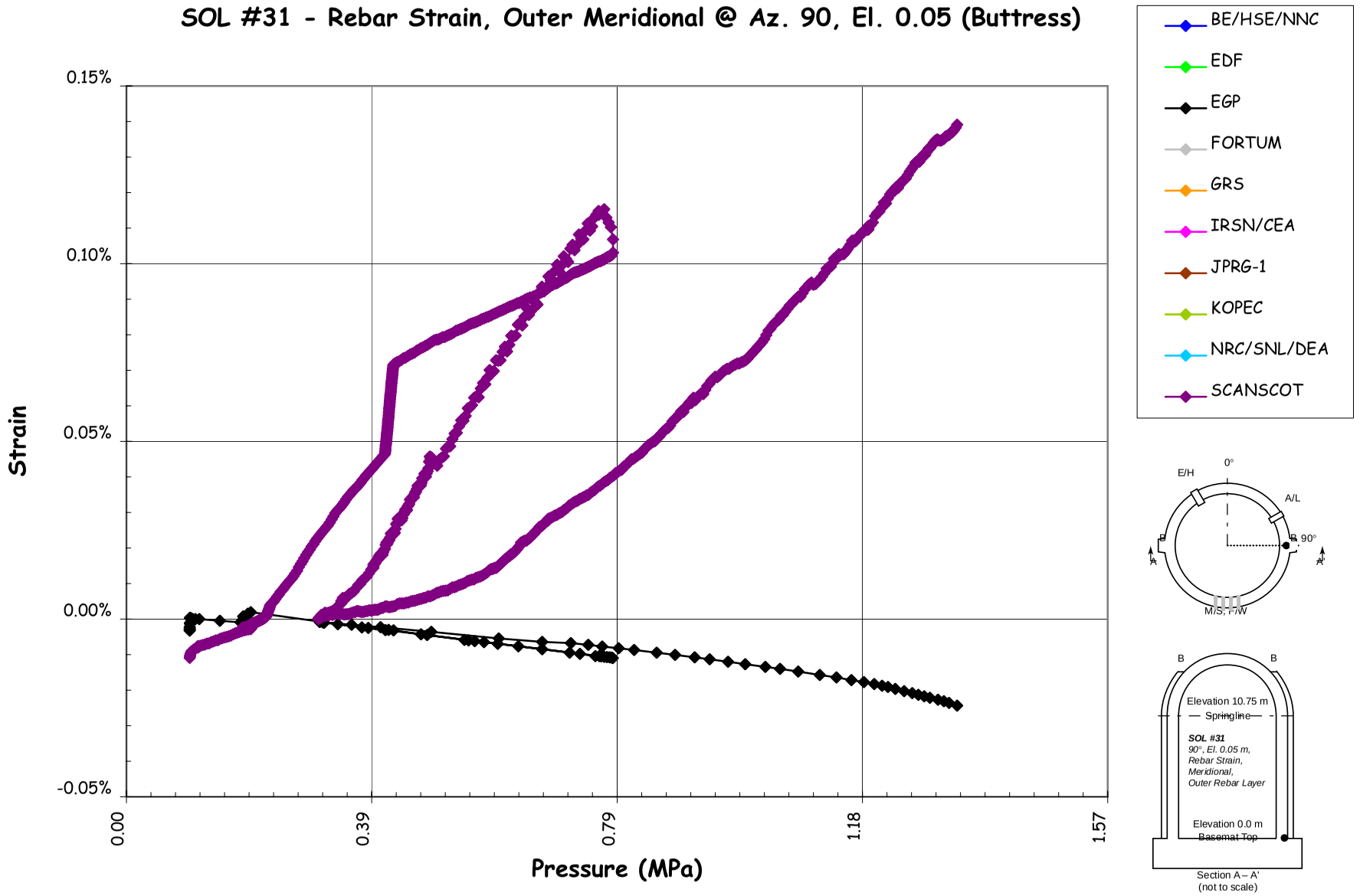
SOL #31 - Rebar Strain, Outer Meridional @ Az. 90, El. 0.05 (Buttress)
Strain
0.15%
0.10%
0.05%
0.00%
-0.05%
0.00
0.39
0.79
1.18
1.57
Pressure (MPa)
BE/HSE/NNC
EDF
EGP
FORTUM
GRS
IRSN/CEA
JPRG-1
KOPEC
NRC/SNL/DEA
SCANSCOT
0°
E/H
A/L
90°
M/S, F/W
B
B
Elevation 10.75 m
Springline
SOL #31
90°, El. 0.05 m,
Rebar Strain,
Meridional,
Outer Rebar Layer
Elevation 0.0 m
Basemat Top
Section A – A'
(not to scale)

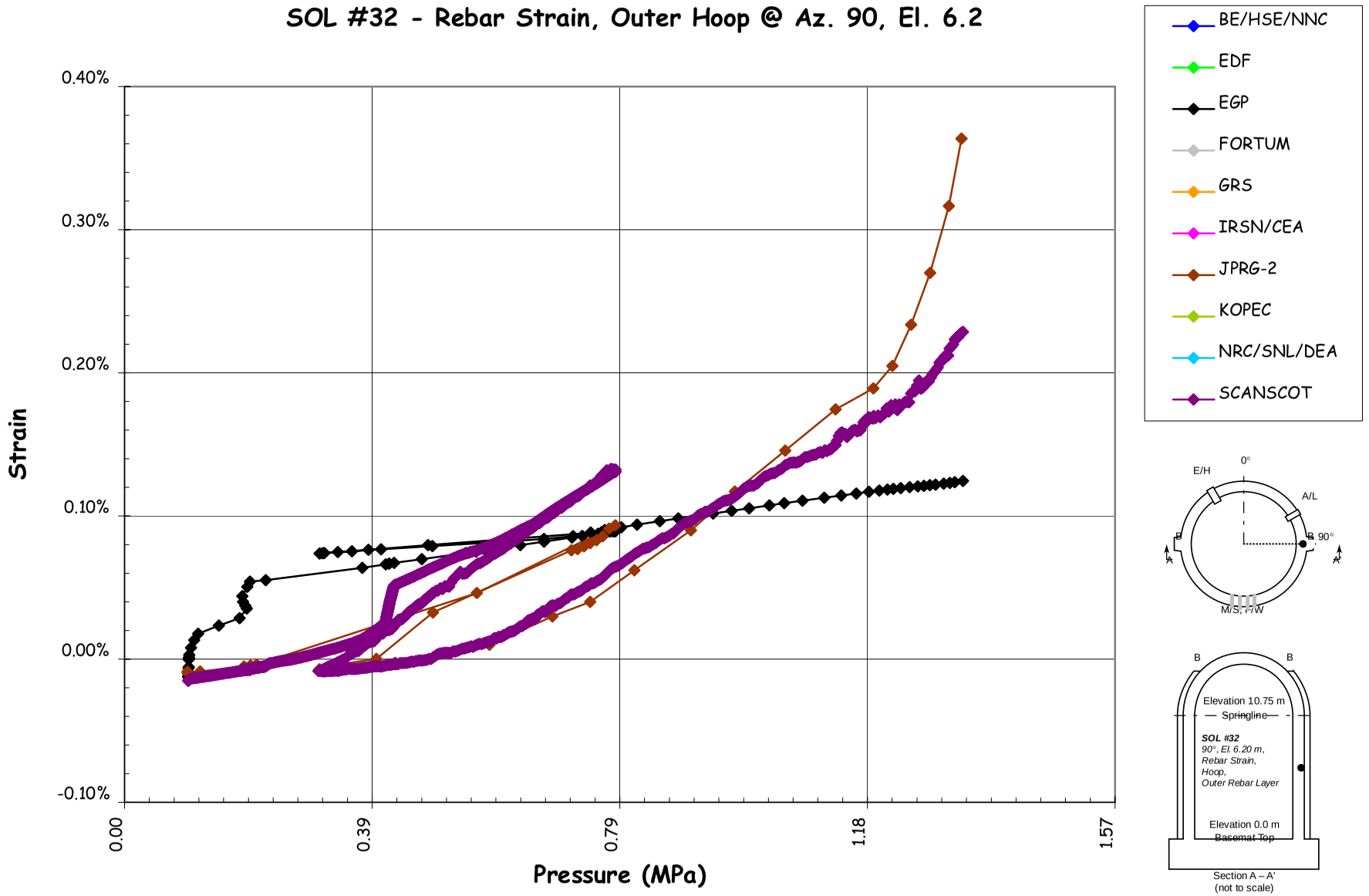
SOL #32 - Rebar Strain, Outer Hoop @ Az. 90, El. 6.2
Strain
0.40%
0.30%
0.20%
0.10%
0.00%
-0.10%
0.00
0.39
0.79
1.18
1.57
Pressure (MPa)
BE/HSE/NNC
EDF
EGP
FORTUM
GRS
IRSN/CEA
JPRG-2
KOPEC
NRC/SNL/DEA
SCANSCOT
0°
E/H
A/L
B
B
90°
A
A'
M/S, F/W
B
B
Elevation 10.75 m
Springline
SOL #32
90°, El. 6.20 m,
Rebar Strain,
Hoop,
Outer Rebar Layer
Elevation 0.0 m
Basemat Top
Section A – A'
(not to scale)

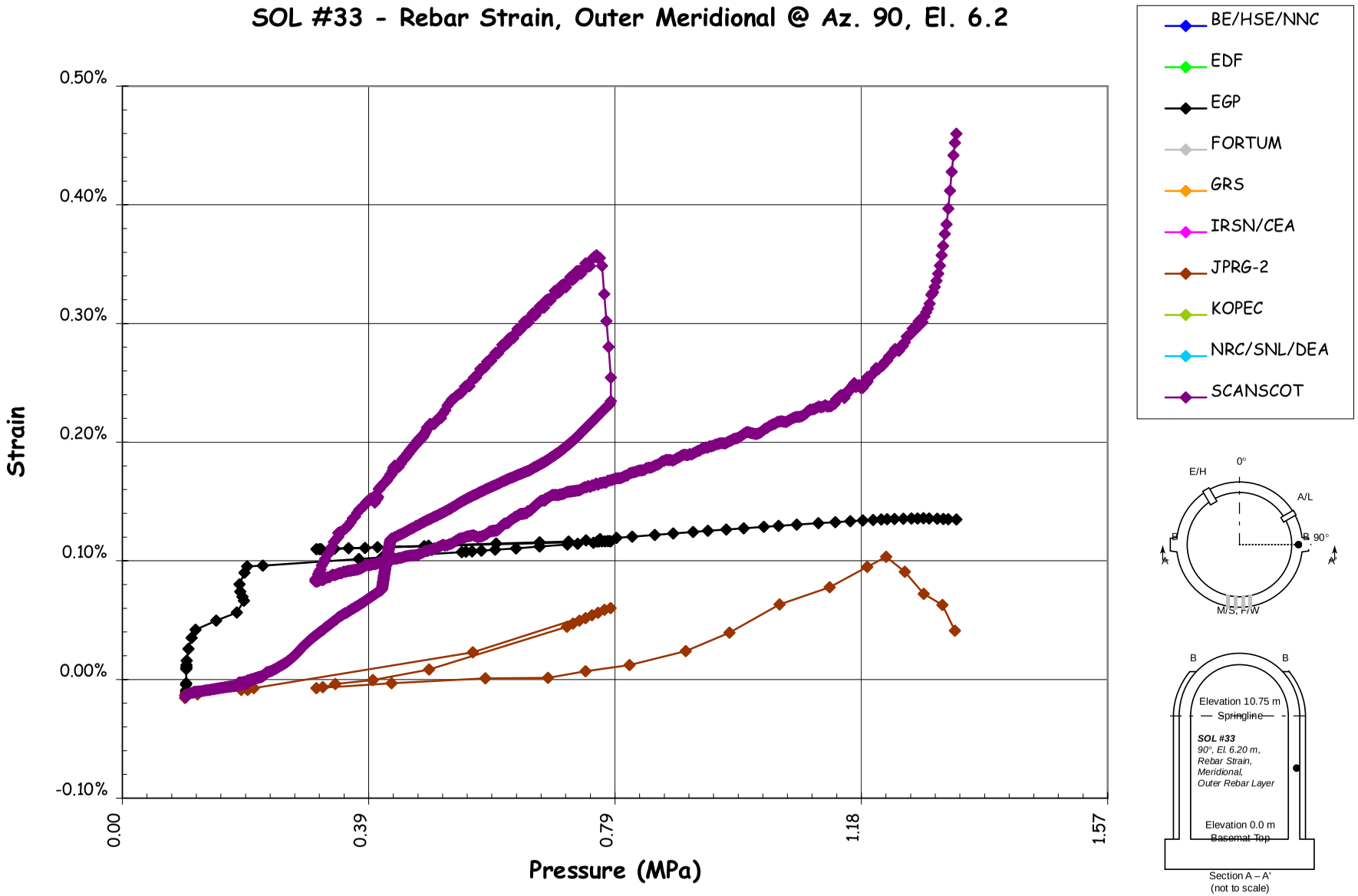
SOL #33 - Rebar Strain, Outer Meridional @ Az. 90, El. 6.2
Strain
0.50%
0.40%
0.30%
0.20%
0.10%
0.00%
-0.10%
0.00
0.39
0.79
1.18
1.57
Pressure (MPa)
BE/HSE/NNC
EDF
EGP
FORTUM
GRS
IRSN/CEA
JPRG-2
KOPEC
NRC/SNL/DEA
SCANSCOT
0°
E/H
A/L
B
B
90°
A
A'
M/S, F/W
B
B
Elevation 10.75 m
Springline
SOL #33
90°, El. 6.20 m,
Rebar Strain,
Meridional,
Outer Rebar Layer
Elevation 0.0 m
Basemat Top
Section A – A'
(not to scale)

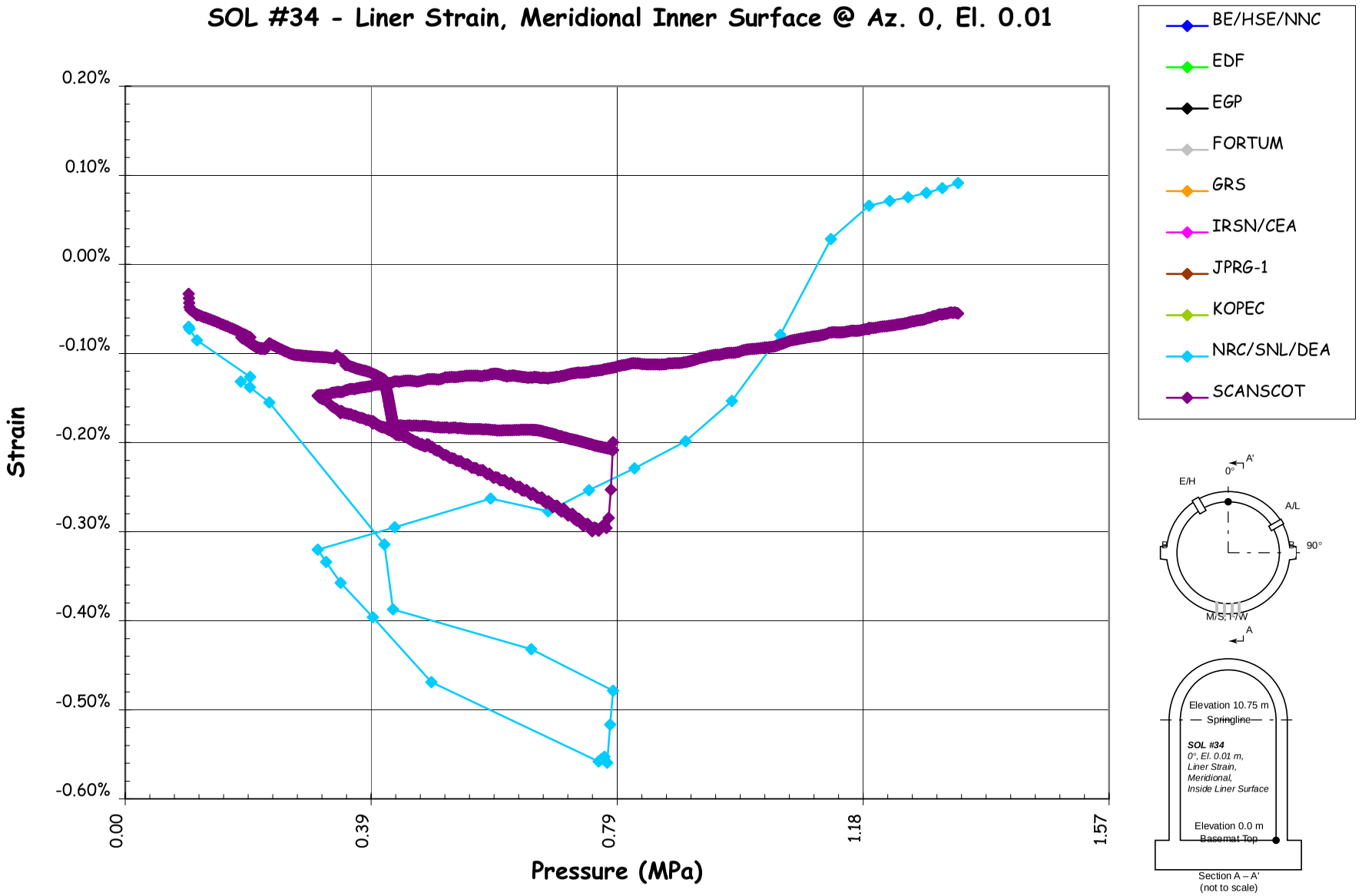
SOL #34 - Liner Strain, Meridional Inner Surface @ Az. 0, El. 0.01
Strain
0.20%
0.10%
0.00%
-0.10%
-0.20%
-0.30%
-0.40%
-0.50%
-0.60%
0.00
0.39
0.79
1.18
1.57
Pressure (MPa)
BE/HSE/NNC
EDF
EGP
FORTUM
GRS
IRSN/CEA
JPRG-1
KOPEC
NRC/SNL/DEA
SCANSCOT
A'
0°
E/H
A/L
90°
M/S, I-W
A
Elevation 10.75 m
Springline
SOL #34
0°, El. 0.01 m,
Liner Strain,
Meridional,
Inside Liner Surface
Elevation 0.0 m
Basemat Top
Section A – A'
(not to scale)

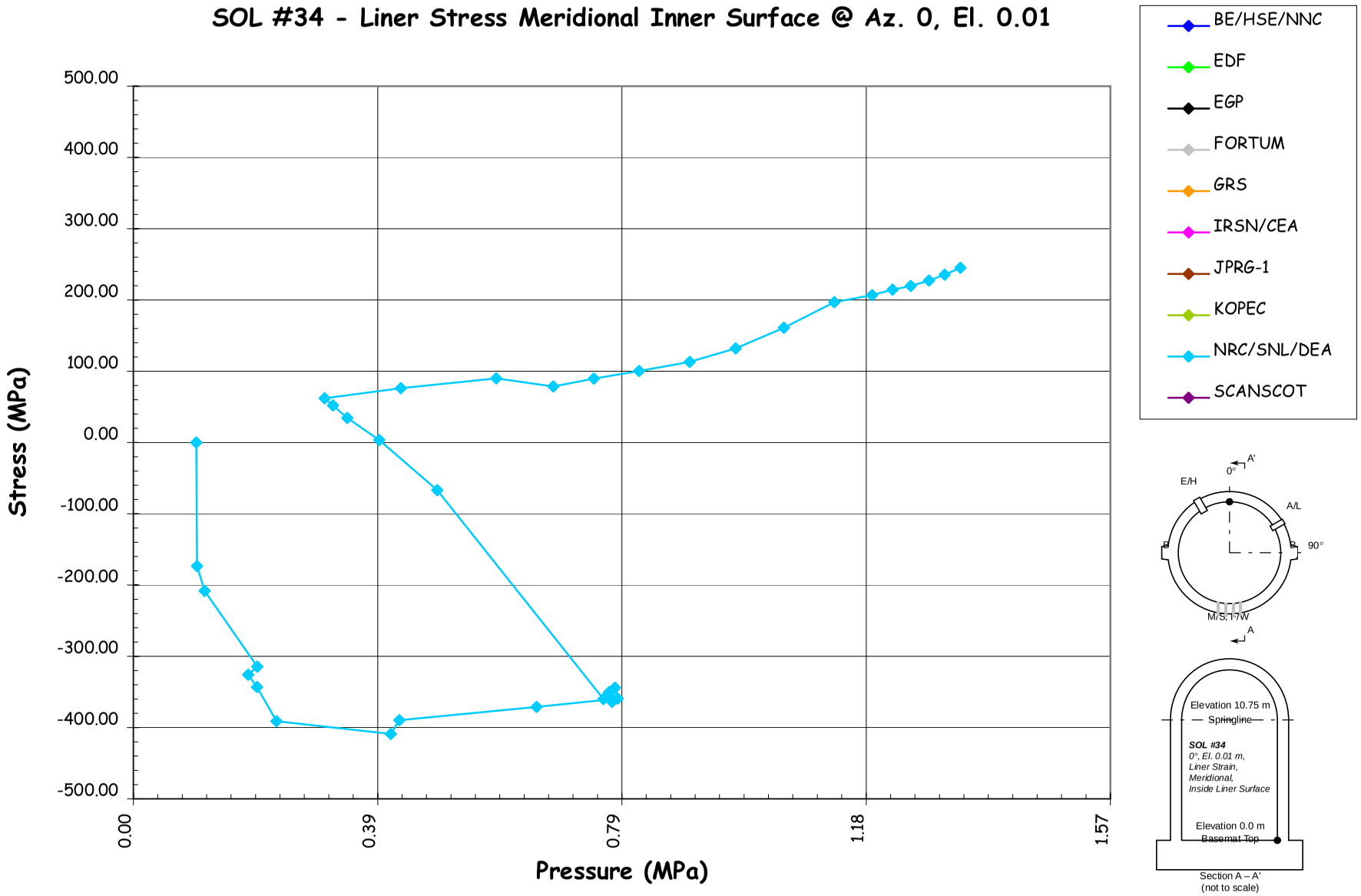
SOL #34 - Liner Stress Meridional Inner Surface @ Az. 0, El. 0.01
Stress (MPa)
500.00
400.00
300.00
200.00
100.00
0.00
-100.00
-200.00
-300.00
-400.00
-500.00
0.00
0.39
0.79
1.18
1.57
Pressure (MPa)
BE/HSE/NNC
EDF
EGP
FORTUM
GRS
IRSN/CEA
JPRG-1
KOPEC
NRC/SNL/DEA
SCANSCOT
A'
0°
E/H
A/L
90°
M/S, I-W
A
Elevation 10.75 m
Springline
SOL #34
0°, El. 0.01 m,
Liner Strain,
Meridional,
Inside Liner Surface
Elevation 0.0 m
Basemat Top
Section A – A'
(not to scale)

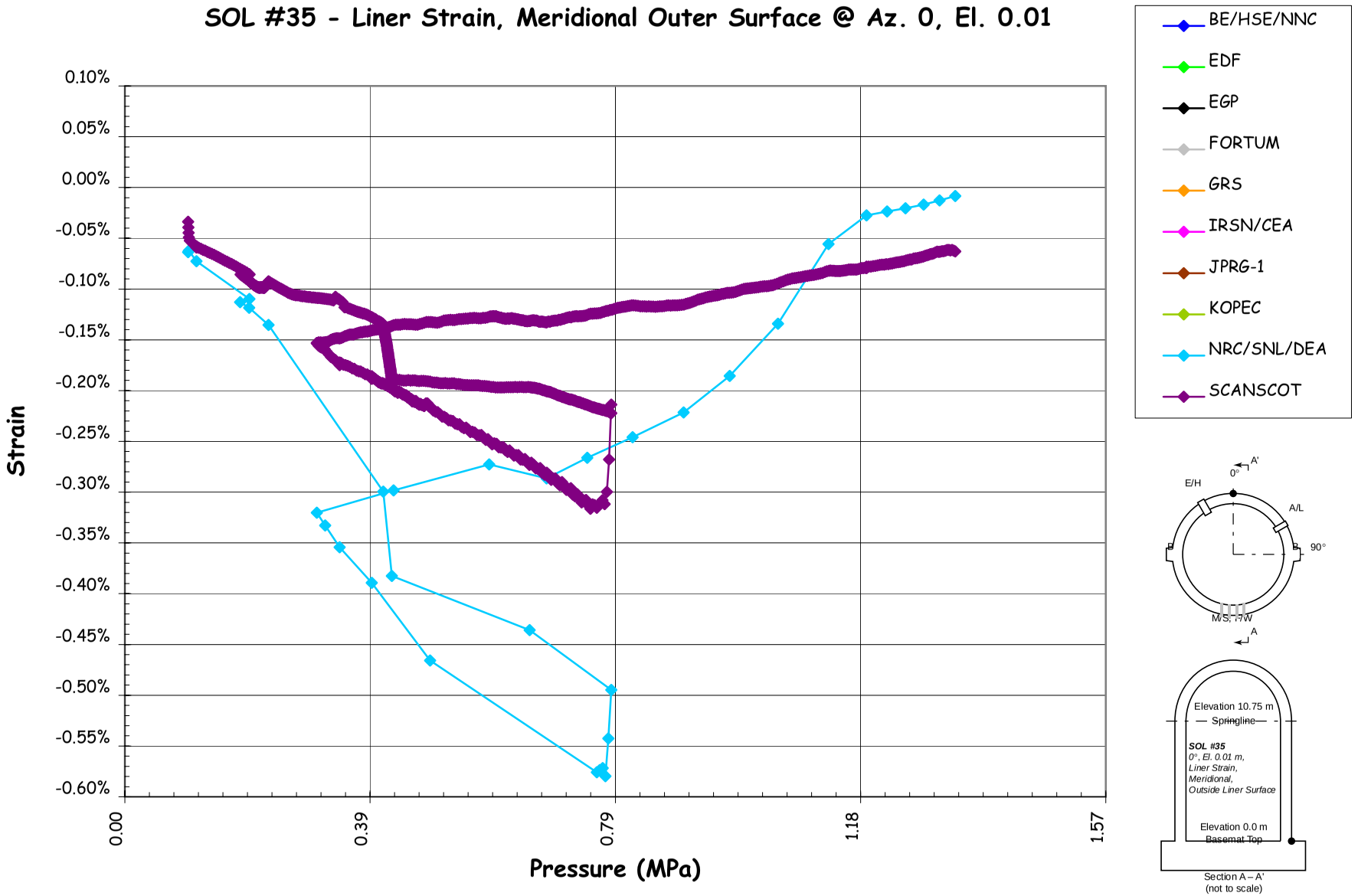
SOL #35 - Liner Strain, Meridional Outer Surface @ Az. 0, El. 0.01
Strain
0.10%
0.05%
0.00%
-0.05%
-0.10%
-0.15%
-0.20%
-0.25%
-0.30%
-0.35%
-0.40%
-0.45%
-0.50%
-0.55%
-0.60%
0.00
0.39
0.79
1.18
1.57
Pressure (MPa)
BE/HSE/NNC
EDF
EGP
FORTUM
GRS
IRSN/CEA
JPRG-1
KOPEC
NRC/SNL/DEA
SCANSCOT
A'
0°
E/H
A/L
B
B
90°
MS, HW
A
Elevation 10.75 m
Springline
SOL #35
0°, El. 0.01 m,
Liner Strain,
Meridional,
Outside Liner Surface
Elevation 0.0 m
Basemat Top
Section A – A'
(not to scale)

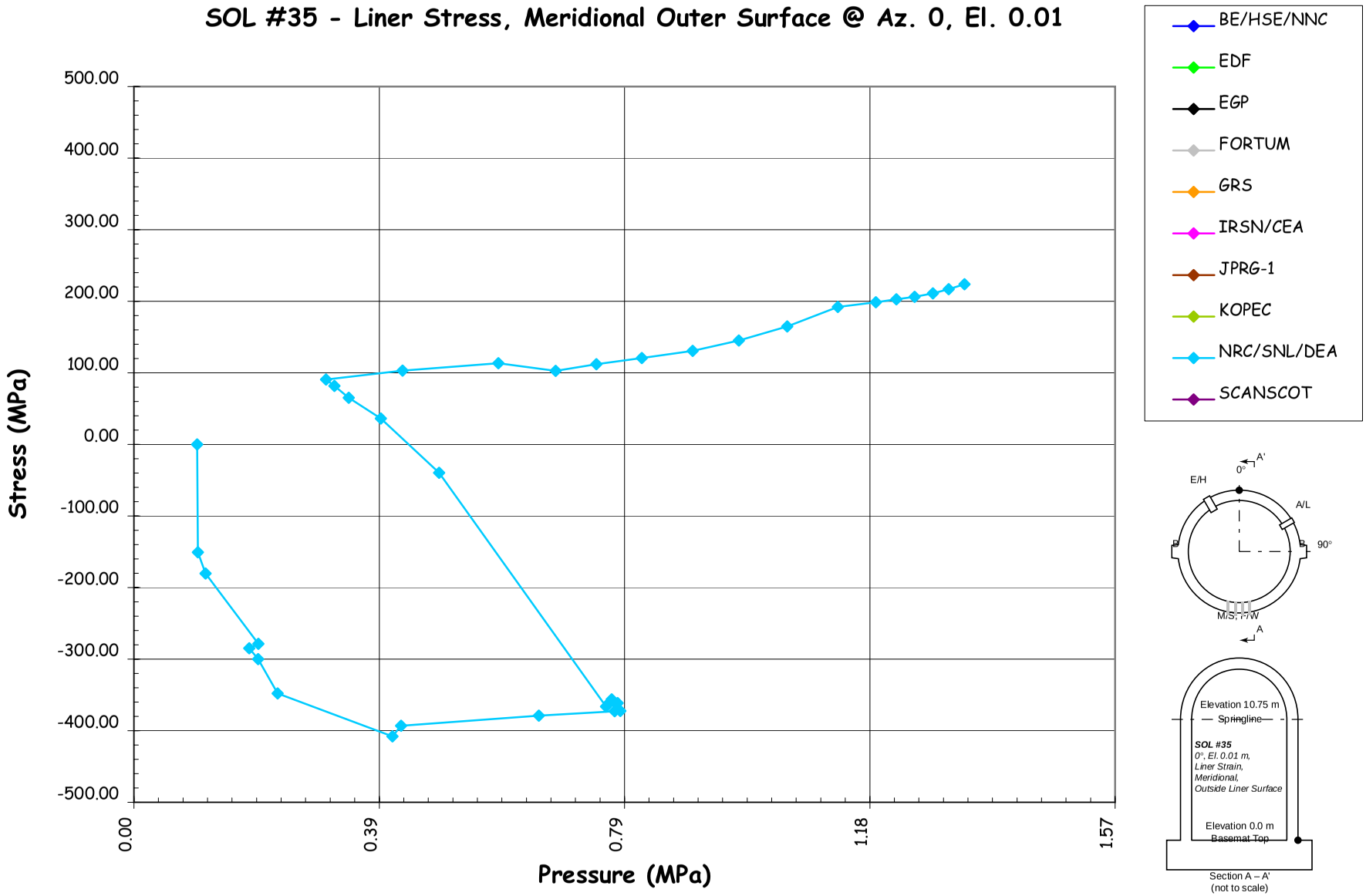
SOL #35 - Liner Stress, Meridional Outer Surface @ Az. 0, El. 0.01
Stress (MPa)
500.00
400.00
300.00
200.00
100.00
0.00
-100.00
-200.00
-300.00
-400.00
-500.00
0.00
0.39
0.79
1.18
1.57
Pressure (MPa)
BE/HSE/NNC
EDF
EGP
FORTUM
GRS
IRSN/CEA
JPRG-1
KOPEC
NRC/SNL/DEA
SCANSCOT
A'
0°
E/H
A/L
90°
M/S
A
Elevation 10.75 m
Springline
SOL #35
0°, El. 0.01 m,
Liner Strain,
Meridional,
Outside Liner Surface
Elevation 0.0 m
Basemat Top
Section A – A'
(not to scale)

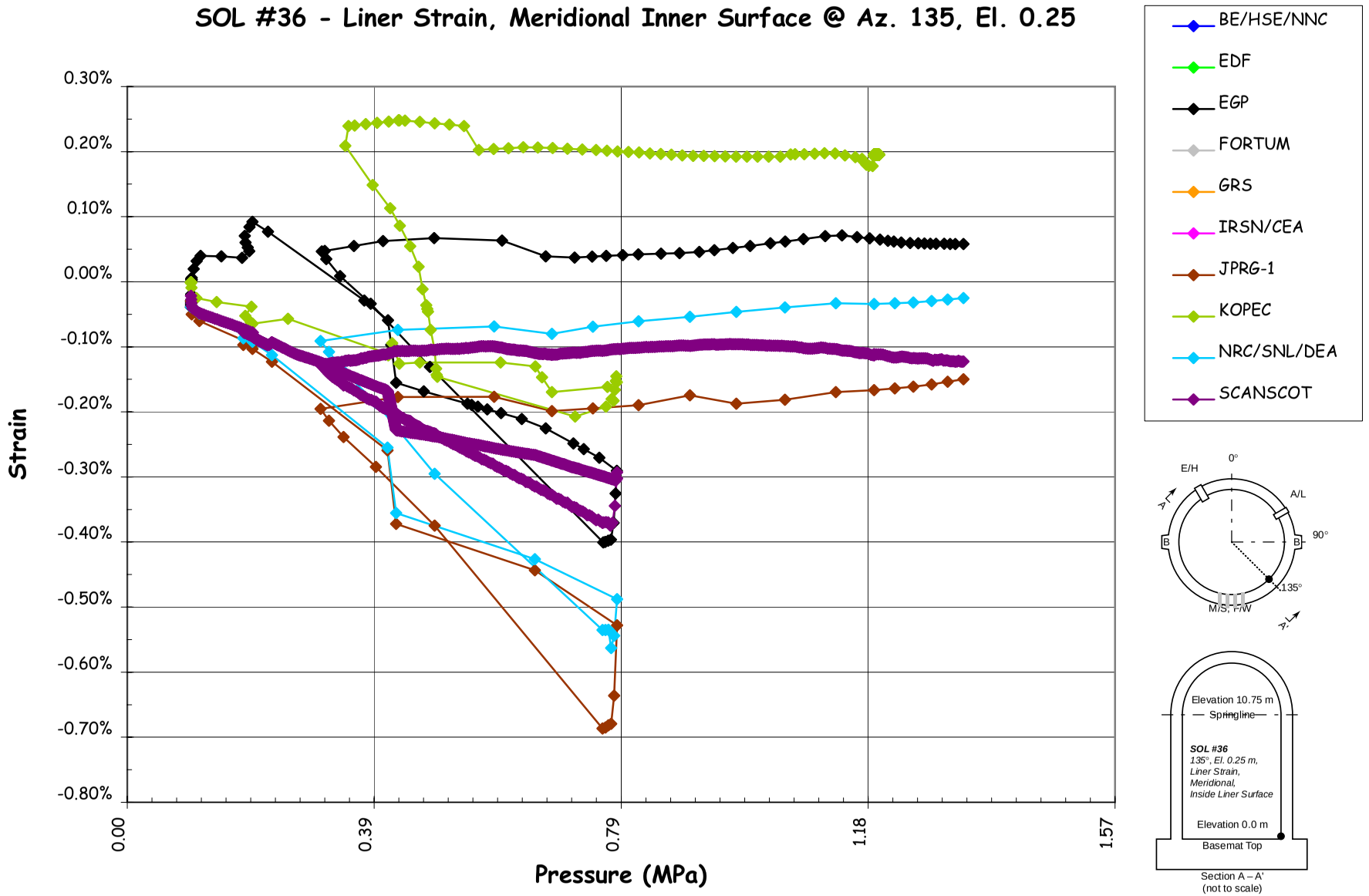
SOL #36 - Liner Strain, Meridional Inner Surface @ Az. 135, El. 0.25
Strain
0.30%
0.20%
0.10%
0.00%
-0.10%
-0.20%
-0.30%
-0.40%
-0.50%
-0.60%
-0.70%
-0.80%
0.00
0.39
0.79
1.18
1.57
Pressure (MPa)
BE/HSE/NNC
EDF
EGP
FORTUM
GRS
IRSN/CEA
JPRG-1
KOPEC
NRC/SNL/DEA
SCANSCOT
0°
E/H
A/L
90°
135°
M/S, P/W
Elevation 10.75 m
Springline
SOL #36
135°, El. 0.25 m,
Liner Strain,
Meridional,
Inside Liner Surface
Elevation 0.0 m
Basemat Top
Section A – A'
(not to scale)

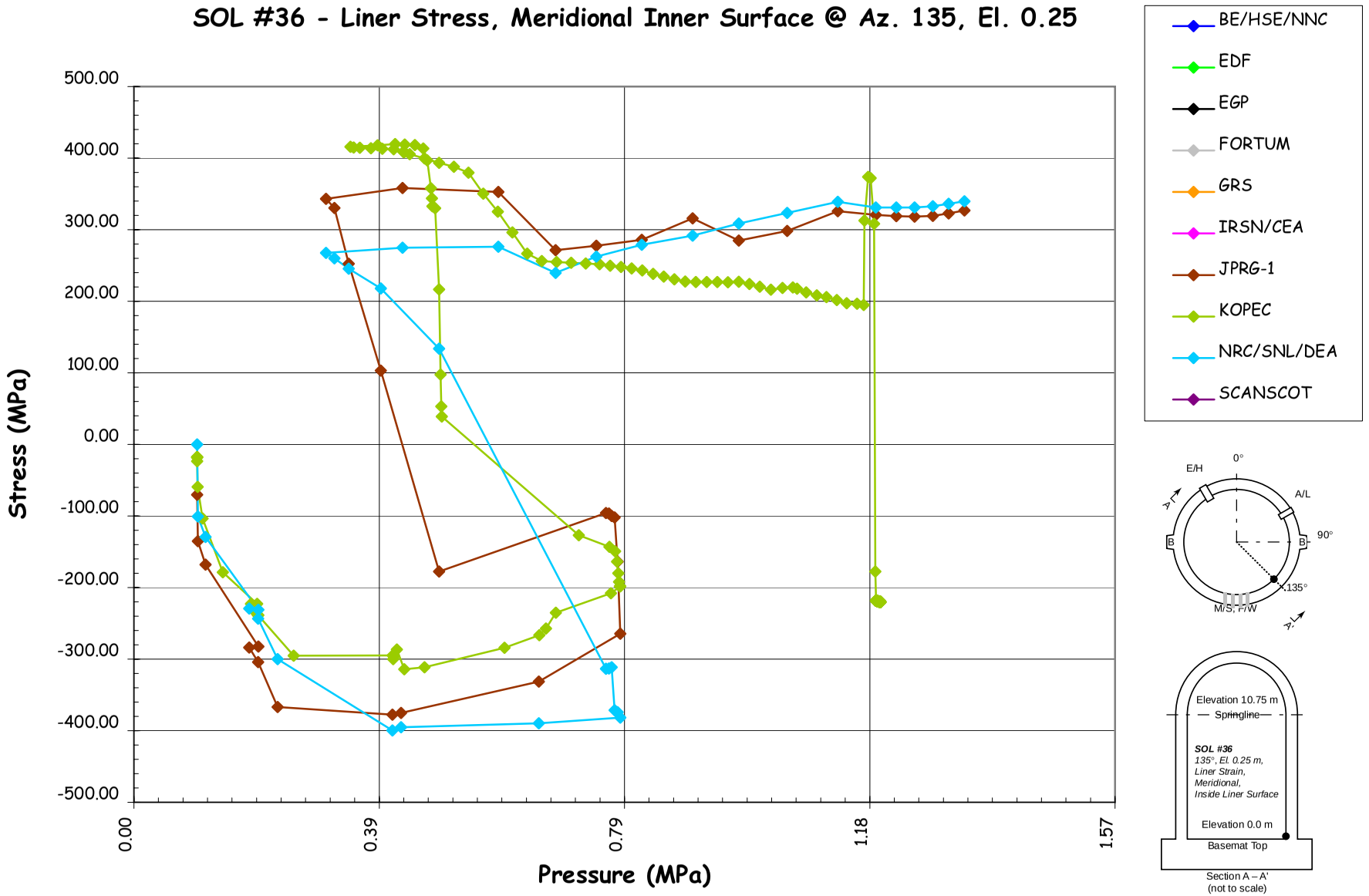
SOL #36 - Liner Stress, Meridional Inner Surface @ Az. 135, El. 0.25
Stress (MPa)
500.00
400.00
300.00
200.00
100.00
0.00
-100.00
-200.00
-300.00
-400.00
-500.00
0.00
0.39
0.79
1.18
1.57
Pressure (MPa)
BE/HSE/NNC
EDF
EGP
FORTUM
GRS
IRSN/CEA
JPRG-1
KOPEC
NRC/SNL/DEA
SCANSCOT
0°
E/H
A/L
90°
135°
M/S, F/W
Elevation 10.75 m
Springline
SOL #36
135°, El. 0.25 m,
Liner Strain,
Meridional,
Inside Liner Surface
Elevation 0.0 m
Basemat Top
Section A – A'
(not to scale)

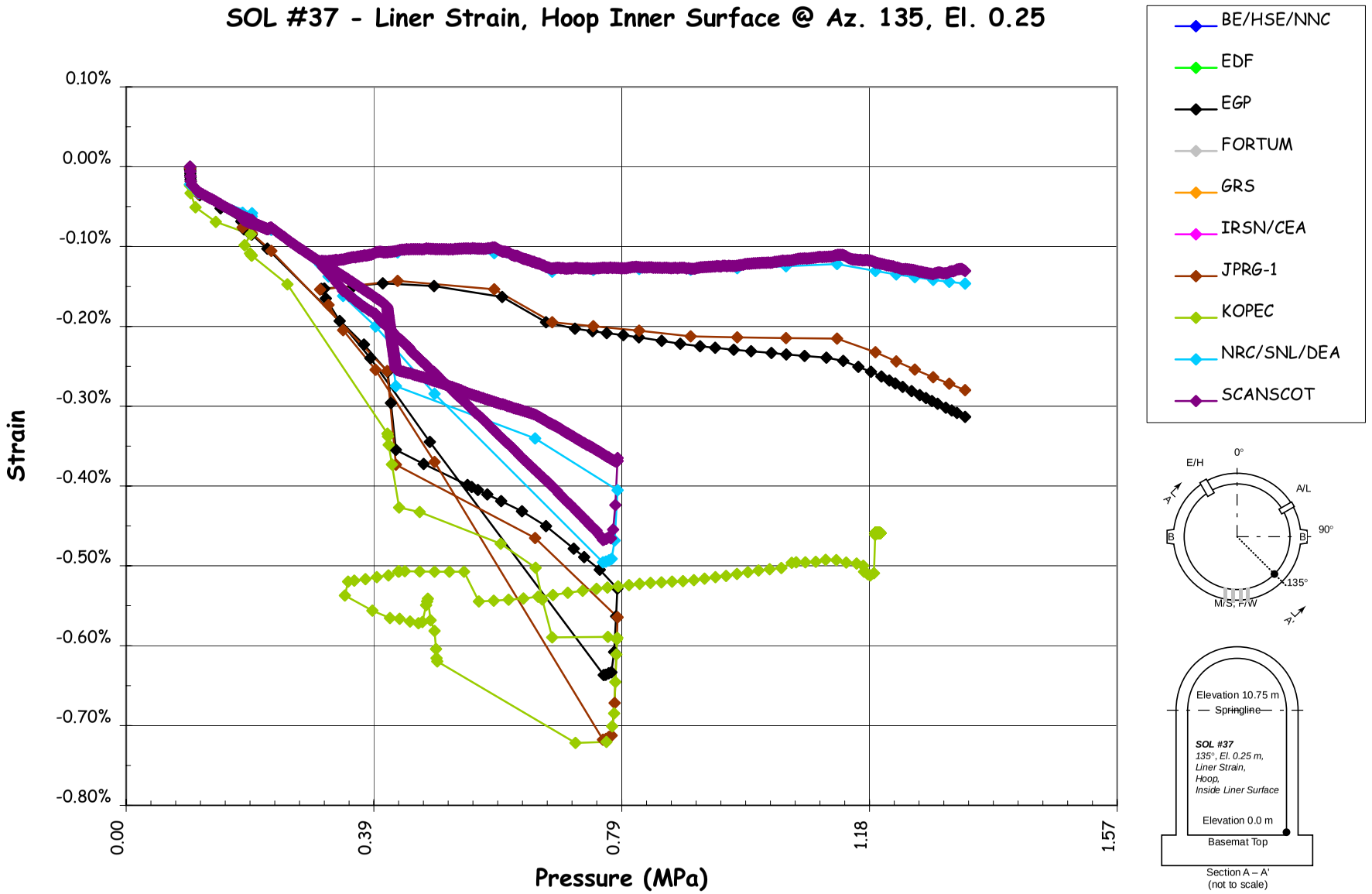
SOL #37 - Liner Strain, Hoop Inner Surface @ Az. 135, El. 0.25
Strain
0.10%
0.00%
-0.10%
-0.20%
-0.30%
-0.40%
-0.50%
-0.60%
-0.70%
-0.80%
0.00
0.39
0.79
1.18
1.57
Pressure (MPa)
BE/HSE/NNC
EDF
EGP
FORTUM
GRS
IRSN/CEA
JPRG-1
KOPEC
NRC/SNL/DEA
SCANSCOT
E/H
0°
A/L
90°
135°
M/S, F/W
Elevation 10.75 m
Springline
SOL #37
135°, El. 0.25 m,
Liner Strain,
Hoop,
Inside Liner Surface
Elevation 0.0 m
Basemat Top
Section A – A'
(not to scale)

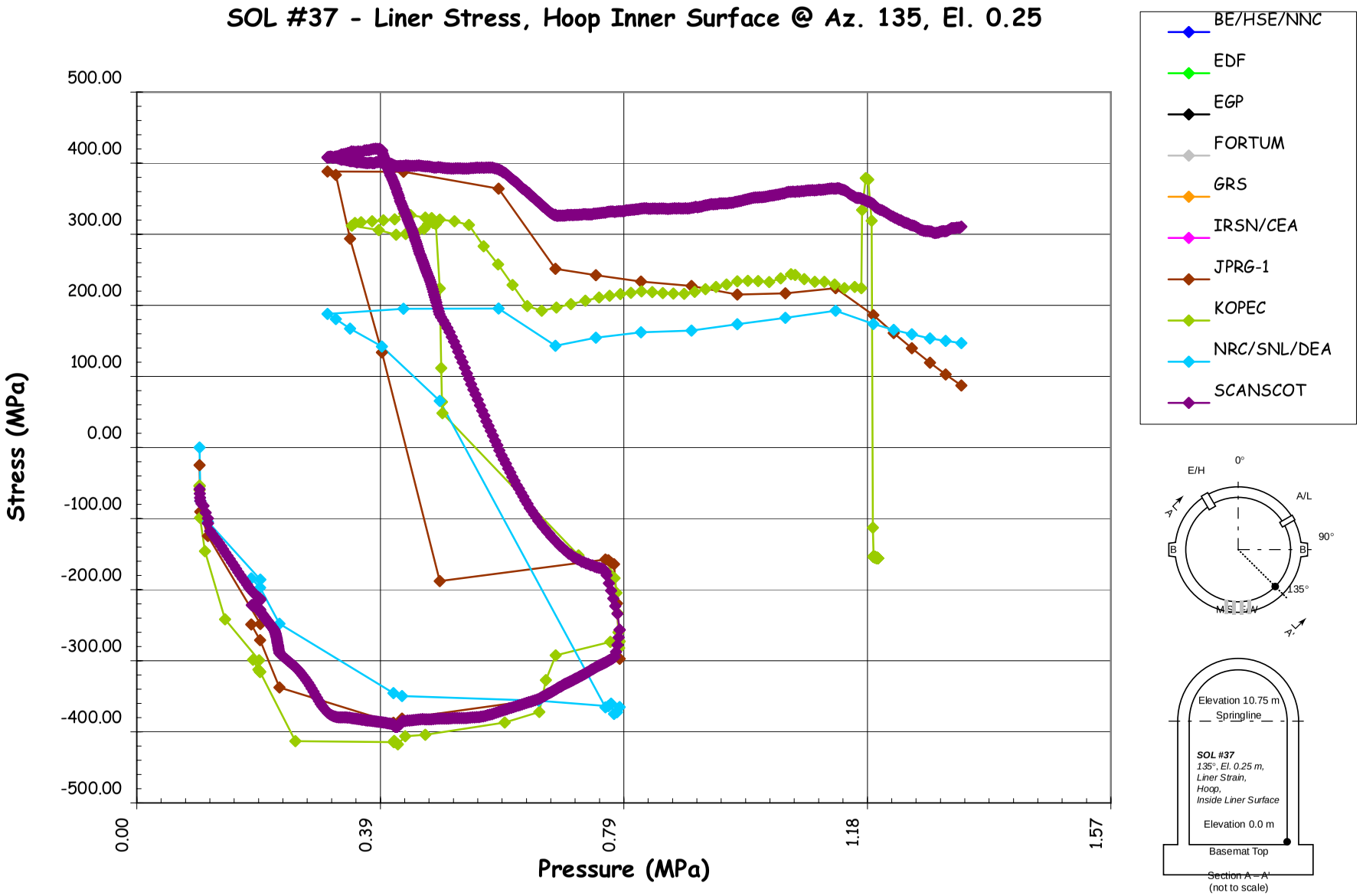
SOL #37 - Liner Stress, Hoop Inner Surface @ Az. 135, El. 0.25
Stress (MPa)
500.00
400.00
300.00
200.00
100.00
0.00
-100.00
-200.00
-300.00
-400.00
-500.00
0.00
0.39
0.79
1.18
1.57
Pressure (MPa)
BE/HSE/NNC
EDF
EGP
FORTUM
GRS
IRSN/CEA
JPRG-1
KOPEC
NRC/SNL/DEA
SCANSCOT
E/H
0°
A/L
90°
135°
Elevation 10.75 m
Springline
SOL #37
135°, El. 0.25 m,
Liner Strain,
Hoop,
Inside Liner Surface
Elevation 0.0 m
Basemat Top
Section A – A'
(not to scale)

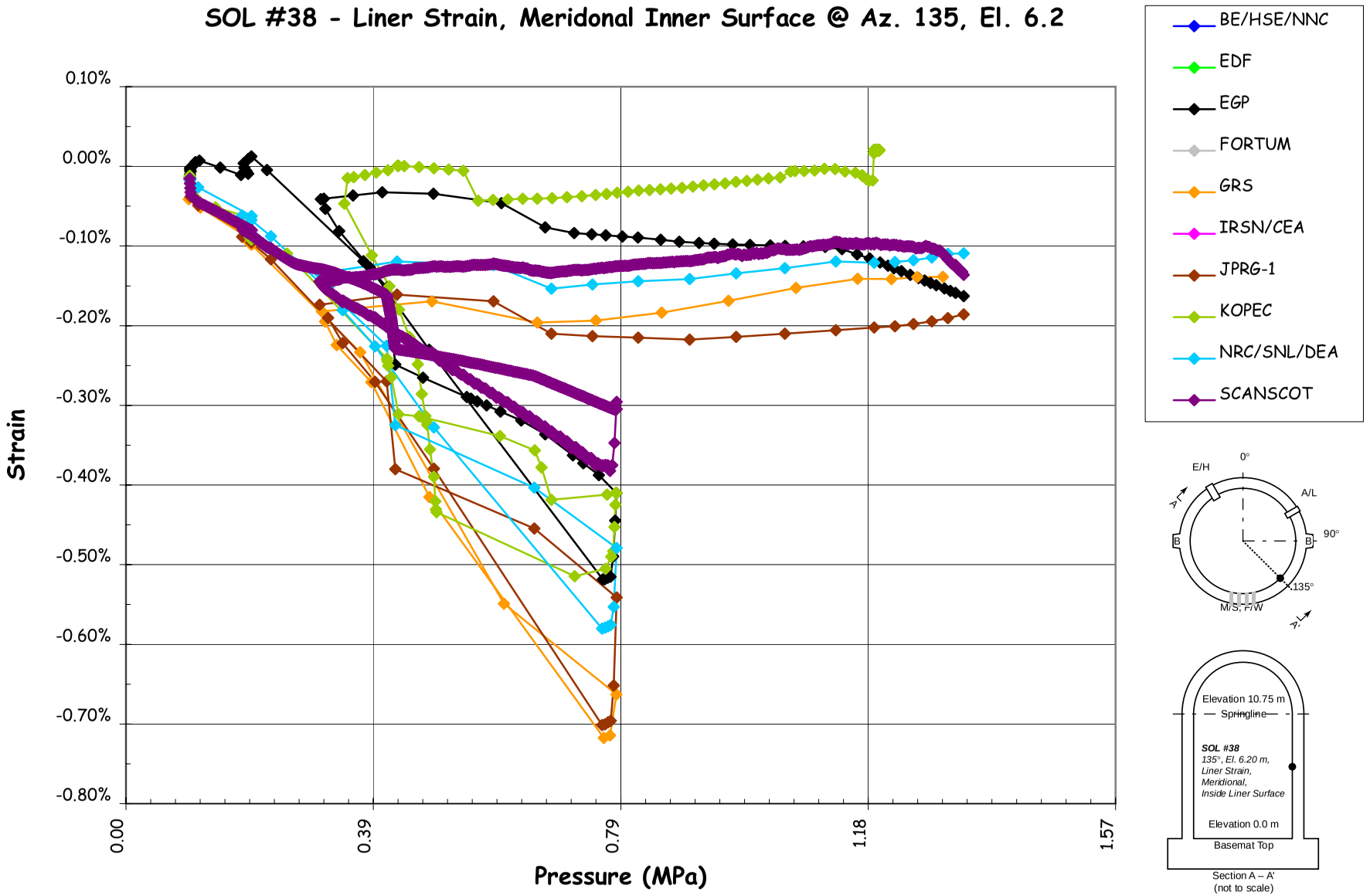
SOL #38 - Liner Strain, Meridonal Inner Surface @ Az. 135, El. 6.2
Strain
0.10%
0.00%
-0.10%
-0.20%
-0.30%
-0.40%
-0.50%
-0.60%
-0.70%
-0.80%
0.00
0.39
0.79
1.18
1.57
Pressure (MPa)
BE/HSE/NNC
EDF
EGP
FORTUM
GRS
IRSN/CEA
JPRG-1
KOPEC
NRC/SNL/DEA
SCANSCOT
E/H
A/L
B
0°
90°
135°
M/S, P/W
Elevation 10.75 m
Springline
SOL #38
135°, El. 6.20 m,
Liner Strain,
Meridional,
Inside Liner Surface
Elevation 0.0 m
Basemat Top
Section A – A'
(not to scale)

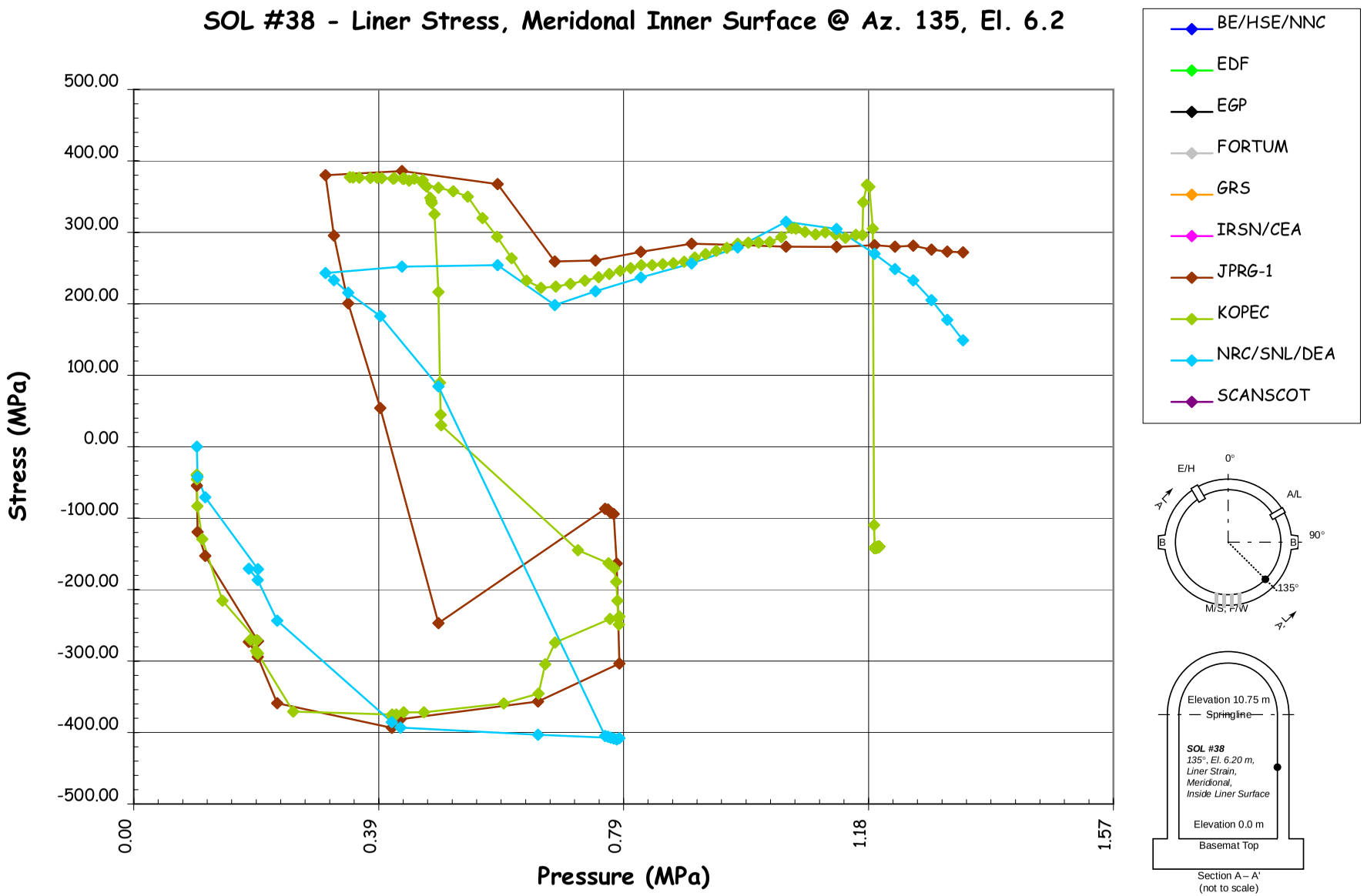
SOL #38 - Liner Stress, Meridonal Inner Surface @ Az. 135, El. 6.2
Stress (MPa)
500.00
400.00
300.00
200.00
100.00
0.00
-100.00
-200.00
-300.00
-400.00
-500.00
0.00
0.39
0.79
1.18
1.57
Pressure (MPa)
BE/HSE/NNC
EDF
EGP
FORTUM
GRS
IRSN/CEA
JPRG-1
KOPEC
NRC/SNL/DEA
SCANSCOT
0°
E/H
A/L
90°
B
B
135°
M/S, F/W
A
A
Elevation 10.75 m
Springline
SOL #38
135°, El. 6.20 m,
Liner Strain,
Meridional,
Inside Liner Surface
Elevation 0.0 m
Basemat Top
Section A – A'
(not to scale)

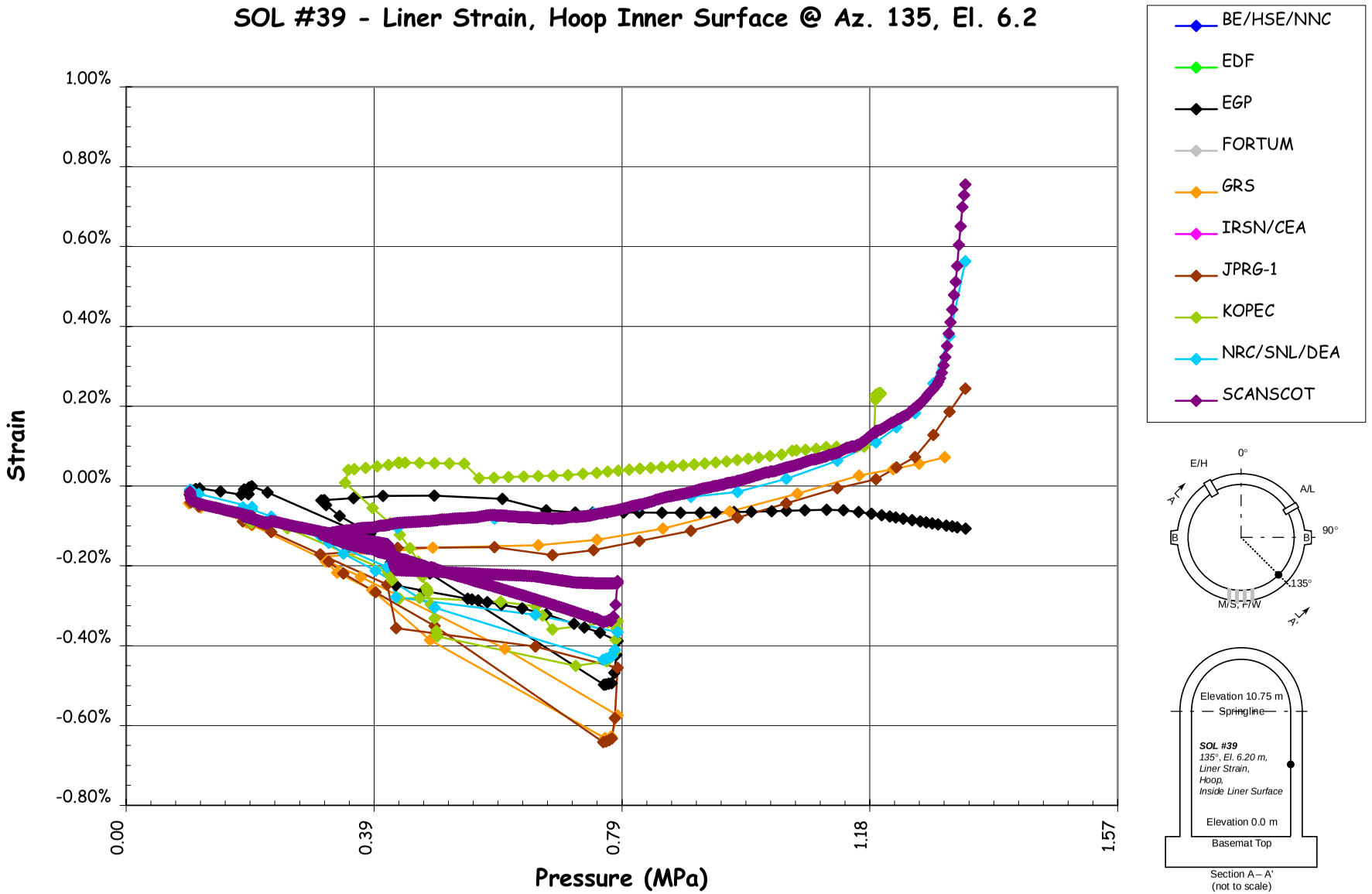
SOL #39 - Liner Strain, Hoop Inner Surface @ Az. 135, El. 6.2
Strain
1.00%
0.80%
0.60%
0.40%
0.20%
0.00%
-0.20%
-0.40%
-0.60%
-0.80%
0.00
0.39
0.79
1.18
1.57
Pressure (MPa)
BE/HSE/NNC
EDF
EGP
FORTUM
GRS
IRSN/CEA
JPRG-1
KOPEC
NRC/SNL/DEA
SCANSCOT
0°
E/H
A/L
90°
135°
M/S, HW
Elevation 10.75 m
Springline
SOL #39
135°, El. 6.20 m,
Liner Strain,
Hoop,
Inside Liner Surface
Elevation 0.0 m
Basemat Top
Section A – A'
(not to scale)

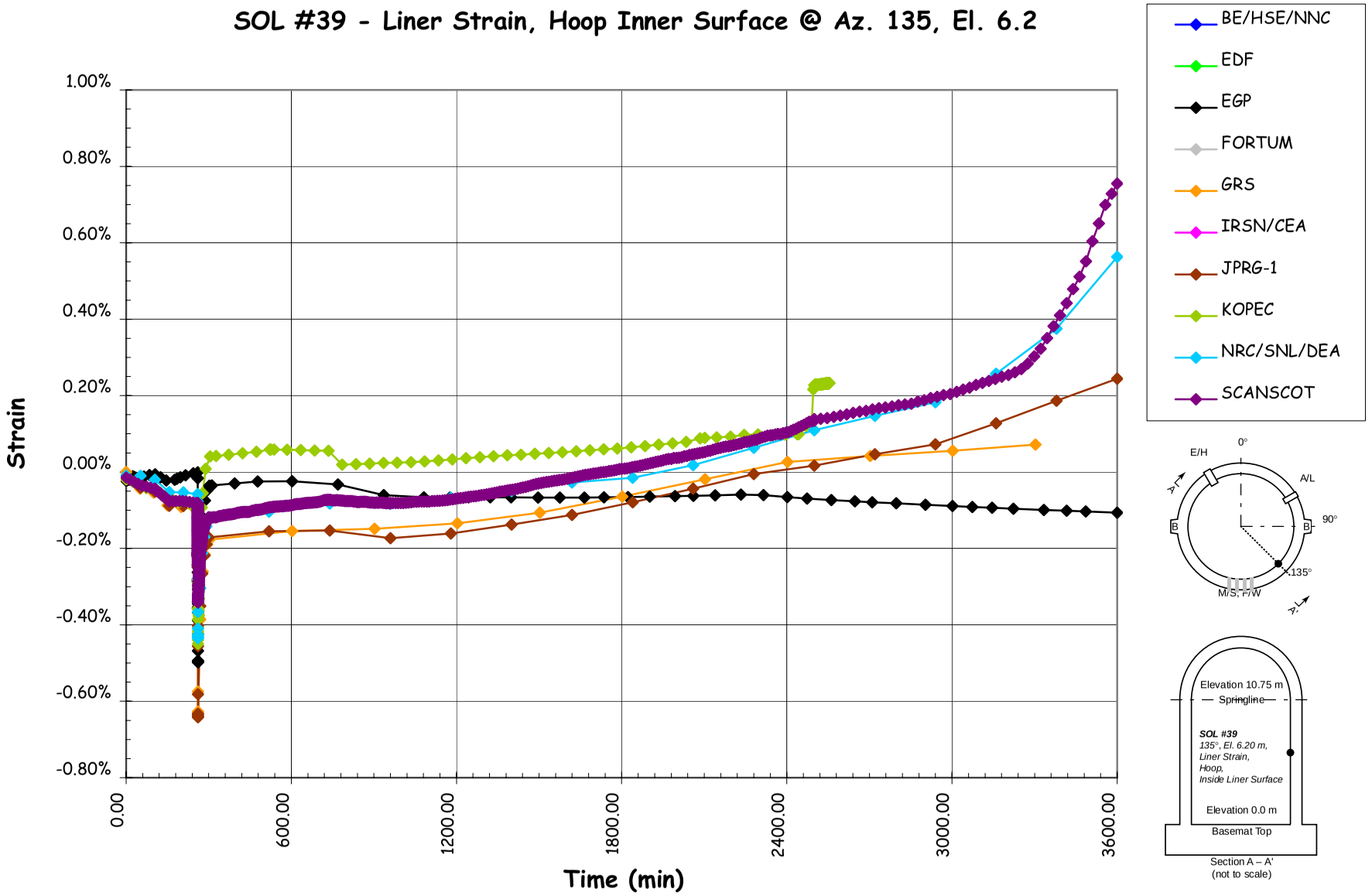
SOL #39 - Liner Strain, Hoop Inner Surface @ Az. 135, El. 6.2
Strain
1.00%
0.80%
0.60%
0.40%
0.20%
0.00%
-0.20%
-0.40%
-0.60%
-0.80%
0.00
600.00
1200.00
1800.00
2400.00
3000.00
3600.00
Time (min)
BE/HSE/NNC
EDF
EGP
FORTUM
GRS
IRSN/CEA
JPRG-1
KOPEC
NRC/SNL/DEA
SCANSCOT
0°
E/H
A/L
90°
135°
M/S, F/W
Elevation 10.75 m
Springline
SOL #39
135°, El. 6.20 m,
Liner Strain,
Hoop,
Inside Liner Surface
Elevation 0.0 m
Basemat Top
Section A – A'
(not to scale)

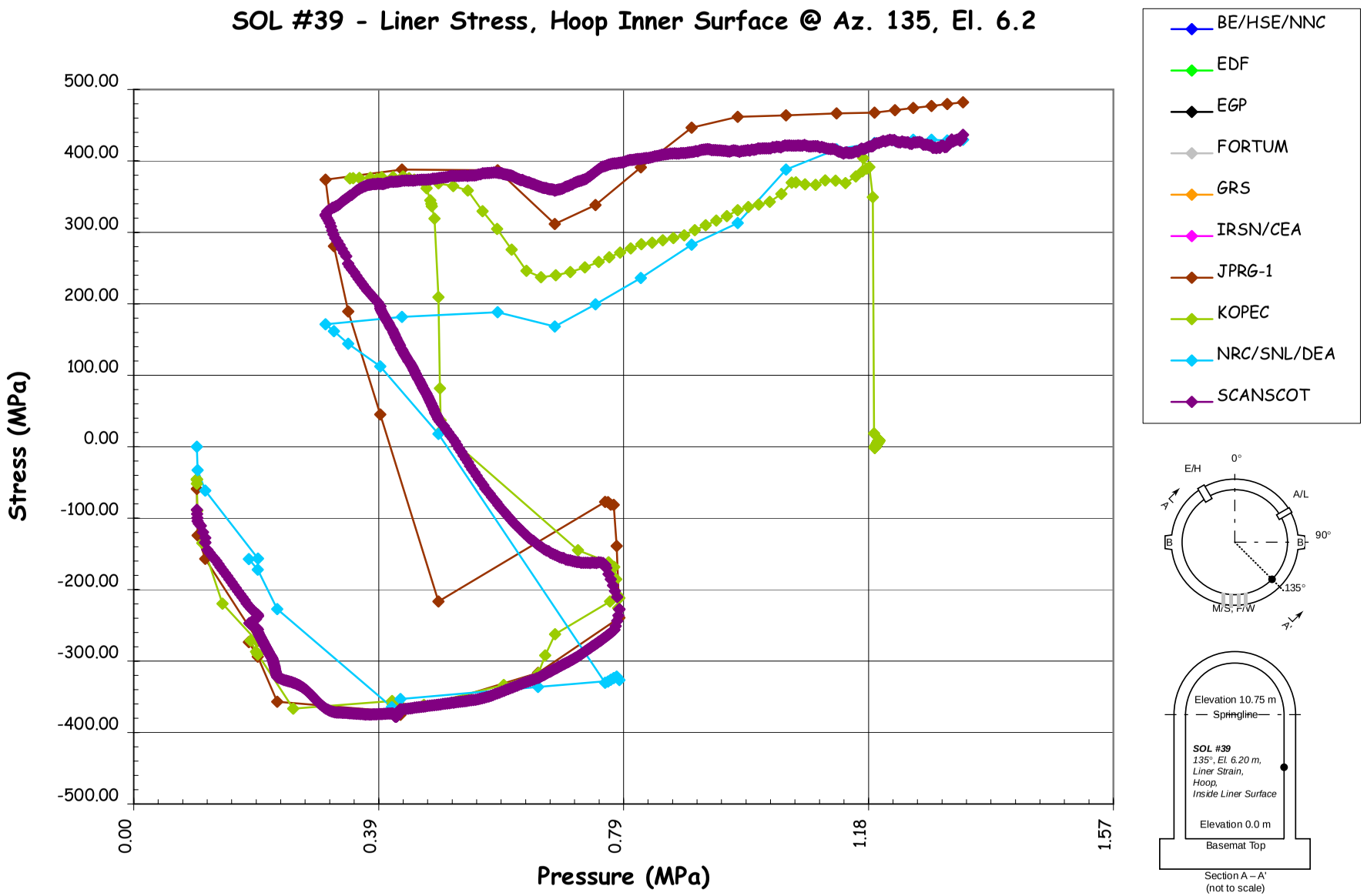
SOL #39 - Liner Stress, Hoop Inner Surface @ Az. 135, El. 6.2
Stress (MPa)
500.00
400.00
300.00
200.00
100.00
0.00
-100.00
-200.00
-300.00
-400.00
-500.00
0.00
0.39
0.79
1.18
1.57
Pressure (MPa)
BE/HSE/NNC
EDF
EGP
FORTUM
GRS
IRSN/CEA
JPRG-1
KOPEC
NRC/SNL/DEA
SCANSCOT
0°
E/H
A/L
90°
135°
M/S, F/W
Elevation 10.75 m
Springline
SOL #39
135°, El. 6.20 m,
Liner Strain,
Hoop,
Inside Liner Surface
Elevation 0.0 m
Basemat Top
Section A – A'
(not to scale)

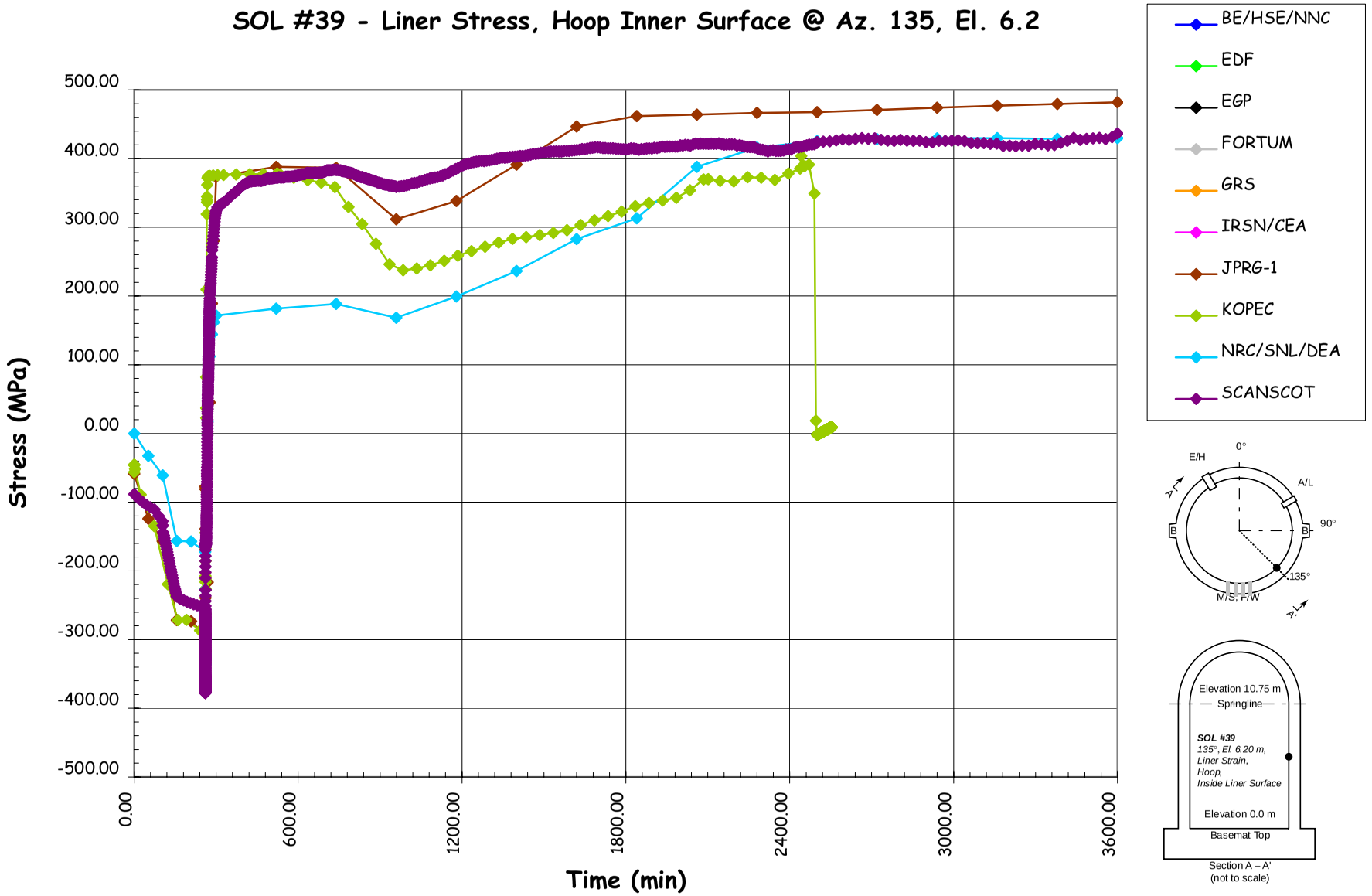
SOL #39 - Liner Stress, Hoop Inner Surface @ Az. 135, El. 6.2
Stress (MPa)
500.00
400.00
300.00
200.00
100.00
0.00
-100.00
-200.00
-300.00
-400.00
-500.00
0.00
600.00
1200.00
1800.00
2400.00
3000.00
3600.00
Time (min)
BE/HSE/NNC
EDF
EGP
FORTUM
GRS
IRSN/CEA
JPRG-1
KOPEC
NRC/SNL/DEA
SCANSCOT
0°
E/H
A/L
90°
135°
M/S, F/W
Elevation 10.75 m
Springline
SOL #39
135°, El. 6.20 m,
Liner Strain,
Hoop,
Inside Liner Surface
Elevation 0.0 m
Basemat Top
Section A – A'
(not to scale)

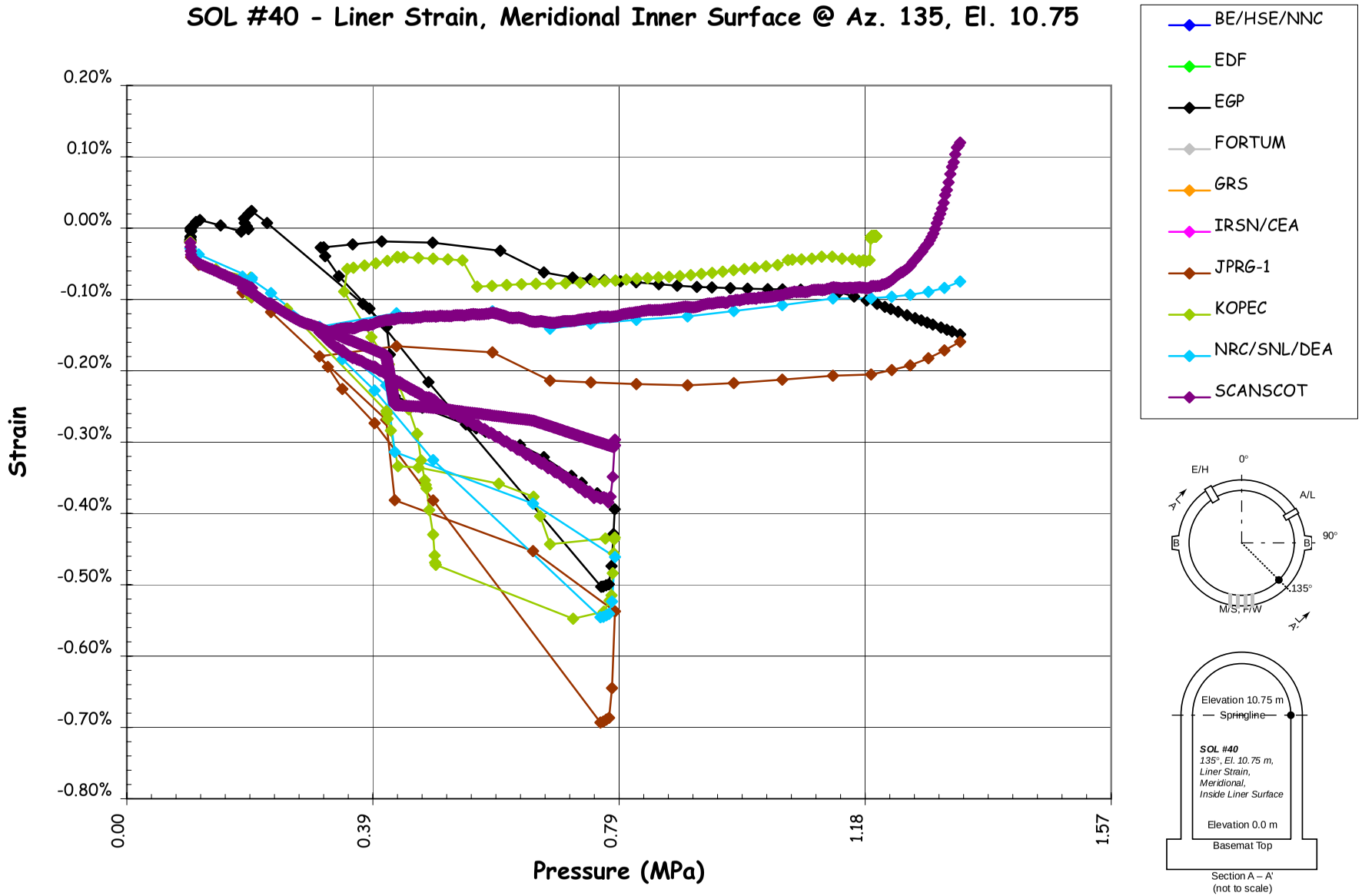
SOL #40 - Liner Strain, Meridional Inner Surface @ Az. 135, El. 10.75
Strain
0.20%
0.10%
0.00%
-0.10%
-0.20%
-0.30%
-0.40%
-0.50%
-0.60%
-0.70%
-0.80%
0.00
0.39
0.79
1.18
1.57
Pressure (MPa)
BE/HSE/NNC
EDF
EGP
FORTUM
GRS
IRSN/CEA
JPRG-1
KOPEC
NRC/SNL/DEA
SCANSCOT
0°
E/H
A/L
90°
135°
M/S, F/W
Elevation 10.75 m
Springline
SOL #40
135°, El. 10.75 m,
Liner Strain,
Meridional,
Inside Liner Surface
Elevation 0.0 m
Basemat Top
Section A – A'
(not to scale)

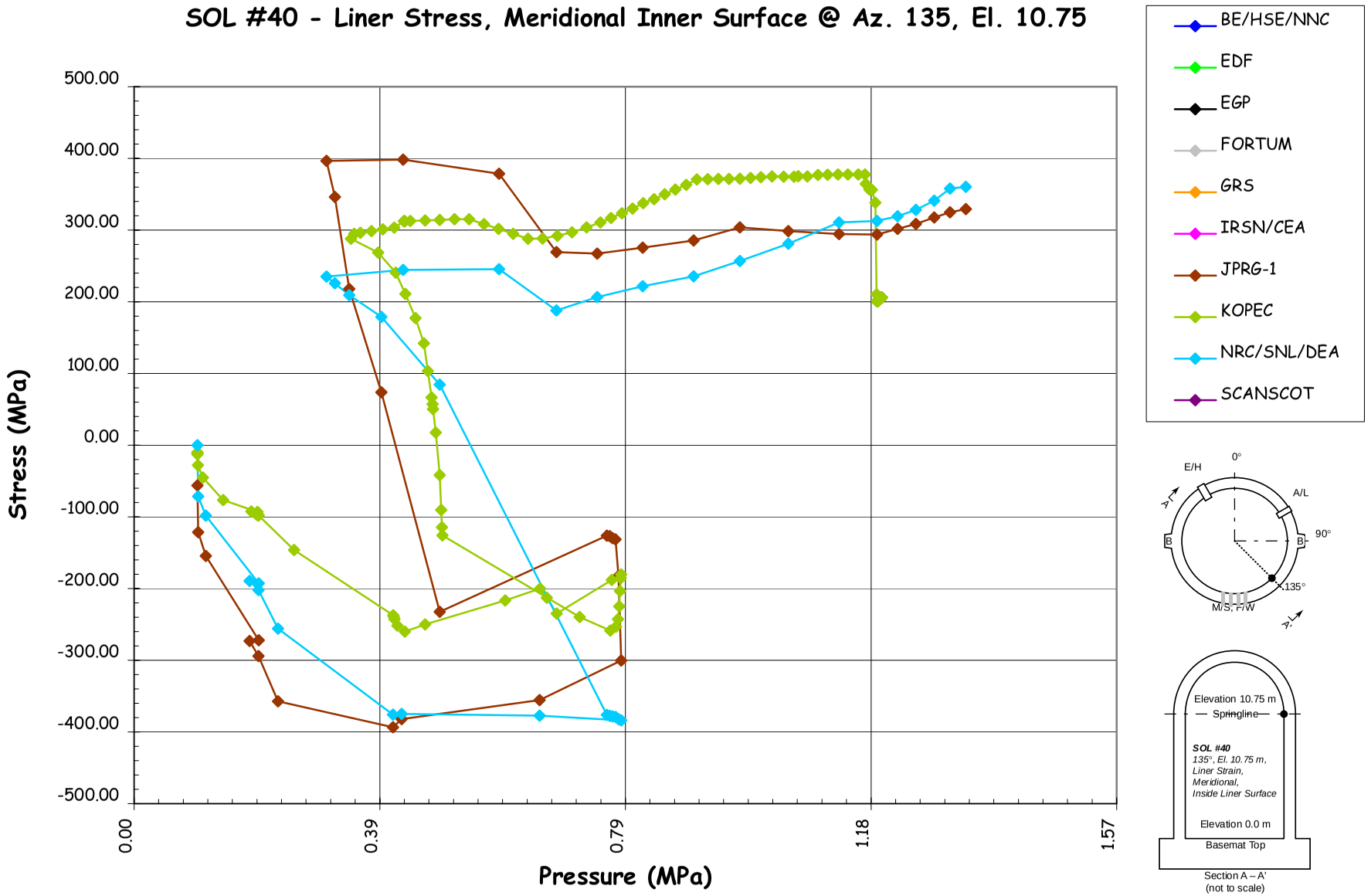
SOL #40 - Liner Stress, Meridional Inner Surface @ Az. 135, El. 10.75
Stress (MPa)
500.00
400.00
300.00
200.00
100.00
0.00
-100.00
-200.00
-300.00
-400.00
-500.00
0.00
0.39
0.79
1.18
1.57
Pressure (MPa)
BE/HSE/NNC
EDF
EGP
FORTUM
GRS
IRSN/CEA
JPRG-1
KOPEC
NRC/SNL/DEA
SCANSCOT
E/H
0°
A/L
90°
135°
M/S, P/W
Elevation 10.75 m
Springline
SOL #40
135°, El. 10.75 m,
Liner Strain,
Meridional,
Inside Liner Surface
Elevation 0.0 m
Basemat Top
Section A – A'
(not to scale)

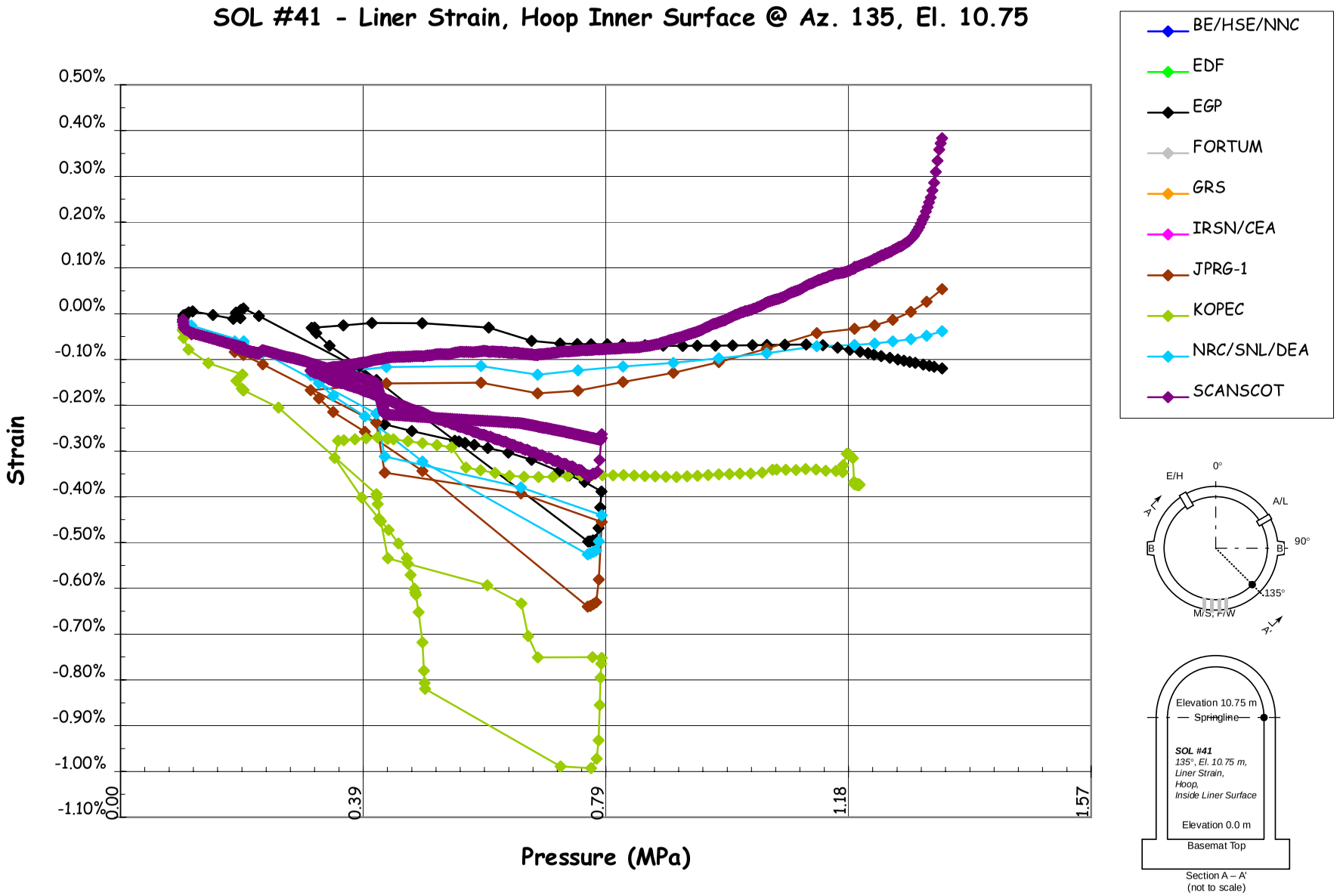
SOL #41 - Liner Strain, Hoop Inner Surface @ Az. 135, El. 10.75
Strain
0.50%
0.40%
0.30%
0.20%
0.10%
0.00%
-0.10%
-0.20%
-0.30%
-0.40%
-0.50%
-0.60%
-0.70%
-0.80%
-0.90%
-1.00%
-1.10%
0.00
0.39
0.79
1.18
1.57
Pressure (MPa)
BE/HSE/NNC
EDF
EGP
FORTUM
GRS
IRSN/CEA
JPRG-1
KOPEC
NRC/SNL/DEA
SCANSCOT
E/H
0°
A/L
90°
B
135°
M/S, F/W
Elevation 10.75 m
Springline
SOL #41
135°, El. 10.75 m,
Liner Strain,
Hoop,
Inside Liner Surface
Elevation 0.0 m
Basemat Top
Section A – A'
(not to scale)

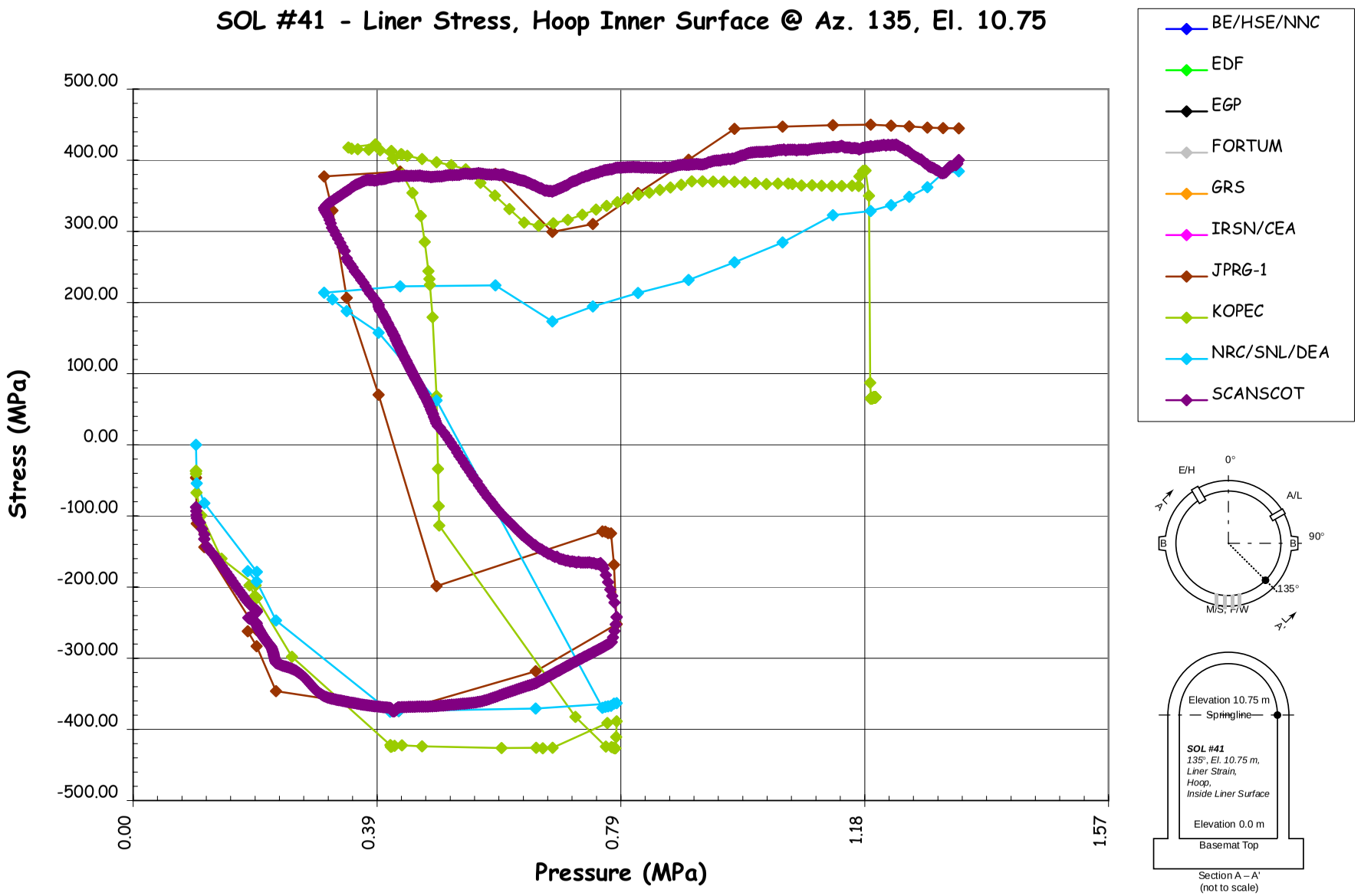
SOL #41 - Liner Stress, Hoop Inner Surface @ Az. 135, El. 10.75
Stress (MPa)
500.00
400.00
300.00
200.00
100.00
0.00
-100.00
-200.00
-300.00
-400.00
-500.00
0.00
0.39
0.79
1.18
1.57
Pressure (MPa)
BE/HSE/NNC
EDF
EGP
FORTUM
GRS
IRSN/CEA
JPRG-1
KOPEC
NRC/SNL/DEA
SCANSCOT
0°
E/H
A/L
90°
135°
M/S, P/W
Elevation 10.75 m
Springline
SOL #41
135°, El. 10.75 m,
Liner Strain,
Hoop,
Inside Liner Surface
Elevation 0.0 m
Basemat Top
Section A – A'
(not to scale)

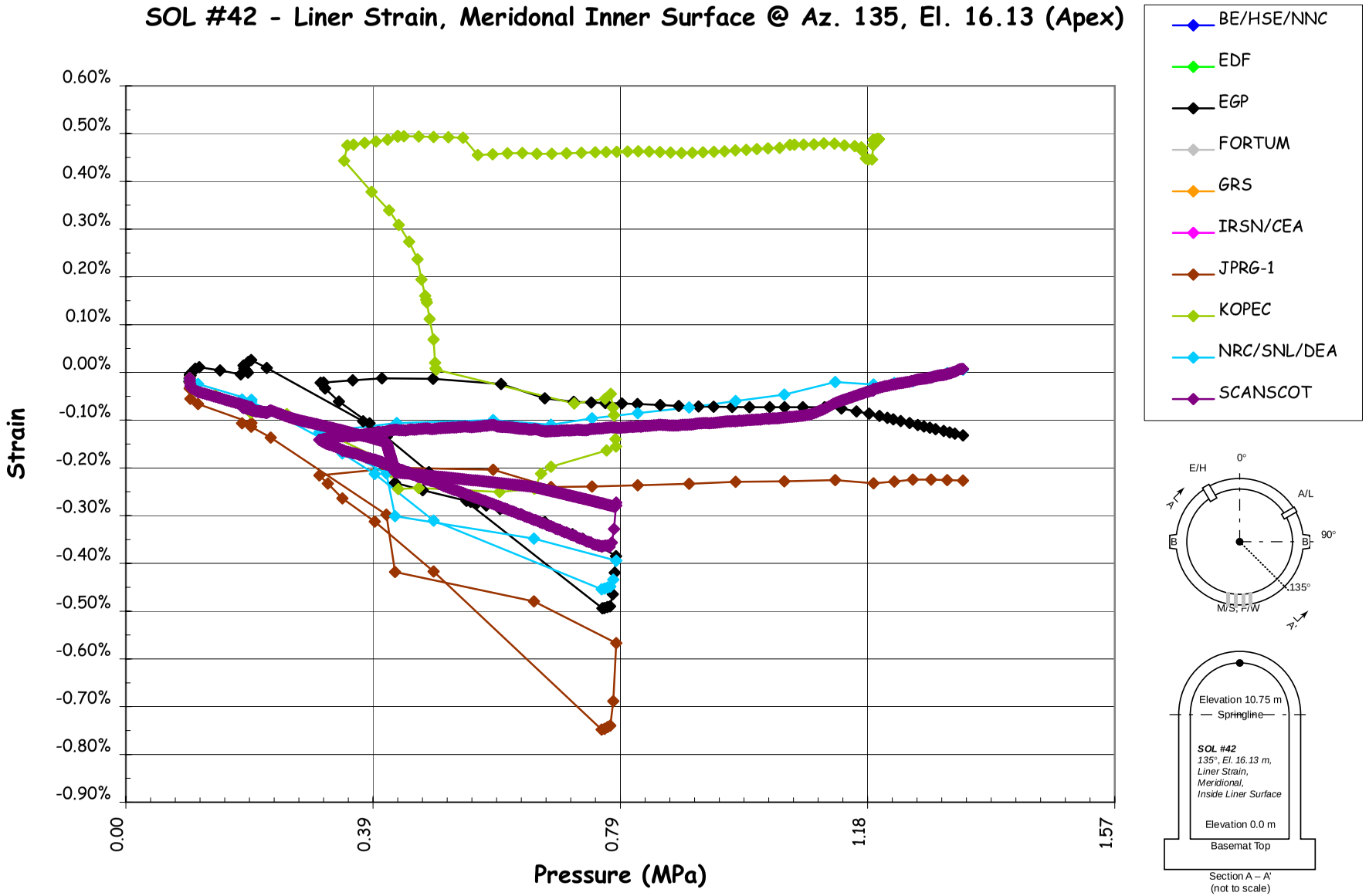
SOL #42 - Liner Strain, Meridonal Inner Surface @ Az. 135, El. 16.13 (Apex)
Strain
0.60%
0.50%
0.40%
0.30%
0.20%
0.10%
0.00%
-0.10%
-0.20%
-0.30%
-0.40%
-0.50%
-0.60%
-0.70%
-0.80%
-0.90%
0.00
0.39
0.79
1.18
1.57
Pressure (MPa)
BE/HSE/NNC
EDF
EGP
FORTUM
GRS
IRSN/CEA
JPRG-1
KOPEC
NRC/SNL/DEA
SCANSCOT
0°
E/H
A/L
90°
135°
M/S, F/W
Elevation 10.75 m
Springline
SOL #42
135°, El. 16.13 m,
Liner Strain,
Meridional,
Inside Liner Surface
Elevation 0.0 m
Basemat Top
Section A – A'
(not to scale)

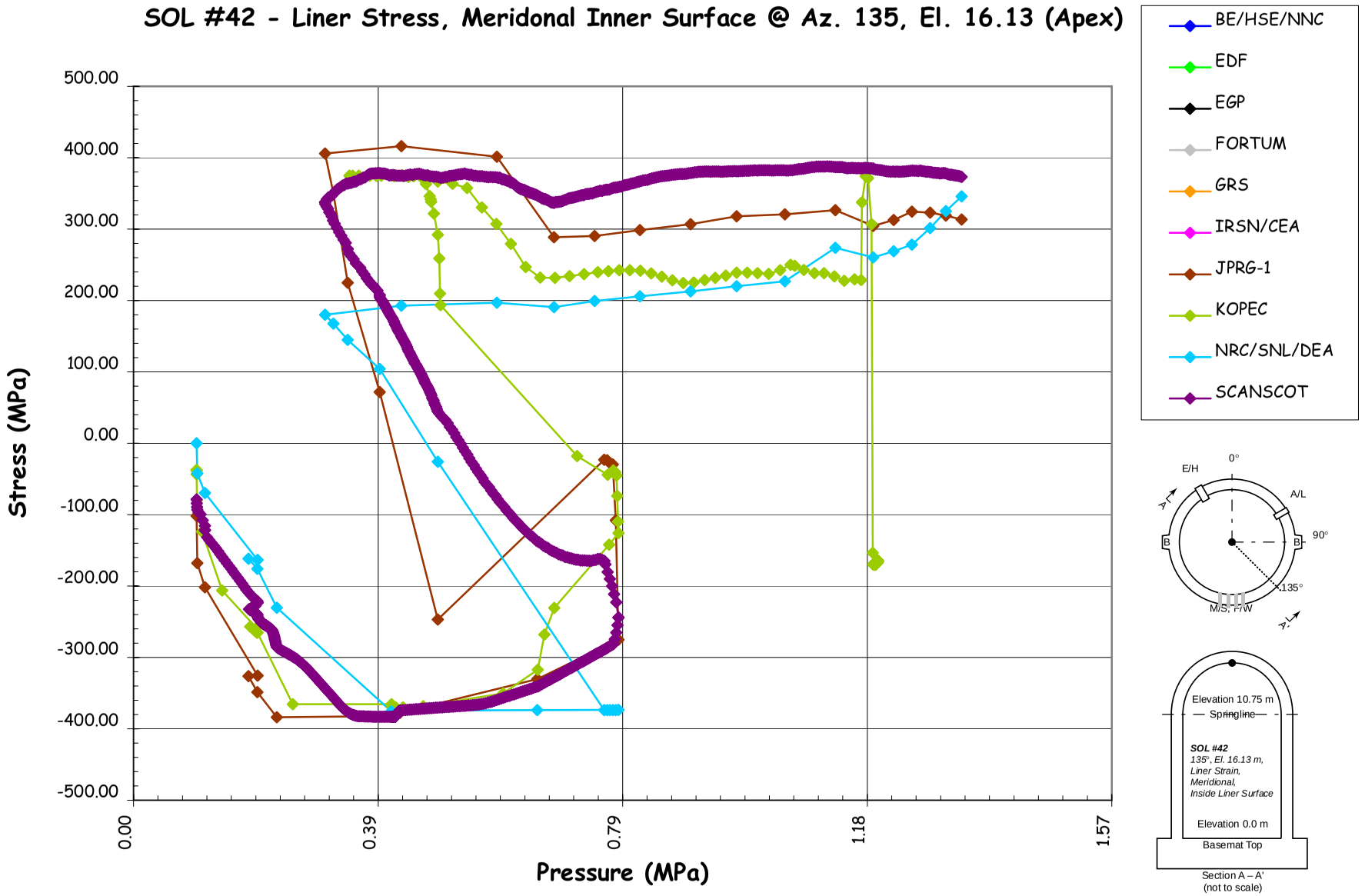
SOL #42 - Liner Stress, Meridonal Inner Surface @ Az. 135, El. 16.13 (Apex)
Stress (MPa)
500.00
400.00
300.00
200.00
100.00
0.00
-100.00
-200.00
-300.00
-400.00
-500.00
0.00
0.39
0.79
1.18
1.57
Pressure (MPa)
BE/HSE/NNC
EDF
EGP
FORTUM
GRS
IRSN/CEA
JPRG-1
KOPEC
NRC/SNL/DEA
SCANSCOT
0°
E/H
A/L
90°
135°
M/S, F/W
Elevation 10.75 m
Springline
SOL #42
135°, El. 16.13 m,
Liner Strain,
Meridional,
Inside Liner Surface
Elevation 0.0 m
Basemat Top
Section A – A'
(not to scale)

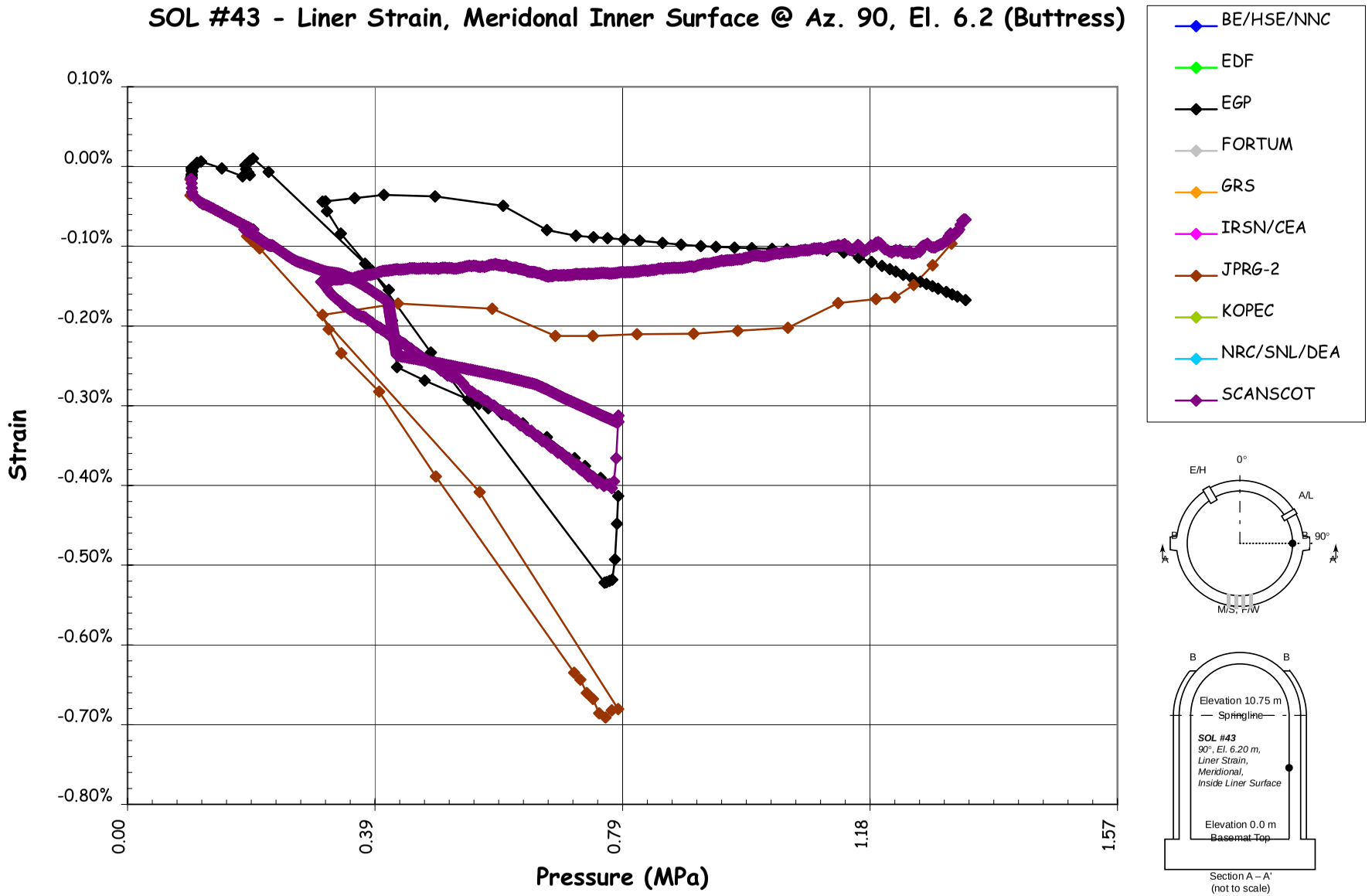
SOL #43 - Liner Strain, Meridonal Inner Surface @ Az. 90, El. 6.2 (Buttress)
Strain
0.10%
0.00%
-0.10%
-0.20%
-0.30%
-0.40%
-0.50%
-0.60%
-0.70%
-0.80%
0.00
0.39
0.79
1.18
1.57
Pressure (MPa)
BE/HSE/NNC
EDF
EGP
FORTUM
GRS
IRSN/CEA
JPRG-2
KOPEC
NRC/SNL/DEA
SCANSCOT
0°
E/H
A/L
90°
M/S, F/W
B
B
Elevation 10.75 m
Springline
SOL #43
90°, El. 6.20 m,
Liner Strain,
Meridional,
Inside Liner Surface
Elevation 0.0 m
Basemat Top
Section A – A'
(not to scale)

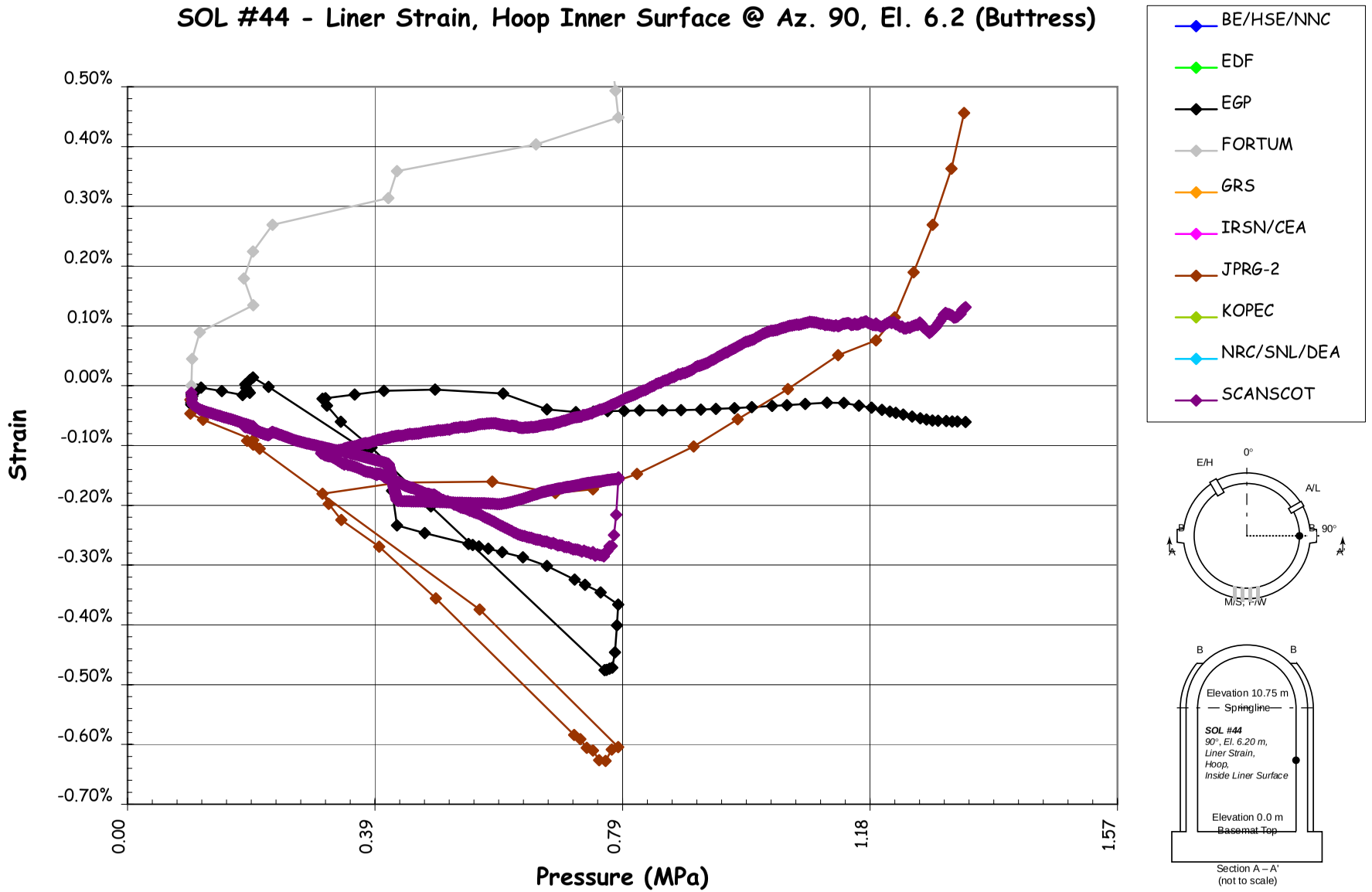
SOL #44 - Liner Strain, Hoop Inner Surface @ Az. 90, El. 6.2 (Buttress)
Strain
0.50%
0.40%
0.30%
0.20%
0.10%
0.00%
-0.10%
-0.20%
-0.30%
-0.40%
-0.50%
-0.60%
-0.70%
0.00
0.39
0.79
1.18
1.57
Pressure (MPa)
BE/HSE/NNC
EDF
EGP
FORTUM
GRS
IRSN/CEA
JPRG-2
KOPEC
NRC/SNL/DEA
SCANSCOT
E/H
0°
A/L
90°
M/S, F/W
B
B
Elevation 10.75 m
Springline
SOL #44
90°, El. 6.20 m,
Liner Strain,
Hoop,
Inside Liner Surface
Elevation 0.0 m
Basemat Top
Section A – A'
(not to scale)

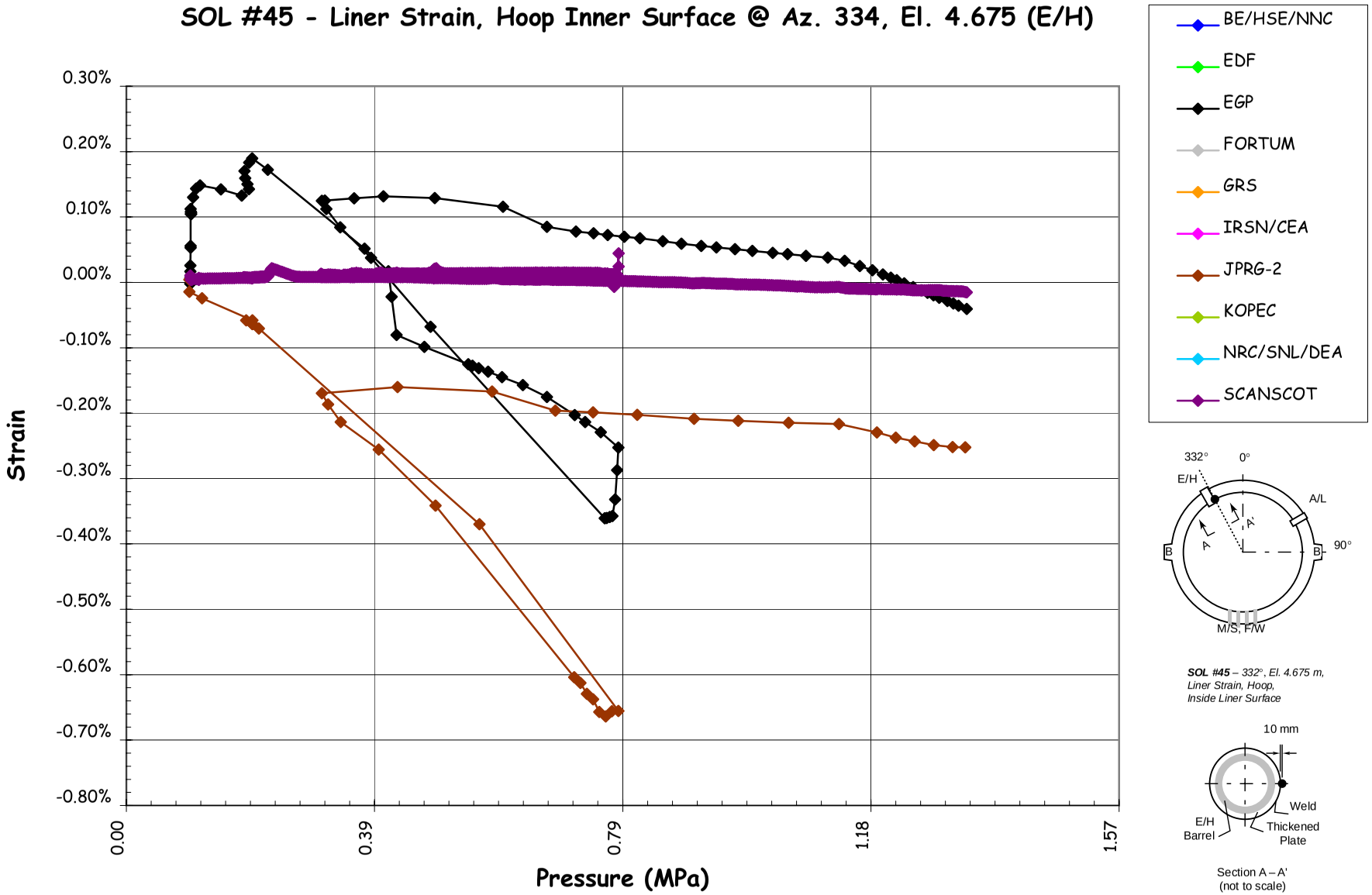
SOL #45 - Liner Strain, Hoop Inner Surface @ Az. 334, El. 4.675 (E/H)
Strain
0.30%
0.20%
0.10%
0.00%
-0.10%
-0.20%
-0.30%
-0.40%
-0.50%
-0.60%
-0.70%
-0.80%
0.00
0.39
0.79
1.18
1.57
Pressure (MPa)
BE/HSE/NNC
EDF
EGP
FORTUM
GRS
IRSN/CEA
JPRG-2
KOPEC
NRC/SNL/DEA
SCANSCOT
332°
0°
E/H
A/L
90°
M/S, F/W
SOL #45 – 332°, El. 4.675 m,
Liner Strain, Hoop,
Inside Liner Surface
10 mm
Weld
E/H
Barrel
Thickened
Plate
Section A – A'
(not to scale)

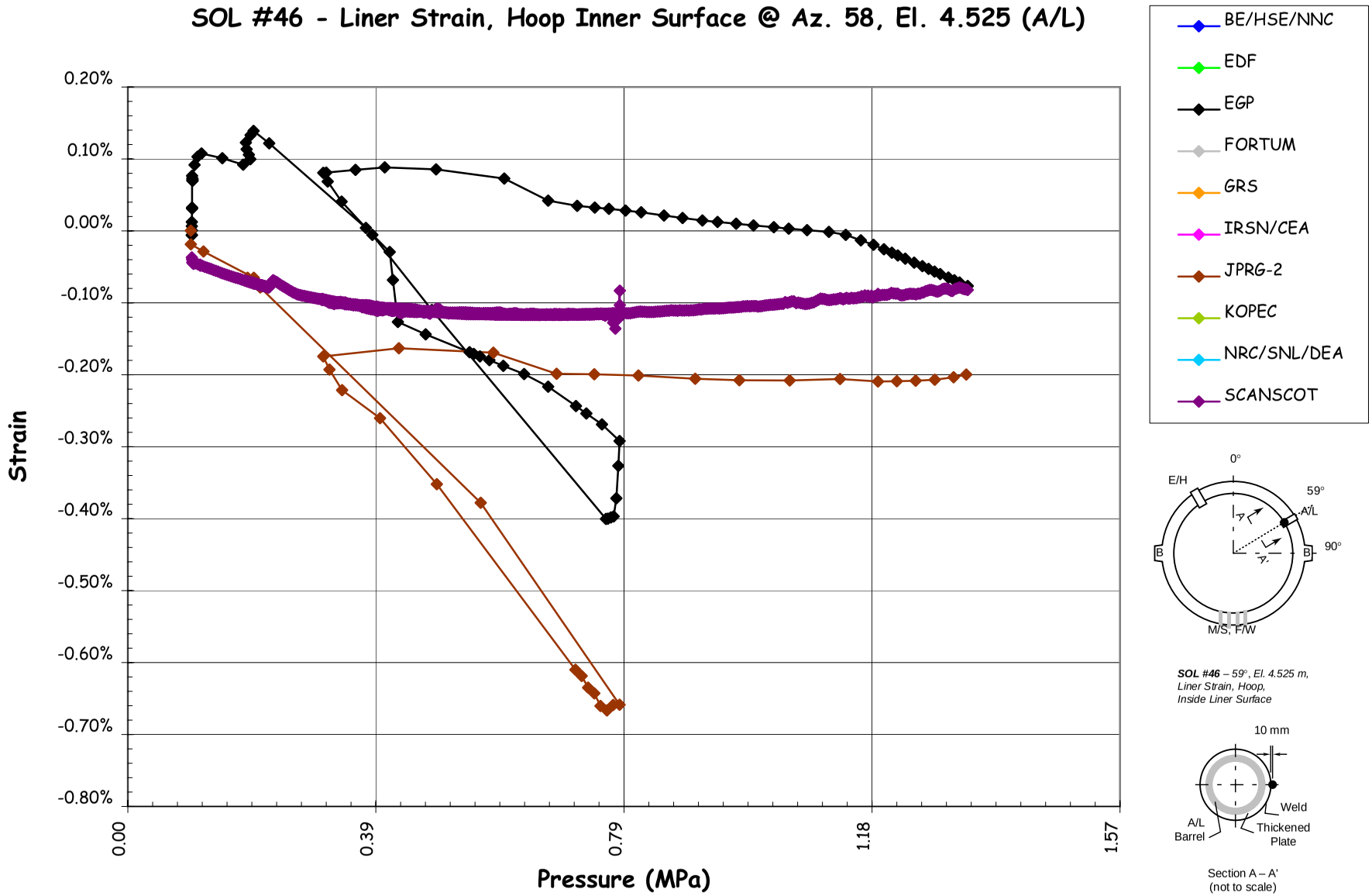
SOL #46 - Liner Strain, Hoop Inner Surface @ Az. 58, El. 4.525 (A/L)
Strain
0.20%
0.10%
0.00%
-0.10%
-0.20%
-0.30%
-0.40%
-0.50%
-0.60%
-0.70%
-0.80%
0.00
0.39
0.79
1.18
1.57
Pressure (MPa)
BE/HSE/NNC
EDF
EGP
FORTUM
GRS
IRSN/CEA
JPRG-2
KOPEC
NRC/SNL/DEA
SCANSCOT
0°
E/H
59°
A/L
90°
B
B
M/S, F/W
SOL #46 – 59°, El. 4.525 m,
Liner Strain, Hoop,
Inside Liner Surface
10 mm
Weld
A/L
Barrel
Thickened
Plate
Section A – A'
(not to scale)

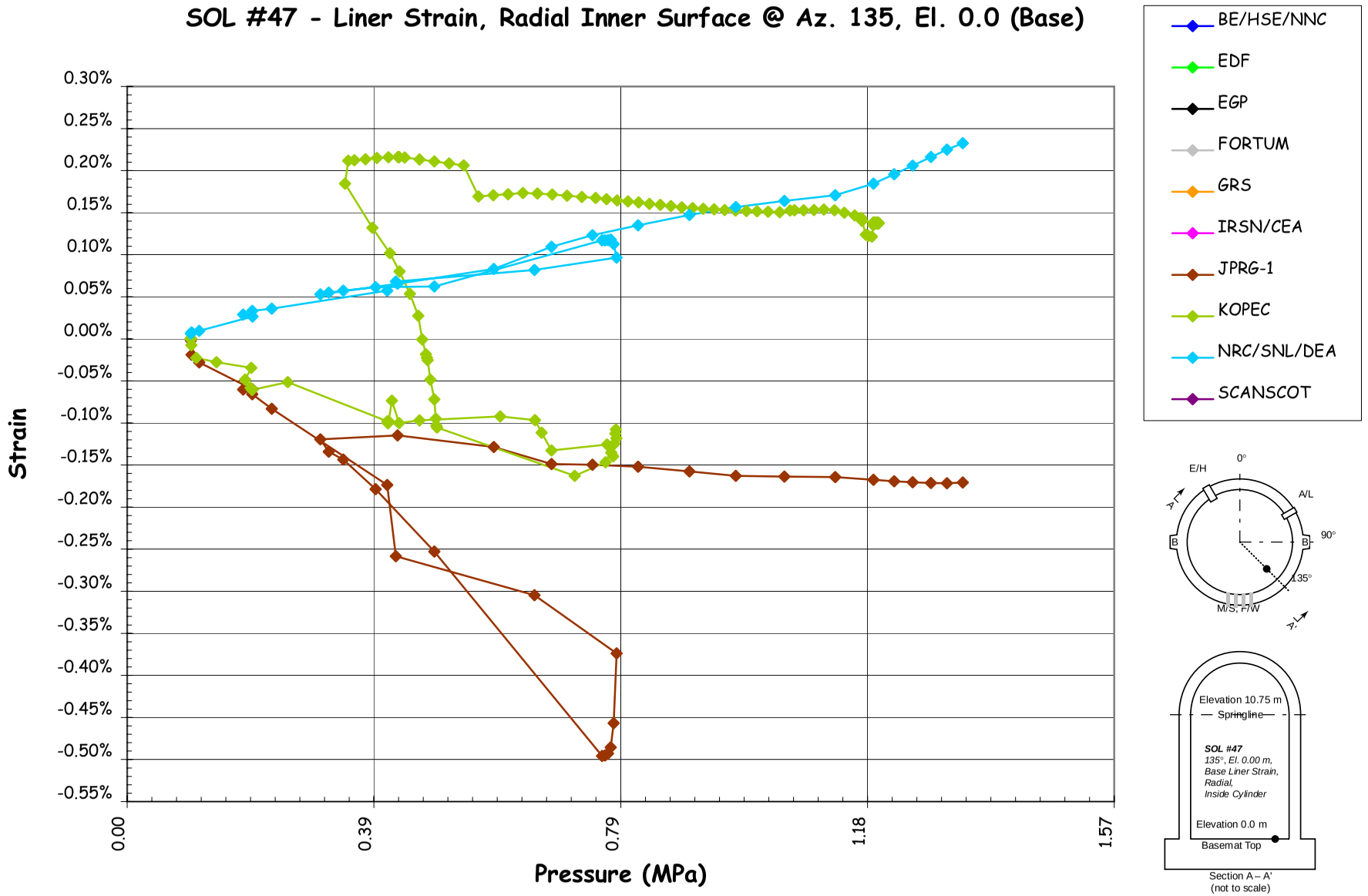
SOL #47 - Liner Strain, Radial Inner Surface @ Az. 135, El. 0.0 (Base)
Strain
0.30%
0.25%
0.20%
0.15%
0.10%
0.05%
0.00%
-0.05%
-0.10%
-0.15%
-0.20%
-0.25%
-0.30%
-0.35%
-0.40%
-0.45%
-0.50%
-0.55%
0.00
0.39
0.79
1.18
1.57
Pressure (MPa)
BE/HSE/NNC
EDF
EGP
FORTUM
GRS
IRSN/CEA
JPRG-1
KOPEC
NRC/SNL/DEA
SCANSCOT
0°
E/H
A/L
90°
135°
M/S, F/W
Elevation 10.75 m
Springline
SOL #47
135°, El. 0.00 m,
Base Liner Strain,
Radial,
Inside Cylinder
Elevation 0.0 m
Basemat Top
Section A – A'
(not to scale)

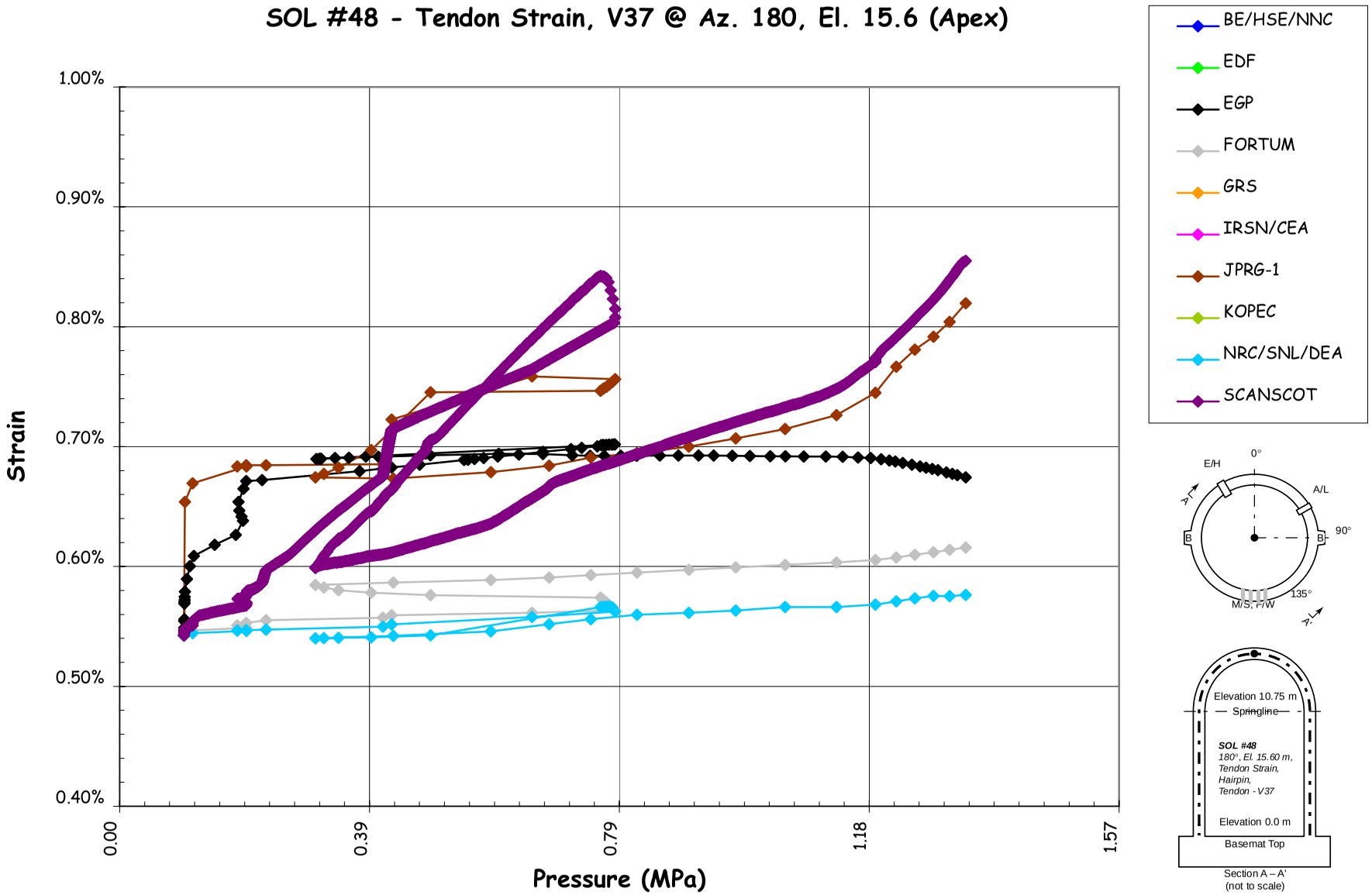
SOL #48 - Tendon Strain, V37 @ Az. 180, El. 15.6 (Apex)
Strain
1.00%
0.90%
0.80%
0.70%
0.60%
0.50%
0.40%
0.00
0.39
0.79
1.18
1.57
Pressure (MPa)
BE/HSE/NNC
EDF
EGP
FORTUM
GRS
IRSN/CEA
JPRG-1
KOPEC
NRC/SNL/DEA
SCANSCOT
0°
E/H
A/L
90°
135°
M/S, F/W
Elevation 10.75 m
Springline
SOL #48
180°, El. 15.60 m,
Tendon Strain,
Hairpin,
Tendon - V37
Elevation 0.0 m
Basemat Top
Section A – A'
(not to scale)

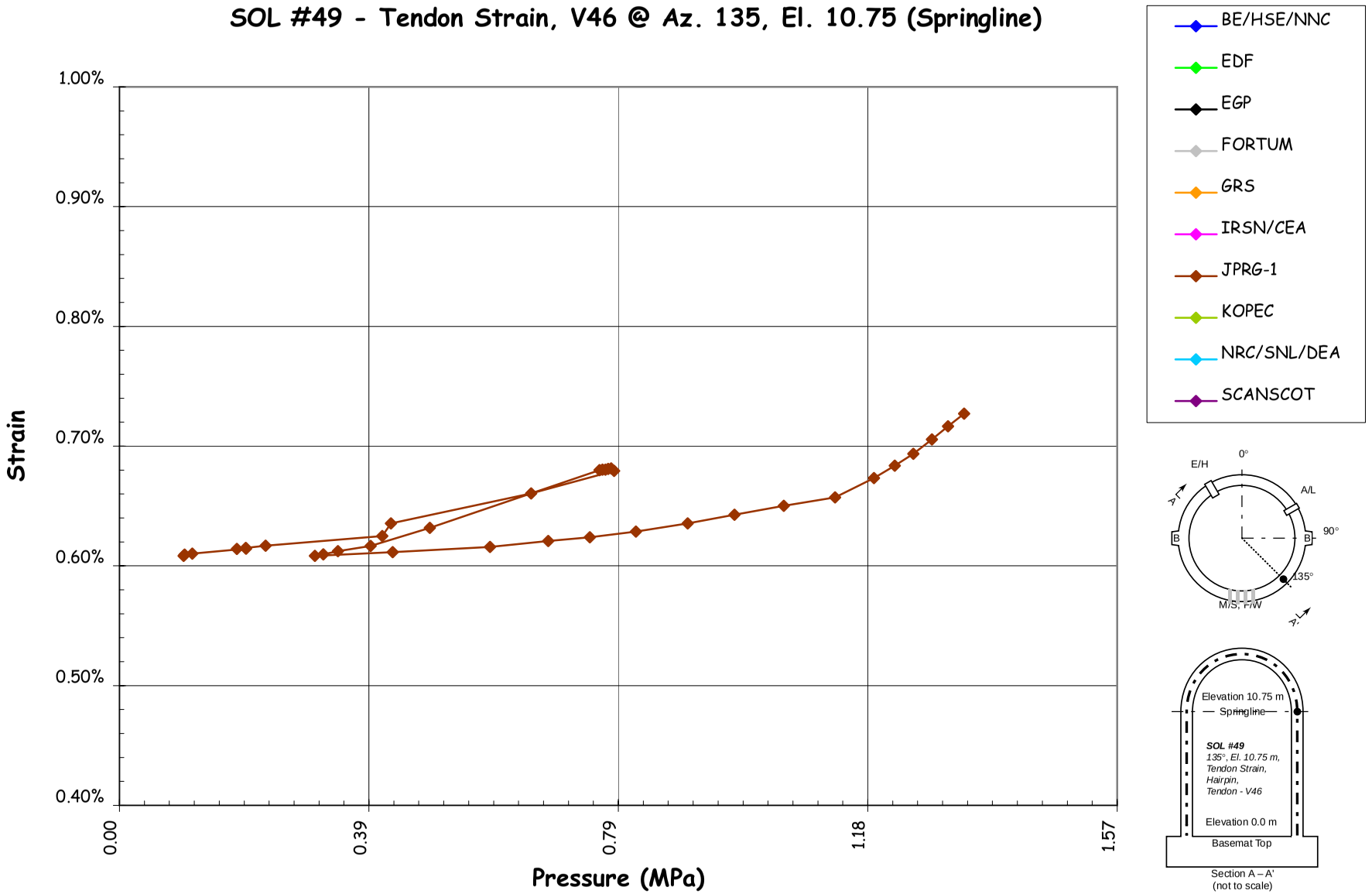
SOL #49 - Tendon Strain, V46 @ Az. 135, El. 10.75 (Springline)
Strain
1.00%
0.90%
0.80%
0.70%
0.60%
0.50%
0.40%
0.00
0.39
0.79
1.18
1.57
Pressure (MPa)
BE/HSE/NNC
EDF
EGP
FORTUM
GRS
IRSN/CEA
JPRG-1
KOPEC
NRC/SNL/DEA
SCANSCOT
E/H
0°
A/L
90°
B
B
135°
M/S, F/W
A
A
Elevation 10.75 m
Springline
SOL #49
135°, El. 10.75 m,
Tendon Strain,
Hairpin,
Tendon - V46
Elevation 0.0 m
Basemat Top
Section A – A'
(not to scale)

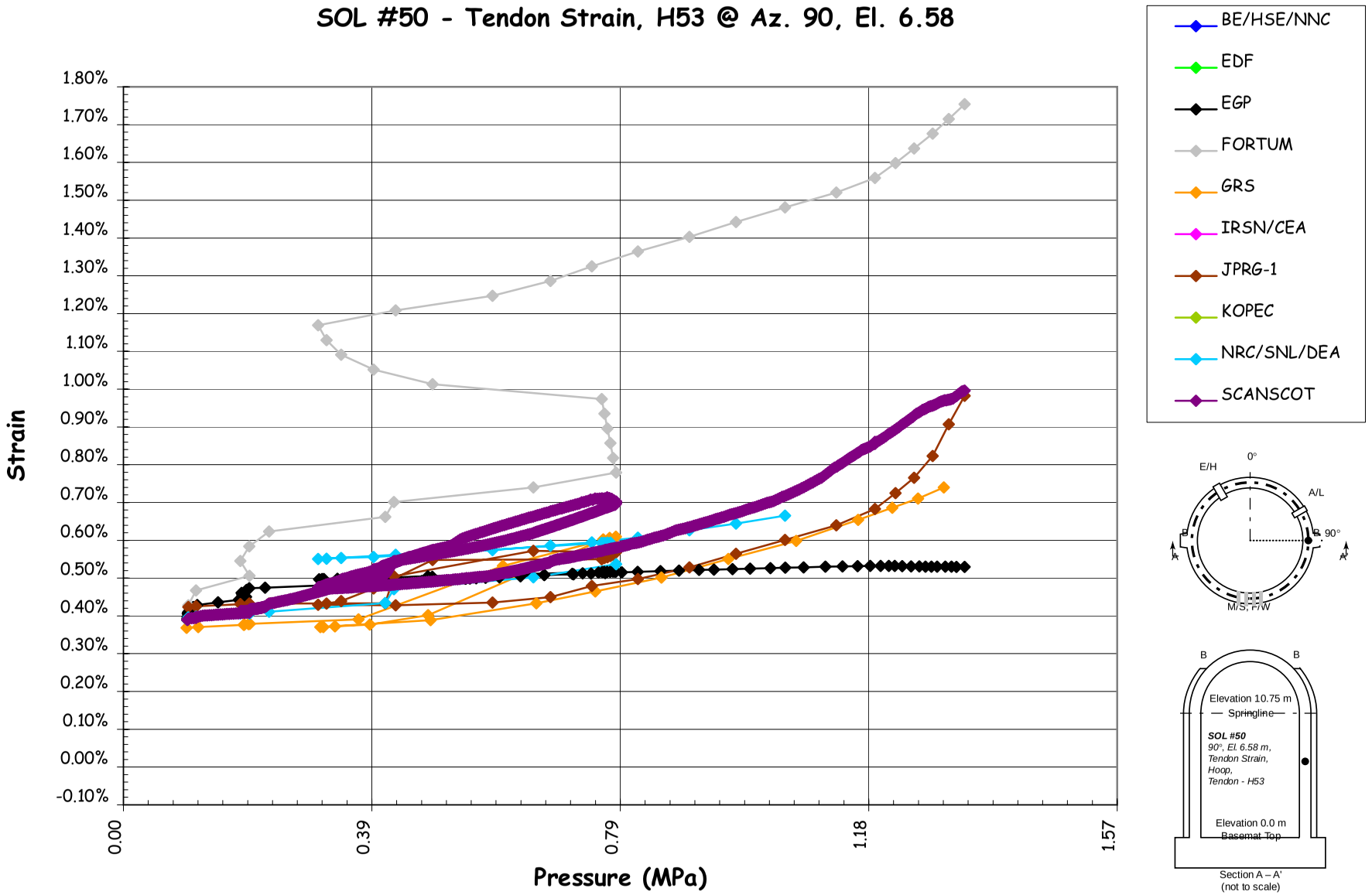
SOL #50 - Tendon Strain, H53 @ Az. 90, El. 6.58
Strain
1.80%
1.70%
1.60%
1.50%
1.40%
1.30%
1.20%
1.10%
1.00%
0.90%
0.80%
0.70%
0.60%
0.50%
0.40%
0.30%
0.20%
0.10%
0.00%
-0.10%
0.00
0.39
0.79
1.18
1.57
Pressure (MPa)
BE/HSE/NNC
EDF
EGP
FORTUM
GRS
IRSN/CEA
JPRG-1
KOPEC
NRC/SNL/DEA
SCANSCOT
E/H
0°
A/L
90°
M/S, F/W
B
B
Elevation 10.75 m
Springline
SOL #50
90°, El. 6.58 m,
Tendon Strain,
Hoop,
Tendon - H53
Elevation 0.0 m
Basemat Top
Section A – A'
(not to scale)

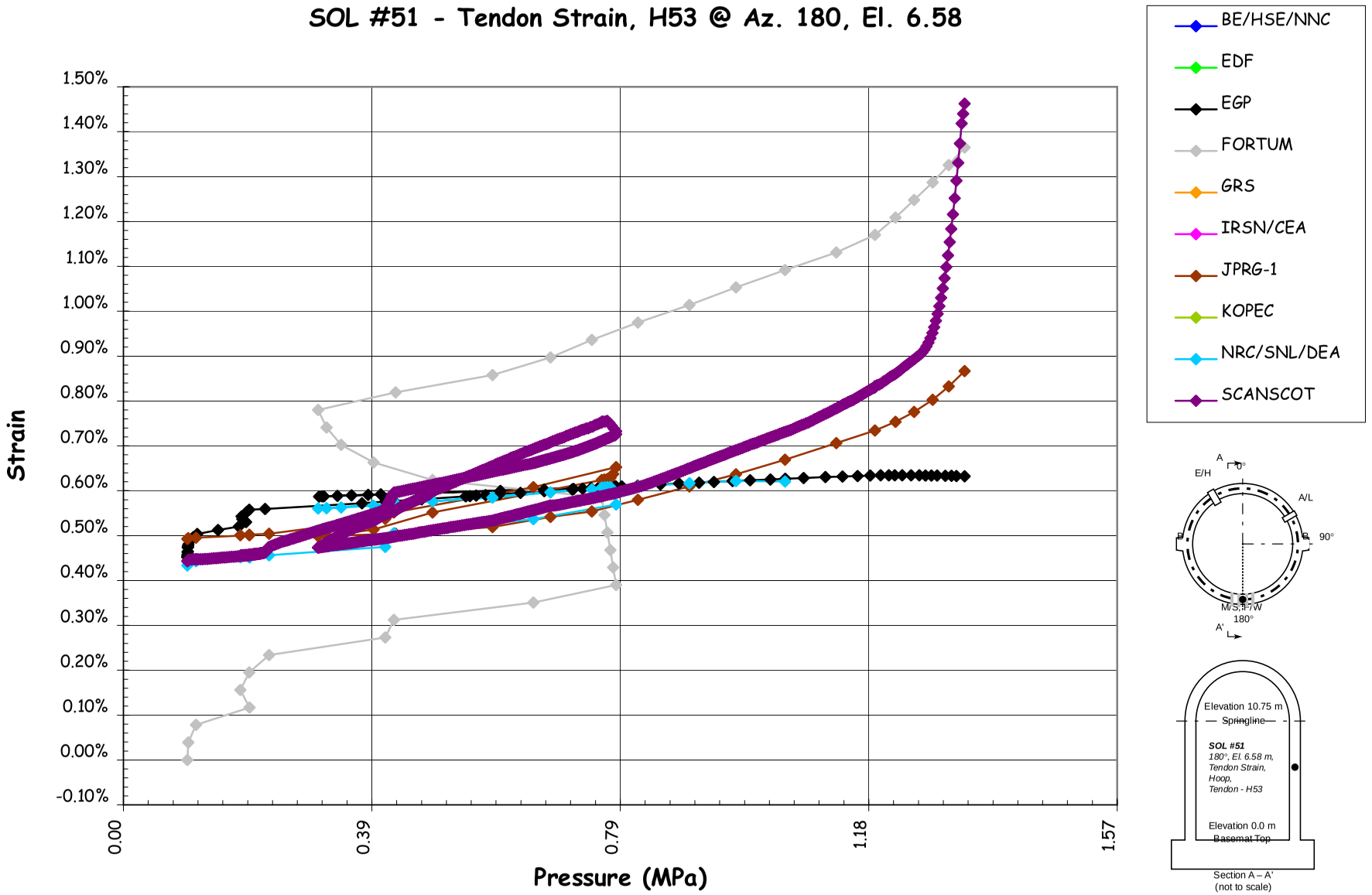
SOL #51 - Tendon Strain, H53 @ Az. 180, El. 6.58
Strain
1.50%
1.40%
1.30%
1.20%
1.10%
1.00%
0.90%
0.80%
0.70%
0.60%
0.50%
0.40%
0.30%
0.20%
0.10%
0.00%
-0.10%
0.00
0.39
0.79
1.18
1.57
Pressure (MPa)
BE/HSE/NNC
EDF
EGP
FORTUM
GRS
IRSN/CEA
JPRG-1
KOPEC
NRC/SNL/DEA
SCANSCOT
A
E/H
0°
A/L
90°
M/S
I-7W
180°
A'
Elevation 10.75 m
Springline
SOL #51
180°, El. 6.58 m,
Tendon Strain,
Hoop,
Tendon - H53
Elevation 0.0 m
Basemat Top
Section A – A'
(not to scale)

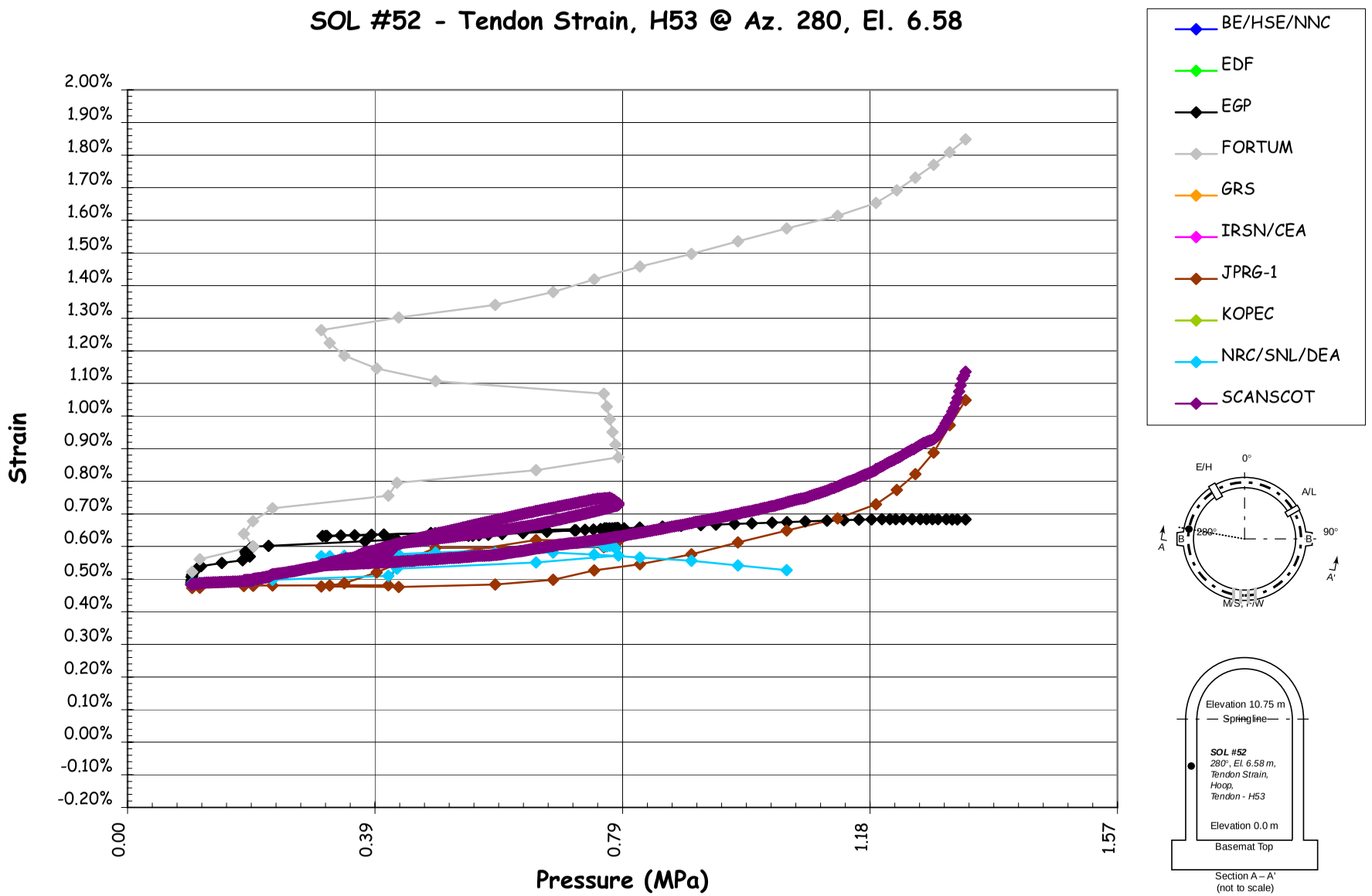
SOL #52 - Tendon Strain, H53 @ Az. 280, El. 6.58
Strain
2.00%
1.90%
1.80%
1.70%
1.60%
1.50%
1.40%
1.30%
1.20%
1.10%
1.00%
0.90%
0.80%
0.70%
0.60%
0.50%
0.40%
0.30%
0.20%
0.10%
0.00%
-0.10%
-0.20%
0.00
0.39
0.79
1.18
1.57
Pressure (MPa)
BE/HSE/NNC
EDF
EGP
FORTUM
GRS
IRSN/CEA
JPRG-1
KOPEC
NRC/SNL/DEA
SCANSCOT
E/H
0°
A/L
280°
90°
A
A'
M/S, I-W
Elevation 10.75 m
Springline
SOL #52
280°, El. 6.58 m,
Tendon Strain,
Hoop,
Tendon - H53
Elevation 0.0 m
Basemat Top
Section A – A'
(not to scale)

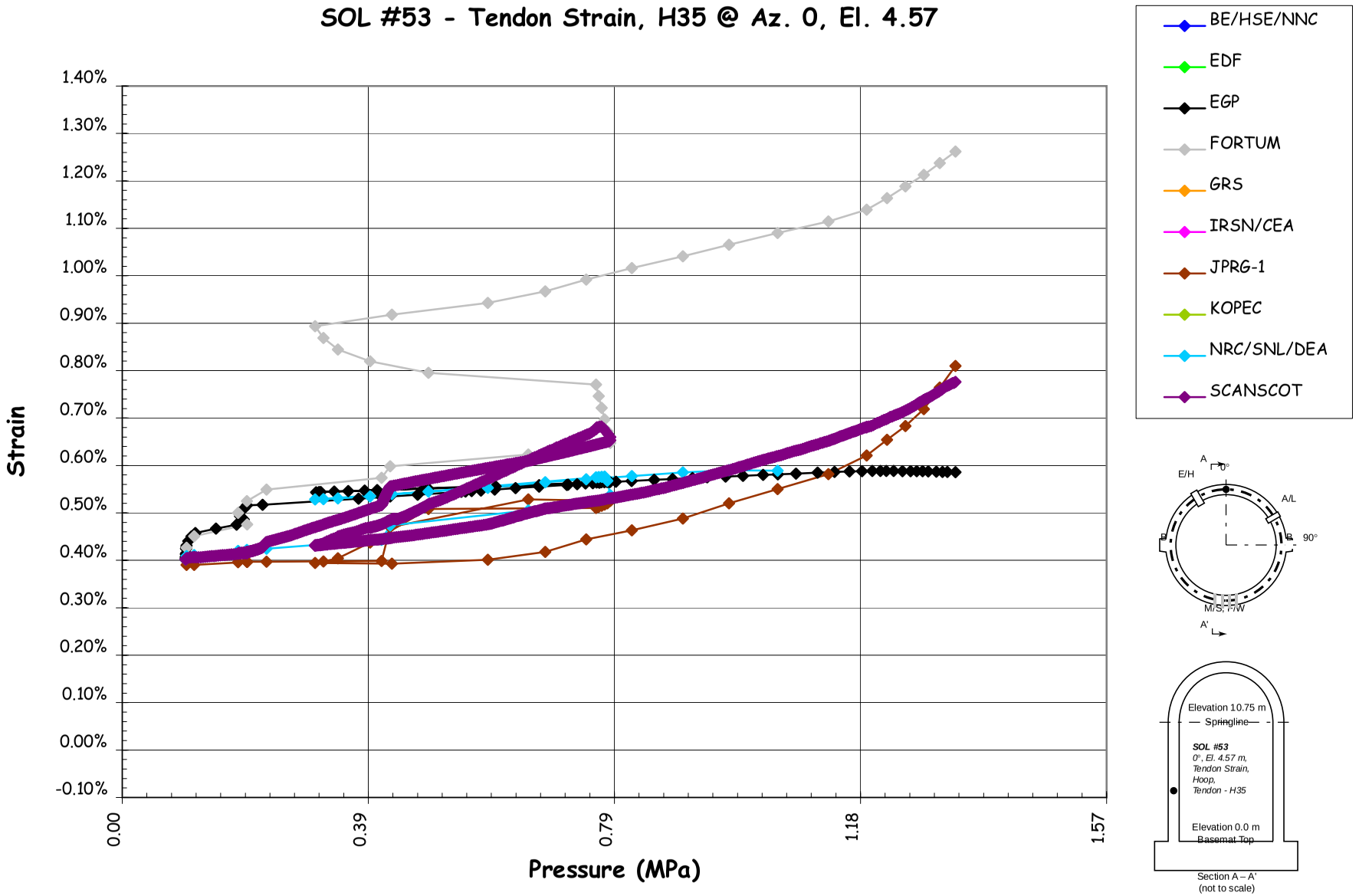
SOL #53 - Tendon Strain, H35 @ Az. 0, El. 4.57
Strain
1.40%
1.30%
1.20%
1.10%
1.00%
0.90%
0.80%
0.70%
0.60%
0.50%
0.40%
0.30%
0.20%
0.10%
0.00%
-0.10%
0.00
0.39
0.79
1.18
1.57
Pressure (MPa)
BE/HSE/NNC
EDF
EGP
FORTUM
GRS
IRSN/CEA
JPRG-1
KOPEC
NRC/SNL/DEA
SCANSCOT
A
E/H
0°
A/L
B
B
90°
M/S, I-W
A'
Elevation 10.75 m
Springline
SOL #53
0°, El. 4.57 m,
Tendon Strain,
Hoop,
Tendon - H35
Elevation 0.0 m
Basemat Top
Section A – A'
(not to scale)

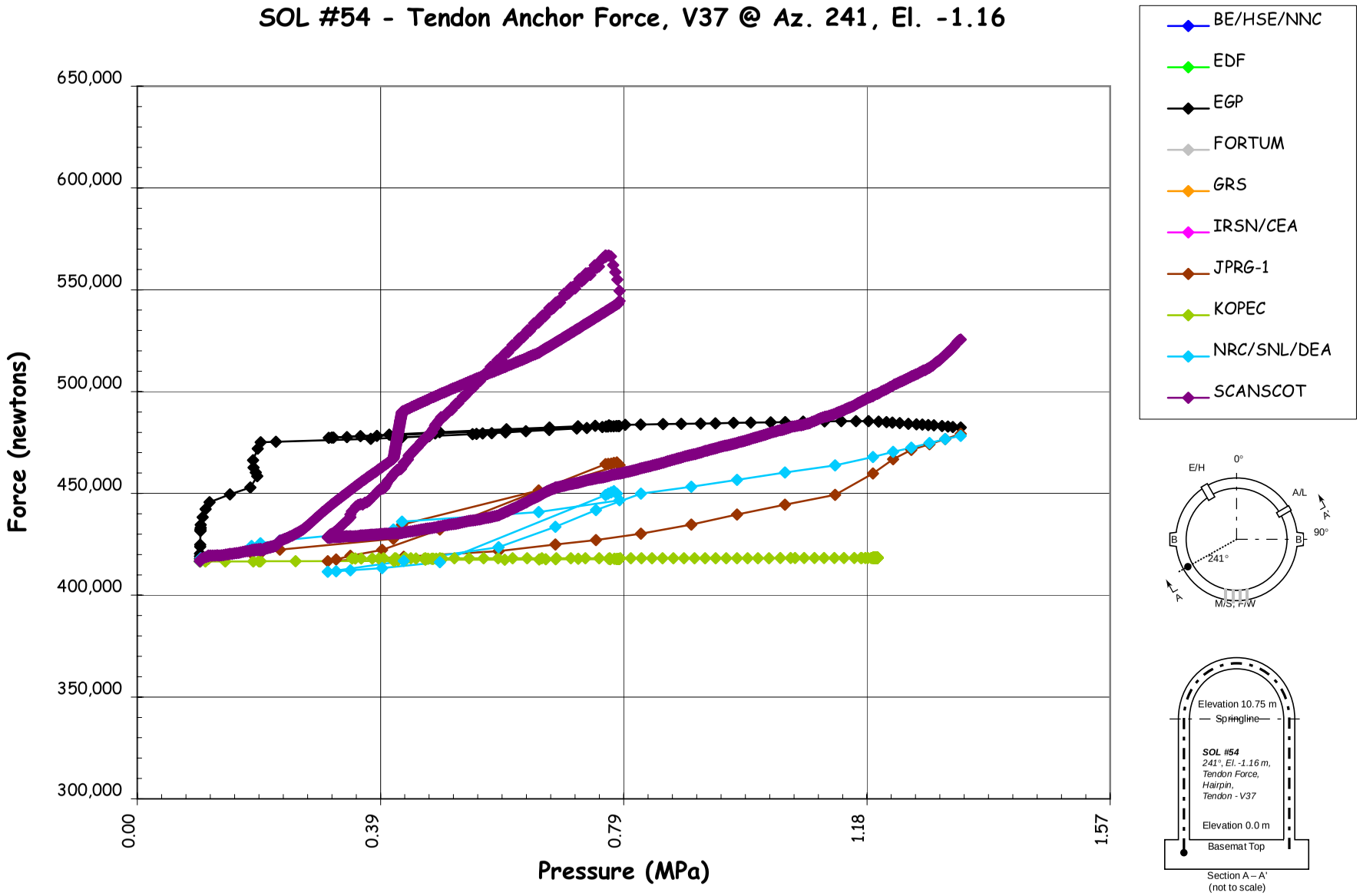
SOL #54 - Tendon Anchor Force, V37 @ Az. 241, El. -1.16
Force (newtons)
650,000
600,000
550,000
500,000
450,000
400,000
350,000
300,000
0.00
0.39
0.79
1.18
1.57
Pressure (MPa)
BE/HSE/NNC
EDF
EGP
FORTUM
GRS
IRSN/CEA
JPRG-1
KOPEC
NRC/SNL/DEA
SCANSCOT
E/H
0°
A/L
90°
241°
M/S, F/W
Elevation 10.75 m
Springline
SOL #54
241°, El. -1.16 m,
Tendon Force,
Hairpin,
Tendon - V37
Elevation 0.0 m
Basemat Top
Section A – A'
(not to scale)

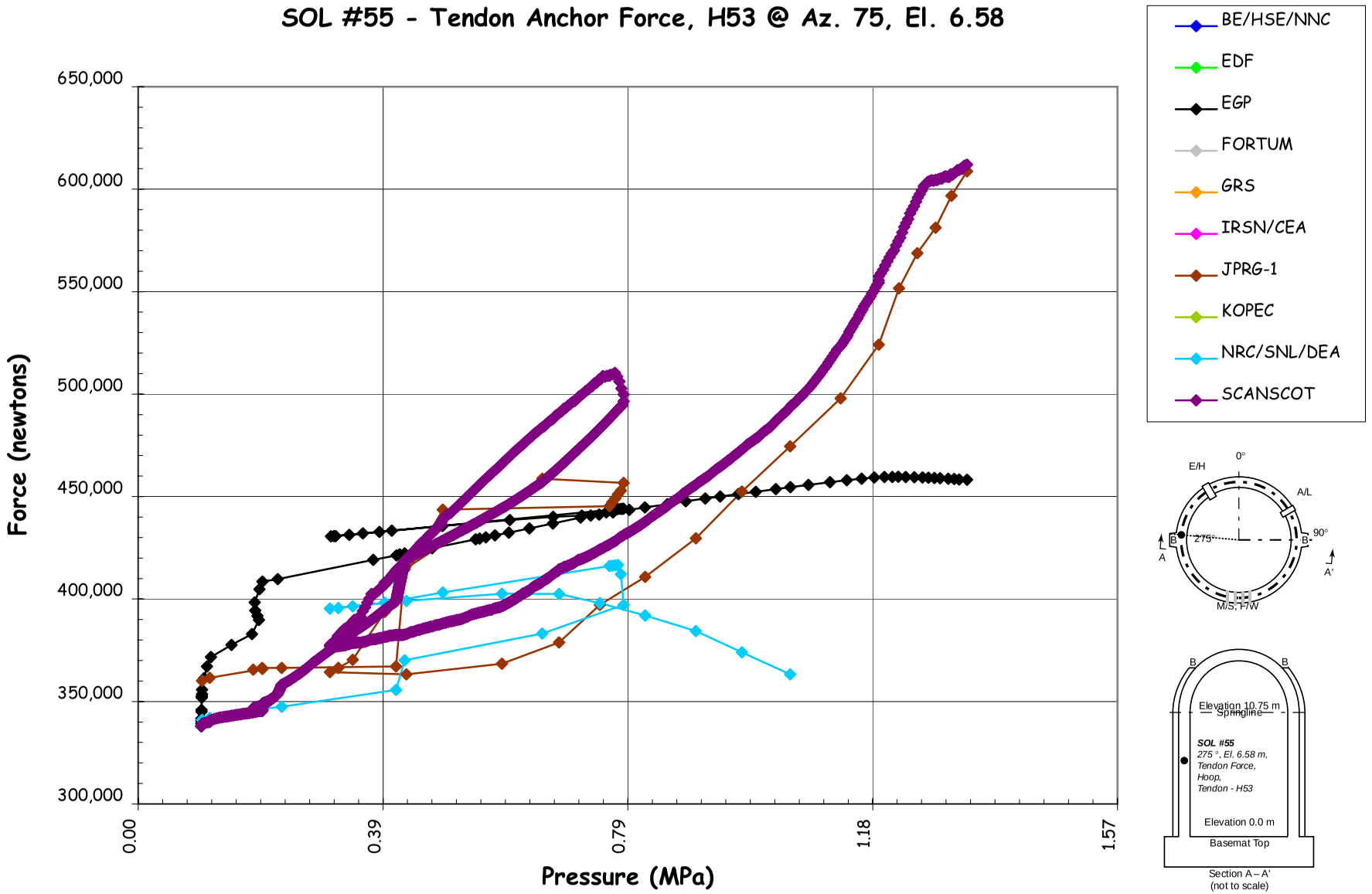
SOL #55 - Tendon Anchor Force, H53 @ Az. 75, El. 6.58
Force (newtons)
650,000
600,000
550,000
500,000
450,000
400,000
350,000
300,000
0.00
0.39
0.79
1.18
1.57
Pressure (MPa)
BE/HSE/NNC
EDF
EGP
FORTUM
GRS
IRSN/CEA
JPRG-1
KOPEC
NRC/SNL/DEA
SCANSCOT
0°
E/H
A/L
90°
275°
B
A
A'
M/S, T-W
Elevation 10.75 m
Springline
SOL #55
275 °, El. 6.58 m,
Tendon Force,
Hoop,
Tendon - H53
Elevation 0.0 m
Basemat Top
Section A – A'
(not to scale)